UNIVERSITY OF SOUTHAMPTON
FACULTY OF ENGINEERING, SCIENCE AND MATHEMATICS
SCHOOL OF ELECTRONICS AND COMPUTER SCIENCE

Hybrid Multi-User OFDM Uplink Systems Using Multiple Antennas

by

Ming Jiang
BEng, MEng

A doctoral thesis submitted in partial fulfilment of the requirements for the award of Doctor of Philosophy at the University of Southampton

December 2005

SUPERVISOR:
Professor Lajos Hanzo
Dip Ing, MSc, PhD, FIEE, FIEEE, DSc, FREng
Chair of Telecommunications
School of Electronics and Computer Science
University of Southampton
Southampton SO17 1BJ
United Kingdom

Dedicated to everyone
who has painted the colorful pictures
in my life...

UNIVERSITY OF SOUTHAMPTON

ABSTRACT

Faculty of Engineering, Science and Mathematics

School of Electronics and Computer Science

Doctor of Philosophy

Hybrid Multi-User OFDM Uplink Systems Using Multiple Antennas

by Ming Jiang

The employment of multiple antennas in Orthogonal Frequency Division Multiplexing (OFDM) based systems constitutes an effective way of improving the systems' performance. Multiple transmitters may be used for achieving a number of design objectives. This thesis explores two different design principles. Firstly, the family of Space-Time Block Codes (ST-BCs) can be exploited, which exhibits a remarkable encoding and decoding simplicity and yet achieves a high transmit diversity gain, when combined with a range of Forward Error Correction (FEC) codes, such as Turbo Convolutional (TC) codes, Low Density Parity Check (LDPC) codes and Coded Modulation (CM) schemes.

Secondly, multiple antennas may be used for supporting a multiplicity of users by differentiating them with the aid of their unique, user-specific Channel Impulse Responses (CIRs). More explicitly, by invoking the Multiple-Input Multiple-Output (MIMO) Space Division Multiple Access (SDMA) techniques, a number of simultaneous users may share the same frequency bandwidth in different geographical locations, which results in an increased bandwidth efficiency. In order to improve the achievable performance of SDMA-OFDM systems, various CM schemes, namely Trellis Coded Modulation (TCM), Turbo TCM (TTCM), Bit-Interleaved Coded Modulation (BICM) and Iteratively Decoded BICM (BICM-ID) can be employed for attaining a substantial coding gain without any bandwidth expansion. Furthermore, classic Walsh-Hadamard Transform Spreading (WHTS) often used in Code Division Multiple Access (CDMA) systems can be invoked across a number of OFDM subcarriers in the frequency domain, for the sake of exploiting the frequency diversity potential offered by frequency-selective fading channels.

Regardless of the specific choice of the FEC schemes, the Multi-User Detector (MUD) invoked at the SDMA base station has a significant effect on the achievable system performance. Specifically, the Maximum-Likelihood (ML) MUD achieves the optimum performance at the cost of a typically excessive computational complexity. By contrast, the Genetic Algorithm (GA) based MUDs attain a near-ML performance, despite having a substantially reduced complexity. Moreover, the GA MUDs can be further enhanced in terms of three different design aspects. Firstly, an iterative detector architecture involving channel decoders can be employed. Secondly, the GA's detection capability can be improved by introducing a novel ge-

netic mutation approach, which we refer to as the Biased Q-function based Mutation (BQM) scheme. Thirdly, it is beneficial to generate soft information as the GA's output, which assists the channel decoders in attaining an increased coding gain.

Furthermore, time-domain Direct-Sequence Spreading (DSS) and a novel subcarrier-based Slow Frequency-Hopping (SFH) technique, referred to as Slow SubCarrier-Hopping (SSCH), can be incorporated into SDMA-OFDM systems. With the aid of the new Uniform SSCH (USSCH) patterns proposed, hybrid DSS/SSCH SDMA-OFDM systems are rendered capable of overcoming a number of disadvantages of the conventional SDMA-OFDM arrangements, benefitting from both a high frequency diversity gain and a robustness against the Multi-User Interference (MUI).

Naturally, in SDMA-OFDM systems accurate channel estimation is required at the receiver for the sake of invoking both coherent demodulation and interference cancellation. Compared to Single-Input Single-Output (SISO) systems, channel estimation in the MIMO scenario becomes more challenging, since a significantly increased number of independent transmitter-receiver channel links have to be estimated simultaneously for each subcarrier. Moreover, the interfering signals of the other transmitter antennas have to be suppressed. This problem, however, may be effectively mitigated by employing joint channel estimation and symbol detection techniques. With the advent of soft-decoded GAs, the proposed iterative Joint Channel Estimation and Multi-User Detection (GA-JCEMUD) approach constitutes an attractive solution to the multi-user channel estimation problem in MIMO SDMA-OFDM systems, especially in the so-called overloaded scenarios, where the number of users exceeds that of the receiver antennas. More specifically, the GA-JCEMUD technique is capable of simultaneously capturing the fading envelope changes of each individual user-receiver link, thus achieving an equally good performance over all the user-receiver links.

Acknowledgement

First of all, I would like to thank my supervisor Professor Lajos Hanzo from the bottom of my heart for his substantial assistance to me. I would like to express my uttermost gratitude for him for his reliable friendship, continual enthusiasm and invaluable encouragement during my work. His efficient guidance, insightful inspiration and impressive perseverance have significantly benefitted me not only in my work but also in my personal life. His loyalty to research has exhibited the right way to be an excellent researcher, which will continue to stimulate me to make progress in my future career.

Especially, my grateful thanks go to Dr. Walter Tuttlebee and the Virtual Centre of Excellence in Mobile and Personal Communications Ltd. (Mobile VCE) for their generous financial support.

Many thanks are also due to the academic staff of the Communications Group, especially to Professor Sheng Chen and Dr. Lie-Liang Yang for their useful guidance in my research. Also special thanks to Denise Harvey for her help in the administrative work. Many personal thanks to all my colleagues of the Communications Group, particularly to Dr. Soon Xin Ng for his kind help in Coded Modulations, and to Mr. Jos Akhtman for his inspirational discussions as well as selfless collaborations during our cooperative VCE project work.

Finally I would like thank my parents back in China for their love and cares since I was born. And special thanks to my beloved wife Yongjie for her love and support during these years.

List of Publications

Book Chapters

1. M. Jiang, J. Akhtman, and L. Hanzo: "Chapter 11: Genetic Algorithm Aided Joint Channel Estimation and MUD for SDMA OFDM", In: L. Hanzo and T. Keller, *An OFDM and MC-CDMA Primer*. IEEE Press - John Wiley & Sons Ltd., 2006.

Journal Papers

2. M. Jiang and L. Hanzo, "Improved Hybrid MMSE Detection for Turbo Trellis Coded Modulation Assisted Multi-User OFDM Systems," *Electronics Letters*, vol. 40, no. 16, pp. 1002-1003, August 2004.

3. M. Jiang, S. X. Ng, and L. Hanzo, "Hybrid Iterative Multi-User Detection for Channel Coded Space Division Multiple Access OFDM Systems," *IEEE Transactions on Vehicular Technology*, vol. 55, no. 1, pp. 115-127, January 2006.

4. M. Jiang, J. Akhtman, and L. Hanzo, "Soft-information Assisted Near-optimum Nonlinear Detection for BLAST-type Space Division Multiplexing OFDM Systems," accepted by *IEEE Wireless Communications Letters*, January 2006.

5. M. Jiang, L.-L. Yang, and L. Hanzo, "Direct-Sequence-Spreading and Slow-Subcarrier-Hopping Aided Multi-User OFDM Systems," submitted to *IEEE Transactions on Vehicular Technology*, June 2005; revised December 2005.

6. M. Jiang and L. Hanzo, "Multi-User MIMO OFDM Systems Using Subcarrier-Hopping," submitted to *IEE Proceedings - Communications*, August 2005; revised March 2006.

7. M. Jiang, J. Akhtman, and L. Hanzo, "Iterative Joint Channel Estimation and Multi-User Detection for Multiple-Antenna Aided OFDM Systems," submitted to *IEEE Transactions on Wireless Communications*, October 2005.

Conference Papers

8. M. Jiang, S. X. Ng, and L. Hanzo, "TCM, TTCM, BICM and BICM-ID Assisted MMSE Multi-User Detected SDMA-OFDM Using Walsh-Hadamard Spreading," in *Proceedings of the 2004 IEEE 59th Vehicular Technology Conference (VTC '04 Spring)*, vol. 2, Milan, Italy, 17-19 May 2004, pp. 1129-1133.

9. M. Jiang and L. Hanzo, "Genetically Enhanced TTCM Assisted MMSE Multi-User Detection for SDMA-OFDM," in *Proceedings of the 2004 IEEE 60th Vehicular Technology Conference (VTC '04 Fall)*, vol. 3, Los Angeles, USA, 26-29 September 2004, pp. 1954-1958.

10. M. Jiang, S. X. Ng, and L. Hanzo, "Slow Subcarrier-Hopped Space Division Multiple Access OFDM Systems," in *Proceedings of the 2005 IEEE 62nd Vehicular Technology Conference (VTC '05 Fall)*, Dallas, USA, 25-28 September 2005.

11. M. Jiang and L. Hanzo, "Iterative Hybrid Multi-User Detection Using Genetic Algorithm and Biased Mutation," in *Proceedings of the 2005 IEE 6th International Conference on 3G and Beyond (3G '05)*, London, UK, 7-9 November 2005, pp. 297-301.

12. M. Jiang, J. Akhtman, and L. Hanzo, "Near-Optimum Nonlinear Soft Detection for Multiple-Antenna Assisted OFDM," accepted by the *2006 IEEE Wireless Communications and Networking Conference (WCNC '06)*, Las Vegas, USA, 3-6 April 2006.

13. M. Jiang, J. Akhtman, F. Guo, and L. Hanzo, "Iterative Joint Channel Estimation and Multi-User Detection for High-Throughput Multiple-Antenna Aided OFDM Systems," accepted by the *2006 IEEE 63rd Vehicular Technology Conference (VTC '06 Spring)*, Melbourne, Australia, 7-10 May 2006.

Technical Company Reports

14. M. Jiang and L. Hanzo, "SDMA-OFDM Using Channel Coding and Spreading," University of Southampton, Southampton, UK, *Mobile VCE Core 3 Programme - Wireless Enablers 2.2: Deliverable D-WE2.2.1(P2)*, December 2003.

15. M. Jiang and L. Hanzo, "Novel MUD Techniques Designed for OFDM/MC-CDMA," University of Southampton, Southampton, UK, *Mobile VCE Core 3 Programme - Wireless Enablers 2.2: Deliverable D-WE2.2.2(P2)*, June 2004.

16. M. Jiang and L. Hanzo, "Subband-Hopped and Subcarrier-Hopped Multi-User SDMA-OFDM Systems," University of Southampton, Southampton, UK, *Mobile VCE Core 3 Programme - Wireless Enablers 2.2: Deliverable D-WE2.2.3(P2)*, December 2004.

17. M. Jiang, J. Akhtman, and L. Hanzo, "Joint Channel Estimation and Multi-User Detection for Multiple-Antenna Aided OFDM," University of Southampton, Southampton, UK, *Mobile VCE Core 3 Programme - Wireless Enablers 2.2: Deliverable D-WE2.2.4(P2)*, October 2005.

Contents

Chapter 1

Introduction

1.1 Historic Background

During the past decades, wireless communication has benefitted from substantial advances and it is considered as the key enabling technique of innovative future consumer products. For the sake of satisfying the requirements of various applications, significant technological achievements are required to ensure that wireless devices have appropriate architectures suitable for supporting a wide range of services delivered to the users.

In the foreseeable future, the large-scale deployment of wireless devices and the requirements of high-bandwidth applications are expected to lead to tremendous new challenges in terms of the efficient exploitation of the achievable spectral resources. New wireless techniques, such as Ultra WideBand (UWB) [1], advanced source and channel encoding as well as various smart antenna techniques, for example Space-Time Codes (STCs) [2], Space Division Multiple Access (SDMA) [3] and beamforming, as well as other Multiple-Input Multiple-Output (MIMO) [4] wireless architectures are capable of offering substantial improvements over classic communication systems. Hence researchers have focused their attention on the next generation of wireless broadband communications systems, which aim for delivering multimedia services requiring data rates beyond 2Mbps. Undoubtedly, supporting such high data rates, while maintaining a high robustness against radio channel impairments, such as multi-path fading and frequency-selective fading, requires further enhanced system architectures.

1.1.1 Orthogonal Frequency Division Multiplexing

In recent years Orthogonal Frequency Division Multiplexing (OFDM) [3, 5–7] has emerged as a successful air-interface technique. In the context of wired environments, OFDM techniques

are also known as Discrete MultiTone (DMT) [8] transmissions and are employed in the American National Standards Institute's (ANSI) Asymmetric Digital Subscriber Line (ADSL) [9], High-bit-rate Digital Subscriber Line (HDSL) [10], and Very-high-speed Digital Subscriber Line (VDSL) [11] standards as well as in the European Telecommunication Standard Institute's (ETSI) [12] VDSL applications. In wireless scenarios, OFDM has been advocated by many European standards, such as Digital Audio Broadcasting (DAB) [13], Digital Video Broadcasting for Terrestrial television (DVB-T) [14], Digital Video Broadcasting for Handheld terminals (DVB-H) [15], Wireless Local Area Networks (WLANs) [16] and Broadband Radio Access Networks (BRANs) [17]. Furthermore, OFDM has been ratified as a standard or has been considered as a candidate standard by a number of standardization groups of the Institute of Electrical and Electronics Engineers (IEEE), such as:

- IEEE 802.11a [18]: An extension to IEEE 802.11 [19] that applies to WLANs and provides a bitrate of up to 54Mbps in the 5GHz band. In comparison to IEEE 802.11, where Frequency-Hopping Spread Spectrum (FHSS) or Direct-Sequence Spread Spectrum (DSSS) are used, IEEE 802.11a employs an OFDM scheme which applies to Wireless Asynchronous Transfer Mode (WATM) networks and access hubs.

- IEEE 802.11g [20]: Offers wireless transmission over relatively short distances at 20-54Mbps in the 2.4GHz band. It also uses an OFDM scheme.

- IEEE 802.11n [21]: Candidate standard for next generation WLANs, which was created from previous IEEE 802.11 standards by incorporating MIMO techniques. It offers high-throughput wireless transmission at 100-200Mbps.

- IEEE 802.15.3a [22]: Candidate standard using MultiBand OFDM (MB-OFDM), which is based on the IEEE 802.15.3 [23] scheme proposed for Wireless Personal Area Networks (WPANs).

- IEEE 802.16 [24]: Defines wireless services operating in the 2-11GHz band associated with Wireless Metropolitan Area Networks (WMANs), providing a communication link between a subscriber and a core network, e.g. the public telephone network and the Internet.

The first OFDM schemes date back in 1960s, which were proposed by Chang [25] and Saltzberg [26]. In the classic parallel data transmission systems [25,26], the Frequency-Domain (FD) bandwidth is divided into a number of non-overlapping subchannels, each of which hosts a specific carrier widely referred to as a subcarrier. While each subcarrier is separately modulated by a data symbol, the overall modulation operation across all the subchannels results in a frequency-multiplexed signal. All of the sinc-shaped subchannel spectra exhibit

zero-crossings at all of the remaining subcarrier frequencies and the individual subchannel spectra are orthogonal to each other. This ensures that the subcarrier signals do not interfere with each other, when communicating over perfectly distortionless channels, as a consequence of their orthogonality [3].

The early OFDM schemes [25–28] required banks of sinusoidal subcarrier generators and demodulators, which imposed a high implementation complexity. This drawback limited the application of OFDM to military systems until 1971, when Weinstein and Ebert [29] suggested that the Discrete Fourier Transform (DFT) can be used for the OFDM modulation and demodulation processes, which significantly reduces the implementation complexity of OFDM. Since then, more practical OFDM research has been carried out. For example, in the early 1980s Peled and Ruiz [30] proposed a simplified FD data transmission method using a cyclic prefix aided technique and exploited reduced-complexity algorithms for achieving a significantly lower computational complexity than that of classic single-carrier time-domain Quadrature Amplitude Modulation (QAM) [31] modems. Around the same era, Keasler *et al.* [32] invented a high-speed OFDM modem for employment in switched networks, such as the telephone network. Hirosaki designed a subchannel-based equalizer for an orthogonally multiplexed QAM system in 1980 [33] and later introduced the DFT-based implementation of OFDM systems [34], based on which a so-called groupband data modem was developed [35]. Cimini [36] and Kalet [37] investigated the performance of OFDM modems in mobile communication channels. Furthermore, Alard and Lassalle [38] applied OFDM in digital broadcasting systems, which was the pioneering work of the European DAB standard [13] established in the mid-1990s. More recent advances in OFDM transmission were summarized in the state-of-the-art collection of works edited by Fazel and Fettweis [39]. Other important recent OFDM references include the books by Hanzo *et al.* [3] and Van Nee *et al.* [7] as well as a number of overview papers [40–42].

OFDM has some key advantages over other widely-used wireless access techniques, such as Time Division Multiple Access (TDMA) [43], Frequency Division Multiple Access (FDMA) [43] and Code Division Multiple Access (CDMA) [44–48]. The main merit of OFDM is the fact that the radio channel is divided into many narrow-band, low-rate, frequency-nonselective subchannels or subcarriers, so that multiple symbols can be transmitted in parallel, while maintaining a high spectral efficiency. Each subcarrier may deliver information for a different user, resulting in a simple multiple access scheme known as Orthogonal Frequency Division Multiple Access (OFDMA) [49–52]. This enables different media such as video, graphics, speech, text, or other data to be transmitted within the same radio link, depending on the specific types of services and their Quality-of-Service (QoS) requirements. Furthermore, in OFDM systems different modulation schemes can be employed for different subcarriers or

even for different users. For example, the users close to the Base Station (BS) may have a relatively good channel quality, thus they can use high-order modulation schemes to increase their data rates. By contrast, for those users that are far from the BS or are serviced in highly-loaded urban areas, where the subcarriers' quality is expected to be poor, low-order modulation schemes can be invoked [53].

Besides its implementational flexibility, the low complexity required in transmission and reception as well as the attainable high performance render OFDM a highly attractive candidate for high data rate communications over time-varying frequency-selective radio channels. For example, in classic single-carrier systems, complex equalizers have to be employed at the receiver for the sake of mitigating the Inter-Symbol Interference (ISI) introduced by multi-path propagation. By contrast, when using a cyclic prefix [30], OFDM exhibits a high resilience against the ISI. Incorporating channel coding techniques into OFDM systems, which results in Coded OFDM (COFDM) [54,55], allows us to maintain robustness against frequency-selective fading channels, where busty errors are encountered at specific subcarriers in the FD.

However, besides its significant advantages, OFDM also has a few disadvantages. One problem is the associated increased Peak-to-Average Power Ratio (PAPR) in comparison to single-carrier systems [3], requiring a large linear range for the OFDM transmitter's output amplifier. In addition, OFDM is sensitive to carrier frequency offset, resulting in Inter-Carrier Interference (ICI) [56].

As a summary of this section, we outline the milestones and the main contributions found in the OFDM literature in Tables 1.1, 1.2 and 1.3, respectively.

1.1.2 Multiple-Input Multiple-Output Assisted OFDM

1.1.2.1 The Benefits of MIMOs

High data-rate wireless communications have attracted significant interest and constitute a substantial research challenge in the context of the emerging WLANs and other indoor multimedia networks. Specifically, the employment of multiple antennas at both the transmitter and the receiver, which is widely referred to as the Multiple-Input Multiple-Output (MIMO) technique, constitutes a cost-effective approach to high-throughput wireless communications.

The concepts of MIMOs have been under development for many years for both wired and wireless systems. One of the earliest MIMO applications for wireless communications dates back to 1984, when Winters [4] published a breakthrough contribution, where he introduced a technique of transmitting data from multiple users over the same frequency/time channel using multiple antennas at both the transmitter and receiver ends. Based on this work, a

Year	Milestone
1966	First OFDM scheme proposed by Chang [25] for dispersive fading channels.
1967	Saltzberg [26] studied a multi-carrier system employing Orthogonal QAM (O-QAM) of the carriers.
1970	U.S. patent on OFDM issued [28].
1971	Weinstein and Ebert [29] applied DFT to OFDM modems.
1980	Hirosaki designed a subchannel-based equalizer for an orthogonally multiplexed QAM system [33].
	Keasler *et al.* [32] described an OFDM modem for telephone networks.
1985	Cimini [36] investigated the feasibility of OFDM in mobile communications.
1987	Alard and Lasalle [38] employed OFDM for digital broadcasting.
1991	ANSI ADSL standard [9].
1994	ANSI HDSL standard [10].
1995	ETSI DAB standard [13]: the first OFDM-based standard for digital broadcasting systems.
1996	ETSI WLAN standard [16].
1997	ETSI DVB-T standard [14].
1998	ANSI VDSL and ETSI VDSL standards [11,12].
	ETSI BRAN standard [17].
1999	IEEE 802.11a WLAN standard [18].
2002	IEEE 802.11g WLAN standard [20].
2003	Commercial deployment of FLASH-OFDM [57,58] commenced.
2004	ETSI DVB-H standard [15].
	IEEE 802.16 WMAN standard [24].
	Candidate for IEEE 802.11n standard for next generation WLAN [21].
	Candidate for IEEE 802.15.3a standard for WPAN (using MB-OFDM) [22].
2005	Candidate for 3.75G mobile cellular standards (3GPP [59] and 3GPP2 [60]).
	Candidate for 4G standards in China, Japan and South Korea (CJK) [61].

Table 1.1: Milestones in the history of OFDM.

Year	Author(s)	Contribution
1966	Chang [25]	Proposed the first OFDM scheme.
1967	Saltzberg [26]	Studied a multi-carrier system employing O-QAM.
1968	Chang and Gibby [27]	Presented a theoretical analysis of the performance of an orthogonal multiplexing data transmission scheme.
1970	Chang [28]	U.S. patent on OFDM issued.
1971	Weinstein and Ebert [29]	Applied DFT to OFDM modems.
1980	Hirosaki [33]	Designed a subchannel-based equalizer for an orthogonally multiplexed QAM system.
	Peled and Ruiz [30]	Described a reduced-complexity FD data transmission method together with a cyclic prefix technique.
	Keasler *et al.* [32]	Invented an OFDM modem for telephone networks.
1981	Hirosaki [34]	Suggested a DFT-based implementation of OFDM systems.
1985	Cimini [36]	Investigated the feasibility of OFDM in mobile communications.
1986	Hirosaki, Hasegawa and Sabato [35]	Developed a groupband data modem using an orthogonally multiplexed QAM technique.
1987	Alard and Lasalle [38]	Employed OFDM for digital broadcasting.
1989	Kalet [37]	Analyzed multitone QAM modems in linear channels.
1990	Bingham [5]	Discussed various aspects of early OFDM techniques in depth.
1991	Cioffi [9]	Introduced the ANSI ADSL standard.
1993-1995	Warner [62], Moose [56] and Pollet [63]	Conducted studies on time and frequency synchronization in OFDM systems.
1994-1996	Jones [64], Shepherd [65] and Wulich [66, 67]	Explored various coding and post-processing techniques designed for minimizing the peak power of the OFDM signal.
1997	Li and Cimini [68, 69]	Revealed how clipping and filtering affect OFDM systems.
	Hara and Prasad [70]	Compared various methods of combining CDMA and OFDM.
1998	Li, Cimini and Sollenberger [71]	Designed a robust Minimum Mean Square Error (MMSE) based channel estimator for OFDM systems.
	May, Rohling and Engels [54]	Carried out a performance analysis of Viterbi decoding in the context of 64-Differential Amplitude and Phase-Shift Keying (64-DAPSK) and 64QAM modulated OFDM signals.
1999	Li and Sollenberger [72]	Focused on parameter estimation invoked by a MMSE diversity combiner designed for adaptive antenna array aided OFDM.
	Armour, Nix and Bull [73–75]	Illustrated the combined OFDM-equalization aided receiver and the design of pre-Fast Fourier Transform (FFT) equalizers.
	Prasetyo and Aghvami [76, 77]	Simplified the transmission frame structure for achieving fast burst synchronization in OFDM systems.
	Cherriman, Keller and Hanzo [78]	Evaluated a packetization and packet acknowledgment scheme assisted H.263 video codec in OFDM scenarios.
	Wong *et al.* [79]	Advocated a subcarrier, bit and power allocation algorithm to minimize the total transmit power of multi-user OFDM.

Table 1.2: Main contributions on OFDM (Part 1).

Year	Author(s)	Contribution
2000	Fazel and Fettweis [39]	A collection of state-of-the-art works on OFDM.
	Van Nee and Prasad [7]	OFDM for wireless multimedia communications.
	Lee, Keller and Hanzo [80]	Studied enhanced turbo-coded OFDM receivers designed for DVB-T systems.
	Keller and Hanzo [40]	Highlighted the adaptive bit allocation and turbo coding schemes in the context of OFDM.
	Lin, Cimini and Chuang [55]	Invoked turbo coding in an OFDM system using diversity.
	Keller and Hanzo [81]	Analyzed the design tradeoffs of turbo-coded burst-by-burst adaptive OFDM wideband transceivers.
2001-2002	Keller *et al.* [82]	Quantified the effect of time-domain and frequency-domain synchronization errors in OFDM systems.
	Lu and Wang [83–86]	Considered channel coded STC-assisted OFDM systems.
	Cherriman, Keller and Hanzo [87]	A range of adaptive OFDM video systems were proposed for interactive communications over wireless channels.
2003	Hanzo, Münster, Choi and Keller [3]	OFDM for broadband multi-user communications, WLANs and broadcasting.
2004	Simeone, Bar-Ness and Spagnolini [88]	Demonstrated a subspace tracking algorithm used for channel estimation in OFDM systems.
	J. Zhang, Rohling and P. Zhang [89]	Adopted an ICI cancellation scheme to combat the ICI in OFDM systems.
	Necker and Stüber [90]	Exploited a blind channel estimation scheme based on the Maximum Likelihood (ML) principle in OFDM systems.
	Doufexi *et al.* [91]	Reflected the benefits of using sectorized antennas in WLANs.
	Alsusa, Lee and McLaughlin [92]	Proposed packet based multi-user OFDM systems using adaptive subcarrier-user allocation.
2005	Williams *et al.* [93]	Evaluated a pre-FFT synchronisation method for OFDM.

Table 1.3: Main contributions on OFDM (Part 2).

patent was filed and approved [94]. Sparked off by Winters' pioneering work [4], Salz [95] investigated joint transmitter/receiver optimization using the MMSE criterion. Since then, Winters and others [96–104] have made further significant advances in the field of MIMOs. In 1996, Raleigh [105] and Foschini [106] proposed new approaches for improving the efficiency of MIMO systems, which inspired numerous further contributions [107–115].

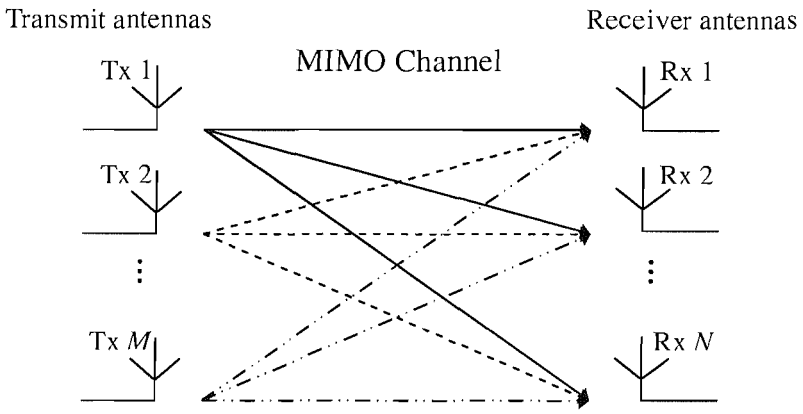

Figure 1.1: Schematic of the generic MIMO system employing M transmitter antennas and N receiver antennas.

As a key building block of next-generation wireless communication systems, MIMOs are capable of supporting significantly higher data rates than the Universal Mobile Telecommunications System (UMTS) and the High Speed Downlink Packet Access (HSDPA) based 3G networks [116]. As indicated by the terminology, a MIMO system employs multiple transmitter and receiver antennas for delivering parallel data streams, as illustrated in Figure 1.1. Since the information is transmitted through different paths, a MIMO system is capable of exploiting both transmitter and receiver diversity, hence maintaining reliable communications. Furthermore, with the advent of multiple antennas, it becomes possible to jointly process/combine the multi-antenna signals and thus improves the system's integrity and/or throughput. Briefly, compared to Single-Input Single-Output (SISO) systems, the two most significant advantages of MIMO systems are:

- A significant increase of both the system's capacity and spectral efficiency. The capacity of a wireless link increases linearly with the minimum of the number of transmitter or the receiver antennas [105, 107]. The data rate can be increased by spatial multiplexing without consuming more frequency resources and without increasing the total transmit power.

- Dramatic reduction of the effects of fading due to the increased diversity. This is particularly beneficial, when the different channels fade independently.

An overview of MIMO techniques covering channel models, performance limits, coding and transceiver designs can be found in [117].

1.1.2.2 MIMO OFDM

The quality of a wireless link can be described by three basic parameters, namely the transmission rate, the transmission range and the transmission reliability. Conventionally, the transmission rate may be increased by reducing the transmission range and reliability. By contrast, the transmission range may be extended at the cost of a lower transmission rate and reliability, while the transmission reliability may be improved by reducing the transmission rate and range [118]. However, with the advent of MIMO assisted OFDM systems, the above-mentioned three parameters may be simultaneously improved [118]. Initial field tests of broadband wireless MIMO OFDM communication systems have shown that an increased capacity, coverage and reliability is achievable with the aid of MIMO techniques [119]. Furthermore, although MIMOs can potentially be combined with any modulation or multiple access technique, recent research suggests that the implementation of MIMO aided OFDM is more efficient, as a benefit of the straightforward matrix algebra invoked for processing the MIMO OFDM signals [118].

MIMO OFDM, which is claimed to be invented by Airgo Networks [120], has formed the foundation of all candidate standards proposed for IEEE 802.11n [21]. In recent years, this topic has attracted substantial research efforts, addressing numerous aspects, such as system capacity [121, 122], space/time/frequency coding [123–127], PAPR control [128–130], channel estimation [131–133], receiver design [134–137], etc. Recently, Paulraj *et al.* [117] and Stüber *et al.* [138] provided compelling overviews of MIMO OFDM communications. Furthermore, Nortel Networks has developed a MIMO OFDM prototype [139] during late 2004, which demonstrates the superiority of MIMO OFDM over today's networks in terms of the achievable data rate. For the reader's convenience, we have summarized the major contributions on MIMO OFDM in Tables 1.4, 1.5 and 1.6 at a glance.

1.1.2.3 SDMA-based MIMO OFDM Systems

As a subclass of MIMO arrangements, recently the Space Division Multiple Access (SDMA) [3, 192–194] based techniques have attracted substantial interest. As one of the most promising techniques aiming at solving the capacity problem of wireless communication systems, SDMA enables multiple users to simultaneously share the same bandwidth in different geographical locations. More specifically, the exploitation of the spatial dimension, namely the so-called spatial signature, makes it possible to identify the individual users, even when they are in the

Year	Author(s)	Contribution
2001	Blum *et al.* [123]	Studied improved space-time coding techniques for MIMO OFDM systems.
	Piechocki *et al.* [140]	Reported on the performance of spatial multiplexing using ML decoding for a Vertical Bell Labs Layered Space-Time (V-BLAST) OFDM system.
2002	Li [131]	Exploited optimum training sequence design and simplified channel estimation for improving the performance and for reducing the complexity of channel parameter estimation in MIMO OFDM systems.
	Bolckei, Gesbert and Paulraj [121]	Analyzed the influence of physical parameters such as the amount of delay spread, cluster angle spread and total angle spread, as well as system parameters such as the number of antennas and the antenna spacing on both the ergodic capacity and outage capacity.
	Chuah *et al.* [141]	Derived and compared the asymptotic growth rate of capacity in multiple-antenna aided systems.
	Catreux *et al.* [142]	Offered an overview of the challenges and promises of link adaptation in future broadband wireless networks.
	Piechocki *et al.* [143]	Presented a performance evaluation of spatial multiplexing and space-frequency coded modulation schemes designed for WLANs.
	Molisch, Win and Winters [144]	Proposed a reduced-complexity method for grouping multiple antennas and space-time codes.
	Li, Winters and Sollenberger [134]	Invoked space-time coding and Successive Interference Cancellation (SIC) in MIMO OFDM systems.
	Stamoulis *et al.* [145]	Revealed the effects of ICI on MIMO OFDM.
	Doufexi *et al.* [146]	Characterized the outdoor physical layer performance of a coded MIMO OFDM system using space-time processing.
	Giangaspero *et al.* [135]	Compared two Co-Channel Interference (CCI) cancellation schemes in the context of MIMO OFDM.
2003	Li, Letaief and Cao [136]	Advocated a CCI cancellation method using angle diversity based on null-steering or minimum variance distortion response beamforming.
	Bölcskei, Borgmann and Paulraj [147]	Measured the impact of the propagation environment on the performance of space-frequency coded MIMO OFDM.
	Barhumi, Leus and Moonen [132]	Described a Least-Squares (LS) channel estimation scheme designed for MIMO OFDM systems based on pilot tones.
	Ganesan and Sayeed [122]	Derived a virtual MIMO framework for single-transmitter, single-receiver multipath fading channels that enables maximal exploitation of channel diversity at both the transmitter and the receiver.
	Gamal *et al.* [124]	Utilized an OFDM technique to transform the MIMO multi-path channel into a MIMO flat block fading channel, where the associated diversity is exploited by employing space-frequency codes.
	Moon *et al.* [128]	Evaluated the PAPR performance in a MIMO OFDM-based WLAN system using a Space-Time Block Code (STBC).
	Cai, Song and Li [148]	Developed a technique based on the auto-correlation function for estimating the Doppler spread in Rayleigh fading channels for mobile OFDM systems using multiple antennas.
	Leus and Moonen [149]	Employed tone-by-tone based equalization techniques in MIMO OFDM systems.
	Lee *et al.* [129]	Investigated the PAPR characteristics in a MIMO OFDM system using the selective mapping approach.
	Piechocki *et al.* [150]	Devised a blind method for joint detection of space-time coded MIMO OFDM.

Table 1.4: Main contributions on MIMO OFDM (Part 1).

Year	Author(s)	Contribution
	Shin, H. Lee and C. Lee [133]	Suggested a cyclic comb-type training structure for reducing the Mean-Square Errors (MSEs) at the edge subcarriers of MIMO OFDM signals.
	Xia, Zhou and Giannakis [151]	Created an adaptive MIMO OFDM transmitter by applying an adaptive two-dimensional coder-beamformer with the aid of partial channel knowledge.
	Huang and Letaief [152]	Portrayed an OFDM symbol based space diversity technique.
	Butler and Collings [153]	Employed an approximate log-likelihood decoding approach based on a Zero-Forcing (ZF) receiver for bit-interleaved coded modulation assisted MIMO OFDM systems.
	Stüber *et al.* [138]	Summarized various physical layer research challenges in MIMO OFDM system design.
	Paulraj *et al.* [117]	Provided an overview of MIMO and/or MIMO OFDM systems.
	Lu, Yue and Wang [154]	Identified the performance of an optimized MIMO OFDM scheme using Low Density Parity Check (LDPC) codes.
	Van Zelst and Schenk [155]	Implemented MIMO OFDM processing and evaluated its performance by both simulations and experimental test results.
	Pascual-Iserte, Pérez-Neira and Lagunas [156]	Conducted studies on maximizing the Signal to Noise and Interference Ratio (SNIR) over the subcarriers subject to a total transmit power constraint.
2004	Zeng and Ng [157]	Contrived a subspace-based semi-blind method for estimating the channel responses of a multi-user and multi-antenna OFDM uplink system.
	Alien *et al.* [158]	Assessed the performance of spatial diversity in an OFDM WLAN for various antenna topologies.
	Dayal, Brehler and Varanasi [125]	Introduced space-time channel-sounding training codes designed for multiple-antenna, noncoherent, multiple block Rayleigh fading channel.
	Park and Kang [137]	Adopted a reduced-complexity iterative algorithm for joint Maximum-A-Posteriori (MAP) detection and CCI suppression in MIMO OFDM systems.
	Tan and Stüber [159]	Combined cyclic delay diversity and MIMO OFDM for achieving full spatial diversity in flat-fading channels.
	Wang, Shayan and Zeng [160]	Illustrated the diversity and coding advantages in terms of the minimum Hamming distance and the minimum squared product distance of the code as well as the relative frequencies.
	Pan, Letaief and Cao [161]	Discussed dynamic spatial subchannel allocation in conjunction with adaptive beamforming in broadband OFDM wireless systems.
	Tepedelenlioğlu and Challagulla [162]	Demonstrated how to achieve high diversity gains in MIMO OFDM systems with the aid of fractional sampling.
	Baek *et al.* [163]	Addressed a time-domain semi-blind channel estimation approach and a PAPR Reduction scheme for MIMO OFDM.
	Dubuc *et al.* [139]	Outlined Nortel Networks' MIMO OFDM concept prototype and provided measured performance results.
	Barriac and Madhow [164]	Offered guidelines for optimizing the antenna spacing in MIMO OFDM systems using feedback of the covariance matrix of the downlink channel.

Table 1.5: Main contributions on MIMO OFDM (Part 2).

Year	Author(s)	Contribution
	Su, Safar and Liu [126, 127]	Designed a general space-frequency block code structure capable of providing full-rate, full-diversity MIMO OFDM transmission.
	Zhang, Kavcic and Wong [165]	Researched an optimal QR decomposition technique designed for a precoded MIMO OFDM system using successive-cancellation detection.
	Yao and Giannakis [166]	Proposed a low-complexity blind Carrier Frequency Offset (CFO) estimator for OFDM systems.
	Zheng *et al.* [167]	Extended Time-Division Synchronous CDMA (TD-SCDMA) to Time-Division Code-Division Multiplexing OFDM (TD-CDM-OFDM) for future 4G systems.
	Yang [168]	Reviewed the state-of-the-art approaches in MIMO OFDM air-interface.
	Zhang and Letaief [169]	Aimed at developing an adaptive resource-allocation approach which jointly allocates subcarriers, power and bits for multi-user MIMO OFDM systems.
	Ma [170]	Established a pilot-assisted modulation scheme for CFO and channel estimation in OFDM transmissions over frequency-selective MIMO fading channels.
	Fozunbal, McLaughlin and Schafer [171]	Calculated a sphere packing lower bound and a pairwise error upper bound of the error probability of space-time-frequency coded OFDM systems using multiple antennas for transmission over block-fading channels.
	Nanda *et al.* [172]	Built a MIMO WLAN prototype that provides data rates over 200Mb/s.
	Kim *et al.* [173]	Invoked a QR-Decomposition combined with the M-algorithm (QRD-M) for joint data detection and channel estimation in MIMO OFDM.
	Qiao *et al.* [174]	Contrived an iterative LS channel estimation algorithm for MIMO OFDM.
	Sampath, Erceg and Paulraj [175]	Validated the properties of the transmit correlation matrix through field trial results obtained from a MIMO OFDM wireless system operated in a macro-cellular environment.
	Rey, Lamarca and Vazquez [176]	Used a Bayesian approach to design transmit prefiltering matrices for closed-loop schemes, which is robust to channel estimation errors.
2005	Sun, Xiong and Wang [177]	Targeted at designing CFO estimator aided Expectation Maximization (EM) based iterative receivers for MIMO OFDM systems.
	Han and Lee [130]	Provided an overview of multicarrier PAPR reduction techniques.
	Lodhi *et al.* [178]	Evaluated the complexity and performance of a MC-CDMA system exploiting STBCs and Cyclic Delay Diversity (CDD).
	Wang, Han and Liu [179]	Advanced MIMO OFDM channel estimation using a scheme based on estimating the Time-of-Arrivals (TOAs).
	Wen, Wang and Chen [180]	Reported on a low-complexity multi-user angle-frequency coding scheme based on the Fourier basis structure for downlink wireless systems.
	Su, Safar and Liu [181]	Performance analysis of MIMO OFDM systems invoking coding in spatial, temporal and frequency domains.
	Tan, Latinović and Bar-Ness [182]	Advocated a scheme of cross-antenna rotation and inversion utilizing additional degrees of freedom by employing multiple antennas in OFDM systems.
	Park and Cho [183]	Characterized a MIMO OFDM technique based on the weighting factor optimization for reducing the ICI caused by time-varying channels.
	Shao and Roy [184]	Maximized the diversity gain achieved over frequency-selective channels by employing a full-rate space-frequency block code for MIMO OFDM systems.
	Schenk *et al.* [185]	Quantified how the transmitter/receiver phase noise affects the performance of a MIMO OFDM system.
	Borgmann and Bölcskei [186]	Contributed to the code designs for noncoherent frequency-selective MIMO OFDM fading links.
	Tarighat and Sayed [187]	Examined the effect of IQ imbalances on MIMO OFDM systems and developed a digital signal processing framework for combating these distortions.
	Jiang, Li and Hager [188]	Formulated a joint transceiver design combining the Geometric Mean Decomposition (GMD) with ZF-type decoders.
	Choi and Heath [189]	Constructed a limited feedback architecture that combines beamforming vector quantization and smart vector interpolation.
	Baek *et al.* [190]	Incorporated multiple antennas into high-rate DAB systems.
2006	Liew and Hanzo [191]	Investigated various space-time codes for OFDM systems.

Table 1.6: Main contributions on MIMO OFDM (Part 3).

same time/frequency/code domains, thus increasing the system's capacity.

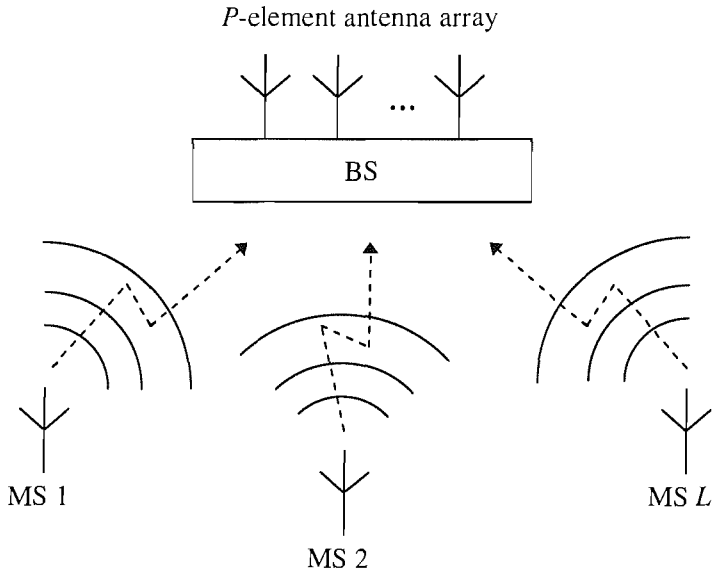

Figure 1.2: Illustration of the generic SDMA system employing a P-element receiver antenna array for supporting L number of mobile users.

In Figure 1.2 we illustrate the concept of SDMA systems. As shown in Figure 1.2, each user exploiting a single transmitter antenna aided Mobile Station (MS) simultaneously communicates with the BS equipped with an array of receiver antennas. Explicitly, SDMA can be considered as a specific branch of the family of MIMO systems, where the transmissions of the multiple transmitter antennas cannot be coordinated, simply because they belong to different users. Briefly speaking, the major advantages of SDMA techniques are [195]:

- *Range extension*: With the aid of antenna array, the coverage area of high-integrity reception can be significantly larger than that of any single-antenna aided systems. In a SDMA system, the number of cells required for covering a given geographic area can be substantially reduced. For example, a ten-element array offers a gain of ten, which typically doubles the radius of the cell and hence quadruples the coverage area.

- *Multi-path mitigation*: Benefitting from the MIMO architecture, in SDMA systems the detrimental effects of multi-path propagations are effectively mitigated. Furthermore, in specific scenarios the multi-path phenomenon can even be exploited for enhancing the desired users' signals by employing efficient receiver diversity schemes.

- *Capacity increase*: Theoretically, SDMA can be incorporated into any existing multiple access standard at the cost of a limited increase in system complexity, while attaining a substantial increase in capacity. For instance, by applying SDMA to a conventional

TDMA system, two or more users can share the same time slots, resulting in a doubled or higher overall system capacity.

- *Interference suppression*: The interference imposed by other systems and by users in other cells can be significantly reduced by exploiting the desired user's unique, user-specific Channel Impulse Responses (CIRs).

- *Compatibility*: SDMA is compatible with most of the existing modulation schemes, carrier frequencies and other specifications. Furthermore, it can be readily implemented using various array geometries and antenna types.

The combination of SDMA and OFDM results in SDMA-OFDM systems [3, 192, 196, 197], which exploit the merits of both SDMA and OFDM, having attracted more and more interest [197–202]. Tables 1.7 and 1.8 summarize the main contributions on SDMA and SDMA-OFDM found in the open literature.

1.2 Organization of the Thesis

Having briefly reviewed the OFDM, MIMO OFDM and SDMA-OFDM literature, let us now outline the organization of the thesis.

- **Chapter 2: Channel Coding Assisted Space-Time Block Coded Systems**
  As an introductory study, in this chapter we discuss various channel coded Space-Time Block Codes (STBCs) in the context of single-user single-carrier and single-user OFDM systems. This work constitutes the background work for the multi-user systems to be investigated in following chapters. More specifically, various Turbo Convolutional (TC) codes, Low Density Parity Check (LDPC) codes and Coded Modulation (CM) schemes are combined with STBCs for improving the performance of the single-user system considered.

- **Chapter 3: Coded Modulation Assisted Multi-User SDMA-OFDM Using Frequency-Domain Spreading**
  In this chapter, we invoke a multi-user MIMO SDMA-OFDM system for uplink communications, where the classic Minimum Mean-Square Error (MMSE) Multi-User Detector (MUD) is employed at the BS for separating the different users' signals. The CM schemes discussed in Chapter 2, namely Trellis Coded Modulation (TCM), Turbo TCM (TTCM), Bit-Interleaved Coded Modulation (BICM) and Iteratively Decoded BICM (BICM-ID), are evaluated and compared in the context of the SDMA-OFDM system. Furthermore, the performance gain arising from invoking Walsh-Hadamard Transform

Year	Author(s)	Contribution
1982	Yeh and Reudink [203]	Illustrated that high spectrum efficiencies can be achieved in mobile radio systems using a modest number of space diversity branches.
1983	Ko and Davis [204]	Early studies on SDMA in the context of satellite communication networks.
1989	Swales, Beach and Edwards [205, 206]	Devised a multi-beam adaptive BS antenna in an attempt to mitigate the problem of limited radio resources.
1990	Agee, Schell and Gardner [207]	Invoked narrowband antenna arrays for blind adaptive signal extraction.
1991	Anderson *et al.* [208]	Adopted adaptive antenna techniques to increase the channel capacity.
1992	Balaban and Salz [209, 210]	Provided a comprehensive characterization of space diversity reception combined with various equalization techniques.
1994	Xu *et al.* [211]	Offered preliminary results of experimental studies on SDMA systems.
	Talwar, Viberg and Paulraj [212]	Described an approach for separating and estimating multiple co-channel signals with the aid of an antenna array.
1995	Van Der Veen *et al.* [213]	Blindly identified Finite Impulse Response (FIR) channels using oversampling and the finite-alphabet property of digital signals.
	Khalaj, Paulraj and Kailath [214]	Estimated the spatio-temporal characteristics of the radio channel in coherent direct-sequence spread-spectrum systems.
	Anand, Mathew and Reddy [215]	Established a method of blind separation of co-channel Binary Phase-Shift Keying (BPSK) signals arriving at an antenna array.
1997	Liu and Xu [216]	Addressed the SDMA uplink blind channel and sequence estimation problem.
	Tsoulos, Beach and McGeehan [217]	Reported the research of the TSUNAMI project that demonstrated the benefits of SDMA in wireless communications.
1998	Deneire and Slock [218]	Derived a subspace fitting and linear prediction method using cyclic statistics of fractionally sampled channels for channel identification in multi-user and multi-antenna systems.
	Tsoulos, McGeehan and Beach [219, 220]	Provided an experimental demonstration of both transmit and receive beamforming supporting SDMA user access.
	Barroso *et al.* [221]	Introduced a blind algorithm referred to as Array Channel Division Multiple Access (AChDMA) for advanced SDMA in mobile communications systems.
	Demmerle and Wiesbeck [222]	Designed a biconical multi-beam antenna structure for SDMA communications.
	Lindmark [223]	Built a dual-polarized antenna array for a SDMA system working in the 1850-1990MHz band.
	Suard *et al.* [224]	Investigated the channel capacity enhancement of a SDMA system.
	Jeng *et al.* [225]	Presented extensive experimental results of spatial signature variation using a smart antenna testbed.
	Petrus, Ertel and Reed [226]	Proved that capacity improvement can be achieved using adaptive arrays at the BS of an Advanced Mobile Phone Service (AMPS) system.
	Xavier, Barroso and Moura [227]	Targeted at designing a closed-form estimator for the SDMA MIMO channel based on second-order statistics.
	Farsakh and Nossek [228]	Developed an approach for jointly calculating array weights in such a way that all users receive their signal at a given SINR level.
1999	Tsoulos [229]	Provided an overview of smart antennas in the context of current and future personal communication systems.
	Piolini and Rolando [230]	Analyzed a channel-assignment algorithm for SDMA mobile systems.
	Vandenameele *et al.* [192, 196, 197]	Advocated a combined SDMA-OFDM approach that couples the capabilities of the two techniques.
	Galvan-Tejada and Gardiner [231, 232]	Calculated the theoretical blocking probability resulting from SDMA technology in two different channel allocation schemes.
	Tsoulos [233]	Focused on TDMA air interface techniques combined with SDMA schemes.
	Vornefeld, C. Walke and B. Walke [234]	Applied SDMA techniques to WATM systems.

Table 1.7: Main contributions on SDMA (Part 1).

Year	Author(s)	Contribution
2000	Djahani and Kahn [235]	Discussed the employment of multi-beam transmitters and imaging receivers in SDMA implementations.
2001	Shad *et al.* [236]	Invoked dynamic slot allocation in packet-switched SDMA systems.
	Kuehner *et al.* [237]	Considered a BS that communicates with smart-antenna aided mobiles operating in multi-beam, packet-switched and SDMA modes.
2002	Jeon *et al.* [238]	Contrived a smart antenna assisted system using adaptive beamforming for broadband wireless communications.
	Bellofiore *et al.* [239, 240]	Emphasized the interaction and integration of several critical components of a mobile communication network using smart-antenna techniques.
	Fang [241]	Carried out a realistic performance analysis of resource allocation schemes for SDMA systems and obtained analytical results for blocking probability.
	Arredondo, Dandekar and Xu [242]	Employed a novel synthesis and prediction filter at the smart-antenna aided BS for predicting vector channels in time-division duplex systems.
	Walke and Oechtering [243]	Conducted investigations on the Cumulative Dstribution Function (CDF) of the uplink carrier-to-interference ratio in a cellular radio network.
	Zwick, Fischer and Wiesbeck [244]	Proposed a stochastic channel model for indoor propagations in future communication systems equipped with multiple antennas.
	Zekavat, Nassar and Shattil [245]	Combined smart antenna arrays and MC-CDMA systems.
	Pan and Djurić [246]	Suggested sectorized multi-beam cellular mobile communications combined with dynamic channel assignment to beams.
	Cavalcante, Cavalcanti and Mota [247]	Exploited a blind adaptive optimisation criterion for SDMA detection.
	Yin and Liu [248]	Developed a Medium Access Control (MAC) protocol for multimedia SDMA/TDMA packet networks.
	Thoen *et al.* [198]	Showed that the performance of OFDM/SDMA processors can be significantly enhanced by adapting the constellation size applied on the individual subcarriers to the channel conditions.
	Rim [249]	Examined the performance of a high-throughput downlink MIMO SDMA technique.
2003	Thoen *et al.* [199]	Utilized a Constrained Least-Squares (CLS) receiver in multi-user SDMA systems.
	Alastalo and Kahola [200]	Reported link-level results of an adaptive antenna array assisted system compatible with IEEE 802.11a WLANs.
	Bradaric, Petropulu and Diamantaras [250]	Characterized a blind nonlinear method for identifying MIMO FIR CDMA and SDMA systems.
	Alias *et al.* [201, 251]	Constructed a Minimum Bit Error Rate (MBER) Multi-User Detector (MUD) for SDMA-OFDM systems.
	Hanzo, Münster, Choi and Keller [3]	Elaborated on channel estimation and multi-user detection techniques designed for SDMA-OFDM systems.
2004	Spencer, Swindlehurst and Haardt [252]	Delivered two constrained solutions referred to as the block-diagonalization and the successive optimization schemes contrived for downlink SDMA systems.
	Li, Letaief and Cao [253]	Explored a low-complexity ML-based detection scheme using a so-called 'sensitive-bits' algorithm.
	Choi and Murch [254]	Formulated a pre-Bell Labs Layered Space-Time (BLAST) decision-feedback equalization technique for downlink MIMO channels.
2005	Ajib and Haccoun [255]	Overviewed the scheduling algorithms proposed for 4G multi-user wireless networks based on MIMO technology.
	Münster and Hanzo [256]	Investigated parallel interference cancellation assisted decision-directed channel estimation in OFDM.
	Dai [202]	Performed an analysis of CFO estimation in SDMA-OFDM systems.
	Nasr, Costen and Barton [257]	Researched the estimation of the local average signal level in an indoor environment based on a 'wall-imperfection' model.

Table 1.8: Main contributions on SDMA (Part 2).

Spreading (WHTS) across a block of OFDM subcarriers in the Frequency Domain (FD) is studied in both the uncoded SDMA-OFDM and the CM-assisted SDMA-OFDM systems.

- **Chapter 4: Hybrid Multi-User Detection for SDMA-OFDM Systems**
  This chapter focuses on the design of MUDs invoked by the SDMA receiver. Specifically, the Maximum Likelihood Detection (MLD) scheme is found to attain the best performance at the cost of a computational complexity that increases exponentially both with the number of users and with the number of Bits Per Symbol (BPS) transmitted by higher-order modulation schemes. By contrast, the MMSE MUD exhibits a lower complexity at the expense of a performance loss. In order to achieve a good performance-complexity tradeoff, Genetic Algorithm (GA) based MUD techniques are proposed for employment in channel coded SDMA-OFDM systems, where TTCM is used. Moreover, a novel Biased Q-function Based Mutation (BQM) assisted iterative GA (IGA) MUD is designed. The performance of the proposed BQM-IGA is compared to both that of the optimum MLD and the linear MMSE MUD in the so-called fully-loaded and overloaded scenarios, respectively, where the number of users is equal to or higher than the number of receiver antenna elements. Additionally, the computational complexity associated with the various MUD schemes is discussed.

- **Chapter 5: Direct-Sequence Spreading and Slow Subcarrier-Hopping Aided Multi-User SDMA-OFDM Systems**
  This chapter commences with a short review of conventional SDMA-OFDM systems, followed by an introduction to hybrid SDMA-OFDM arrangements, which incorporate Direct-Sequence Spreading (DSS) and/or Frequency-Hopping (FH) techniques into conventional SDMA-OFDM. A novel FH technique referred to as Slow SubCarrier-Hopping (SSCH) is designed for hybrid DSS/FH SDMA-OFDM systems using a TTCM scheme. Furthermore, two types of SSCH pattern are discussed, namely the Random SSCH (RSSCH) and the Uniform SSCH (USSCH) patterns. The performance of the proposed TTCM-assisted DSS/SSCH SDMA-OFDM system is evaluated and compared to the conventional SDMA-OFDM and various hybrid SDMA-OFDM configurations.

- **Chapter 6: Iterative Joint Channel Estimation and Multi-User Detection for High-Throughput Multiple-Antenna Aided OFDM Systems**
  The objective of this chapter is to develop an efficient solution to the channel estimation problem of multi-user MIMO OFDM systems. It is well-known that compared to Single-Input Single-Output (SISO) systems, channel estimation in the MIMO scenario becomes more challenging, owing to the increased number of independent transmitter-receiver links to be estimated. Against this background, an iterative, joint channel estimation

and symbol detection approach is proposed for LDPC-coded MIMO SDMA-OFDM systems. More specifically, the method modifies the GA MUD advocated in Chapter 4 so that it becomes capable of jointly optimizing the Frequency-Domain CHannel Transfer Functions (FD-CHTFs) and the multi-user data symbols. Moreover, an efficient algorithm is derived, which enables the GA to output soft bits for the sake of improving the performance of the LDPC channel decoder.

- **Chapter 7: Conclusions and Future Work**
  The major findings of our work are summarized in this chapter, including our suggestions for future research.

1.3 Novel Contributions

The novel contributions of this thesis are summarized as follows:

- A CM-assisted and MMSE multi-user detected SDMA-OFDM system combined with WHTS across a number of subcarriers was proposed [258,259]. The various CM schemes used were TCM, TTCM, BICM and BICM-ID, which constitute bandwidth efficient schemes that combine the functions of coding and modulation. It was shown that by invoking the WHTS technique the average Bit Error Rate (BER) performance of the CM-SDMA-OFDM system can be further improved, since the bursty error effects imposed by the frequency-domain fading encountered are spread over the entire WHTS block length, therefore increasing the chances of correcting the transmission errors by the CM decoders.

- A GA-aided MUD was proposed for a TTCM-assisted SDMA-OFDM system [260,261], which is capable of achieving a similar performance to that attained by its MLD-aided counterpart at a significantly lower complexity, especially at high user loads.

- Furthermore, the performance of the GA MUD can be significantly improved with the aid of an iterative detection framework and/or a novel BQM technique [262–264]. The iterative BQM-aided GA MUD was capable of achieving a high performance even in overloaded scenarios, where the degree of detection freedom at the SDMA receiver becomes insufficient.

- A novel GA having the capability of providing soft outputs was proposed, which is the first known scheme overcoming the limitations of conventional hard-decoded GAs. The proposed GA's performance was evaluated in a TC-coded Space Division Multiplexing (SDM) aided OFDM system [265,266], where it was shown that the performance of the

currently known GA-assisted systems can be improved by about 2dB with the aid of the GA's soft solution, approaching the optimum performance of the soft-information assisted MLD, while exhibiting a lower complexity, especially in high-throughput scenarios.

- A novel hybrid DSS and/or SSCH assisted TTCM-aided multi-user SDMA-OFDM scheme was proposed [267–270]. It was demonstrated that by using the USSCH pattern, the Multi-User Interference (MUI) experienced by the high-throughput SDMA-OFDM system can be effectively suppressed, resulting in a significant performance improvement. The hybrid system employing the USSCH pattern was capable of outperforming a range of SDMA-OFDM systems considered, including the conventional SDMA-OFDM system dispensing with the employment of hopping techniques, particularly in high-throughput scenarios, while maintaining a similar complexity.

- A novel iterative GA-assisted Joint Channel Estimation and Multi-User Detection (GA-JCEMUD) approach was designed for multi-user MIMO SDMA-OFDM systems [271–273] [274, Chapter 11], which provides an effective solution to the multi-user MIMO channel estimation problem in overloaded scenarios, where none of the known channel estimation techniques is capable of operating. Our research demonstrated that the proposed iterative GA-JCEMUD was capable of *simultaneously* capturing the fading envelope changes of *each* individual user-receiver link, regardless of its instant variety of fading, and thus achieving an equally good performance over all the user-receiver links.

1.4 Chapter Summary

In this chapter, we briefly reviewed the history of OFDM in Section 1.1.1, spanning from the early studies to its recent applications. Furthermore, the historic development of various MIMO techniques was summarized in Section 1.1.2.1, followed by the introduction to MIMO OFDM systems in Section 1.1.2.2. In Section 1.1.2.3 a concise review of various SDMA and SDMA-OFDM techniques was given.

Having provided an outline of the thesis in Section 1.2 as well as the novel contributions in Section 1.3, respectively, let us now commence our discourse with an introductory study on channel coding and space-time coding assisted single-user systems.

Chapter 2

Channel Coding Assisted Space-Time Block Coded Systems

2.1 Introduction

Increasing market expectations for third-generation mobile radio systems show a great demand for a wider range of services spanning from voice to high-rate data services required for supporting mobile multimedia communications. This leads to higher technical specifications for existing and future communication systems, which have to support data rates as high as 144Kb/s in vehicular, 384Kb/s in outdoor-to-indoor and 2Mb/s in indoor and picocelluar environments [275].

The employment of multiple antennas constitutes an effective way of achieving an increased capacity. The classic approach is to use multiple receiver antennas and exploit Maximum Ratio Combining (MRC) of the received signals for the sake of improving the system's performance [276, 277]. However, the performance improvement of MRC is achieved at the cost of increasing the complexity of the Mobile Stations (MSs). Alternatively, MRC may be employed at the Base Stations (BSs), which support numerous MSs. While this scheme provides diversity gain for the BSs' receivers, the MSs cannot benefit from it.

Employing multiple transmitters, rather than receiver antennas at the BSs constitutes a further design option in this context. Since transmitter diversity techniques are proposed for employment at the BSs, it is possible to enhance the system's integrity by upgrading the BSs. Alamouti [278] introduced an attractive scheme, which uses two transmitters in conjunction with an arbitrary number of receivers for communications in non-dispersive Rayleigh fading channels. Tarokh *et al.* [279, 280] generalized Alamouti's scheme to an arbitrary number of transmitters. These schemes introduced Space-Time Block Codes (STBCs), which show

remarkable encoding and decoding simplicity, while achieving a good performance.

2.2 Space-Time Block Codes

In this section we will present the basic principles of space-time block codes. Before providing more details, let us first consider a simple space-time block coded system communicating over uncorrelated Rayleigh fading channels, as shown in Figure 2.1.

2.2.1 Alamouti's G_2 Space-Time Block Code

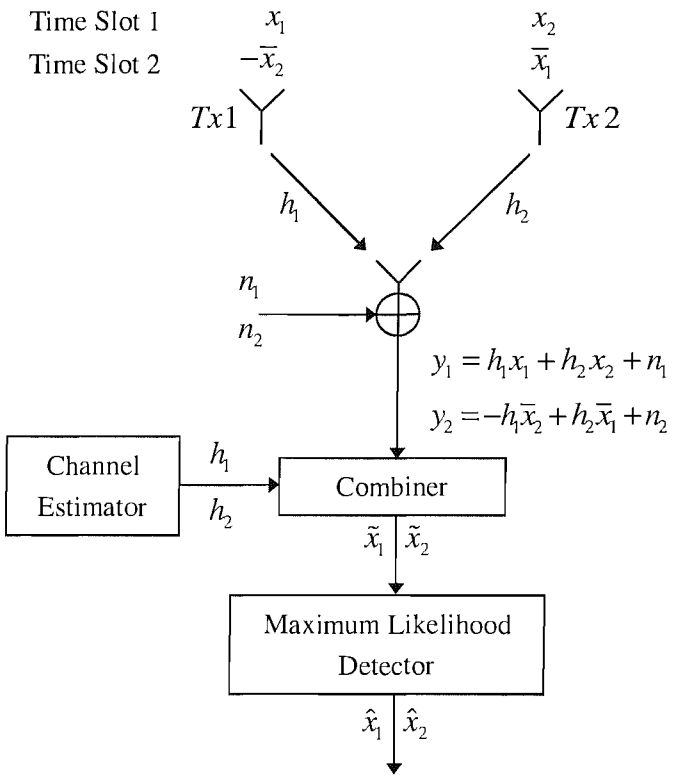

Figure 2.1: Schematic of Alamouti's G_2 space-time block code.

The system contains two transmitter antennas and one receiver antenna. The philosophy of Alamouti's G_2 space-time block code is as follows.

In a conceptually simple approach we could argue that the achieveable throughput of the system may be doubled with the aid of the two transmitter antennas, if their signal could be separated by the receiver. This task may be viewed as analogous to multiuser detection, where the two signals would arrive at the BS's receiver from two geographically separated users. From a simple conceptual perspective the Bell Labs Layered Space-Time (BLAST)

transmission scheme [106] adopts a similar principle for increasing the achievable throughput of multiple transmitter antenna based systems.

By contrast, Alamouti's approach is different, since the aim is to achieve a diversity gain rather than to increase the achievable throughput. This is achieved by extending the duration of time allocated to the transmission of a symbol by a factor of two and transmitting two independently faded and 'appropriately transformed' replicas of the symbol using each of the two antennas. The independence of the two channels may be ascertained by positioning the transmitter antennas Tx 1 and Tx 2 sufficiently far apart, for example at a distance of 10λ, where λ is the wavelength. Thus, during the first time slot, the information symbols x_1 and x_2 are transmitted by transmitter antenna Tx 1 and Tx 2, respectively, and again each of the two symbols is transmitted through an independently faded channel. For the sake of avoiding the channel-induced inter-symbol interference between the two time slots, both channels' path gains are assumed to be constituted by a single propagation path given by:

$$h_1 = |h_1| e^{j\alpha_1} \tag{2.1}$$

$$h_2 = |h_2| e^{j\alpha_2}, \tag{2.2}$$

where $|h_1|$, $|h_2|$ are the fading magnitudes and α_1, α_2 are the corresponding phase rotations. The complex fading envelopes are assumed to remain constant during the two consecutive time slots [2], which is expressed as:

$$h_1 = h_1(t = 1) = h_1(t = 2) \tag{2.3}$$

$$h_2 = h_2(t = 1) = h_2(t = 2). \tag{2.4}$$

Therefore we receive the composite signal y_1 constituted by the superposition of the two transmitted symbols through both channels:

$$y_1 = h_1 x_1 + h_2 x_2 + n_1, \tag{2.5}$$

where n_1 is a complex noise sample. As mentioned above, during the second time slot, a transformed version of the signals x_1 and x_2 is transmitted. Since the consecutive time slots are not faded independently, no diversity gain would be achieved, if we mapped these 'transformed' replicas of x_1 and x_2 to the same transmitter antenna as during the first time slot. Hence we now swap the assignment of the time slots to transmitter antennas, since this way their independent fading may be ascertained. More explicitly, during the second time slot, the negative version of the conjugate of x_2 and the conjugate of x_1 are sent by transmitter antenna Tx 1 and Tx 2, respectively. However, as mentioned above, the envelopes of each of the channels associated with the two transmitters are assumed to be the same as during the first time slot, hence we get the second transmitter's signal y_2 as:

$$y_2 = -h_1 \bar{x}_2 + h_2 \bar{x}_1 + n_2, \tag{2.6}$$

where n_2 is a complex noise sample. If the channels' characteristics are known to the receiver, i.e. we have a perfect channel estimator, the information symbols x_1 and x_2 can be readily separated in the combiner of Figure 2.1, yielding:

$$\begin{aligned}\tilde{x}_1 &= \bar{h}_1 y_1 + h_2 \bar{y}_2 \\ &= \bar{h}_1 h_1 x_1 + \bar{h}_1 h_2 x_2 + \bar{h}_1 n_1 - h_2 \bar{h}_1 x_2 + h_2 \bar{h}_2 x_1 + h_2 \bar{n}_2 \\ &= \left(|h_1|^2 + |h_2|^2\right) x_1 + \bar{h}_1 n_1 + h_2 \bar{n}_2 \end{aligned} \tag{2.7}$$

$$\begin{aligned}\tilde{x}_2 &= \bar{h}_2 y_1 - h_1 \bar{y}_2 \\ &= \bar{h}_2 h_1 x_1 + \bar{h}_2 h_2 x_2 + \bar{h}_2 n_1 + h_1 \bar{h}_1 x_2 - h_1 \bar{h}_2 x_1 - h_1 \bar{n}_2 \\ &= \left(|h_1|^2 + |h_2|^2\right) x_2 + \bar{h}_2 n_1 - h_1 \bar{n}_2, \end{aligned} \tag{2.8}$$

where $\tilde{x}_1$ and $\tilde{x}_2$ are the extracted noisy signals. Then $\tilde{x}_1$ and $\tilde{x}_2$ will be forwarded to the maximum likelihood detector of Figure 2.1, which determines the most likely transmitted symbols, namely $\hat{x}_1$ and $\hat{x}_2$ by simply outputting the specific legitimate transmitted symbol, which has the lowest Euclidean distance from the received channel-impaired symbol [2].

The equations above, which are based on the one-receiver scheme, can be generalized to multiple-receiver aided schemes, where the received signal y_t^j arriving at receiver j during time slot t is [2]:

$$y_t^j = \sum_{i=1}^{p} h_{i,j} x_t^i + n_t^j, \tag{2.9}$$

where p is the number of transmitters, $h_{i,j}$ is the complex-valued path gain between the transmitter i and receiver j, x_t^i is the space-time coded symbol transmitted by transmitter i during time slot t, and n_t^j is the noise sample at receiver j in time slot t. Accordingly, the extracted noisy signals become [2]:

$$\tilde{x}_1 = \sum_{j=1}^{q} \left[\left(|h_{1,j}|^2 + |h_{2,j}|^2\right) x_1 + \bar{h}_{1,j} n_1^j - h_{2,j} \bar{n}_2^j \right] \tag{2.10}$$

$$\tilde{x}_2 = \sum_{j=1}^{q} \left[\left(|h_{1,j}|^2 + |h_{2,j}|^2\right) x_2 + \bar{h}_{2,j} n_1^j - h_{1,j} \bar{n}_2^j \right]. \tag{2.11}$$

2.2.2 Encoding Algorithm

In last section, we have provided an example of a simple space-time block coded communication system. Let us now discuss space-time block codes in more depth.

2.2.2.1 Transmission Matrix

A generic space-time block code is defined by a $(n \times p)$-dimensional transmission matrix G, where the entries of the matrix G are linear combinations of the k input symbols $x_1, x_2, \cdots, x_k$

and their conjugates. Each symbol x_i $(i = 1, \cdots, k)$ conveys b original information bits according to the relevant signal constellation that has $M = 2^b$ constellation points, and hence can be regarded as information symbols. Thus, $(k \times b)$ input bits are conveyed by each $(n \times p)$ block. The general form of the transmission matrix of space-time block codes is given by Equation (2.12):

$$G = \begin{bmatrix} g_{11} & g_{12} & \cdots & g_{1p} \\ g_{21} & g_{22} & \cdots & g_{2p} \\ \cdots & \cdots & \cdots & \cdots \\ g_{n1} & g_{n2} & \cdots & g_{np} \end{bmatrix}, \tag{2.12}$$

where the entries g_{ij} $(i = 1, \cdots, n;\ j = 1, \cdots, p)$ represent the linear combinations of the information symbols x_i $(i = 1, \cdots, k)$ and their conjugates. In the transmission matrix G, which can be viewed as a space-time encoding block, the number of rows (namely n) is equal to the number of time slots, while the number of columns (namely p) is equal to the number of transmitter antennas. For example, during time slot $i = 1$, the encoded symbols $g_{11}, g_{12}, \cdots, g_{1p}$ are transmitted simultaneously from transmitter antennas $Tx\ 1, Tx\ 2, \cdots, Tx\ p$, respectively.

References [278, 279] have defined a range of space-time block codes. Different designs of the transmission matrix seen in Equation (2.12) will result in different encoding algorithms and code rates. Generally, the code rate is defined as:

$$R = k/n, \tag{2.13}$$

where k is the number of possible input information symbols, and n is the number of time slots.

2.2.2.2 Encoding Algorithm of the Space-Time Block Code G_2

From Section 2.2.1 and Equation (2.12) we can readily derive the G_2 transmission matrix in the form of:

$$G_2 = \begin{bmatrix} g_{11} & g_{12} \\ g_{21} & g_{22} \end{bmatrix} \tag{2.14}$$

or more specifically, as:

$$G_2 = \begin{bmatrix} x_1 & x_2 \\ -\bar{x}_2 & \bar{x}_1 \end{bmatrix}. \tag{2.15}$$

From Equation (2.15), it can be readily seen that there are $n = 2$ rows in the G_2 matrix associated with two time slots and $p = 2$ columns corresponding to two transmitter antennas, as we have already seen in the example of Figure 2.1. Since there are $k = 2$ input symbols, namely x_1 and x_2, the code rate of G_2 is $R = k/n = 1$.

2.2.2.3 Other Space-Time Block Codes

The G_2 space-time block code was first proposed by Alamouti [278] in 1998. This code has attracted much attention because of its appealing simplicity compared to the family of Space-Time Trellis Codes (STTCs) proposed in [281–284], although this simplicity was achieved at the cost of a performance loss. Later, Tarokh *et al.* [279] extended Alamouti's scheme to multiple transmitters, which led to other space-time block codes, such as the three-transmitter code G_3 and four-transmitter code G_4. The transmission matrix of G_3 [279] is defined as:

$$G_3 = \begin{bmatrix} x_1 & x_2 & x_3 \\ -x_2 & x_1 & -x_4 \\ -x_3 & x_4 & x_1 \\ -x_4 & -x_3 & x_2 \\ \bar{x}_1 & \bar{x}_2 & \bar{x}_3 \\ -\bar{x}_2 & \bar{x}_1 & -\bar{x}_4 \\ -\bar{x}_3 & \bar{x}_4 & \bar{x}_1 \\ -\bar{x}_4 & -\bar{x}_3 & \bar{x}_2 \end{bmatrix}, \tag{2.16}$$

and the transmission matrix of G_4 [279] is defined as:

$$G_4 = \begin{bmatrix} x_1 & x_2 & x_3 & x_4 \\ -x_2 & x_1 & -x_4 & x_3 \\ -x_3 & x_4 & x_1 & -x_2 \\ -x_4 & -x_3 & x_2 & x_1 \\ \bar{x}_1 & \bar{x}_2 & \bar{x}_3 & \bar{x}_4 \\ -\bar{x}_2 & \bar{x}_1 & -\bar{x}_4 & \bar{x}_3 \\ -\bar{x}_3 & \bar{x}_4 & \bar{x}_1 & -\bar{x}_2 \\ -\bar{x}_4 & -\bar{x}_3 & \bar{x}_2 & \bar{x}_1 \end{bmatrix}. \tag{2.17}$$

From Equations (2.16) and (2.17), we may notice that the code rates of G_3 and G_4 are reduced to a half, which degrades the bandwidth efficiency. However, the space-time block codes H_3 and H_4 of [279] mitigate this problem, since their code rate is 3/4. The transmission matrices of H_3 and H_4 [279] are defined as follows:

$$H_3 = \begin{bmatrix} x_1 & x_2 & \frac{x_3}{\sqrt{2}} \\ -\bar{x}_2 & \bar{x}_1 & \frac{x_3}{\sqrt{2}} \\ \frac{\bar{x}_3}{\sqrt{2}} & \frac{\bar{x}_3}{\sqrt{2}} & \frac{(-x_1-\bar{x}_1+x_2-\bar{x}_2)}{2} \\ \frac{\bar{x}_3}{\sqrt{2}} & -\frac{\bar{x}_3}{\sqrt{2}} & \frac{(x_2+\bar{x}_2+x_1-\bar{x}_1)}{2} \end{bmatrix} \tag{2.18}$$

$$H_4 = \begin{bmatrix} x_1 & x_2 & \frac{x_3}{\sqrt{2}} & \frac{x_3}{\sqrt{2}} \\ -\bar{x}_2 & \bar{x}_1 & \frac{x_3}{\sqrt{2}} & -\frac{x_3}{\sqrt{2}} \\ \frac{\bar{x}_3}{\sqrt{2}} & \frac{\bar{x}_3}{\sqrt{2}} & \frac{(-x_1-\bar{x}_1+x_2-\bar{x}_2)}{2} & \frac{(-x_2-\bar{x}_2+x_1-\bar{x}_1)}{2} \\ \frac{\bar{x}_3}{\sqrt{2}} & -\frac{\bar{x}_3}{\sqrt{2}} & \frac{(x_2+\bar{x}_2+x_1-\bar{x}_1)}{2} & \frac{(-x_1-\bar{x}_1-x_2+\bar{x}_2)}{2} \end{bmatrix}. \quad (2.19)$$

In conclusion, the parameters of the space-time block codes mentioned above are summarized in Table 2.1.

Space-time block code	Code rate (R)	Number of transmitters (p)	Number of input symbols (k)	Number of time slots (n)
G_2	1	2	2	2
G_3	1/2	3	4	8
G_4	1/2	4	4	8
H_3	3/4	3	3	4
H_4	3/4	4	3	4

Table 2.1: Parameters of the space-time block codes.

2.2.3 Decoding Algorithm

In this section, two algorithms are briefly discussed, which are widely used for decoding space-time block codes. The maximum likelihood (ML) decoding algorithm generates hard-decision outputs, while the Maximum-A-Posteriori (MAP) decoding algorithm is capable of providing soft outputs, which readily lend themselves to channel coding for the sake of achieving further performance improvements.

2.2.3.1 Maximum Likelihood Decoding

Maximum Likelihood (ML) decoding of space-time block codes can be achieved using simple linear processing at the receiver, thus maintaining a low decoding complexity. As mentioned in Section 2.2.1, when the space-time coded symbols are transmitted over different channels and arrive at the receiver during time slot t ($t = 1, \cdots, n$), we will have the received signal y_t^j expressed in Equation (2.9). With the proviso of having a perfect channel estimator, the receiver computes the decision metric

$$\sum_{t=1}^{n} \sum_{j=1}^{q} \left| y_t^j - \sum_{i=1}^{p} h_{i,j} x_t^i \right|^2 \quad (2.20)$$

over all indices $i = 1, \cdots, n$; $j = 1, \cdots, p$ and decides in favor of the specific entry that minimizes the sum.

Alamouti [278] first proposed a simple maximum likelihood decoding algorithm for the G_2 space-time block code. Tarokh *et al.* [280] extended it for the space-time block codes summarized in Table 2.1. The algorithm exploits the orthogonal structure of the space-time block codes for decoupling the signals transmitted from different antennas rather than requiring their joint detection. According to [280], low complexity signal processing may be invoked for separating the channel-impaired transmitted signal y_t^j into k decision metrics, each of which corresponding to the channel-impaired version of a specific information symbol of the set x_i, $i = 1, \cdots, k$. For example, for the G_2 space-time block code, we will minimize the decision metric

$$\left| \left[\sum_{j=1}^{q} \left(y_1^j \bar{h}_{1,j} + \bar{y}_2^j h_{2,j} \right) \right] - x_1 \right|^2 + \left(\sum_{j=1}^{q} \sum_{i=1}^{2} |h_{i,j}|^2 - 1 \right) |x_1|^2 \tag{2.21}$$

for decoding x_1 and the decision metric

$$\left| \left[\sum_{j=1}^{q} \left(y_1^j \bar{h}_{2,j} - \bar{y}_2^j h_{1,j} \right) \right] - x_2 \right|^2 + \left(\sum_{j=1}^{q} \sum_{i=1}^{2} |h_{i,j}|^2 - 1 \right) |x_2|^2 \tag{2.22}$$

for decoding x_2. The relevant decision metrics for decoding other STBC codes can be found in [280].

2.2.3.2 Maximum-A-Posteriori Decoding

As seen in Equations (2.21) and (2.22), hard decisions would have to be made in order to generate the decoded outputs, which are the most likely transmitted information symbols. In other words, the usual ML detection is a hard-decoding method. However, in most practical systems various channel codes, such as Low Density Parity Check (LDPC) codes [285] or turbo codes [2, 286, 287], may have to be combined with STBC codes for the sake of further improving the system's performance. In this case, the space-time decoder must provide soft outputs, which can be efficiently utilized by the channel decoder.

Bauch [288] presented a simple symbol-by-symbol Maximum-A-Posteriori (MAP) algorithm for decoding space-time block codes. According to [288], the aposteriori probability of each information symbol x_i ($i = 1, \cdots, k$) is:

$$\ln P\left(x_i \,|\mathrm{y}_1, \mathrm{y}_2, \cdots, \mathrm{y}_q\right) = \text{const} + \ln P\left(\mathrm{y}_1, \mathrm{y}_2, \cdots, \mathrm{y}_q \,|x_i\right) + \ln P\left(x_i\right), \tag{2.23}$$

where $\mathrm{y}_j = [\ y_1^j,\ y_2^j,\ \cdots,\ y_n^j\ ]$ $(j = 1, \cdots, q)$ represents the received signal vector at receiver j during the period spanning from time slot 1 to time slot n. For example, for the space-time

block code G_2 $(k = 2, n = 2)$ the aposteriori probabilities are:

$$\ln P\left(x_1 \left| \mathrm{y}_1, \mathrm{y}_2, \cdots, \mathrm{y}_q \right.\right) = \text{const} + \\ -\frac{1}{2\sigma^2}\left\{\left|\left[\sum_{j=1}^{q}\left(y_1^j \bar{h}_{1,j} + \bar{y}_2^j h_{2,j}\right)\right] - x_1\right|^2 + \left(\sum_{j=1}^{q}\sum_{i=1}^{2}|h_{i,j}|^2 - 1\right)|x_1|^2\right\} + \ln P\left(x_1\right) \tag{2.24}$$

$$\ln P\left(x_2 \left| \mathrm{y}_1, \mathrm{y}_2, \cdots, \mathrm{y}_q \right.\right) = \text{const} + \\ -\frac{1}{2\sigma^2}\left\{\left|\left[\sum_{j=1}^{q}\left(y_1^j \bar{h}_{2,j} - \bar{y}_2^j h_{1,j}\right)\right] - x_2\right|^2 + \left(\sum_{j=1}^{q}\sum_{i=1}^{2}|h_{i,j}|^2 - 1\right)|x_2|^2\right\} + \ln P\left(x_2\right). \tag{2.25}$$

We notice that Equations (2.24) and (2.25) are quite similar to Equations (2.21) and (2.22), respectively. In fact, it can be shown that Bauch's MAP algorithms can be extended for decoding other space-time block codes, such as the G_3, G_4, H_3 and H_4 and the corresponding algorithms also resemble the ML algorithms [2] discussed in Section 2.2.3.1. Given the aposteriori probabilities of the symbols, we can derive the corresponding aposteriori probabilities of the bits (i.e. the corresponding soft outputs) using the symbol-to-bit probability conversion of:

$$P\left(d_i = 0\right) = \sum_j P\left(x_j \left| \mathrm{y}_1, \mathrm{y}_2, \cdots, \mathrm{y}_q \right.\right), \quad \forall x_j = \left(d_1 \cdots d_i \cdots d_b\right), \quad d_i = 0, \tag{2.26}$$

$$P\left(d_i = 1\right) = \sum_j P\left(x_j \left| \mathrm{y}_1, \mathrm{y}_2, \cdots, \mathrm{y}_q \right.\right), \quad \forall x_j = \left(d_1 \cdots d_i \cdots d_b\right), \quad d_i = 1, \tag{2.27}$$

where $P(d_i = 0)$ or $P(d_i = 1)$ represents the probability of the i^{th} bit, namely d_i, of the b-bit symbol being zero and one, respectively. Let us consider the QPSK modulation scheme for example. The phasor constellation of QPSK is shown in Figure 2.2:

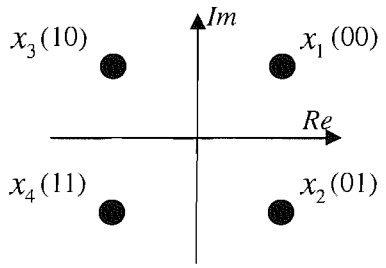

Figure 2.2: Gray-coded QPSK constellation.

As seen in Figure 2.2, each constellation point consists of two bits, hence the constellation points can be represented as:

$$x_j = (d_2 d_1), \quad j = \{1, \cdots, 4\}, \tag{2.28}$$

where $d_i = \{0, 1\}$. With the aid of Equations (2.26) and (2.27), we generate the aposteriori probabilities of each bit, taking into account that d_1 assumes a value of zero only in x_1 and x_3, while d_2 in x_1 and x_2, etc. yielding:

$$\begin{cases} P(d_1 = 0) = P(x_1 | y_1, y_2, \cdots, y_q) + P(x_3 | y_1, y_2, \cdots, y_q) \\ P(d_1 = 1) = P(x_2 | y_1, y_2, \cdots, y_q) + P(x_4 | y_1, y_2, \cdots, y_q) \\ P(d_2 = 0) = P(x_1 | y_1, y_2, \cdots, y_q) + P(x_2 | y_1, y_2, \cdots, y_q) \\ P(d_2 = 1) = P(x_3 | y_1, y_2, \cdots, y_q) + P(x_4 | y_1, y_2, \cdots, y_q) \end{cases} . \tag{2.29}$$

Then the relevant soft outputs can be forwarded to the channel decoders, which will make a hard decision to finally decode the received signals.

In practical applications, however, the Max-Log-MAP [289, 290] or Log-MAP [291] algorithms are usually preferred [2], since either can lower the computational complexity to some degree. The Max-Log-MAP algorithm was proposed by both Koch and Baier [289] and Erfanian *et al.* [290] for reducing the complexity of the MAP algorithm. This technique transfers the computation into the logarithmic domain and invokes an approximation for dramatically reducing the complexity imposed. As a consequence of using an approximation, its performance is sub-optimal. However, Robertson *et al.* [291] later proposed the Log-MAP algorithm, which partially corrected the approximation invoked in the Max-Log-MAP algorithm. Hence the performance of the Log-MAP algorithm is similar to that of the MAP algorithm, which is achieved at a significantly lower complexity. More details of the Max-Log-MAP and Log-MAP algorithms may be found in [2]. In our STBC soft decoder, the Log-MAP algorithm is employed. In the rest of this section we will characterize the achievable performance of a range of space-time block coding schemes.

2.2.4 System Overview

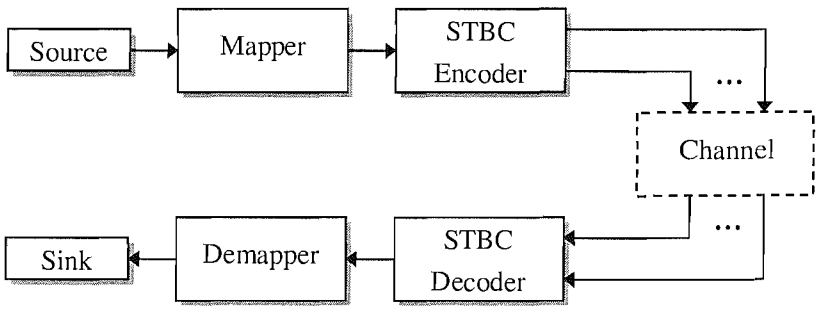

Figure 2.3: Schematic diagram of a simple system employing space-time block codes.

Figure 2.3 shows the structure of the simulation system used. As seen in the figure, the mapper maps the source information bits to relevant phasor constellation points employed

by the specific modulation scheme used. Then the symbols are forwarded to the space-time encoder. The encoded symbols are then transmitted through different antennas and arrive the receiver(s), where the received signals will be decoded by the space-time decoder. Finally, the demapper converts the STBC-decoded symbols back to the information bits and the Bit Error Ratio (BER) is calculated. The parameters of all the space-time block codes studied are summarized in Table 2.1. The following assumptions were used:

- Signals are transmitted over non-dispersive Rayleigh fading channels;
- The channels are quasi-static so that the path gains are constant across n consecutive time slots, corresponding to the n rows of the space-time block codes' transmission matrix;
- The different transmitter-receiver channel links are subject to independent fading;
- The average signal power received from each transmitter antenna is the same;
- The receiver has a perfect knowledge of the channels' fading amplitudes.

These assumptions simplify the simulations to a degree, therefore the system concerned is not a realistic one. However, since the experimental circumstances are identical for all performance comparisons, the results characterize the relative performance of various space-time block codes.

2.2.5 Simulation Results

In the past sections, the basic principles of space-time block codes as well as the simulation conditions were presented. In this section, our simulation results will be provided for the sake of comparatively studying the performance of the various STBCs of Table 2.1. In the uncorrelated channel scenario of Section 2.2.5.1, the channel fades between consecutive STBC blocks are assumed to be uncorrelated, while they are assumed to be correlated in the channel scenario of Section 2.2.5.2.

2.2.5.1 Performance over Uncorrelated Rayleigh Fading Channels

Performance at the Throughput of 1 BPS Figure 2.4 compares the performance of the G_2, G_3, and G_4 space-time block codes in conjunction with one receiver at the throughput of 1 BPS over the uncorrelated Rayleigh fading channel. Binary Phase-Shift Keying (BPSK) modulation is employed in conjunction with the space-time code G_2, while QPSK modulation is considered with the half-rate space-time codes G_3 and G_4 so that the system throughput

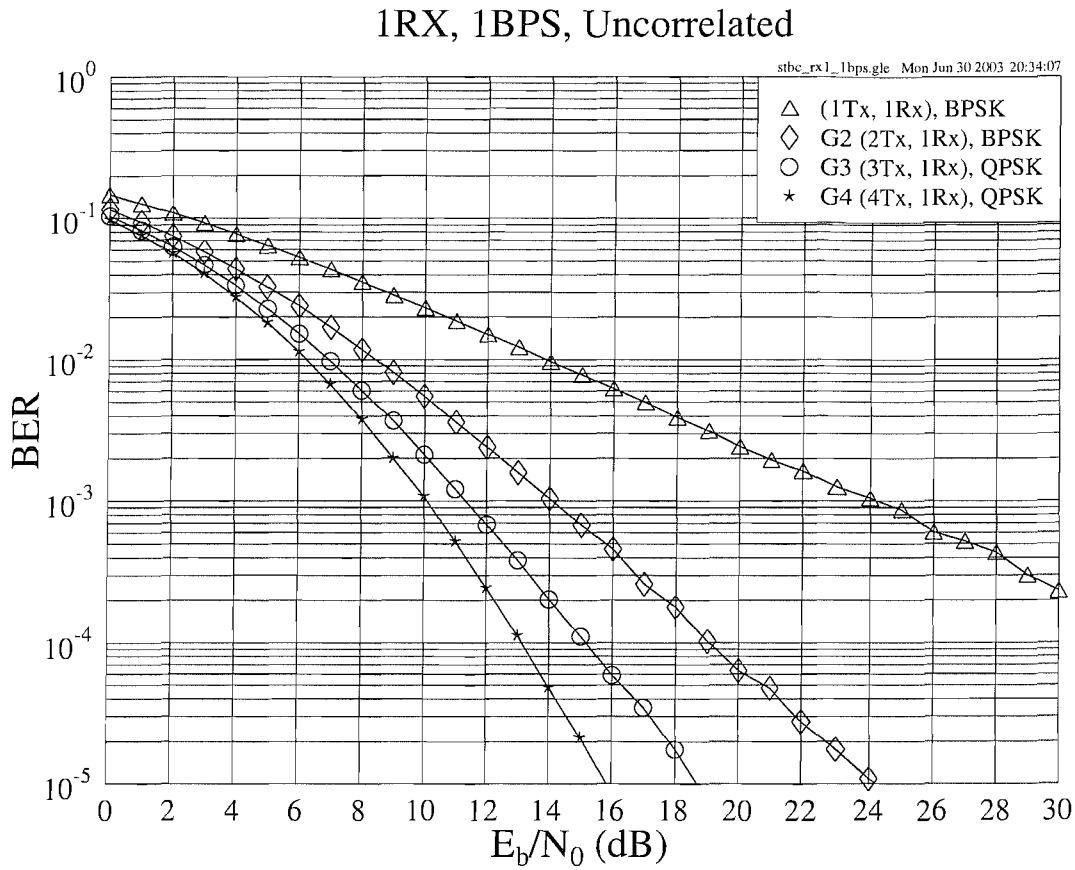

Figure 2.4: The BER versus E_b/N_0 performance of the $\mathbf{G_2}$, $\mathbf{G_3}$, and $\mathbf{G_4}$ space-time block codes of Table 2.1 at an effective throughput of **1 BPS** using **one receiver** over **uncorrelated** Rayleigh fading channels.

remains 1 BPS. From Figure 2.4 we can see that at the BER of 10^{-5} the G_3 and G_4 codes provide an approximately 5.5 and 7.5 dB gain over the G_2 code, respectively. If we add one more receiver in the context of all of these schemes, as seen in Figure 2.5, the relevant E_b/N_0 gain of the G_3 and G_4 schemes over the G_2 arrangement reduces to 2.5 and 3.5 dB, respectively. This may suggest that the G_2 code using two receivers has achieved most of the attainable diversity gain [2], and hence even if we further increase the number of transmitter antennas, the performance cannot be significantly improved.

Performance at the Throughput of 2 BPS In Figure 2.6 the performances of the space-time block codes using one receiver and having a throughput of about 2 BPS over uncorrelated Rayleigh fading channels are compared. In order to meet the 2 BPS throughput criteria, QPSK modulation is used for the G_2 code, while 16QAM modulation is employed for the G_3 and G_4 arrangements, as the latter ones are half rate codes. However, for the $\frac{3}{4}$-rate codes H_3 and H_4, an exact throughput of 2 BPS cannot be achieved. Thus we chose 8PSK and the throughput of the H_3 and H_4 schemes became 2.25 BPS, which is close to 2 BPS.

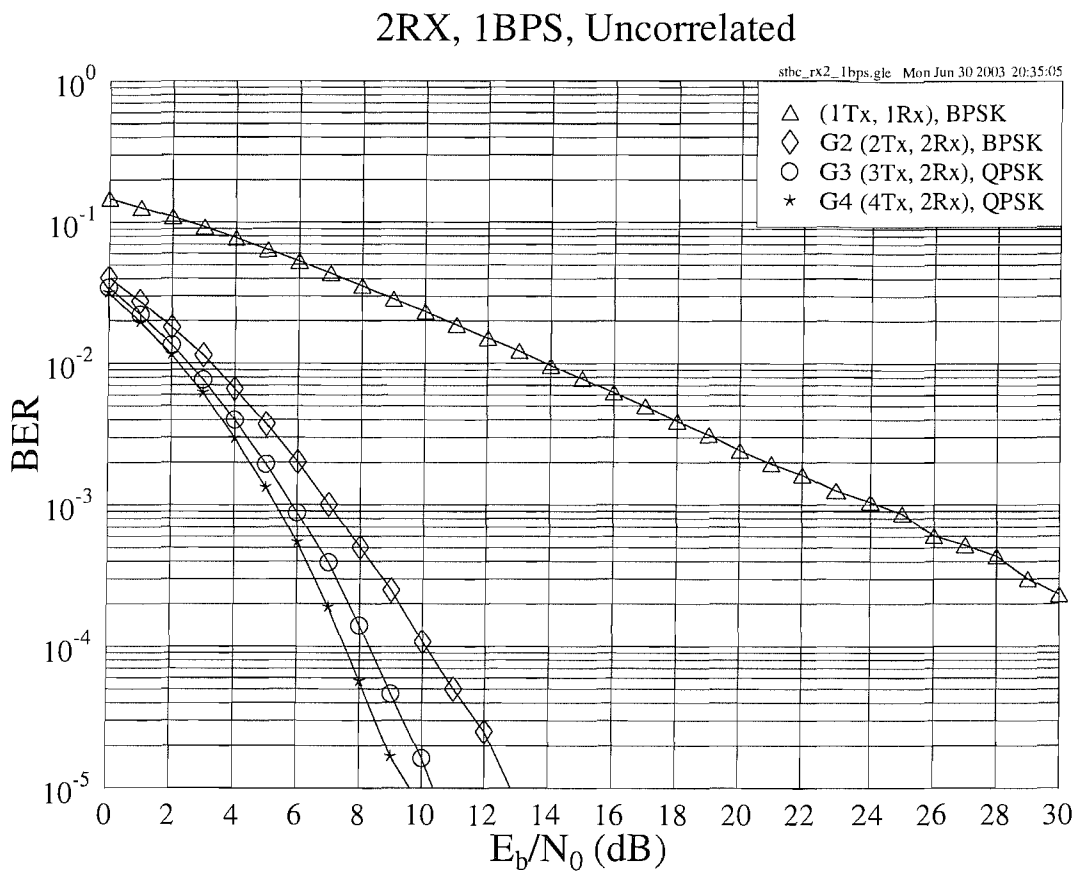

Figure 2.5: The BER versus E_b/N_0 performance of the $\mathbf{G_2}$, $\mathbf{G_3}$, and $\mathbf{G_4}$ space-time block codes of Table 2.1 at an effective throughput of **1 BPS** using **two receivers** over **uncorrelated** Rayleigh fading channels.

From Figure 2.6 we can see that when the Signal-to-Noise Ratio (SNR) is low, i.e. E_b/N_0 is below 12.5 dB, the space-time block code G_2 performs better than other codes, although the performance difference is not significant. When E_b/N_0 increases to a value higher than 12.5 dB, however, the G_4 code outperforms other codes, having an approximately 1 dB gain over the H_4 code at the BER of 10^{-5}. Similarly, the G_3 code achieves an approximately 1 dB gain over the H_3 code at the BER of 10^{-5}. We may note that although the G_3 and G_4 codes employ a higher-order 16QAM modulation scheme, which is more vulnerable to channel effects than the lower-order 8PSK modulation scheme used by the H_3 and H_4 codes, the former performs slightly better than the latter.

In the scenario of using two receivers, however, the G_2 code stands out in comparison to all the candidates, as Figure 2.7 indicates. This result suggests that the attainable diversity gain has already been achieved by the G_2 code using two receivers. Furthermore, the potential benefit of using more transmitters is eroded by the employment of higher throughput, but more vulnerable modulation schemes, which are more prone to transmission errors.

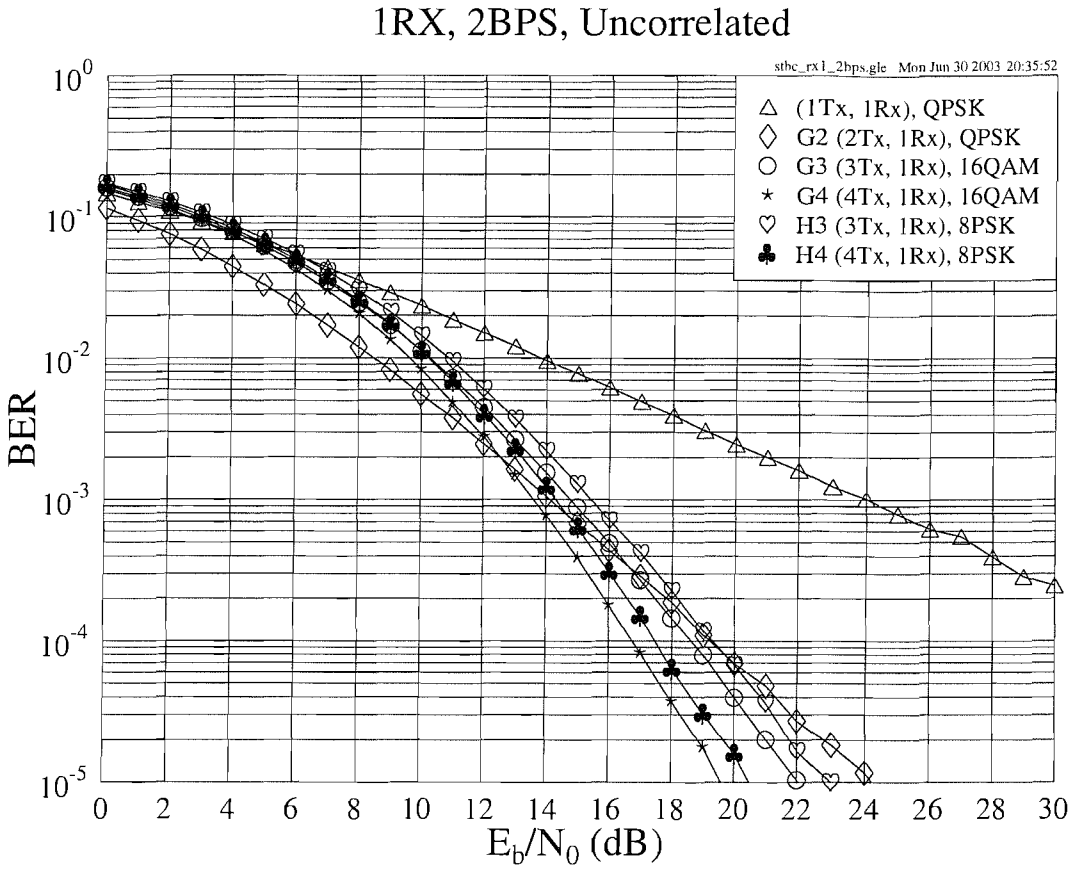

Figure 2.6: The BER versus E_b/N_0 performance of the $\mathbf{G_2}$, $\mathbf{G_3}$, $\mathbf{G_4}$, $\mathbf{H_3}$, and $\mathbf{H_4}$ space-time block codes of Table 2.1 at an effective throughput of about **2 BPS** using **one receiver** over **uncorrelated** Rayleigh fading channels.

Performance at the Throughput of 3 BPS The performances of the space-time block codes using one receiver and having a throughput of 3 BPS over uncorrelated Rayleigh fading channels are compared in Figure 2.8. Again, similarly to the scenario of having a throughput of 2 BPS, the G_2 code performs best at a low SNR, namely below about 10 dB, although the performance difference between G_2 and other codes is even smaller than it is in Figure 2.6. As shown in Figure2.8, at the BER of 10^{-5}, the H_3 and H_4 codes achieve a gain of about 3 dB over the G_3 and G_4 codes, respectively. Since the space-time block codes themselves do not have an error-correction capability which would allow them to correct the extra errors induced by employing a more vulnerable, higher-order modulation scheme [2], this results in a poorer performance. Furthermore, since the relative increase of the constellation density when changing from 16QAM to 64QAM is higher than that from 8PSK to 16QAM, the performance degradation imposed by reverting from 16QAM to 64QAM is more severe than that imposed by opting for 16QAM instead of 8PSK. Therefore it is not surprising that the best code to be used for high-SNR situations becomes the H_4 instead of the G_4 code,

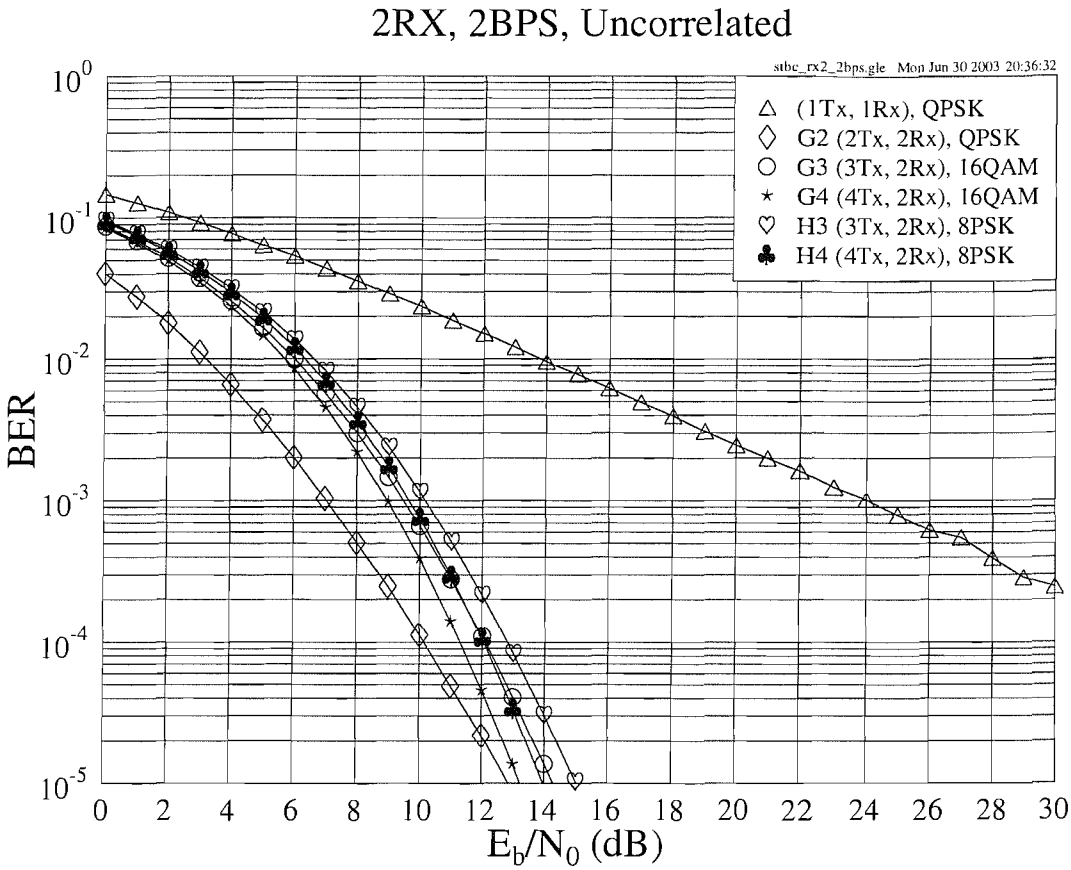

Figure 2.7: The BER versus E_b/N_0 performance of the $\mathbf{G_2}$, $\mathbf{G_3}$, $\mathbf{G_4}$, $\mathbf{H_3}$, and $\mathbf{H_4}$ space-time block codes of Table 2.1 at an effective throughput of about **2 BPS** using **two receivers** over **uncorrelated** Rayleigh fading channels.

which was the best code according to Figure 2.6 at high-SNR scenarios, since the G_4 and H_4 codes are used in conjunction with 64QAM and 16QAM, respectively. Moreover, we note that the H_3 code gives approximately 0.4 dB gain over the G_4 code, although the former has a lower diversity order.

If the number of receivers is doubled, as seen in Figure 2.9, the performance degradations of the G_3 and G_4 codes are much more dramatic. In this scenario, even the lower-diversity space-time code G_2 is capable of outperforming the space-time code G_4 having a higher-order diversity by about 1.7 dB at the BER of 10^{-5}.

2.2.5.2 Performance over Correlated Rayleigh Fading Channel

We have compared the performances of the space-time block codes of Table 2.1 for transmission over uncorrelated Rayleigh fading channels in Section 2.2.5.1. In this section, the performance of the STBCs will be studied based on the same assumptions noted on page 30, except that the

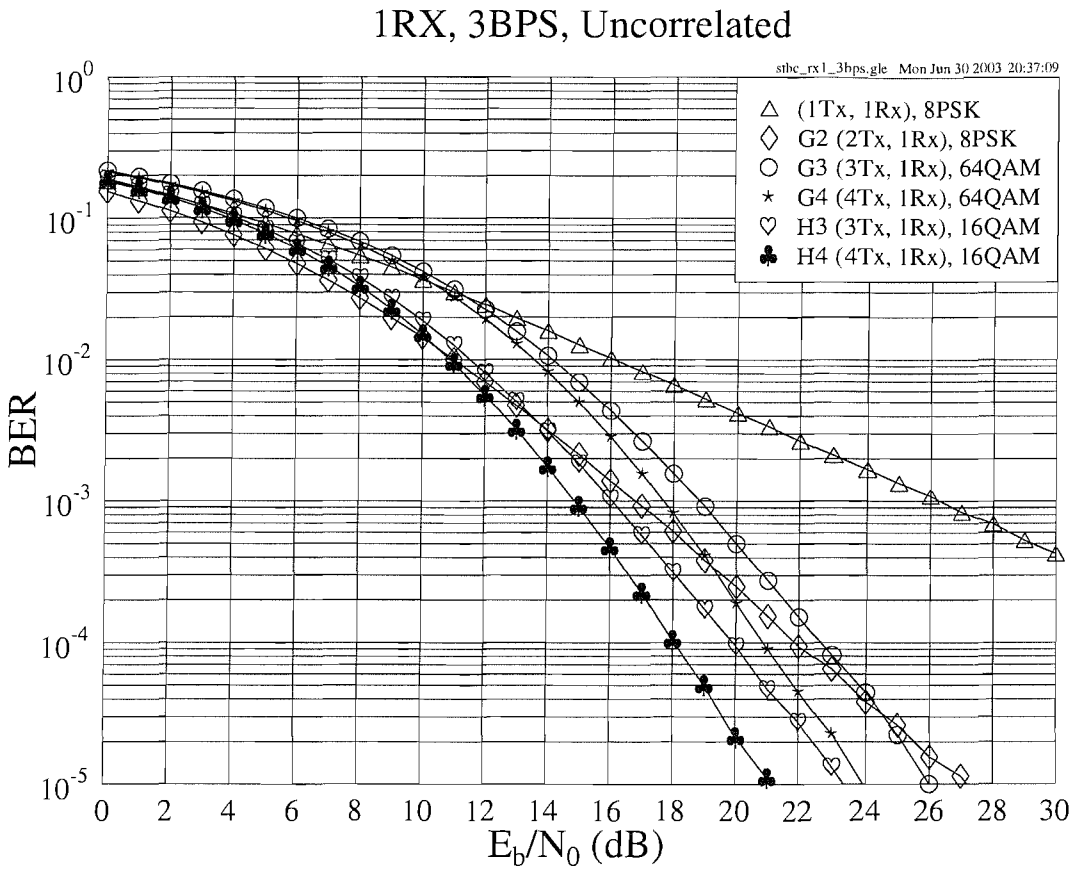

Figure 2.8: The BER versus E_b/N_0 performance of the $\mathbf{G_2}$, $\mathbf{G_3}$, $\mathbf{G_4}$, $\mathbf{H_3}$, and $\mathbf{H_4}$ space-time block codes of Table 2.1 at an effective throughput of **3 BPS** using **one receiver** over **uncorrelated** Rayleigh fading channels.

channel is assumed to be a correlated Rayleigh fading channel associated with the normalized Doppler frequency of 3.25×10^{-5}.

Specifically, Figure 2.10 compares the performance of the G_2, G_3, and G_4 space-time block codes in conjunction with one receiver at the throughput of 1 BPS, when communicating over a correlated Rayleigh fading channel. If we compare Figure 2.10 with Figure 2.4, which shows the relevant codes' performance over uncorrelated Rayleigh fading channels, we will note that the performances recorded in these cases are almost the same. This is because the receiver is aided by a perfect channel estimator that provides full knowledge of the path gains, and thus the effect imposed on the transmitted signals by the different path gains, regardless whether they are correlated or uncorrelated, is efficiently counteracted. When the throughput increases to 2 BPS and even further to 3 BPS, it can also be shown that the achievable performances of STBC codes communicating over a correlated Rayleigh channel are the same as those of their corresponding counterparts transmitting over uncorrelated Rayleigh channels, respectively.

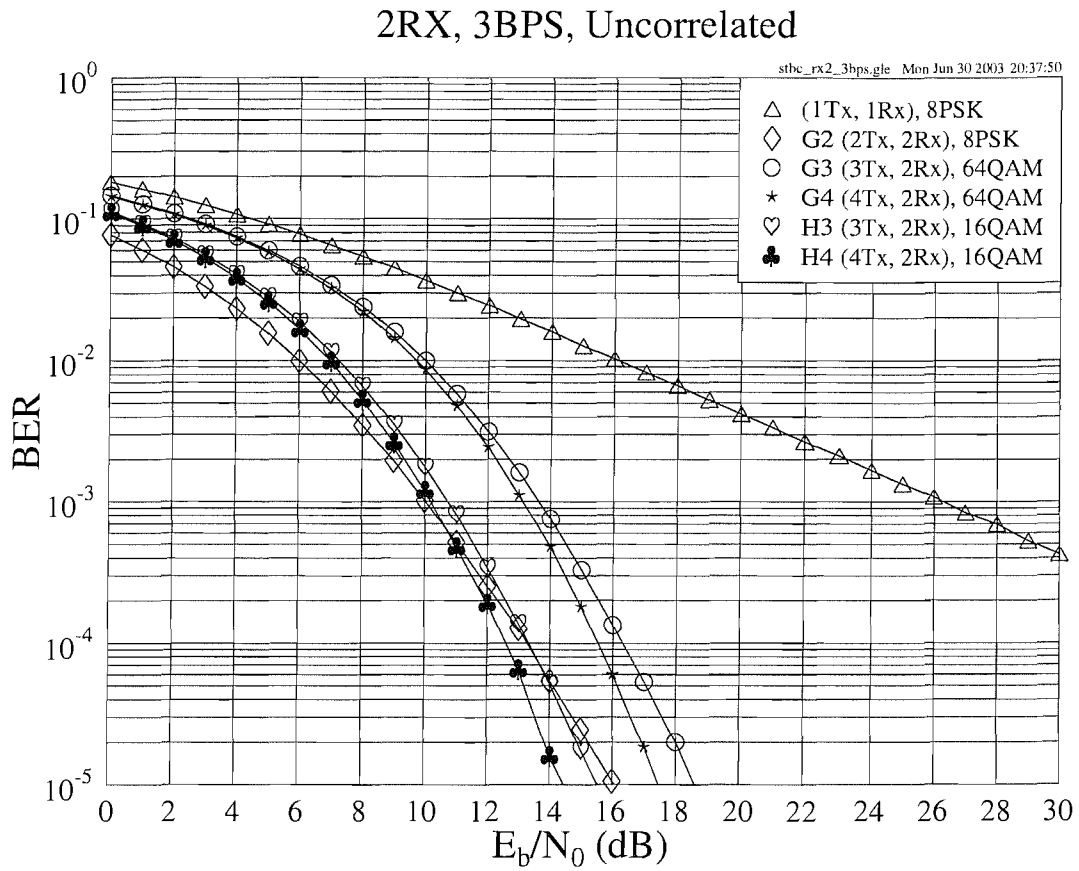

Figure 2.9: The BER versus E_b/N_0 performance of the $\mathbf{G_2}$, $\mathbf{G_3}$, $\mathbf{G_4}$, $\mathbf{H_3}$, and $\mathbf{H_4}$ space-time block codes of Table 2.1 at an effective throughput of **3 BPS** using **two receivers** over **uncorrelated** Rayleigh fading channels.

2.2.6 Conclusions

From the discussions and simulation results of Sections 2.2.5.1 and 2.2.5.2, several conclusions can be inferred. Firstly, the encoding and decoding of space-time block codes has a low complexity. At the receiver end, the maximum likelihood decoder requires low-complexity linear processing for decoding.

Secondly, from Figures 2.4, 2.6 and 2.8 we note that when the effective throughput is increased, the phasor-constellation has to be extended for accommodating the increased number of bits. Hence the performances of the half-rate codes G_3 and G_4 degrade in comparison to that of the unity-rate code G_2.

Thirdly, at the even higher effective throughput of 3 BPS, the H_3 and H_4 codes perform better than the G_3 and G_4 codes, respectively, as shown in Figure 2.8. Moreover, according to Figures 2.4, 2.5, 2.8 and 2.9, when the number of receivers is increased, the performance gain of the G_3, G_4, H_3 and H_4 codes over the G_2 code becomes more modest because much

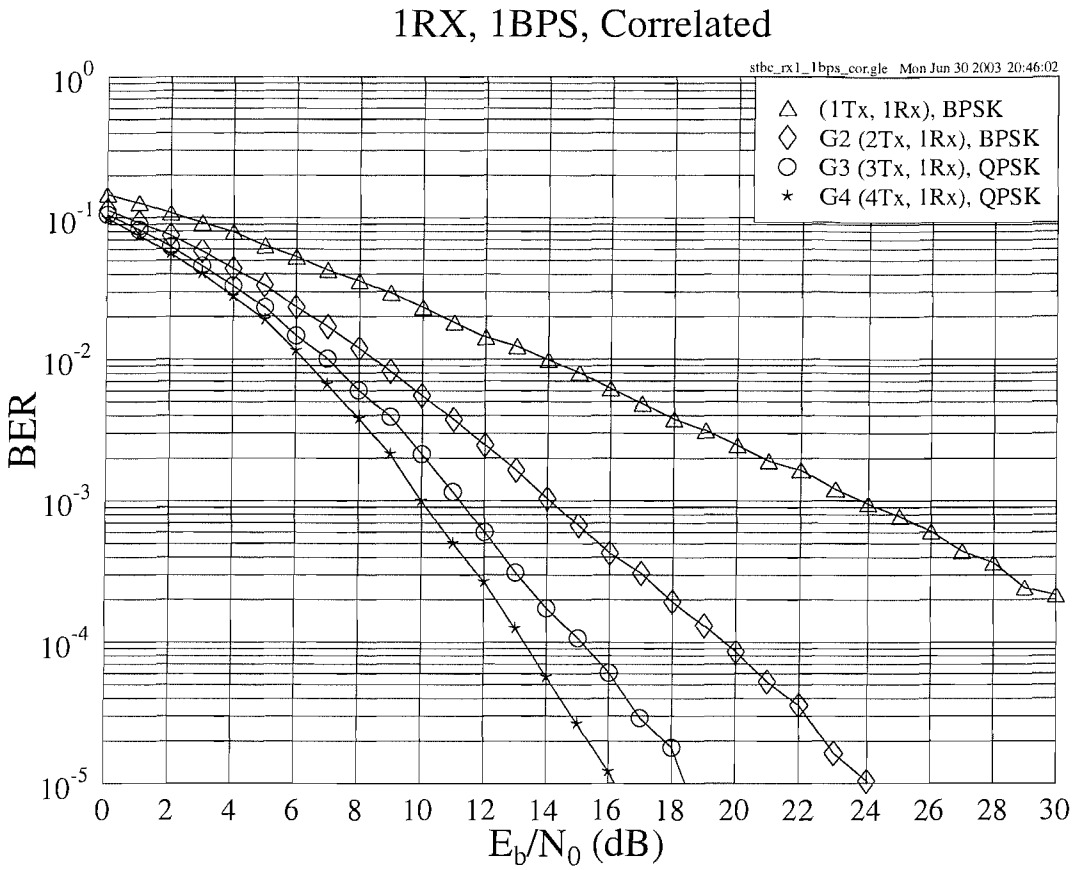

Figure 2.10: The BER versus E_b/N_0 performance of the $\mathbf{G_2}$, $\mathbf{G_3}$, and $\mathbf{G_4}$ space-time block codes of Table 2.1 at an effective throughput of **1 BPS** using **one receiver** over **correlated** Rayleigh fading channels. The normalized Doppler frequency is 3.25×10^{-5}.

of the attainable diversity gain has already been achieved using the G_2 code employing two receivers.

Last but not least, it was also found that the performances of the space-time codes communicating over uncorrelated and correlated Rayleigh fading channels are similar, provided that the effective throughput is the same.

The achievable coding gains of the space-time block codes are summarized in Table 2.2. The coding gain is defined as the E_b/N_0 difference, expressed in terms of decibels, at a BER of 10^{-5} between the various space-time block coded and uncoded single-transmitter systems having the same throughput. The best schemes at the effective throughput of 1, 2, and 3 BPS are printed in bold, respectively.

BPS	Code	Code Rate	Modem	E_b/N_0 (dB)		Gain (dB)	
				BER			
				10^{-3}	10^{-5}	10^{-3}	10^{-5}
1.00	Uncoded	1	BPSK	24.22	44.00	0.00	0.00
	G_2	1	BPSK	14.08	24.22	10.14	19.78
	G_3	1/2	QPSK	11.33	18.71	12.89	25.29
	G_4	1/2	QPSK	**10.10**	**15.85**	**14.12**	**28.15**
2.00	Uncoded	1	QPSK	24.22	44.00	0.00	0.00
	G_2	1	QPSK	14.12	24.22	10.10	19.78
	G_3	1/2	16QAM	14.78	22.06	9.44	21.94
	G_4	1/2	16QAM	**13.61**	**19.58**	**10.61**	**24.42**
2.25	H_3	3/4	8PSK	15.43	23.00	8.79	21.00
≈ 2.00	H_4	3/4	8PSK	14.31	20.48	9.91	23.52
3.00	Uncoded	1	8PSK	26.30	46.26	0.00	0.00
	G_2	1	8PSK	16.80	27.21	9.50	19.05
	G_3	1/2	64QAM	18.83	26.00	7.47	20.26
	G_4	1/2	64QAM	17.69	23.92	8.61	22.34
	H_3	3/4	16QAM	16.06	23.36	10.24	22.90
	H_4	3/4	16QAM	**14.87**	**21.10**	**11.43**	**25.16**

Table 2.2: Coding gains of the space-time block codes using one receiver when communicating over uncorrelated and correlated Rayleigh fading channels. The performance of the best scheme for a specific effective throughput is printed in bold.

2.3 Channel Coded Space-Time Block Codes

In Section 2.2, we have presented the basic concepts of the space-time block codes and provided a range of characteristic performance results. Furthermore, the MAP algorithm invoked for decoding STBC codes has also been briefly highlighted. This enables a space-time decoder to provide soft outputs that can be exploited by concatenated channel decoders for further improving the system's performance. In this section, we will concatenate the space-time block codes with various Low Density Parity Check (LDPC) channel codes [285] and with a Turbo Convolutional (TC) code [286, 287]. The performances of the different schemes will also be evaluated.

2.3.1 Space-Time Block Codes with LDPC Channel Codes

LDPC codes were devised by Gallager [285] in 1962. During the early evolutionary phase of channel coding, LDPC schemes made a limited impact on the research of the channel coding community, although they showed an unprecedented performance prior to the turbo coding era. This was because LDPC codes required a relatively high storage space and complexity. However, owing to their capability of approaching Shannon's predicted performance limits [292], research interests in LDPC codes have been rekindled during recent years [292–296].

LDPC codes [285] belong to the family of linear block codes, which are defined by a parity check matrix having M rows and N columns. The column weight j and row weight k is typically significantly lower than the dimension M and N of the parity check matrix. The construction of the parity check matrix is referred to as regular or irregular, depending on whether the Hamming weight per column or row is identical. Reference [294] shows that carefully designed irregular LDPC codes may perform better than their regular counterparts. Furthermore, when the block length is increased, irregular LDPC codes may become capable of outperforming turbo codes [292] at the cost of a higher complexity. Since the details of the decoding of LDPC codes can be found in [297], in the forthcoming sections we are more interested in the performance of LDPC codes than the LDPC decoding algorithm itself.

The number of columns N is given by the number of coded bits hosted by a LDPC codeword, while the number of rows M corresponds to the number of parity check constraints imposed by the design of the LDPC code. The number of information bits encoded by a LDPC codeword is denoted by $K = N - M$, yielding a coding rate of K/M [297]. Thus, the LDPC code rate can be adjusted by changing K and/or M.

Figure 2.11 characterizes the performance of several LDPC codes for transmission over both uncorrelated and correlated Rayleigh fading channels. The normalized Doppler frequency of the correlated Rayleigh channel was 3.25×10^{-5}. It was found that the LDPC codes perform far better over uncorrelated than over correlated Rayleigh channels, since the codeword length is short. This characteristic predetermines the expected performance of the LDPC-STBC coded concatenated system to be introduced in the next section and characterized in Section 2.3.1.2.2.

2.3.1.1 System Overview

Figure 2.12 shows the schematic diagram of the system. The source bits are first encoded by the LDPC encoder, whose outputs are modulated and forwarded to the STBC encoder. At the receiver, the noise-contaminated received symbols are decoded by the STBC soft decoder. As discussed in Section 2.2.3.2, the soft outputs constituted by the aposteriori probabilities of the

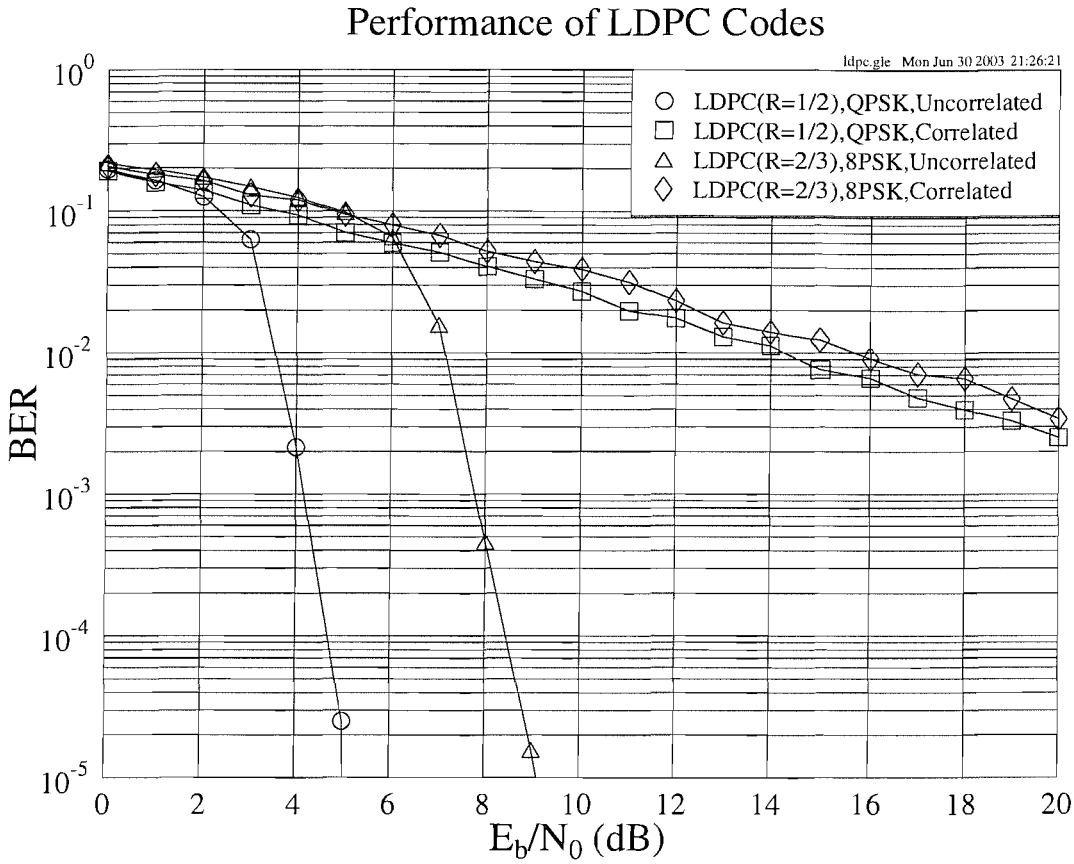

Figure 2.11: The BER versus E_b/N_0 performance of several LDPC codes communicating over both uncorrelated and correlated Rayleigh fading channels. The parameters of the LDPC codes are given in Tables 2.3 and 2.4. The normalized Doppler frequency of the correlated Rayleigh fading channels was 3.25×10^{-5}. The effective throughput of the QPSK and 8PSK schemes were 1 BPS and 2 BPS, respectively.

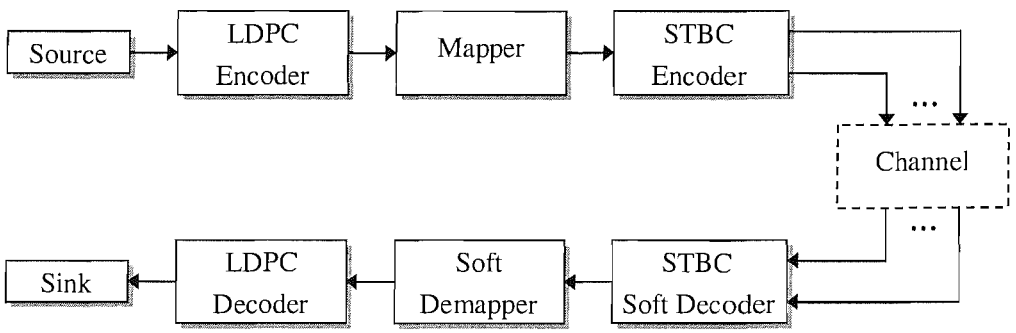

Figure 2.12: System overview of LDPC channel coding aided space-time block codes.

STBC-decoded symbols will be passed on to the soft demapper, where the symbol probabilities are used for generating the resultant bit probabilities. Finally, the LDPC decoder decodes the soft inputs and the channel decoded information bits are obtained.

In Section 2.3.1.2, we will provide a range of simulation results and compare the achievable performances of the different schemes designed for transmission over both uncorrelated and correlated Rayleigh fading channels. According to [297], when using different column weights j and/or a different number of LDPC decoding iterations, the performance of LDPC codes will change correspondingly. In our system, we fix the column weight and the number of iterations to 3 and 25, respectively. For the scenarios of communicating over correlated Rayleigh fading channels, a fix-length random channel interleaver was used. Furthermore, for the sake of fair comparisons, we comply with the assumptions outlined on page 30 so that the simulation results of Section 2.2.5 remain comparable in this new context.

BPS	STBC		LDPC					Modem
	Code	Code Rate	Code Rate	Input Bits Block Size	Output Bits Block Size	Column Weight	Iter-ations	
1.00	G_2	1	1/2	1008	2016	3	20	QPSK
	G_3	1/2	1/2	1008	2016	3	20	16QAM
	G_4	1/2	1/2	1008	2016	3	20	16QAM
	H_3	3/4	2/3	1344	2016	3	20	QPSK
	H_4	3/4	2/3	1344	2016	3	20	QPSK
2.00	G_2	1	2/3	1344	2016	3	20	8PSK
	G_2	1	1/2	1008	2016	3	20	16QAM
	G_2	1	1/3	672	2016	3	20	64QAM
	G_3	1/2	2/3	1344	2016	3	20	64QAM
	G_4	1/2	2/3	1344	2016	3	20	64QAM
2.25	H_3	3/4	1/2	1008	2016	3	20	64QAM
$\approx$ 2.00	H_4	3/4	1/2	1008	2016	3	20	64QAM
3.00	G_2	1	3/4	1512	2016	3	20	16QAM
	G_2	1	1/2	1008	2016	3	20	64QAM
	H_3	3/4	2/3	1344	2016	3	20	64QAM
	H_4	3/4	2/3	1344	2016	3	20	64QAM

Table 2.3: The parameters used in the LDPC-STBC coded concatenated schemes for transmissions over **uncorrelated** Rayleigh fading channels.

The parameters used in our LDPC-STBC coded concatenated system are given in Tables 2.3 and 2.4, while the parameters of the space-time block codes have been given in Table 2.1. For the sake of maintaining the same effective throughput, the LDPC codec's parameters have to be harmonized with the STBC codec's parameters.

BPS	STBC		LDPC					Channel Interleaver Depth	Modem
	Code	Code Rate	Code Rate	Input Bits Block Size	Output Bits Block Size	Column Weight	Iterations		
1.00	G_2	1	1/2	10080	20160	3	20	20160	QPSK
	G_3	1/2	1/2	10080	20160	3	20	20160	16QAM
	G_4	1/2	1/2	10080	20160	3	20	20160	16QAM
	H_3	3/4	2/3	13440	20160	3	20	20160	QPSK
	H_4	3/4	2/3	13440	20160	3	20	20160	QPSK
2.00	G_2	1	2/3	13440	20160	3	20	20160	8PSK
	G_2	1	1/2	10080	20160	3	20	20160	16QAM
	G_2	1	1/3	6720	20160	3	20	20160	64QAM
	G_3	1/2	2/3	13440	20160	3	20	20160	64QAM
	G_4	1/2	2/3	13440	20160	3	20	20160	64QAM
2.25	H_3	3/4	1/2	10080	20160	3	20	20160	64QAM
$\approx$ 2.00	H_4	3/4	1/2	10080	20160	3	20	20160	64QAM
3.00	G_2	1	3/4	15120	20160	3	20	20160	16QAM
	G_2	1	1/2	10080	20160	3	20	20160	64QAM
	H_3	3/4	2/3	13440	20160	3	20	20160	64QAM
	H_4	3/4	2/3	13440	20160	3	20	20160	64QAM

Table 2.4: The parameters used in the LDPC-STBC coded concatenated schemes for transmissions over **correlated** Rayleigh fading channels.

2.3.1.2 Simulation Results

Similarly to Section 2.2.5, we will compare the performances of different schemes in the context of the same effective throughput, when communicating over both uncorrelated and correlated Rayleigh fading channels.

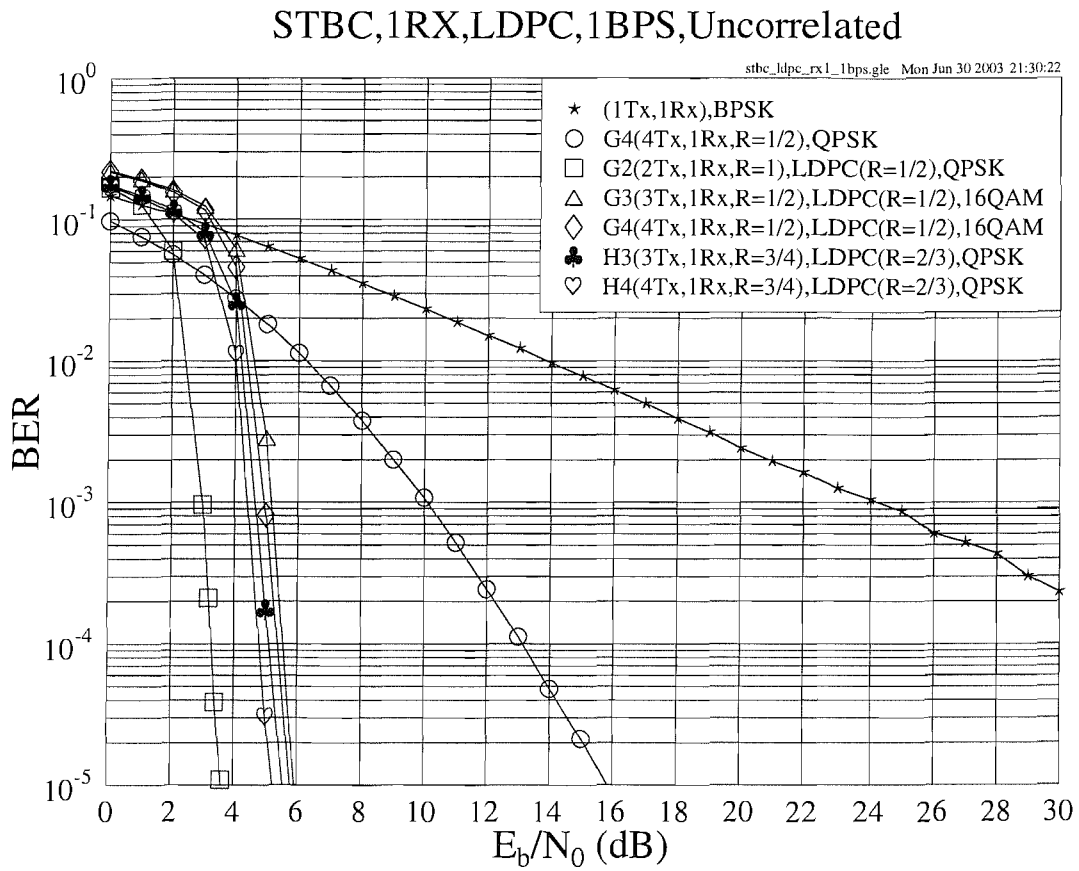

Figure 2.13: The BER versus E_b/N_0 performance of the $\mathbf{G_2}$, $\mathbf{G_3}$, $\mathbf{G_4}$, $\mathbf{H_3}$ and $\mathbf{H_4}$ space-time block codes of Table 2.1 in conjunction with the different-rate LDPC codes of Table 2.3 at an effective throughput of **1 BPS** using **one receiver** over **uncorrelated** Rayleigh fading channels.

2.3.1.2.1 Performance over Uncorrelated Rayleigh Fading Channels

Performance at the Throughput of 1 BPS Figure 2.13 compares the achievable performance of the G_2, G_3, G_4, H_3 and H_4 space-time block codes, which are combined with various LDPC codes, in the context of using one receiver and maintain a throughput of 1 BPS, while communicating over uncorrelated Rayleigh fading channels. We can see that when E_b/N_0 is lower than about 2.7dB, the half-rate space-time bock code G_4 using QPSK modulation, which constituted the best system at the throughput of 1 BPS according to Table 2.2, gives the best performance. But when the SNR increases, the situation reverses since the performance of the LDPC-assisted STBC codes becomes significantly better than that of the G_4 scheme using no channel coding. Moreover, the scheme constituted by the G_2 code and half-rate LDPC code excels among all the LDPC-coded STBC schemes by a margin of about 2dB gain over others. Note that in order to maintain the same effective throughput of 1 BPS, the unity-rate space-time block code G_2 is combined with the half-rate LDPC code

employing QPSK modulation, while the half-rate space-time codes G_3 and G_4 assisted by half-rate LDPC code use 16QAM modulation. For the $\frac{3}{4}$-rate codes H_3 and H_4, the $\frac{2}{3}$-rate LDPC code is introduced and QPSK modulation is used for meeting the criteria of having the same throughput of 1 BPS.

From Figure 2.13, we may arrive at the following conclusions. Provided that a fixed block size of the LDPC codeword is used, a lower LDPC code rate implies that more parity check bits are attached to the original bits sequence, which leads to a better performance. On the other hand, as seen in Figure 2.13, when QPSK modulation is used, the G_2 code employing the half-rate LDPC code outperforms the H_3 and H_4 codes in conjunction with the $\frac{2}{3}$-rate LDPC code, despite the fact that the former has a lower diversity order. Therefore we may surmise for the set of LDPC-coded STBC schemes considered that when using a specific modulation scheme, the system's performance is predominantly determined by the LDPC code employed instead of the space-time code's diversity order. Another observation informed from the figure is, that the number of bits per symbol used by the specific modulation scheme is a more decisive factor in terms of determining the achievable performance, than the diversity order, when the same LDPC code is used. In other words, if we want to improve the system's performance, it is more beneficial to reduce the number of bits per symbol instead of increasing the number of transmitter antennas. For example, when employing a half-rate LDPC code, the G_3 and G_4 space-time codes employing 16QAM perform about 2.2dB worse than the G_2 code employing QPSK, despite that the fact that the former one has a higher diversity order.

Performance at the Throughput of 2 BPS In Figure 2.14 the performance of the LDPC-aided space-time block codes using one receiver and having a throughput of about 2 BPS, while communicating over uncorrelated Rayleigh fading channels is studied. Specially, the $\frac{3}{4}$-rate codes H_3 and H_4 are employed in conjunction with the half-rate LDPC code using 64QAM modulation, and thus achieve an effective throughput of 2.25 BPS, which is close to our target of 2 BPS.

The curves seen in Figure 2.14 can be divided into two groups based on their relative performances. The first group contains the three schemes employing the G_2 code in conjunction with various LDPC codes and gives an average gain of about 3dB over the members of the second group, in which the $G_3/G_4/H_3/H_4$ schemes are grouped. The performance difference between the two groups tallies with our conclusions derived in the case of aiming for a throughput of 1 BPS. As seen in Figure 2.14, the schemes of the second group suffer performance degradations as a consequence of employing the densely-packed 64QAM constellation, which is more prone to transmission errors than the other modulation schemes. Furthermore, the 64QAM-based scheme of the first group, i.e. the arrangement employing the G_2 code as well as the $\frac{1}{3}$-rate LDPC code, also performs better than any member scheme of the second

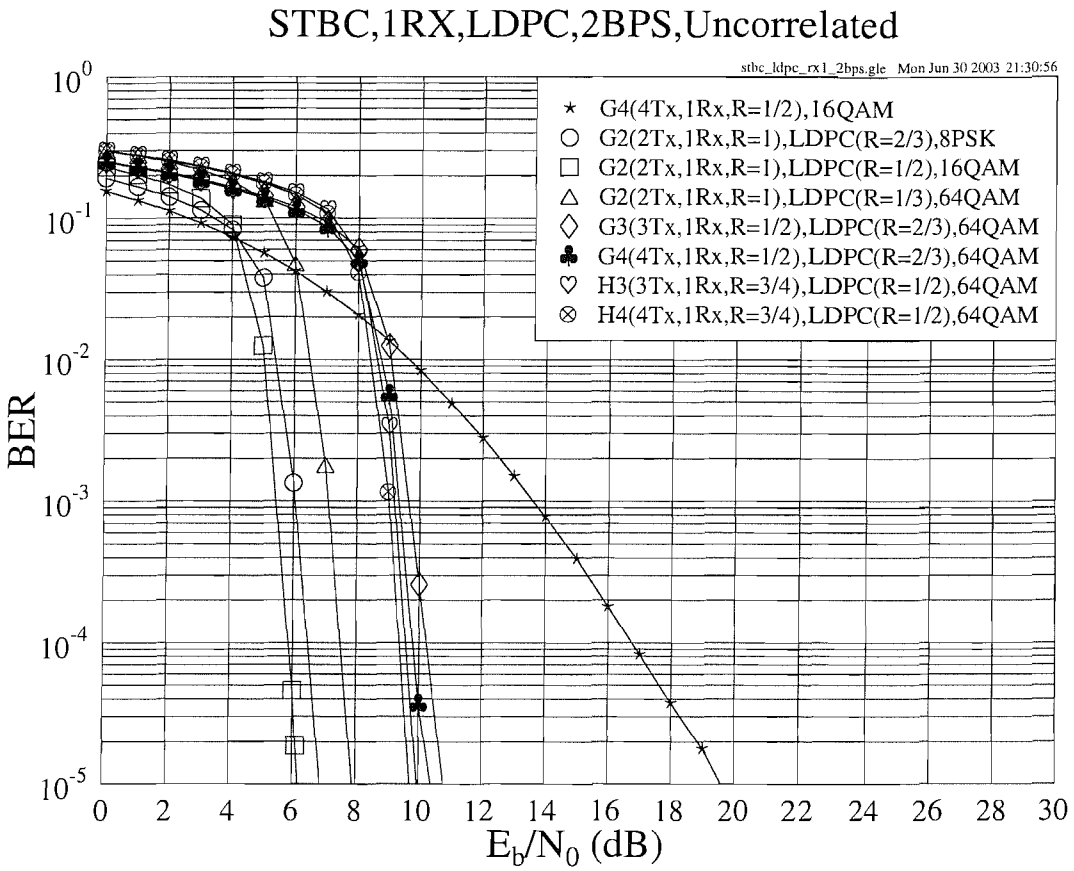

Figure 2.14: The BER versus E_b/N_0 performance of the $\mathbf{G_2}$, $\mathbf{G_3}$, $\mathbf{G_4}$, $\mathbf{H_3}$ and $\mathbf{H_4}$ space-time block codes of Table 2.1 in conjunction with the different-rate LDPC codes of Table 2.3 at an effective throughput of about **2 BPS** using **one receiver** over **uncorrelated** Rayleigh fading channels.

group as a benefit of its lower LDPC code rate.

Ass seen in Figure 2.14, in all the three G_2-based schemes of the superior group, the best design option is the compromise scheme employing the half-rate LDPC-aided G_2 code using 16QAM modulation. The reason for this phenomenon can be explained from two different aspects. On one hand, when the number of bits per symbol is moderate, as in relatively lower-order 8PSK and 16QAM, for example, the performance trends imposed by the different LDPC codes outweigh those caused by the different modulation schemes. In this case, as expected, if the system uses a lower-rate LDPC code, it will achieve a better performance. This is why the half-rate LDPC coded scheme using 16QAM modulation is superior to the $\frac{2}{3}$-rate LDPC coded scheme using 8PSK modulation, as seen in Figure 2.14. On the other hand, when the modulation level is increased to 64, for example, as in 64QAM, the situation is reversed and the number of bits per symbol conveyed by the modulation schemes will become the predominant factor. In this case, the combination of lower-rate LDPC codes with high-order modulation arrangements will no longer outperform the scheme that uses higher-rate LDPC

codes in conjunction with lower-order modulation constellations. Hence the $\frac{1}{3}$-rate LDPC coded 64QAM modulation scheme is outperformed by the half-rate LDPC coded 16QAM modulation arrangement, as indicated by Figure 2.14.

Performance at the Throughput of 3 BPS The performance of the LDPC-assisted space-time block codes using one receiver and having a throughput of 3 BPS for transmissions over uncorrelated Rayleigh fading channels is shown in Figure 2.15. When the half-rate space-time codes G_3 and G_4 are used in conjunction with LDPC codes, even if we employ a high-throughput 64QAM scheme, the system's effective throughput will be lower than 3 BPS, because the code rate of the LDPC code is below unity. For employment in conjunction with the G_3 and G_4 codes, a high-rate LDPC code has to be used in order to maintain a throughput close to 3 BPS. However, as discussed before, when the high-order 64QAM scheme is used, the achievable performance improvement of LDPC coding remains modest, regardless of the rate of the LDPC code. Hence in this scenario the performance of the LDPC-aided G_3 and G_4 codes is not considered here.

In Figure 2.15, similarly to the 2-BPS throughput scenario, it is also found that the four LDPC-aided STBC schemes can be divided into two groups. The G_2 space-time code aided by the $\frac{3}{4}$-rate LDPC code using 16QAM performs best in high SNR situations and it only suffers a low performance degradation over the scheme using no channel coding when SNR is low.

When we increase the number of receiver antennas, the performance gap between the two groups remains still obvious as shown in Figure 2.16. In this scenario, the best scheme is again the one employing the half-rate LDPC-aided G_2 code using 16QAM. However, the gain achieved by the best LDPC-STBC scheme over the best unprotected STBC scheme using two receivers decreases to about 10dB compared to the 12.5dB achieved, while using a single receiver.

2.3.1.2.2 Performance over Correlated Rayleigh Fading Channels

We have compared the performance of the LDPC-aided space-time block codes when communicating over uncorrelated Rayleigh fading channels in Section 2.3.1.2.1. In this section, the performance of the STBC codes will be studied based on the same assumptions summarized on page 30, except that the channel is assumed to be a correlated Rayleigh fading channel obeying the normalized Doppler frequency of 3.25×10^{-5}. The corresponding parameters are given in Table 2.4.

In Section 2.2.5.2 it was found that if the effective throughput is a fixed constant, the performance of the various space-time codes used for transmission over uncorrelated and cor-

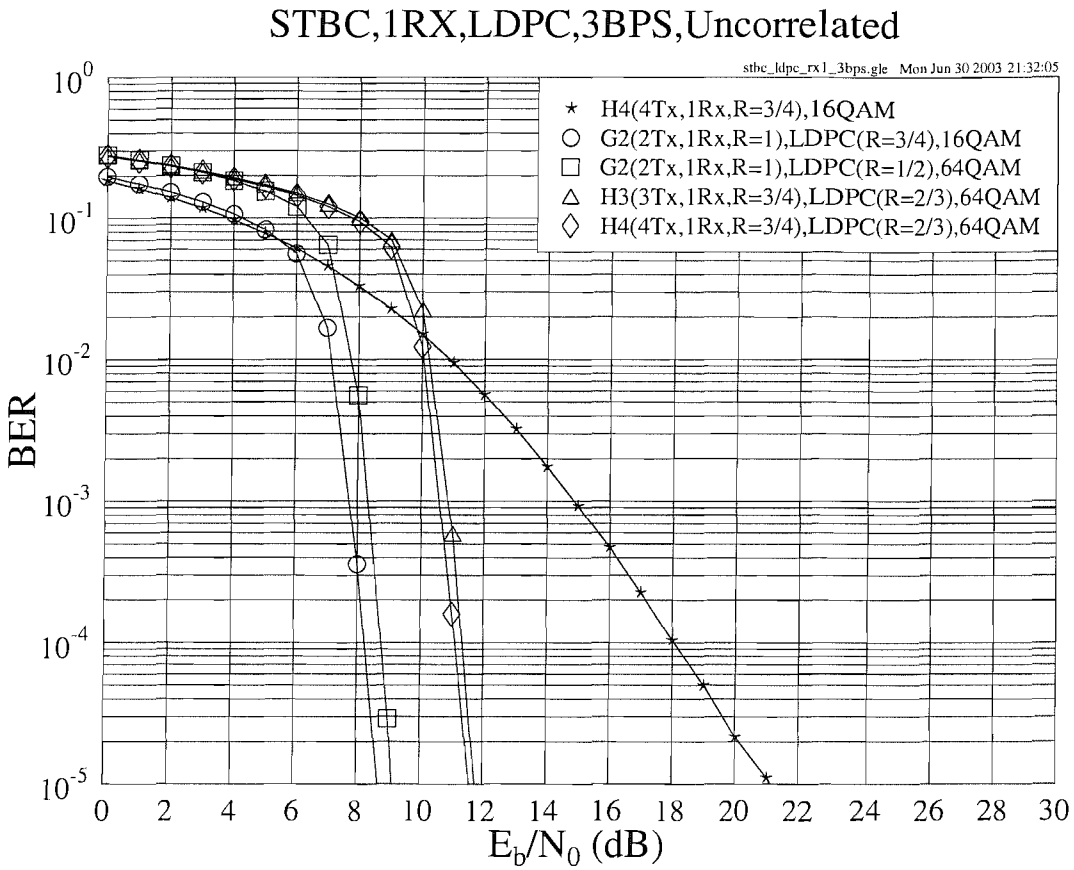

Figure 2.15: The BER versus E_b/N_0 performance of the $\mathbf{G_2}$, $\mathbf{H_3}$, and $\mathbf{H_4}$ space-time block codes of Table 2.1 in conjunction with the different-rate LDPC codes of Table 2.3 at an effective throughput of **3 BPS** using **one receiver** over **uncorrelated** Rayleigh fading channels.

related Rayleigh fading channels is similar. However, in the context of the LDPC-assisted STBC-coded system, the achievable performances are different over uncorrelated and correlated Rayleigh fading channels. This can be clearly seen by comparing Figures 2.17, 2.18 and 2.19 of this section to Figures 2.13, 2.14 and 2.15 of Section 2.3.1.2.1, respectively. The reason for this phenomenon is that the LDPC codes perform better over uncorrelated rather than correlated Rayleigh fading channels, unless their codeword length is extremely high or long channel interleavers are used. This will be demonstrated during our further discourse.

Performance at the Throughput of 1 BPS Figure 2.17 shows the achievable performance of the LDPC-assisted G_2, G_3, G_4, H_3 and H_4 codes of Table 2.1 using one receiver at the effective throughput of 1 BPS when communicating over correlated Rayleigh fading channels. We can see that the $\frac{2}{3}$-rate LDPC-coded H_4 and H_3 codes outperform the $\frac{2}{3}$-rate LDPC-coded G_4 and G_3 codes by about 1dB, respectively. However, when E_b/N_0 is lower than about 8dB, we notice that the scheme employing the unprotected G_4 code, which is the best design option at the throughput of 1 BPS according to Table 2.2, performs better

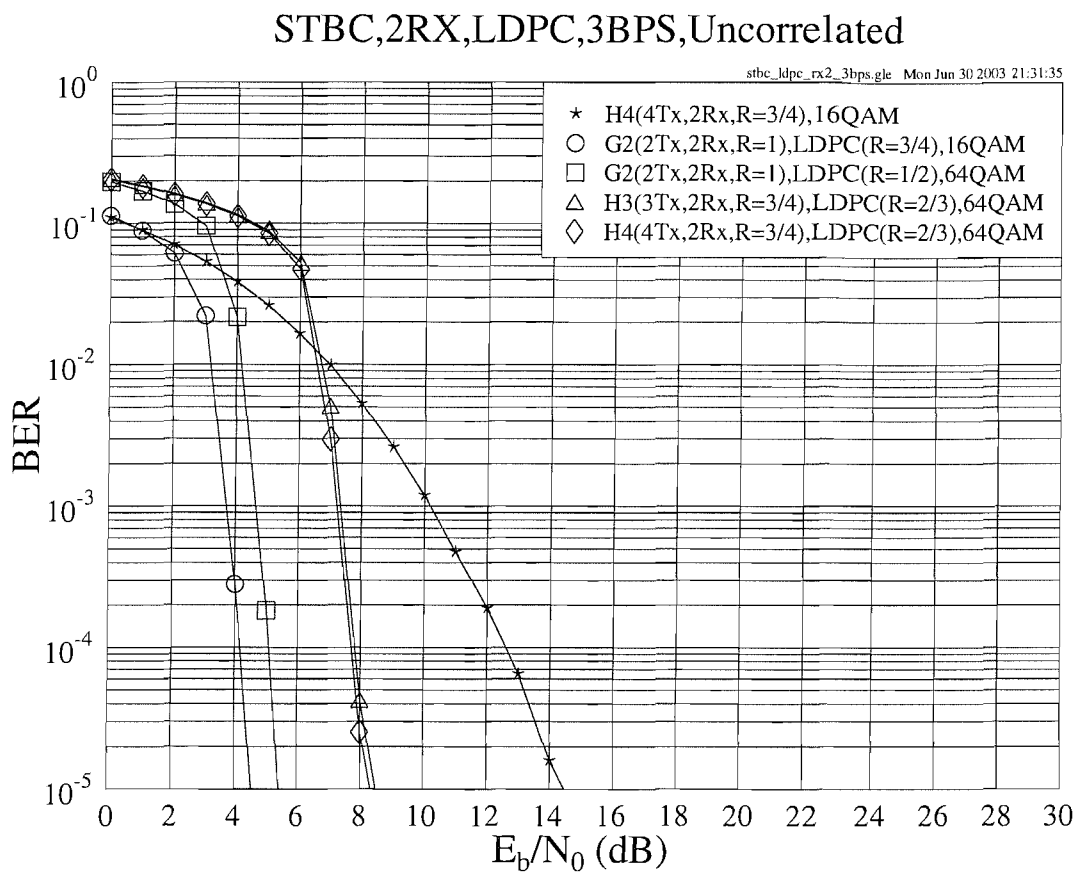

Figure 2.16: The BER versus E_b/N_0 performance of the $\mathbf{G_2}$, $\mathbf{H_3}$, and $\mathbf{H_4}$ space-time block codes of Table 2.1 in conjunction with the different-rate LDPC codes of Table 2.3 at an effective throughput of **3 BPS** using **two receivers** over **uncorrelated** Rayleigh fading channels.

than the scheme employing the $\frac{2}{3}$-rate LDPC-aided H_4 code. When the SNR is increased to 15dB, the situation is reversed, since the unprotected G_4 scheme is outperformed by the best LDPC-STBC scheme, namely the $\frac{2}{3}$-rate LDPC-assisted H_4 coded scheme, with about 1dB E_b/N_0 degradation at the BER of 10^{-5}.

Performance at the Throughput of 2 BPS At an effective throughput of approximately 2 BPS, the relevant schemes' performances are given in Figure 2.18. It is seen in the figure that the performance of the schemes employing the H_4 and H_3 codes of Table 2.1 is similar to those of the schemes employing the G_4 and G_3 codes, respectively, although we may bear in mind that the $\frac{3}{4}$-rate H_4 and H_3 codes have an effective throughput of 2.25 BPS, rather than exactly 2 BPS. Furthermore, an important phenomenon found in Figure 2.18 is that the best unprotected STBC scheme of Figure 2.6 also attains the best performance in this new scenario.

This result may be explained as follows. The performance of the unprotected space-time

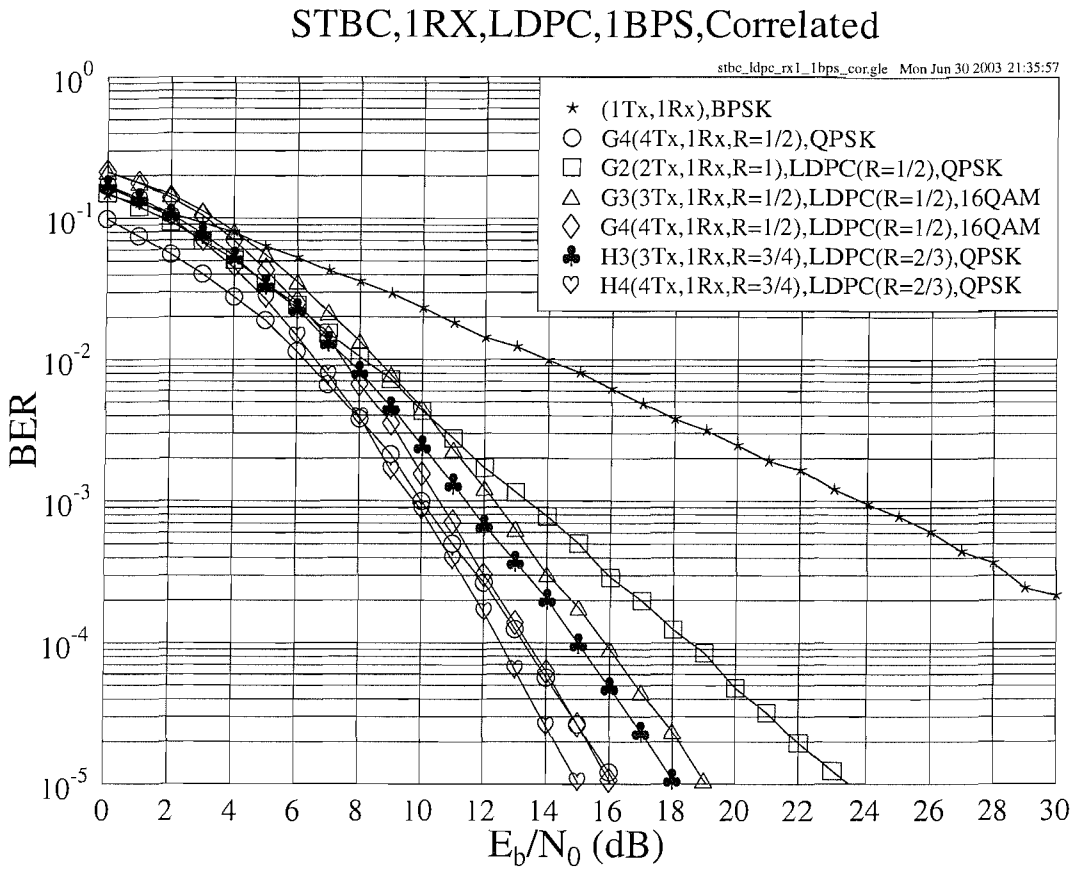

Figure 2.17: The BER versus E_b/N_0 performance of the $\mathbf{G_2}$, $\mathbf{G_3}$, $\mathbf{G_4}$, $\mathbf{H_3}$, and $\mathbf{H_4}$ space-time block codes of Table 2.1 in conjunction with the different-rate LDPC codes of Table 2.4 at an effective throughput of **1 BPS** using **one receiver** over **correlated** Rayleigh fading channels. The normalized Doppler frequency is 3.25×10^{-5}.

block codes remains similar over uncorrelated or correlated Rayleigh fading channels, as it was indicated in Section 2.2.5.2. Furthermore, the performance of the LDPC codes degrades when communicating over correlated rather than uncorrelated Rayleigh fading channels, as seen in Figure 2.11. Hence it is not surprising that the LDPC-STBC coded concatenated system will suffer a performance degradation in the context of correlated Rayleigh channels. In this case, the LDPC codes' relatively poor performance recorded over correlated Rayleigh channels disadvantageously affects the entire system. In other words, the LDPC codes improve the system's performance less dramatically over correlated Rayleigh fading channels than over uncorrelated Rayleigh fading channels, unless the LDPC codeword length is very high or long interleavers are used.

Performance at the Throughput of 3 BPS The performance of the LDPC-assisted space-time block codes using one receiver and having a throughput of 3 BPS while communicating over correlated Rayleigh fading channel is portrayed in Figure 2.19. Similar to

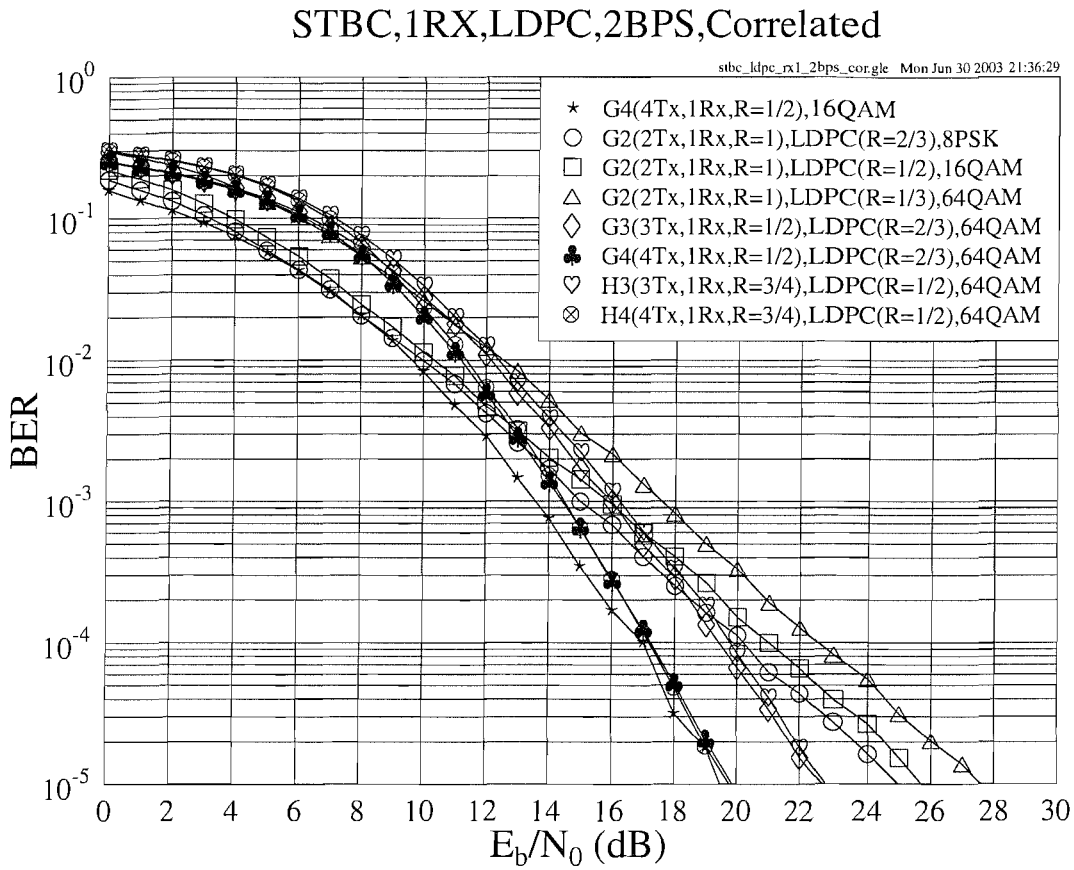

Figure 2.18: The BER versus E_b/N_0 performance of the $\mathbf{G_2}$, $\mathbf{G_3}$, $\mathbf{G_4}$, $\mathbf{H_3}$, and $\mathbf{H_4}$ space-time block codes of Table 2.1 in conjunction with the different-rate LDPC codes of Table 2.4 at an effective throughput of about **2 BPS** using **one receiver** over **correlated** Rayleigh fading channels. The normalized Doppler frequency is 3.25×10^{-5}.

Figure 2.15, the schemes which employ the half-rate space-time codes G_3 and G_4 of Table 2.1 are not considered in this scenario, since they are incapable of achieving an effective throughput of 3 BPS, nor can they achieve a better performance than the candidate schemes characterized in Figure 2.19.

As Figure 2.19 shows, the unprotected STBC H_4 using 16QAM modulation performs best, giving an approximately 1dB gain over the best LDPC-aided scheme, namely the STBC H_4 combined with the $\frac{2}{3}$-rate LDPC code using 64QAM modulation at the BER of 10^{-5}. Similar to the scenario maintaining an effective throughput of 2 BPS, at a relatively lower E_b/N_0 value, i.e. below 14.5dB, the best STBC-LDPC concatenated scheme is the one that employs the G_2 ST code combined with a low-order modulation, namely the $\frac{3}{4}$-rate LDPC-coded 16QAM.

Furthermore, when the number of receivers is increased to two, the $\frac{3}{4}$-rate LDPC-assisted G_2 code outperforms all the other schemes considered, provided that the E_b/N_0 value is

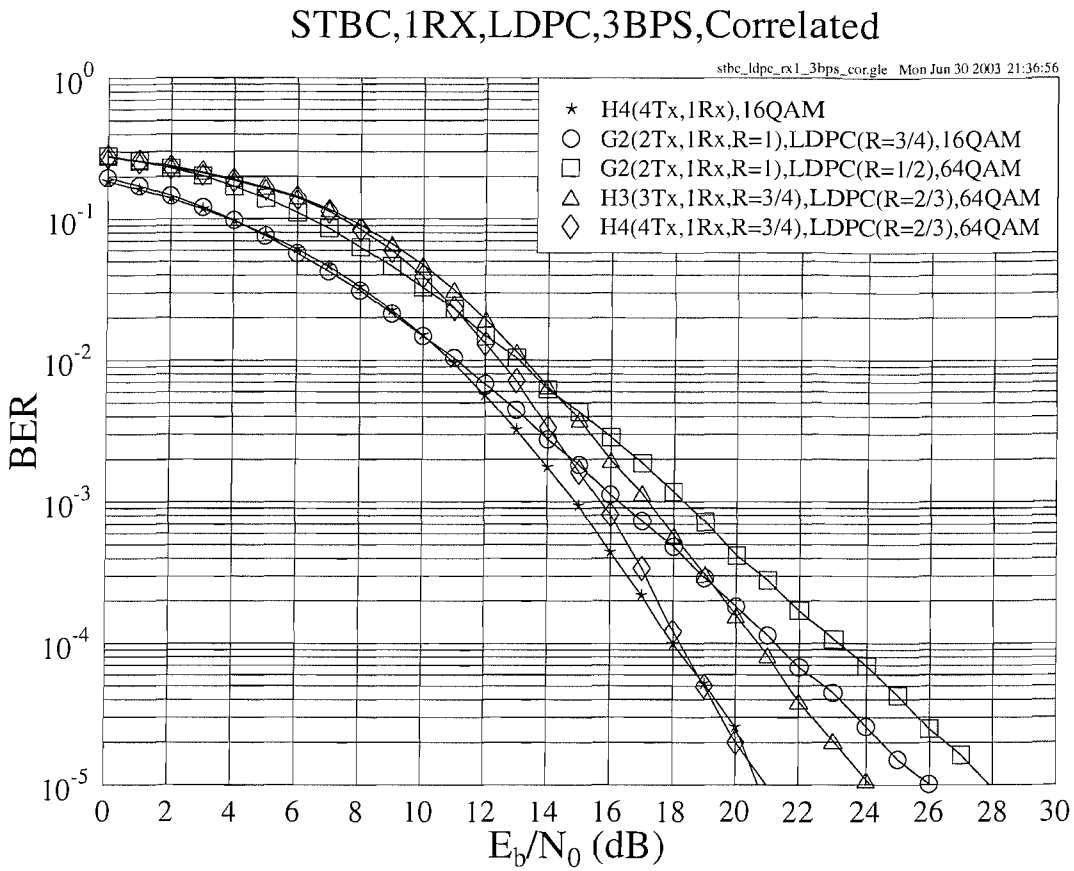

Figure 2.19: The BER versus E_b/N_0 performance of the $\mathbf{G_2}$, $\mathbf{H_3}$, and $\mathbf{H_4}$ space-time block codes of Table 2.1 in conjunction with the different-rate LDPC codes of Table 2.4 at an effective throughput of **3 BPS** using **one receiver** over **correlated** Rayleigh fading channels. The normalized Doppler frequency is 3.25×10^{-5}.

below 12dB, as observed in Figure 2.20. At even higher E_b/N_0 values, namely in excess of 12dB, the $\frac{2}{3}$-rate LDPC-assisted H_4 code exhibits the best performance, although it uses the highest-order 64QAM modem. It can be also observed from Figure 2.20 that the curves are significantly closer to one another compared to the scenario of using one receiver, which is shown in Figure 2.19.

2.3.1.3 Complexity Issues

In Section 2.3.1.2, we have compared the performance of various LDPC-STBC coded concatenated systems. The best scheme was also identified for each scenario. However, these choices have been made based purely on the achievable performance, and the complexity issue of implementation has not been taken into consideration. In this section, we will briefly address the associated complexity issues.

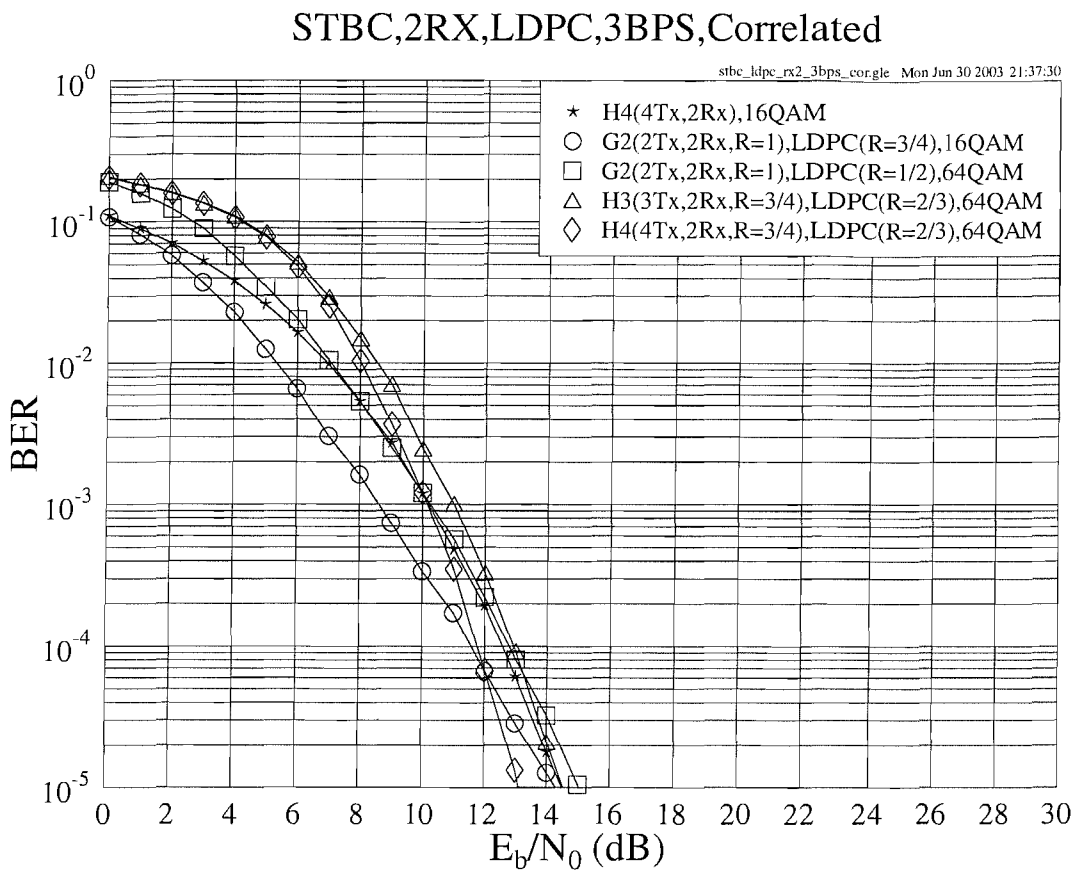

Figure 2.20: The BER versus E_b/N_0 performance of the $\mathbf{G_2}$, $\mathbf{H_3}$, and $\mathbf{H_4}$ space-time block codes of Table 2.1 in conjunction with the different-rate LDPC codes of Table 2.4 at an effective throughput of **3 BPS** using **two receivers** over **correlated** Rayleigh fading channels. The normalized Doppler frequency is 3.25×10^{-5}.

As discussed in Section 2.2.3.2, the soft decoder of the space-time block codes employs the Log-MAP algorithm summarized for example in [2]. With the advent of the Log-MAP algorithm, the high-complexity complicated exponential operations are substituted by additions and subtractions carried out in the logarithmic domain. Hence the complexity of the STBC decoder is significantly reduced, while closely matching the performance of the MAP algorithm. In our following discussions, the decoding complexity of the space-time bock codes is considered to be sufficiently low for it to be ignored for the sake of simplifying our comparisons. This will not affect our conclusions, since we will show in the rest of this section that the LDPC-assisted G_2 code, which has the lowest decoding complexity among all the space-time block codes of Table 2.1, gives the best performance as seen in Figures 2.21, 2.22 and 2.23. Hence, even if the decoding complexity of the space-time block codes is considered, the G_2 code will still be superior to the other STBCs in the context of the coding gain versus complexity performance.

The decoding complexity per information bit per iteration of the LDPC codes can be calculated as follows [297]:

$$comp\{LDPC\} = \left(\frac{5-R}{1-R}\right) \cdot j^2, \tag{2.30}$$

where R is the LDPC code's code rate and j is the column weights of the parity check matrix. In our system the value of column weights was fixed to 3, thus Equation (2.30) is simplified to:

$$comp\{LDPC\} = \left(\frac{45-9R}{1-R}\right). \tag{2.31}$$

According to Equation (2.31), the decoding complexity is essentially based on the code rate of the LDPC code employed. Thus for the rate 1/3, 1/2, 2/3 and 3/4 LDPC codes used in our system, the associated decoding complexity per bit per iteration becomes 63, 81, 117 and 153 additions and subtractions, respectively, as summarized in Table 2.5.

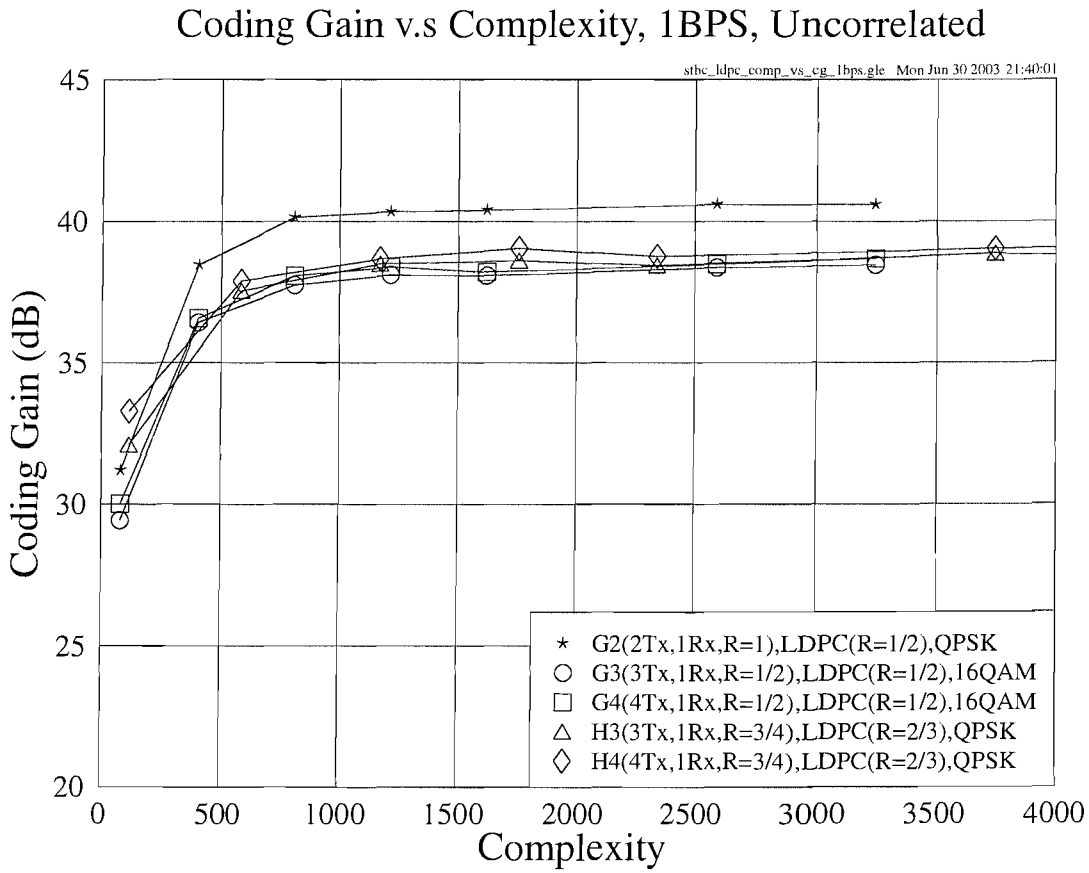

Figure 2.21: Coding gain versus estimated complexity for the LDPC-STBC coded concatenated schemes using one receiver, when communicating over uncorrelated Rayleigh fading channels at the effective throughput of **1 BPS**. The simulation parameters are given in Table 2.3.

Let us now compare the coding gain versus complexity characteristics of the different schemes considered, as seen from Figures 2.21 to 2.23, where the parameters used are given

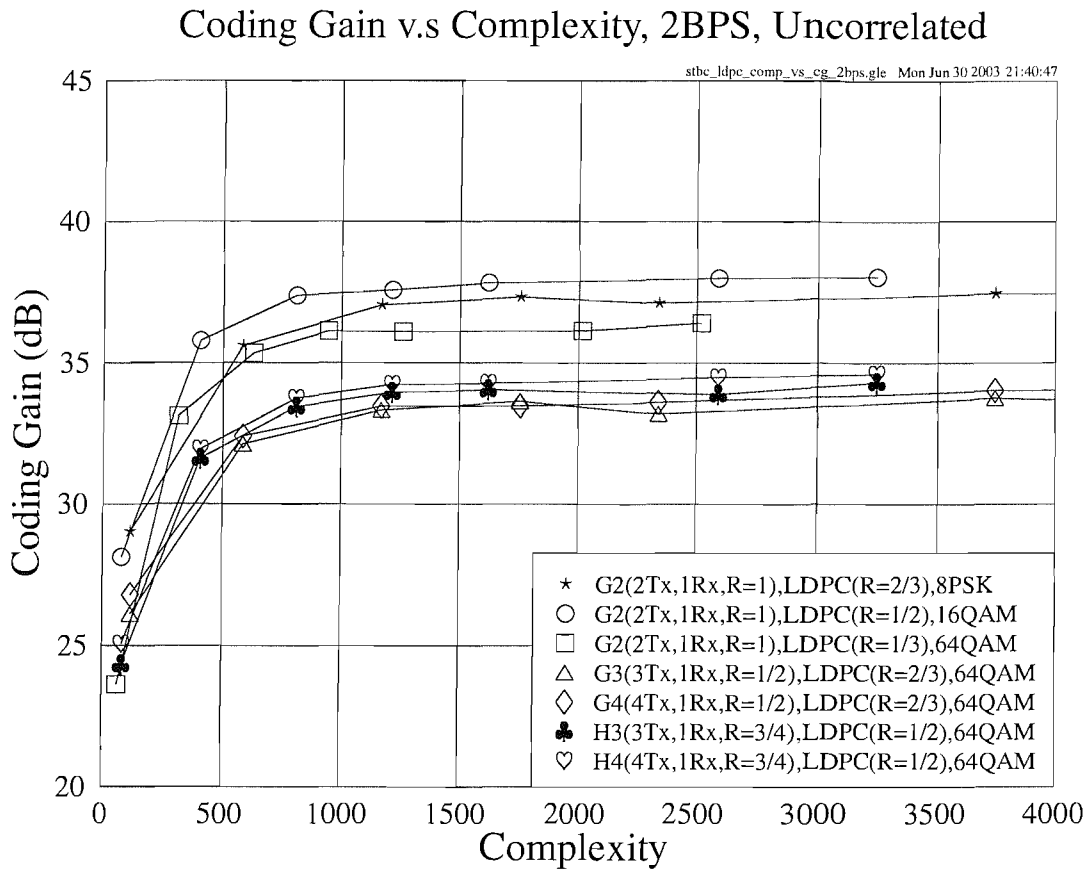

Figure 2.22: Coding gain versus estimated complexity for the LDPC-STBC coded concatenated schemes using one receiver, when communicating over uncorrelated Rayleigh fading channels at the effective throughput of **2 BPS**. The simulation parameters are given in Table 2.3.

in Table 2.3. The coding gain here is defined as the E_b/N_0 difference, expressed in terms of decibels, at a BER of 10^{-5} between the various channel codes assisted space-time block coded systems and the uncoded single-transmitter systems having the same throughput. All the estimated implementational complexities were calculated based on Equation (2.31), using different number of iterations ranging from 1 to 40 with a step of about 5.

At an effective throughput of 1 and 2 BPS, as seen in Figures 2.21 and 2.22, it was found that the best scheme was the half-rate LDPC-coded G_2 space-time code. In the scenario of having an effective throughput of 3 BPS, the performance curves of the half-rate and $\frac{3}{4}$-rate LDPC-coded G_2 space-time code are close to each other, although the former performs slightly better. We may also note that the coding gain increases dramatically in the low-complexity range and tends to saturate in the vicinity of an estimated complexity of about 1200, which corresponds to approximately 19, 15, 10 and 8 iterations for the LDPC codes having a code rate of $\frac{1}{3}$, $\frac{1}{2}$, $\frac{2}{3}$ and $\frac{3}{4}$, respectively. As Figure 2.24 shows, for example, when the number of iterations is increased to about 10 in terms of the half-rate LDPC-aided G_2

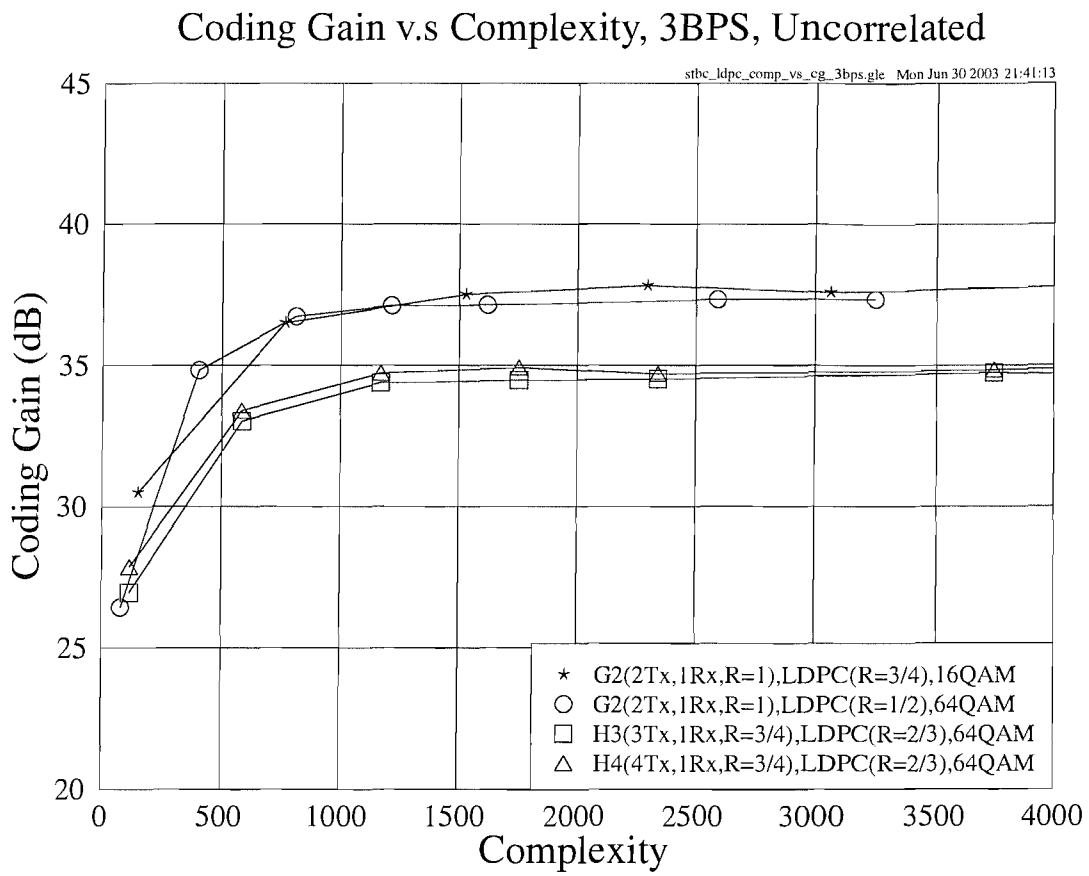

Figure 2.23: Coding gain versus estimated complexity for the LDPC-STBC coded concatenated schemes using one receiver, when communicating over uncorrelated Rayleigh fading channels at the effective throughput of **3 BPS**. The simulation parameters are given in Table 2.3.

code, the performance is already close to the achievable maximum coding gain. This result can be considered as a rule of thumb for setting the number of iterations for the LDPC-STBC coded concatenated schemes, when aiming for a good tradeoff in terms of the achievable performance-to-complexity relationships.

In Figure 2.25, we show the E_b/N_0 value required for maintaining a BER of 10^{-5} versus the effective throughput BPS for the unprotected space-time block codes and the half-rate LDPC-assisted G_2 code, while the associated simulation parameters are summarized in Tables 2.1 and 2.3. The simulation results were obtained using one receiver for communicating over uncorrelated Rayleigh fading channels. It can be observed in Figure 2.25 that the E_b/N_0 value required for maintaining a BER of 10^{-5} increases near-linearly, as the effective BPS throughput increases. This conclusion was valid for both the unprotected STBC-aided schemes and for the half-rate LDPC-assisted G_2 coded scheme. Furthermore, the half-rate LDPC-G_2 concatenated scheme achieves a gain of about 15dB over the best unprotected STBC scheme at the effective throughput values of 1, 2 and 3 BPS, respectively.

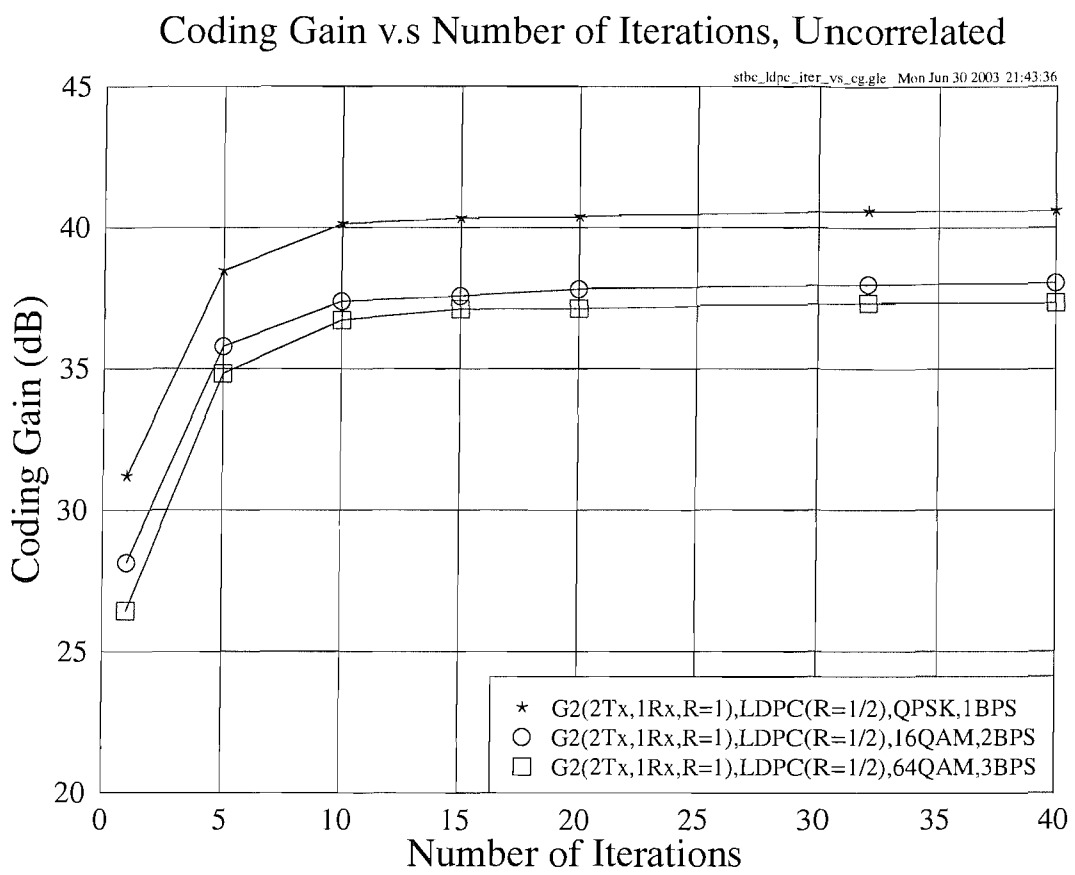

Figure 2.24: Coding gain versus the number of iterations for the half-rate LDPC-assisted G_2 space-time block coded schemes using one receiver, when communicating over uncorrelated Rayleigh fading channels at the effective throughput of 1, 2 and 3 BPS. The parameters used are given in Table 2.3.

2.3.1.4 Conclusions

Having studied Figures 2.13 to 2.19, we may arrive at the following conclusions. First of all, as expected, the LDPC-aided STBC-coded schemes perform significantly better than the unprotected STBC schemes, when transmitting over uncorrelated Rayleigh fading channels. However, over correlated Rayleigh fading channels the performance improvements achieved by the LDPC codes are not as significant as in uncorrelated Rayleigh fading channels, as seen in Figures 2.17 to 2.20. This is because the LDPC codes suffer from their finite codeword length and for a limited tolerable channel interleaver delay, as evidenced by Figure 2.11. This affects the attainable performance of the LDPC-STBC coded concatenated system to some degree. If we use an extremely long codeword or employ a long channel interleaver, however, the achievable performance of the LDPC-STBC concatenated schemes can be improved in the context of correlated Rayleigh fading channels.

Another observation inferred from Figures 2.13 to 2.19 is that when the number of receiver

BPS	STBC Code	LDPC Rate	LDPC *Compl.*	E_b/N_0 (dB) BER 10^{-3}	E_b/N_0 (dB) BER 10^{-5}	Gain (dB) BER 10^{-3}	Gain (dB) BER 10^{-5}	Modem
1.00	Uncoded	-	-	24.22	44.00	0.00	0.00	BPSK
	G_4	-	-	10.10	15.85	14.12	28.15	QPSK
	G_2	1/2	81	**2.99**	**3.61**	**21.23**	**40.39**	QPSK
	G_3	1/2	81	5.17	5.92	19.05	38.08	16QAM
	G_4	1/2	81	4.95	5.79	19.27	38.21	16QAM
	H_3	2/3	117	4.65	5.56	19.57	38.44	QPSK
	H_4	2/3	117	4.41	5.24	19.81	38.76	QPSK
2.00	Uncoded	-	-	24.22	44.00	0.00	0.00	QPSK
	G_4	-	-	13.61	19.58	10.61	24.42	16QAM
	G_2	2/3	117	6.05	6.89	18.17	37.11	8PSK
	G_2	1/2	81	**5.45**	**6.18**	**18.77**	**37.82**	16QAM
	G_2	1/3	63	7.10	7.90	17.12	36.10	64QAM
	G_3	2/3	117	9.65	10.81	14.57	33.19	64QAM
	G_4	2/3	117	9.34	10.40	14.88	33.60	64QAM
2.25	H_3	1/2	81	9.20	9.96	15.02	34.04	64QAM
$\approx$ 2.00	H_4	1/2	81	9.02	9.73	15.20	34.27	64QAM
3.00	Uncoded	-	-	26.30	46.26	0.00	0.00	8PSK
	H_4	-	-	14.87	21.10	11.43	25.16	16QAM
	G_2	3/4	153	**7.73**	**8.68**	**18.57**	**37.58**	16QAM
	G_2	1/2	81	8.33	9.13	17.97	37.13	64QAM
	H_3	2/3	117	10.85	11.75	15.45	34.51	64QAM
	H_4	2/3	117	10.58	11.57	15.72	34.69	64QAM

Table 2.5: Coding gains of the LDPC-STBC coded concatenated schemes using one receiver, when communicating over uncorrelated Rayleigh fading channels. With reference to Figures 2.21, 2.22 and 2.23, the performance of the best scheme is printed in bold for the scenarios of having different effective throughputs, respectively.

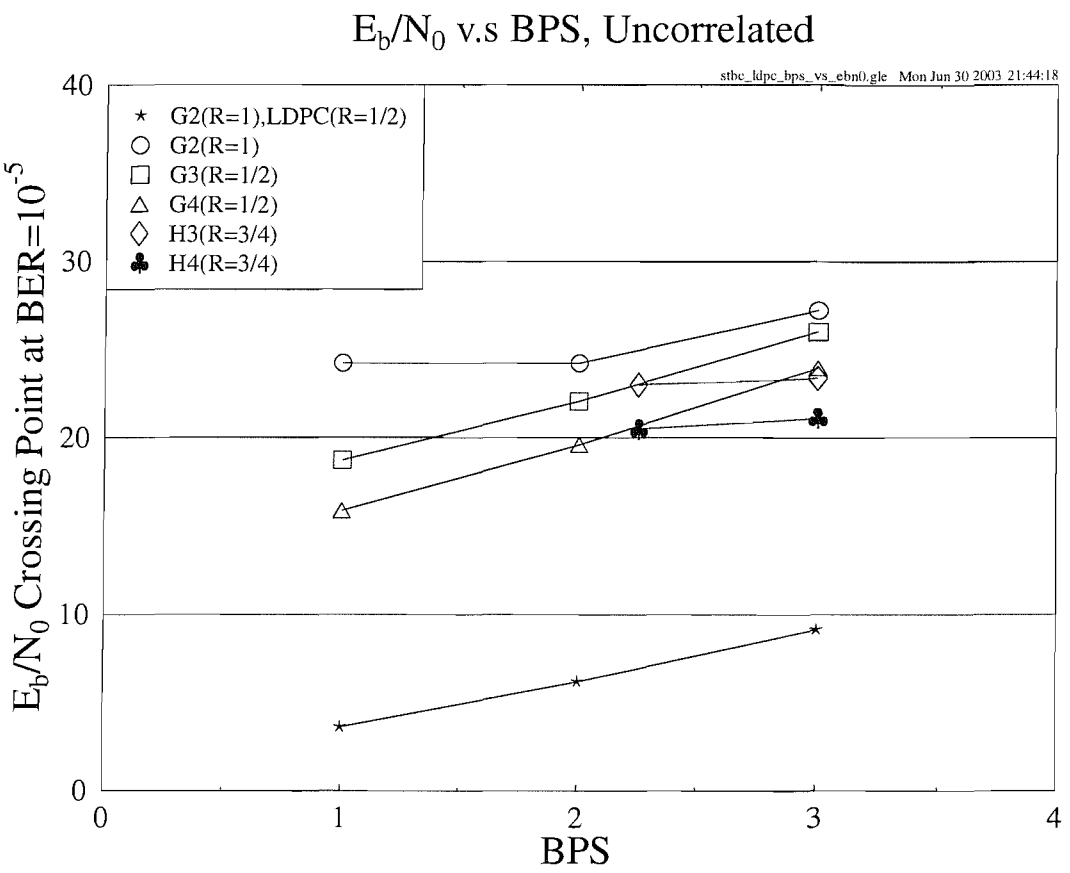

Figure 2.25: The E_b/N_0 value required for maintaining BER=10^{-5} versus the effective BPS throughput for the space-time block codes of Table 2.1 and for the half-rate LDPC-assisted G_2 code of Table 2.3, when using one receiver and communicating over uncorrelated Rayleigh fading channels.

antennas is increased, most of the attainable diversity gain has already been achieved by the LDPC-G_2 coded concatenated schemes. Hence, the employment of a space-time block code using more transmitter antennas will introduce a higher-throughput modulation mode, which in turn will require an increased E_b/N_0 value and hence degrades the achievable performance.

Furthermore, in the context of uncorrelated Rayleigh fading channels and using a specific modulation scheme, the LDPC-STBC coded system's performance is mainly decided by the code-rate and error correction capability of the LDPC code employed, instead of the space-time codes' diversity order. In this case, using a lower-rate LDPC code will achieve a more substantial performance improvement than increasing the number of transmitters and the associated diversity gain. On the other hand, if the same LDPC code is employed, the throughput of the modulation scheme has more influence on the system's performance than the diversity order. In other words, the benefits brought about by the employment of low-throughput modulation schemes will be more substantial than that offered by a high-order space-time block code, provided that both schemes are assisted by the same LDPC code.

The reason behind this phenomenon is that when the higher-order STBC codes are used in conjunction with a high number of antennas, more vulnerable high-throughput modulation schemes have to be used, for the sake of maintaining the same effective throughput. Therefore the employment of the latter scenario would result in performance degradations. In summary, the best candidate schemes are the ones using the LDPC-aided G_2 code when communicating over uncorrelated Rayleigh fading channels. When using the same space-time block code, the complexity of the STBC code can be ignored during our comparisons.

Another useful conclusion can be drawn from Figure 2.24. As seen in the figure, the coding gains of the LDPC-aided schemes tend to remain unimproved, even if the affordable complexity increases to a certain degree, although the validity of this statement depends on the specific choice of the LDPC code used. This result assists us in deciding on the appropriate number of iterations to be used by the LDPC-STBC concatenated schemes, so that the achievable best possible performance-to-complexity tradeoff can be achieved.

Before concluding this section, we summarize the achievable performance of the different schemes used in our various candidate systems communicating over uncorrelated Rayleigh fading channels in Table 2.5. For the scenarios of having an effective throughput of 1, 2 and 3 BPS, respectively, the corresponding bold numbers denote the best scheme based on the criterion of achieving the best coding gain versus complexity tradeoff, as seen in Figures 2.21, 2.22 and 2.23. As a result, the half-rate LDPC-coded space-time block code G_2 was found to be the best scheme in the scenarios having an effective throughput of 1 and 2 BPS, while the $\frac{3}{4}$-rate LDPC-coded G_2 code performs best in the scenario of having an effective throughput of 3 BPS.

2.3.2 LDPC-Aided and TC-Aided Space-Time Block Codes

In Section 2.3.1, we have studied the performance of various LDPC-aided space-time block coded systems. It has been found that the LDPC codes considerably improve the STBC-coded system's performance over uncorrelated Rayleigh fading channels. However, besides LDPC channel codes, the space-time block codes can also be concatenated with a range of other channel codes, such as Convolutional Codes (CC), Turbo Convolutional (TC) codes [286, 287], Turbo Bose-Chaudhuri-Hocquenghem (TBCH) codes [298], etc. The performance of these various channel-coded G_2 schemes designed for transmission over uncorrelated Rayleigh fading channels has been studied in [2], where the best scheme found was the half-rate TC(2,1,4) code in conjunction with the space-time block code G_2. Hence, in this section, we will compare the performance of the best LDPC-STBC coded concatenated scheme found in Section 2.3.1.2, namely that of the half-rate LDPC-aided G_2 code, with the half-rate TC(2,1,4)-aided space-time block coded schemes.

2.3.2.1 System Overview

In 1993, Berrou *et al.* [286,287] proposed a novel channel code, referred to as a turbo code. As detailed in [2], the turbo encoder consists of two component encoders. Generally, convolutional codes are used as the component encoders and the corresponding turbo codes are termed here as TC codes. For a TC(n, k, K) code, the three parameters n, k and K have the same meaning as in a convolutional code CC(n, k, K), where k is the number of input bits, n is the number of coded bits and K is the constraint length of the code. More details about TC codes can be found in [2]. The schematic of our experimental system, where the half-rate TC(2,1,4) code is employed, is given in Figure 2.26.

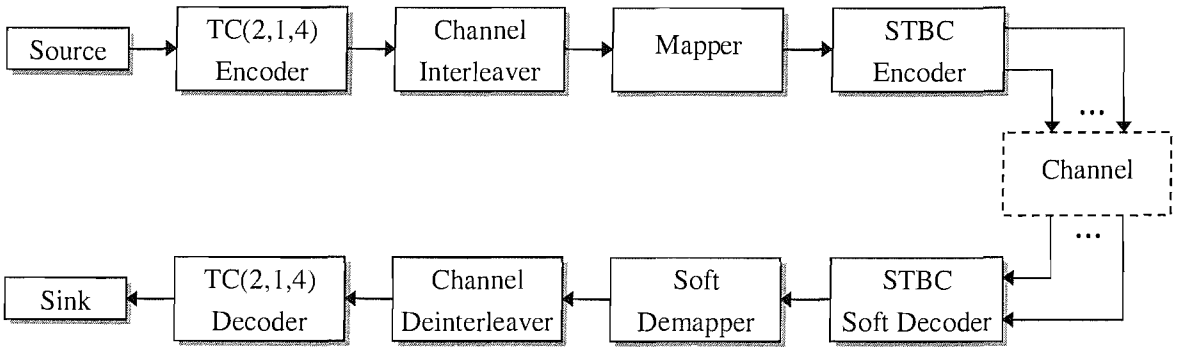

Figure 2.26: Overview of the space-time block coded and TC(2,1,4) channel coded system.

The source bits are first encoded by the half-rate TC(2,1,4) encoder. The Log-MAP decoding algorithm [2] is utilized for iterative turbo decoding, since it operates in the logarithmic domain and thus significantly reduces the computational complexity imposed by the MAP algorithm [291]. The number of turbo iterations is set to eight, since this yields a performance close to the achievable performance associated with an infinite number of iterations. The TC-encoded bits will be interleaved by the channel interleaver, as seen in Figure 2.26. In this case, a random interleaver having a depth of about 20,000 is used. The interleaved bits will then be forwarded to the mapper, followed by the STBC encoder. At the receiver side, the corresponding inverse operations are invoked, as seen in Figure 2.26. The simulation parameters of the TC-STBC coded concatenated system are given in Table 2.6.

2.3.2.2 Complexity Issues

For the sake of fair comparisons, we should calculate and take into account the complexity of the LDPC and TC(2,1,4) codes. The total estimated complexity of the TC codes per information bit per iteration in terms of additions and subtractions to be carried out is [299]:

$$comp\{TC(n,1,K)\} = 40\left(2^{K-1}\right) + 12n - 22. \quad (2.32)$$

BPS	STBC		TC(2,1,4)						Modem
	Code	Code Rate	Random Turbo Interleaver Depth	Random Channel Interleaver Depth	Code Rate	Puncturing Pattern	Iterations	Total *Compl.*	
1.00	G_2	1	10000	20000	1/2	10,01	8	2576	QPSK
	G_3	1/2	10000	20000	1/2	10,01	8	2576	16QAM
	G_4	1/2	10000	20000	1/2	10,01	8	2576	16QAM
2.00	G_2	1	10000	20000	1/2	10,01	8	2576	16QAM
3.00	G_2	1	10002	20004	1/2	10,01	8	2576	64QAM

Table 2.6: The parameters used in the TC(2,1,4)-STBC coded concatenated schemes.

According to Equation (2.32), the complexity of the TC(2,1,4) code is 322 per information bit per iteration. Since the number of iterations has been set to eight, the total complexity of the TC(2,1,4) code per bit is $322 \times 8 = 2576$ in the context of additions and subtractions, as shown in Table 2.6.

On the other hand, the complexity of the LDPC codes per information bit per iteration can be calculated according to Equation (2.31). Therefore, we can multiply the result of Equation (2.31) with the appropriately selected number of iterations required by the different-rate LDPC codes, so that a similar complexity per bit is used for both the LDPC codes and for the TC(2,1,4) code. For the half-rate LDPC-coded G_2 scheme, the number of iterations was set to 32 so that the total complexity becomes $81 \times 32 = 2592$, which is close to the estimated complexity of 2576 encountered by the TC(2,1,4) scheme. The parameters of the LDPC-G_2 coded concatenated scheme used in this new scenario are given in Table 2.7.

BPS	STBC		LDPC						Interleaver Depth	Modem
	Code	Code Rate	Code Rate	Input Bits Block Size	Output Bits Block Size	Column Weight	Iterations	Total *Compl.*		
1.00	G_2	1	1/2	10000	20000	3	32	2592	20000	QPSK
2.00	G_2	1	1/2	10000	20000	3	32	2592	20000	16QAM
3.00	G_2	1	1/2	10002	20004	3	32	2592	20004	64QAM

Table 2.7: The parameters used in the LDPC-G_2 coded concatenated schemes invoked for comparison with the TC(2,1,4)-G_2 coded concatenated schemes.

2.3.2.3 Simulation Results

In this section, the performance of the LDPC- and TC-aided space-time block coded schemes communicating over uncorrelated Rayleigh fading channels will be studied and compared. The parameters of the space-time block codes, the half-rate TC(2,1,4) code and the LDPC codes are given in Tables 2.1, 2.6 and 2.7, respectively. The simulation results are based on the same assumptions which were outlined in Section 2.2.4 on page 30.

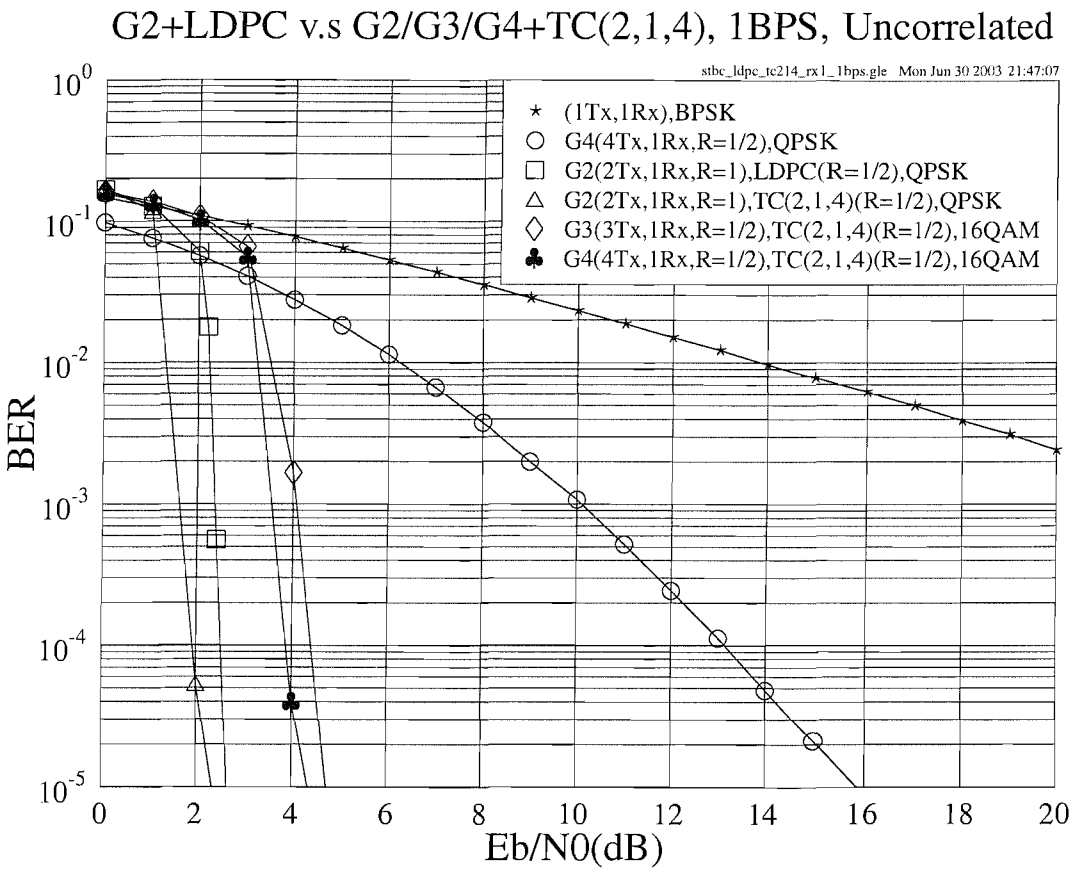

Figure 2.27: The BER versus E_b/N_0 performance of the $\mathbf{G_2}$, $\mathbf{G_3}$ and $\mathbf{G_4}$ space-time block codes of Table 2.1 in conjunction with the LDPC codes of Table 2.7 or the half-rate TC(2,1,4) code of Table 2.6 at an effective throughput of **1 BPS** using one receiver over uncorrelated Rayleigh fading channels.

Figure 2.27 compares the performance of the candidate schemes using the parameters summarized in Tables 2.6 and 2.7 operating at an effective throughput of 1 BPS over uncorrelated Rayleigh fading channels. For the half-rate TC(2,1,4) coded scheme combined with the half-rate G_3 and G_4 codes, the 16QAM modem is used for maintaining a throughput of 1 BPS. As seen in Figure 2.27, the TC(2,1,4)-aided G_2 code outperforms the others. However, at the BER of 10^{-5}, it only provides an approximately 0.1dB gain over the LDPC-aided G_2 code, which is the best LDPC-STBC coded concatenated scheme according to Table 2.5. It is

also observed that the schemes in which the G_3 and G_4 codes are employed exhibit an inferior performance in comparison to their G_2-code based counterpart as well as in comparison to the LDPC-aided scheme, because the more densely-packed 16QAM phasor constellation is used.

Figure 2.28 compares the performance of the candidate schemes using the parameters summarized in Tables 2.6 and 2.7 operating at an effective throughput of 2 and 3 BPS over uncorrelated Rayleigh fading channels. As suggested by Figure 2.28, the TC(2,1,4)-aided schemes perform slightly better, than the LDPC-aided schemes providing an approximately 0.1dB and 0.4dB gain at the BER of 10^{-5} in the scenarios of having a throughput of 2 and 3 BPS, respectively.

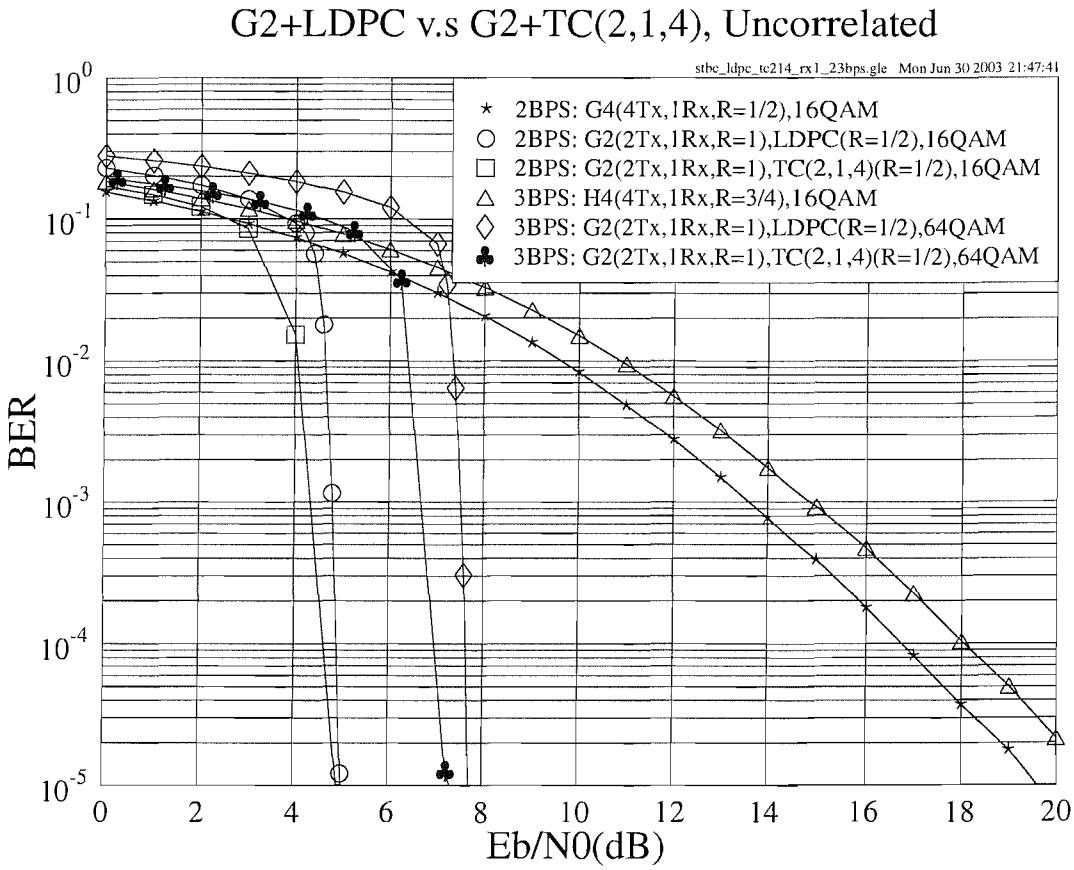

Figure 2.28: The BER versus E_b/N_0 performance of the $\mathbf{G_2}$ space-time block code of Table 2.1 in conjunction with the LDPC codes of Table 2.7 or the half-rate TC(2,1,4) code of Table 2.6 at an effective throughput of **2** and **3 BPS** using one receiver over uncorrelated Rayleigh fading channels.

In Figure 2.29 the achievable coding gain versus complexity is characterized. The coding gains were recorded at the BER of 10^{-5}, as presented in Section 2.3.1.3. From Figure 2.29, we infer that the curves associate with the TC(2,1,4) code are close to those of the LDPC codes, although the former ones perform slightly better than the latter ones in the context of having the same effective throughput of 1, 2 and 3 BPS, respectively. However, in the low

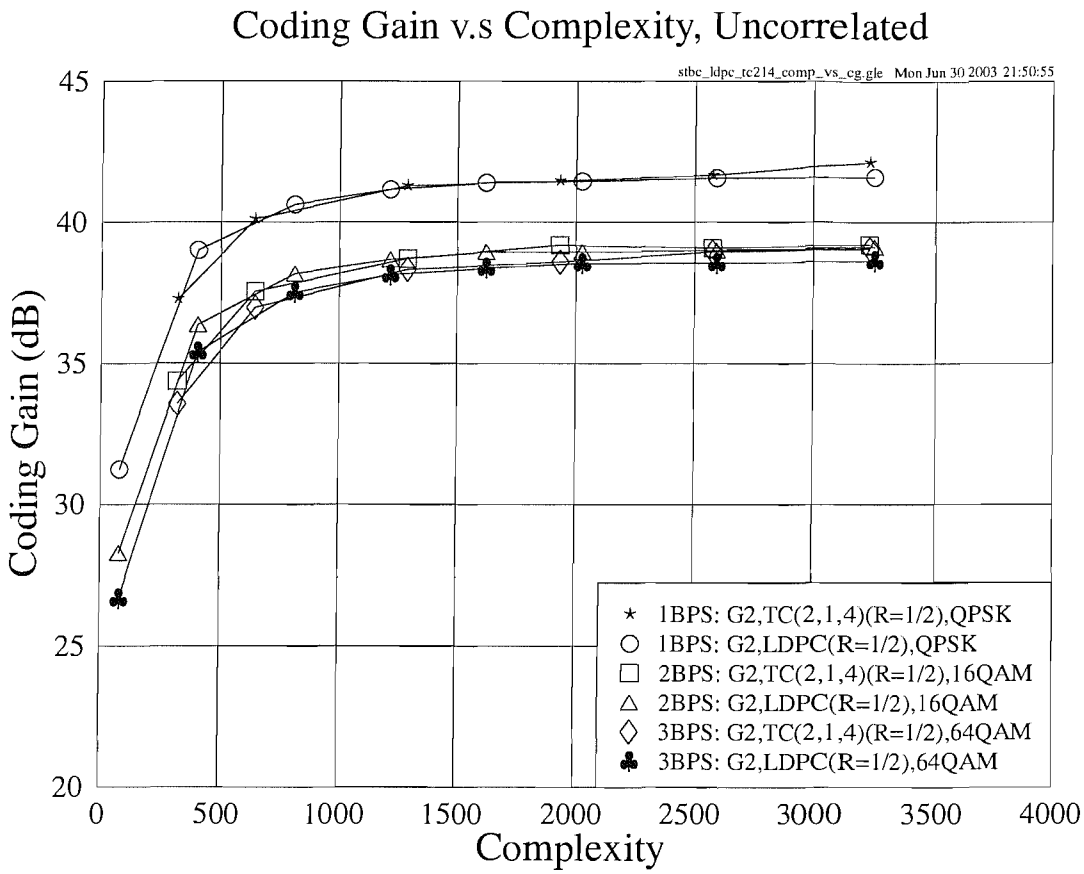

Figure 2.29: Coding gain versus complexity for the LDPC-G_2 concatenated arrangements and for the TC(2,1,4)-G_2 concatenated schemes using one receiver for communicating over uncorrelated Rayleigh fading channels. The associated parameters are given in Tables 2.6 and 2.7.

complexity range, namely in the complexity range spanning from 0 to 600, the LDPC codes perform better than the TC(2,1,4) code. On one hand, the achievable lowest complexity of the half-rate TC(2,1,4) code is 322, which is attained when the number of iterations is set to one, while the LDPC codes are capable of providing an even lower complexity down to 81, again, as seen in Figure 2.29. On the other hand, for the LDPC schemes, the achievable coding gain dramatically increases, when the affordable complexity is increased within the range spanning from 0 to about 600. Therefore, the employment of the LDPC-aided schemes may be more attractive in scenarios, where the affordable complexity is the most important concern, while the system's performance does not necessarily have to be the best.

2.3.2.4 Conclusions

In Section 2.3.2.3 we have presented a range of performance comparisons in the context of the attainable coding gain versus complexity for the various TC(2,1,4)-STBC and the

LDPC-STBC coded concatenated schemes for transmission over uncorrelated Rayleigh fading channels. As a conclusion, the TC(2,1,4)-assisted space-time block code G_2 outperforms its LDPC-assisted counterparts for all the three scenarios having different effective throughputs. However, it was found that the associated performance difference is insignificant, namely less than 0.3dB. Furthermore, the LDPC-STBC coded concatenated schemes considered may be preferred for employment in systems, where the severity of complexity constraint outweighs the importance of achieving the highest possible performance.

Finally, the performance of the different schemes studied is summarized in Table 2.8. All the results were generated using a single receiver, when communicating over uncorrelated Rayleigh fading channels. The performance of the best scheme at the effective throughputs of 1, 2 and 3 BPS is printed in bold, respectively.

BPS	STBC Code	LDPC Rate	TC(2,1,4) Rate	E_b/N_0 (dB) BER 10^{-3}	E_b/N_0 (dB) BER 10^{-5}	Gain (dB) BER 10^{-3}	Gain (dB) BER 10^{-5}	Modem
1.00	Uncoded	-	-	24.22	44.00	0.00	0.00	BPSK
	G_4	-	-	10.10	15.85	14.12	28.15	QPSK
	G_2	1/2	-	2.36	2.44	21.86	41.56	QPSK
	G_2	-	1/2	**1.62**	**2.34**	**22.60**	**41.66**	QPSK
	G_3	-	1/2	4.07	4.73	20.15	39.27	16QAM
	G_4	-	1/2	3.55	4.35	20.67	39.65	16QAM
2.00	Uncoded	-	-	24.22	44.00	0.00	0.00	QPSK
	G_4	-	-	13.61	19.58	10.61	24.42	16QAM
	G_2	1/2	-	4.81	5.01	19.41	38.99	16QAM
	G_2	-	1/2	**4.34**	**4.92**	**19.88**	**39.08**	16QAM
3.00	Uncoded	-	-	26.30	46.26	0.00	0.00	8PSK
	H_4	-	-	14.87	21.10	11.43	25.16	16QAM
	G_2	1/2	-	7.52	7.72	18.78	38.54	64QAM
	G_2	-	1/2	**6.68**	**7.32**	**19.62**	**38.94**	64QAM

Table 2.8: Coding gains of the LDPC-STBC concatenated schemes and the TC(2,1,4)-STBC concatenated schemes using one receiver for communicating over uncorrelated Rayleigh fading channels. For the scenarios having different effective throughputs, the performance of the best scheme is printed in bold.

2.4 Channel Coding Aided Space-Time Block Coded OFDM

In Section 2.3, we have investigated various LDPC channel coding assisted space-time block coded schemes communicating over narrowband fading channels, followed by the performance study of LDPC-aided and TC-aided STBC schemes. Naturally, a range of channel codes can also be combined with the family of space-time block codes for the sake of improving the system's performance. In this section, various Coded Modulation (CM) [2] assisted STBC schemes will be studied for transmission over multipath Rayleigh fading channels. Specifically, Trellis-Coded Modulation (TCM) [2, 300], Turbo Trellis-Coded Modulation (TTCM) [2, 301], Bit-Interleaved Coded Modulation (BICM) [2, 302] and iterative joint decoding and demodulation assisted BICM (BICM-ID) [2, 303] will be investigated. Furthermore, the above CM-assisted STBC aided schemes will be studied in the context of a single-user Orthogonal Frequency Division Multiplexing (OFDM) [3, 5–7] system. As a well-established technique, OFDM has exhibited a number of advantages over more traditional multiplexing techniques, and has been adopted for both Digital Audio and Video Broadcasting (DAB and DVB) in Europe. It has also been selected as the IEEE 802.11 standards for Wireless Local Area Network (WLAN). Let us now embark on the investigation of the CM-assisted space-time coded single-user OFDM system.

2.4.1 Coded Modulation Assisted Space-Time Block Codes

Since the signal bandwidth available for wireless communications is limited, one of the most important objectives in the design of digital mobile systems is to make the most of the attainable bandwidth, for example with the aid of the CM schemes.

2.4.1.1 Coded Modulation Principles

The basic principle of CM [2] is that we attach a parity bit to each uncoded information symbol formed by m information bits according to the specific modulation scheme used, hence doubling the number of constellation points to 2^{m+1} compared to that of 2^m in the original modem constellation. This is achieved by extending the modulation constellation, rather than expanding the required bandwidth, while maintaining the same effective throughput of m bits per symbol, as in the case of no channel coding. In other words, the signalling rate remains the same, since the redundant parity bit can be absorbed by the expansion of the constellation. Therefore, when the achievable coding gain of the CM scheme becomes higher than the E_b/N_0 degradation imposed by the more vulnerable higher-order modulation scheme employed, a useful effective coding gain can be achieved.

Among the various CM schemes, TCM [300] was originally designed for transmission over Additive White Gaussian Noise (AWGN) channels. TTCM [301] is a more recent joint coding and modulation scheme which has a structure similar to that of the family of binary turbo codes, but employs TCM schemes as component codes. Both TCM and TTCM employ set partitioning based constellation mapping [2], while using symbol-based turbo interleavers and channel interleavers. Another CM scheme referred to as BICM [302], invokes bit-based channel interleavers in conjunction with gray constellation mapping. Furthermore, iteratively decoded BICM [303] using set partitioning was also proposed. More details about the various CM schemes used can be found in [2]. In this section, we will mostly focus on the performance of the proposed CM-assisted STBC coded OFDM schemes communicating over wideband Rayleigh fading channels.

2.4.1.2 Inter-Symbol Interference and OFDM Basics

If the modulation bandwidth exceeds the coherence bandwidth of the channel, Inter-Symbol Interference (ISI) will be introduced and the consecutive transmitted symbols are distorted, since the past and current symbols of the signals are overlapped. Hence, at the receiver, channel equalizers have to be employed for the sake of removing the effects of ISI [2].

An alternative way of mitigating the effects of ISI is to employ OFDM, which effectively mitigates the detrimental effects of the frequency-selective fading, when transmitting over high-rate wideband channels. The basic principle of OFDM is to split a high-rate data stream into a number of low-rate streams which are transmitted simultaneously over a number of subcarriers. Hence the symbol duration is rendered longer for each of the parallel subcarriers, and thus the relative effects of imposed by the multipath channel's delay spread is reduced. In other words, since the system's data throughput is the sum of all the parallel sub-channels' throughputs, the data rate per sub-channel is only a small fraction of the total data rate of a conventional single-carrier system having the same throughput. This results in the phenomenon that the symbol duration becomes significantly longer than the channel's impulse response, thus it has the potential to disperse with channel equalization. Specifically, if an appropriate-duration cyclic OFDM symbol extension is selected, the ISI between consecutive OFDM symbols can be almost completely eliminated. Furthermore, for a given delay spread, the implementation complexity of an OFDM modem may be significantly lower than that of a single carrier system employing an equalizer [7].

The schematic of an OFDM modem is shown in Figure 2.30. The source bit stream is first encoded by a STBC or channel encoder and forwarded to the interleaver and the mapper, where the bits are interleaved and may be mapped to non-binary symbols. Some pilot subcarriers may be inserted for the sake of assisting the estimation of the channel's

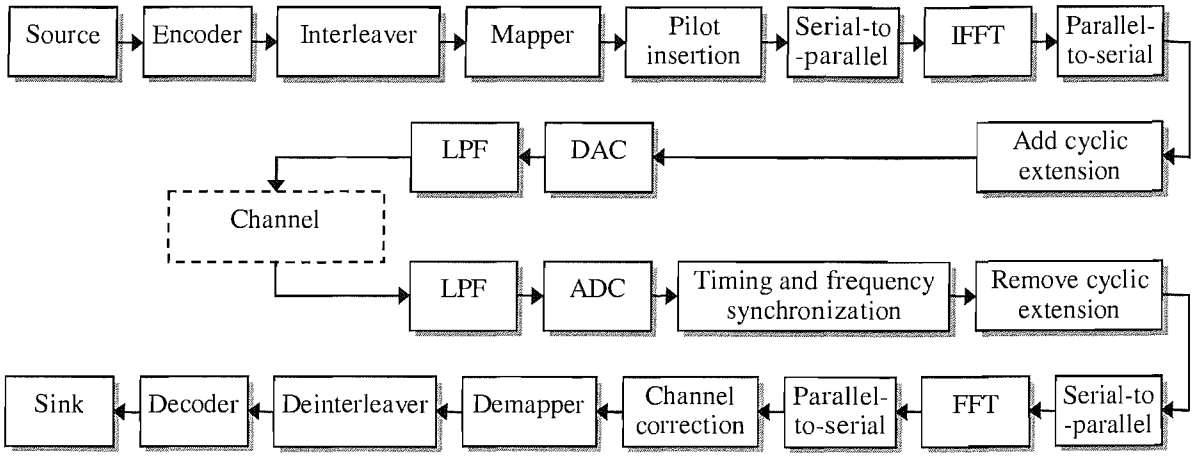

Figure 2.30: Schematic diagram of an OFDM modem.

frequency-domain transfer function, which is required for the receiver to counteract the effects of the channel's frequency-domain fading. The serial data stream is then converted into a parallel symbol sequence and forwarded to the Inverse Fast Fourier Transform (IFFT) modulator for the sake of forming the time-domain modulated signal. Again, in order to eliminate the ISI between consecutive OFDM symbols a cyclic extension has to be added to each OFDM symbol. Then the Digital-to-Analogue Converter (DAC) converts the cyclically extended OFDM signal to the analogue domain, which is finally filtered by a Low-Pass Filter (LPF) and transmitted through the wideband channel. At the receiver side, the Analogue-to-Digital Converter (ADC) converts the LPF-filtered received signal to the digital domain, where symbol timing and frequency synchronization are the first processing steps [7]. Then the cyclic extension attached to each OFDM symbol is removed and the recovered signal is forwarded to the Fast Fourier Transform (FFT) based demodulator, whose output will be processed by the pilot-based frequency-domain channel equalizer in order to compensate the frequency-domain fading imposed by the channel. After symbol-demapping and deinterleaving the received signal is finally passed to the space-time or channel decoder, which outputs the decoded information bits.

2.4.1.3 System Overview

Figure 2.31 shows the schematic of the CM-assisted space-time block coded OFDM system investigated [2, 3]. As observed in Figure 2.31, the source information bits are first encoded and modulated by the CM encoder followed by the space-time encoder. In our schemes, the space-time block code employed was the G_2 code of Table 2.1, which invokes two transmitter antennas, and the two space-time coded samples are mapped to two consecutive OFDM subcarriers and OFDM modulated. Then the frequency-domain symbols are converted to

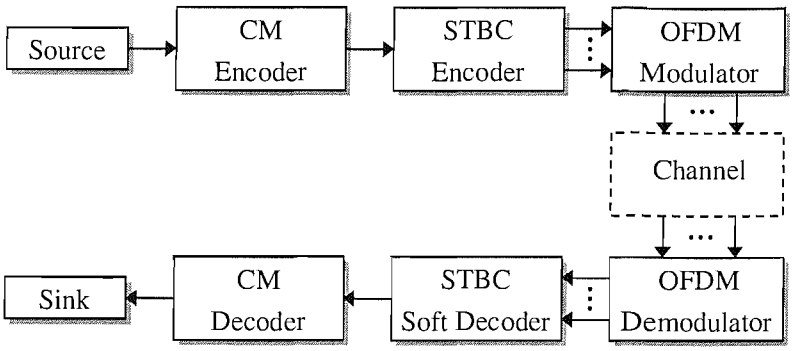

Figure 2.31: Schematic diagram of the proposed CM-assisted space-time block coded OFDM system.

time-domain OFDM symbols by the IFFT-based modulator and the cyclic extension is appended to each individual OFDM symbol. The OFDM symbols are then transmitted via the multipath fading channel, and the received noise-contaminated symbols are forwarded to the OFDM demodulator, where the FFT operation will be employed for converting the channel-impaired time-domain symbols to their frequency-domain counterparts. The recovered signal is then space-time soft-decoded and the soft outputs are fed to the CM decoder for recovering the most-likely transmitted information bits.

2.4.1.3.1 Complexity Issues

In order to compare the different candidate schemes under fair conditions, we chose the system parameters so that the decoding complexity of the various CM schemes employed became similar. The complexity imposed by the STBC codec was neglected, since the same G_2 space-time block code was used for all the CM-STBC concatenated schemes.

The symbol-based Log-MAP decoder [2] is utilized in all the CM schemes considered in our system, namely in the TCM, TTCM, BICM and BICM-ID codecs, for the sake of reducing the computational complexity imposed by the MAP algorithm [2]. Therefore, the multiplication and and addition operations are substituted by additions and by the Jacobian sum operations [291] carried out in the logarithmic domain, respectively. As a result, in terms of the number of additions and subtractions, the total decoding complexity per bit per iteration for the TTCM scheme studied is as follows [297]:

$$comp\{TTCM\} = \frac{10M\left(2^{\nu+1}-1\right)}{m}, \tag{2.33}$$

where m is the number of information bits in a coded information symbol, $M = 2^m$ is the number of legitimate symbols in the mapping constellation set, and ν is the code memory. For example, for the QPSK-based TTCM scheme having a code memory of $\nu = 3$, the associated complexity per bit per iteration is $\frac{10\cdot 2^1\cdot\left(2^{3+1}-1\right)}{1} = 300$, since in this case m is equal to 1. If

the number of iterations is 4, the total decoding complexity per bit becomes $300 \cdot 4 = 1200$, as seen in Table 2.9. For the remaining CM schemes used, namely for TCM/BICM/BICM-ID, the corresponding decoding complexity per bit per iteration is:

$$comp\{TCM/BICM/BICM-ID\} = \frac{5M\left(2^{\nu+1}-1\right)}{m}, \tag{2.34}$$

which is half the complexity of that in Equation (2.33). The reason for this is that the TTCM scheme utilizes two Log-MAP decoders, while TCM/BICM/BICM-ID schemes only use one [2], hence the associated complexity of TTCM is doubled. The parameters used by the various CM-STBC concatenated schemes investigated are provided in Table 2.9. From the table, we may see that the total decoding complexity per bit - rather than per bit per iteration - of the four CM schemes are similar.

BPS	STBC		CM							Modem
	Code	Code Rate	CM Scheme	Code Rate	Data Bits	ν	Iterations	Symbol-based Cw. Length	Total *Compl.*	
1.00	G_2	1	-	-	-	-	-	1024	-	QPSK
	G_2	1	TCM	1/2	1	6	-	1024	1270	QPSK
	G_2	1	TTCM	1/2	1	3	4	1024	1200	QPSK
	G_2	1	BICM	1/2	1	6	-	1024	1270	QPSK
	G_2	1	BICMID	1/2	1	3	8	1024	1200	QPSK
2.00	G_2	1	-	-	-	-	-	1024	-	8PSK
	G_2	1	TCM	2/3	2	6	-	1024	1270	8PSK
	G_2	1	TTCM	2/3	2	3	4	1024	1200	8PSK
	G_2	1	BICM	2/3	2	6	-	1024	1270	8PSK
	G_2	1	BICMID	2/3	2	3	8	1024	1200	8PSK
3.00	G_2	1	-	-	-	-	-	1024	-	16QAM
	G_2	1	TCM	3/4	3	6	-	1024	1693	16QAM
	G_2	1	TTCM	3/4	3	3	4	1024	1600	16QAM
	G_2	1	BICM	3/4	3	6	-	1024	1693	16QAM
	G_2	1	BICMID	3/4	3	3	8	1024	1600	16QAM

Table 2.9: The parameters of the various CM-assisted space-time block coded schemes. The parameters of the STBC G_2 are given in Table 2.1.

2.4.1.3.2 Channel Model

As mentioned earlier, we will investigate the proposed system when communicating over dispersive wideband Rayleigh fading channels. Specifically, we consider the Short Wireless Asynchronous Transfer Mode (SWATM) Channel Impulse Response (CIR) given on page 78 of [3], although the Doppler frequency may assume a range of different values. The three-tap SWATM channel is a truncated version of the five-tap Wireless Asynchronous Transfer Mode (WATM) CIR, retaining only the first three impulses [3]. This reduces the total length of the impulse response, where the last path arrives at a delay of 48.9ns, which corresponds to 11 sample periods. For our simulations each of the three paths experiences independent Rayleigh fading having the normalized Doppler frequency of $f'_d = 1.235 \times 10^{-5}$. Figure 2.32 displays the impulse response of the SWATM channel, while the associated parameters are given in Table 2.10.

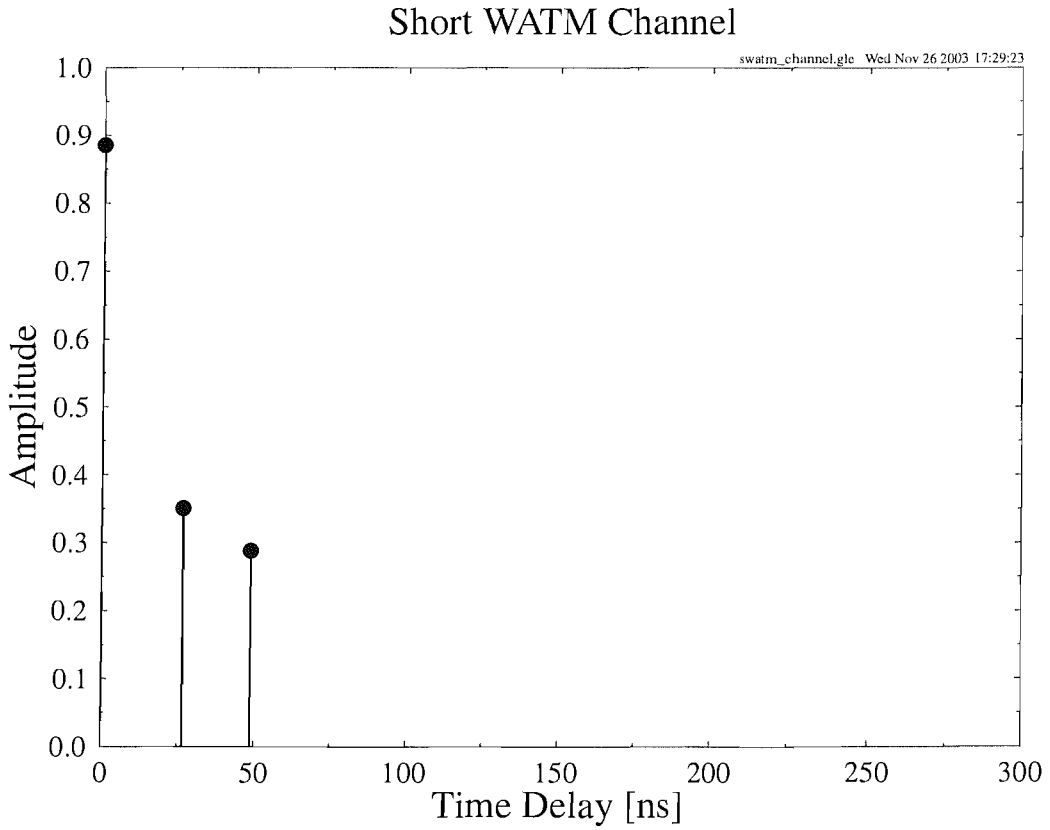

Figure 2.32: The impulse response of the SWATM channel [3]. The corresponding parameters of the channel are summarized in Table 2.10.

For the sake of combating the effects of ISI when communicating over the multipath Rayleigh fading channel, as discussed in Section 2.4.1, we employ an OFDM modem having 512 subcarriers, while each OFDM symbol is extended by a cyclic prefix of $512/8 = 64$

$1/T_s$	τ_{max}	f_d	f'_d	n	K	cp
225 MHz	48.9 ns	2278 Hz	1.235×10^{-5}	3	512	64

Table 2.10: Sampling Rate $1/T_s$, maximum path delay τ_{max}, maximum Doppler frequency f_d, normalized Doppler frequency f'_d, number of paths n, FFT length K and cyclic prefix length cp of the SWATM channel of Figure 2.32.

time-domain samples [3]. Therefore, the length of an OFDM symbol becomes $512 + 64 = 576$ samples. Since the number of subcarriers is sufficiently high, we may assume that each OFDM subcarrier experiences narrowband channel conditions in the frequency domain.

2.4.1.3.3 Assumptions

When the space-time block codes were employed for transmissions over uncorrelated Rayleigh fading channels, as mentioned in Section 2.2.4, we assumed that the channel was quasi-static so that its path gains remained constant across for example $n = 2$ consecutive STBC time slots for the G_2 space-time block code, corresponding to the $n = 2$ rows of the G_2 code's transmission matrix. However, in this new context we can no longer assume that the corresponding frequency-domain subcarrier gains remain identical as a consequence of the wideband channel's frequency-domain fading profile, an issue, which will be further discussed in Section 2.4.1.4. This results in a residual error floor for the unprotected G_2 space-time block coding scheme, as seen for example in Figure 2.35. For the concatenated CM-STBC schemes, however, the error floor experienced may be significantly reduced to a neglectable level.

In Section 2.4.1.4, the performance of the proposed CM-assisted space-time block coded OFDM schemes will be compared. All our simulation results achieved were based on the following assumptions:

- Each path of the multipath channel employed experiences independent Rayleigh fading;
- The average signal power received from each transmitter antenna is the same;
- The receiver has a perfect knowledge of the channels' fading amplitudes.

These assumptions simplify the simulations to a degree, therefore the system concerned is not a realistic one. However, again, since the experimental circumstances are identical for all performance comparisons, the results may be expected to adequately characterize the relative performance of the various schemes used.

2.4.1.4 Simulation Results

In this section, the performance of the CM-assisted space-time block coded OFDM system considered will be studied. The simulation parameters have been given in Table 2.9. All schemes utilized two transmitter antennas for the G_2 space-time block code and one receiver antenna. Each OFDM symbol has 512 subcarriers and a cyclic extension of 64 samples.

Performance at an effective throughput of 1 BPS Figure 2.33 shows the performance of the various CM-assisted G_2 space-time block coded OFDM schemes communicating over the SWATM channel. In our system, we employ gray-coding based constellation mapping for the BICM scheme, while using set-partitioning based constellation mapping for the TCM, TTCM and BICM-ID arrangements [2]. For the sake of achieving an effective throughput of 1 BPS, QPSK modulation is used for all the half-rate CM-assisted schemes. As seen in Figure 2.33, the CM-G_2 coded concatenated schemes perform significantly better than the unprotected G_2 scheme, achieving an E_b/N_0 gain of about 14dB at the BER of 10^{-5}. Among all the CM-assisted schemes, the TTCM-aided arrangement gives the best performance by achieving about 0.5dB to 1dB gain over the other CM-assisted schemes at the BER of 10^{-5}.

Performance at an effective throughput of 2 BPS The performance comparison of the different CM-STBC concatenated schemes having an effective throughput of 2 BPS for transmissions over the SWATM channel is shown in Figure 2.34. It is seen in Figure 2.34 that when the E_b/N_0 value encountered is relatively low, namely below about 7.5dB, the unprotected G_2 scheme performs better than the CM-assisted G_2 schemes. However, when the E_b/N_0 value experienced is higher than approximate 7.5dB, the TTCM-aided G_2 scheme outperforms all the other candidates, achieving a gain of about 1.3dB and 12.5dB over the other CM-aided G_2 schemes and over the unprotected G_2 scheme, respectively, at the BER of 10^{-5}.

Performance at an effective throughput of 3 BPS If we increase the system's effective throughput to 3 BPS, a residual BER of approximate 6×10^{-5} is observed for the performance curve of the unprotected G_2 scheme, as seen in Figure 2.35. This phenomenon can be explained as follows. In the context of the single-path uncorrelated Rayleigh fading channels mentioned in Section 2.2.4, we assumed that the channel is quasi-static so that the channel's path gains are constant across n consecutive STBC time slots. For example, we have $n = 2$ for the G_2 space-time block code, corresponding to the $n = 2$ rows of the space-time block codes' transmission matrix. In the context of wideband channels, for instance the SWATM channel of Figure 2.32, however, the channel's delay spread will have an effect on the associated frequency-domain transfer functions. More specifically, the fading amplitudes vary more rapidly, when the delay spread is increased [2]. Since the maximum delay spread of the

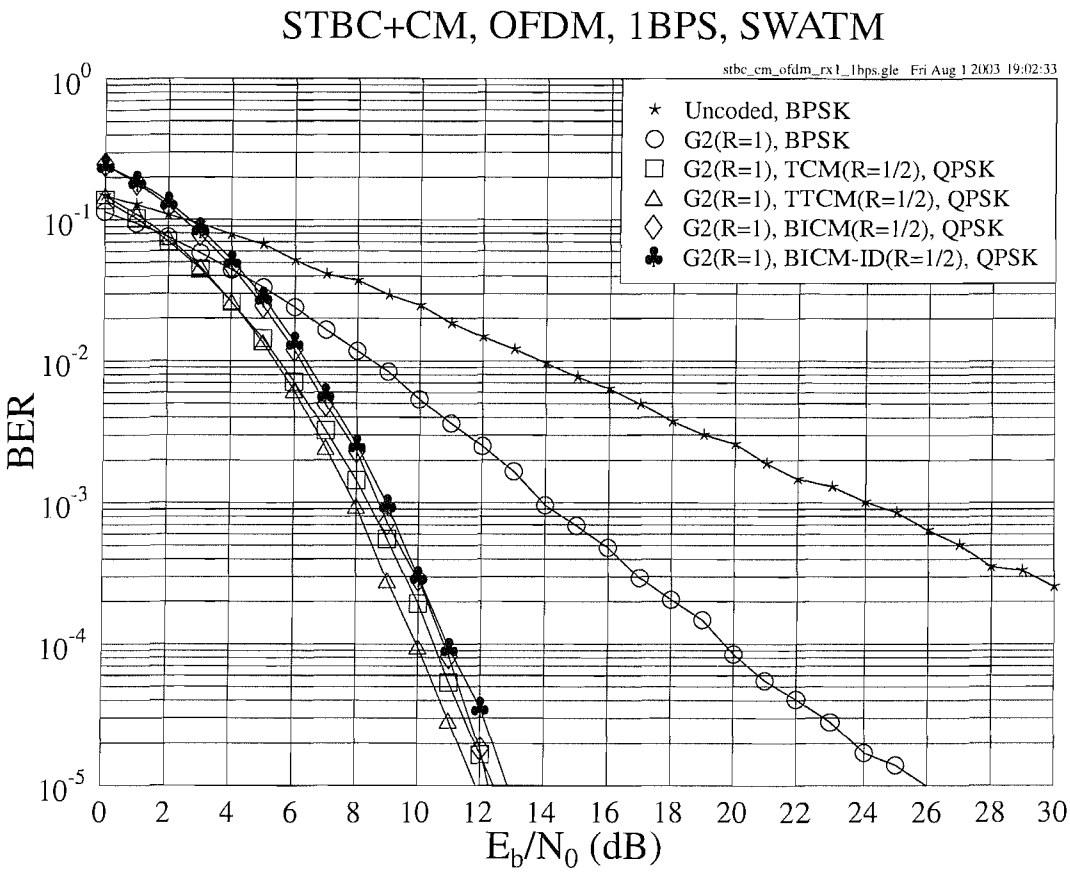

Figure 2.33: The BER versus E_b/N_0 performance of the G_2 space-time block code of Table 2.1 in conjunction with the various Coded Modulation schemes of Table 2.9 at an effective throughput of **1 BPS** using one receiver when communicating over the SWATM channel. An OFDM scheme having 512 subcarriers and a cyclic extension of 64 samples is employed.

SWATM channel is as high as $\tau_{max} = 48.9ns$, the variation of the frequency-domain fading amplitudes is so dramatic that we can no longer assume that the path gains remain constant during two consecutive STBC time slots. In this case, for the unprotected STBC schemes, the rapid variation of the channel's frequency-domain fading envelope will seriously erode the orthogonality of the G_2 space-time block code's two components, resulting in a residual error floor, as seen for example in Figure 2.35.

Furthermore, if a higher-order modulation scheme such as 16QAM is employed, as shown in Figure 2.35, since the signal is mapped to more densely-packed constellation phasors which are prone to transmission errors, the error floor imposed by the channel is expected to be higher than that in the scenarios, where a lower-order modulation scheme, such as QPSK or 8PSK is used, as exhibited by Figures 2.33 and 2.34. More explicitly, comparing Figures 2.33 and 2.34 to Figure 2.35, we can see that the BER error floors observed in Figures 2.33 and 2.34 are below 10^{-5}, while in Figure 2.35 the error floor encountered is about 6×10^{-5}.

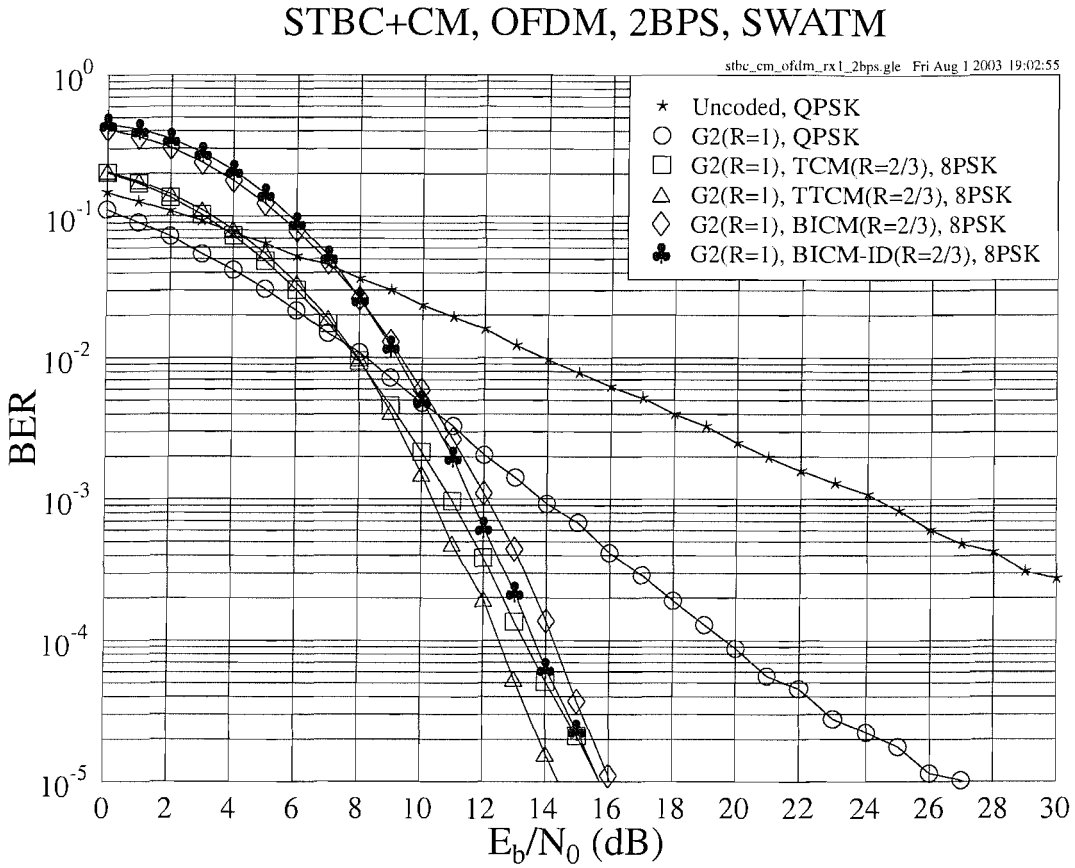

Figure 2.34: The BER versus E_b/N_0 performance of the G_2 space-time block code of Table 2.1 in conjunction with the various Coded Modulation schemes of Table 2.9 at an effective throughput of **2 BPS** using one receiver when communicating over the SWATM channel. An OFDM scheme having 512 subcarriers and a cyclic extension of 64 samples is employed.

With the advent of employing the CM schemes, however, the error floor can be eliminated or reduced to a significantly lower level. As Figure 2.35 shows, the CM schemes significantly improve the space-time block coded OFDM system's performance and the BER error floor exhibited by the unprotected G_2 scheme has been essentially eliminated. Similar to the scenarios of having an effective throughput of 1 and 2 BPS, the TTCM-G_2 concatenated scheme was found to give the best performance among all the CM-assisted schemes studied, although the E_b/N_0 gain achieved over the other candidate schemes is not significant.

2.4.1.5 Conclusions

In the previous sections we have investigated the achievable performance of the various CM-assisted space-time block coded OFDM schemes for transmissions over the SWATM channel. We first briefly reviewed the basic principles of the CM schemes in Section 2.4.1.1. In Sec-

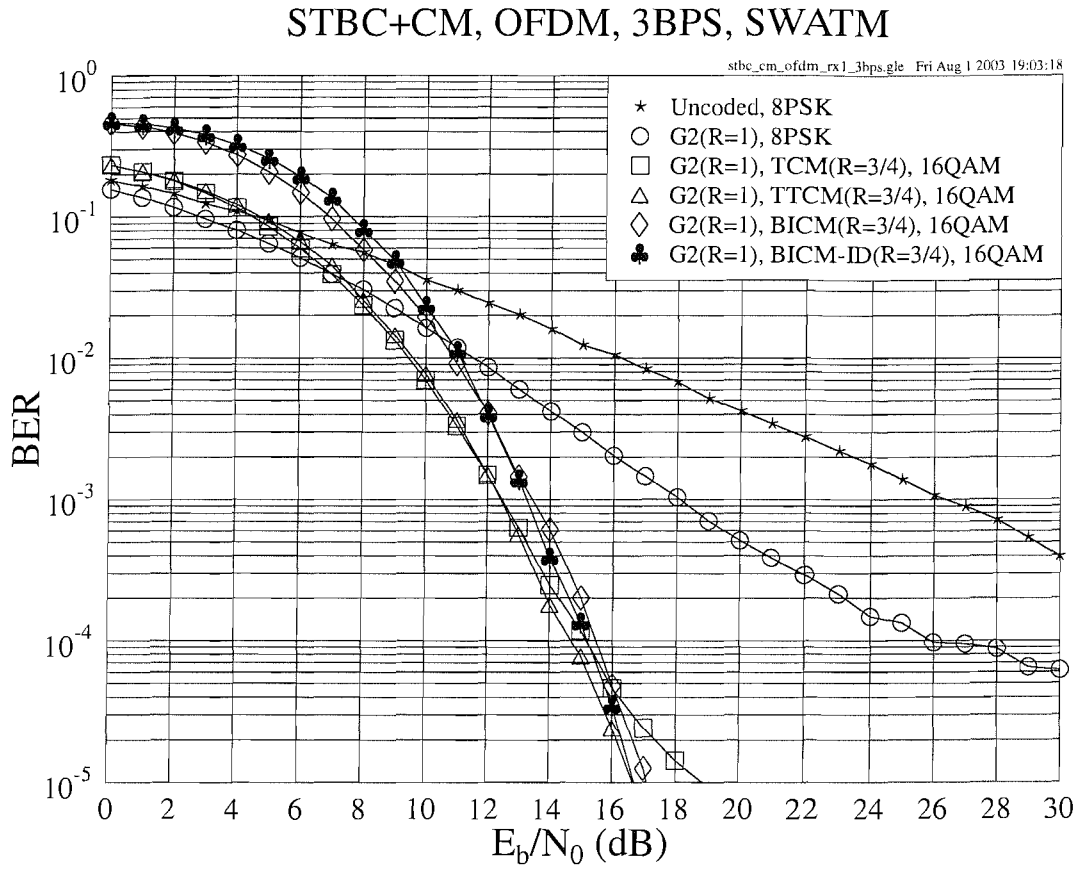

Figure 2.35: The BER versus E_b/N_0 performance of the G_2 space-time block code of Table 2.1 in conjunction with the various Coded Modulation schemes of Table 2.9 at an effective throughput of **3 BPS** using one receiver when communicating over the SWATM channel. An OFDM scheme having 512 subcarriers and a cyclic extension of 64 samples is employed.

tion 2.4.1.2 a rudimentary introduction to OFDM was provided, which was followed by the overview of the simulation arrangement, as detailed in Section 2.4.1.3. Our performance analysis was presented in Section 2.4.1.4, where the CM-assisted STBC schemes were found to significantly improve the system's achievable performance, eliminating the BER floor of the unprotected STBC scheme. Furthermore, the TTCM-STBC coded concatenated scheme was observed to give the best performance among all the CM-STBC coded concatenated schemes.

In conclusion, we summarized the performance of the evaluated CM-STBC concatenated schemes in Table 2.11. The coding gains summarized in Table 2.11 were defined as the E_b/N_0 difference, expressed in terms of decibels, at a BER of 10^{-5} between the various channel coding assisted space-time block coded OFDM systems and the uncoded single-transmitter OFDM system having the same effective throughput. All the results were recorded by using one receiver, while communicating over the SWATM channel of Section 2.4.1.3.2.

BPS	STBC Scheme	CM Scheme	CM Code Rate	E_b/N_0 (dB) BER 10^{-3}	E_b/N_0 (dB) BER 10^{-5}	Gain (dB) BER 10^{-3}	Gain (dB) BER 10^{-5}	Modem
1.00	Uncoded	-	-	24.06	44.27	0.00	0.00	BPSK
	G_2	-	-	13.92	25.97	10.14	18.30	BPSK
	G_2	TCM	1/2	8.38	12.44	15.68	31.83	QPSK
	G_2	TTCM	1/2	**7.94**	**11.87**	**16.12**	**32.40**	QPSK
	G_2	BICM	1/2	8.72	12.28	15.34	31.99	QPSK
	G_2	BICM-ID	1/2	8.96	12.89	15.10	31.38	QPSK
2.00	Uncoded	-	-	24.06	44.27	0.00	0.00	QPSK
	G_2	-	-	13.81	27.08	10.25	17.19	QPSK
	G_2	TCM	2/3	10.95	15.73	13.11	28.54	8PSK
	G_2	TTCM	2/3	**10.36**	**14.43**	**13.70**	**29.84**	8PSK
	G_2	BICM	2/3	12.10	16.05	11.96	28.22	8PSK
	G_2	BICM-ID	2/3	11.60	15.73	12.46	28.54	8PSK
3.00	Uncoded	-	-	26.36	47.17	0.00	0.00	8PSK
	G_2	-	-	18.09	-	8.27	-	8PSK
	G_2	TCM	3/4	12.46	18.86	13.90	28.31	16QAM
	G_2	TTCM	3/4	**12.42**	**16.67**	**13.94**	**30.50**	16QAM
	G_2	BICM	3/4	13.43	17.11	12.93	30.06	16QAM
	G_2	BICM-ID	3/4	13.25	16.71	13.11	30.46	16QAM

Table 2.11: Performance of the CM-STBC concatenated OFDM schemes using one receiver, when communicating over the SWATM channel. The STBC and CM parameters were given in Table 2.1 and Table 2.9, respectively. An OFDM scheme having 512 subcarriers and a cyclic extension of 64 samples was employed. For the scenarios of having a different effective throughput, the performance of the best scheme is printed in bold.

2.4.2 CM-Aided and LDPC-Aided Space-Time Block Coded OFDM

In Section 2.4.1, we have studied the performance of different CM-assisted space-time block coded schemes for transmissions over the SWATM channel [3] of Figure 2.32. Instead of the joint coding modulation schemes of Table 2.9, separate channel codes such as LDPC codes [285], can also be incorporated into our space-time block coded OFDM system for the sake of improving the achievable performance. Hence, in this section we will compare the CM-assisted G_2 space-time coded schemes of Section 2.4.1 to those in which the LDPC codes are combined with the space-time block code G_2.

2.4.2.1 System Overview

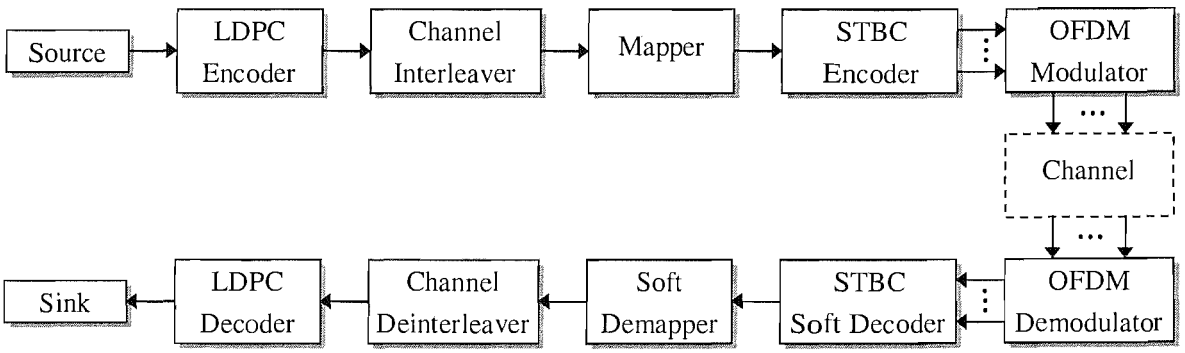

Figure 2.36: Schematic diagram of the proposed LDPC-assisted space-time block coded OFDM system.

The LDPC-assisted space-time block coded OFDM system's schematic is given in Figure 2.36. Compared to Figure 2.31, where the CM-assisted space-time block coded OFDM system was introduced, we substituted the CM encoder and decoder by a LDPC encoder and decoder, respectively. For the CM schemes, the associated symbol-based channel interleaver and deinterleaver have been integrated in the CM encoder and decoder, respectively. For the LDPC schemes, however, an external bit-based channel interleaver and deinterleaver has to be employed for the sake of further improving the system's performance, as seen in Figure 2.36.

Assisted by Equations (2.31), (2.33), and (2.34), we can calculate the corresponding decoding complexity per bit per iteration for the LDPC and CM schemes, respectively. For the sake of fair comparisons, we have to select the appropriate parameters, so that the CM-STBC schemes and the LDPC-STBC schemes exhibit a similar decoding complexity. Specifically, similar to Section 2.4.1.3, the space-time block code was also chosen to be the G_2 code in all the LDPC-STBC concatenated OFDM schemes investigated, and thus again the related decoding complexity of the G_2 code was neglected in order to simplify our comparisons. Furthermore, the symbol-based codeword length of the LDPC-STBC concatenated schemes was

fixed to 1024, which is equal to that of the CM-STBC concatenated schemes. Specifically, the same channel model, namely the SWATM channel of Section 2.4.1.3, and the same OFDM modem having 512 subcarriers and a cyclic prefix of 64 samples were employed in this new context.

As mentioned in Section 2.4.1.4, at a specific effective throughput, it was found that the TTCM-assisted G_2 coded scheme gave the best performance. Hence we used the TTCM scheme as the representative of the CM family, while half-rate and $\frac{3}{4}$-rate LDPC codes were chosen for representing the LDPC code family. As a summary, the parameters of the various CM-STBC concatenated OFDM systems are given in Table 2.9, while the parameters of the LDPC-STBC concatenated OFDM systems are provided in Table 2.12.

BPS	STBC		LDPC								Modem
	Code	Code Rate	Code Rate	Column Weight	Iterations	In. Bits Block Size	Out. Bits Block Size	Interleaver Depth	Symbol-based Cw. Length	Total *Compl.*	
1.00	G_2	1	1/2	3	15	1024	2048	2048	1024	1215	QPSK
2.00	G_2	1	1/2	3	15	2048	4096	4096	1024	1215	16QAM
3.00	G_2	1	3/4	3	10	3072	4096	4096	1024	1530	16QAM

Table 2.12: Parameters of the various LDPC-assisted space-time block coded OFDM schemes. The parameters of the G_2 space-time block code are given in Table 2.1.

2.4.2.2 Simulation Results

In this section we compare the TTCM- and LDPC-assisted space-time block coded OFDM schemes, which are characterized in Figure 2.37. All schemes utilized two transmitter antennas for the G_2 space-time block code and one receiver antenna. All simulation results were generated based on the assumptions outlined in Section 2.4.1.3.

As seen from Figure 2.37, the TTCM- and LDPC-assisted G_2 coded OFDM schemes have a similar performance. Specifically, when the effective throughput is 1 BPS, the TTCM-assisted scheme performs slightly better than the LDPC-aided candidate system. In the scenario of having an effective throughput of 2 BPS, the former outperforms the latter again. In this context, however, we may see that the performance gap between the two competing schemes is larger than that in the scenario of having a throughput of 1 BPS. This is because in order to achieve the same effective throughput of 2 BPS, the TTCM-aided scheme employs 8PSK modulation in conjunction with set partitioning, while the LDPC-aided candidate has to employ the more vulnerable 16QAM gray mapping based constellation, since the code rate

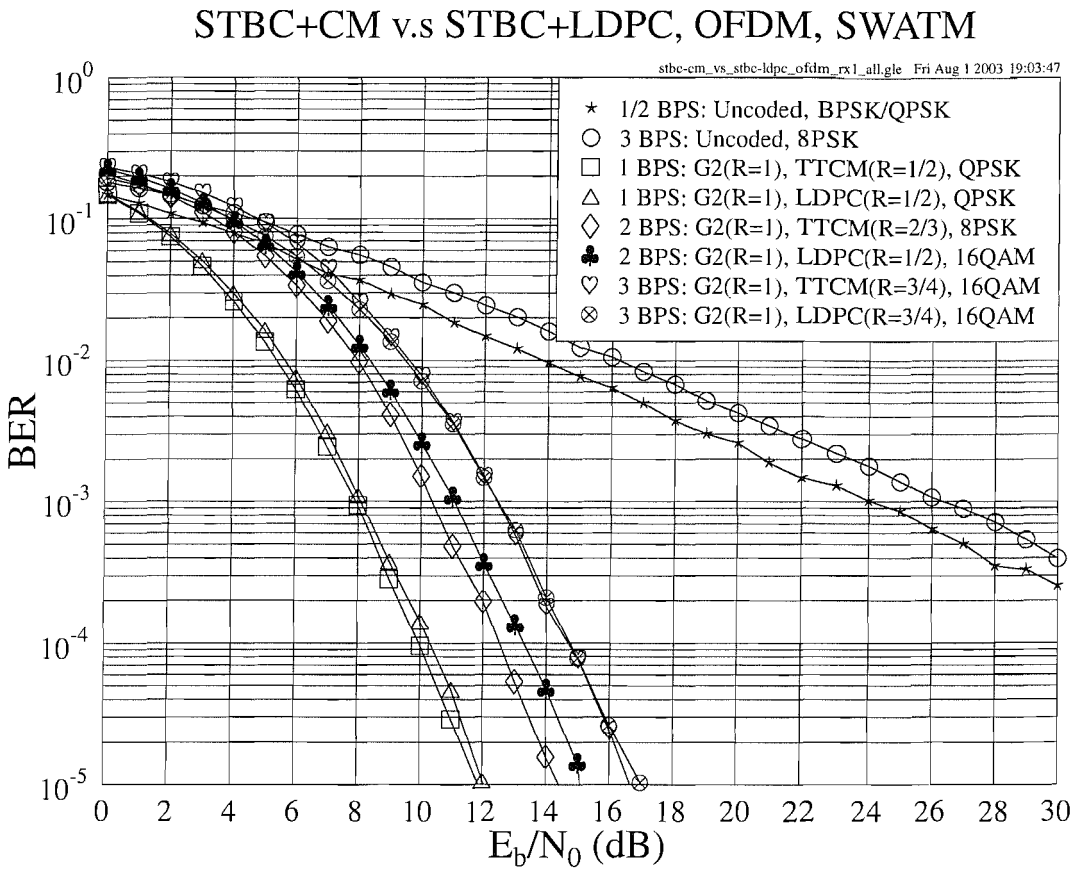

Figure 2.37: The BER versus E_b/N_0 performance of the G_2 space-time block code of Table 2.1 in conjunction with the TTCM of Table 2.9 or the LDPC codes of Table 2.12 at different effective throughputs using one receiver when communicating over the SWATM channel of Figure 2.32. An OFDM scheme having 512 subcarriers and a cyclic extension of 64 samples is employed.

of the TTCM and the LDPC code are $\frac{2}{3}$ and $\frac{1}{2}$, respectively. Nonetheless, it is found in Figure 2.37 that the two corresponding competitors exhibit a similar performance, when the throughput is increased to 3 BPS. In this case, however, the LDPC-aided scheme is marginally superior to the TTCM-aided scheme, when the E_b/N_0 value is relatively low, namely below 11dB.

In Figure 2.38, the associated coding gain versus complexity results are provided. The coding gain was defined in Section 2.4.1.5, while the complexity of the CM schemes and LDPC codes can be calculated with the aid of Equations (2.33) and (2.31), respectively. Given the same effective throughput, it is found that the coding gain performance of the TTCM-aided G_2 schemes surpasses that of the LDPC-aided G_2 schemes, when the affordable complexity is higher than approximate 500, as observed in Figure 2.38. At a low complexity, namely below a value of about 500, however, the LDPC-aided schemes tend to achieve a higher coding gain than the TTCM-aided schemes at the specific throughput values considered.

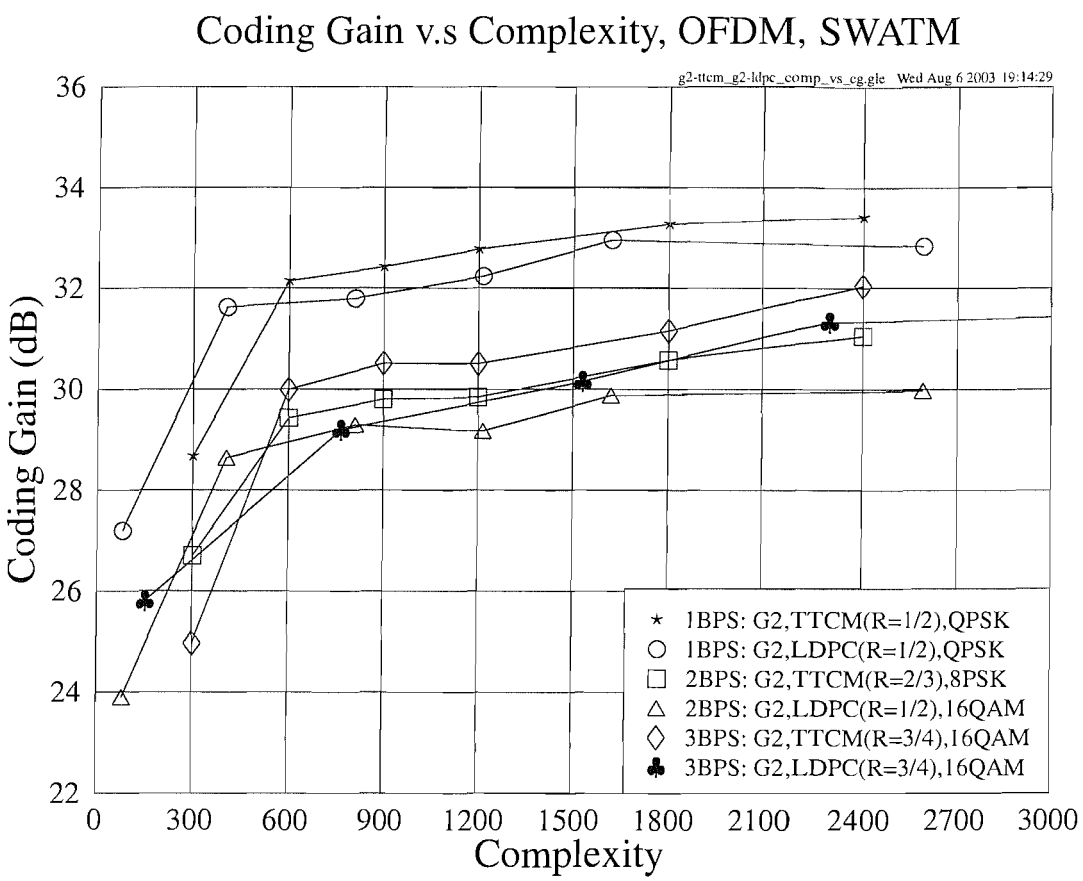

Figure 2.38: Coding gain versus complexity for the TTCM-G_2 concatenated and LDPC-G_2 concatenated schemes using one receiver, when communicating over the SWATM channel of Figure 2.32. An OFDM scheme having 512 subcarriers and a cyclic extension of 64 samples is employed. The simulation parameters are given in Tables 2.9 and 2.12.

2.4.2.3 Conclusions

In Section 2.4.2.2 the performance of the different TTCM- and LDPC-assisted G_2 coded OFDM schemes has been studied and compared. As seen from Figure 2.37, the TTCM-assisted G_2 scheme gives a better performance than the LDPC-assisted G_2 scheme. Furthermore, in the context of the achievable coding gain versus complexity performance, it was found that the TTCM-assisted schemes are capable of achieving higher coding gains in the relatively high complexity range, than the LDPC-assisted candidate schemes.

In conclusion, we summarize the achievable performance of the various schemes discussed in Table 2.13.

BPS	STBC Scheme	TTCM Code Rate	LDPC Code Rate	E_b/N_0 (dB) BER 10^{-3}	E_b/N_0 (dB) BER 10^{-5}	Gain (dB) BER 10^{-3}	Gain (dB) BER 10^{-5}	Modem
1.00	Uncoded	-	-	24.06	44.27	0.00	0.00	BPSK
	G_2	-	-	13.92	25.97	10.14	18.30	BPSK
	G_2	1/2	-	**7.94**	**11.87**	**16.12**	**32.40**	QPSK
	G_2	-	1/2	8.09	12.04	15.97	32.23	QPSK
2.00	Uncoded	-	-	24.06	44.27	0.00	0.00	QPSK
	G_2	-	-	13.81	27.08	10.25	17.19	QPSK
	G_2	2/3	-	**10.36**	**14.43**	**13.70**	**29.84**	8PSK
	G_2	-	1/2	11.07	15.10	12.99	29.17	16QAM
3.00	Uncoded	-	-	26.36	47.17	0.00	0.00	8PSK
	G_2	-	-	18.09	-	8.27	-	8PSK
	G_2	3/4	-	**12.42**	**16.67**	**13.94**	**30.50**	16QAM
	G_2	-	3/4	12.44	17.02	13.92	30.15	16QAM

Table 2.13: Performance of the TTCM- and LDPC-STBC coded concatenated OFDM schemes using one receiver, when communicating over the SWATM channel of Figure 2.32. The STBC, CM and LDPC parameters were given in Tables 2.1, 2.9 and 2.12, respectively. An OFDM scheme having 512 subcarriers and a cyclic extension of 64 samples was employed. For the scenarios of having a different effective throughput, the performance of the best scheme is printed in bold.

2.5 Chapter Summary

The state-of-the-art of various transmission schemes based on multiple transmitters and receivers was briefly reviewed in Section 2.1. A simple communication system invoking the space-time block code G_2 was introduced in Section 2.2.1, leading to further discussions on various other space-time block codes. More specifically, Section 2.2.2.1 defined the STBC transmission matrix, while the encoding algorithm of the G_2 and a range of other space-time block codes was given in Sections 2.2.2.2 and 2.2.2.3, respectively. Section 2.2.3 presented the decoding algorithm of the space-time block codes considered. More specifically, Section 2.2.3.1 introduced the Maximum Likelihood algorithm, while Section 2.2.3.2 discussed the Maximum-A-Posteriori algorithm, which enables the STBC decoder to provide soft outputs. Thus various channel codes can be concatenated with the space-time block codes for the sake of improving the system's performance. In Section 2.2.4, the schematic of the proposed system was presented, and some assumptions used in our simulations were outlined.

The performances of the various space-time block codes were studied and compared in

Section 2.2.5. Specifically, in Sections 2.2.5.1 and 2.2.5.2 the performances of different space-time block coded schemes communicating over both uncorrelated and correlated Rayleigh fading channels were compared, respectively. It was found that the performances of the half-rate codes G_3 and G_4 degraded in comparison to that of the unity-rate code G_2, when the effective throughput was increased. The reason is that in order to maintain the same effective throughput, higher-throughput modulation schemes have to be employed in conjunction with the half-rate codes G_3 and G_4 which are more vulnerable to errors. This hence degrades the performance of the system. The $\frac{3}{4}$-rate codes H_3 and H_4 suffer a lower degradation in this case, as their code rate is higher than that of the G_3 and G_4 codes, therefore a moderate-throughput modulation scheme can be employed. This in turn assists in maintaining the performance advantage achieved by the space-time codes. Additionally, when the number of receivers is increased, the achievable performance gain of the G_3, G_4, H_3 and H_4 codes over the G_2 code becomes lower, as seen in Figures 2.4, 2.5, 2.8 and 2.9. This is because much of the attainable diversity gain has already been achieved using the G_2 code employing two receivers. Another important conclusion is that the performances of the space-time codes communicating over both uncorrelated and correlated Rayleigh fading channels are the same, provided that the effective throughput is the same. The performances of all the space-time block codes are summarized in Table 2.2 at the end of Section 2.2.6.

The schemes employing space-time block codes in conjunction with channel codes were studied in Section 2.3, which were divided into two parts, namely the performance study of LDPC-aided space-time block codes was presented in Section 2.3.1, while our performance comparisons between LDPC-assisted and TC(2,1,4)-aided STBC schemes were provided in Section 2.3.2.

In Section 2.3.1.1 the LDPC-based system was introduced and the associated simulation parameters were given. The performances of the LDPC-STBC concatenated schemes were provided in Section 2.3.1.2, including the scenarios of both uncorrelated and correlated Rayleigh fading channels in Section 2.3.1.2.1 and Section 2.3.1.2.2, respectively. The implementation complexity issues of the schemes studied were discussed in Section 2.3.1.3, where the coding gain versus complexity at different effective throughputs was shown in Figures 2.21, 2.22 and 2.23. It was found that the LDPC-aided STBC schemes performed significantly better than the STBC-only schemes when communicating over uncorrelated Rayleigh fading channels, while the achievable performance improvement was insignificant, when communicating over correlated Rayleigh fading channels. This is because the attainable performances of the LDPC codes were found to be worse, when comminucating over correlated Rayleigh channels than over uncorrelated Rayleigh channels, unless the LDPC codeword length was sufficiently long enough or a sufficiently long channel interleaver was used. The phenomenon of achieving

different performances over uncorrelated and correlated Rayleigh fading channels was also observed in the context of the LDPC-STBC concatenated system. On the other hand, when the number of receiver antennas was increased, the schemes employing a space-time block code of a higher-diversity order were found to provide an inferior performance, since most of the attainable diversity gain has already been achieved by the LDPC-aided G_2 coded scheme. It was also found that for transmission over the uncorrelated Rayleigh fading channels, when the same modulation scheme was used, a lower-rate LDPC code benefited the system more than a space-time code of a higher-diversity order did. Furthermore, when the same LDPC code was used, a lower-order modulation scheme tended to offer a higher performance improvement, than a space-time block code of a higher diversity order did. The performance of different LDPC-aided space-time block coded schemes was summarized in Table 2.5, where the half-rate LDPC-coded space-time block code G_2 was found to be the best option among all the LDPC-STBC concatenated schemes.

Following Section 2.3.1, where the LDPC-aided space-time coded system was studied, our comparative study between LDPC-aided and TC(2,1,4)-assisted STBC schemes transmitting over uncorrelated Rayleigh fading channels was presented in Section 2.3.2. The TC(2,1,4)-aided system was introduced in Section 2.3.2.1, while the associated complexity issues were discussed in Section 2.3.2.2, which was followed by the performance analysis in Section 2.3.2.3. From our coding gain versus complexity performance comparisons, it was concluded that the half-rate TC(2,1,4)-assisted space-time block code G_2 slightly outperforms the LDPC-assisted space-time block coded schemes. However, the LDPC-STBC concatenated schemes may be considered as better design options for complexity-sensitive systems, where the achievable performance does not necessarily have to be the highest possible, since the LDPC-aided schemes are capable of maintaining a lower complexity than the TC(2,1,4)-aided scheme is. In conclusion, the performance of the different schemes studied was summarized in Table 2.8.

Furthermore, channel coding assisted space-time block coded single-user OFDM systems were studied in Section 2.4. This research was divided into two parts. The first part is the investigation of the various CM-assisted space-time block coded OFDM schemes detailed in Section 2.4.1. The basic OFDM system was introduced in Section 2.4.1.2, followed by the whole system's overview in Section 2.4.1.3. More specifically, a brief complexity analysis was provided in Section 2.4.1.3.1, and the introduction of the SWATM channel model was the subject of Section 2.4.1.3.2. Our simulation results were discussed in Section 2.4.1.4, which were summarized in Table 2.11. The latter part of Section 2.4 focused on the performance comparison of the CM- and LDPC-assisted space-time block coded systems considered, which was detailed in Section 2.4.2. The BER versus E_b/N_0 as well as the coding gain versus complexity performances of the two groups of candidate schemes were compared in Section 2.4.2.2, fol-

lowed by our conclusions in Section 2.4.2.3, where the results were summarized in Table 2.13.

The family of STBCs is readily applicable to employment in downlink systems, where the multiple transmitter antennas are installed at the BS. However, in the context of uplink systems it is impractical to use high-order STBCs at the MSs, since the MSs are expected to have a low implementation complexity and thus cannot afford the added cost of a high number of transmitter antennas. In the next chapter, Space Division Multiple Access (SDMA) type uplink multi-user OFDM systems will be investigated, which invoke multiple receiver antenna elements for supporting a multiplicity of MSs, each of which employs a single transmitter antenna only.

Chapter 3

Coded Modulation Assisted Multi-User SDMA-OFDM Using Frequency-Domain Spreading

3.1 Introduction

In recent years Orthogonal Frequency Division Multiplexing (OFDM) [3, 5, 7, 31] has emerged as a successful air-interface technology for both broadcast and Wireless Local Area Network (WLAN) applications, whilst Wideband Code Division Multiple Access (WCDMA) has emerged as the winning candidate for 3G mobile systems. Our research therefore includes an exploration of the performance versus complexity tradeoffs of a generic class of Multi-Carrier Code Division Multiple Access (MC-CDMA) [45] systems, which are capable of supporting the interworking of existing as well as future broadcast and personal communication systems.

Space Division Multiple Access (SDMA) based OFDM [3, 192, 304] communication invoking Multi-User Detection (MUD) [305] techniques has recently attracted intensive research interests. In SDMA Multiple-Input Multiple-Output (MIMO) systems the transmitted signals of L simultaneous uplink mobile users - each equipped with a single transmitter antenna - are received by the P different receiver antennas of the base station (BS). At the BS the individual users' signals are separated with the aid of their unique, user-specific spatial signature constituted by their channel transfer functions or, equivalently, Channel Impulse Responses (CIRs). A variety of MUD schemes, such as the Least-Squares (LS) [3, 305, 306] and Minimum Mean-Square Error (MMSE) [3, 192, 196, 305, 306] detectors, or Successive Interference Cancellation (SIC) [3, 192, 196, 305–307], Parallel Interference Cancellation (PIC) [3, 305, 307, 308] and Maximum Likelihood Detection (MLD) [3, 192, 196, 197, 305] schemes may be invoked for

the sake of separating the different users at the BS on a per-subcarrier basis. Among these schemes, the MLD arrangement was found to give the best performance, although this was achieved at the cost of a dramatically increased computational complexity, especially in the context of a high number of users and higher-order modulation schemes, such as 16QAM [307]. By contrast, MMSE combining exhibits the lowest complexity in this set of detectors, while suffering from a performance loss [3, 307].

In order to improve the achievable performance by exploiting the multi-path diversity potential offered by wideband channels, a further technique that is often used in the context of CDMA systems is constituted by the spreading of the subcarrier signals over a number of adjacent subcarriers with the aid of orthogonal spreading codes, such as Walsh-Hadamard Transform (WHT) based codes [39]. This technique may also be employed in multi-user SDMA-OFDM systems in the context of spreading across all or a fraction of the subcarriers [309]. Spreading across all subcarriers using a single Walsh-Hadamard Transform Spreading (WHTS) [3] code is expected to result in a better averaging of the bursty error effects at the cost of a higher WHT complexity.

Furthermore, the achievable performance can be significantly improved, if Forward Error Correction (FEC) schemes, such as for example Turbo Convolutional (TC) codes are incorporated into the SDMA system [3]. Among a number of FEC schemes, Trellis Coded Modulation (TCM) [2, 300], Turbo TCM (TTCM) [2, 301], Bit-Interleaved Coded Modulation (BICM) [2, 302] and Iteratively Decoded BICM (BICM-ID) [2, 303] have attracted intensive research interests, since they are capable of achieving a substantial coding gain without bandwidth expansion.

In this section, we combine the above-mentioned various Coded Modulation (CM) schemes with a multi-user SDMA-OFDM system, in which WHT-based subcarrier spreading is used. The structure of this section is as follows. The SDMA MIMO channel model is described in Section 3.2.1, while an overview of the CM-assisted multi-user SDMA-WHTS-OFDM system is provided in Section 3.2.2, where the basic principles of CM, MUD and WHT-based spreading (WHTS) are also introduced. Our simulation results are provided in Section 3.3, while our conclusions are summarized in Section 3.4.

3.2 System Model

3.2.1 SDMA MIMO Channel Model

Figure 3.1 shows a SDMA uplink MIMO channel model, where each of the L simultaneous mobile users employs a single transmitter antenna at the mobile station (MS), while the BS's

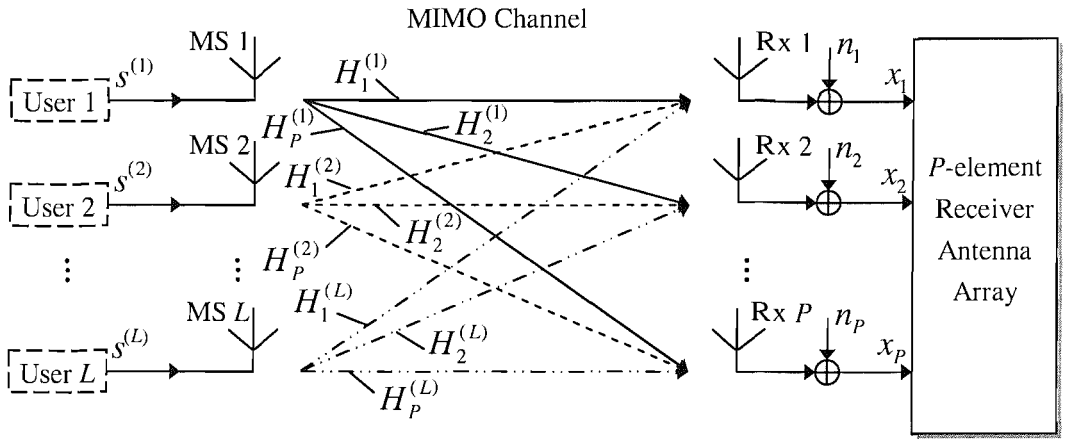

Figure 3.1: Schematic of the SDMA uplink MIMO channel model [3], where each of the L mobile users is equipped with a single transmitter antenna and the BS's receiver is assisted by a P-element antenna front-end.

receiver exploits P antennas. At the k^{th} subcarrier of the n^{th} OFDM symbol received by the P-element receiver antenna array we have the complex received signal vector $\mathbf{x}[n,k]$, which is constituted by the superposition of the independently faded signals associated with the L mobile users and contaminated by the Additive White Gaussian Noise (AWGN), expressed as:

$$\mathbf{x} = \mathbf{H}\mathbf{s} + \mathbf{n}, \tag{3.1}$$

where the $(P \times 1)$-dimensional vector $\mathbf{x}$, the $(L \times 1)$-dimensional vector $\mathbf{s}$ and the $(P \times 1)$-dimensional vector $\mathbf{n}$ are the received, transmitted and noise signals, respectively. Here we have omitted the indices $[n,k]$ for each vector for the sake of notational convenience. Specifically, the vectors $\mathbf{x}$, $\mathbf{s}$ and $\mathbf{n}$ are given by:

$$\mathbf{x} = [\, x_1,\ x_2,\ \cdots,\ x_P \,]^T, \tag{3.2}$$

$$\mathbf{s} = [\, s^{(1)},\ s^{(2)},\ \cdots,\ s^{(L)} \,]^T, \tag{3.3}$$

$$\mathbf{n} = [\, n_1,\ n_2,\ \cdots,\ n_P \,]^T. \tag{3.4}$$

The $(P \times L)$-dimensional matrix $\mathbf{H}$, which contains the Frequency-Domain CHannel Transfer Functions (FD-CHTFs) of the L users, is given by:

$$\mathbf{H} = [\, \mathbf{H}^{(1)},\ \mathbf{H}^{(2)},\ \cdots,\ \mathbf{H}^{(L)} \,], \tag{3.5}$$

where $\mathbf{H}^{(l)}$ $(l = 1, \cdots, L)$ is the vector of the FD-CHTFs associated with the transmission paths from the l^{th} user's transmitter antenna to each element of the P-element receiver antenna array, which is expressed as:

$$\mathbf{H}^{(l)} = [\, H_1^{(l)},\ H_2^{(l)},\ \cdots,\ H_P^{(l)} \,]^T, \quad l = 1, \cdots, L. \tag{3.6}$$

In Equations (3.1) to (3.6), we assume that the complex signal $s^{(l)}$ transmitted by the l^{th} user has zero-mean and a variance of σ_l^2. The AWGN noise signal n_p also exhibits a zero-mean and a variance of σ_n^2. The FD-CHTFs $H_p^{(l)}$ of the different receivers or users are independent, stationary, complex Gaussian distributed processes with zero-mean and unit variance [309].

3.2.2 CM-assisted SDMA-OFDM Using Frequency Domain Spreading

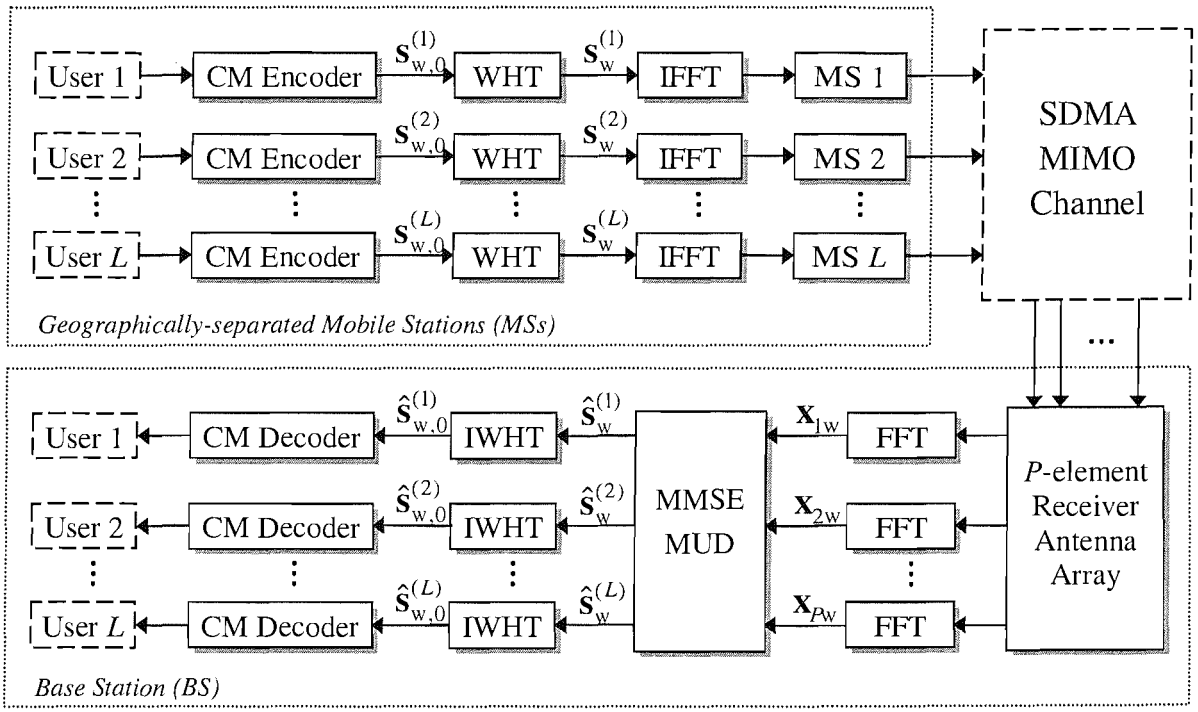

Figure 3.2: Schematic of the CM-assisted and multi-user detected SDMA-OFDM uplink system employing subcarrier-based WHT spreading.

In Section 3.2.1 we have briefly reviewed the SDMA MIMO channel model, as shown in Figure 3.1. In Figure 3.2, we present the schematic of the proposed CM-assisted and multi-user detected SDMA-OFDM uplink system employing WHT spreading. At the transmitter end, as seen at the top of Figure 3.2, the information bit sequences of the geographically-separated L simultaneous mobile users are forwarded to the CM encoders, where they are encoded into symbols. Each user's encoded signal is divided into a number of WHT signal blocks, denoted by $\mathbf{s}_{\mathrm{w},0}^{(l)}$ $(l = 1, \cdots, L)$, which are then forwarded to the subcarrier-based WHT spreader, followed by the OFDM-related Inverse Fast Fourier Transform (IFFT) based modulator, which converts the frequency-domain signals to the time-domain modulated OFDM symbols. The OFDM symbols are then transmitted by the MSs to the BS over the SDMA MIMO channel. Then each element of the receiver antenna array shown at the bottom of Figure 3.2 receives the superposition of the AWGN-contaminated transmitted signals and performs Fast Fourier

Transform (FFT) based OFDM demodulation. The demodulated outputs $\mathbf{x}_{p_W}$ $(p = 1, \cdots, P)$ seen in Figure 3.2 are forwarded to the multi-user detector for separating the different users' signals. The separated signals $\hat{\mathbf{s}}_W^{(l)}$ $(l = 1, \cdots, L)$, namely the estimated versions of the transmitted signals, are independently despread based on the inverse WHT (IWHT), resulting in the despread signals of $\hat{\mathbf{s}}_{W,0}^{(l)}$ $(l = 1, \cdots, L)$ which are then decoded by the CM decoders of Figure 3.2.

The further structure of this section is as follows. A brief description of the MMSE MUD employed in our SDMA-OFDM system is given in Section 3.2.2.1. The subcarrier-based WHTS is then introduced in Section 3.2.2.2.

3.2.2.1 Minimum Mean-Square Error Multi-User Detector

As mentioned earlier, MUD schemes have to be invoked at the receiver of the SDMA-OFDM system for the sake of detecting the received signals of different users. From the family of various MUD techniques, represented for example by the Maximum Likelihood Detection (MLD) [3, 192, 196, 197, 305], Parallel Interference Cancellation (PIC) [3, 305, 307, 308], Successive Interference Cancellation (SIC) [3, 192, 196, 305–307], Minimum Mean-Square Error (MMSE) [3, 192, 196, 305, 306] and Least-Squares (LS) [3, 305, 306] detectors, ML detection is known to exhibit the optimum performance, although this is achieved at the highest complexity. In order to avoid the potentially excessive complexity of optimum ML detection, sub-optimum detection techniques such as the MMSE-MUD have been devised. Specifically, the MMSE detector exhibits the lowest detection complexity in the set of detectors mentioned above, although this comes at the cost of a Bit Error Ratio (BER) degradation [3, 307].

In the MMSE-based MUD the estimates of the different users' transmitted signals are generated with the aid of the linear MMSE combiner. More specifically, the estimated signal vector $\hat{\mathbf{s}} \in \mathbb{C}^{(L \times 1)}$ generated from the transmitted signal $\mathbf{s}$ of the L simultaneous users, as shown in Figure 3.2, is obtained by linearly combining the signals received by the P different receiver antenna elements with the aid of the array weight matrix, as follows [3]:

$$\hat{\mathbf{s}} = \mathbf{W}_{\text{MMSE}}^H \mathbf{x}, \tag{3.7}$$

where the superscript H denotes the Hermitian transpose, and $\mathbf{W}_{\text{MMSE}} \in \mathbb{C}^{(P \times L)}$ is the MMSE-based weight matrix given by [3]:

$$\mathbf{W}_{\text{MMSE}} = (\mathbf{H}\mathbf{H}^H + \sigma_n^2 \mathbf{I})^{-1} \mathbf{H}, \tag{3.8}$$

while $\mathbf{I}$ is the identity matrix and σ_n^2 is the AWGN noise variance.

3.2.2.2 Subcarrier-based Walsh-Hadamard Transform Spreading

In single- and multi-carrier CDMA systems, the employment of orthogonal codes is vital for the sake of supporting multiple access [39]. In the context of multi-user SDMA-OFDM systems, orthogonal codes may be employed for the sake of randomizing the wideband channel's frequency-selective fading, rather than for supporting multiple users, since the multiple users are supported with the aid of the SDMA-OFDM system employing a P-element antenna array and appropriate multi-user detection techniques.

A prominent class of orthogonal codes often used in CDMA systems is the family of orthogonal Walsh codes [39], which are particularly attractive, since the operation of spreading with the aid of these codes can be implemented in form of a 'fast' transform, which takes advantage of the codes' recursive structure, similarly to the FFT [3].

Let us now provide a deeper insight into the operation of the subcarrier-based WHTS [3]. During every OFDM symbol period prior to transmission of the independent user signals, the K data samples associated with the subcarriers, where K is the FFT length, may be spread with the aid of the WHT having a block size of K. This is achieved by left-multiplying the WHT signal block $\mathbf{s}_{\mathrm{W},0}^{(l)}$ $(l = 1, \cdots, L)$ of Figure 3.2 with the K-order WHT matrix $\mathbf{U}_{\mathrm{WHT}_K}$ for each user separately:

$$\mathbf{s}_{\mathrm{W}}^{(l)} = \mathbf{U}_{\mathrm{WHT}_K} \mathbf{s}_{\mathrm{W},0}^{(l)}, \quad l = 1, \cdots, L, \tag{3.9}$$

where $\mathbf{s}_{\mathrm{W}}^{(l)}$ is the l^{th} user's spread signal block, and $\mathbf{U}_{\mathrm{WHT}_K}$ is given in a recursive form as:

$$\mathbf{U}_{\mathrm{WHT}_K} = \frac{1}{\sqrt{2}} \begin{bmatrix} 1 \cdot \mathbf{U}_{\mathrm{WHT}_{K/2}} & 1 \cdot \mathbf{U}_{\mathrm{WHT}_{K/2}} \\ 1 \cdot \mathbf{U}_{\mathrm{WHT}_{K/2}} & -1 \cdot \mathbf{U}_{\mathrm{WHT}_{K/2}} \end{bmatrix}, \tag{3.10}$$

while the lowest-order WHT unitary matrix is defined by:

$$\mathbf{U}_{\mathrm{WHT}_2} = \frac{1}{\sqrt{2}} \begin{bmatrix} 1 & 1 \\ 1 & -1 \end{bmatrix}. \tag{3.11}$$

When the WHT block size is long, for example identical to the FFT length of $K = 512$, the computational complexity imposed by the length-K WHTS may be very high. Therefore a more practical solution is to further divide the K samples into K/M_{WHT} number of interleaved blocks, each of which has a block size of $M_{\mathrm{WHT}} < K$. Specifically, the i^{th} WHT block is constituted by the samples selected from the subcarriers having the indices [3, 309]:

$$j = i + r\frac{K}{M_{\mathrm{WHT}}}, \ 0 \leq i \leq \frac{K}{M_{\mathrm{WHT}}} - 1, \ 0 \leq r \leq M_{\mathrm{WHT}} - 1, \tag{3.12}$$

where i is the index of the WHT blocks within the same OFDM symbol. In Figure 3.3 we illustrate the operation of the subcarrier-based WHTS, where the number of OFDM subcarriers is 512 and the WHT block size is 32. Therefore in each OFDM symbol we have

512/32 = 16 frequency-domain interleaved WHT blocks. At the top of Figure 3.3 an OFDM symbol is shown with the subcarriers' indices displayed, while the bottom illustration of the figure shows the WHT blocks generated, which contain subcarriers of the specified indices, as given by Equation (3.12). As Figure 3.3 shows, for example, the signal sample carried by the second ($r = 1$) slot within the WHT block of index $i = 0$ is selected from the subcarrier of index $j = 16$ within the original OFDM symbol. After the WHT blocks are formed, the WHTS is then invoked with the aid of the length-M_{WHT} WHT matrix given in Equation (3.10).

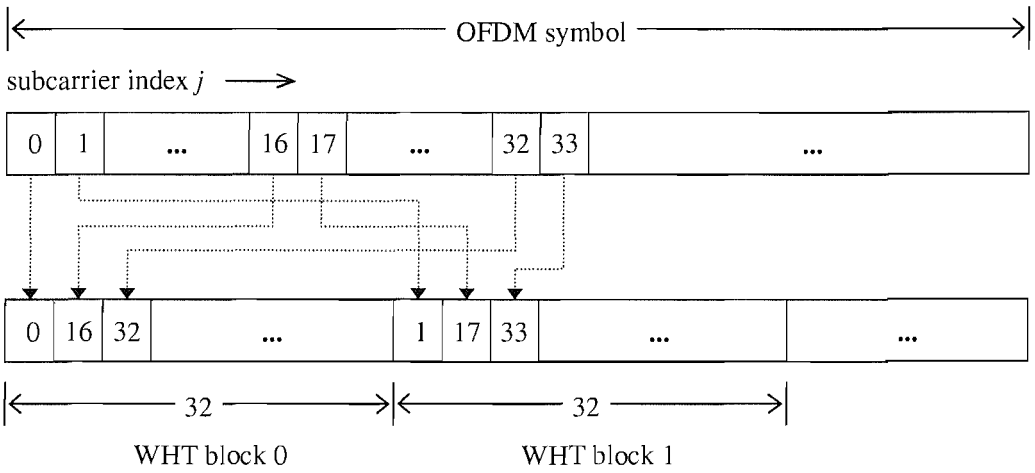

Figure 3.3: Example of the subcarrier-based WHT blocks' generation using a WHT block size of 32, where the total number of OFDM subcarriers is 512.

At the BS receiver seen in Figure 3.2, the despreading operation follows the inverse procedure of that portrayed in Figure 3.3, which is invoked independently for the separated signal of each user. More specifically, we have:

$$\hat{\mathbf{s}}_{\text{W},0}^{(l)} = \mathbf{U}_{\text{WHT}_K} \hat{\mathbf{s}}_{\text{W}}^{(l)}, \quad l = 1, \cdots, L, \tag{3.13}$$

where $\hat{\mathbf{s}}_{\text{W},0}^{(l)}$ and $\hat{\mathbf{s}}_{\text{W}}^{(l)}$ are the estimated version of $\mathbf{s}_{\text{W},0}^{(l)}$ and $\mathbf{s}_{\text{W}}^{(l)}$, respectively, while $\hat{\mathbf{s}}_{\text{W}}^{(l)}$ is achieved by applying Equation (3.7) at each subcarrier of every length-M_{WHT} WHT block. Upon employing the WHTS technique, the detrimental effects imposed on the system's average BER performance by the specific subcarriers corrupted by deep frequency-domain channel fades can be potentially improved, since the effects of the fades are spread over the entire WHT block. Hence the receiver has a high chance of recovering the impaired transmitted signals of the badly affected subcarriers.

3.3 Simulation Results

In this section, we characterize the performance of the proposed CM-assisted MMSE-SDMA-OFDM schemes in conjunction with WHTS. The channel is assumed to be OFDM-symbol-

invariant, implying that the taps of the impulse response are assumed to be constant for the duration of one OFDM symbol, but they are faded at the beginning of each symbol [6]. Each user's associated transmit power or signal variance is assumed to be the same and normalized to unity, while the complex-valued fading envelope of the different users' signal is assumed to be uncorrelated. For the sake of simplifying the experimental conditions, the channel's frequency-domain transfer function is assumed to be perfectly known in all simulations. Nonetheless, these performance trends are expected to remain unchanged in case of imperfect channel estimation, in particular, when the turbo-style PIC aided Recursive Least-Squares (RLS) channel estimators of Chapter 16 in reference [3] are used. This may be made plausible by noting that turbo-style iterative detection techniques have been reported to be capable of achieving a virtually indistinguishable performance from the idealistic system using perfect channel estimation [2,3]. In addition, the transmitted signals of the different users are assumed to be perfectly synchronized.

3.3.1 MMSE-SDMA-OFDM Using WHTS

We commence by considering a multi-user SDMA-OFDM system operating without the assistance of CM communicating over the Short Wireless Asynchronous Transfer Mode (SWATM) channel of [6]. The impulse response of the three-tap SWATM channel was given in Figure 2.32, while the specific channel parameters used were given in Table 2.10. Each of the three paths experiences independent Rayleigh fading having the same normalized Doppler frequency of $f'_d = 1.235 \times 10^{-5}$. A total of 512 subcarriers and a cyclic prefix of 64 samples were used for the OFDM modem.

Figure 3.4 compares the BER versus E_b/N_0 performance of the MMSE-SDMA-OFDM system equipped with two receiver antenna elements, while supporting one or two users both with and without WHTS, respectively. Furthermore, the performance of the unprotected single-user BPSK scheme communicating over an AWGN channel is also provided for reference. As expected, the WHTS-assisted schemes perform better than their non-spread counterparts, both for one and two users. It is also beneficial to view the subcarrier BERs as a function of both the subcarrier index and the E_b/N_0, which was portrayed in Figure 3.5 for the SDMA-OFDM system equipped with two BS receiver antennas for supporting two users. The subcarrier BER is defined as the BER averaged over a specific subcarrier of all the consecutive OFDM symbols transmitted by the users. It was found that at a specific E_b/N_0 value, the subcarrier BER curves shown at the top of Figures 3.5, exhibit undulations across the frequency domain owing to deep channel fades at certain subcarriers, which could be potentially eliminated with the aid of WHTS, as observed at the bottom of the figure. This suggests that the system's average BER performance can be potentially improved by using

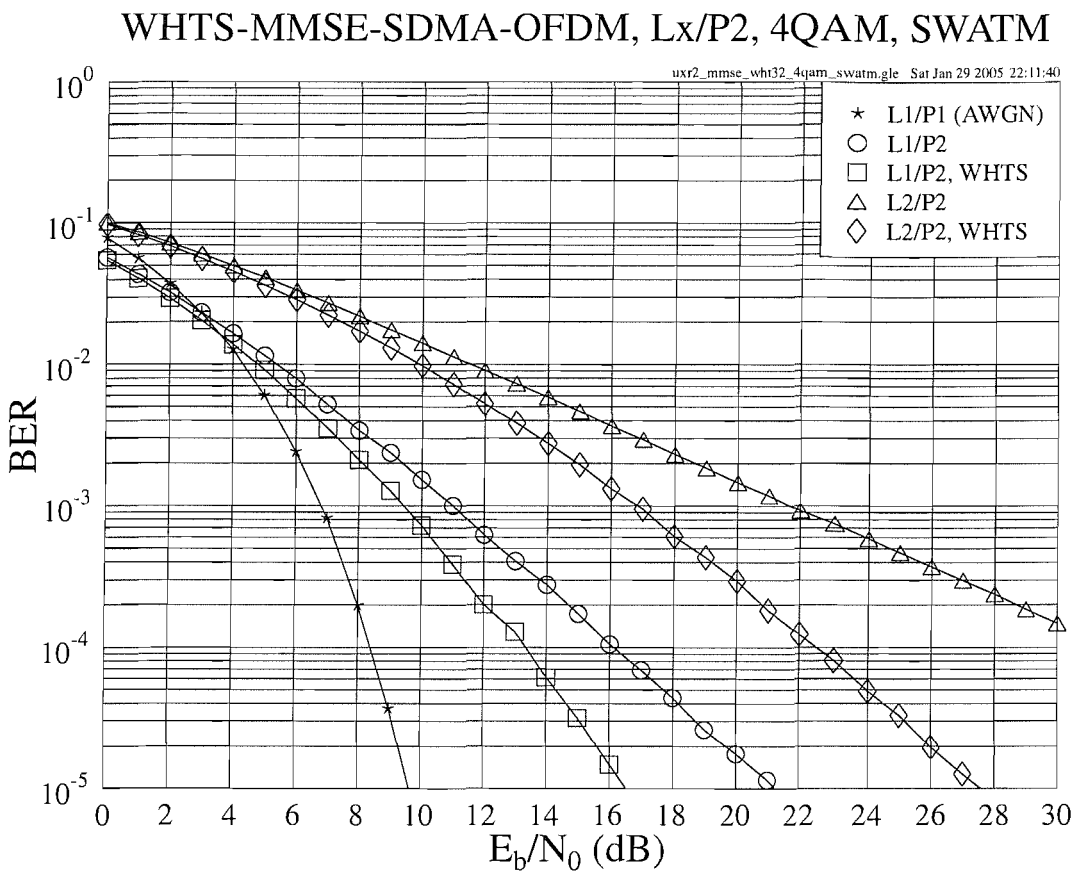

Figure 3.4: **BER** versus E_b/N_0 performance of the **WHTS-assisted MMSE-SDMA-OFDM** system employing a 4QAM scheme for transmission over the **SWATM** channel, where **L=1, 2** users are supported with the aid of **P=2** receiver antenna elements. The WHT block size used is **32**.

WHTS, since the bursty subcarrier errors can be effectively spread across the subcarriers of the entire WHT block.

3.3.2 CM- and WHTS-assisted MMSE-SDMA-OFDM

Similarly to the previous sections, let us first investigate the SDMA-OFDM system's performance while communicating over the SWATM channel [6].

3.3.2.1 Performance Over the SWATM Channel

For the various CM schemes used, we select the parameters so that all schemes have the same effective throughput and the same number of decoding states, hence have a similar decoding complexity. More specifically, the code memory ν is fixed to 6 for the non-iterative TCM and BICM schemes, so that the number of decoding states becomes $S = 2^{\nu} = 64$. For the iterative

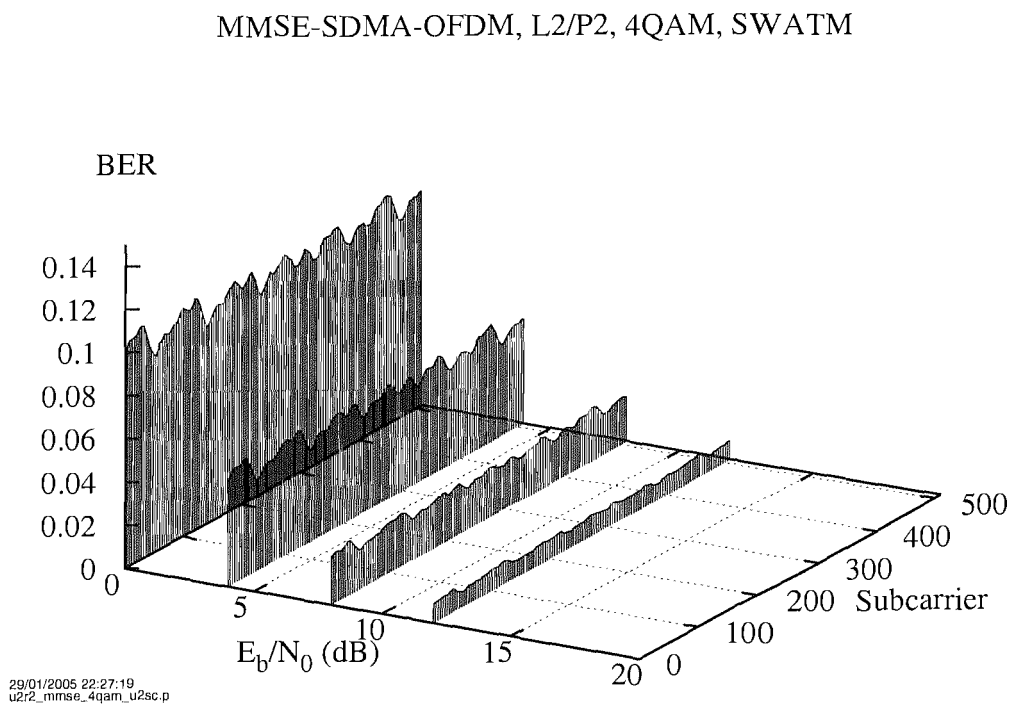

Figure 3.5: **BER** versus E_b/N_0 performance as a function of the subcarrier index of the **MMSE-SDMA-OFDM (top)** and **WHTS-assisted MMSE-SDMA-OFDM (bottom)** systems employing a 4QAM scheme for transmission over the **SWATM** channel, where **L=2** users are supported with the aid of **P=2** receiver antenna elements. The WHT block size used is **32**.

TTCM and BICM-ID schemes, however, ν is fixed to 3, while the number of iterations for these schemes is set to 4 and 8, respectively. Hence the total number of trellis states is $2^3 \cdot 4 \cdot 2 = 64$ for TTCM and $2^3 \cdot 8 \cdot 1 = 64$ for BICM-ID, since there are two 8-state decoders, which are invoked in four iterations in the scenario of TTCM, while only one 8-state decoder is employed in the context of BICM-ID. The generator polynomials expressed in octal format for TCM, TTCM, BICM and BICM-ID are [117 26], [13 6], [133 171] and [15 17], respectively. The parameters of the various CM schemes used are summarized in Table 3.1.

CM Scheme	Code Rate	Data Bits	Parity Bits	Code Memory	Iterations	Codeword Length	Modem
TCM	1/2	1	1	6	-	1024	4QAM
TTCM	1/2	1	1	3	4	1024	4QAM
BICM	1/2	1	1	6	-	1024	4QAM
BICMID	1/2	1	1	3	8	1024	4QAM

Table 3.1: The parameters of the various CM schemes used in the multi-user SDMA-OFDM system for communicating over the SWATM channel of Figure 2.32.

3.3.2.1.1 Two Receiver Antenna Elements

In Section 3.3.1 the beneficial effects of WHTS on the MMSE-SDMA-OFDM system's performance have been demonstrated. Let us now combine the various CM schemes considered with the multi-user MMSE-SDMA-OFDM system. The corresponding simulation results are portrayed in Figure 3.6, where the top and bottom of the figure illustrate the BER and CodeWord Error Ratio (CWER) versus E_b/N_0 performance of the proposed CM-MMSE-SDMA-OFDM schemes, respectively.

Here we define the user load of an L-user and P-receiver SDMA-OFDM system as:

$$\alpha_P = \frac{L}{P}, \tag{3.14}$$

which assumes a value of unity in case of full user load, when the number of users is equal to the number of receiver antenna elements. The simulation results generated in the context of $\alpha_2 = 0.5$ and $\alpha_2 = 1$ are plotted at the left and right side of Figure 3.6, respectively. The BER performance of the 32-state TC code assisted MMSE-SDMA-OFDM [3] system is also portrayed as a reference. Furthermore, the performance of the unprotected 4QAM SDMA-OFDM system and that of the single-user BPSK scheme communicating over an AWGN channel is also provided as a benchmarker. As observed in Figure 3.6, the TC-assisted arrangement and the various CM-assisted schemes provide a similar BER performance in both scenarios.

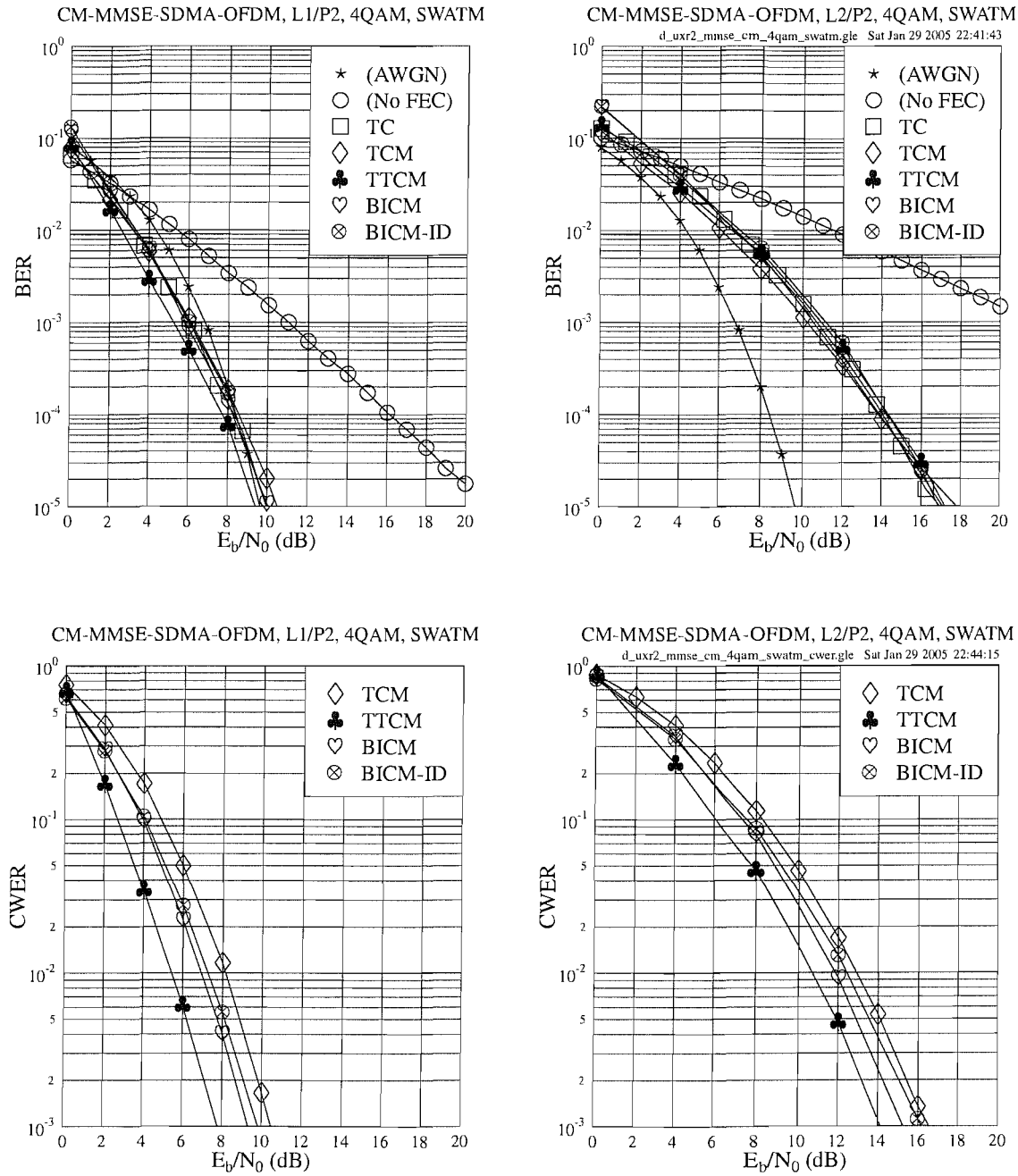

Figure 3.6: **BER (top)** and **CWER (bottom)** versus E_b/N_0 performance of the **CM-assisted MMSE-SDMA-OFDM** system employing a 4QAM scheme for transmission over the **SWATM** channel, where **L=1 (left)** or **L=2 (right)** users are supported with the aid of **P=2** receiver antenna elements. The CM parameters are given in Table 3.1. The CM codeword length is **1024** symbols. The BER performance of the same 4QAM MMSE-SDMA-OFDM system assisted by the half-rate TC code [3] (the curves with the legend of □) is also provided for reference.

As expected, all the FEC-aided schemes perform significantly better than their unprotected counterparts in the BER performance investigations. Furthermore, the TTCM-aided scheme is found to give the best CWER performance from the set of all CM-aided schemes in both the half-loaded and fully-loaded scenarios, where α_2 is equal to 0.5 and 1, respectively. This suggests that more transmission errors can be eliminated by TTCM than by the other three CM schemes, although the burst errors inflicted by deep frequency-domain channel fades cannot be recovered completely. However, this effect may be potentially mitigated by employing WHTS, as discussed in Section 3.2.2.2.

As expected, for each of the schemes evaluated, we may notice that the performance achieved in the context of $\alpha_2 = 0.5$, is better than that attained, when we have $\alpha_2 = 1$. This phenomenon may be explained as follows. Since P receiver antenna elements are invoked at the BS, there are P uplink paths for each MS user having one transmitter antenna. Hence the achievable spatial diversity order provided by the P paths remains the same for each user, regardless of the total number of simultaneous users supported. However, when the user load is lower, i.e. the number of users supported is lower, the MMSE combiner will benefit from a higher degree of freedom in terms of the choice of the array weights optimized for differentiating the different users' transmitted signal, and thus the system becomes more efficient in terms of suppressing the reduced Multi-User Interference (MUI).

In Figure 3.7, we provide the subcarrier based BER versus E_b/N_0 performance of the TTCM-assisted MMSE-SDMA-OFDM system in the context of two users and two receiver antenna elements. Comparing Figure 3.5 to Figure 3.7, where the beneficial effects of WHTS have been characterized, we may notice that the achievable performance improvement attained by TTCM, or more generally by the CM schemes, is typically higher than that achieved by WHTS.

Having discussed the beneficial effects of WHTS and those of CM on the SDMA-OFDM system, as described in Section 3.3.1 and earlier in this section, respectively, we now combine the MMSE-SDMA-OFDM system with CM and WHTS. The corresponding simulation results are portrayed in Figure 3.8, where the left and right side of the figure illustrate the scenarios of $\alpha_2 = 0.5$ and $\alpha_2 = 1$, while the top and bottom of the figure shows the BER and CWER performance, respectively. Again, the TTCM-aided scheme was found to give the best CWER performance among all the CM-aided schemes considered. Comparison of Figure 3.6 and Figure 3.8 shows that in the CM-aided MMSE-SDMA-OFDM system the employment of WHTS having a block size of 32 only insignificantly improves the system's BER and CWER performance, since most of the achievable diversity gain may have already been achieved by using the CM schemes. However, the employment of WHTS has the potential of further enhancing the CM-SDMA-OFDM system's performance in highly-dispersive propagation environments,

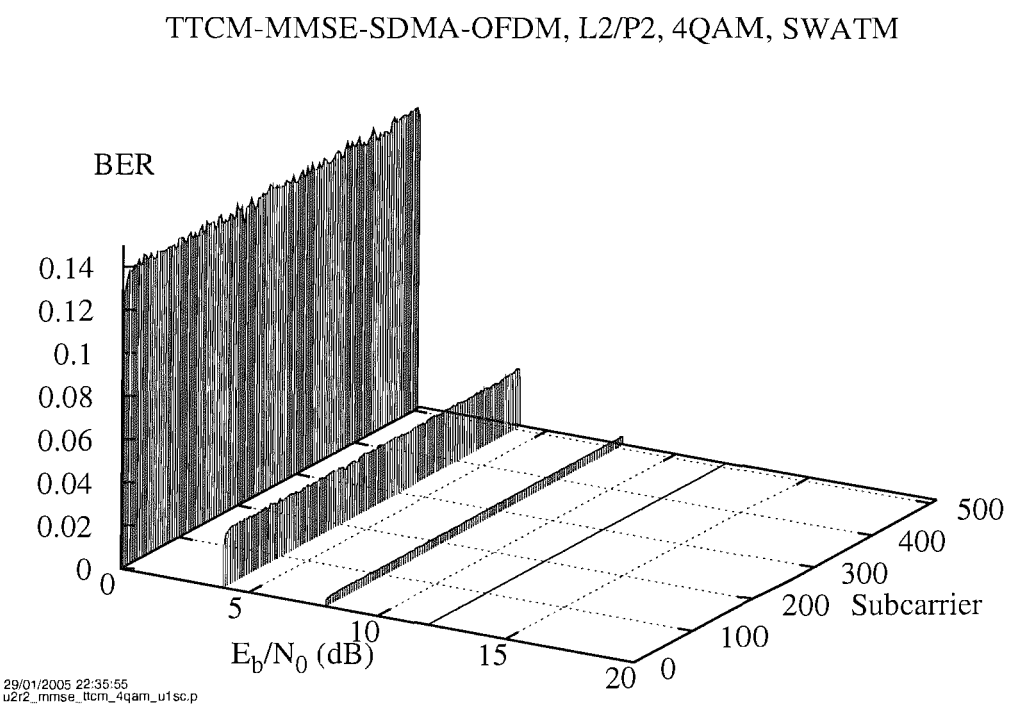

Figure 3.7: **BER** versus E_b/N_0 performance as a function of the subcarrier index of the **TTCM-assisted MMSE-SDMA-OFDM** system employing a 4QAM scheme for transmission over the **SWATM** channel, where **L=2** users are supported with the aid of **P=2** receiver antenna elements. The TTCM codeword length is **1024** symbols.

an issue which will be further discussed in Section 3.3.2.2.

Furthermore, if a longer CM codeword length is used, the system's performance can be further improved at the cost of a higher computational complexity. The effects of different CM codeword lengths can be seen in Figure 3.9. As expected, when a higher codeword length is employed, the system's performance becomes better, since a longer CM codeword is capable of better averaging the bursty error effects. However this performance improvement is achieved at a substantially higher complexity. For examples of the associated complexity issues, the interested reader is referred to Chapter 9 of [2].

3.3.2.1.2 Four Receiver Antenna Elements

In Section 3.3.2.1.1, we have compared the various CM- and WHTS-aided schemes in the context of one or two users and two receiver antenna elements. In this section, we investigate a higher-order spatial diversity assisted scenario by increasing the number of receiver antenna

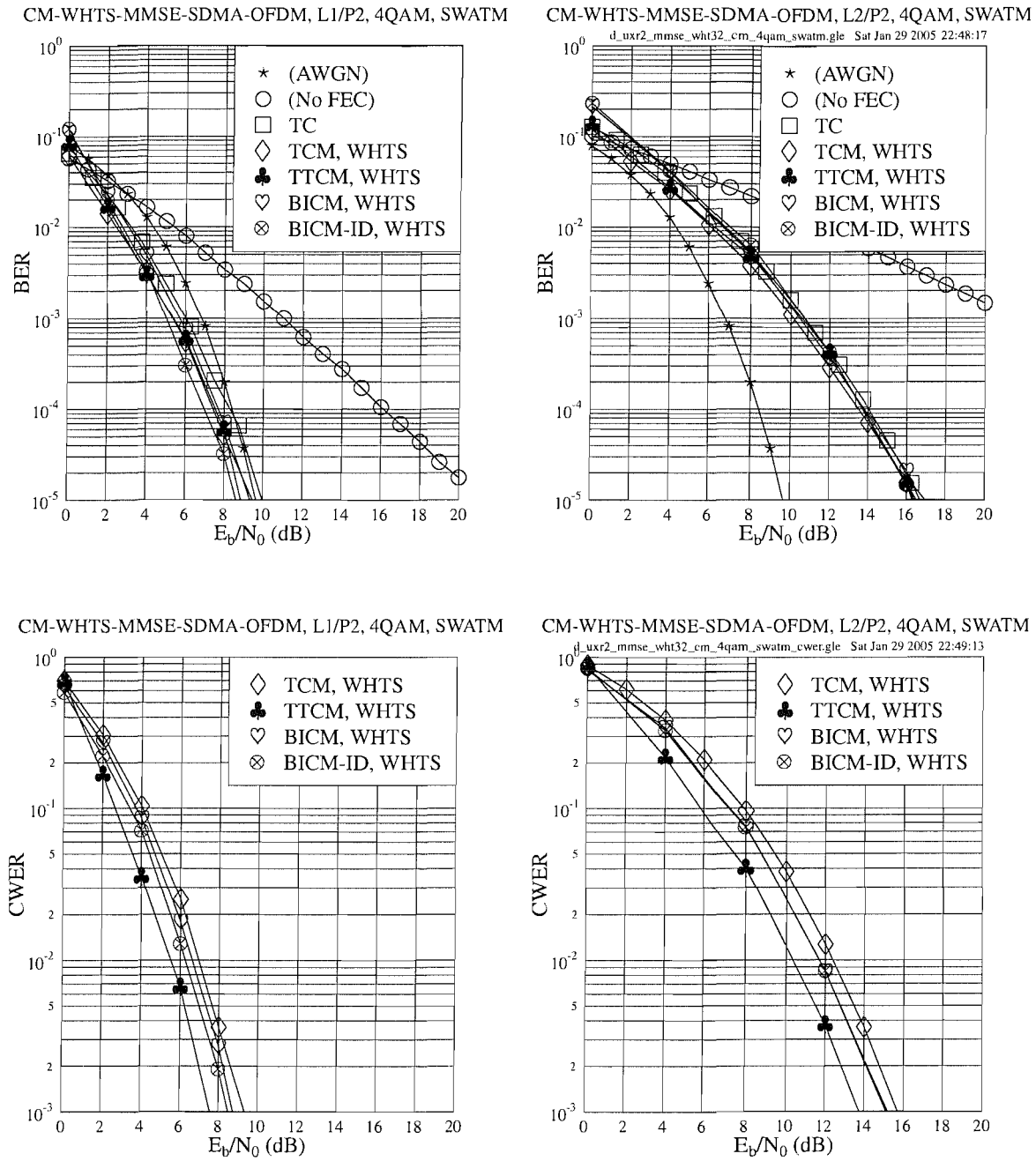

Figure 3.8: **BER (top)** and **CWER (bottom)** versus E_b/N_0 performance of the **CM- and WHTS-assisted MMSE-SDMA-OFDM** system employing a 4QAM scheme for transmission over the **SWATM** channel, where **L=1 (left)** or **L=2 (right)** users are supported with the aid of **P=2** receiver antenna elements. The CM parameters are given in Table 3.1. The CM codeword length is **1024** symbols and the WHT block size used is **32**. The BER performance of the 4QAM MMSE-SDMA-OFDM system assisted by the half-rate TC code [3] (the curves with the legend of □) is also provided for reference.

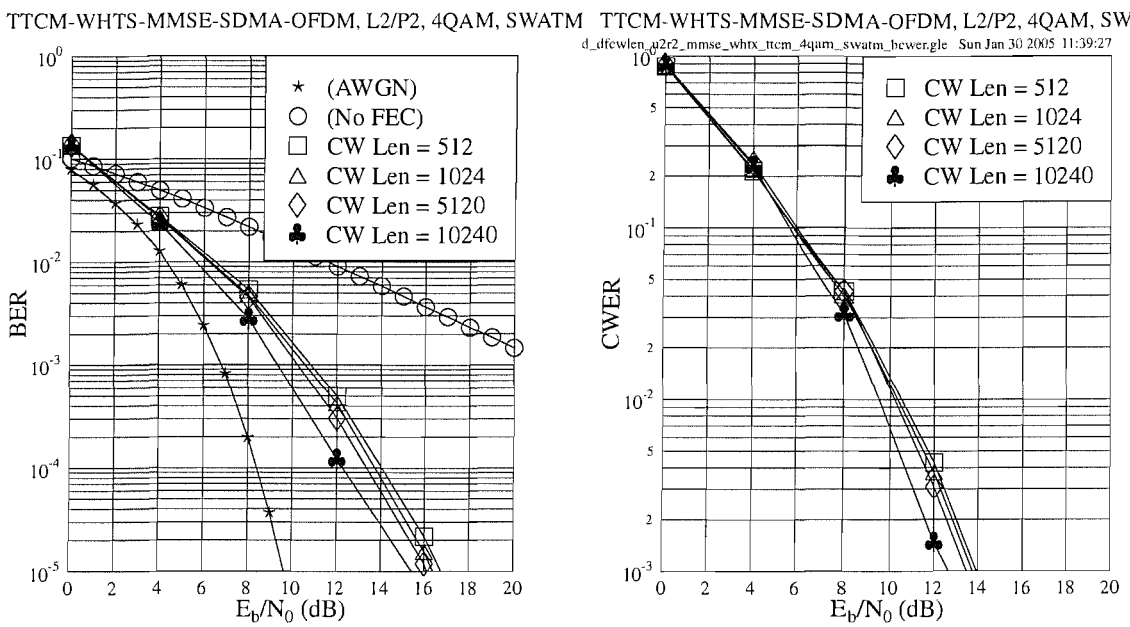

Figure 3.9: **BER (left)** and **CWER (right)** versus E_b/N_0 performance of the **TTCM- and WHTS-assisted MMSE-SDMA-OFDM** system employing a 4QAM scheme for transmission over the **SWATM** channel, where **L=2** users are supported with the aid of **P=2** receiver antenna elements. The TTCM parameters are given in Table 3.1, although a range of **different codeword lengths** is employed. The WHT block size used is **32**.

elements, and thus supporting a higher number of simultaneous users.

Figures 3.10 and 3.11 show the BER and CWER performance achieved by the CM- and WHTS-aided MMSE-SDMA-OFDM schemes in the scenario, where there are four receivers supporting a maximum number of four users. The BER performance of the 32-state TC code assisted MMSE-SDMA-OFDM [3] system is also provided as a reference. As seen in Figure 3.10, similar to the two-receiver scenario of Figure 3.8, the TC-assisted arrangement and the various CM-aided schemes achieve a similar BER performance at a specific user load. However, again, the TTCM-aided scheme stands out of all CM-aided schemes by attaining a better CWER performance.

Furthermore, comparing Figure 3.8 to Figure 3.10, where there are two receivers supporting a maximum of two users, we find that at the same user load level, for example at $\alpha_4 = \alpha_2 = 0.5$ or $\alpha_4 = \alpha_2 = 1.0$, the E_b/N_0 performance achieved by the four-receiver system is approximately 4.5dB better than that of the two-receiver system, provided that the same CM-assisted scheme is used. This is because, when the number of the BS receiver antenna elements is increased, the SDMA-MIMO system becomes capable of providing a higher diversity gain, which may be expected to improve the system's performance for each user.

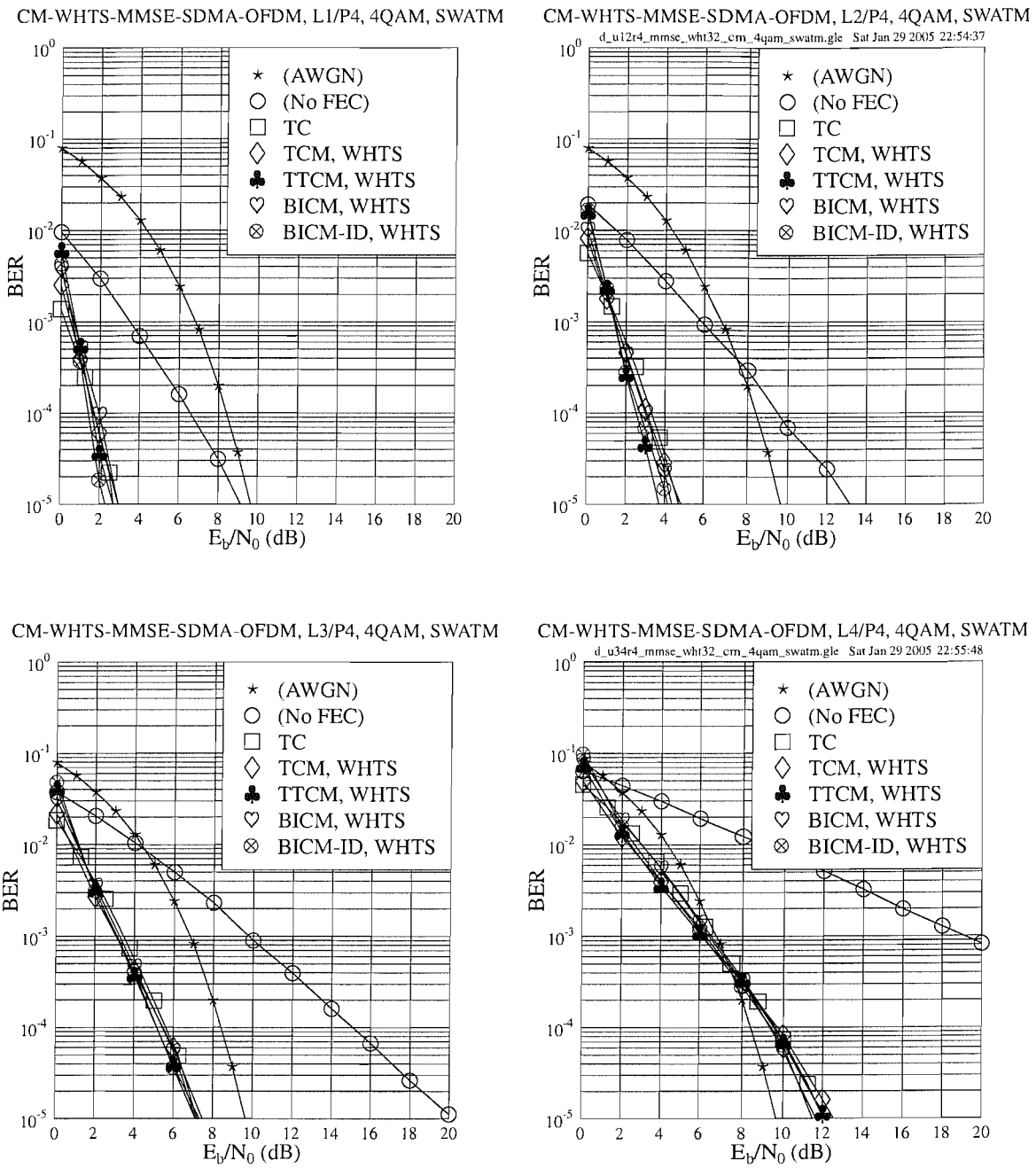

Figure 3.10: **BER** versus E_b/N_0 performance of the **CM- and WHTS-assisted MMSE-SDMA-OFDM** system employing a 4QAM scheme for transmission over the **SWATM** channel, where **L=1 (top left)**, **L=2 (top right)**, **L=3 (bottom left)** or **L=4 (bottom right)** users are supported with the aid of **P=4** receiver antenna elements. The CM parameters are given in Table 3.1. The CM codeword length is **1024** symbols and the WHT block size used is **32**. The BER performance of the 4QAM MMSE-SDMA-OFDM system assisted by the half-rate TC code [3] (the curves with the legend of □) is also provided for reference.

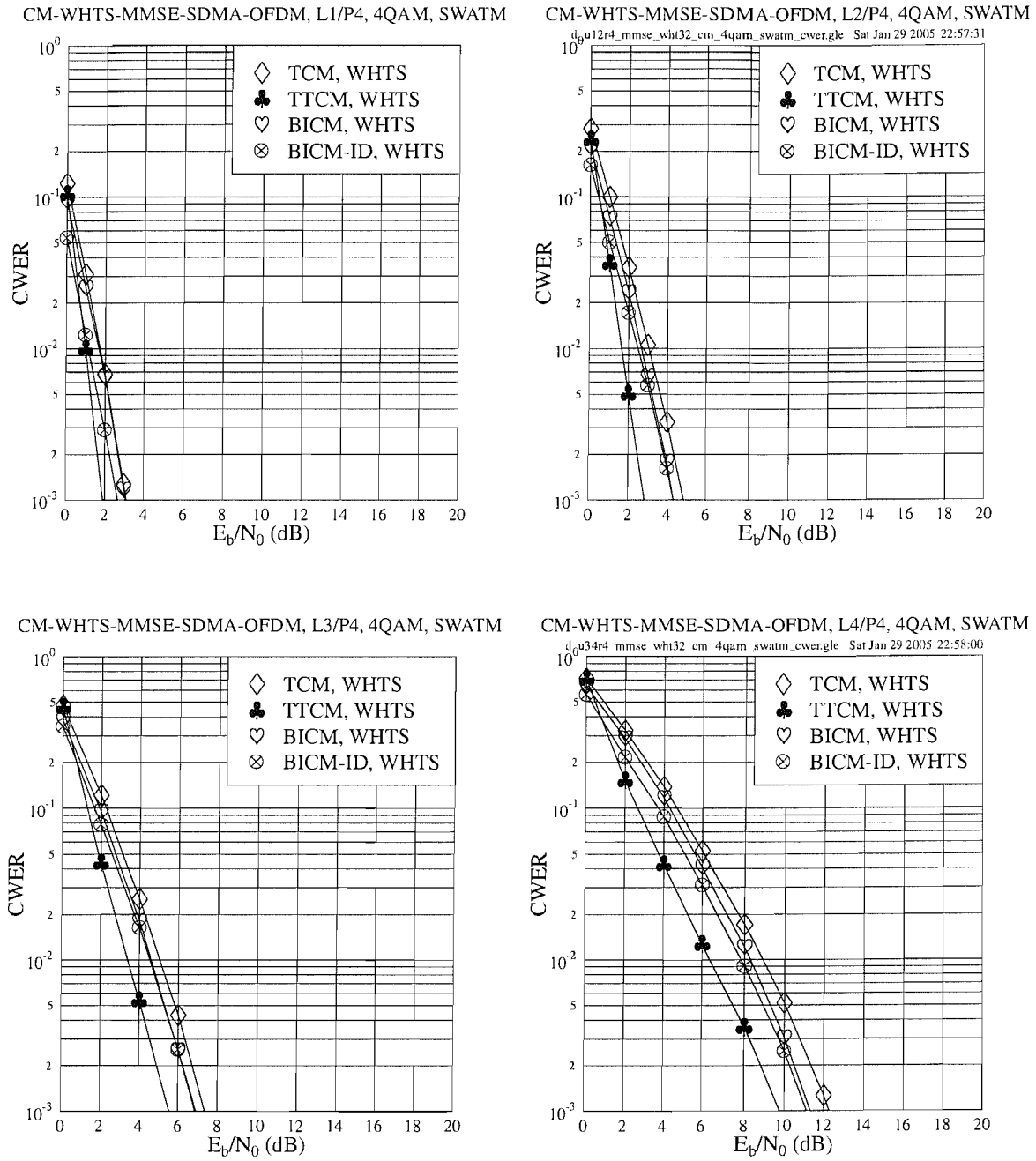

Figure 3.11: **CWER** versus E_b/N_0 performance of the **CM- and WHTS-assisted MMSE-SDMA-OFDM** system employing a 4QAM scheme for transmission over the **SWATM** channel, where **L=1 (top left)**, **L=2 (top right)**, **L=3 (bottom left)** or **L=4 (bottom right)** users are supported with the aid of **P=4** receiver antenna elements. The CM parameters are given in Table 3.1. The CM codeword length is **1024** symbols and the WHT block size used is **32**.

3.3.2.2 Performance Over the COST207 HT Channel

In this section, we will investigate the performance of the CM- and WHTS-assisted MMSE-SDMA-OFDM schemes, while communicating over a more dispersive channel, namely over the 12-path COST207 [310] Hilly Terrain (HT) channel. The impulse response of the channel model is portrayed in Figure 3.12, while the specific channel parameters are given in Table 3.2. Each of the twelve paths experiences independent Rayleigh fading having the same normalized Doppler frequency of $f'_d = 1.0 \times 10^{-5}$. Compared to the 512-subcarrier OFDM modem used for communication over the SWATM channel investigated in Section 3.3.2.1, we now employ a higher number of 2048 subcarriers and a cyclic prefix of 256, since the maximum path delay of the COST207 HT channel is longer than that of the SWATM channel, hence it requires a longer cyclic prefix for combatting the effects of Inter-Symbol Interference (ISI) [3, 31].

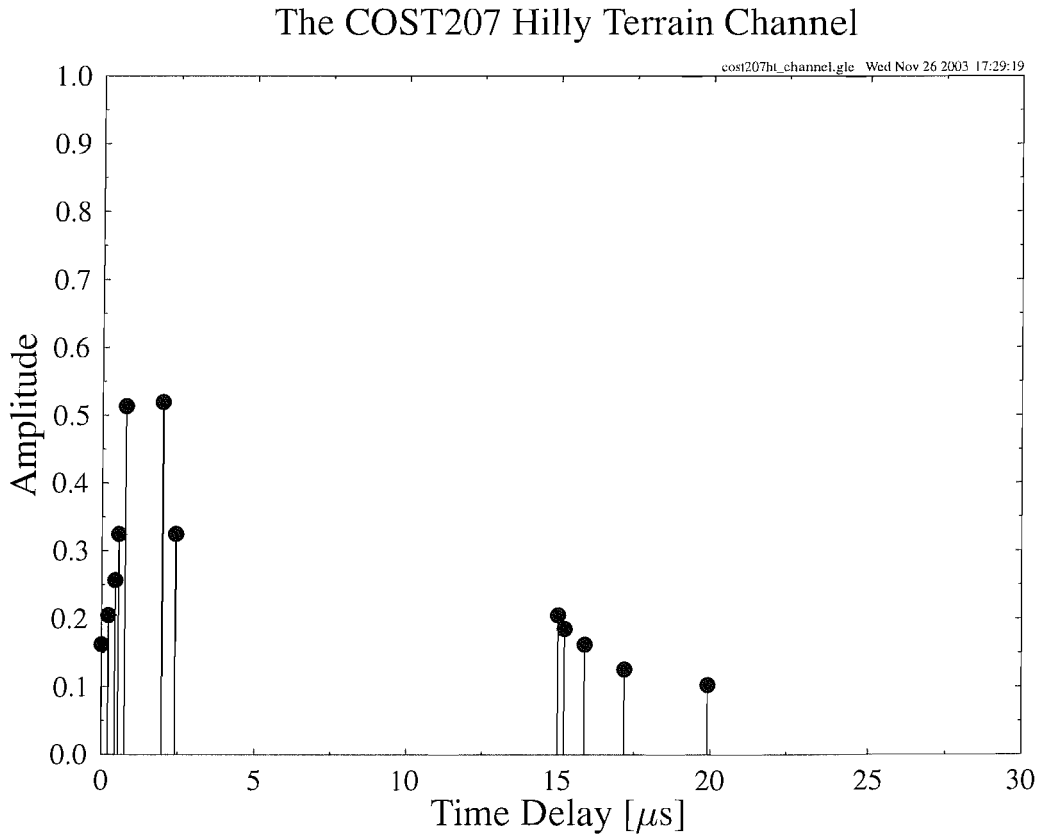

Figure 3.12: COST207 Hilly Terrain (HT) channel impulse response. The corresponding parameters of the channel are summarized in Table 3.2.

In Sections 3.3.2.2.1 and 3.3.2.2.2, we will compare the corresponding performance of the various CM- and WHTS-assisted MMSE-SDMA-OFDM schemes, when communicating over the COST207 HT channel. The parameters of the CM schemes used are summarized in Table 3.3.

$1/T_s$	τ_{max}	f_d	f'_d	n	K	cp
9.14 MHz	19.9 μs	92.6 Hz	1.0×10^{-5}	12	2048	256

Table 3.2: Sampling Rate $1/T_s$, maximum path delay τ_{max}, maximum Doppler frequency f_d, normalized Doppler frequency f'_d, number of paths n, FFT length K and cyclic prefix length cp of the COST207 Hilly Terrain (HT) channel of Figure 3.12.

CM Scheme	Code Rate	Data Bits	Parity Bits	Code Memory	Iterations	Codeword Length	Modem
TCM	1/2	1	1	6	-	2048	4QAM
TTCM	1/2	1	1	3	4	2048	4QAM
BICM	1/2	1	1	6	-	2048	4QAM
BICMID	1/2	1	1	3	8	2048	4QAM

Table 3.3: The parameters of the various CM schemes used in the multi-user SDMA-OFDM system communicating over the COST207 HT channel of Figure 3.12.

3.3.2.2.1 Two Receiver Antenna Elements

We present the BER and CWER performance of the CM-assisted MMSE-SDMA-OFDM system dispensing with WHTS for transmission over the COST207 HT channel at the top of Figures 3.13 and 3.14, respectively. Two receiver antenna elements are employed for supporting a maximum of two users. The simulation results show that the TTCM-aided scheme constitutes the best design option in terms of both the BER and CWER, attaining a coding gain ranging from 2dB to 4dB over the other three CM-aided schemes at the BER of 10^{-5} without the assistance of WHTS. Furthermore, when WHTS is incorporated into the CM-MMSE-SDMA-OFDM system, as seen in the bottom of Figures 3.13 and 3.14, a further useful E_b/N_0 gain is achieved by most of the four schemes, especially by the TCM-aided arrangement. However, recall that in Section 3.3.2.1 where the SWATM channel was employed, the additional E_b/N_0 gain achieved by spreading in the context of the various CM- and WHTS-assisted schemes was rather modest. This result may suggest that in highly dispersive environments, such as that characterized by the 12-path COST207 HT channel, the channel-coded SDMA-OFDM system's performance may be further improved by employing WHTS. This spreading-induced E_b/N_0 gain was achieved, because the detrimental effects imposed on the system's average BER performance by the deeply-faded subcarriers has been spread over the entire WHT block, and these randomized or dispersed channel errors may be more readily corrected by the CM decoders.

It transpires from Figures 3.13 and 3.14 that the four CM-aided schemes communicating

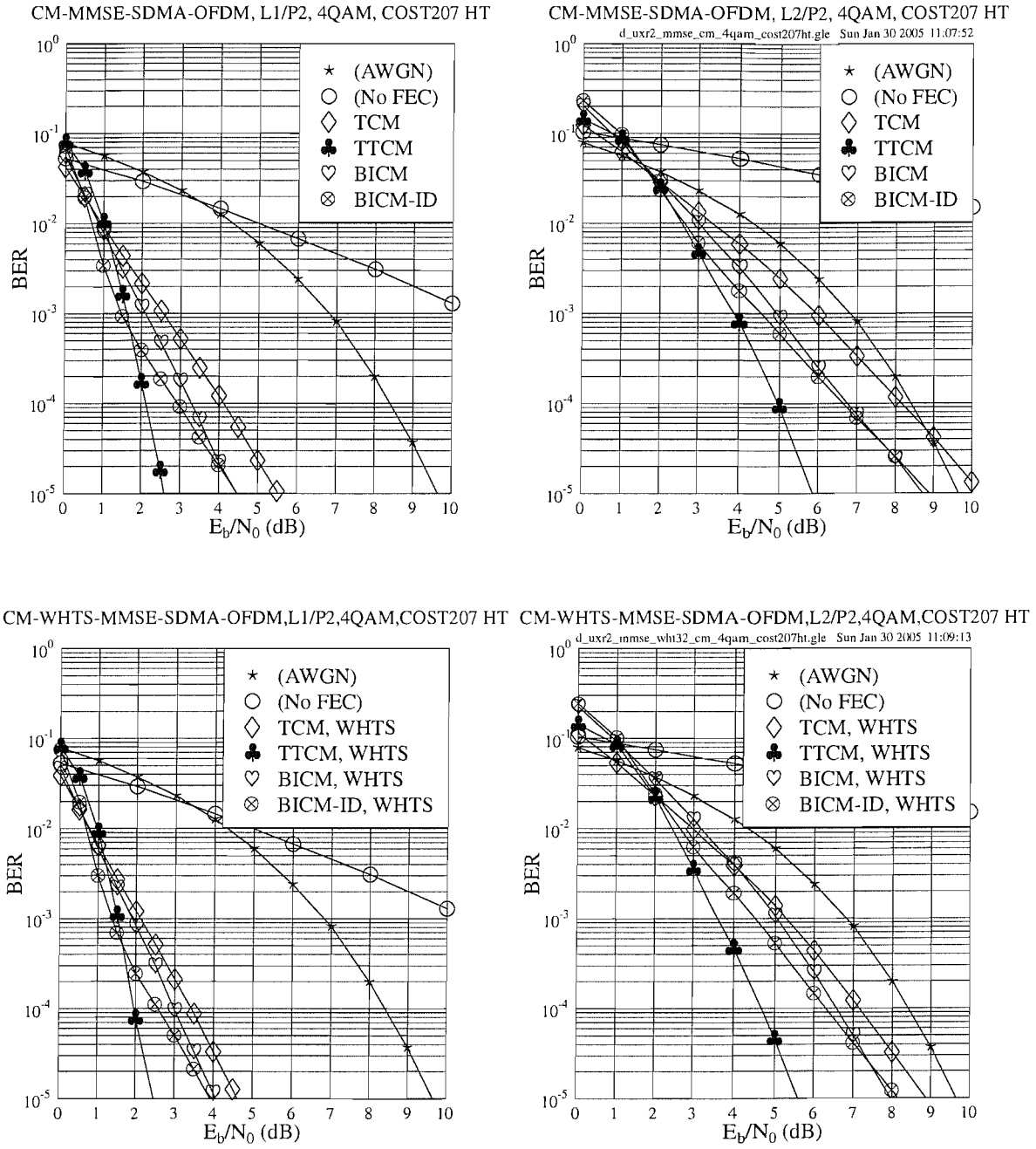

Figure 3.13: **BER** versus E_b/N_0 performance of the **CM-assisted MMSE-SDMA-OFDM (top)** and **CM- and WHTS-assisted MMSE-SDMA-OFDM (bottom)** systems employing a 4QAM scheme for transmission over the **COST207 HT** channel, where **L=1 (left)** or **L=2 (right)** users are supported with the aid of **P=2** receiver antenna elements. The CM parameters are given in Table 3.3. The CM codeword length is **2048** symbols and the WHT block size used is **32**.

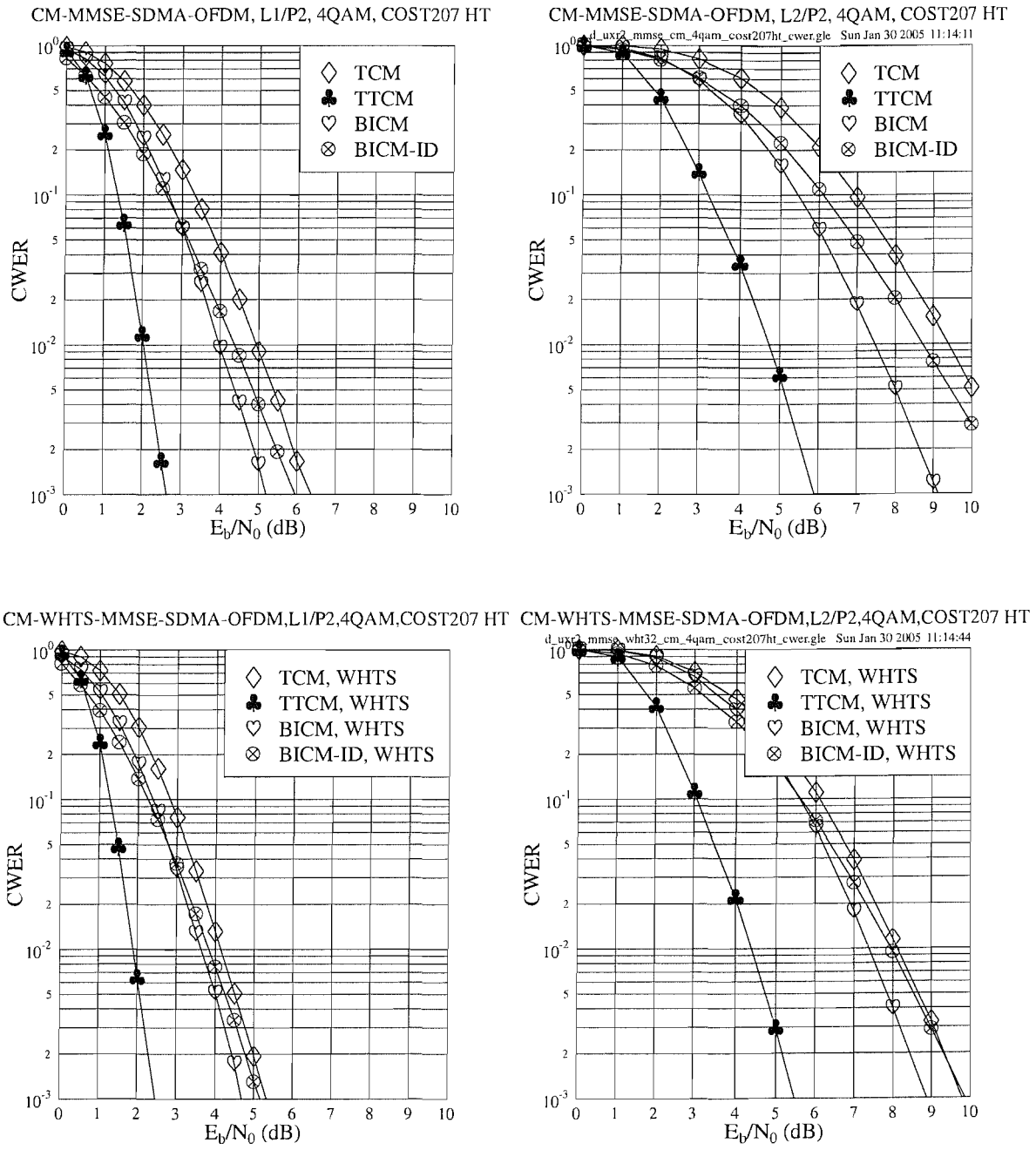

Figure 3.14: **CWER** versus E_b/N_0 performance of the **CM-assisted MMSE-SDMA-OFDM (top)** and **CM- and WHTS-assisted MMSE-SDMA-OFDM (bottom)** systems employing a 4QAM scheme for transmission over the **COST207 HT** channel, where **L=1 (left)** or **L=2 (right)** users are supported with the aid of **P=2** receiver antenna elements. The CM parameters are given in Table 3.3. The CM codeword length is **2048** symbols and the WHT block size used is **32**.

over the COST207 HT channel attain a different performance. This observation is different from what was noted in Figures 3.6 and 3.8, where the performance of the various CM-aided schemes communicating over the SWATM channel was more similar. The reason for this phenomenon is that the amplitude variation of the FD-CHTFs becomes both more frequent and more dramatic, when the channel exhibits a longer path delay [2]. Since the COST207 HT channel's maximum path delay is $19.9\mu s$, which is significantly longer than the $48.9ns$ maximum dispersion of the SWATM channel, the fades occur more frequently in the FD-CHTF of the COST207 HT channel, as indicated by Figure 3.15. Apparently, in the COST207 HT channel displayed at the left hand side of Figure 3.15, the frequency domain separation between the neighbouring fades is proportionately lower than that in the SWATM channel shown at the right side of Figure 3.15. This characteristic will result in more uniformly distributed corrupted subcarrier symbols which can be more readily corrected by the channel codes. More specifically, when a deep fade occurs in the FD-CHTF of the SWATM channel, a number of consecutive subcarriers which are located in the corresponding faded block of subcarriers may be seriously affected by the fade.

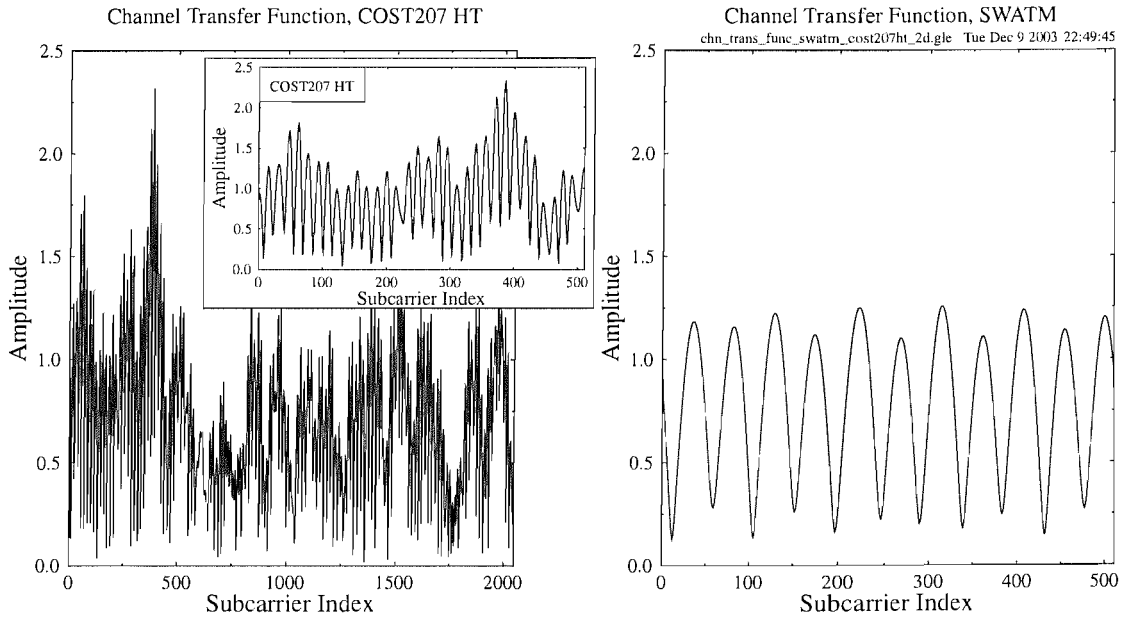

Figure 3.15: The FD-CHTF amplitudes of the **COST207 HT (left)** and **SWATM (right)** channels plotted for the duration of one OFDM symbol.

This implies that the channel codes, for example one of the four CM schemes, may have a lower chance of correcting less-frequently occurring but prolonged error bursts, than more frequently encountered isolated errors. The more prolonged error bursts imposed by the SWATM channel often overload the error correction capability of the CM schemes, regardless

of which of the four CM schemes is used, since owing to the preponderance of transmission errors their trellis decoder often opts for choosing the wrong trellis path. This is particularly true for CM schemes using short channel interleavers. Therefore, this phenomenon results in a similar performance for the various CM-aided schemes, when communicating over the SWATM channel, as seen in Figures 3.6 and 3.8.

By contrast, in the context of the COST207 HT channel such prolonged error bursts are unlikely to occur, since the faded subcarriers result in more frequent but less prolonged error bursts, which are reminiscent of the error distributions experienced in AWGN channels and therefore may have a higher chance of being corrected by the CM decoders used at the receiver. Hence, the different error-correcting capability of the various CM schemes becomes more explicit, as revealed in Figures 3.13 and 3.14.

3.3.2.2.2 Four Receiver Antenna Elements

As mentioned in Section 3.3.2.1.2, when the number of receiver antenna elements is increased to four, the performance of the system becomes better, than that experienced in the two-receiver scenario, which was discussed in Section 3.3.2.2.1. In Figures 3.16 and 3.17, we compare both the BER and CWER performance of the different CM- and WHTS-assisted schemes for transmissions over the COST207 HT channel, while employing four receiver antenna elements at user loads of $\alpha_4 = 0.5$ and $\alpha_4 = 1.0$, as shown at the left and right hand sides of Figures 3.16 and 3.17, respectively. Again, it can be seen in the figures that the performance achieved by the four-receiver SDMA-OFDM system, which has a higher diversity order, is better than that attained by the two-receiver system both at the user loads of $\alpha_{2,4} = 0.5$ and $\alpha_{2,4} = 1.0$, averaging at an approximately 3dB E_b/N_0 improvement for a specific CM-aided scheme. Hence a plausible conclusion is that at a specific user load α_P, the more receivers the SDMA-MIMO system employs, the higher attainable grade of diversity and thus an improved performance may be achieved. However, the relative performance improvement achieved by an already high-order system upon doubling the number of receivers is expected to be lower than that in a lower-order system, since most of the attainable gain may have already been achieved, which results in a near-Gaussian performance.

3.3.2.2.3 Performance Comparisons

Table 3.4 summarizes the E_b/N_0 values required by the various CM- and WHTS-assisted MMSE-SDMA-OFDM schemes for achieving a BER of 10^{-5}. The corresponding spreading-induced E_b/N_0 gains achieved by the WHTS-assisted schemes are also provided, which are defined as the E_b/N_0 difference, expressed in terms of dBs, at a BER of 10^{-5} between the

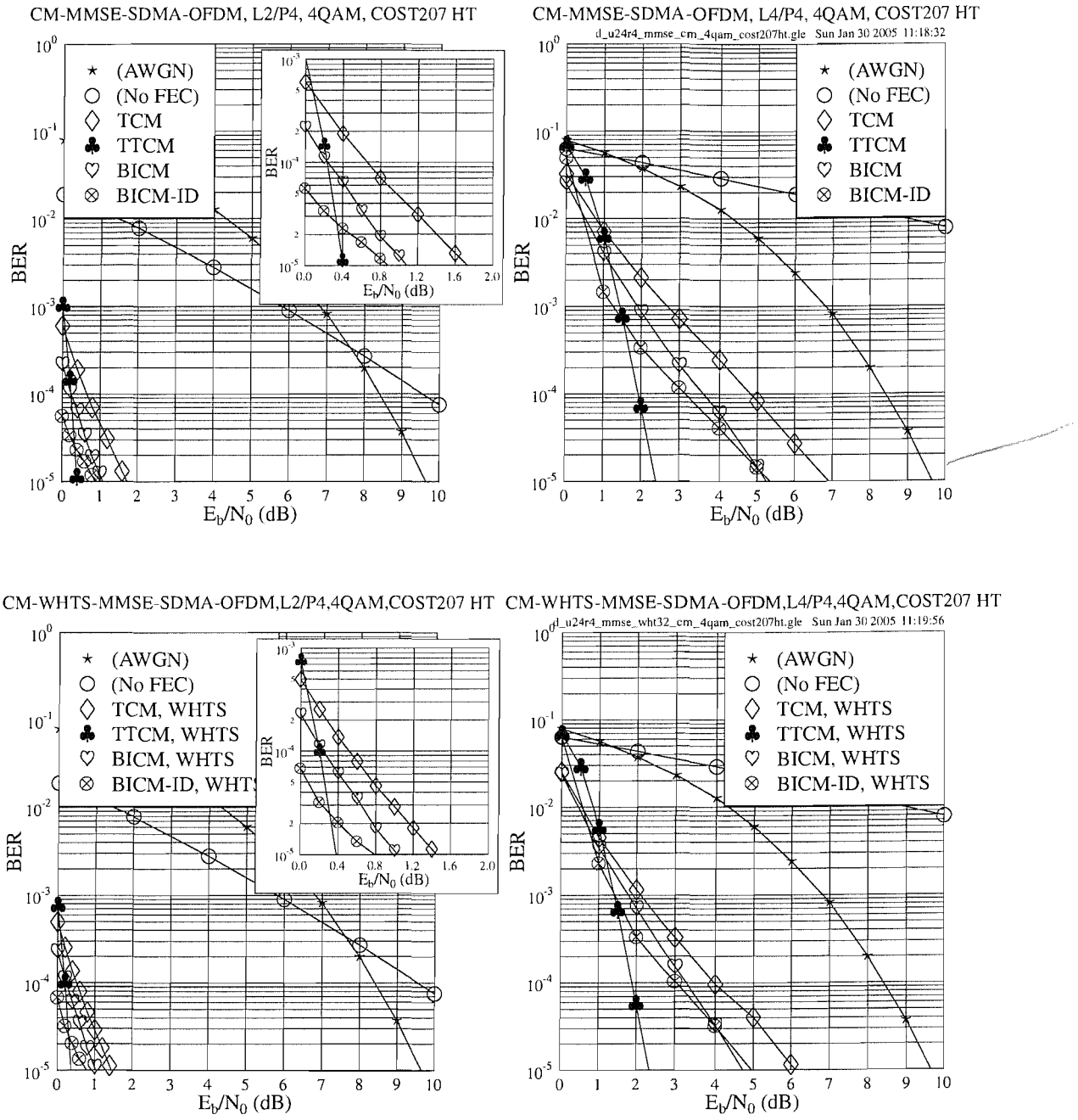

Figure 3.16: **BER** versus E_b/N_0 performance of the **CM-assisted MMSE-SDMA-OFDM (top)** and **CM- and WHTS-assisted MMSE-SDMA-OFDM (bottom)** systems employing a 4QAM scheme for transmission over the **COST207 HT** channel, where **L=2 (left)** or **L=4 (right)** users are supported with the aid of **P=4** receiver antenna elements. The CM parameters are given in Table 3.3. The CM codeword length is **2048** symbols and the WHT block size used is **32**.

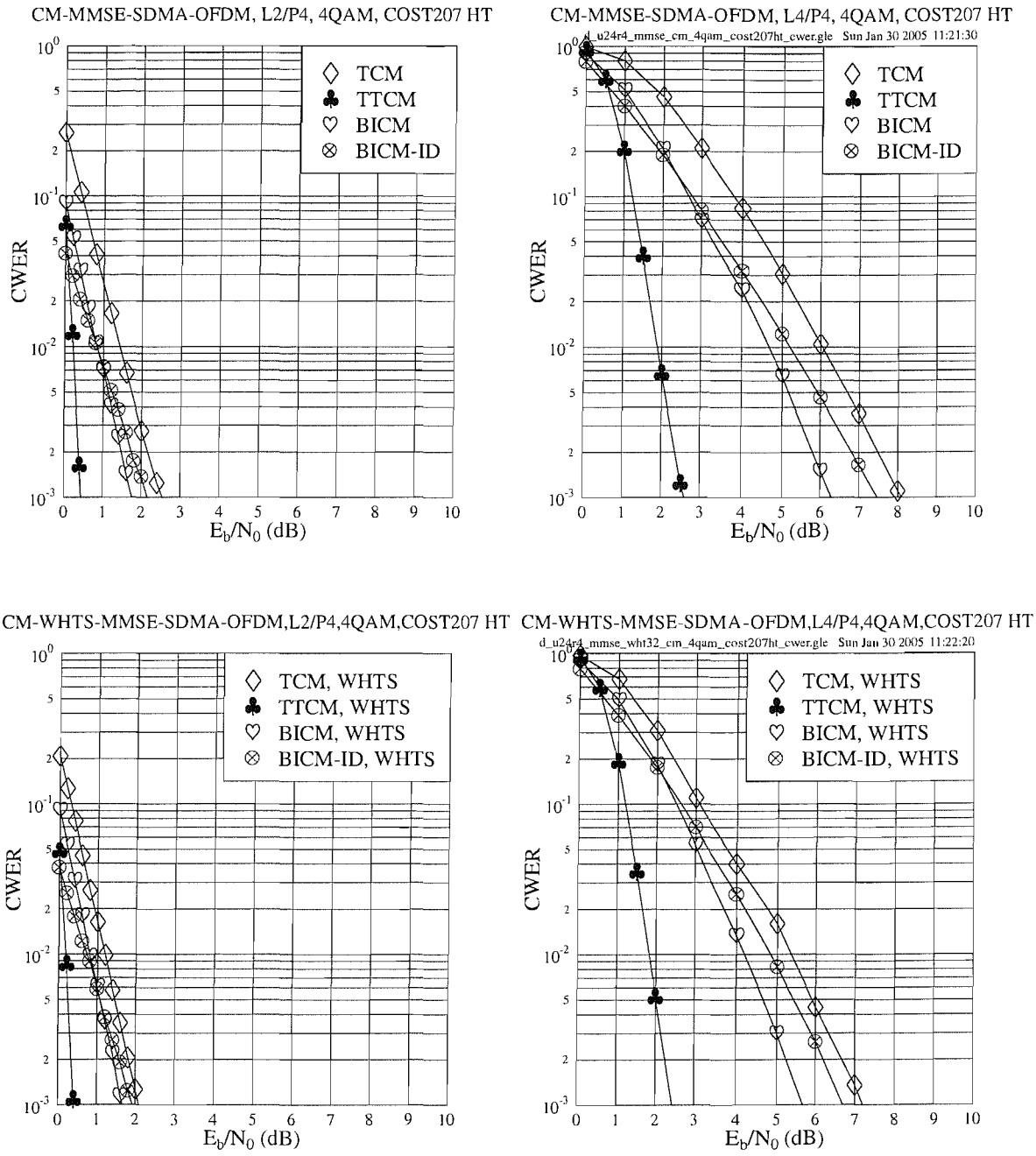

Figure 3.17: **CWER** versus E_b/N_0 performance of the **CM-assisted MMSE-SDMA-OFDM (top)** and **CM- and WHTS-assisted MMSE-SDMA-OFDM (bottom)** systems employing a 4QAM scheme for transmission over the **COST207 HT** channel, where **L=2 (left)** or **L=4 (right)** users are supported with the aid of **P=4** receiver antenna elements. The CM parameters are given in Table 3.3. The CM codeword length is **2048** symbols and the WHT block size used is **32**.

CM Schemes	Spreading	$\alpha_{2,4} = 0.5$		$\alpha_{2,4} = 1.0$	
		U1R2	U2R4	U2R2	U4R4
(No FEC)	No WHTS	20.85	12.99	41.97	38.85
	WHTS	14.53	9.53	23.30	20.78
	E_b/N_0 Gain	**6.32**	**3.46**	**18.67**	**18.07**
TCM	No WHTS	5.53	1.73	10.28	6.91
	WHTS	4.62	1.45	8.88	6.11
	E_b/N_0 Gain	**0.91**	**0.28**	**1.40**	**0.80**
TTCM	No WHTS	2.60	0.41	5.87	2.41
	WHTS	2.47	0.38	5.61	2.35
	E_b/N_0 Gain	**0.13**	**0.03**	**0.26**	**0.06**
BICM	No WHTS	4.47	1.08	8.72	5.25
	WHTS	4.06	1.03	7.97	4.73
	E_b/N_0 Gain	**0.41**	**0.05**	**0.75**	**0.52**
BICM-ID	No WHTS	4.48	0.88	8.89	5.35
	WHTS	3.92	0.79	8.15	4.96
	E_b/N_0 Gain	**0.56**	**0.09**	**0.74**	**0.39**

Table 3.4: The E_b/N_0 values required and the spreading-induced gains achieved at the BER of 10^{-5} of the various CM- and WHTS-assisted MMSE-SDMA-OFDM schemes for communicating over the COST207 HT channel. The CM parameters are given in Table 3.3. The CM codeword length is 2048 symbols and the WHT block size used is 32. All data are in dB.

WHTS-assisted and the unspreading system having the same effective throughput.

Several useful points can be concluded from Table 3.4. Firstly, when we have a specific user load, the spreading-induced E_b/N_0 gain achieved by a system having a lower diversity order is higher, regardless whether CM is employed or not. For example, when we have a user load of $\alpha_{2,4} = 0.5$, the spreading-induced E_b/N_0 gains achieved in the No-FEC-, TCM-, TTCM-, BICM- and BICM-ID-assisted two-receiver systems are 6.32, 0.91, 0.13, 0.41 and 0.56dB, respectively. By contrast, lower spreading-induced E_b/N_0 gains of 3.46, 0.28, 0.03, 0.05 and 0.09dB are achieved in the corresponding four-receiver systems, respectively. In other words, in relatively lower diversity-order scenarios, the subcarrier-based WHTS technique may be expected to attain a higher system performance improvement.

Furthermore, if the number of users supported is fixed but the number of receiver antenna elements is varied, similar conclusions may be drawn. When there are two simultaneous users, for example, the spreading-induced E_b/N_0 gains achieved in the two-receiver scenario, are higher than those achieved in the four-receiver scenario, as observed in Table 3.4. A

plausible explanation for this fact may be as follows. In the SDMA-MIMO system, when a higher number of receiver antenna elements is employed, a potentially higher space diversity can be achieved. In this scenario, the benefits of spreading may be less substantial, especially in the CM-aided system, since most of the attainable gain has already been achieved by using the channel codes.

Secondly, when the BS employs a given number of receiver antenna elements, the spreading-induced E_b/N_0 gains achieved in the context of the fully-loaded systems are higher than in the half-loaded systems, regardless of the employment of channel codes. For instance, if we have two receivers installed in the BS, the various schemes having a user load of $\alpha_2 = 1.0$ attain a higher spreading-induced E_b/N_0 gain, than their half-loaded counterparts, as seen in Table 3.4. This suggests that more benefits may arise from WHTS, especially in the fully-loaded scenarios, where the MUD suffers from a relatively low efficiency in differentiating the different users' signals. Furthermore, if a longer WHT block size is used, the E_b/N_0 gain of WHTS may even be higher, since the detrimental bursty error effects degrading the system's average BER performance will be spread over a higher block length, hence increasing the chances of correcting a higher number of errors, as it will be presented in Section 3.3.2.3.

In order to characterize the system's performance at different user loads, as an example, we portray the BER performance of the TTCM- and WHTS-aided scheme at a range of different user loads in Figure 3.18. As expected, the system's performance improves, when the user load is lower, since the MUD will have a better chance of separating the different users' signals. It is also observed in Figure 3.18 that the relevant E_b/N_0 gain achieved by a lower-load scheme over a higher-load arrangement reduces, when the user load decreases. This again shows that most of the achievable E_b/N_0 gain has already been attained at a medium user load.

Figure 3.19 shows the E_b/N_0 crossing points of the various CM-WHTS-MMSE-SDMA-OFDM schemes at the BER of 10^{-5}. It is shown explicitly that the performance gap between the different CM-aided schemes increases as the user load increases. Furthermore, from Figure 3.19 we see that the TTCM-aided scheme performs best in high user-load scenarios, namely for $\alpha_4 \geq 0.5$. In other words, the other three CM schemes, namely the TCM, BICM and BICM-ID arrangements will suffer a higher performance degradation than TTCM, when the MUD's user-separation capability erodes owing to the increased MUI.

In Figure 3.20 we compare the total gain achieved by the four different CM-aided schemes, which includes both the coding gain and the spreading-induced E_b/N_0 gain. As the figure indicates, the TTCM-aided scheme achieved a further E_b/N_0 gain of 3.76dB, 2.38dB and 2.61dB over the TCM, BICM and BICM-ID aided schemes in the fully-loaded scenario, respectively. At a relatively low user load, namely for $\alpha_4 \leq 0.5$, the various schemes provide a similar performance, because most of the attainable gain in the four-receiver SDMA-OFDM system

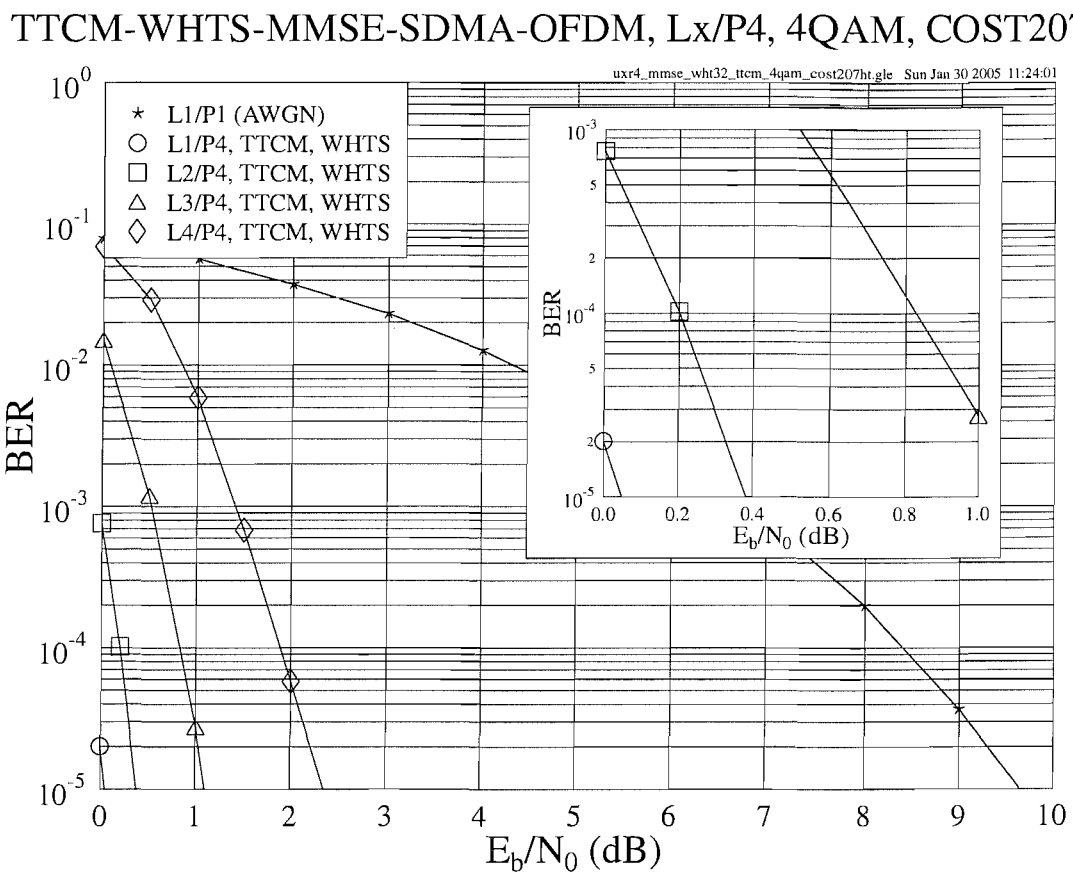

Figure 3.18: **BER** versus E_b/N_0 performance of the **TTCM- and WHTS-assisted MMSE-SDMA-OFDM** system employing a 4QAM scheme for transmission over the **COST207 HT** channel, where **L=1, 2, 3, 4** users are supported with the aid of **P=4** receiver antenna elements. The TTCM parameters are given in Table 3.3. The TTCM codeword length is **2048** symbols and the WHT block size used is **32**.

has already been achieved, as discussed earlier in this section.

3.3.2.3 Effects of the WHT Block Size

In Sections 3.3.2.1 and 3.3.2.2 we have investigated the CM- and WHTS-assisted MMSE-SDMA-OFDM system for transmission over the SWATM and COST207 HT channel, respectively. In this section, we will study how the variation of the WHT block size affects the system's performance, when communicating over the above two channel models.

As mentioned in Section 3.3.2.2.3, when a larger WHT block size is used for the SDMA-OFDM system, the system's performance may potentially be improved, since the signals carried by the subcarriers that are badly-affected by deep channel fades could be spread over a larger set of subcarriers, which may mitigate the detrimental channel effects and thus

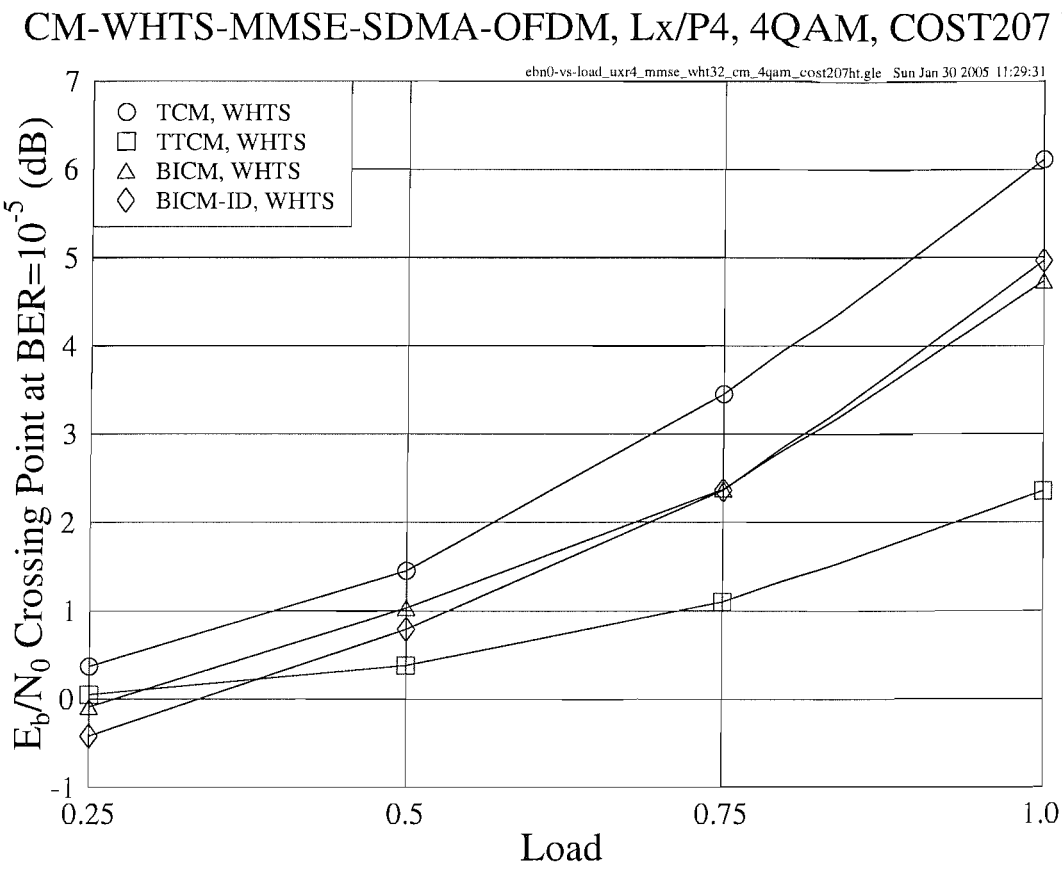

Figure 3.19: **E_b/N_0 Crossing Point** at the BER of 10^{-5} versus user load performance of the **CM- and WHTS-assisted MMSE-SDMA-OFDM** system employing a 4QAM scheme for transmission over the **COST207 HT** channel, where **L=1, 2, 3, 4** users are supported with the aid of **P=4** receiver antenna elements. The CM parameters are given in Table 3.3. The CM codeword length is **2048** symbols and the WHT block size used is **32**.

assists the receiver in achieving a better performance. In order to show the effects imposed by different-length WHTS schemes, we provide simulation results generated in the context of different WHT block sizes in both the No-CM and CM-aided scenarios, as shown in the left and right hand sides of Figure 3.21, respectively. As expected, the system's performance was improved upon increasing the WHT block size, regardless whether CM was employed or not. In the context of the COST207 HT channel of Figure 3.12, similarly, a performance improvement is observed, when an increased WHT block size is employed as portrayed in Figure 3.22.

Furthermore, we may notice that the spreading-induced E_b/N_0 gains achieved by the No-CM schemes, when using a larger WHT block size, are significantly higher than those attained by the TTCM-aided schemes, as observed in Figures 3.21 and 3.22. This suggests that in the SDMA-OFDM system employing no CM, the performance improvement potential

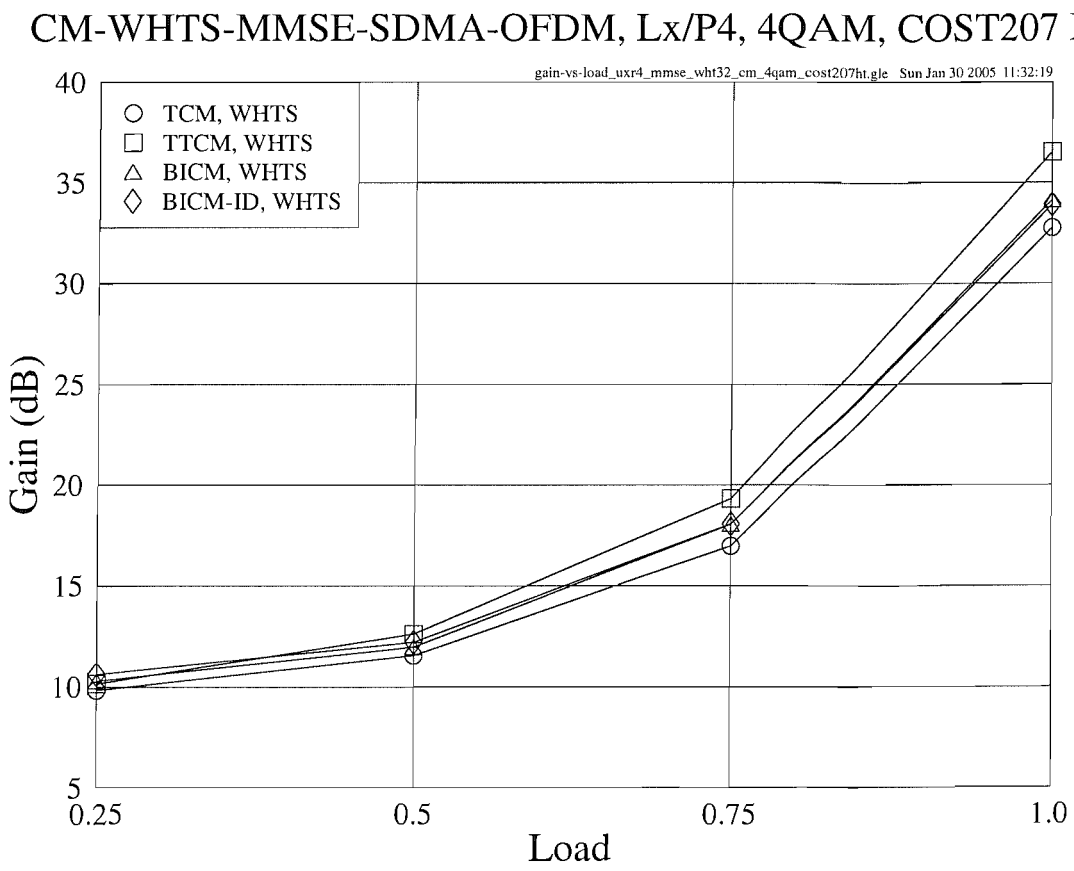

Figure 3.20: **Gain** at the BER of 10^{-5} versus user load performance of the **CM- and WHTS-assisted MMSE-SDMA-OFDM** system employing a 4QAM scheme for transmission over the **COST207 HT** channel, where **L=1, 2, 3, 4** users are supported with the aid of **P=4** receiver antenna elements. The CM parameters are given in Table 3.3. The CM codeword length is **2048** symbols and the WHT block size used is **32**.

owing to the employment of a larger WHT block size is higher than that in the CM-aided system, where most of the achievable diversity gain has been attained by the time-diversity of the CM schemes. However, as suggested by Table 3.2, the other three CM-aided schemes, for example the TCM-aided arrangement, may be capable of achieving a higher spreading-induced gain than the TTCM-aided scheme with the aid of WHTS. Therefore, owing to their lower time-diversity and relatively more modest unspread performance, a potentially higher spreading-induced E_b/N_0 gain may be achieved by combining WHTS with the TCM, BICM and BICM-ID assisted schemes than in conjunction with the TTCM-aided arrangement, when a larger WHT block size is used. Having studied the effects of different WHT block sizes, let us now consider the impact of varying the Doppler frequency.

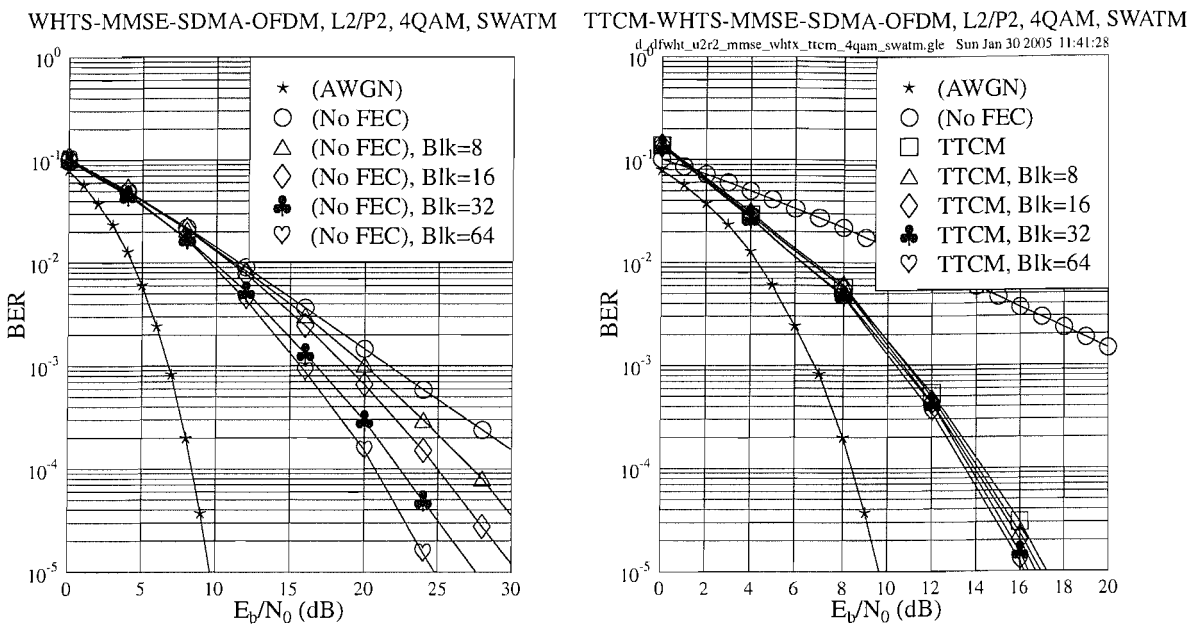

Figure 3.21: **BER** versus E_b/N_0 performance of the **WHTS-assisted MMSE-SDMA-OFDM (left)** and **TTCM- and WHTS-assisted MMSE-SDMA-OFDM (right)** systems using **different WHT block size** and employing a 4QAM scheme for transmission over the **SWATM** channel, where **L=2** users are supported with the aid of **P=2** receiver antenna elements. The TTCM parameters are given in Table 3.1 and the TTCM codeword length is **1024** symbols.

3.3.2.4 Effects of the Doppler Frequency

In our further investigations we have generated the BER versus E_b/N_0 curves of the TTCM- and WHTS-assisted MMSE-SDMA-OFDM system communicating over the COST207 HT channel, when the maximum Doppler frequency was fixed to a range of different values. For simplicity, here we have assumed perfect channel estimation. As before, the CIR of the 12-path COST207 HT channel of Figure 3.12 was used. For the sake of presenting these results in a compact form, the E_b/N_0 values required for maintaining a BER of 10^{-5} were extracted. In Figure 3.23, we show the E_b/N_0 crossing point at BER=10^{-5} versus the maximum Doppler frequency for the WHTS-assisted MMSE-SDMA-OFDM system both with and without the aid of TTCM, where two receivers were used for supporting two users. We conclude from the near-horizontal curves shown in Figure 3.23 that the maximum Doppler frequency does not significantly affect the performance of the WHTS-assisted MMSE-SDMA-OFDM system, regardless of the employment of TTCM. This may be a desirable benefit of the error-randomizing effect of WHTS, resulting in a robustness against the variation of the mobile speed. Moreover, as expected, the performance of the TTCM-aided scheme was consistently better, than that

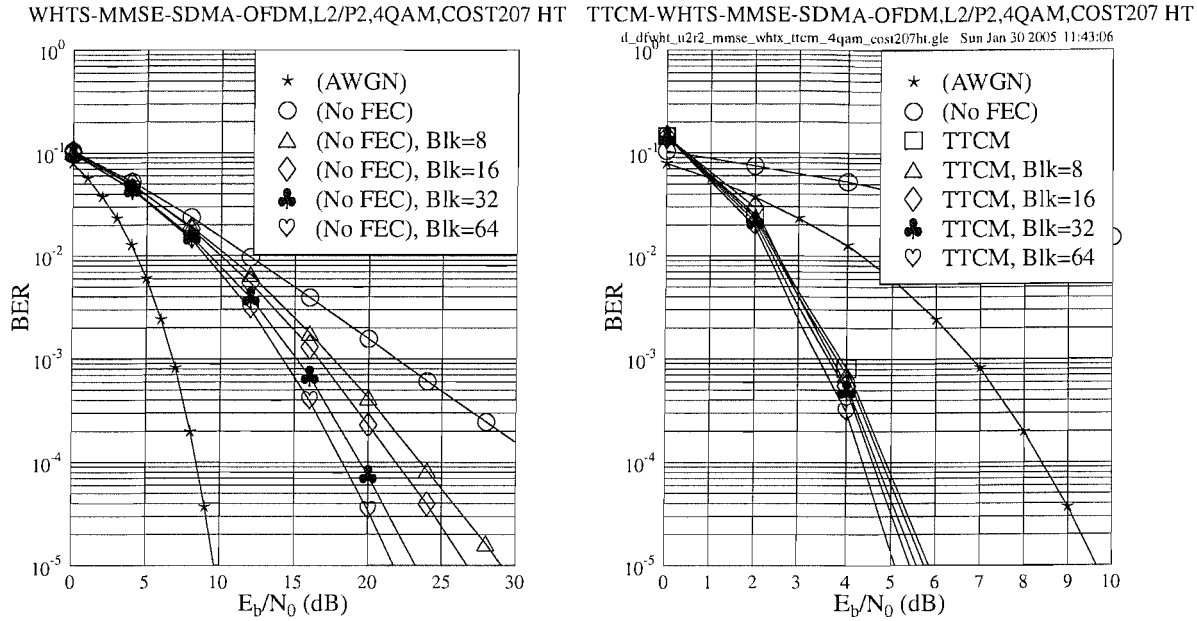

Figure 3.22: **BER** versus E_b/N_0 performance of the **WHTS-assisted MMSE-SDMA-OFDM (left)** and **TTCM- and WHTS-assisted MMSE-SDMA-OFDM (right)** systems using **different WHT block size** and employing a 4QAM scheme for transmission over the **COST207 HT** channel, where **L=2** users are supported with the aid of **P=2** receiver antenna elements. The TTCM parameters are given in Table 3.3 and the TTCM codeword length is **2048** symbols.

of the scheme using no channel coding, as evidenced by Figure 3.23.

It is worth noting that when the channel's Doppler frequency is high, the effects of Inter-Carrier Interference (ICI) may become significant[1], as argued on page 81 of [3]. In this case for example the ICI-cancellation techniques of Chapter 4 in [3] may be invoked for combating the ICI effects.

3.4 Chapter Summary

The system model of our multi-user uplink SDMA-based OFDM system was presented in Section 3.2, where the SDMA-MIMO channel model was introduced in Section 3.2.1, followed by the detailed description of the CM-assisted multi-user SDMA-OFDM system employing

[1]Since the ICI is caused by the variation of the channel impulse response during the transmission of each OFDM symbol, we introduce the OFDM-symbol-normalized Doppler frequency F_d [3]. In the case of a maximum Doppler frequency of 200Hz, for example, the corresponding OFDM-symbol-normalized Doppler frequency F_d will become as high as $F_d = f_d \cdot NT_s = f'_d \cdot N = 0.023$, where N is the cyclically-extended OFDM symbol's total duration expressed as $N = K + cp$, while the associated values of f_d, f'_d, T_s, K and cp are given in Table 3.2.

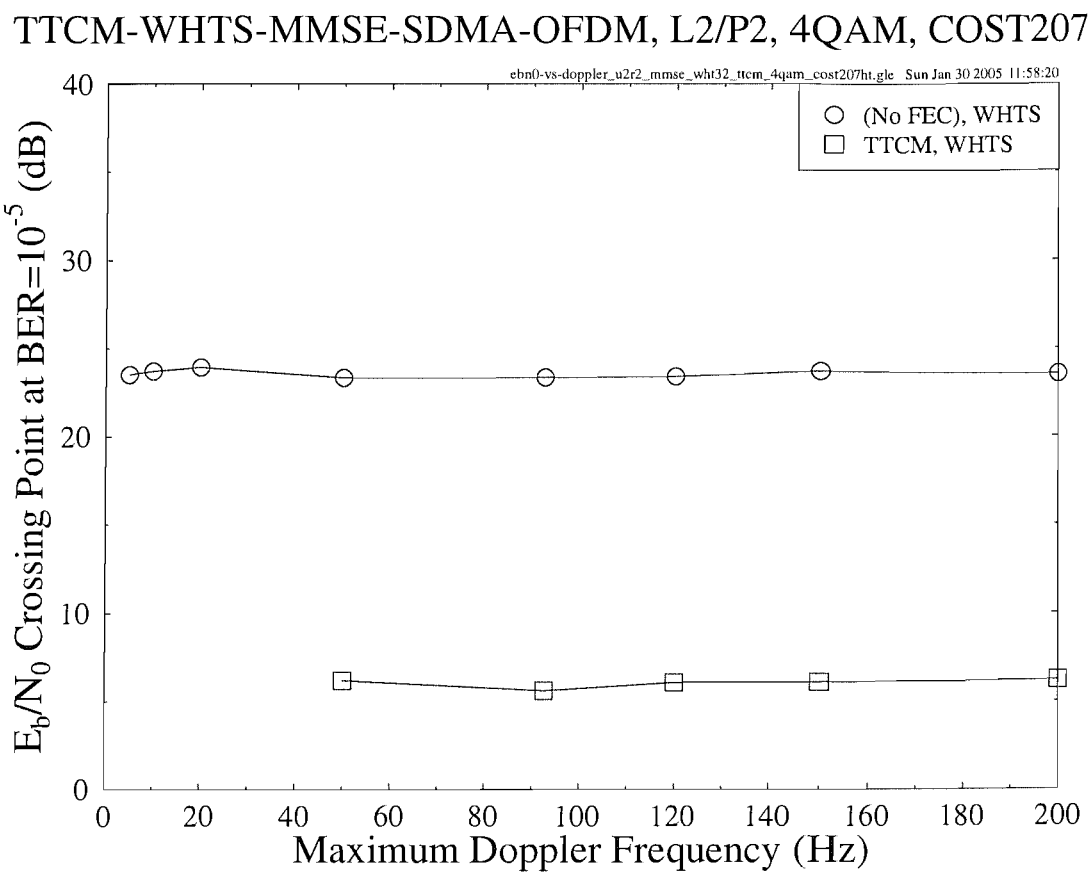

Figure 3.23: **E_b/N_0 Crossing Point** at the BER of 10^{-5} versus maximum Doppler frequency performance of the **TTCM- and WHTS-assisted MMSE-SDMA-OFDM** system employing a 4QAM scheme for transmission over the **COST207 HT** channel, where **L=2** users are supported with the aid of **P=2** receiver antenna elements. The TTCM parameters are given in Table 3.3. The TTCM codeword length is **2048** symbols and the WHT block size used is **32**.

the frequency-domain subcarrier-based WHTS scheme of Section 3.2.2. The theoretical foundations of the Minimum Mean-Square Error based Multi-User Detector were provided in Section 3.2.2.1. Furthermore, a detailed discussion of the WHTS technique was presented in Section 3.2.2.2.

In Section 3.3 the performance of the various CM- and WHTS-assisted MMSE-SDMA-OFDM schemes was studied and compared. The uncoded MMSE-SDMA-OFDM system was first investigated in Section 3.3.1, where it was found that WHTS was capable of improving the system's performance, since the bursty subcarrier errors can be pseudo-randomly spread across the subcarriers of the entire WHT block. In the investigations outlined in Section 3.3.2 our performance comparison among the different CM- and WHTS-assisted MMSE-SDMA-OFDM schemes was detailed. Specifically, the unspread CM-aided SDMA-OFDM system using two receiver antenna elements was studied in Section 3.3.2.1.1, whose performance was compared

to that of the WHTS-assisted system dispensing with the employment of CM. Firstly, it was found that the performance achieved by all half-loaded schemes was better than that attained by the fully-loaded arrangements. This is because, when the user load is lower, the MUD will achieve a higher efficiency in differentiating the different users' transmitted signal, since the multi-user interference is lower. Therefore, the system becomes more efficient in terms of suppressing the detrimental fading channel effects. Secondly, it was also noticed that the achievable performance improvement attained by CM was typically higher than that achieved by WHTS, as evidenced by comparing Figure 3.5 to Figure 3.7.

Furthermore, we combined the MMSE-SDMA-OFDM system with both CM and WHTS in Section 3.3.2.1.1. The corresponding simulation results portrayed in Figure 3.8 showed that the TTCM-aided scheme achieved the best CWER performance among all the CM- and WHTS-assisted schemes considered. Moreover, the comparison of Figure 3.6 and Figure 3.8 suggested that in the CM-aided MMSE-SDMA-OFDM system the employment of WHTS having a block size of 32 subcarriers only insignificantly improved the system's BER and CWER performance, since most of the achievable diversity gain may have already been achieved by the time-diversity of the CM schemes. It was also found that when a higher CM codeword length was used, the system's performance was further improved, as observed in Figure 3.9, since a longer CM codeword is capable of more efficiently dispersing and averaging the bursty error effects.

In Section 3.3.2.1.2, the system's performance evaluated in the four-receiver CM scenarios was compared, when communicating over the SWATM channel of Figure 2.32. Comparing Figure 3.8 to Figure 3.10, we found that at the same user load level, for example at $\alpha_4 = \alpha_2 = 0.5$ or $\alpha_4 = \alpha_2 = 1.0$, the E_b/N_0 performance achieved by the four-receiver system was better than that of the two-receiver system, provided that the same CM-assisted scheme was used. The reason for this phenomenon is that when the SDMA-MIMO system's space-diversity order is increased by employing a higher number of receiver antenna elements, it becomes capable of providing a higher diversity gain, which may be expected to improve the system's performance for each user.

The performance of the various CM- and WHTS-assisted MMSE-SDMA-OFDM systems was evaluated in the context of the COST207 HT channel of Figure 3.12 in Section 3.3.2.2, which included the two- and four-receiver scenarios in Section 3.3.2.2.1 and Section 3.3.2.2.2, respectively. It was found that without the assistance of WHTS the TTCM-aided scheme constituted the best design option in terms of both the BER and CWER in comparison to the other three CM-aided schemes. When WHTS was incorporated into the CM-MMSE-SDMA-OFDM system, a further E_b/N_0 gain was achieved by all the schemes, which was different from the scenario of Section 3.3.2.1 recorded for transmission over the SWATM channel, where

the additional E_b/N_0 gain achieved by WHTS in the context of the various CM- and WHTS-assisted schemes was rather modest. This may suggest that in highly dispersive environments, such as that characterized by the 12-path COST207 HT channel of Figure 3.12, the channel-coded SDMA-OFDM system's performance may be further improved by employing WHTS. This is because the detrimental fading-induced bursty error effects degrading the system's average BER performance owing to the deeply-faded subcarriers can be spread over the entire WHT block, and these dispersed and randomized channel errors may be more readily corrected by the CM decoder.

Furthermore, the four CM-aided schemes communicating over the COST207 HT channel of Figure 3.12 attain a different performance, as shown in Figures 3.13 and 3.14. This conclusion is different from what was noted in Figures 3.6 and 3.8, where the performance of the various CM-aided schemes communicating over the SWATM channel of Figure 2.32 was more similar. This is owing to the more frequent and more dramatic amplitude variation of the FD-CHTF in the COST207 HT channel, which exhibits a significantly longer maximum path delay than that of the SWATM channel, as indicated by Figure 3.15. This characteristic resulted in more randomly dispersed rather than burstily corrupted subcarrier symbols, which can be more readily corrected by the channel codes. Hence, in the context of the COST207 HT channel of Figure 3.12, the different error-correcting capability of the various CM schemes becomes more explicit, than that exhibited in the scenario of the SWATM channel of Figure 2.32.

In Table 3.4 of Section 3.3.2.2.3 we summarized the E_b/N_0 values required by the various CM- and WHTS-assisted MMSE-SDMA-OFDM schemes for achieving a BER of 10^{-5}, also showing the corresponding gains attained by the WHTS-assisted schemes. We observed that on one hand, when we had a specific user load, the spreading-induced E_b/N_0 gain achieved by a system having a lower diversity order was higher, regardless of the employment of CM. In other words, the subcarrier-based WHTS technique may be expected to attain a higher system performance improvement in relatively lower diversity-order scenarios. Moreover, if we supported a fixed number of users but varied the number of receiver antenna elements, similar conclusions may be drawn. A plausible explanation for this fact may be that in the SDMA-MIMO system, a potentially higher space diversity gain may be achieved, when a higher number of receiver antenna elements is employed, and thus the benefits of WHTS may be less substantial. This may be particularly true in the context of the CM-aided systems, since most of the attainable gain has already been achieved by using the channel codes. On the other hand, when a given number of receiver antenna elements was used, the spreading-induced E_b/N_0 gains achieved in the context of the fully-loaded systems were higher than in the half-loaded systems, regardless of the employment of channel codes. This suggests that more benefits may arise from WHTS, especially in the fully-loaded scenarios, where the MUD

suffers from a relatively low efficiency in differentiating the different users' signals.

Additionally, we provided the E_b/N_0 crossing points and the corresponding total gain achieved by the various CM-WHTS-MMSE-SDMA-OFDM schemes at the BER of 10^{-5}, in Figures 3.19 and 3.20 of Section 3.3.2.2.3, respectively. It was demonstrated that the performance gap between the different CM-aided schemes increased, as the user load increased. Furthermore, it was observed in Figures 3.19 and 3.20 that the TCM, BICM and BICM-ID-aided schemes suffered a higher performance degradation than the TTCM arrangement, when the MUD's user-separation capability eroded owing to the increased multi-user interference. At a relatively low user load the various schemes provided a similar performance, because most of the attainable gain of the four-receiver SDMA-OFDM system had already been achieved, as discussed earlier in Section 3.3.2.2.3.

The effects of using different WHT block sizes was studied in Section 3.3.2.3, in both the SWATM and COST207 HT channel scenarios, as seen in Figures 3.21 and 3.22, respectively. As expected, it was found that the system's performance was improved, while the WHT block size used was increased. This is because when a larger WHT block size is used by the SDMA-OFDM system, the data symbols carried by the subcarriers that are badly-affected by deep channel fades could be spread over a larger WHT length, which may mitigate the detrimental channel effects and thus assists the receiver in terms of achieving a better error correction capability. Furthermore, it was suggested by the simulation results of Section 3.3.2.3 that in the SDMA-OFDM system operating without the aid of CM, the performance improvement potential owing to the employment of a larger WHT block size was higher than that in the CM-aided system, where most of the achievable diversity gain has been attained by using CM.

Finally, we studied the effects of the Doppler frequency in Section 3.3.2.4. It was concluded that the maximum Doppler frequency does not significantly affect the performance of the WHTS-assisted MMSE-SDMA-OFDM system, regardless of the employment of CM, as for example portrayed in Figure 3.23.

From the investigations conducted, we conclude that the various CM schemes, namely TCM, TTCM, BICM and BICM-ID are capable of substantially improving the achievable performance of uncoded SDMA-OFDM systems. The employment of WHTS has the potential of further enhancing the system's performance in highly dispersive propagation environments. As a result, the TTCM- and WHTS-assisted scheme was found to have the best CWER performance in all the scenarios investigated. Furthermore, it was also the best design option in terms of the achievable E_b/N_0 gain expressed in dB, when communicating in highly dispersive environments, for example over the COST207 HT channel of Figure 3.12, while carrying a high user load of $\alpha_p \geq 0.5$.

In the next chapter, our research is targeted at contriving a more sophisticated MUD,

namely the Genetic Algorithm (GA) assisted MUD, in order to further improve the SDMA-OFDM system's achievable performance.

Chapter 4

Hybrid Multi-User Detection for SDMA-OFDM Systems

4.1 Introduction

In the previous chapter, the MMSE MUD has been investigated in the context of various CM schemes assisted SDMA-OFDM systems. Furthermore, the WHT-based frequency-domain spreading technique has been incorporated into the CM-assisted MMSE-SDMA-OFDM system for the sake of attaining performance enhancements. However, the SDMA system's performance is somewhat limited due to the employment of the low-complexity MMSE MUD, which is devised based on the sub-optimal linear MMSE algorithm. On the other hand, the high-complexity optimum Maximum Likelihood (ML) MUD is capable of achieving the best performance owing to invoking an exhaustive search. However, the computational complexity of the ML MUD typically increases exponentially with the number of simultaneous users supported by the SDMA-OFDM system, which may render its implementation prohibitive. In the literature, a range of sub-optimal nonlinear MUDs have been proposed, such as for example the MUDs based on Successive Interference Cancellation (SIC) [3, 192, 196, 305–307] or Parallel Interference Cancellation (PIC) [3, 305, 307, 308] techniques. Instead of detecting and demodulating the users' signals in a sequential manner, as the MMSE MUD does, the PIC and SIC MUDs invoke an iterative processing technique that combines detection and demodulation. More specifically, the output signal generated during the previous detection iteration is demodulated and fed back to the input of the MUD for the next iterative detection step. Similar techniques invoking decision-feedback have been applied also in the context of classic channel equalization. However, since the philosophy of both the PIC and SIC MUDs is based on the principle of removing the effects of the interfering users during each detection

stage, they are prone to error propagation occurring during the consecutive detection stages due to the erroneously detected signals of the previous stages [3]. In order to mitigate the effects of error propagation, an attractive design alternative is to *simultaneously* detect all the users' signals, rather than invoking iterative interference cancellation schemes. Recently, another branch of multi-user detection schemes referred to as Sphere Decoder (SD) [311–317] has also been proposed for multi-user systems, which is capable of achieving ML performance at a lower complexity.

As far as we are concerned, most of the above-mentioned techniques were proposed for the systems, where the number of users is less than or equal to the number of receivers, referred to here as the underloaded or fully-loaded scenarios, respectively. However, in practical applications it is possible that the number of users L to be supported exceeds that of the receiver antennas P, which is often referred to as an *overloaded* scenario. In overloaded systems, the $(P \times L)$-dimensional MIMO channel matrix representing the $(P \times L)$ number of channel links becomes singular, thus rendering the degree of freedom of the detector insufficient. This will catastrophically degrade the performance of numerous known detection approaches, such as for example the Vertical Bell Labs Layered Space-Time architecture (V-BLAST) [106,109,318] detector of [135], the MMSE algorithm of [3, 305] and the QR Decomposition combined with the M-algorithm (QRD-M) algorithm of [173].

Based on this motivation, in this chapter a sophisticated nonlinear MUD is devised, which exploits the power of genetic algorithms. Genetic Algorithms (GAs) [319–323] have been applied to a number of problems, such as machine learning and modeling adaptive processes. Moreover, GA-based multiuser detection has been proposed by Juntti *et al.* [324] and Wang *et al.* [325], where the analysis was based on the AWGN channel in the absence of diversity techniques. The proposal by Ergün *et al.* [326] utilized GAs as the first stage of a multistage multiuser detector, in order to provide good initial guesses for the subsequent stages. Its employment in Rayleigh fading channels was considered by Yen *et al.* in [45, 327] and [45, 328] in diverse scenarios both with and without the aid of diversity techniques, respectively.

However, most of the GA-aided transceiver research mentioned above was conducted in the context of Code Division Multiple Access (CDMA) systems [45, 329]. By contrast, in this chapter, we apply GAs in the context of multi-user OFDM schemes, rather than CDMA systems. More specifically, we combine GAs with the MMSE MUD for the sake of contriving a more powerful concatenated MMSE-GA MUD, which is capable of maintaining near-optimum performance in the above-mentioned overloaded systems. Furthermore, TTCM is selected as the FEC scheme for the proposed MMSE-GA multi-user detected SDMA-OFDM system, since it generally provides the best performance in the family of CM schemes in the context of

MMSE-SDMA-OFDM systems, as demonstrated in Chapter 3. We will show in this chapter that the proposed MMSE-GA assisted TTCM-SDMA-OFDM system is capable of achieving a similar performance to that attained by its optimum ML MUD assisted counterpart at a significantly lower computational complexity, especially at high user loads. Furthermore, the performance of the proposed GA-aided system can be further improved, if an enhanced iterative GA MUD is employed. This improvement is achieved at the cost of an increased complexity, which is however still substantially lower than that imposed by the ML MUD.

The structure of this chapter is as follows. The overview of the GA-assisted TTCM-aided MMSE-SDMA-OFDM system is given in Section 4.2.1, followed by the introduction of the basic principles of the concatenated MMSE-GA MUD of Section 4.2.2. Our simulation results are provided in Section 4.2.3, while the associated complexity issues are discussed in Section 4.2.4. The enhanced GA MUD is introduced in Section 4.3, including the improved mutation scheme of Section 4.3.1 and the enhanced GA MUD framework of Section 4.3.2, while the associated simulation results are provided in Sections 4.3.1.3 and 4.3.2.2, respectively, followed by the associated complexity analysis in Section 4.3.3. Our final conclusions are summarized in Section 4.4.

4.2 Genetical Algorithm Assisted Multi-User Detection

4.2.1 System Overview

In Figure 4.1, we present the schematic of the proposed concatenated MMSE-GA MUD aided SDMA-OFDM uplink system. At the transmitter end, as seen at the top of Figure 4.1, the information bit sequences of the geographically separated L simultaneous mobile users are forwarded to the TTCM [2] encoders, where they are encoded into symbols. The encoded signals $s^{(l)}$ $(l = 1, \cdots, L)$ of the L users are then forwarded to the OFDM-related Inverse Fast Fourier Transform (IFFT) based modulator, which converts the frequency-domain signals to the time-domain modulated OFDM symbols. The OFDM symbols are then transmitted by the independent Mobile Stations (MSs) to the Base Station (BS) over the SDMA MIMO channel, which has been presented in Section 3.2.1. Then each element of the receiver antenna array shown at the bottom of Figure 4.1 receives the superposition of the transmitted signals faded and contaminated by the channel and performs Fast Fourier Transform (FFT) based OFDM demodulation. The demodulated outputs x_p $(p = 1, \cdots, P)$ seen in Figure 4.1 are forwarded to the proposed concatenated MMSE-GA MUD for separating the different users' signals. The separated signals $\hat{s}^{(l)}$ $(l = 1, \cdots, L)$, namely the estimated versions of the L users' transmitted signals, are then independently decoded by the TTCM decoders of Figure 4.1.

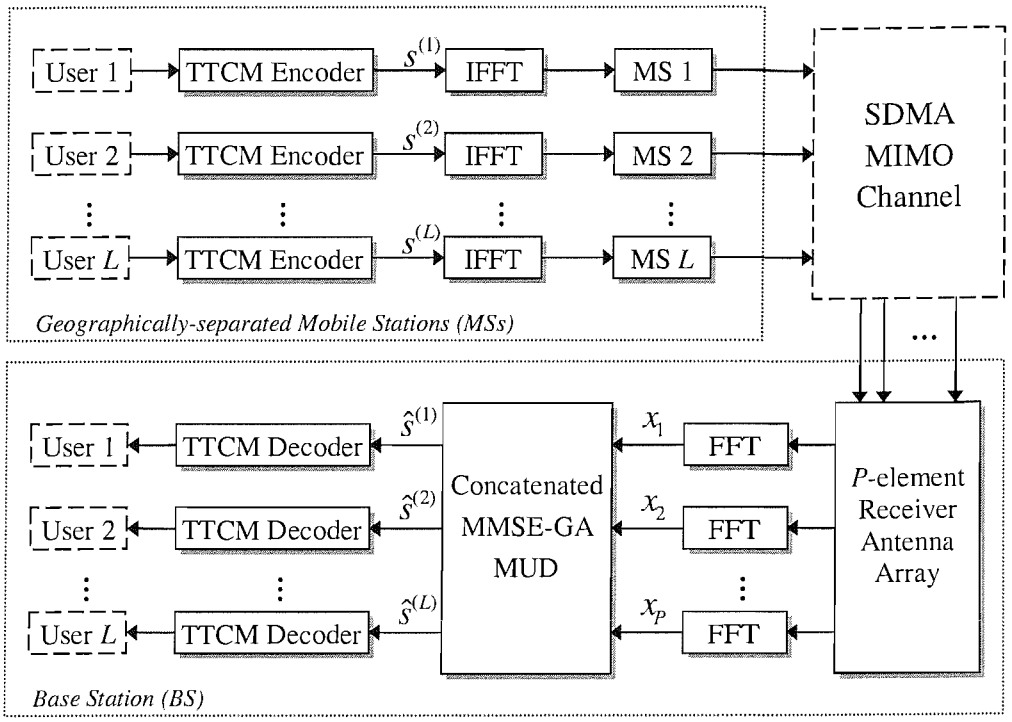

Figure 4.1: Schematic of the MMSE-GA-concatenated multi-user detected SDMA-OFDM uplink system.

4.2.2 MMSE-GA-concatenated Multi-User Detector

4.2.2.1 Optimization Metric for the GA MUD

The optimum ML MUD [3] uses an exhaustive search for finding the most likely transmitted signals. More explicitly, for a ML-detection assisted SDMA-OFDM system supporting L simultaneous users, a total of 2^{mL} metric evaluations has to be invoked, where m denotes the number of bits per symbol (BPS), in order to detect the L-user symbol vector $\hat{\mathbf{s}}_{\mathrm{ML}}$ that consists of the most likely transmitted symbols of the L users at a specific subcarrier, given by:

$$\hat{\mathbf{s}}_{\mathrm{ML}} = \arg\left\{ \min_{\check{\mathbf{s}} \in \mathcal{M}^L} ||\mathbf{x} - \mathbf{H}\check{\mathbf{s}}||^2 \right\}, \tag{4.1}$$

where the $(P \times 1)$-dimensional received signal vector $\mathbf{x}$ and the $(P \times L)$-dimensional Frequency-Domain CHannel Transfer Function (FD-CHTF) matrix $\mathbf{H}$ are defined by Equations (3.2) and (3.5), respectively. The set $\mathcal{M}^L$ in Equation (4.1), which is constituted by 2^{mL} number of trial vectors, is formulated as:

$$\mathcal{M}^L = \left\{ \check{\mathbf{s}} = \left[\check{s}^{(1)}, \check{s}^{(2)}, \cdots, \check{s}^{(L)} \right]^T \middle| \check{s}^{(1)}, \check{s}^{(2)}, \cdots, \check{s}^{(L)} \in \mathcal{M}_c \right\}, \tag{4.2}$$

where $\mathcal{M}_c$ denotes the set containing the 2^m number of legitimate complex constellation points associated with the specific modulation scheme employed. Explicitly, the number of

metric evaluations required for detecting the optimum vector increases exponentially with the number of users L.

Furthermore, the optimum ML-based decision metric of Equation (4.1) may also be used in the GA-based MUD for the sake of detecting the estimated transmitted symbol vector $\hat{\mathbf{s}}_{\mathrm{GA}}$. In the context of the SDMA-OFDM system employing P receiver antenna elements, the decision metric required for the p^{th} receiver antenna, namely the antenna-specific *objective function (OF)* [45] can be derived from Equation (4.1), yielding:

$$\Omega_p(\check{\mathbf{s}}) = |x_p - \mathbf{H}_p\check{\mathbf{s}}|^2, \tag{4.3}$$

where x_p is the received symbol at the input of the p^{th} receiver at a specific OFDM subcarrier, while $\mathbf{H}_p$ is the p^{th} row of the channel transfer function matrix $\mathbf{H}$. Therefore the decision rule for the optimum multiuser detector associated with the p^{th} antenna is to choose the specific L-symbol vector $\check{\mathbf{s}}$, which minimizes the metric given in Equation (4.3). Thus, the estimated transmitted symbol vector of the L users based on the knowledge of the received signal at the p^{th} receiver antenna and a specific subcarrier is given by:

$$\hat{\mathbf{s}}_{\mathrm{GA}_p} = \arg\left\{\min_{\check{\mathbf{s}}}\left[\Omega_p(\check{\mathbf{s}})\right]\right\}. \tag{4.4}$$

However, it transpires from above derivation that we will have P metrics in total for the P receiver antennas. Since the channel impulse responses of each of the P antennas are statistically independent, the L-symbol vector that is considered optimum at antenna 1 may not be considered optimum at antenna 2, etc. In other words, this implies that a decision conflict is encountered, which may be expressed as:

$$\arg\left\{\min_{\check{\mathbf{s}}}\left[\Omega_i(\check{\mathbf{s}})\right]\right\} = \hat{\mathbf{s}}_{\mathrm{GA}_i} \neq \hat{\mathbf{s}}_{\mathrm{GA}_j} = \arg\left\{\min_{\check{\mathbf{s}}}\left[\Omega_j(\check{\mathbf{s}})\right]\right\}, \tag{4.5}$$

where $\forall\, i,j \in \{1,\cdots,P\},\ i \neq j$. This decision conflict therefore leads to a so-called multi-objective optimization problem, since the optimization of the P metrics may result in more than one possible L-symbol solutions. A similar decision conflict resolution problem was studied in [330] in an attempt to reconcile the decision conflicts of multiple antennas resulting in a decision dilemma. In order to resolve this problem we may adopt a similar approach and may amalgamate the P number of antenna-specific L-symbol metrics into a joint metric as follows:

$$\Omega(\check{\mathbf{s}}) = \sum_{p=1}^{P}\Omega_p(\check{\mathbf{s}}). \tag{4.6}$$

Hence, the decision rule of the GA MUD is to find the specific estimated transmitted L-symbol vector $\hat{\mathbf{s}}_{\mathrm{GA}}$ that minimizes $\Omega(\mathbf{s})$ in Equation (4.6) for every OFDM subcarrier considered.

4.2.2.2 Concatenated MMSE-GA Multi-User Detection

The BER performance of the MMSE MUD is somewhat limited, since it is the total mean-square estimation error imposed by the different simultaneous users that is minimized, rather than directly optimizing the BER performance. Therefore, the MMSE-SDMA-OFDM system's BER performance may be potentially further improved with the aid of a concatenated GA-aided MUD, which is capable of exploiting the output provided by the MMSE MUD of Section 3.2.2.1 in its initial population. For the sake of brevity, we will portray the philosophy of the proposed system in as simple terms as possible. However, the readers who are unfamiliar with GAs might like to consult Appendix A.1 for a rudimentary introduction to GA-based optimization in the context of multi-user SDMA-OFDM systems.

The GA invoked in the SDMA-OFDM system commences its search for the optimum L-symbol solution at the initial *generation* with the aid of the MMSE combiner. In other words, using GA parlance, the so-called *individuals* of the $y = 1^{st}$ generation having a *population* size of X are created from the estimated length-L transmitted symbol vector provided by the MMSE combiner, where the x^{th} $(x = 1, \cdots, X)$ individual is expressed as $\tilde{\mathbf{s}}_{(y,x)} = [\ \tilde{s}^{(1)}_{(y,x)},\ \tilde{s}^{(2)}_{(y,x)},\ \cdots,\ \tilde{s}^{(L)}_{(y,x)}\ ]$, and we have $\tilde{s}^{(l)}_{(y,x)} \in \mathcal{M}_c$ $(l = 1, \cdots, L)$. Note that here a complex symbol representation of the individuals is employed, which is derived from the classic *binary encoding* technique [45], where a binary vector constituted by binary zeros and ones is used to represent an individual. Then the GA-based optimization selects some of the L-symbol candidates from a total of X legitimate individuals in order to create a so-called *mating pool* of T number of L-symbol *parent* vectors [45]. Two L-symbol parent vectors are then combined using specific GA operations for the sake of creating two L-symbol *offspring* [45] and this 'genetic evolution-like' process of generating new L-symbol offspring continues over Y number of consecutive generations, so that the optimum L-symbol solution may be found.

The selection of the L-symbol individuals for creating the mating pool containing T number of L-symbol parents is vital in determining the GA's achievable quality of optimization [331]. In our research the individual-selection strategy based on the concept of the so-called *Pareto Optimality* [320] was employed. This strategy favours the so-called *non-dominated* individuals and ignores the so-called *dominated* individuals [45]. More specifically, the u^{th} L-symbol individual is considered to be dominated by the v^{th} individual, if we have [332]:

$$\begin{aligned} &\forall i \in \{1, \cdots, P\}:\ \Omega_i\big(\tilde{\mathbf{s}}_{(y,v)}\big) \leq \Omega_i\big(\tilde{\mathbf{s}}_{(y,u)}\big) \\ \wedge\ &\exists j \in \{1, \cdots, P\}:\ \Omega_j\big(\tilde{\mathbf{s}}_{(y,v)}\big) < \Omega_j\big(\tilde{\mathbf{s}}_{(y,u)}\big). \end{aligned} \tag{4.7}$$

If an individual is not dominated in the sense of Equation (4.7) by any other individuals in the

population, then it is considered to be non-dominated. All the non-dominated individuals are then selected and placed in the mating pool, which will have a size of $2 < T \leq X$ [45]. Two of the T number of L-symbol individuals in the mating pool are then selected as parents based on their corresponding diversity-based *fitness* values calculated with the aid of Equation (4.6) according to the so-called *fitness-proportionate* selection scheme [45], which is described as follows. First the so-called *windowing-mapping* [325] technique is invoked in order to get the fitness value $f_{(y,x)}$ associated with the x^{th} individual, which is given by:

$$f_{(y,x)} = \Omega_{y,T} - \Omega\left(\tilde{\mathbf{s}}_{(y,x)}\right) + c, \tag{4.8}$$

where

$$\Omega_{y,T} = \max_{t\in\{1,\cdots,T\}} \left\{\Omega\left(\tilde{\mathbf{s}}_{(y,t)}\right)\right\} \tag{4.9}$$

is the maximum *Objective Score (OS)*[1] achieved by evaluating the T number of individuals in the mating pool at the y^{th} generation, and c is a small positive constant, which is used for the sake of ensuring the positiveness of $f_{(y,x)}$. Then the fitness-proportionate selection probability p_x of the x^{th} individual can be formulated as:

$$p_x = \frac{f_{(y,x)}}{\sum_{t=1}^{T} f_{(y,t)}}. \tag{4.10}$$

When two L-symbol parents are selected, the so-called *uniform cross-over*, *mutation* and *elitism* operations [45] are invoked for offering a chance of evolving the parents' one or more element symbols to other symbols of the set $\mathcal{M}_c$, resulting in two offspring. The above operation is repeated, until a new population consisting of X offspring is created. Furthermore, the so-called *incest prevention* [45] technique was invoked during the selection process, which only allows different individuals to be selected for the cross-over operation. Finally, the GA terminates after Y number of generations and thus the L-symbol individual having the highest diversity-based fitness value will be considered as the detected L-user transmitted symbol vector corresponding to the specific OFDM subcarrier considered.

From the above arguments, we note that in the GA MUD the different users' signals are jointly detected. This mechanism is different from that of the SIC or PIC MUDs, where each user's estimated transmitted signal is inferred by removing the interference imposed by the others. Therefore, there is no error propagation between the different users' signal detections in the GA MUD.

[1]Note that the individual having the maximum OS out of the pool of the T candidates is considered as the worst solution in the context of the current mating pool, since the GA searches for the optimum solution which minimizes Equation (4.6).

4.2.3 Simulation Results

In this section, we characterize the performance of the proposed TTCM-assisted SDMA-OFDM system using the concatenated MMSE-GA MUD. The channel is assumed to be 'OFDM-symbol-invariant', implying that the taps of the impulse response are assumed to be constant for the duration of one OFDM symbol, but they are faded at the beginning of each OFDM symbol [3]. The simulation results were obtained using a 4QAM scheme communicating over the SWATM CIR of Figure 2.32, assuming that the channels' transfer functions are perfectly known. Each of the paths experiences independent Rayleigh fading having the same normalized Doppler frequencies of $f'_d = 1.235 \times 10^{-5}$. The OFDM modem employed $K = 512$ subcarriers and a cyclic prefix of 64 samples, which is longer than the maximum channel delay spread. For the iterative TTCM scheme [2] employed, the code memory ν is fixed to 3, while the number of iterations is set to 4. Hence the total number of trellis states is $2^3 \cdot 4 \cdot 2 = 64$, since there are two 8-state decoders which are invoked in four iterations. The generator polynomial expressed in octal format for the TTCM scheme considered is [13 6], while the codeword length and channel interleaver depth are fixed to 1024 symbols. The various techniques and parameters used in our simulations discussed in this section are summarized in Table 4.1.

The BER performance of the TTCM-assisted MMSE-GA-SDMA-OFDM system employing a 4QAM scheme for transmission over the SWATM channel, where six users are supported with the aid of six receiver antenna elements, is portrayed in Figure 4.2. The performance of the TTCM-assisted MMSE-detected SDMA-OFDM system, the TTCM-aided optimum ML-detected system, and the uncoded single-user scheme employing either a single receiver or invoking Maximum Ratio Combining (MRC) when communicating over an AWGN channel are also provided for reference, respectively. The numbers in the round brackets seen in the legends of Figure 4.2 represent the total GA or ML complexity[2]. It is observed from Figure 4.2 that the BER performance of the TTCM-assisted MMSE-SDMA-OFDM system was significantly improved with the aid of the GA having a sufficiently large population size X and/or a larger number of generations Y. This improvement was achieved, since a larger population may contain a higher variety of L-symbol individuals, and similarly, a larger number of generations implies that again, a more diverse set of individuals may be evaluated, thus extending the GA's search space, which may be expected to increase the chance of finding a lower-BER solution. On the other hand, it may be observed that when we have the same total number of $(X \times Y)$ correlation metric evaluations according to Equation (4.3), the performance improvement achieved by increasing the population size X was more substantial than that upon increasing the Y number of generations. For example, when we have $X \times Y = 100$, the

[2]The quantification of the GA or ML complexity will be given in Section 4.2.4.

TTCM	Modem	4QAM
	Code rate	0.5
	Code memory ν	3
	Octal generator polynomial	[13 6]
	Codeword length	1024 symbols
	Channel interleaver depth	1024 symbols
	Number of turbo iterations	4
GA	Population initialization method	MMSE
	Mating pool creation strategy	Pareto-Optimality
	Selection method	Fitness-Proportionate
	Cross-over	Uniform cross-over
	Mutation	M-ary mutation
	Mutation probability p_m	0.1
	Elitism	Enabled
	Incest prevention	Enabled
	Population size X	Varied
	Generations Y	Varied
Channel	CIRs	SWATM [3]
	Paths	3
	Maximum path delay	48.9 ns
	Normalized Doppler frequency f_d	1.235×10^{-5}
	Subcarriers K	512
	Cyclic prefix	64

Table 4.1: The various techniques and parameters used in the simulations of Section 4.2.3.

GA-assisted scheme employing a population size $X = 20$ and $Y = 5$ number of generations achieved about 1.5dB E_b/N_0 gain over its corresponding counterpart that has $X = 10$ and $Y = 10$, as evidenced by Figure 4.2. This may suggest that in the TTCM-assisted MMSE-SDMA-OFDM system investigated, the GA's convergence speed tends to be faster, when we have a larger population size X instead of a higher number of generations Y. However, when the affordable complexity increases, the improvement achieved by a larger-population GA at a certain value of $(X \times Y)$ becomes modest. For instance, given the maximum affordable complexity of $X \times Y = 400$, the system associated with $X = 80$ and $Y = 5$ brought about a modest E_b/N_0 improvement of 0.25dB over the system associated with $X = 40$ and $Y = 10$, as shown in Figure 4.2. This is because most of the achievable performance gain of the system is likely to have been attained.

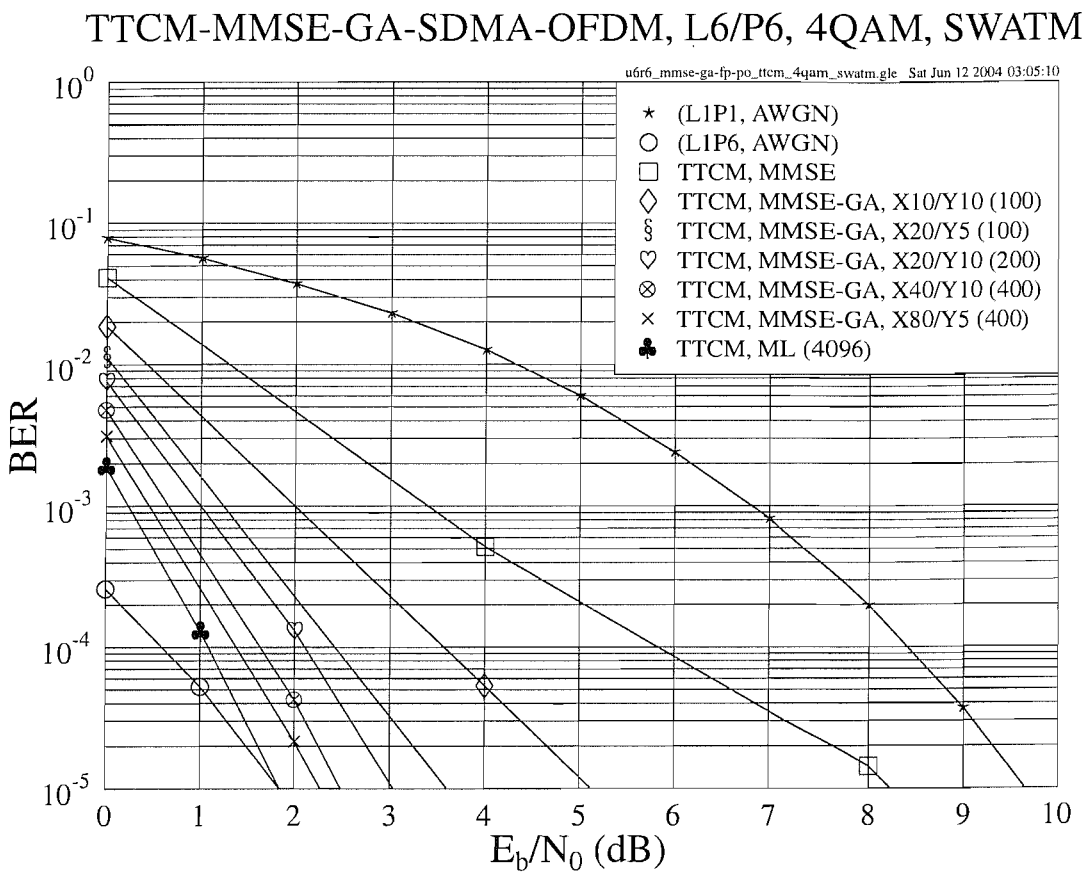

Figure 4.2: **BER** versus E_b/N_0 performance of the **TTCM-assisted MMSE-GA-SDMA-OFDM** system employing a 4QAM scheme for transmission over the SWATM channel, where **L=6** users are supported with the aid of **P=6** receiver antenna elements. The basic simulation parameters are given in Table 4.1.

Figure 4.3 shows the performance achieved by the proposed TTCM-MMSE-GA-SDMA-OFDM system in the scenario, where the number of supported users and receiver antenna elements was increased to eight. As shown in Figure 4.3, again, the TTCM-aided MMSE-SDMA-OFDM system's performance was significantly improved by employing the GA. We may also note that at a specific computational complexity, the E_b/N_0 gain achieved by the GA MUD was decreased, when compared to that attained in the six-user-six-receiver scenario of Figure 4.2. For example, when we have $X = Y = 10$ and $L = P = 6$, the E_b/N_0 gain achieved by the TTCM-MMSE-GA-SDMA-OFDM system over the TTCM-MMSE-SDMA-OFDM system was about 3dB, as seen in Figure 4.2. By contrast, Figure 4.3 shows that this gain decreased to about 1.8dB, when we used the same GA and $L = P = 8$. This phenomenon may be explained as follows. On one hand, when the number of users increases, the separation of the different users' signal becomes more challenging, since the interference imposed by the undesired users becomes stronger. Therefore, a higher-complexity GA MUD has to be

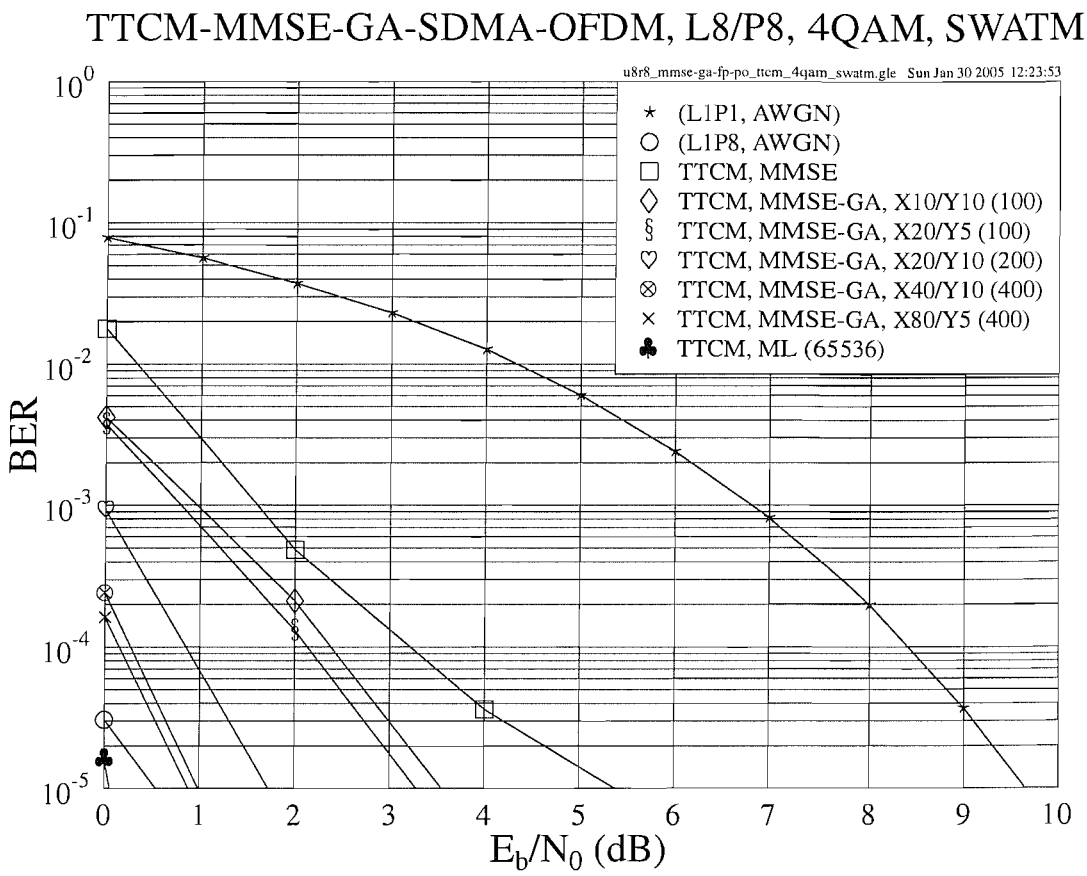

Figure 4.3: **BER** versus E_b/N_0 performance of the **TTCM-assisted MMSE-GA-SDMA-OFDM** system employing a 4QAM scheme for transmission over the SWATM channel, where **L=8** users are supported with the aid of **P=8** receiver antenna elements. The basic simulation parameters are given in Table 4.1.

employed, if we aim for maintaining the same E_b/N_0 gain achieved by the system having a lower user load. On the other hand, when we have more receiver antenna elements installed at the BS, namely when using a 'higher-order' SDMA system, a higher spatial diversity gain may be achieved. Hence, in a 'higher-order' SDMA system, a higher probability of achieving the total attainable gain may be expected than in a 'lower-order' SDMA system, potentially approaching the best possible AWGN performance. Hence, this trend also results in a less significant GA-induced performance gain.

Furthermore, it can be seen in Figures 4.2 and 4.3 that the MMSE-GA-detected TTCM-SDMA-OFDM system was slightly outperformed by its optimum ML-detected counterpart, since the GAs are unable to guarantee that the optimum ML solution would be found [45]. However, the near-optimum performance of the GA-aided TTCM-SDMA-OFDM system was achieved at a significantly lower computational complexity than that imposed by the ML-aided system, as it will be demonstrated in Section 4.2.4.

4.2.4 Complexity Analysis

In this section, an analysis of the associated computational complexity imposed by the optimum ML MUD aided SDMA-OFDM system and the GA-aided MMSE-SDMA-OFDM system will be presented. For the sake of simplicity, we only compare the optimum ML MUD's complexity to that of the GA MUD, since the simple MMSE MUD is used for providing a single initial solution for the GA's initial population and imposes a significantly lower complexity than that of its concatenated GA-aided counterpart. More specifically, since the proposed GA-aided MUD optimizes the metric of Equation (4.3)[3], we will quantify the complexity imposed in terms of the number of metric computations required by the optimization process.

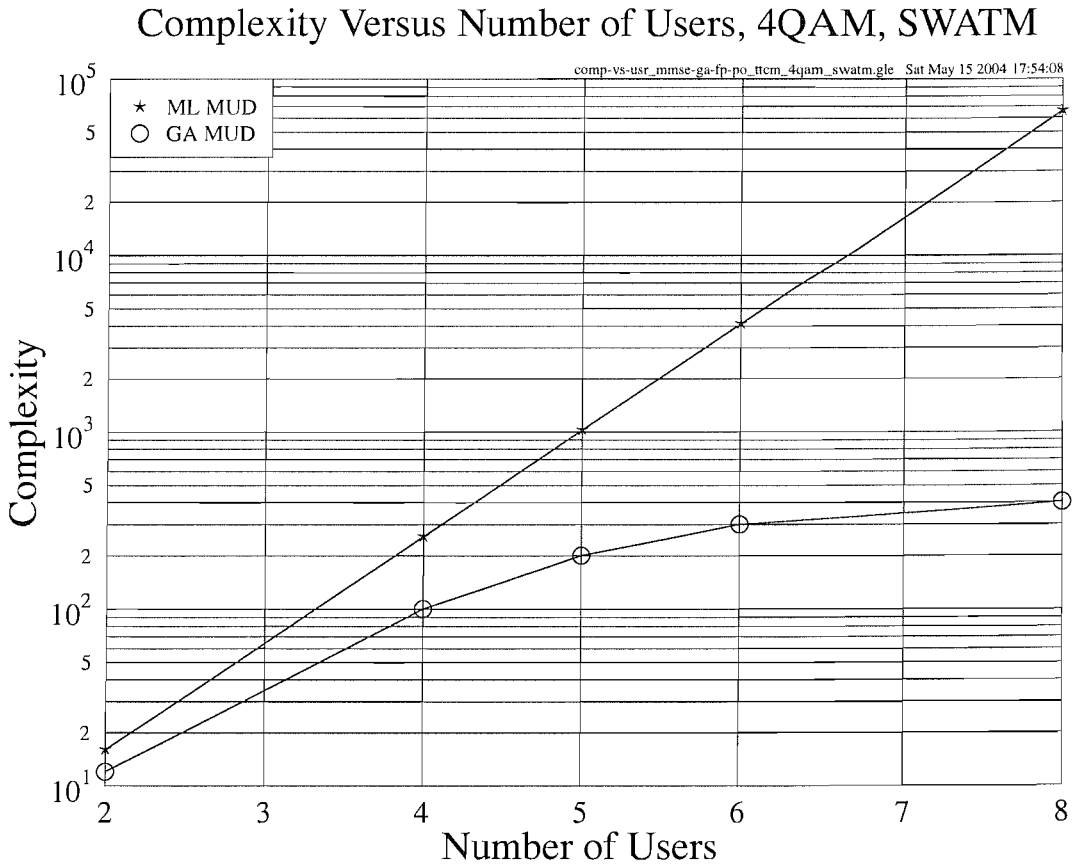

Figure 4.4: Comparison of the **MUD complexity** in terms of the number of metric evaluations, versus the number of users performance of the 4QAM **TTCM-MMSE-GA-SDMA-OFDM** and **TTCM-ML-SDMA-OFDM systems**. The number of receiver antenna elements employed is equivalent to the number of users supported, i.e. $L = P$.

As mentioned in Section 4.2.2.1, for the ML MUD, 2^{mL} number of metric computations have to be carried out for finding the optimum solution [3], namely the most likely transmitted

[3]Similarly, the ML-aided MUD optimizes the metric of Equation (4.1), from which Equation (4.3) is derived.

L-user vector, where m denotes the number of bits per symbol. By contrast, our proposed GA MUD requires a maximum of $(X \times Y)$ metric evaluations, since X number of L-symbol vectors are evaluated during each of the Y number of generations, as shown in round brackets in the legends of Figures 4.2 and 4.3. Furthermore, the number of such metric evaluations may readily be reduced by avoiding repeated evaluations of identical individuals, either within the same generation or across the entire iterative process, provided that the receiver has the necessary memory for storing the corresponding evaluation history. In Figure 4.4, we compare both the ML- and the GA-aided schemes in terms of their complexity, i.e. the number of metric computations. At a specific user load, we always select an appropriate GA-aided scheme for comparison, which suffers from less than 1dB E_b/N_0 loss at the BER of 10^{-5} compared to the ML-aided system. As shown in Figure 4.4, the ML-aided system imposes an exponentially increasing complexity on the order of $O(2^{mL})$, when the number of users increases, while the complexity of the GA-aided system required for maintaining a near-optimum performance increases only slowly.

4.2.5 Conclusions

From the investigations conducted, we conclude that the GA-assisted TTCM-aided MMSE-SDMA-OFDM system is capable of achieving a similar performance to that of the optimum ML-assisted TTCM-SDMA-OFDM system. Furthermore, this is attained at a significantly lower computational complexity than that imposed by the ML-assisted system, especially when the number of users is high. For example, a complexity reduction in excess of a factor of 100 can be achieved by the proposed system for $L = P = 8$, as evidenced by Figure 4.4.

4.3 Enhanced GA-based Multi-User Detection

In Section 4.2, we have presented a detailed characterization of the concatenated MMSE-GA MUD designed for the TTCM-assisted multi-user SDMA-OFDM system. In this section, an enhanced GA-based multi-user detector will be introduced, which is capable of further improving the proposed system's performance.

As discussed in Section 4.2, the proposed MMSE-GA-assisted TTCM-SDMA-OFDM system achieves a close-to-optimum performance at a significantly lower computational complexity than its optimum ML-assisted counterpart. Moreover, the GA-aided system can be further improved in each or both of the following two aspects:

- By optimizing the component(s) of the GA MUD for the sake of finding a better configuration that may improve the GA's performance in the context of the SDMA-OFDM

system;

- By invoking an iterative detection framework so that the system's performance may be improved iteration by iteration.

In the following sections we will discuss the techniques that may be applied in terms of the above-mentioned two aspects for achieving an improved system performance.

4.3.1 Improved Mutation Scheme

In the context of GA-based detection techniques, the efficiency of the mutation scheme employed is important for the success of the entire evolution procedure, since it provides a chance for the individuals of the current population to influence the forthcoming ones, so that new areas of the total search space may be explored and thus the chance of finding the optimum solution increases [333]. An efficient mutation scheme is expected to be capable of guiding the search process in the correct direction for the sake of finding the global optimum, rather than the local ones. In the context of the GA-assisted multi-user SDMA-OFDM system, when the number of users L increases or a high-throughput modulation scheme is used, the total search space consisting of 2^{mL} number of L-user symbol vectors would become excessive. In such cases, the role of mutation may become vital for the success of the overall system, since the GA may get trapped in local optima without appropriate assistance of the mutation scheme.

In Section 4.3.1.1, we will first discuss a widely-used conventional mutation scheme as well as its drawbacks, which is followed by the introduction of an improved new mutation mechanism in Section 4.3.1.2.

4.3.1.1 Conventional Uniform Mutation

In Section 4.2.3, M-ary mutation was employed by the GA MUD. More specifically, each *gene* $\hat{s}^{(l)}$ $(l = 1, \cdots, L)$ of a length-L GA individual $\hat{\mathbf{s}}$ in the X-element population is represented by a specific symbol in $\mathcal{M}_c$, where $\mathcal{M}_c$ is the set containing the 2^m number of legitimate constellation points. In other words, the l^{th} gene denotes the l^{th} user's estimated transmitted symbol - which is a hard-decoded version of the complex signal - at the subcarrier considered. During the genetic evolution, when a gene is subjected to mutation, it will be substituted by a different symbol in $\mathcal{M}_c$ based on a uniform *mutation-induced transition probability* $p_{mt}^{(ij)}$ [4], which quantifies the probability of the i^{th} legitimate symbol becoming the j^{th}. For the sake of brevity, from now on we refer to this probability as the *transition probability*. Furthermore,

[4]Note that the mutation probability p_m of Table 4.1 is different from the probability $p_{mt}^{(ij)}$ of mutating to a specific symbol in $\mathcal{M}_c$. The former denotes the probability of how likely it is that a gene will mutate, while the latter specifies, how likely it is that a specific symbol in $\mathcal{M}_c$ becomes the mutated gene.

we shall refer to the mutation scheme employing uniformly distributed $p_{mt}^{(ij)}$ values as *Uniform Mutation (UM)*, which is a widely-used conventional mutation scheme known in the literature and was also employed by the GAs invoked in [45].

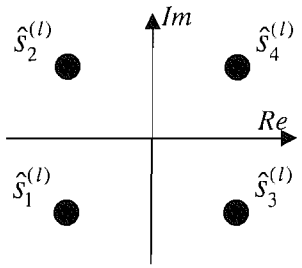

Figure 4.5: A 4QAM constellation.

More specifically, UM mutates to all the candidate symbols in $\mathcal{M}_c$ with the same probability. For example, let us consider the 4QAM modem constellation shown in Figure 4.5, where $\hat{s}_i^{(l)} \in \mathcal{M}_c$ $(i = 1, \cdots, 4)$ are the constellation points as well as possible gene candidates for the l^{th} user at a specific subcarrier. When $\hat{s}_i^{(l)}$ is subjected to mutation, we have:

$$\hat{s}_j^{(l)} = MUTATION\left(\hat{s}_i^{(l)} \mid p_{mt}^{(ij)}\right), \quad i, j \in \{1, \cdots, 4\},\ i \neq j. \tag{4.11}$$

For the UM scheme, the transition probability $p_{mt}^{(ij)} = 1/(2^m - 1)$ is equal for all $i, j \in \{1, \cdots, 4\}$, $i \neq j$.

Based on the mechanism of UM, the GA has a chance of successfully identifying the actually transmitted symbol of the l^{th} user at the subcarrier considered. However, UM has a drawback that may prevent the GA from rapid convergence under certain conditions. To explain this further, again, let us consider the example of Figure 4.5. Without loss of generality, let us make the following assumptions:

a) $\hat{s}_1^{(l)}$ is the received symbol, which is the original gene to be mutated, and

b) $\hat{s}_1^{(l)}$ is *not* the transmitted symbol.

Hence, the task of mutation is to find the actually transmitted symbol from the set of three candidates, namely $\hat{s}_i^{(l)}$ $(i = 2, \cdots, 4)$. According to UM, the probability that $\hat{s}_1^{(l)}$ hops to $\hat{s}_2^{(l)}$, $\hat{s}_3^{(l)}$ or $\hat{s}_4^{(l)}$ is equal. In other words, in this case the chance of finding the true transmitted symbol of the specific user during a single UM operation is 1/3. However, this fixed uniform transition probability fails to reflect the realistic channel condition that the system is subjected to. More precisely, at different Signal-to-Noise Ratio (SNR) levels, some symbols in $\mathcal{M}_c$ should not constitute high-probability mutation targets. For example, at high SNRs, the chances are that $\hat{s}_2^{(l)}$ or $\hat{s}_3^{(l)}$ is more likely to be the transmitted symbol, rather than $\hat{s}_4^{(l)}$, since the noise

effects are insignificant and thus the signal corruption from the most distant symbol $\hat{s}_4^{(l)}$ to the received symbol $\hat{s}_1^{(l)}$ is rare. Hence, it may be more reasonable to consider $\hat{s}_2^{(l)}$ and $\hat{s}_3^{(l)}$ only as the potential mutation candidates, and assign a modified transition probability $p_{mt}^{(1j)} = 0.5$ $(j \in \{2,3\})$. This fact implies that at different SNR levels we may restrict the *effective* GA search space with the aid of a biased mutation, which ignores the constellation points that are far from the received symbol. This is especially beneficial for the system employing high-throughput modulation schemes such as 16QAM, where the total search space is exponentially expanded as a function of the number of BPS compared to lower-throughput modems. In such a system, the UM-aided GA which allows mutation to all legitimate symbols may suffer from a slow convergence speed and might result in a high residual error floor, since a considerable portion of the GA's searching power may be wasted on mutating to highly unlikely gene candidates, especially in high-SNR scenarios. By contrast, the above-mentioned biased mutation guided GA is expected to achieve a better performance, since it searches for the optimum solution in a more efficient way, as it will be demonstrated in Section 4.3.1.2.

4.3.1.2 Biased Q-function Based Mutation

The conventional UM and its drawbacks have been discussed in Section 4.3.1.1. In this section, an improved novel mutation scheme will be presented, which we shall refer to as *Biased Q-function Based Mutation (BQM).*

4.3.1.2.1 Theoretical Foundations

As discussed in Section 4.3.1.1, for an original gene to be mutated, a SNR-related *biased* transition probability $p_{mt}^{(ij)}$ has to be assigned to each of the target candidate symbols in $\mathcal{M}_c$. The calculation of $p_{mt}^{(ij)}$ may be carried out with the aid of the widely-known Q-function [334]:

$$Q(x) = \frac{1}{\sqrt{2\pi}} \int_x^\infty e^{-t^2/2} dt, \quad x \geq 0. \tag{4.12}$$

For the sake of easy explanation, let us first consider a simple one-dimensional (1D) scenario. In Figure 4.6 we plotted the 1D real component of the constellation symbols $\hat{s}_i^{(l)}$ in the context of the 4QAM modem constellation seen in Figure 4.5. The horizontal axis is then divided into two zones, each of which represents one specific 1D constellation symbol s_{Ri} $(i = 1, \cdots, 2)$, as separated by the vertical dashed line of Figure 4.6. If s_{R1} is the original gene to be mutated, the Gaussian distribution $N(0, \sigma)$ may be centered at the position of s_{R1}, where σ is the noise variance at a given SNR level. In this specific example, s_{R2} is the only mutation target and the 1D transition probability of mutating from s_{R1} to s_{R2}, i.e. $p_{mt}^{(12)}$, is

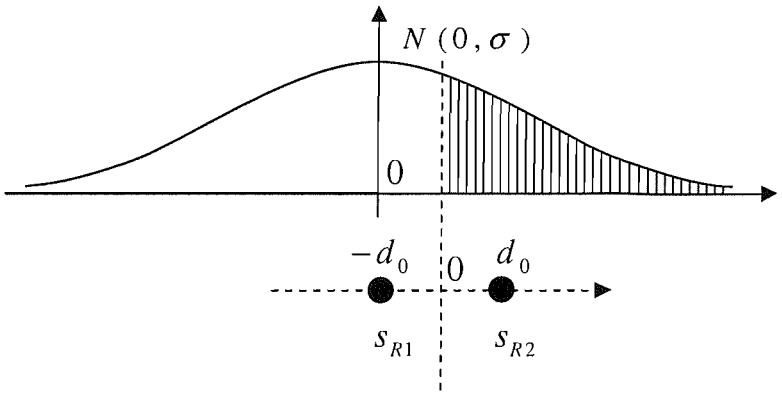

Figure 4.6: Illustration of the 1D transition probability $p_{mt}^{(ij)}$ for 4QAM.

characterized by the shadow area shown in Figure 4.6, which is given by:

$$p_{mt}^{(12)} = Q(\frac{d_0}{\sigma}), \tag{4.13}$$

where d_0 is half of the distance between the neighbouring constellation symbols. Similarly, we have:

$$p_{mt}^{(21)} = Q(\frac{d_0}{\sigma}). \tag{4.14}$$

Furthermore, we also have a certain probability for the original gene to remain unchanged, which can also be expressed in terms of the Gaussian distribution as:

$$p_{mt}^{(11)} = p_{mt}^{(22)} = 1 - Q(\frac{d_0}{\sigma}). \tag{4.15}$$

$\{ij\}$	$p_{mt}^{(ij)}$
$\{12\},\{21\}$	$Q(\frac{d_0}{\sigma})$
$\{11\},\{22\}$	$1-Q(\frac{d_0}{\sigma})$

Table 4.2: The 1D transition probabilities for 4QAM.

The above-mentioned 1D transition probabilities are summarized in Table 4.2. The corresponding two-dimensional (2D) symbol transition probability $p_{mt}^{(ij)}$ can be derived by combining the 1D real and imaginary transition probabilities[5]. Let us again consider the 4QAM modem of Figure 4.5 as an example, which is replotted in Figure 4.7. In Figure 4.7, for instance, the 2D transition probability of mutating from the constellation symbol $\hat{s}_1^{(l)}$ to $\hat{s}_2^{(l)}$, namely $p_{mt}^{(12)}$, can be calculated by multiplying the two relevant 1D transition probabilities

[5]Note that the 1D transition probability $p_{mt}^{(ij)}$ is different from the transition probability $p_{mt}^{(ij)}$, which is based on the 2D constellation symbols.

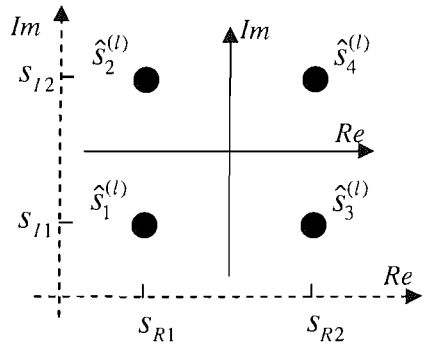

Figure 4.7: Illustration of the 2D transition probability $p_{mt}^{(ij)}$ for 4QAM, which is the product of the relevant 1D transition probabilities. s_{Ri} and s_{Ii} ($i \in \{1,2\}$) denote the 1D constellation symbols in the context of the real and imaginary components of the 4QAM constellation symbols, respectively.

according to[6]:

$$p_{mt}^{(12)} = p_{mt}^{(\underline{11})} \cdot p_{mt}^{(\underline{12})} = \left[1 - Q(\frac{d_0}{\sigma})\right] \cdot Q(\frac{d_0}{\sigma}), \tag{4.16}$$

while the associated 2D probability of remaining in the current state is:

$$p_{mt}^{(11)} = p_{mt}^{(\underline{11})} \cdot p_{mt}^{(\underline{11})} = \left[1 - Q(\frac{d_0}{\sigma})\right]^2. \tag{4.17}$$

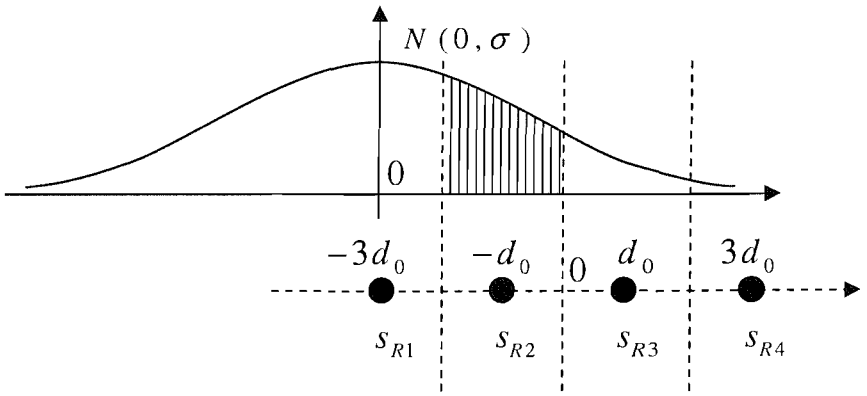

Figure 4.8: Illustration of the 1D transition probability $p_{mt}^{(\underline{ij})}$ for 16QAM.

For higher-throughput modems, for example for 16QAM and 64QAM, the same algorithm can be invoked for calculating the corresponding 1D and 2D transition probabilities. In Figure 4.8 an example associated with 16QAM is provided. According to Figure 4.8, assuming that s_{R1} is the original gene to be mutated, while s_{R2} is the mutation target, we have the

[6]Note that the superscripts i and j of the 2D transition probability $p_{mt}^{(ij)}$ denote the 2D constellation symbols $\hat{s}_i^{(l)}$ and $\hat{s}_j^{(l)}$, while the underlined superscripts i and j of the 1D transition probability $p_{mt}^{(\underline{ij})}$ represent the 1D constellation symbols s_{Ri} and s_{Rj}, respectively.

following 1D transition probability of:

$$p_{mt}^{(12)} = Q(\frac{d_0}{\sigma}) - Q(\frac{3d_0}{\sigma}). \quad (4.18)$$

Similarly, we can derive the remaining 1D transition probabilities for 16QAM, which are summarized in Table 4.3. For the sake of brevity, here we omit the derivation of the corresponding 2D transition probabilities. Note that the proposed BQM scheme can be readily extended to M-dimensional (MD) constellations, since the MD transition probability associated with a specific MD symbol can be readily derived upon multiplying the M number of corresponding 1D transition probabilities.

$\{ij\}$	$p_{mt}^{(ij)}$
$\{34\},\{21\}$	$Q(\frac{d_0}{\sigma})$
$\{24\},\{31\}$	$Q(\frac{3d_0}{\sigma})$
$\{14\},\{41\}$	$Q(\frac{5d_0}{\sigma})$
$\{11\},\{44\}$	$1-Q(\frac{d_0}{\sigma})$
$\{22\},\{33\}$	$1-2Q(\frac{d_0}{\sigma})$
$\{12\},\{23\},\{32\},\{43\}$	$Q(\frac{d_0}{\sigma})-Q(\frac{3d_0}{\sigma})$
$\{13\},\{42\}$	$Q(\frac{3d_0}{\sigma})-Q(\frac{5d_0}{\sigma})$

Table 4.3: The 1D transition probabilities for 16QAM.

However, when a mutation takes place during the evolution, the mutating gene or constellation symbol should not be allowed to be mutated to itself. Hence, the effect of the probability of mutating a symbol to itself should be removed. This can be achieved by normalizing the 2D transition probability $p_{mt}^{(ij)}$ $(i \neq j)$ with the aid of the original gene's probability of remaining unchanged, namely $p_{mt}^{(ii)}$, following the principles of conditional probability theory [335]. For more details concerning the normalization process, the interested reader is referred to Appendix A.2.

4.3.1.2.2 Simplified BQM

In Section 4.3.1.2.1 we have provided a detailed explanation of the mechanism of BQM. Furthermore, the proposed BQM scheme can be effectively simplified, when only a subset of all the theoretically-possible mutation target symbols are considered. More precisely, for the original gene subjected to mutation, we may only consider its adjacent neighbouring constellation symbols as mutation target candidates, since the original transmitted symbol is less unlikely to be corrupted to a relatively distant constellation symbol.

An example of the simplified BQM designed for 16QAM is provided in Figure 4.9. As

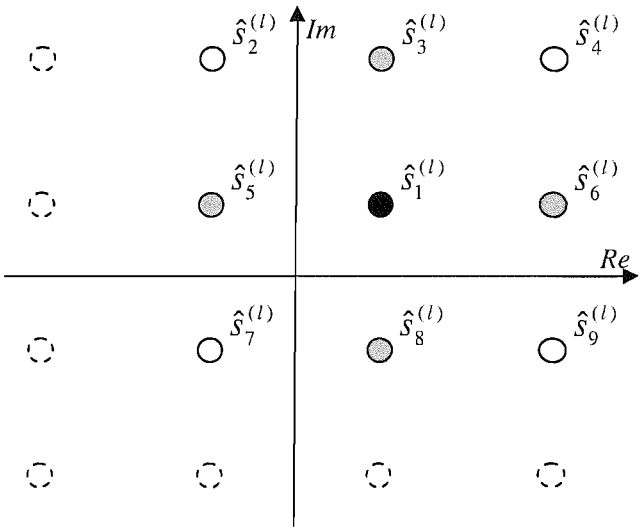

Figure 4.9: An example of the simplified BQM for 16QAM.

shown in Figure 4.9, for example, we assume that $\hat{s}_1^{(l)}$ is the original gene subjected to mutation, and $\hat{s}_i^{(l)}$ $(i = 2, \cdots, 9)$ represents the adjacent neighbours of $\hat{s}_1^{(l)}$, while the symbols represented by the dashed-line circles are ignored. Therefore, the GA's entire search space is reduced. Moreover, the search space can be further compressed, when we only consider the nearest neighbours of $\hat{s}_1^{(l)}$. In this case, only the symbols $\hat{s}_i^{(l)}$ $(i = 3, 5, 6, 8)$ printed in grey in Figure 4.9 will be regarded as the legitimate mutation candidates, each of which is assigned an equal 2D transition probability $p_{mt}^{(1j)} = 1/4$ $(j = 3, 5, 6, 8)$, while all other constellation symbols printed in white are neglected. Since the transition probability for each selected mutation candidate is equally fixed, the BQM scheme is simplified to a scheme similar to UM, which we may refer to as the *Closest-Neighbour Uniform Mutation (CNUM)* scheme. Note that similar to the scenario of BQM, in CNUM the corresponding transition probability value is also dependent on the location of the original gene. For instance, if the original gene is located in one of the four corners of the constellation map plotted in Figure 4.9, the relevant transition probability $p_{mt}^{(ij)}$ becomes 1/2, since in this case only two nearest-neighbour symbols exist. The CNUM-related transition probability values of the different modems are summarized in Table 4.4. Hence, by introducing the simplified BQM scheme or the CNUM arrangement, the computational complexity of BQM can be reduced. This issue will be discussed in Section 4.3.3.

4.3.1.3 Simulation Results

In this section, we provide our simulation results characterizing the achievable performance of the TTCM-assisted MMSE-GA-SDMA-OFDM system employing UM or BQM. For the BQM-

Modem	Transition probability value set
4QAM	1/2
16QAM	1/2, 1/3, 1/4
64QAM	1/2, 1/3, 1/4

Table 4.4: Possible transition probability values for the CNUM scheme.

based schemes, all the parameters used, including the TTCM-, GA- and channel-related ones, are the same as those specified in Table 4.1, except that the UM component was substituted by the BQM in the GA MUD.

4.3.1.3.1 BQM Versus UM

In Figure 4.10, the BER performance of the UM- and BQM-aided GA-assisted TTCM-MMSE-SDMA-OFDM systems employing a 4QAM scheme for transmission over the SWATM channel of Table 2.10 are compared, where six users are supported with the aid of six receiver antenna elements. Again, the performance of the TTCM-assisted MMSE-SDMA-OFDM system, the TTCM-aided optimum ML-detected system and the uncoded single-user scheme employing either a single receiver or invoking MRC when communicating over an AWGN channel are also provided for reference, respectively. As expected, we can see from Figure 4.10 that the BER performance of the TTCM-assisted MMSE-SDMA-OFDM system was further improved at relatively higher SNRs, when BQM rather than UM was used.

Furthermore, a higher performance improvement can be achieved by the BQM-aided scheme, when we have a higher user load or higher throughput, as seen in Figure 4.11. More specifically, the left hand side of Figure 4.11 shows the simulation results attained in the scenario, where a higher number of $L = 10$ users is supported. In this case, an E_b/N_0 gain of about 1dB was attained by the employment of BQM for a GA having a size of $X = 20$ and $Y = 5$ at the BER of 10^{-5}. This E_b/N_0 gain was achieved, since a higher user load results in a larger search space and hence the conventional UM suffers more from its inefficient mutation mechanism, while BQM may more readily be able to guide the mutation in the desirable directions even at low SNRs, especially in the scenarios having higher user loads. On the other hand, when a high-throughput modem such as for example 16QAM is employed, BQM may significantly outperform UM, as evidenced at the right hand side of Figure 4.11. As seen in the figure, the UM-aided scheme yielded a high residual error floor, since the GA apparently settled in local minima during its search due to the less efficient mutation strategy. By contrast, BQM significantly improved the GA's performance by lowering the error floor by about two magnitudes to the BER of 10^{-5}. Note that at SNRs higher

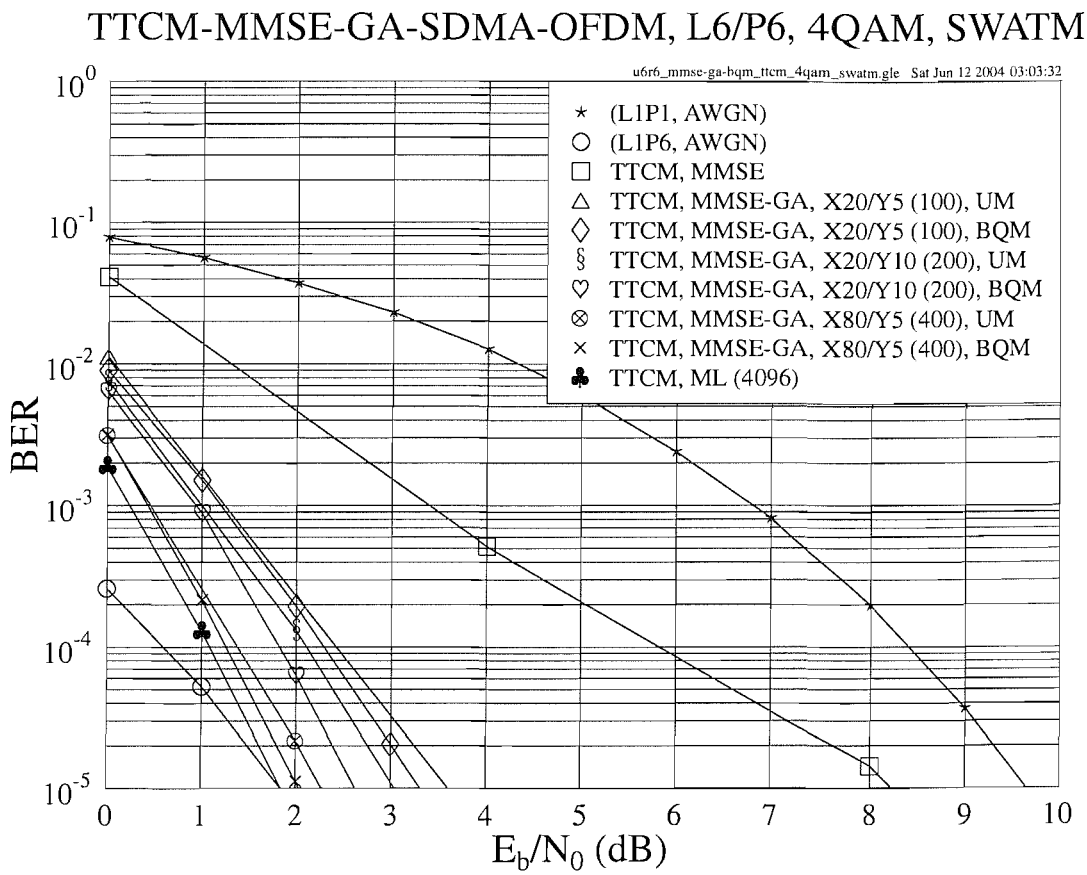

Figure 4.10: **BER** versus E_b/N_0 performance comparison of the **TTCM-assisted MMSE-GA-SDMA-OFDM** system using **UM** or **BQM**, while employing a **4QAM** scheme for transmission over the SWATM channel, where **L=6** users are supported with the aid of **P=6** receiver antenna elements. The basic simulation parameters are given in Table 4.1.

than 20dB, however, a cross-over point appeared on the curves, where a GA having $X = 160$ and $Y = 5$ could no longer improve the MMSE-aided system's performance, when the SNR was increased. The reason for encountering this phenomenon at a high SNR level is that it becomes more difficult for a moderate-complexity GA to mitigate the associated symbol errors, amongst the increased number of the 16QAM constellation symbols in comparison to the 4QAM constellation symbols. Hence, for the sake of improving the attainable performance of systems employing high-throughput modems, we may either use a more complex GA, which is less attractive for complexity-sensitive systems, or invoke an improved MUD framework, as it will be discussed in Section 4.3.2.

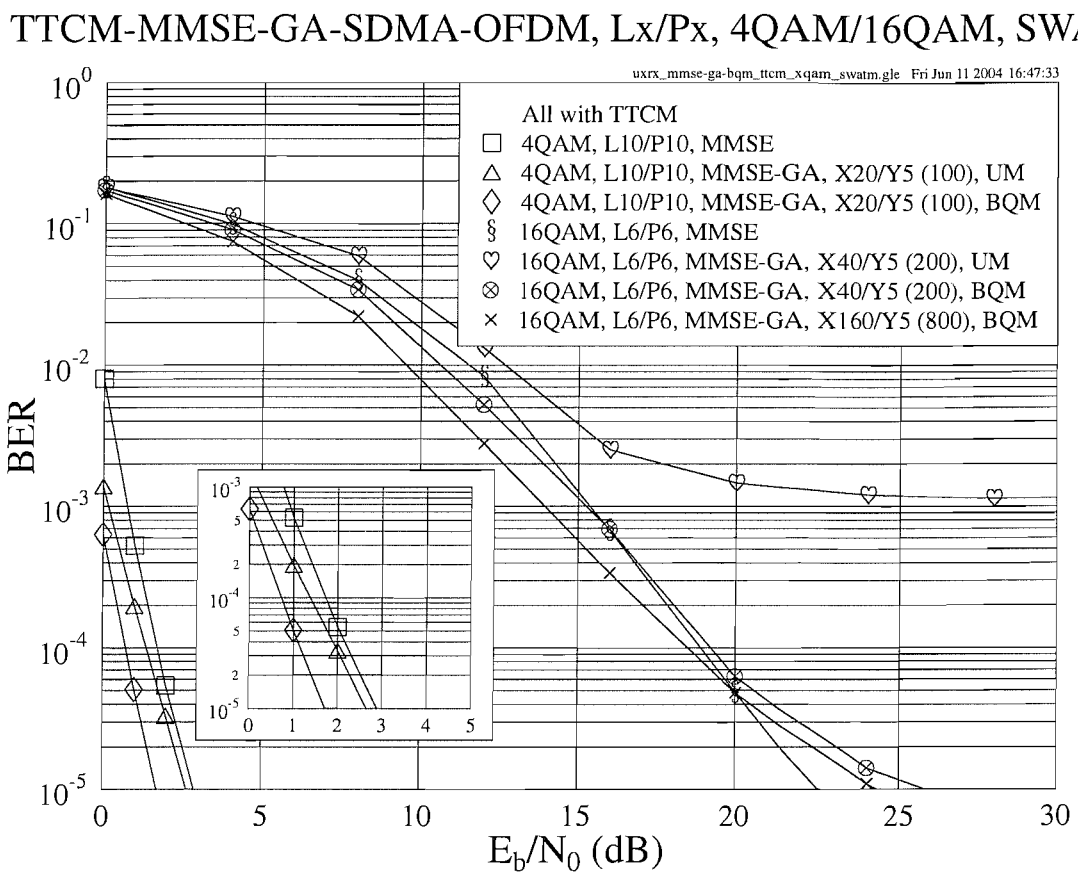

Figure 4.11: **BER** versus E_b/N_0 performance comparison of the **TTCM-assisted MMSE-GA-SDMA-OFDM** system using **UM** or **BQM**, while employing a **4QAM** or **16QAM** scheme for transmission over the SWATM channel, where **L=6** or **L=10** users are supported with the aid of **P=6** or **P=10** receiver antenna elements, respectively. The basic simulation parameters are given in Table 4.1.

4.3.1.3.2 BQM Versus CNUM

As discussed in Section 4.3.1.2.2, the BQM scheme may be simplified to the CNUM arrangement, which mutates to only one of the closest neighbours of the original gene, thus incurring a lower complexity in comparison to BQM. However, CNUM does not necessarily degrade the system's performance dramatically. Figure 4.12 provides a comparison of CNUM and BQM for both low- and high-throughput systems. As observed in Figure 4.12, the BQM-GA-assisted system achieved a slightly better performance than its CNUM-GA-assisted counterpart. This may suggest that in such scenarios the CNUM scheme may become an attractive alternative to the BQM scheme for the sake of further decreasing the complexity imposed.

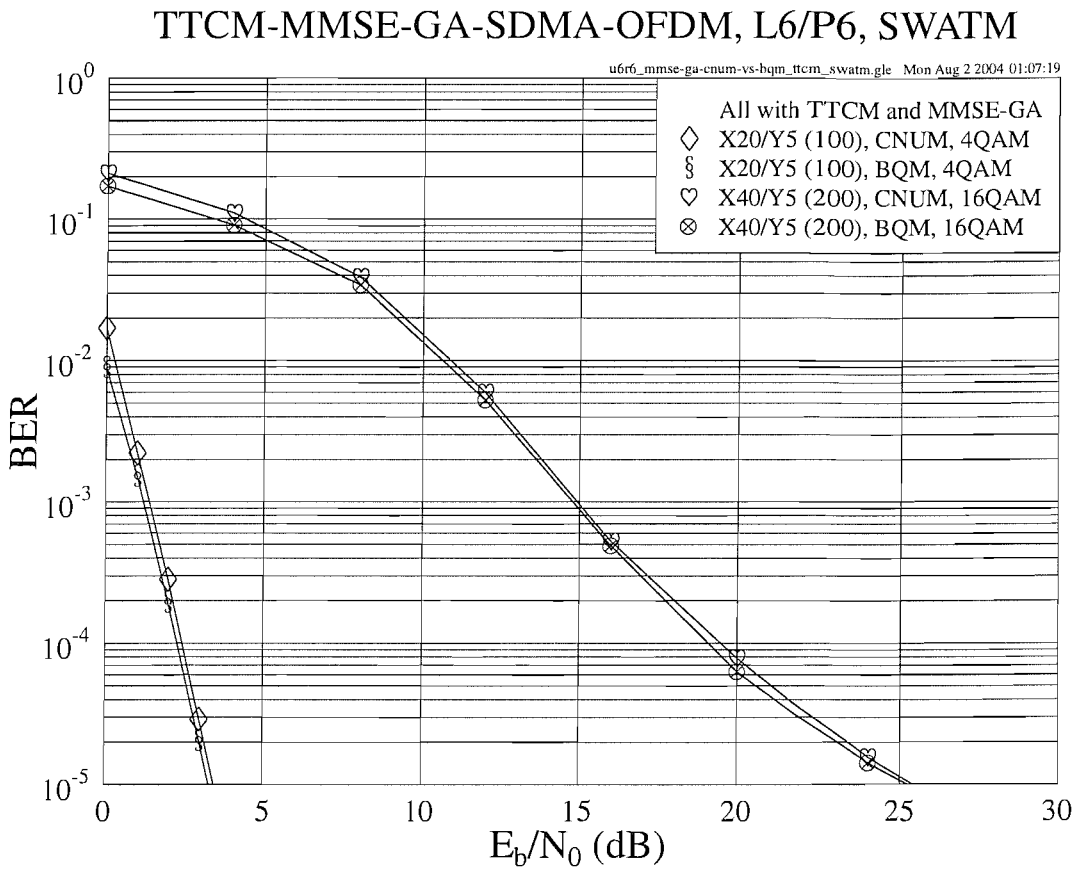

Figure 4.12: **BER** versus E_b/N_0 performance comparison of the **TTCM-assisted MMSE-GA-SDMA-OFDM** system using **CNUM** or **BQM**, while employing a **4QAM** or **16QAM** scheme for transmission over the SWATM channel, where **L=6** users are supported with the aid of **P=6** receiver antenna elements, respectively. The basic simulation parameters are given in Table 4.1.

4.3.2 Iterative MUD Framework

In Section 4.3.1, we have presented an enhanced mutation scheme, namely BQM, which is capable of improving the GA MUD's performance, especially in systems having high user loads and/or employing high-throughput modems. This may be regarded as GA-related improvement in the context of the GA MUD. In this section, we will focus our attention on an enhanced iterative MUD framework, so that the system's performance may be further improved in all the scenarios considered so far.

4.3.2.1 MMSE-initialized Iterative GA MUD

In the literature, iterative techniques such as Successive Interference Cancellation (SIC) [196, 305–307] and Parallel Interference Cancellation (PIC) [305, 307, 308], have been designed for multi-user OFDM systems. Following the philosophy of iterative detections, we propose a

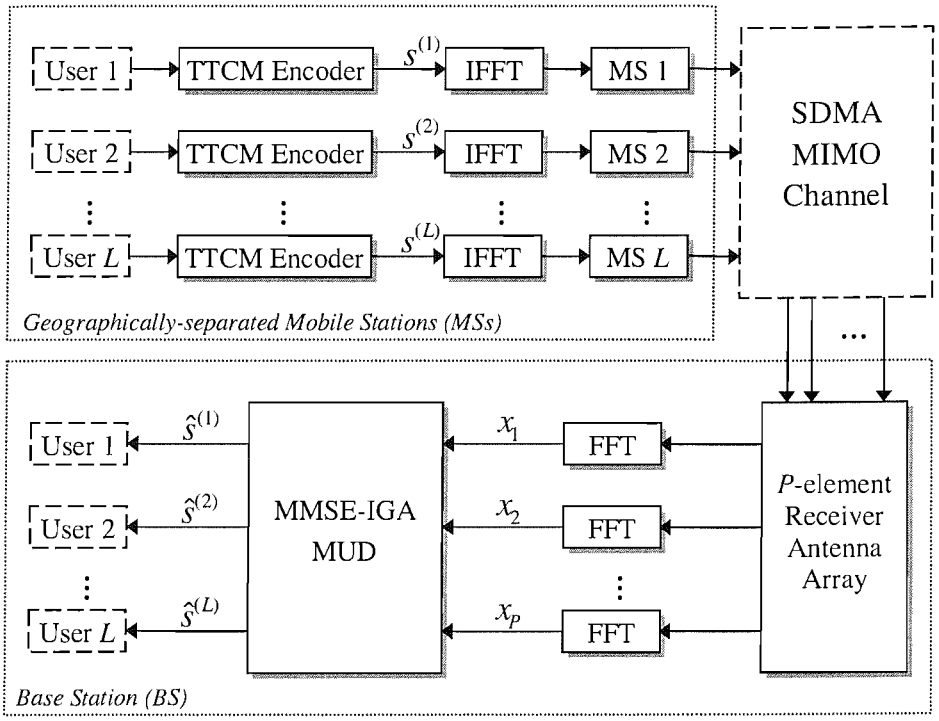

Figure 4.13: Schematic of the IGA MUD assisted multi-user SDMA-OFDM uplink system.

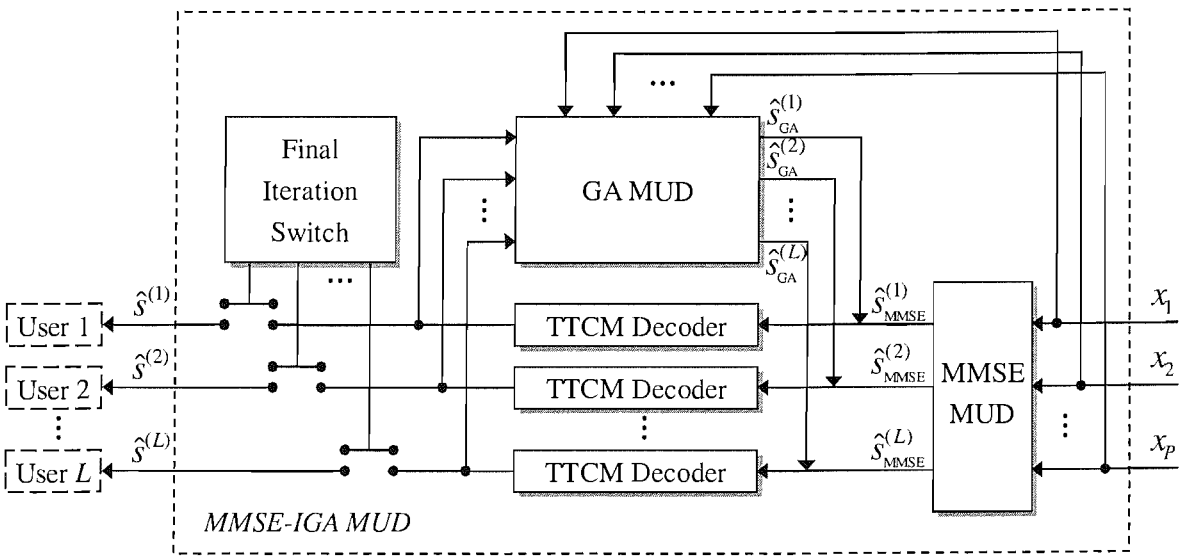

Figure 4.14: Structure of the MMSE-initialized iterative GA MUD used at the BS.

MMSE-initialized iterative GA (IGA) MUD for multi-user SDMA-OFDM systems. Figure 4.13 shows the proposed IGA MUD assisted multi-user SDMA-OFDM uplink system. Upon comparing Figure 4.1 and Figure 4.13, we can observe that the concatenated MMSE-GA MUD used in the BS of Figure 4.1 is replaced by the MMSE-assisted IGA MUD seen in the middle-bottom part of Figure 4.13, while the detailed structure of the IGA MUD is outlined in Figure 4.14. More specifically, the received length-P symbol vector $\mathbf{x}$ of Equation (3.2) is first detected by the MMSE MUD, which outputs the L MMSE-detected symbols $\hat{s}^{(l)}_{\text{MMSE}}$ $(l = 1, \cdots, L)$ of the L users, and forwards them to L number of independent TTCM decoders. The TTCM-decoded L-symbol vector, which is more reliable than the MMSE MUD's output, is then fed into the concatenated GA MUD for assisting the creation of the initial population. Then the genetically enhanced output symbol vector $\hat{\mathbf{s}}_{\text{GA}}$, which may be expected to become more reliable, will be fed back to the TTCM decoders in order to further improve the signal's quality, invoking a number of iterations. Following the last iteration, the final GA solution will be decoded by the TTCM decoders, and the hard-decision version of the estimated information bits of the L independent users is forwarded to the output, which is only enabled at the final iteration by the switch seen in Figure 4.14.

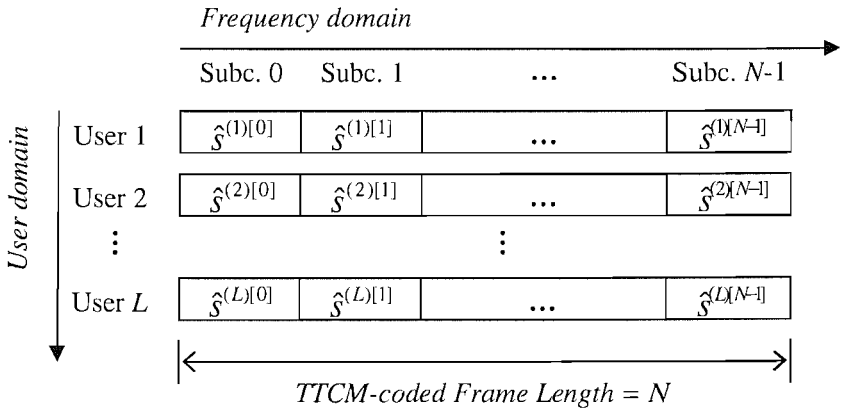

Figure 4.15: The 2D optimization provided by the MMSE-IGA MUD of Figure 4.14. The square brackets [·] denote the subcarrier indices in the TTCM-coded frame of length N.

Therefore, two improvements have been achieved by the MMSE-IGA MUD. Firstly, a more accurate initial knowledge of the transmitted signals, namely the output of the TTCM decoders rather than that of the MMSE MUD, is supplied for the GA MUD. This reliable improvement therefore offers a better starting point for the GA's search. Secondly, the iterative processing ensures that the detected L-user symbol vector can be optimized in two dimensions, as demonstrated in Figure 4.15. During every iteration, on one hand, each L-symbol vector at a specified subcarrier slot is optimized by the GA in the context of the *user domain*. On the other hand, the entire TTCM-coded frame of each user is optimized by the TTCM decoder in the context of the TTCM-related *codeword domain*, or more specifically

the *frequency domain*. Hence, as the iterative processing continues, an information exchange takes place between the two domains, resulting in a 2D optimization which may be expected to improve the system's performance.

4.3.2.2 Simulation Results

In this section, we combine the IGA MUD with BQM, which has been presented in Section 4.3.1.2, and compare the associated simulation results with our previous results. Note that for the sake of fairness, we halved the number of TTCM decoding iterations for the IGA-aided scheme, so that the total TTCM-related complexity remains approximately the same as in the non-iterative system. For the convenience of the reader, in Table 4.5 we summarize the basic simulation parameters used for generating the results provided in this section.

4.3.2.2.1 Performance in Underloaded and Fully-loaded Scenarios

In this section, we will investigate the system's achievable performance generated in the so-called underloaded and fully-loaded scenarios, respectively, where the number of users L is less than or is equal to the number of receiver antennas P.

4.3.2.2.1.1 BQM-IGA Performance

Figure 4.16 shows the BER performance achieved by the various schemes considered. The numbers in the round brackets seen in the legends of Figure 4.16 denote the associated number of IGA MUD iterations and the total GA or ML complexity, respectively. From the results of Figure 4.16 two conclusions may be arrived at. Firstly, an improved performance can be achieved, when the GA commences its operation from a better initial population, regardless of the different mutation schemes used. For example, at the same GA complexity, the single-iteration IGA MUD assisted systems outperformed their non-iterative GA aided counterparts, since the initial GA population of the former systems were created based on the first-iteration outputs of the TTCM decoders, rather than on the less reliable MMSE MUD regardless, whether UM or BQM was employed.

Secondly, the system employing the BQM-aided two-iteration IGA MUD was capable of achieving the same performance as the optimum ML-aided system at an even lower complexity compared to the UM- or BQM-aided non-iterative GA MUD, which was characterized in Figure 4.10. For instance, Figure 4.16 shows that the two-iteration BQM-IGA MUD having a complexity of 200 achieved virtually indistinguishable performance in comparison to its ML-aided counterpart, while the non-iterative UM/BQM-GA MUD having a complexity of

TTCM	Modem	4QAM
	Code rate	0.5
	Code memory ν	3
	Octal generator polynomial	[13 6]
	Codeword length	1024 symbols
	Channel interleaver depth	1024 symbols
	Number of turbo iterations	2
GA	Population initialization method	MMSE
	Mating pool creation strategy	Pareto-Optimality
	Selection method	Fitness-Proportionate
	Cross-over	Uniform cross-over
	Mutation	UM or BQM
	Mutation probability p_m	0.1
	Elitism	Enabled
	Incest prevention	Enabled
	Population size X	Varied
	Generations Y	Varied
	Number of IGA iterations	Varied
Channel	CIRs	SWATM [3]
	Paths	3
	Maximum path delay	48.9 ns
	Normalized Doppler frequency f_d	1.235×10^{-5}
	Subcarriers K	512
	Cyclic prefix	64

Table 4.5: The various techniques and parameters used in the simulations of Section 4.3.2.2.

400 attained a slightly inferior performance in comparison to the ML-aided arrangement, as observed in Figure 4.10.

Having investigated the system using the 4QAM modem, let us now consider various high-throughput scenarios. As mentioned in Section 4.3.1.3, the non-iterative GA MUD may result in a high residual error floor in high-throughput scenarios, even if BQM is employed. However, with the aid of the IGA MUD, the error floor can be effectively reduced, as seen in Figure 4.17. 16QAM modem was employed by all the schemes[7] characterized in Figure 4.17, except for the uncoded single-user benchmark scheme communicating over the AWGN channel, which

[7]Note that in this case the associated complexity of the ML-aided scheme is as high as on the order of $O(2^{mL}) = O(2^{4\cdot 6}) = O(16,777,216)$, which imposes an excessive complexity and hence cannot be simulated.

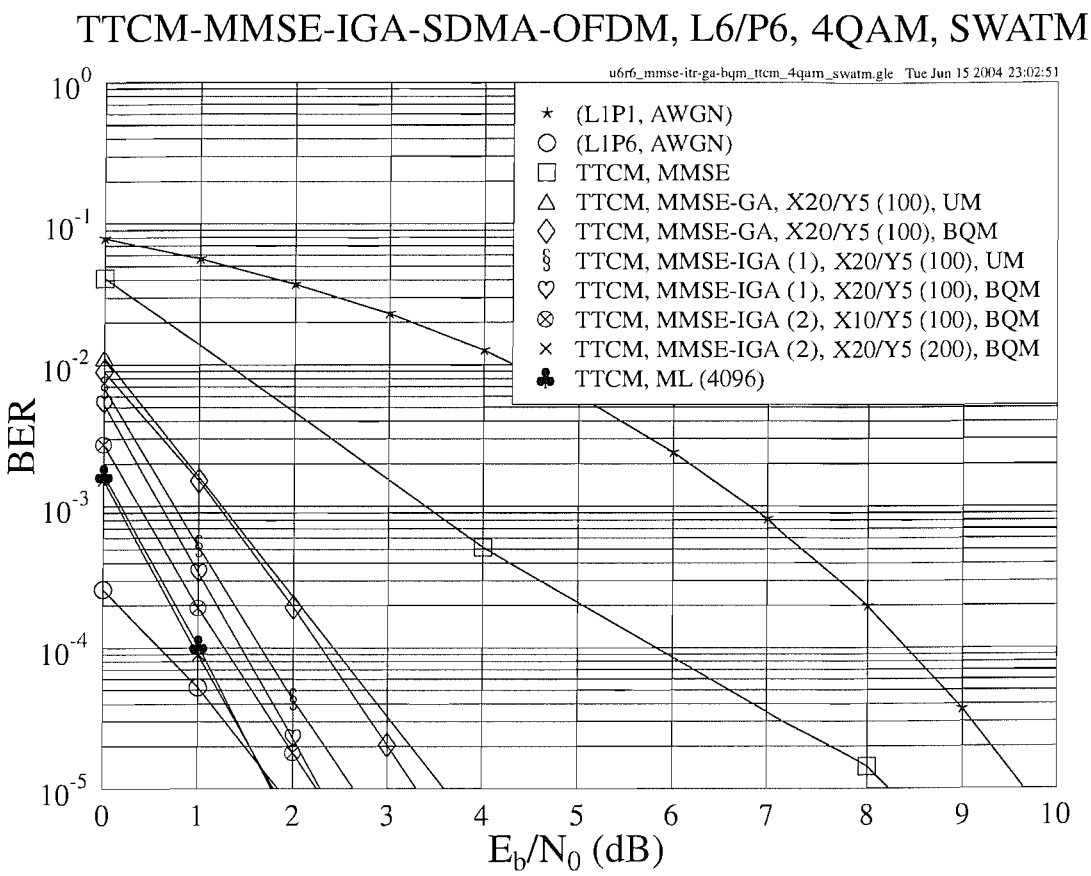

Figure 4.16: **BER** versus E_b/N_0 performance comparison of the **iterative** or **non-iterative TTCM-assisted MMSE-GA-SDMA-OFDM** system using **UM** or **BQM**, while employing a **4QAM** scheme for transmission over the SWATM channel, where **L=6** users are supported with the aid of **P=6** receiver antenna elements, respectively. The basic simulation parameters are given in Table 4.5.

used 8PSK for the sake of maintaining the same effective throughput of 3BPS as the other TTCM-coded schemes. Similarly to the 4QAM scenario of Figure 4.16, it can be seen in Figure 4.17 that a better initial population resulted in an improved performance in both the UM- and BQM-aided systems. However, we may notice that even when assisted by a reliable initial knowledge of the transmitted symbols, the UM-aided single-iteration IGA MUD was unable to substantially decrease the error floor. Even when we increased the number of UM-IGA MUD iterations, the situation remained the same, except for the modest improvements achieved at SNRs lower than 16dB. By contrast, the BQM-aided scheme is capable of substantially exploiting the benefits arising from both a better initial GA population and from an increased number of IGA MUD iterations. More specifically, on one hand, the improved initial population provides a good starting point for the GA, thus assisting the BQM, which in turn benefits the entire detection process, resulting in a substantial performance improvement. On the other hand, the iterative processing invoked by the IGA MUD further enhances

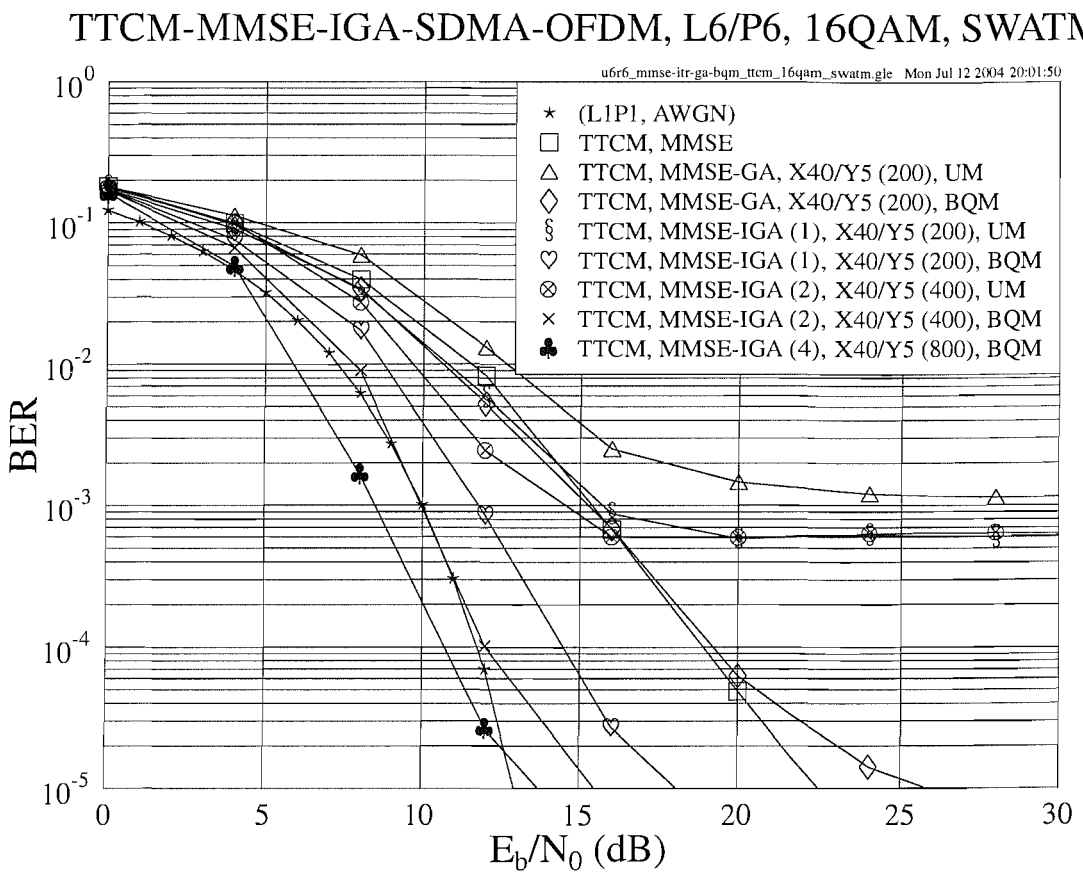

Figure 4.17: **BER** versus E_b/N_0 performance comparison of the **iterative** or **non-iterative TTCM-assisted MMSE-GA-SDMA-OFDM** system using **UM** or **BQM**, while employing a **16QAM** scheme for transmission over the SWATM channel, where **L=6** users are supported with the aid of **P=6** receiver antenna elements, respectively. The basic simulation parameters are given in Table 4.5.

the system's performance with the aid of the 2D optimization, as discussed in Section 4.3.2.1, since the beneficial information exchange between the user domain and the frequency domain assists both the GA MUD and the TTCM decoder in eliminating more and more errors found in the received signal, as the iterative procedure continues.

4.3.2.2.1.2 Effects of the Number of IGA MUD Iterations

Figure 4.18 shows the E_b/N_0 gain achieved by the BQM-IGA assisted TTCM-MMSE-SDMA-OFDM systems employing 16QAM at the BER of 10^{-5}, while using different number of IGA MUD iterations. The E_b/N_0 gain is defined here as the E_b/N_0 difference measured at the BER of 10^{-5} between the systems employing the BQM-IGA MUD or the MMSE MUD. As expected, when we had a higher number of IGA MUD iterations, a higher E_b/N_0 gain was attained. It is also found in Figure 4.18 that most of the achievable gain may be attained,

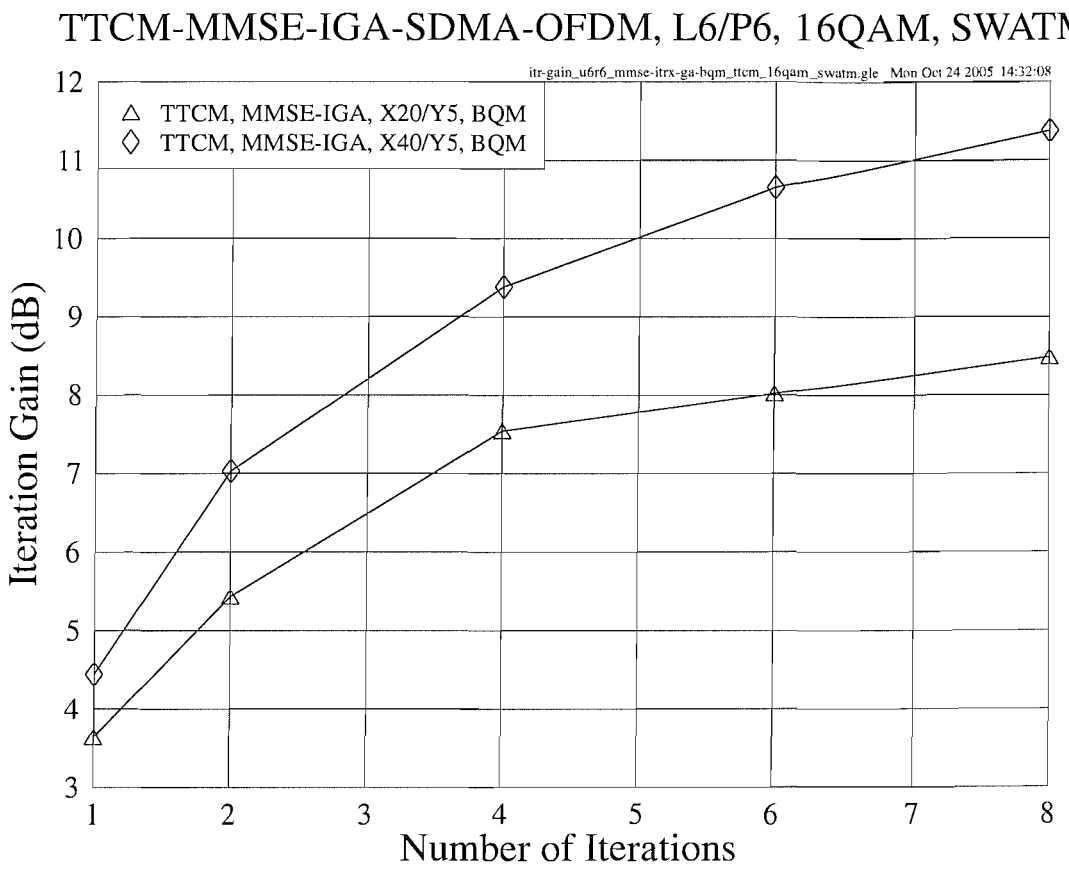

Figure 4.18: **Iteration gain** at the BER of 10^{-5} versus number of IGA MUD iterations performance of the **TTCM-assisted MMSE-IGA-SDMA-OFDM** system using **BQM**, while employing a **16QAM** scheme for transmission over the SWATM channel, where **L=6** users are supported with the aid of **P=6** receiver antenna elements. The basic simulation parameters are given in Table 4.5.

when the number of IGA MUD iterations reaches 8. Furthermore, when the complexity of the GA MUD increases, because for example a higher population size is employed, a higher gain can be achieved, as seen in Figure 4.18. Moreover, we may also notice that when the number of IGA MUD iterations was increased, the difference between the E_b/N_0 gains achieved by the higher-complexity and the lower-complexity IGAs tends to be larger. For example, as observed in Figure 4.18, when we had only one IGA MUD iteration, the E_b/N_0 gain difference between the two curves was about 1dB, while this value increased to about 3dB, when the number of iterations was increased to 8. This suggests that a high-complexity IGA may benefit more from a higher number of IGA MUD iterations than its lower-complexity counterpart.

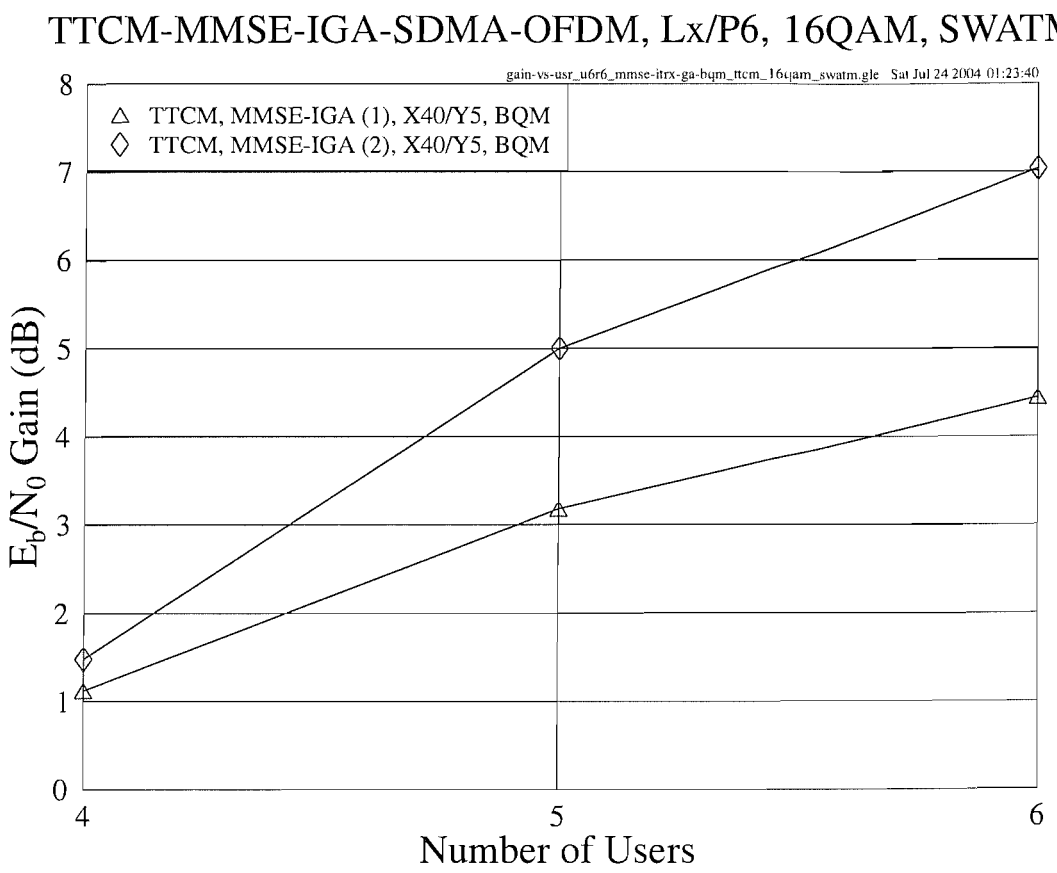

Figure 4.19: **E_b/N_0 gain** at the BER of 10^{-5} versus number of users performance of the **TTCM-assisted MMSE-IGA-SDMA-OFDM** system using **BQM**, while employing a **16QAM** scheme for transmission over the SWATM channel, where **L=4, 5, 6** users are supported with the aid of **P=6** receiver antenna elements, respectively. The basic simulation parameters are given in Table 4.5.

4.3.2.2.1.3 Effects of the User Load

Figure 4.19 exhibits the corresponding E_b/N_0 gains achieved by the SDMA-OFDM system exploiting $P = 6$ receiver antenna elements at the BER of 10^{-5} in the scenarios, where the user load varies. The user load of SDMA-OFDM systems was defined by Equation (3.14) in Section 3.3.2.1.1. As observed in Figure 4.19, firstly, it is shown that when the user load becomes higher, a higher gain can be attained. For example, for the single-iteration IGA-aided system, a further gain of about 3.5dB is achieved, when the number of users increases from four to six. This is because when more users were accommodated by the SDMA-OFDM system, the reference MMSE MUD suffered a higher performance degradation than the IGA MUD, and thus a higher E_b/N_0 gain was attained by the IGA MUD. Secondly, a higher number of IGA MUD iterations provides a higher E_b/N_0 gain for the system. For instance, in the full-user-load scenario, namely for $L = P = 6$, the two-iteration IGA-aided system achieves a

further gain of about 2.7dB over its single-iteration counterpart, providing an overall E_b/N_0 gain of 7dB over the base-line TTCM-MMSE-SDMA-OFDM benchmark system dispensing with the GA MUD.

4.3.2.2.2 Performance in Overloaded Scenarios

Recall that in Section 4.1 we pointed out that in practical applications the number of users L may be higher than that of the receiver antennas P, resulting in the overloaded scenario. However, most of the existing MUD techniques, such as for example the MMSE algorithm of [3,305] and the QRD-M algorithm of [173], suffer from a significant performance degradation in overloaded scenarios, owing to the insufficient degree of detection freedom at the receiver. By contrast, we will show in this section that the proposed IGA MUD is capable of adequately performing in overloaded scenarios.

4.3.2.2.2.1 Overloaded BQM-IGA

Figure 4.20 shows the performance achieved by the BQM-IGA aided TTCM-SDMA-OFDM system using 4QAM, when six, seven and eight users are supported by six receiver antenna elements, respectively. It is seen in Figure 4.20 that in the so-called overloaded scenarios, where the number of users exceeds the number of receiver antenna elements, the linear MMSE MUD suffered from an insufficient degree of freedom for separating the different users, since the high number of users incurred an excess Multi-User Interference (MUI). This results in a significant performance degradation in the context of the system using the MMSE MUD, when the number of users increased from six to eight, as observed in Figure 4.20. However, in such cases the system employing the proposed BQM-IGA MUD was still capable of maintaining a near-ML performance. For example, when we had $L = 8$, the two-iteration based BQM-IGA MUD reduced the BER measured at 3dB by four orders of magnitude in comparison to the MMSE-aided benchmark system, as evidenced by Figure 4.20. This result characterizes the robustness of the BQM-IGA MUD, which has successfully suppressed the high MUI experienced in overloaded scenarios.

Figure 4.21 shows the iteration gain achieved by the BQM-IGA assisted TTCM-MMSE-SDMA-OFDM system employing 4QAM at the BER of 10^{-5}, while using different number of IGA MUD iterations. The iteration gain is defined here as the E_b/N_0 difference of the systems employing different number of IGA MUD iterations measured at the BER of 10^{-5} in comparison to the baseline system employing a single IGA MUD iteration. It is found in Figure 4.21 that when more users are supported, higher iteration gains may be obtained by iterative detection. For example, a gain of about 6dB was attained by the eight-user system

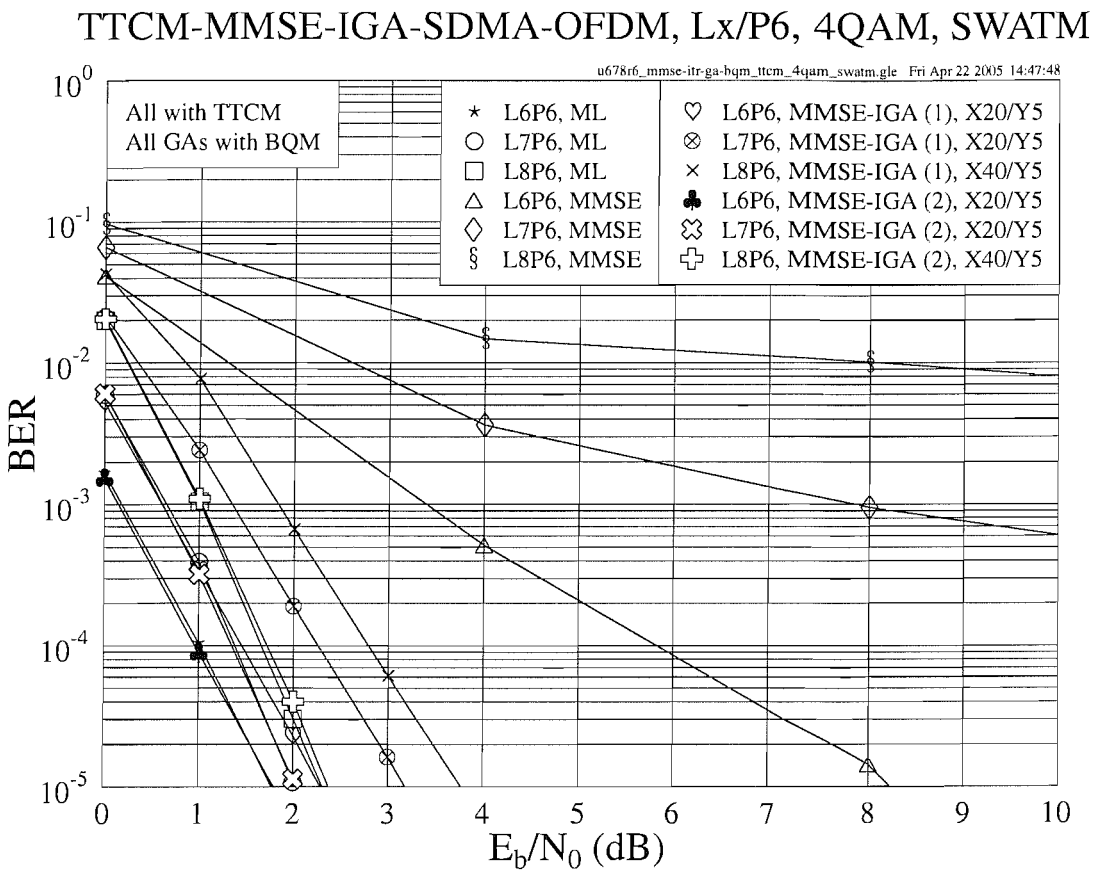

Figure 4.20: **BER** versus E_b/N_0 performance comparison of the **TTCM-assisted MMSE-IGA-SDMA-OFDM** system using **BQM**, while employing a **4QAM** scheme for transmission over the SWATM channel, where **L=6, 7, 8** users are supported with the aid of **P=6** receiver antenna elements, respectively. The basic simulation parameters are given in Table 4.5.

at the second IGA MUD iteration, while that attained by the six-user system was only about 0.5dB. Furthermore, as the number of iterations was increased from two to six, the former scheme provided a further gain of about 1dB, while no explicit gain was achieved by the latter arrangement, as shown in Figure 4.21. It is also seen in Figure 4.21 that most of the achievable iteration gain has been attained at the second IGA MUD iteration for all the schemes.

4.3.2.2.2.2 BQM Versus CNUM

In Section 4.3.1.3.2, we have shown the performance of the CNUM arrangement discussed in Section 4.3.1.2.2 in a fully-loaded scenario. In Figure 4.22, we characterize the CNUM aided system's performance achieved in an overloaded scenario, where six receiver antennas were used. As seen in Figure 4.22, the BQM-IGA aided system slightly outperformed the CNUM-IGA aided system. This suggests that similar to the case of fully-loaded scenarios,

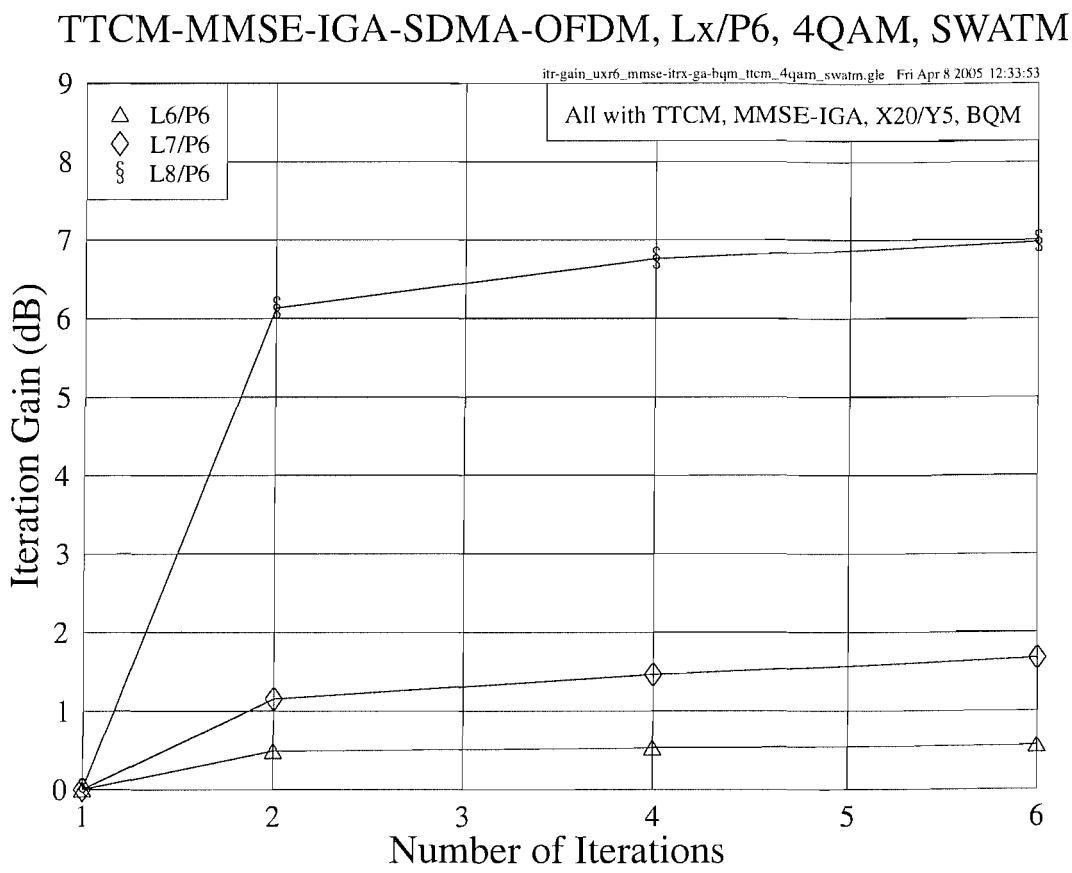

Figure 4.21: **Iteration gain** at the BER of 10^{-5} versus number of IGA MUD iterations performance of the **TTCM-assisted MMSE-IGA-SDMA-OFDM** system using **BQM**, while employing a **4QAM** scheme for transmission over the SWATM channel, where **L=6, 7, 8** users are supported with the aid of **P=6** receiver antenna elements, respectively. The basic simulation parameters are given in Table 4.5.

the CNUM scheme may also be employed in overloaded scenarios for achieving a further complexity reduction over the BQM scheme without suffering from a significant performance loss.

4.3.2.2.2.3 Convergence

As an investigation on the GA's convergence characteristics, in Figure 4.23 the performance of the 8×6 overloaded TTCM-aided MMSE-BQM-IGA-SDMA-OFDM system is illustrated, while using two IGA MUD iterations at a fixed E_b/N_0 value of 2dB. More specifically, at the left-hand side of Figure 4.23 the population size X was varied with the number of generations fixed at $Y = 5$, while at the right-hand side of Figure 4.23 the effect of a different number of generations Y was evaluated at a fixed population size of $X = 20$. Explicitly, as

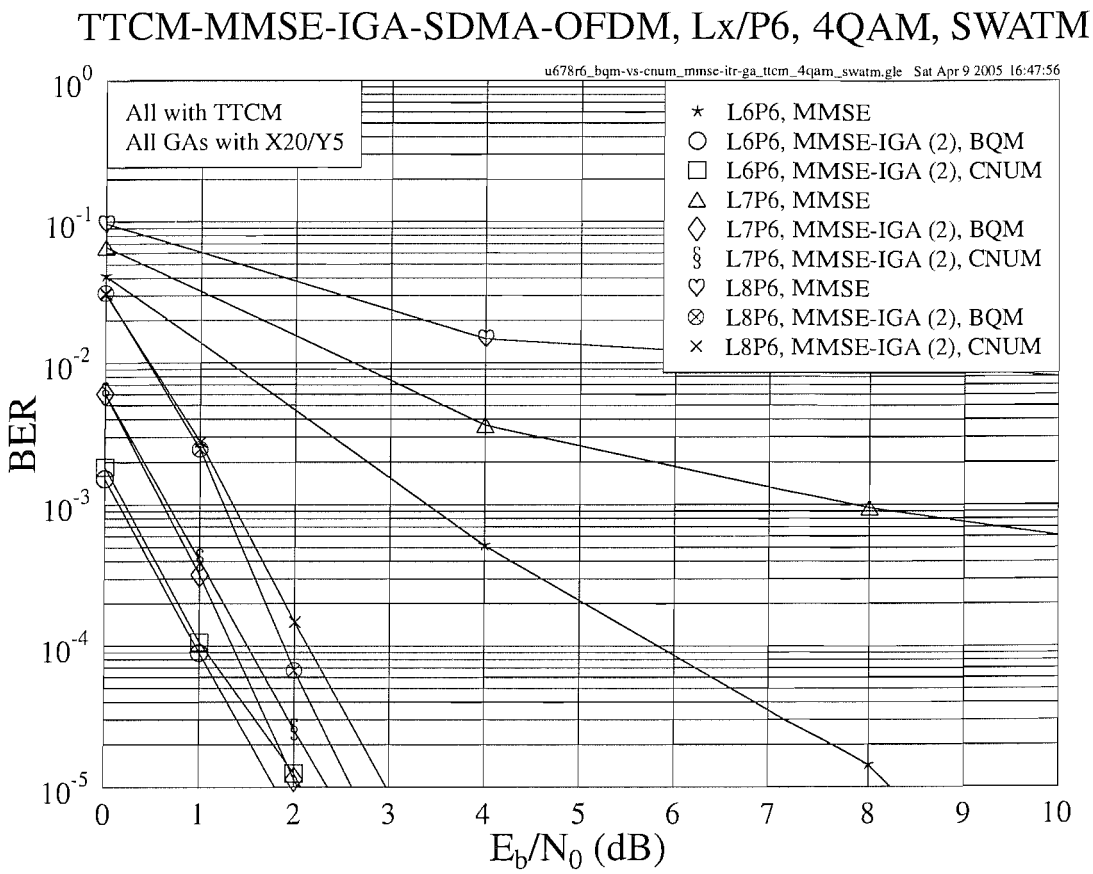

Figure 4.22: **BER** versus E_b/N_0 performance comparison of the **TTCM-assisted MMSE-IGA-SDMA-OFDM** system using **BQM** or **CNUM**, while employing a **4QAM** scheme for transmission over the SWATM channel, where **L=6, 7, 8** users are supported with the aid of **P=6** receiver antenna elements, respectively. The basic simulation parameters are given in Table 4.5.

X or Y increases, a consistently reduced BER is observed, which approaches the optimum ML performance. Furthermore, we show in Figure 4.24 the corresponding Probability Distribution Function (PDF) curves of the IGA-aided system's BER performance using a similar configuration as that associated with Figure 4.23, except that the population size was fixed at $X = 40$. Each of the five PDFs was plotted based on the statistical distribution of the BER results generated by 300 independent simulation runs. As shown in Figure 4.24, the peak of the PDF curve, which indicates the IGA-aided system's most-likely attainable BER performance, is 'shifted' closer to the average ML performance represented by the vertical dashed line seen at the left side of the figure, as the number of generations Y increases. This fact demonstrates that the performance of the IGA MUD *will* converge to the optimum one in overloaded scenarios, provided that a sufficiently high value of Y is used. We also point out that in underloaded or fully-loaded scenarios, a similar convergence having the same trend is expected.

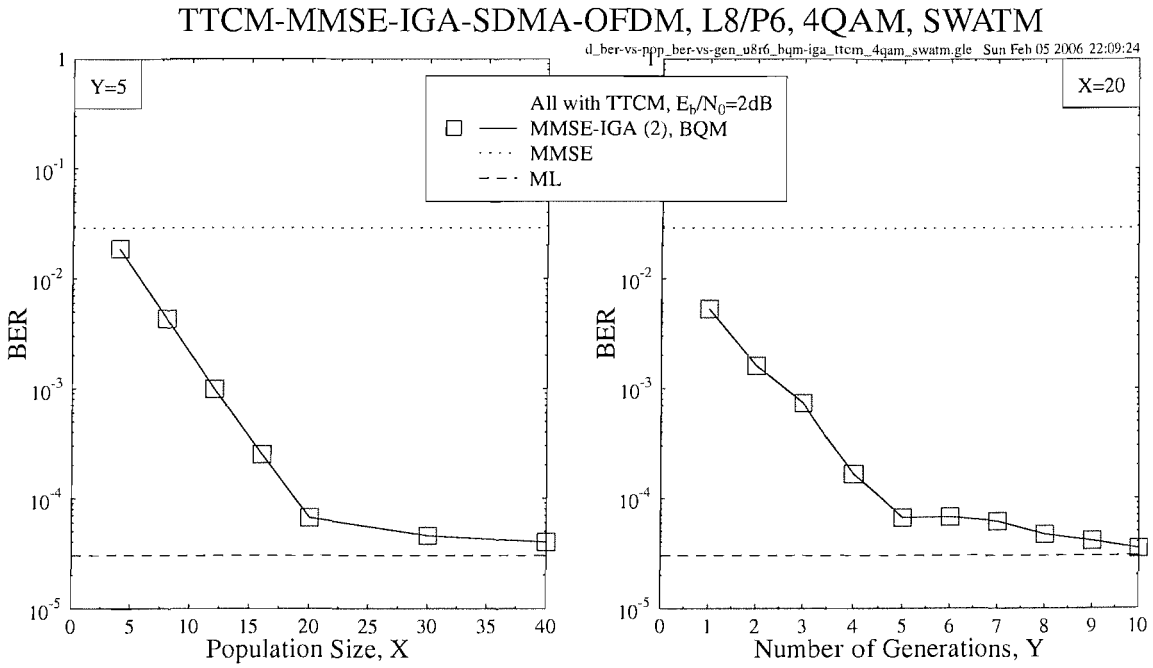

Figure 4.23: BER versus E_b/N_0 performance of the TTCM-assisted MMSE-IGA-SDMA-OFDM system using BQM, while employing a 4QAM scheme for transmission over the SWATM channel, where $L = 8$ users are supported with the aid of $P = 6$ receiver antenna elements. An E_b/N_0 value of 2dB was assumed. Left: a variable population size X with the number of generations fixed at $Y = 5$; right: a different number of generations Y with the population size fixed at $X = 20$.

4.3.2.2.3 Performance Under Imperfect Channel Estimation

As a further investigation, we provide the simulation results generated in the scenario, where the Channel State Information (CSI) was assumed to be imperfect. The estimated CIRs $\hat{h}_i$ were generated by adding random Gaussian noise to the true CIR taps h_i as:

$$\hat{h}_i[n] = h_i[n] + \sqrt{\frac{\sigma_n^2}{\varepsilon}} n_i[n], \quad i = 1, \cdots, \mathcal{L}, \tag{4.19}$$

where ε is the effective noise factor, σ_n^2 is the noise variance at the specific SNR level, n_i is an AWGN sample having zero-mean and a variance of unity, $\mathcal{L}$ is the number of CIR taps and $[n]$ denotes the n^{th} OFDM symbol. In the scenarios associated with imperfect CIRs, ε was set to 64 and $\mathcal{L}$ was set to 3 for the three-path SWATM channel used. In this case, the effective noise power added to the true CIR taps during each OFDM symbol for the sake of simulating imperfect channel estimation was $\sigma_n^2 \cdot \mathcal{L}/\varepsilon = \sigma_n^2 \times 4.69\%$. A snap shot of the SWATM channel is portrayed in Figure 4.25, which shows both the real and imaginary components of the FD-CHTFs associated with both perfect and imperfect CIRs.

Our performance comparison of the proposed BQM-IGA aided TTCM-MMSE-SDMA-

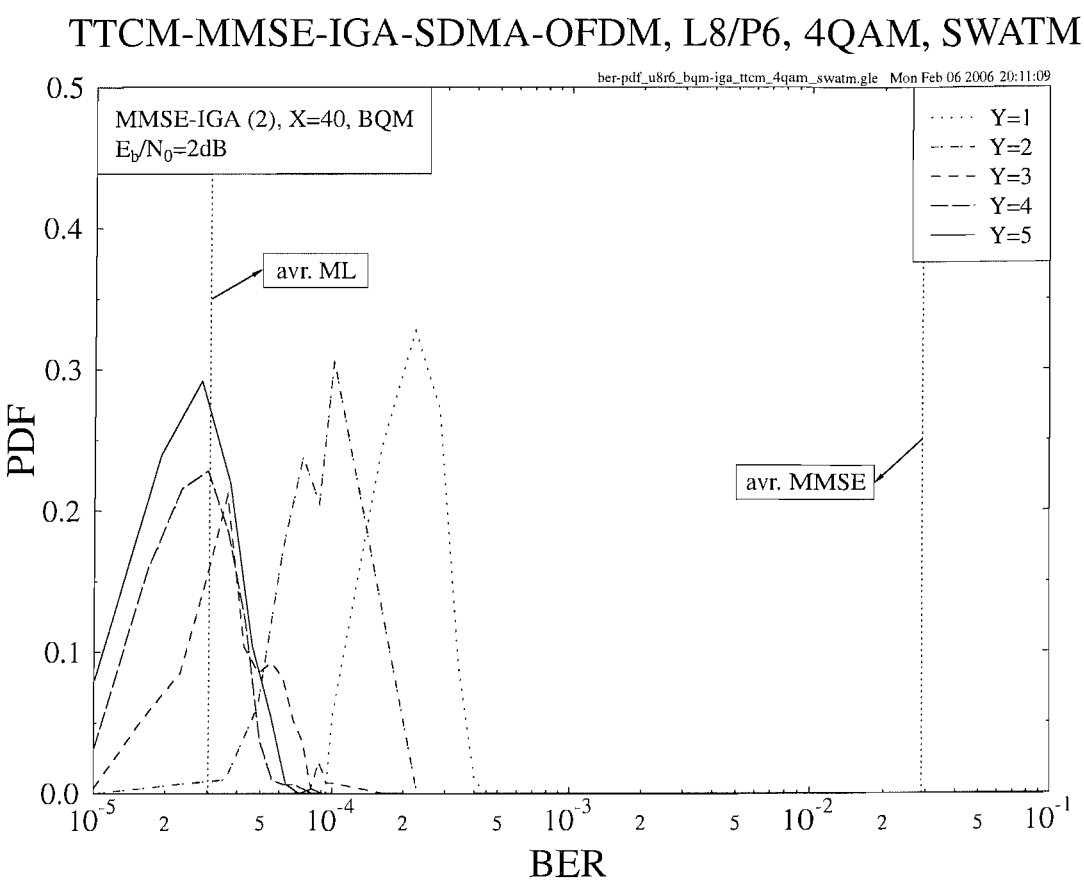

Figure 4.24: Probability Distribution Function (PDF) versus BER performance of the TTCM-assisted MMSE-IGA-SDMA-OFDM system using BQM, while employing a 4QAM scheme for transmission over the SWATM channel, where $L = 8$ users are supported with the aid of $P = 6$ receiver antenna elements. An E_b/N_0 value of 2dB was assumed.

OFDM system under the assumptions both of perfect and imperfect CSI is provided in Figure 4.26. As seen in Figure 4.26, the proposed system was capable of attaining an acceptable performance even without accurate channel knowledge. Moreover, it was found that when imperfect channel estimation was assumed, the BQM-IGA aided system outperformed its ML-aided counterpart, especially in the scenarios associated with higher user loads. This phenomenon may be explained as follows. When the CSI is imperfect, the ML-detected signal becomes less reliable than that detected in the scenario benefitting from perfect CSI. The relatively unreliable output of the ML MUD may readily mislead the TTCM decoder due to error propagation, resulting in a performance degradation. However, the detrimental effects of imperfect CSI may be mitigated by the proposed IGA MUD. More specifically, the IGA MUD optimizes the detected signal in two dimensions, namely in both the user domain as well as in the frequency domain, as discussed in Section 4.3.2.1. The beneficial information exchange offered by the IGA MUD between the two domains may effectively assist the con-

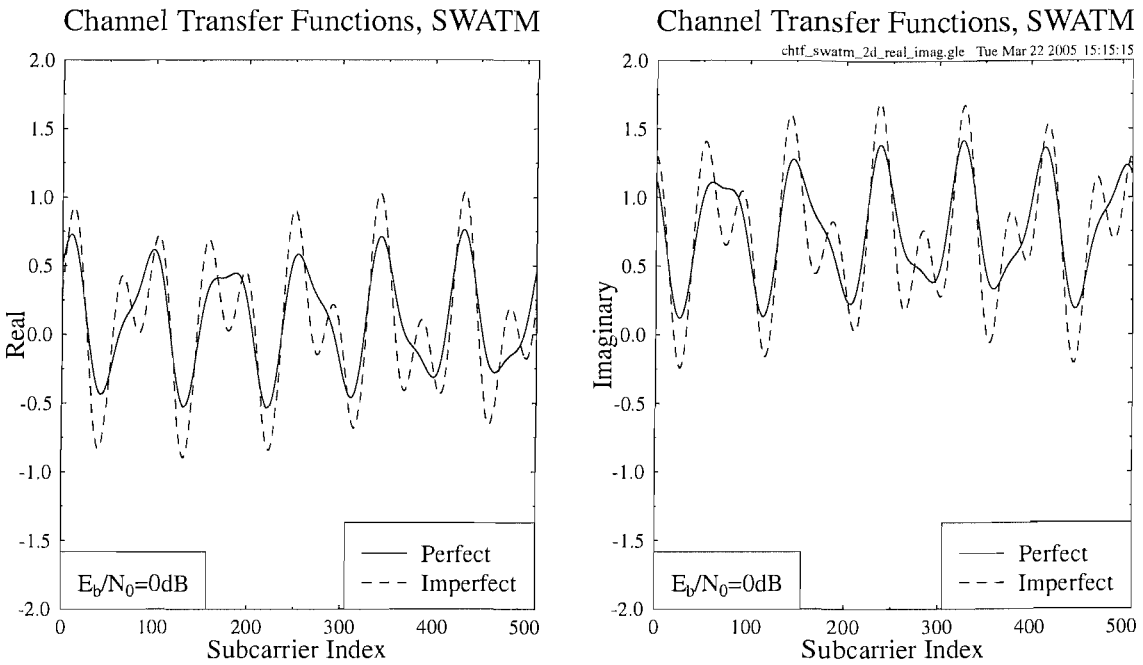

Figure 4.25: The real and imaginary components of the FD-CHTFs of the SWATM channel measured during one OFDM symbol at a E_b/N_0 value of 0dB in terms of both perfect and imperfect CIRs.

catenated detection-decoding procedure in counteracting the detrimental effects of imperfect channel estimation. This therefore results in a better system performance in comparison to that achieved by the ML-aided system. Furthermore, when a higher number of users had to be supported, the ML-aided system using imperfect CSI suffered more from the inaccurate multi-user detection, while a more robust behaviour was exhibited by the IGA-aided system, as shown in Figure 4.26.

4.3.3 Complexity Analysis

Compared to the conventional UM scheme, BQM is capable of significantly improving the GA's performance, especially in high-throughput or high-SNR scenarios, as discussed in Section 4.3.1.3.1. Furthermore, this performance improvement was achieved at the cost of a modest complexity increase and a modest memory requirement. More specifically, at different SNR levels, for each of the 2^m constellation symbols, a specific set containing $(2^m - 1)$ number of normalized 2D transition probabilities has to be created. However, this only imposes a modest "once-for-all" calculation, since we can derive the associated transition probabilities with the aid of off-line experiments for a number of typical SNR levels, where the calculated data can be stored in the base station's memory, hence incurring no further computational complexity. Furthermore, by introducing the simplified BQM scheme of Section 4.3.1.2.2, the

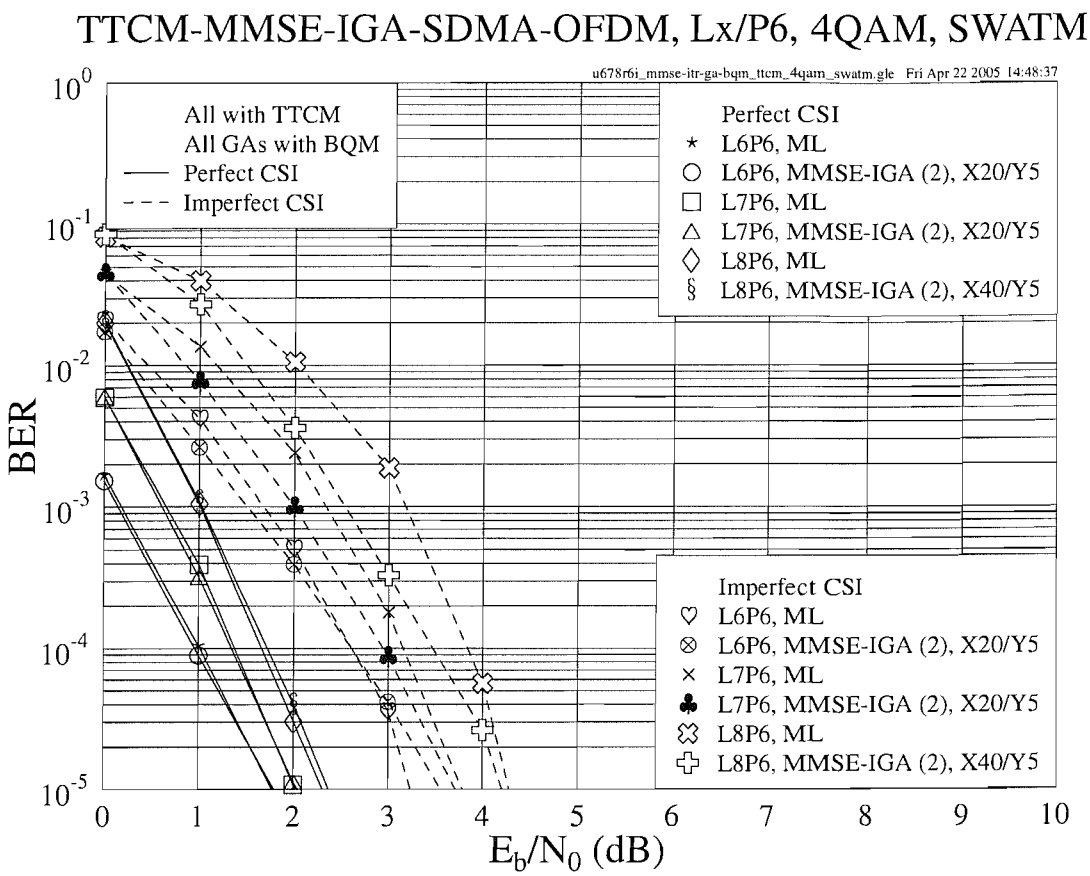

Figure 4.26: **BER** versus E_b/N_0 performance comparison of the **TTCM-assisted MMSE-IGA-SDMA-OFDM** system using **BQM** with perfect or imperfect CSI , while employing a **4QAM** scheme for transmission over the SWATM channel, where **L=6, 7, 8** users are supported with the aid of **P=6** receiver antenna elements, respectively. The basic simulation parameters are given in Table 4.5.

associated complexity and memory cost may be dramatically reduced, especially for high-throughput modems such as 16QAM or 64QAM, since the number of mutation target candidates decreases and thus fewer transition probability calculations are required. Moreover, if the CNUM scheme is employed, the associated complexity can be further decreased, since in this case there is no need to calculate the transition probabilities, which are already available in Table 4.4. This may significantly reduce the associated complexity and memory requirement, while still maintaining a similar performance to that of the BQM scheme, as seen in Figures 4.12 and 4.22.

As shown in Figures 4.18 and 4.21, the system's performance can be further improved, when the number of IGA MUD iterations is increased. When the other parameters remain the same, using a higher number of IGA MUD iterations will result in a further increased complexity. However, this may still be significantly lower than that imposed by the ML-aided scheme. Figure 4.27 provides our comparison of the TTCM-assisted MMSE-SDMA-

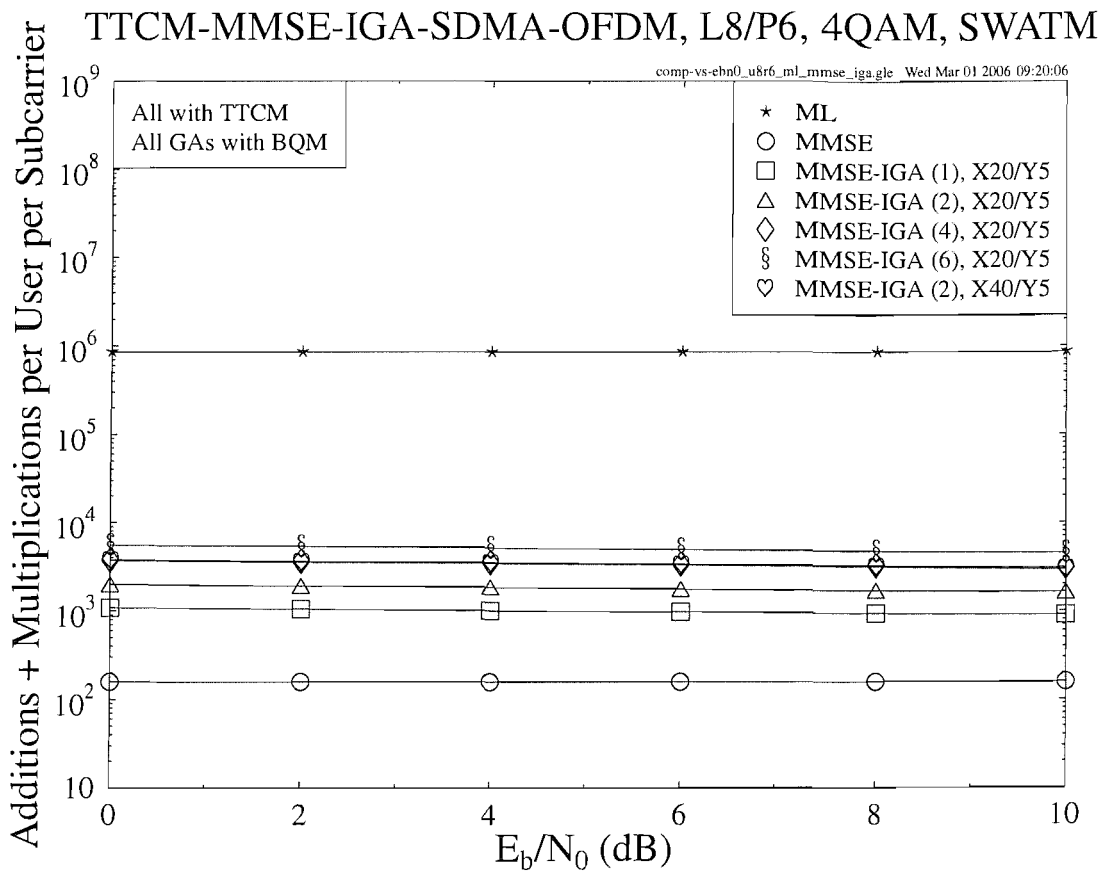

Figure 4.27: **Complexity** per user per subcarrier versus E_b/N_0 performance comparison of the **TTCM-assisted MMSE-SDMA-OFDM**, **ML-SDMA-OFDM**, and **MMSE-BQM-IGA-SDMA-OFDM** systems, while employing a **4QAM** scheme for transmission over the SWATM channel, where **L=8** users are supported with the aid of **P=6** receiver antenna elements. The basic simulation parameters are given in Table 4.5.

OFDM, ML-SDMA-OFDM and MMSE-BQM-IGA-SDMA-OFDM systems in the context of their MUD complexity, which was quantified in terms of the number of complex additions and multiplications imposed by the different MUDs on a per user per subcarrier basis. As illustrated in Figure 4.27, the complexity of the ML MUD is significantly higher than that of the MMSE MUD or the IGA MUD. Furthermore, the IGA MUD's complexity does not significantly vary at different E_b/N_0 values and depends on the number of IGA MUD iterations as well as on the GA's parameters, for example the population size. In Figure 4.28 the complexity of the various systems is compared in terms of different user loads at an E_b/N_0 value of 0dB. At a specific user load, we always select an appropriate GA-aided scheme for comparison, which achieved a similar performance compared to the ML-aided system at the BER of 10^{-5}. As seen in Figure 4.28, the ML-aided system imposes a linearly increasing complexity on a logarithmic scale, which corresponds to an exponential increase when the

number of users increases. By contrast, the complexity of the IGA-aided system required for maintaining a near-optimum performance increases only moderately.

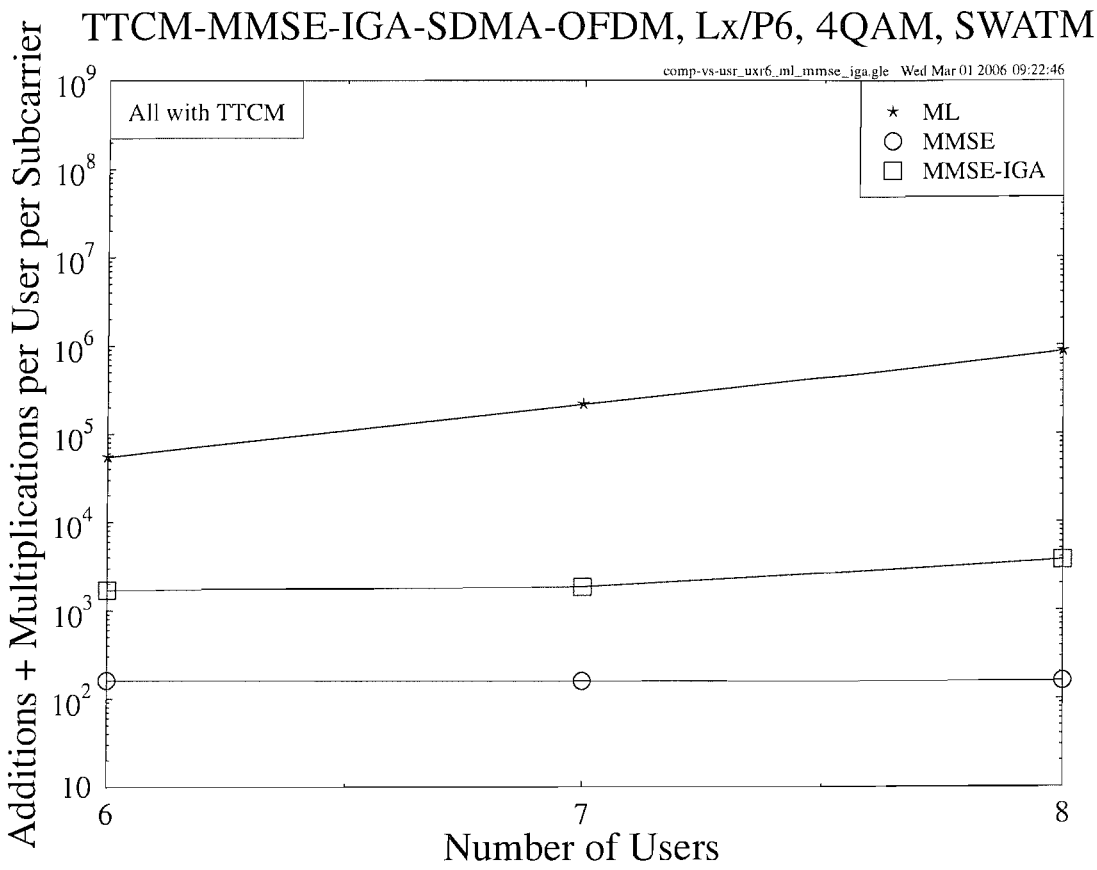

Figure 4.28: **Complexity** per user per subcarrier versus number of users performance comparison of the **TTCM-assisted MMSE-SDMA-OFDM**, **ML-SDMA-OFDM** and **MMSE-BQM-IGA-SDMA-OFDM** systems, while employing a **4QAM** scheme for transmission over the SWATM channel, where **L=6, 7, 8** users are supported with the aid of **P=6** receiver antenna elements. The basic simulation parameters are given in Table 4.5.

In order to characterize the advantage of the BQM-IGA scheme in terms of the performance-versus-complexity tradeoff, in Table 4.6 we summarize the computational complexity imposed by the different MUDs assuming an E_b/N_0 value of 3dB. As observed in Table 4.6, the complexity of the ML MUD is significantly higher than that of the MMSE MUD or the IGA MUD, especially in highly overloaded scenarios. By contrast, the IGA MUD reduced the BER by up to five orders of magnitude in comparison to the MMSE MUD at a moderate complexity.

L	MUD	+	×	BER
6	ML	2.8×10^4	2.7×10^4	1.8×10^{-7}
	IGA	8.1×10^2	7.9×10^2	2.2×10^{-7}
	MMSE	7.1×10^1	9.0×10^1	1.5×10^{-3}
7	ML	1.1×10^5	1.1×10^5	5.1×10^{-7}
	IGA	8.7×10^2	8.5×10^2	6.2×10^{-7}
	MMSE	7.1×10^1	8.8×10^1	7.5×10^{-3}
8	ML	4.3×10^5	4.2×10^5	8.5×10^{-7}
	IGA	1.8×10^3	1.7×10^3	9.8×10^{-7}
	MMSE	7.1×10^1	8.7×10^1	2.2×10^{-2}

Table 4.6: Comparison of MUD complexity in terms of number of complex additions and multiplications measured at $E_b/N_0 = 3$dB on a per user per subcarrier basis in the 4QAM TTCM-SDMA-OFDM system.

4.3.4 Conclusions

In Sections 4.3.1 and 4.3.2 we proposed specific techniques designed for further enhancing the achievable performance of the TTCM-assisted MMSE-GA-SDMA-OFDM system. The novel BQM scheme is capable of improving the GA's search at a modest complexity increase, thus significantly increasing the chances of finding the optimum GA solution in high-SNR and/or high-throughput scenarios. On the other hand, the 2D optimization provided by the proposed IGA MUD has been shown to be beneficial for the SDMA-OFDM system in both the frequency and user domains. Finally, the scheme that combines BQM with the IGA MUD yields the best and near-optimum performance in all scenarios considered, including the so-called overloaded scenario, where the performance of most of the conventional detection techniques such as the classic linear MMSE MUD significantly degrades, owing to the insufficiently high degree of freedom. Furthermore, this superior performance of the proposed scheme is achieved at a significantly lower computational complexity than that imposed by the ML-assisted system, especially when the number of users is high. For example, a complexity reduction of three orders of magnitude can be achieved by the proposed BQM-IGA aided system in the overloaded scenario associated with $L = 8$, as evidenced by Figure 4.28. Moreover, we demonstrate that the proposed scheme is capable of providing a satisfactory performance even when the channel estimation is imperfect.

4.4 Chapter Summary

In this chapter, we proposed a TTCM-assisted MMSE-GA MUD designed for SDMA-OFDM systems. In Section 4.2.1 we provided a system overview of the proposed GA-assisted TTCM-MMSE-SDMA-OFDM system. The optimization metric designed for the proposed GA MUD was described in Section 4.2.2.1. Section 4.2.2.2 outlined the concatenated MMSE-GA MUD, while its performance was evaluated in Section 4.2.3, where the GA-based schemes were shown to be capable of achieving a near-optimum performance. Furthermore, a complexity comparison between the proposed GA MUD and the optimum ML MUD was provided in Section 4.2.4, where we showed that the complexity of the GA MUD was significantly lower than that of the ML MUD.

For the sake of further improving the performance of the TTCM-assisted MMSE-GA-SDMA-OFDM system, an enhanced GA MUD was proposed in Section 4.3. This was described in two steps. Firstly, the novel BQM scheme was proposed in Section 4.3.1, including a review of the conventional UM scheme, followed by the detailed explanation of the BQM mechanism, which were the subjects of Sections 4.3.1.1 and 4.3.1.2, respectively. The BQM-aided GA MUD exploits an effective mutation strategy and thus it is capable of achieving a better performance in comparison to its UM-aided counterpart, especially at high SNRs or high user loads, as evidenced by the simulation results given in Section 4.3.1.3. Moreover, this was achieved at a modest complexity increase. Secondly, a MMSE-initialized IGA MUD was introduced in Section 4.3.2. The theoretical foundations of the IGA MUD were presented in Section 4.3.2.1, where the IGA framework as well as its optimization capability were characterized. Our related simulation results were provided in Section 4.3.2.2, where the combined BQM-IGA assisted system was found to give the best performance in all scenarios considered, while maintaining a modest computational complexity. In low-throughput scenarios, for example a six-user system employing a 4QAM modem, a two-iteration BQM-IGA MUD associated with $X = 20$ and $Y = 5$ was capable of achieving the same performance as the optimum ML-aided system at a complexity of 200, which is only about 50% and 5% of the MUD-related complexity imposed by the conventional UM-aided single-iteration IGA MUD and the optimum ML MUD, respectively. On the other hand, in high-throughput six-user systems employing for example a 16QAM modem, a two-iteration BQM-IGA MUD associated with $X = 40$ and $Y = 5$ achieved an E_b/N_0 gain of about 7dB over the MMSE MUD benchmarker at the BER of 10^{-5}, while the UM-aided GA or IGA MUDs suffered from a high residual error floor even when the iterative framework was employed. Furthermore, the associated E_b/N_0 gain was attained at a modest complexity of 400, which is only 0.00238% of the excessive complexity imposed by the ML MUD that cannot be simulated in this case.

Moreover, the proposed BQM-IGA MUD is capable of providing a near-optimum perfor-

mance even in the so-called overloaded scenarios, where the number of users is higher than the number of receiver antenna elements, while many conventional detection techniques suffer from an excessively high error floor. For example, when we had $L = 8$ users and $P = 6$ receivers, the two-iteration based BQM-IGA MUD reduced the BER recorded at an E_b/N_0 value of 3dB by four orders of magnitude in comparison to the classic MMSE MUD aided benchmarker system, as shown in Figure 4.20. This result characterizes the robustness of the BQM-IGA MUD, which has successfully suppressed the high MUI experienced in overloaded scenarios. As a further investigation, we demonstrated in Section 4.3.2.2.3 that the proposed system is capable of achieving a satisfactory performance even in the case of imperfect channel estimation. Furthermore, the complexity of the proposed detection scheme is only moderately higher than that imposed by the linear MMSE MUD, and is substantially lower than that imposed by the optimum ML MUD, as discussed in Section 4.3.3. We also showed that in both the fully-loaded scenario of Section 4.3.1.3.2 and in the overloaded scenario of Section 4.3.2.2.2.2 the complexity of the BQM approach can be further reduced by employing its simplified version, namely the CNUM scheme of Section 4.3.1.2.2, at the cost of a slightly degraded system performance.

Note that the system parameters of the IGA framework, such as the number of TTCM iterations, the number of IGA MUD iterations and the GA-related parameter settings, are all readily configurable, enabling us to strike an attractive tradeoff between the achievable performance and the complexity imposed. For specific scenarios, the TTCM scheme used in the system can also be conveniently substituted by other FEC schemes, for example the TC codes. Therefore, the facility provided by the proposed IGA MUD may make it possible to applications in multi-mode terminals, where good performance, low complexity and easy flexibility are all important criterions. It is also worth pointing out that the proposed BQM-aided IGA MUD can be readily incorporated into the multi-user CDMA systems, for example those of [45]. In this case, the initial detected signal supplied to the GA MUD for creating the first GA population is provided by the bank of matched filters installed at the CDMA BS, rather than by the MMSE MUD. However, the BQM scheme may remain unchanged.

In the next chapter, our attention will be focused on a TTCM-assisted MMSE-IGA multi-user detected SDMA-OFDM system employing a new type of Frequency-Hopping (FH) technique for the sake of achieving further performance enhancements.

Chapter 5

Direct-Sequence Spreading and Slow Subcarrier-Hopping Aided Multi-User SDMA-OFDM Systems

5.1 Conventional SDMA-OFDM Systems

In Chapters 3 and 4, Coded Modulation (CM) [2] assisted SDMA-OFDM systems invoking both Minimum Mean-Square Error (MMSE) and Genetic Algorithm (GA) based Multi-User Detection (MUD) have been investigated, respectively. Specifically, in terms of the bandwidth sharing strategy the SDMA-OFDM systems discussed in these chapters are referred to here as the *conventional* SDMA-OFDM systems [3, 192], where all the users exploit the entire system bandwidth for their communications. However, this bandwidth sharing strategy exhibits a few drawbacks.

On one hand, the conventional SDMA-OFDM systems can exploit little frequency diversity, since each user activates all available subcarriers. This limitation can be mitigated by combining both Frequency-Hopping (FH) and SDMA-OFDM techniques, resulting in the FH/SDMA-OFDM systems. In FH/SDMA-OFDM systems the total system bandwidth is divided into several sub-bands, each of which hosts a number of consecutive subcarriers, and a so-called FH pattern is used for controlling the sub-band allocation for the different users. Since each user activates different sub-bands from time to time, the achievable frequency diversity improves, as the width of the sub-bands is reduced.

On the other hand, when the number of users becomes higher in conventional SDMA-OFDM systems, a higher Multi-User Interference (MUI) is expected across the entire band-

width and hence all users will suffer from a performance degradation. Unfortunately, the same phenomenon is encountered also in FH/SDMA-OFDM systems at those sub-bands that are shared by excessive number of users. Undoubtedly, the best solution to eliminate the MUI is to avoid sub-band collisions between the different users by assigning each sub-band exclusively to a single user. This "one-subband-for-one-user" scheme will inevitably reduce the system's overall throughput. The attainable system throughput can be increased with the aid of higher-order modems, which are more vulnerable to transmission errors as well as impose an increased MUD complexity at the receivers, which is undesirable. Therefore, subcarrier-reuse based SDMA-OFDM using efficient frequency-hopping techniques is preferable, since it is capable of maintaining a sufficiently high overall system throughput even with the employment of a relatively low-order, low-complexity modem, while effectively suppressing the associated high MUI.

In this chapter, we will introduce a new bandwidth-efficient approach for employment in SDMA-OFDM systems designed for solving the two problems mentioned above.

5.2 Introduction to Hybrid SDMA-OFDM

During last decades, a range of Time Division Multiple Access (TDMA) [43], Frequency Division Multiple Access (FDMA) [43] and Code Division Multiple Access (CDMA) [44–48] schemes have found employment in the first-, second- and third-generation wireless systems. Spread-Spectrum Multiple Access (SSMA) [336–339] schemes have been widely investigated, since they exhibit a range of attractive properties, including the ability of combating various types of interference. The well-known Direct-Sequence Code Division Multiple Access (DS-CDMA) [45] is resilient against both narrow-band interference and multi-path fading. Another classic SSMA scheme is constituted by Frequency-Hopped SSMA (FH/SSMA) [45, 340–343], where the total available system bandwidth is divided into a number of sub-bands shared by a number of simultaneous users. An appropriate number of subcarriers can be assigned to each of these sub-bands, which may experience different channel qualities and hence may deliver different type of services. The so-called FH pattern is used to control a frequency synthesizer involved for the sake of activating different subcarrier frequencies. The data of each of the simultaneous users modulates the subcarriers independently, and the entire system bandwidth can be allocated on a demand basis. The bandwidth of the sub-bands may be arbitrarily small or large, depending on the type of services to be delivered or the bit rate to be supported. This flexibility is attractive when aiming for supporting future multimedia services, where variable bit rates associated with different Quality-of-Service (QoS) are required by different applications. Moreover, in FH-aided systems the different sub-bands of a particular user do

not necessarily have to be contiguously allocated. This flexibility is attractive in scenarios, where several systems operated by different service providers have to coexist and/or fractional bandwidths have to be exploited.

FH can be effectively amalgamated with a range of well-established techniques, for example the family of CDMA systems, resulting in the FH/CDMA systems [45,344–347]. Furthermore, OFDM [3, 5, 7, 31] also benefits from invoking various FH schemes [348, 349]. The FH-aided OFDM systems may also be combined with time-domain Direct-Sequence Spreading (DSS) techniques for creating hybrid systems, where the multiple users' modulated DSS signals are frequency-hopped according to their user-specific frequency-hopping patterns. Hybrid DSS/FH systems are attractive, because the advantages of both the DSS and FH techniques may be combined, while eliminating or mitigating some of their disadvantages [346, 350]. For example, a hybrid DSS/FH system is capable of combining the interference resilience of DS/Spread-Spectrum (SS) systems with the attractive partial-band-jamming mitigation features of FH/SS systems [346].

More specifically, hybrid DSS/FH systems can be beneficially amalgamated with the conventional SDMA-OFDM systems [3, 192] invoking Multi-User Detection (MUD) [305] techniques, which exhibit a number of advantages over more traditional multiple access techniques, resulting in hybrid DSS/FH aided SDMA-OFDM systems. Furthermore, the performance of the hybrid system can be significantly improved, if the proposed novel type of Slow Frequency-Hopping (SFH) technique, referred to here as the Slow SubCarrier-Hopping (SSCH) scheme is employed. From a general point of view, the philosophy of the SubCarrier-Hopping (SCH) technique is reminiscent of the concept of Clustered OFDM (ClOFDM) [351–353] and Orthogonal Frequency Division Multiple Access (OFDMA) [49–52], both of which are conceptually similar. In contrast to the systems, which combine OFDM with traditional multiple access schemes, the intrinsic nature of the orthogonal subcarriers enables OFDM itself to support multiple access, where the subcarriers are allocated to a number of sub-bands and assigned to different simultaneous users [49, 50, 354], resulting in the concept of OFDMA. OFDMA was initially proposed for cable TV (CATV) systems [355] and now has been ratified as the IEEE 802.16 standard for Broadband Wireless Multiple Access (BWMA) systems [24].

In the proposed hybrid DSS/SSCH SDMA-OFDM system, each subcarrier is shared by a certain number of users in the context of the OFDM symbol's frequency-domain representation, while each user's time-domain OFDM signal is further spread with the aid of DSS. Moreover, using a simple but efficient Uniform SSCH (USSCH) pattern, the hybrid DSS/SSCH-aided SDMA-OFDM system is capable of achieving a high frequency diversity and hence exhibits a high robustness to the MUI experienced, resulting in a significant performance improvement. In the literature, substantial research efforts have been invested in

designing subcarrier allocation algorithms for Single-Input Single-Output (SISO) OFDM systems, which are subjected to various design constraints, such as requiring the minimal overall transmit power [79, 356–360], achieving the maximum capacity [360–362] or complying with specific QoS criterions [363], etc. A subcarrier and bit allocation algorithm designed for minimizing the overall transmit power for a MIMO OFDM systems was proposed in [364]. A number of sub-band/subcarrier allocation schemes were also proposed for systems based on ClOFDM [351–353] or OFDMA [365–369]. However, many of these algorithms were derived under the assumption that a sub-band or a subcarrier can be used by one user only, resulting in a MUI-free scenario. By contrast, our proposed USSCH algorithm allows multiple constant-rate users to activate the same subcarrier. More explicitly, each subcarrier can be activated by different users during different hopping intervals, while it is desirable to ensure that the average Frequency-Domain (FD) separation of the subcarriers activated by the same user is sufficiently large, in order to experience uncorrelated fading and hence a high diversity gain. Furthermore, the number of users activating each subcarrier should ideally be similar so as to ensure that the MUI encountered at each subcarrier becomes similar, hence eliminating the MUI "peaks" across the system bandwidth. Moreover, each subcarrier may be "overloaded"[1] by being shared by a high number of users for the sake of maintaining a high overall system throughput.

In order to fully exploit the potential benefits of the USSCH pattern, the employment of Forward Error Correction (FEC) schemes is necessary. For the sake of convenient performance comparisons, again, the Turbo Trellis Coded Modulation (TTCM) [2, 301] scheme used in Chapters 3 and 4 is selected, although we point out that other FEC schemes are also applicable. It will be shown in our forthcoming discourse that with the aid of the advocated USSCH pattern, the MUI experienced by the TTCM-aided conventional SDMA-OFDM system can be effectively suppressed, resulting in a significant performance improvement, especially in high-throughput or overloaded scenarios, while a computational complexity similar to that of the conventional SDMA-OFDM systems can be maintained.

The structure of the rest of this chapter is as follows. A comparison of various frequency resource allocation strategies used in the conventional SDMA-OFDM, the SFH/SDMA-OFDM and the SSCH/SDMA-OFDM systems is provided in Section 5.3, followed by the introduction of the proposed hybrid DSS/SSCH aided SDMA-OFDM scheme in Section 5.4. More specifically, a system overview is presented in Section 5.4.1, while the transmitter and receiver structures of the proposed system are elaborated on in Sections 5.4.1.1 and 5.4.1.2, respectively. In Section 5.4.2, two different SSCH pattern assignment strategies are discussed.

[1]The terminology of an overloaded system in this chapter is slightly different from that discussed in Chapter 4. The former indicates that each of specific subcarriers used in the DSS/SSCH SDMA-OFDM system is shared by a sufficiently high number of users, while the latter refers to the overloaded conventional SDMA-OFDM system, where the number of users supported exceeds that of the receiver antenna elements.

Section 5.4.3 provides an insight into the DSS despreading and SSCH demapping processes invoked at the SDMA receiver, followed by a brief description of the multi-user detection process in the context of the presence of DSS/SSCH. The numerical results characterizing a range of different SDMA-OFDM systems in different scenarios are provided in Section 5.5, while the complexity issues are discussed in Section 5.6. Finally, Section 5.7 concludes our findings.

5.3 Subband-Hopping Versus Subcarrier-Hopping

Figure 5.1 shows the frequency resource allocation strategies of conventional SDMA-OFDM [3, 192], SFH/SDMA-OFDM and SSCH/SDMA-OFDM systems. As illustrated in Figure 5.1, in conventional SDMA-OFDM systems, which do not employ any hopping techniques, the total available system bandwidth W is partitioned into a total of $Q_c = W/W_{sc}$ subcarriers, where W_{sc} is the subcarrier bandwidth[2], and each user activates all the Q_c subcarriers for communication.

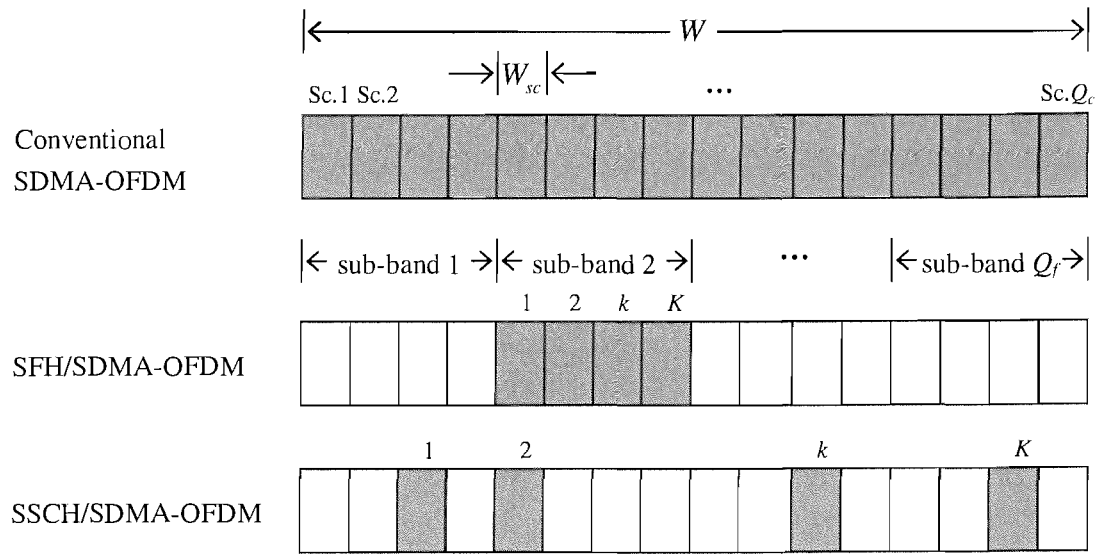

Figure 5.1: Comparison between the conventional SDMA-OFDM, the SFH/SDMA-OFDM and the SSCH/SDMA-OFDM in the context of frequency resource allocation for a single user. Each block in the figure represents a subcarrier, while those in gray denote the user-activated subcarriers. In this example, random hopping patterns are used for both the SFH and the SSCH aided systems.

However, in the SFH-assisted OFDM systems the total system bandwidth W is divided into a number of sub-bands denoted by $q = 1, \cdots, Q_f$, as seen in Figure 5.1. Each sub-band is assigned a carrier frequency f_q, which is used for carrying the OFDM signal to be transmitted

[2]The subcarrier bandwidth W_{sc} represents the FD bandwidth hosting the main spectral lobe of the sinc-function shaped subcarrier spectrum.

in this sub-band, when it is activated. Furthermore, each of the Q_f sub-bands has K number of subcarriers, each having a subcarrier bandwidth of W_{sc}, and we have $W = W_{sc} \times K \times Q_f$. In the context of the SFH/SDMA-OFDM system, during a FH dwell time T_h, each of the L simultaneous users supported is assigned one of the Q_f sub-bands associated with a specific carrier frequency f_q, which is activated by a frequency synthesizer according to either a pseudo-random or a deterministic user-specific hopping pattern set used. In contrast to Fast Frequency-Hopping (FFH) systems, where the symbol duration T_s obeys $\beta_F = T_s/T_h > 1$, in SFH systems we have $\beta_S = T_h/T_s > 1$, where both β_F and β_S are integers, while T_h is the hopping dwell period. Using SFH makes it feasible to use coherent demodulation at the receiver side, since the hopping rate is slower than the data rate.

Note that the SFH sub-bands are not necessarily contiguously allocated in the frequency domain. However, if a sub-band is activated by a user, all the K subcarriers within this sub-band are assigned to the specific user. While each user can only activate one sub-band during each frequency-hopping dwell time T_h, the same sub-band can be exploited by more than one user. Therefore, if an excessive number of users happens to activate the same sub-band, resulting in heavy MUI, a severe signal corruption will occur across all the consecutive subcarriers within this specific sub-band.

In comparison to SFH/SDMA-OFDM systems, where sub-band based SFH is employed, in the proposed SSCH/SDMA-OFDM system a subcarrier based SFH technique is invoked. Similar to conventional SDMA-OFDM systems, in SSCH/SDMA-OFDM systems we also have a total of $Q_c = W/W_{sc}$ subcarriers. However, each user activates only K of the Q_c available subcarriers, where $0 < K < Q_c$. While a SFH user exploits all the K subcarriers of a SFH sub-band during the hopping dwell time of T_h, a SSCH user employing the same number of K subcarriers can potentially select any K of the Q_c available subcarriers without decreasing the throughput, as seen in Figure 5.1. Furthermore, in SSCH/SDMA-OFDM systems a high MUI is expected to contaminate the dispersed subcarriers activated by a number of users, which is different from the situation experienced in the SFH/SDMA-OFDM scenario, where potentially all the consecutive subcarriers of a sub-band hosting a number of users may be at a risk of being severely corrupted. Moreover, the SSCH scheme is capable of more efficiently exploiting the benefits of frequency diversity in comparison to the SFH arrangement, since a deep fade which may corrupt many consecutive subcarriers of a SFH user, may only affect a small fraction of the subcarriers used by a SSCH user, as an added bonus of the employment of discontinuous subcarriers. Explicitly, when an appropriately designed hopping pattern is used, the "interleaving-like" FD fading randomization characteristic of the SSCH system disperses the originally bursty FD errors and hence enhances the chances of the channel decoder to correct the residual errors.

The SSCH-aided OFDM may be viewed as being somewhat similar to OFDM/OFDMA with interleaving, since both of these techniques provide a method to exploit the achievable frequency diversity. However, they are different in that in the former system different subcarriers are assigned to different users at different hopping dwell instants, while in the latter system each user employs all the subcarriers (or the same set of subcarriers in the case of OFDMA), although the signal carried by each subcarrier is interleaved. In hostile propagation scenarios some subcarriers may consistently encounter deep channel fades despite using the above-mentioned anti-fading measures, thus the specific user of the interleaved OFDM/OFDMA system, who happens to activate these bad subcarriers, may suffer from a consistently poor performance. By contrast, in the SSCH-aided OFDM system this rarely happens, since each user will be assigned different subcarriers from time to time.

We point out that by assigning a different number of subcarriers to different users, a flexible multi-rate system can be created, which is capable of satisfying the users' QoS profiles. For the sake of simplicity, in this chapter we assume that each user has the same constant bitrate.

5.4 System Architecture

Having outlined the basic concepts of the SSCH technique, let us now focus our attention on the structure of the proposed TTCM-assisted hybrid DSS/SSCH aided SDMA-OFDM system. The organization of this section is as follows. In Section 5.4.1 an overview of a basic TTCM-assisted DSS/SSCH aided SDMA-OFDM system employing the classic MMSE MUD is provided, followed by an introduction of the associated transmitter and receiver structures, which are detailed in Sections 5.4.1.1 and 5.4.1.2, respectively. The SSCH pattern design is discussed in Section 5.4.2. Furthermore, the operations of DSS despreading and SSCH demapping invoked at the receiver are elaborated on in Section 5.4.3. The last part of this section focuses on the MUD design in the context of the SSCH/SDMA-OFDM system, as detailed in Section 5.4.4.

5.4.1 System Overview

In Figure 5.2 we portray the schematic of a TTCM-assisted hybrid DSS/SSCH aided SDMA-OFDM system. As an example, the MMSE-based MUD [3] of Chapter 3 is used. As seen in the top of Figure 5.2, for each of the L number of geographically dispersed mobile users, the information bit sequence is first mapped into Quadrature Amplitude Modulation (QAM) [31] symbols with the aid of the TTCM encoder. The encoded QAM symbols $\mathbf{s}^{(l)} = [\, s_1^{(l)},\ s_2^{(l)},\ \cdots,\ s_K^{(l)}\,]^T$ $(l = 1, \cdots, L)$, where $K < Q_c$ is the number of subcarriers activated by each user, are then forwarded to the SSCH mapper under the control of a specific

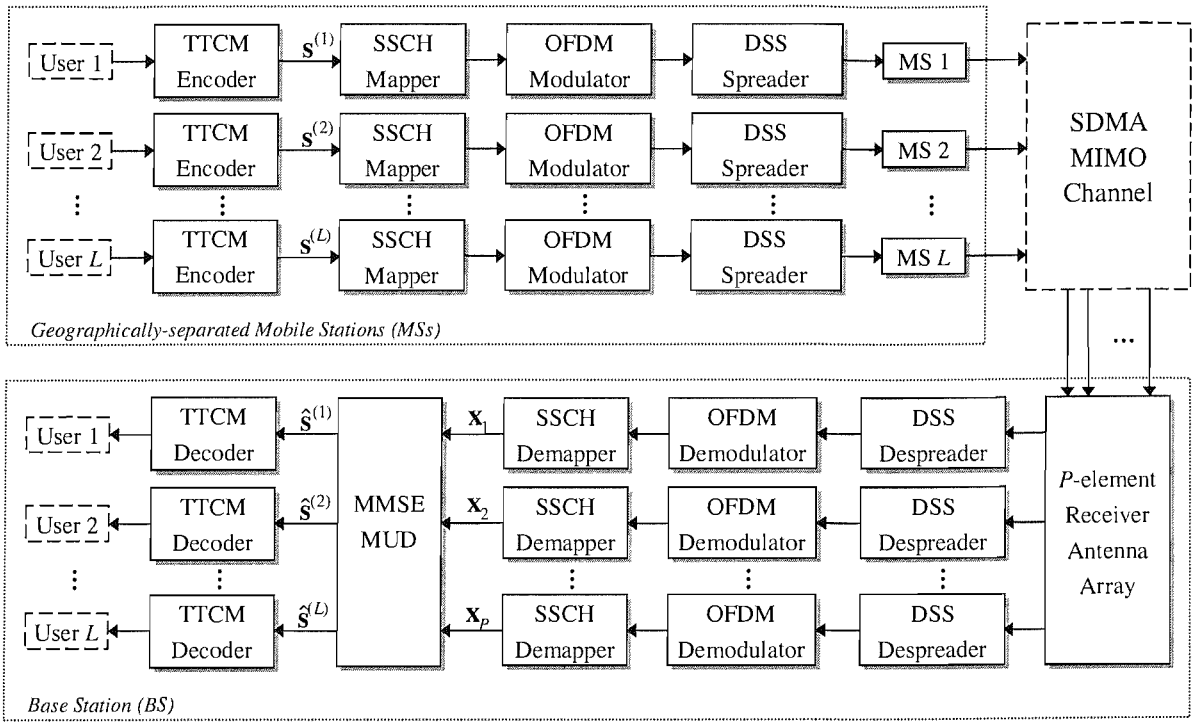

Figure 5.2: Schematic of a TTCM-assisted multi-user DSS/SSCH aided SDMA-OFDM uplink system using the classic MMSE MUD.

SSCH pattern. The mapped symbols are then forwarded to the OFDM modulator, where they are converted to OFDM symbols based on the Q_c-point Inverse Fast Fourier Transform (IFFT) algorithm. The OFDM-modulated signal is then delivered to the DSS spreader for time-domain based spreading. Afterwards, this subcarrier-hopped and spread signal is transmitted to the BS by the single-antenna aided MS over the SDMA MIMO channel described by Figure 3.1. At the BS shown in the bottom part of Figure 5.2, P number of receiver antenna elements are employed, where the despreading process is first invoked, followed by the OFDM demodulation using the Fast Fourier Transform (FFT) algorithm. Given the knowledge of the user-specific SSCH patterns, the despread signal is dehopped by the SSCH demapper. The resultant outputs $\mathbf{x}_p = [\ x_{p,1},\ x_{p,2},\ \cdots,\ x_{p,K}\ ]^T$ $(p = 1, \cdots, P)$ are then forwarded to the MMSE-based MUD for separating the different users' signals. The multi-user detected signals $\hat{\mathbf{s}}^{(l)} = [\ \hat{s}_1^{(l)},\ \hat{s}_2^{(l)},\ \cdots,\ \hat{s}_K^{(l)}\ ]^T$ $(l = 1, \cdots, L)$, namely the estimated versions of the transmitted signals are then independently channel decoded by the TTCM decoders of Figure 5.2.

In Sections 5.4.1.1 and 5.4.1.2, we will provide further insights into the transmitter and receiver structures of the hybrid DSS/SSCH MMSE-SDMA-OFDM system, respectively. Note that for the sake of simplicity, the procedures of adding and removing the cyclic OFDM prefix [3, 31] were omitted in both sections.

5.4.1.1 Transmitter Structure

The transmitter structure of the TTCM-assisted DSS/SSCH SDMA-OFDM system is portrayed in Figure 5.3. As seen in Figure 5.3, the TTCM-coded symbols are first S/P-converted and forwarded to the SSCH mapper. More specifically, the K number of information symbols $s_{g_l,k}^{(l)}$ $(l = 1, \cdots, L;\ k = 1, \cdots, K)$ of a user are mapped to K out of Q_c SSCH subcarriers, where the activation strategy of the set of K subcarriers depends on the specific SSCH pattern used. For example, if pseudo-random hopping is employed, each user can independently select K subcarriers according to the action of a pseudo-random subcarrier selector, as illustrated in Figure 5.3. Since each of the L users activates $K < Q_c$ subcarriers, there will be $Q_c - K$ deactivated subcarriers for each user. Therefore, an ON-OFF type signaling scheme may be invoked [344], where the activated and deactivated status of specific subcarriers represent the ON and OFF states, respectively. Then the total number of Q_c subcarriers can be processed by a Q_c-point IFFT. Since the deactivated subcarriers deliver no information, the transmit power of each SSCH user is the same as that of a SFH user, if the same K number of activated subcarriers is employed by both of them. In order to exploit coherent demodulation at the receiver, the SSCH dwell period T_h should be longer than the symbol duration T_s. In the example of Figure 5.3, each user's SSCH pattern remains constant during the period of T_h for two consecutive symbol periods.

Following the IFFT-based OFDM modulation, the user's signal is forwarded to the DSS spreader seen in Figure 5.3, where the time-domain spreading operation is invoked with the aid of orthogonal spreading sequences for achieving time diversity. In this thesis Walsh-Hadamard Transform Spreading (WHTS) based codes are considered. The G-order Walsh-Hadamard Transform (WHT) matrix $\mathbf{U}_{\mathrm{WHT}_G}$ is given in a recursive form as stated in Equation (3.10), which is repeated here for the convenience of the reader:

$$\mathbf{U}_{\mathrm{WHT}_G} = \frac{1}{\sqrt{2}} \begin{pmatrix} 1 \cdot \mathbf{U}_{\mathrm{WHT}_{G/2}} & 1 \cdot \mathbf{U}_{\mathrm{WHT}_{G/2}} \\ 1 \cdot \mathbf{U}_{\mathrm{WHT}_{G/2}} & -1 \cdot \mathbf{U}_{\mathrm{WHT}_{G/2}} \end{pmatrix}, \tag{5.1}$$

while the lowest-order WHT unitary matrix $\mathbf{U}_{\mathrm{WHT}_2}$ is defined by Equation (3.11). More specifically, a total of L users are supported by the DSS/SSCH system, who are divided into G number of DSS user groups, each of which is assigned a different DSS code vector $\mathbf{c}_{g_l}$ based on WHTS, which is carried out according to one of the G rows in the WHT matrix $\mathbf{U}_{\mathrm{WHT}_G}$ of Equation (5.1), as shown in the DSS spreader block of Figure 5.3. The number of users in one DSS group may be different from that in another, however the users within the same group will share the same DSS code. From the point of the users' view, the l^{th} user's DSS code may or may not be the same as the other users', depending on whether they belong to the same DSS group or not. Explicitly, the users employing the same DSS code cannot be differentiated in the time domain. However, they are separable in the context of

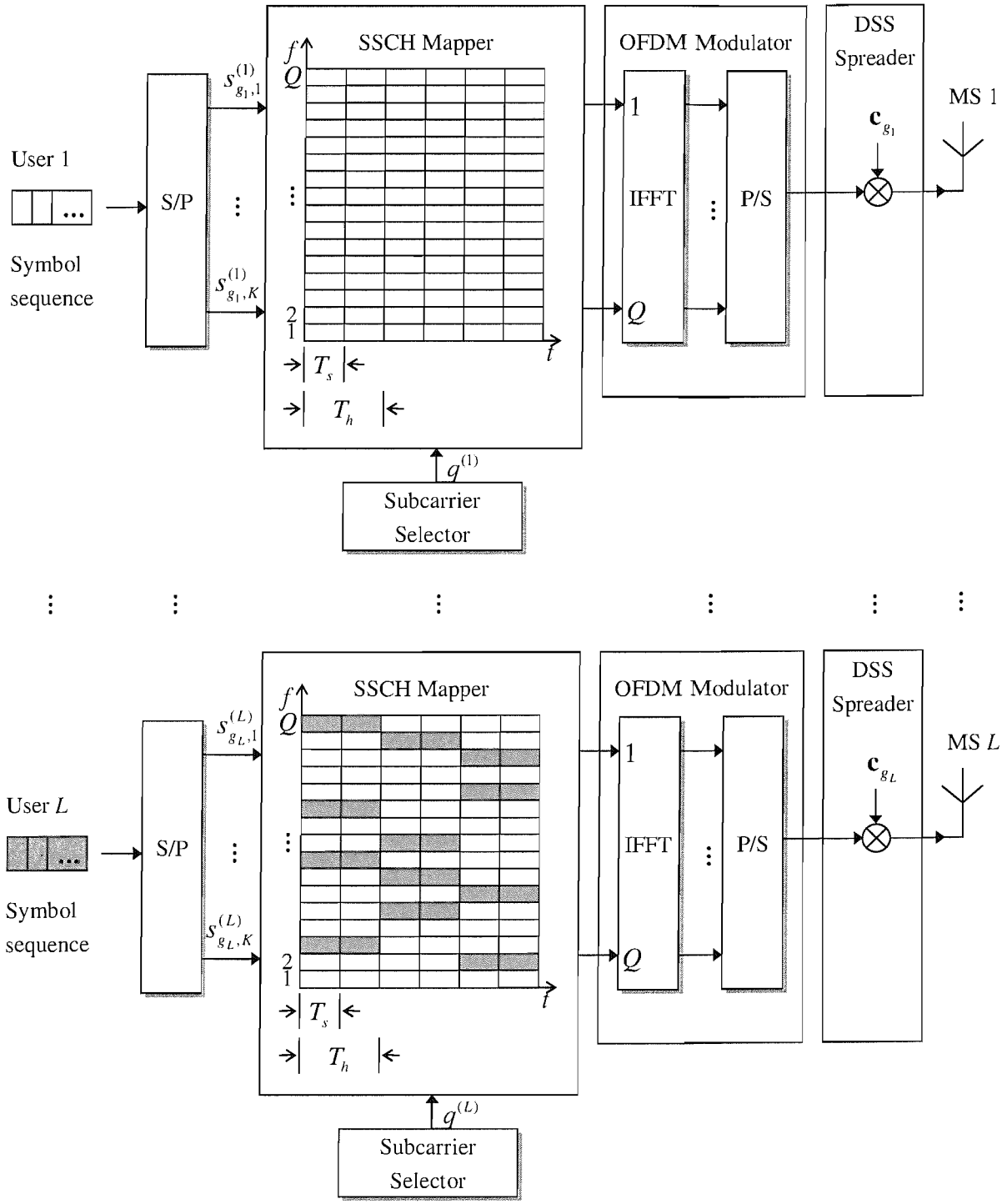

Figure 5.3: Illustration of the L-users' DSS/SSCH SDMA-OFDM transmitters. As an example, random SSCH patterns are used.

the SDMA architecture with the aid of their unique user-specific spatial signatures, namely by their CIRs [3]. More precisely, this is achieved by the employment of the SDMA MUD, for example the MMSE MUD of Section 3.2.2.1. Following the DSS process, the spread OFDM signal will be transmitted by the MS over the channel using a specific carrier frequency f_c.

Note that the quasi-synchronous uplink operation of MSs may be established with the aid of sufficiently accurate timing advance control by advancing the mobiles' transmission instants according to their estimated time delays [370]. Furthermore, the single-user OFDM synchronization techniques of [3] may be further developed for multi-user systems. Alternatively, the techniques of [371–373] may also be applicable to the SSCH/SDMA-OFDM system.

5.4.1.2 Receiver Structure

The receiver structure of the DSS/SSCH SDMA-OFDM system follows the inverse of the transmitter structure, as illustrated in Figure 5.4. The received signal is the superposition of all users' transmitted signals plus the Additive White Gaussian Noise (AWGN). At each of the P number of SDMA BS receiver antenna elements, first the received signal r_p $(p = 1, \cdots, P)$ is despread with the aid of the different DSS codes, resulting in the corresponding G number of different despread signal groups, each of which is constituted by the received signals of the users that employ the same specific DSS code. Note that each subcarrier may be activated[3] by different users employing either the same or different DSS codes, depending on the SSCH pattern assignment strategy used. Hence, with the knowledge of the SSCH patterns, an active subcarrier selector can be employed at the BS for controlling the despreading operation, so that the appropriate DSS codes are used at the different subcarriers. For example, Figure 5.4 shows the processing invoked for the g^{th} $(g \in \{1, \cdots, G\})$ DSS group, where the g^{th} DSS code is used for separating this DSS group's signal from the others'. Then, FFT-based OFDM demodulation is invoked for each of the different DSS groups at each of the P receiver antenna elements, followed by SSCH demapping. The BS's active subcarrier selector simultaneously selects the active subcarriers at the P receivers, and the resultant composite multi-user output signal is forwarded to the multi-user detector for multi-user detection. As an example, the MMSE MUD is pictured in Figure 5.4, but other MUDs such as for example the MMSE-IGA MUD of Chapter 4 are equally applicable. The separated different users' signals are then P/S-converted and forwarded to the user-specific TTCM channel decoders.

[3]A subcarrier is referred to as being *activated*, if it is assigned to at least one user for transmission.

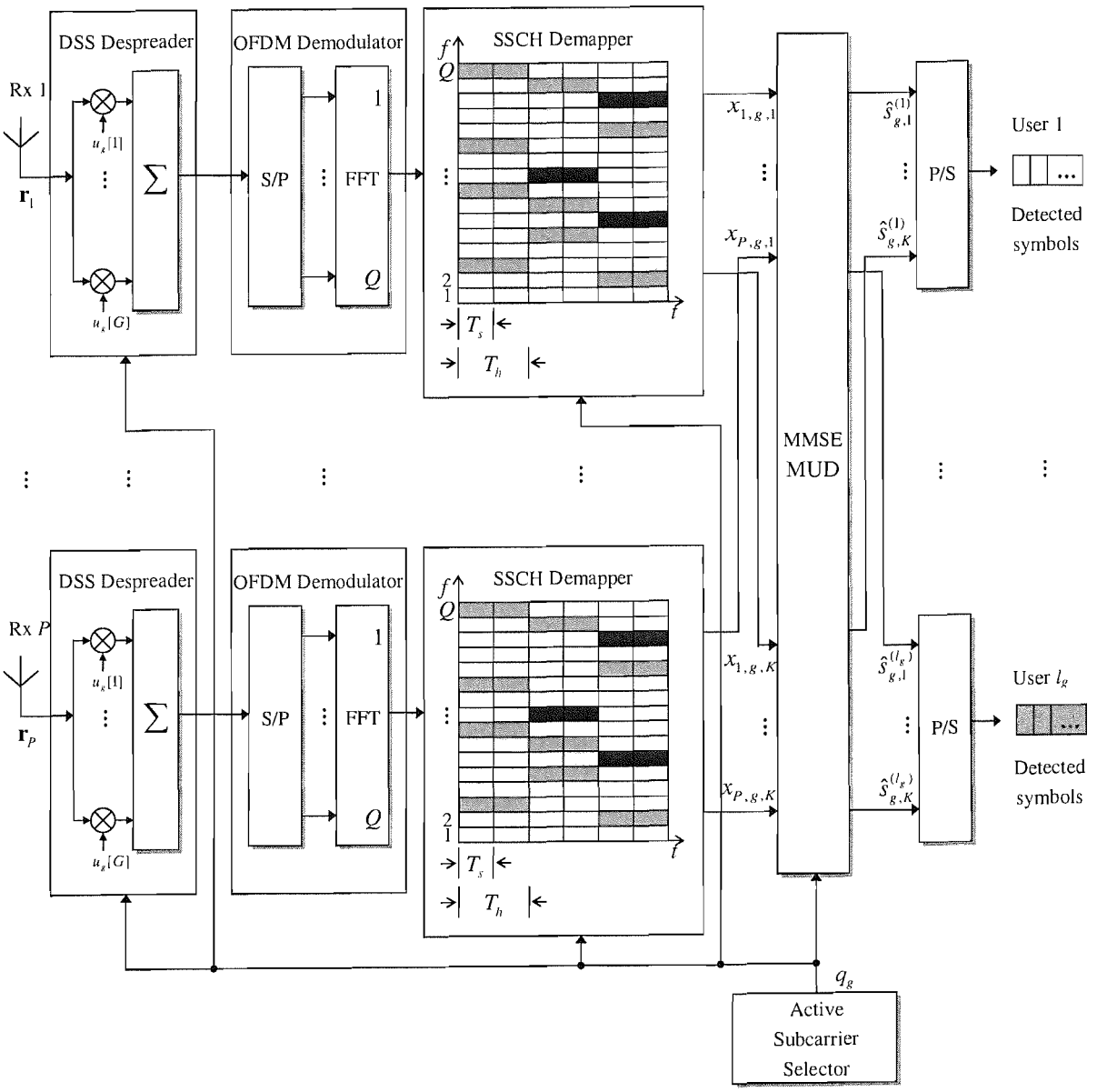

Figure 5.4: Illustration of the L-users' DSS/SSCH SDMA-OFDM receivers. As an example, the MMSE MUD and random SSCH patterns are used. In this figure, the processing invoked in the context of the g^{th} ($g \in \{1, \cdots, G\}$) DSS group containing l_g number of users is portrayed.

5.4.2 Subcarrier-Hopping Strategy Design

In the SSCH/SDMA-OFDM system, the appropriate choice of the SSCH strategy is a crucial factor of the system design. The SSCH pattern decides upon the choice of the subcarriers to which the different users' signals are mapped and thus has a direct impact on the amount of MUI inflicted. In order to eliminate the MUI, the best solution is to avoid subcarrier collisions between the different users by assigning each subcarrier exclusively to a single user, as proposed for a number of systems based on ClOFDM [351] or OFDMA [365–368]. However, we prefer a subcarrier-reuse system, where the system's overall throughput can be further increased. Furthermore, to design an appropriate SSCH pattern the following two aspects should be taken into account. On one hand, for the sake of combatting the MUI, a meritorious SSCH pattern should ensure that each user's high-MUI subcarriers are dispersed across the FD, rather than being concentrated in the FD. On the other hand, in order to mitigate FD fading, the subcarriers activated by the same user should be uniformly distributed across the entire bandwidth, rather than being consecutively mapped to a small fraction of the entire bandwidth, so that frequency diversity can be efficiently exploited and hence the detrimental effects of deep FD fades can be mitigated. Both of these requirements result in a more random distribution of the originally bursty FD errors incurred either by a high MUI or a deep FD fade, thus enhancing the chances of the channel decoder to correct the residual errors.

Based on the above motivation, two types of SSCH pattern will be considered in this section.

5.4.2.1 Random SSCH

We refer to the first scheme as the Random SSCH (RSSCH) pattern, where each user independently select *any* K out of the total Q_c available subcarriers during each SSCH dwell time period of T_h. Employing a random hopping strategy is a convenient solution for the simultaneous mobile users, since each user may activate any of the available subcarriers without restrictions imposed by the others. However, the RSSCH strategy also has some drawbacks. Specifically, in RSSCH-based systems some subcarriers may be activated by a smaller number of users, hence the MUI level is low at these subcarriers, which in turn benefits all the active users that use them. Unfortunately, this benefit is achieved at the cost of increasing the MUI imposed on the other subcarriers, which are assigned to an excessive number of users. Therefore, those disadvantaged users will suffer from a high MUI. Furthermore, the benefits gained from the high-quality subcarriers may not be expected to compensate for the detrimental effects arising from the severely-corrupted ones, and thus result in an increased average Bit Error Ratio (BER).

5.4.2.2 Uniform SSCH

For the sake of mitigating the above-mentioned deficiencies of the RSSCH scheme, we will introduce another SSCH strategy referred to as the Uniform SSCH (USSCH) scheme, which is capable of effectively counteracting the above problem. In the proposed USSCH-based systems all users' hopping patterns are jointly designed so that the number of interfering users at each subcarrier - which also depends on the total number of users L supported by the SSCH system - is as similar as possible, and thus the users can be uniformly distributed to the Q_c subcarriers, which in turn satisfies both requirements mentioned above.

In Section 5.4.2.2.1, we will provide a detailed discussion on the design of the proposed USSCH pattern.

5.4.2.2.1 Design of the USSCH Pattern

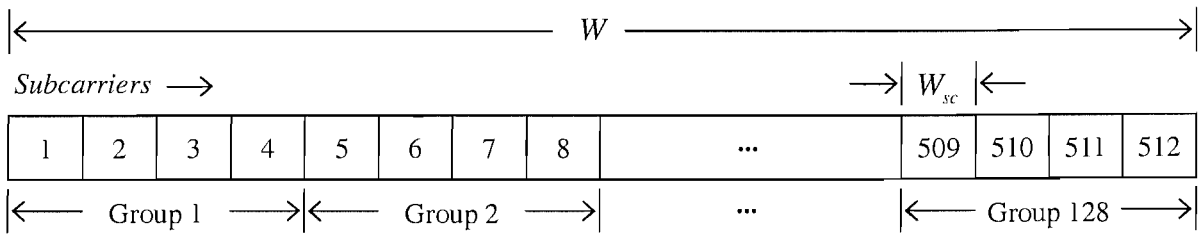

Figure 5.5: An example showing the formation of the subcarrier groups, where the system bandwidth W is shared by a total of $Q_c = 512$ subcarriers, while each user activates $K = 128$ subcarriers for transmission, and each of the 128 subcarrier groups has $Q_g = 4$ subcarriers.

During each SSCH dwell interval of T_h, the algorithm used to create a set of USSCH patterns for all the users is as follows. Recall that in SSCH systems the total bandwidth W is shared by Q_c subcarriers, each of which has a subcarrier bandwidth of $W_{sc} = W/Q_c$. Now we partition the Q_c subcarriers into K subcarrier groups, where each group has $Q_g = Q_c/K$ number of subcarriers. For example, if we have a total of $Q_c = 512$ available subcarriers, where each user activates $K = 128$ subcarriers for transmission, this will result in $K = 128$ subcarrier groups, each of which has $Q_g = 512/128 = 4$ subcarriers, as illustrated in Figure 5.5. Then an L-iteration USSCH pattern assignment algorithm is invoked for each of the K groups, namely from the first to the K^{th} group, for the sake of generating a specific length-K pattern set for each of the L users. Note that this principle is different from that of the RSSCH scheme, where each user is randomly assigned K subcarriers. By contrast, in the USSCH arrangement each of the K subcarriers assigned to a specific user is chosen from a different subcarrier group. In other words, each user's specific set of K activated subcarriers is uniformly distributed across the entire system bandwidth.

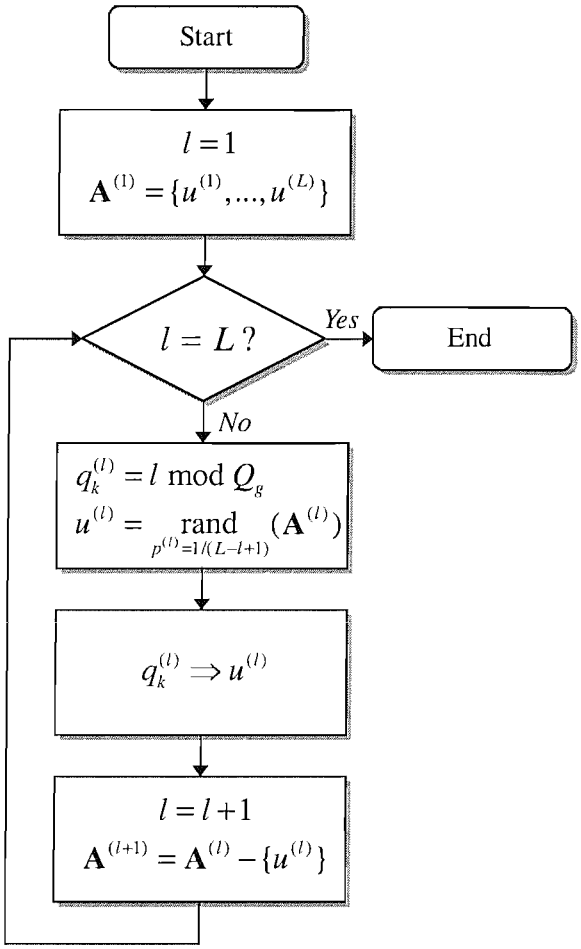

Figure 5.6: Flowchart of the USSCH pattern assignment algorithm invoked in the k^{th} subcarrier group.

Figure 5.6 illustrates the proposed algorithm invoked in the k^{th} ($k = 1, \cdots, K$) subcarrier group for assigning the Q_g subcarriers to the L users. More precisely, initially a *remaining user set* $\mathbf{A}^{(1)}$ containing all the L users is created, as shown in Figure 5.6. During the l^{th} ($l = 1, \cdots, L$) iteration, a subcarrier index $q_k^{(l)}$ is generated by calculating l *mod* Q_g, where *mod* represents the modulo operation. A user $u^{(l)}$ is then randomly selected from $\mathbf{A}^{(l)}$ based on the uniform probability of:

$$p^{(l)} = \frac{1}{L-l+1}, \tag{5.2}$$

and the $(q_k^{(l)})^{th}$ subcarrier within this specific subcarrier group will be assigned to user $u^{(l)}$. The remaining user set $\mathbf{A}^{(l)}$ is then updated by removing user $u^{(l)}$ from it, resulting in $\mathbf{A}^{(l+1)}$, which contains the remaining $(L-l)$ number of users. Then the subcarrier assignment process proceeds to the next, i.e. to the $(l+1)^{th}$ iteration, allocating the next subcarrier to the next randomly selected user, as seen in Figure 5.6. This iterative subcarrier to user assignment process continues, until the L^{th} iteration is completed. By this time, each of the L users

has been assigned a single subcarrier of the k^{th} subcarrier group. Hence, a vector $\mathbf{q}_k = [\, q_k^{(1)},\ q_k^{(2)},\ \cdots,\ q_k^{(L)}]$ is generated, where $q_k^{(l)}$ $(l = 1, \cdots, L)$ constitutes the k^{th} subcarrier of the l^{th} user's length-K USSCH pattern set[4]. Then the vector-generating routine described above is invoked for the next, i.e. for the $(k+1)^{th}$ subcarrier group. When all the K subcarrier groups have been processed, a set containing K number of length-L vectors $\mathbf{q}_k$ $(k = 1, \cdots, K)$ has been generated, explicitly indicating, which specific subcarrier of group k has been assigned to which of the L users. Viewing this subcarrier allocation from the users' perspective, the l^{th} user's specific length-K USSCH pattern set $\mathbf{q}^{(l)}$ is created by choosing that specific subcarrier corresponding to the l^{th} element of each of the K vectors, which has been assigned to user l, resulting in $\mathbf{q}^{(l)} = [\, q_1^{(l)},\ q_2^{(l)},\ \cdots,\ q_K^{(l)}\ ]$, $l \in \{1, \cdots, L\}$.

Note that the above subcarrier group based algorithm employs the full permutation theory [374]. More explicitly, each of the K number of length-L vectors $\mathbf{q}_k$ $(k = 1, \cdots, K)$ associated with the k^{th} subcarrier group is an element of the L-order full permutation set [374], and is generated at a constant probability of:

$$\begin{aligned} p_L &= \prod_{l=1}^{L} p^{(l)} \\ &= \frac{1}{L} \cdot \frac{1}{L-1} \cdot \cdots \cdot \frac{1}{2} \cdot 1 \\ &= \frac{1}{L!}, \end{aligned} \tag{5.3}$$

where $(\cdot)!$ represents the factorial operation. More explicitly, given a total number of L users, the associated L-order full permutation set can be expressed as:

$$\mathbf{Q}_L = \left\{ \mathbf{q}_1,\ \mathbf{q}_2,\ \cdots,\ \mathbf{q}_{L!} \right\}, \tag{5.4}$$

where the element vectors are given by $\mathbf{q}_k = [\, q_k^{(1)},\ q_k^{(2)},\ \cdots,\ q_k^{(L)}\ ]$ $(k = 1, \cdots, L!)$. Thus, the employment of the USSCH pattern assignment algorithm of Figure 5.6 is conceptually equivalent to invoking the algorithm, which randomly selects one element vector from the set $\mathbf{Q}_L$ described by Equation (5.4) for each of the K subcarrier groups, based on the probability given by Equation (5.3).

In order to offer an insight into the relation between the USSCH pattern assignment algorithm and the full permutation theory, an example is provided in Figure 5.7, which illustrates the USSCH pattern assignment operation invoked for the k^{th} subcarrier group of the example given by Figure 5.5, where we have $K = 128$ and $Q_g = 4$. Without loss of generality, in this example we assume that $L = 6$ users are supported by the system. According to the algorithm of Figure 5.6, during the l^{th} $(l = 1, \cdots, 6)$ iteration a user $u^{(l)}$ is randomly selected from the

[4]Recall that each user activates K subcarriers for transmission and thus has to be assigned a length-K USSCH pattern set.

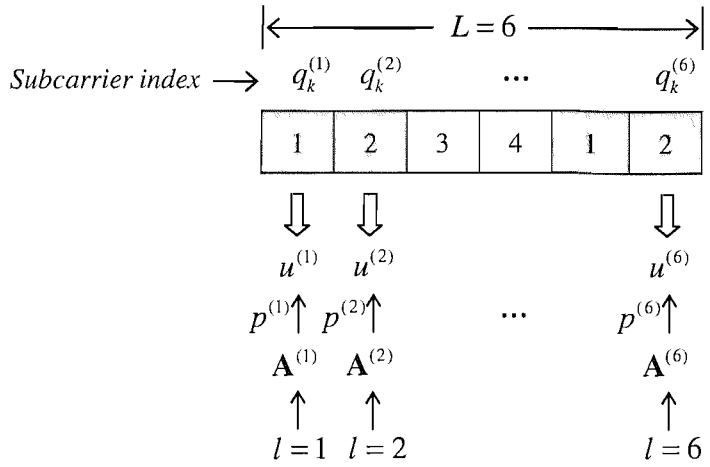

Figure 5.7: An example showing the USSCH pattern assignment operation invoked for the first subcarrier group of Figure 5.5, where we have $L = 6$ and $Q_g = 4$. For the notations used in this figure we refer to Figure 5.6.

remaining user set $\mathbf{A}^{(l)}$ based on the selection probability $p^{(l)}$ calculated by Equation (5.2) and is assigned the subcarrier with the index of $q_k^{(l)}$, as observed in Figure 5.7. Note that since $L = 6 > Q_g = 4$, each of the last two users has to activate a subcarrier that has already been assigned to a previous user. The subcarriers activated by more than one user are printed in gray color in Figure 5.7. After $L = 6$ iterations, a vector $\mathbf{q}_k$ having six elements is generated. Furthermore, the probability of generating $\mathbf{q}_k$ is the product of the user-selection probability $p^{(l)}$, expressed as:

$$\begin{aligned} p &= p^{(1)} \cdot p^{(2)} \cdot \ldots \cdot p^{(5)} \cdot p^{(6)} \\ &= \frac{1}{6} \cdot \frac{1}{5} \cdot \ldots \cdot \frac{1}{2} \cdot 1 \\ &= \frac{1}{6!}, \end{aligned} \tag{5.5}$$

which yields the same result as that calculated by Equation (5.3) in conjunction with $L = 6$. In other words, the generation of the vector $\mathbf{q}_k$ has the same effect as selecting it from the six-order full permutation set $\mathbf{Q}_6$ based on the probability given by Equation (5.3), as pointed out previously.

5.4.2.2.2 Discussions

As informed by Figure 5.7, when we have $L > Q_g$ and $L \ mod \ Q_g \neq 0$, in each of the K subcarrier groups, there will be $(L \ mod \ Q_g)$ number of subcarriers that have to be activated by *one* more user than the other subcarriers in the same group. Thus, a higher MUI is expected at these subcarriers. However, since the users that are assigned to the higher-MUI subcarriers are randomly selected, it is unlikely for these more-MUI contaminated subcarriers of different

subcarrier groups to be always assigned to the same user. In other words, from each user's point of view, among its total K activated subcarriers, the specific subcarriers that encounter a higher MUI can be uniformly dispersed across the entire system bandwidth. Furthermore, since in USSCH/SDMA-OFDM systems each user's activated subcarriers are uniformly distributed over the entire bandwidth, frequency diversity can be efficiently exploited. Thus, both requirements mentioned at the beginning of Section 5.4.2 are satisfied by employing the proposed USSCH pattern assignment algorithm.

On the other hand, if we have $L \ mod \ Q_g = 0$, each subcarrier is activated by the same number of L/Q_g users. Moreover, when we have $L < Q_g$, the USSCH system is actually MUI-free, since each subcarrier is assigned to at most one user. In both of these two scenarios, the MUI encountered in the USSCH/SDMA-OFDM system is identical at all the activated subcarriers, since each subcarrier hosts the same number of users. This situation is similar to that encountered in conventional SDMA-OFDM systems [3, 192] in terms of the amount of MUI inflicted at each subcarrier. However, the USSCH/SDMA-OFDM system benefits from the USSCH pattern assignment algorithm of Figure 5.6, which has the ability to efficiently exploit the achievable frequency diversity offered by the system, and hence becoming capable of outperforming conventional SDMA-OFDM systems. Furthermore, the advantage of the USSCH pattern design will become even more significant in overloaded scenarios, where an excessively high MUI is expected, as we will demonstrate in Section 5.5.

5.4.2.3 Random and Uniform SFH

Note that the principles of the RSSCH and USSCH strategies can also be applied to SFH/SDMA-OFDM, resulting in Random SFH (RSFH) and Uniform SFH (USFH) aided SDMA-OFDM systems, respectively. More specifically, in USFH/SDMA-OFDM systems sub-bands of subcarriers rather than individual subcarriers are jointly assigned to the different users, following a philosophy similar to that of Figure 5.6.

It is worth pointing out that the USFH/SDMA-OFDM scheme is capable of outperforming the conventional SDMA-OFDM arrangement, as a benefit of the proposed uniform pattern assignment algorithm. However, given the same system bandwidth and the same total system throughput, the USFH/SDMA-OFDM system is unable to outperform its USSCH-aided counterpart. This is because in USFH-aided systems a sub-band - which accommodates a number of subcarriers and may be viewed as an "entire" bandwidth for a "reduced-size" conventional SDMA-OFDM system - is still more vulnerable both to high MUI and to deep fades than a subcarrier of USSCH-aided systems. The above arguments will be corroborated by our simulation results to be shown in Section 5.5.

5.4.2.4 Offline Pattern Pre-computation

It is also worth pointing out that the USFH/USSCH patterns can be acquired by offline pre-computation, since their choice is not based on any channel knowledge. Furthermore, the patterns can be reused, provided that the reuse time interval is sufficiently long, so that the frequency diversity can be sufficiently exploited. The reuse intervalis defined by:

$$T_r = \mu T_h, \tag{5.6}$$

where the reuse factor μ is a positive integer. More explicitly, during the offline pattern pre-computation, μ number of USFH/USSCH patterns are generated for each of the L users, each of which is associated with one of the μ number of FH dwell time periods during the time interval of T_r. These USFH/USSCH pattern sets can then be reused during every reuse interval T_r, implying that the real-time signaling of the USFH/USSCH patterns from the transmitters to the receivers is unnecessary. This imposes a significantly lower computational complexity than that required by other adaptive algorithms exploiting the real-time channel knowledge.

Having discussed the design of SSCH patterns, in the next section we will detail the DSS despreading and SSCH demapping processes invoked at the DSS/SSCH SDMA-OFDM receiver.

5.4.3 DSS Despreading and SSCH Demapping

In the L-user TTCM-assisted DSS/SSCH SDMA-OFDM system employing P receiver antenna elements, the l^{th} $(l = 1, \cdots, L)$ user's transmitted signal at the q^{th} $(q = 1, \cdots, Q)$ subcarrier can be expressed as:

$$\begin{aligned} s'^{(l)}_{g_l,q}(t) &= \sqrt{2P_T}\Lambda^{(l)}_q(t)s^{(l)}_{g_l,q}(t)c_{g_l}(t)\cos(2\pi f_c t + \varphi^{(l)}), \\ & l \in \{1, \cdots, L\}, \quad g_l \in \{1, \cdots, G\}, \quad q \in \{1, \cdots, Q\}, \end{aligned} \tag{5.7}$$

where P_T is the transmitted power, $s^{(l)}_{g_l,q}(t)$ is the user's information signal, f_c is the carrier frequency and $\varphi^{(l)}$ is the phase angle introduced by carrier modulation, while $\Lambda^{(l)}_q(t)$ is the subcarrier activation function defined as:

$$\Lambda^{(l)}_q(t) = \begin{cases} 1, & \text{the } q^{th} \text{ subcarrier activated by the } l^{th} \text{ user} \\ 0, & \text{otherwise} \end{cases}, \quad 0 \le t < T_s. \tag{5.8}$$

Furthermore, $c_{g_l}(t)$ of Equation (5.7) denotes the DSS signature sequence assigned to the l^{th} user and associated with the g^{th} DSS group, given by:

$$c_{g_l}(t) = \sum_{c=1}^{G} u_{g_l}[c]\Gamma_{T_c}(t - cT_c), \quad 0 \le t < T_s, \quad g_l \in \{1, \cdots, G\}, \tag{5.9}$$

where T_c is the chip duration, T_s is the OFDM symbol duration and $\Gamma_\tau(t)$ is a rectangular pulse[5] defined as:

$$\Gamma_\tau(t) = \begin{cases} 1, & 0 \leq t < \tau \\ 0, & \text{otherwise} \end{cases}, \tag{5.10}$$

while $u_{g_l}[c]$ of Equation (5.9) is the c^{th} element of the g^{th} row in the $(G \times G)$-dimensional WHT matrix defined by Equation (5.1). Therefore, the received signal at the p^{th} receiver antenna element is:

$$r_p(t) = \sum_{q=1}^{Q} \sum_{l=1}^{L} H_{p,q}^{(l)} s'^{(l)}_{g_l,q}(t) + n_p(t), \quad p \in \{1, \cdots, P\}, \tag{5.11}$$

where $H_{p,q}^{(l)}$ represents the Frequency-Domain CHannel Transfer Functions (FD-CHTFs) associated with the specific link between the l^{th} user and the p^{th} receiver antenna element in the context of the q^{th} subcarrier, which is assumed to remain constant during the period of T_s, while $n_p(t)$ denotes the AWGN at the p^{th} receiver. For the sake of separating the signals of the G different DSS groups, the despreading operation is then invoked with the aid of the DSS codes at each of the P receiver antennas, yielding:

$$x_{p,g}(t) = \int_0^{T_s} c_g(t) r_p(t) dt, \quad g \in \{1, \cdots, G\}. \tag{5.12}$$

Note that the above despreading operation can be restricted to the activated subcarriers only, if RSSCH patterns are used, or if USSCH patterns are employed under the condition of $L < Q_g$. In either scenario there exists inactivated subcarriers which do not carry any information signal and thus do not need to be processed. If USSCH patterns are used and we have $L \geq Q_g$, all subcarriers are activated and thus despreading is required across the entire bandwidth. As a generalized case, let us assume that the q^{th} subcarrier is activated by L_q number of users, where we have $1 \leq L_q \leq L$. Furthermore, at this specific subcarrier, a total of G_q $(1 \leq G_q \leq G)$ different DSS codes are used by the L_q users, where each user's code may or may not be the same as the others'. Without loss of generality, we assume that the g^{th} $(g = 1, \cdots, G_q)$ of the G_q different DSS groups contains l_g number of users, where we have:

$$L_q = \sum_{g=1}^{G_q} l_g. \tag{5.13}$$

Thus, the discrete signal received at the q^{th} subcarrier of the p^{th} receiver during an OFDM symbol duration can be represented as:

$$r_{p,q} = \bar{\mathbf{c}}_{G_q} \bar{\mathbf{H}}_{p,q} \bar{\mathbf{s}}_q + n_{p,q}, \quad p \in \{1, \cdots, P\}, \tag{5.14}$$

[5]In practical systems, the chip pulse shape of $\Gamma_\tau(t)$ is a bandlimited waveform, such as a raised cosine Nyquist pulse. However, for the sake of simplicity in our analysis and simulation, here we will assume that $\Gamma_\tau(t)$ is an ideal rectangular pulse.

where the $(1 \times L_q)$-dimensional DSS code vector $\bar{\mathbf{c}}_{G_q}$ and the L_q users' $(L_q \times 1)$-dimensional information signal vector $\bar{\mathbf{s}}_q$ are given by:

$$\bar{\mathbf{c}}_{G_q} = [\underbrace{\mathbf{c}_1, \mathbf{c}_1, \cdots, \mathbf{c}_1}_{l_1}, \underbrace{\mathbf{c}_2, \mathbf{c}_2, \cdots, \mathbf{c}_2}_{l_2}, \cdots, \underbrace{\mathbf{c}_{G_q}, \mathbf{c}_{G_q}, \cdots, \mathbf{c}_{G_q}}_{l_{G_q}}], \tag{5.15}$$

$$\bar{\mathbf{s}}_q = [\, s_{1,q}^{(1)}, s_{1,q}^{(2)}, \cdots, s_{1,q}^{(l_1)}, s_{2,q}^{(1)}, s_{2,q}^{(2)}, \cdots, s_{2,q}^{(l_2)}, s_{G_q,q}^{(1)}, s_{G_q,q}^{(2)}, \cdots, s_{G_q,q}^{(l_{G_q})} \,]^T \tag{5.16}$$

where $(\cdot)^T$ denotes the transposition operation. The corresponding spreading code sequence $\mathbf{c}_g$ $(g \in \{1, \cdots, G_q\})$ specified in Equation (5.15), which is associated with the g^{th} DSS group in the context of the q^{th} subcarrier, is defined by:

$$\mathbf{c}_g = [\, u_g[1], u_g[2], \cdots, u_g[G] \,], \quad g = 1, \cdots, G_q. \tag{5.17}$$

Furthermore, the L_q users' $(L_q \times L_q)$-dimensional diagonal FD-CHTF matrix associated with the q^{th} subcarrier at the p^{th} receiver antenna, namely $\bar{\mathbf{H}}_{p,q}$ of Equation (5.14), is expressed as:

$$\bar{\mathbf{H}}_{p,q} = \text{diag}\left[H_{p,1,q}^{(1)}, H_{p,1,q}^{(2)}, \cdots, H_{p,1,q}^{(l_1)}, H_{p,2,q}^{(1)}, H_{p,2,q}^{(2)}, \cdots, H_{p,2,q}^{(l_2)}, H_{p,G_q,q}^{(1)}, H_{p,G_q,q}^{(2)}, \cdots, H_{p,G_q,q}^{(l_{G_q})}\right]. \tag{5.18}$$

Therefore, the corresponding despread signal associated with the q^{th} subcarrier of the p^{th} receiver antenna can be given by:

$$\begin{aligned} \bar{\mathbf{x}}_{p,q} &= \check{\mathbf{c}}_{G_q} r_{p,q} \\ &= \bar{\mathbf{R}}_{G_q} \bar{\mathbf{H}}_{p,q} \bar{\mathbf{s}}_q + \bar{\mathbf{n}}_{p,q}, \quad p \in \{1, \cdots, P\}, \end{aligned} \tag{5.19}$$

where the $(G_q \times 1)$-dimensional despread received signal vector $\bar{\mathbf{x}}_{p,q}$ and the $(G_q \times 1)$-dimensional effective noise vector $\bar{\mathbf{n}}_{p,q}$ are expressed as:

$$\bar{\mathbf{x}}_{p,q} = [\, x_{p,1,q}, x_{p,2,q}, \cdots, x_{p,G_q,q} \,]^T, \tag{5.20}$$

$$\bar{\mathbf{n}}_{p,q} = [\, n_{p,1,q}, n_{p,2,q}, \cdots, n_{p,G_q,q} \,]^T, \tag{5.21}$$

while the $(G_q \times 1)$-dimensional DSS code vector $\check{\mathbf{c}}_{G_q}$ is given by:

$$\check{\mathbf{c}}_{G_q} = [\, \mathbf{c}_1, \mathbf{c}_2, \cdots, \mathbf{c}_{G_q} \,]^T. \tag{5.22}$$

Moreover, $\bar{\mathbf{R}}_{G_q}$ in Equation (5.19) is the $(G_q \times L_q)$-dimensional cross-correlation matrix of the L_q users' DSS code sequences, represented as:

$$\bar{\mathbf{R}}_{G_q} = \begin{bmatrix} \underbrace{\omega_{11}\ \omega_{11}\ \cdots\ \omega_{11}}_{l_1} & \underbrace{\omega_{12}\ \omega_{12}\ \cdots\ \omega_{12}}_{l_2} & \cdots & \underbrace{\omega_{1G_q}\ \omega_{1G_q}\ \cdots\ \omega_{1G_q}}_{l_{G_q}} \\ \omega_{21}\ \omega_{21}\ \cdots\ \omega_{21} & \omega_{22}\ \omega_{22}\ \cdots\ \omega_{22} & \cdots & \omega_{2G_q}\ \omega_{2G_q}\ \cdots\ \omega_{2G_q} \\ \vdots & \vdots & \vdots & \vdots \\ \underbrace{\omega_{G_q1}\ \omega_{G_q1}\ \cdots\ \omega_{G_q1}}_{l_1} & \underbrace{\omega_{G_q2}\ \omega_{G_q2}\ \cdots\ \omega_{G_q2}}_{l_2} & \cdots & \underbrace{\omega_{G_qG_q}\ \omega_{G_qG_q}\ \cdots\ \omega_{G_qG_q}}_{l_{G_q}} \end{bmatrix}, \tag{5.23}$$

where ω_{ij} is the cross-correlation coefficient of the i^{th} DSS group's and the j^{th} DSS group's signature sequence, defined as:

$$\omega_{ij} = \int_0^{T_s} c_i(t)c_j(t)dt, \quad i,j \in \{1,\cdots,G_q\}. \tag{5.24}$$

Therefore, for each of the G_q DSS groups at the q^{th} subcarrier, the despread signals can be combined from all the P receiver antenna elements and then be forwarded to the SDMA MUD, where the signals of different users in the same DSS group are separated in the spatial domain.

5.4.4 Multi-User Detection

In Chapters 3 and 4, we have investigated the MMSE and the GA based MUDs, respectively. The MMSE MUD [3] of Chapter 3 exhibits a rather low complexity, while suffering from a performance loss. By contrast, the GA-based MUD of Chapter 4 is capable of achieving a similar performance to that attained by the optimum Maximum Likelihood (ML) MUD at a significantly lower complexity, especially at high user loads. Furthermore, the MMSE-assisted Iterative GA (IGA) MUD of Chapter 4 employing Biased Q-function based Mutation (BQM) was found to outperform the conventional GA-based MUDs [45] at a similar computational complexity, especially in high-throughput scenarios.

The concatenated MMSE-IGA MUD can also be employed in the hybrid DSS/SSCH SDMA-OFDM system for the sake of improving the attainable performance. This is achieved by further processing the output provided by the MMSE MUD as the GA's initial detection knowledge at the active subcarriers, and then invoking the GA-assisted iterative detection technique. More specifically, at the first step of the iterative detection procedure, an initial estimate of the different users' transmitted signals is generated with the aid of the linear MMSE MUD. This operation is similar to that invoked in the GA-aided conventional SDMA-OFDM systems described in Chapter 4. However, in the context of the SDMA-OFDM system employing DSS and SSCH techniques, typically only the signals that arrive at the active subcarriers rather than spread across the entire system bandwidth will be processed.

More specifically, at the q^{th} subcarrier of each of the G_q DSS groups, an initial estimated signal vector $\hat{\mathbf{s}}_{\mathrm{MMSE}_{g,q}} \in \mathbb{C}^{(l_g \times 1)}$ $(g = 1,\cdots,G_q)$ associated with the l_g users of this group is generated by linearly combining the $(P \times 1)$-dimensional despread signal vector $\mathbf{x}_{g,q}$, which is constituted by the specific despread symbols generated from the g^{th} DSS group at all the P receiver antennas with the aid of the MMSE MUD's array weight matrix, as follows:

$$\hat{\mathbf{s}}_{\mathrm{MMSE}_{g,q}} = \mathbf{W}^H_{\mathrm{MMSE}_{g,q}} \mathbf{x}_{g,q}, \tag{5.25}$$

where:

$$\hat{\mathbf{s}}_{\mathrm{MMSE}_{g,q}} = \left[\hat{s}^{(1)}_{\mathrm{MMSE}_{g,q}}, \hat{s}^{(2)}_{\mathrm{MMSE}_{g,q}}, \cdots, \hat{s}^{(l_g)}_{\mathrm{MMSE}_{g,q}} \right]^T, \quad g = 1, \cdots, G_q, \tag{5.26}$$

$$\mathbf{x}_{g,q} = \left[x_{1,g,q}, x_{2,g,q}, \cdots, x_{P,g,q} \right]^T, \quad g = 1, \cdots, G_q. \tag{5.27}$$

The MMSE-based weight matrix $\mathbf{W}_{\mathrm{MMSE}_{g,q}} \in \mathbb{C}^{(P \times l_g)}$ of Equation (5.25) is given by [3]:

$$\mathbf{W}_{\mathrm{MMSE}_{g,q}} = (\mathbf{H}_{g,q}\mathbf{H}^H_{g,q} + \sigma_n^2\mathbf{I})^{-1}\mathbf{H}_{g,q}, \tag{5.28}$$

where $\mathbf{I}$ is the identity matrix and σ_n^2 is the AWGN's variance, while the $(P \times l_g)$-dimensional FD-CHTF matrix associated with the g^{th} DSS group is expressed as:

$$\mathbf{H}_{g,q} = (\mathbf{H}^{(1)}_{g,q}, \mathbf{H}^{(2)}_{g,q}, \cdots, \mathbf{H}^{(l_g)}_{g,q}), \quad g = 1, \cdots, G_q, \tag{5.29}$$

where $\mathbf{H}^{(l)}_{g,q}$ $(l = 1, \cdots, l_g)$ is the vector of the FD-CHTFs associated with the transmission paths between the l^{th} user's transmitter antenna and each element of the P-element receiver antenna array, which is expressed as:

$$\mathbf{H}^{(l)}_{g,q} = (H^{(l)}_{1,g,q}, H^{(l)}_{2,g,q}, \cdots, H^{(l)}_{P,g,q})^T, \quad l = 1, \cdots, l_g. \tag{5.30}$$

Once the MMSE-based multi-user detection is completed, the resultant output can be forwarded to the concatenated IGA MUD of Chapter 4 for the second-stage iterative detection in the context of the g^{th} DSS group at the q^{th} subcarrier.

More precisely, the IGA MUD evaluates a decision metric associated with the P receivers, which is derived from the optimum ML-based decision metric [3], in order to detect the symbol vector $\hat{\mathbf{s}}_{\mathrm{GA}_{g,q}}$ that consists of the estimated transmitted signals of the l_g users in the g^{th} DSS group, which is expressed as:

$$\hat{\mathbf{s}}_{\mathrm{GA}_{g,q}} = (\hat{s}^{(1)}_{\mathrm{GA}_{g,q}}, \hat{s}^{(2)}_{\mathrm{GA}_{g,q}}, \cdots, \hat{s}^{(l_g)}_{\mathrm{GA}_{g,q}})^T, \quad g = 1, \cdots, G_q. \tag{5.31}$$

The decision metric required for evaluation at the p^{th} receiver antenna is defined by:

$$\Omega_{p,g,q}(\mathbf{s}_g) = |x_{p,g,q} - \mathbf{H}_{p,g,q}\mathbf{s}_g|^2, \tag{5.32}$$

where $x_{p,g,q}$ is the despread symbol of the g^{th} DSS group at the q^{th} subcarrier of the p^{th} receiver, while $\mathbf{H}_{p,g,q}$ is the p^{th} row of the matrix $\mathbf{H}_{g,q}$ related to the same subcarrier, which is defined by Equation (5.29). Therefore, the decision rule for the optimum multiuser detector associated with the p^{th} antenna is to choose that specific length-l_g symbol vector $\mathbf{s}_g$, which minimizes the metric given in Equation (5.32). Since there are P number of receivers, the following combined metric is invoked:

$$\Omega_{g,q}(\mathbf{s}_g) = \sum_{p=1}^{P} \Omega_{p,g,q}(\mathbf{s}_g). \tag{5.33}$$

Hence, the joint decision rule is to find that specific estimated transmitted l_g-symbol vector $\hat{\mathbf{s}}_{\mathrm{GA}_{g,q}}$ associated with the g^{th} DSS group, which minimizes $\Omega_{g,q}(\mathbf{s}_g)$ in Equation (5.33) for the q^{th} active subcarrier, which is formulated as:

$$\hat{\mathbf{s}}_{\mathrm{GA}_{g,q}} = \arg\left\{\min_{\mathbf{s}_g}\left[\Omega_{g,q}(\mathbf{s}_g)\right]\right\}. \tag{5.34}$$

Hence, after multi-user detection invoked independently for each of the G_q DSS groups at the q^{th} subcarrier, all the estimated signals of the L_q users that activate this subcarrier will be attained. Here we point out that the IGA-based detection process is similar to that discussed in Chapter 4, except that the operations are separately invoked for each of the G_q DSS groups at the q^{th} activated subcarrier.

5.5 Simulation Results

In this section, we characterize the performance of the TTCM-assisted DSS/SSCH SDMA-OFDM system using the MMSE-IGA MUD of Chapter 4. Its performance is compared to that of its counterparts employing the RSSCH, RSFH and USFH patterns as well as to that of a conventional SDMA-OFDM system [3, 192] dispensing with the employment of any FH techniques. It was assumed in all SFH- or SSCH-aided schemes that the BS has a perfect knowledge of the hopping patterns. The simulation results were obtained using a 4QAM scheme communicating over the 3-path Short Wireless Asynchronous Transfer Mode (SWATM) CIR of Figure 2.32, assuming that the channels' transfer functions were perfectly known. Each of the paths experiences independent Rayleigh fading having the same normalized Doppler frequencies of $f'_d = 1.235 \times 10^{-5}$. The channel is assumed to be 'OFDM-symbol-invariant', implying that the taps of the impulse response are assumed to be constant for the duration of one OFDM symbol, but they are faded at the beginning of each OFDM symbol [3].

The GA-related parameters used were fixed in all the simulations, where the MMSE-IGA MUD was employed. Specifically, the BQM scheme of Section 4.3.1.2 was used, while the IGA MUD invoked a single iteration. For the iterative TTCM scheme [2] employed, the associated parameters were the same as those specified in Table 4.5 of Section 4.3.2.2. For the convenience of the reader, the basic simulation parameters are summarized in Table 5.1.

Recall that in SFH or SSCH aided SDMA-OFDM systems the number of activated subcarriers $K < Q_c$ is lower than that of the conventional SDMA-OFDM system [3, 192], where all the users employ all the Q_c number of available subcarriers for communication. For the sake of fair comparisons, the total system bandwidth was fixed and the number of users L supported by the various SFH/SSCH aided systems was increased, so that the same total

TTCM	Modem	4QAM
	Code rate	0.5
	Code memory ν	3
	Octal generator polynomial	[13 6]
	Codeword length	1024 symbols
	Channel interleaver depth	1024 symbols
	Number of turbo iterations	2
GA	Population initialization method	MMSE
	Mating pool creation strategy	Pareto-Optimality
	Selection method	Fitness-Proportionate
	Cross-over	Uniform cross-over
	Mutation	BQM
	Mutation probability p_m	0.1
	Elitism	Enabled
	Incest prevention	Enabled
	Population size X	20
	Generations Y	5
	Number of IGA iterations	1
Channel	CIRs	SWATM [3]
	Paths	3
	Maximum path delay	48.9 ns
	Normalized Doppler frequency	1.235×10^{-5}
	Total available subcarriers Q_c	128/256/512
	Cyclic prefix	16/32/64

Table 5.1: Basic simulation parameters used in Section 5.5.

system throughput of B_{T} bits per OFDM symbol was maintained, which is calculated by:

$$B_{\mathrm{T}} = K \cdot L \cdot BPS \text{ [bits/OFDM symbol]}, \tag{5.35}$$

where BPS represents the number of Bits Per Symbol per subcarrier. When 4QAM is employed, we have $BPS = 2$. For the reader's convenience, the notations used in the figures of this section are summarized in Table 5.2.

Furthermore, according to the classic spread-spectrum philosophy [375], in order to maintain a fixed OFDM symbol duration of T_s while employing time-domain DSS, the bandwidth of the OFDM symbols will have to be proportionately expanded according to the DS spreading factor, since the DSS codes' chip duration T_c is shorter than T_s [45]. Therefore, in the DSS-assisted SDMA-OFDM systems investigated in this section, where a fixed total system

Notation	Description
K	Number of subcarriers employed by each user
L	Number of users
P	Number of receiver antenna elements
Q_f	Number of available sub-bands in SFH systems
Q_c	Number of available subcarriers in SSCH systems
B_T	Total throughput per OFDM symbol of the L-user system
RSFH	Random-SFH systems
USFH	Uniform-SFH systems
RSSCH	Random-SSCH systems
USSCH	Uniform-SSCH systems

Table 5.2: Notations used in the figures of simulation results presented in Section 5.5.

bandwidth was assumed, the total number of available subcarriers Q_c was decreased. Equivalently, the subcarrier bandwidth W_{sc} was increased, when a longer DSS code was used for the sake of supporting more DSS groups. For example, compared to a SSCH system having $Q_c = 512$ subcarriers and dispensing with the employment of DSS, a hybrid DSS/SSCH system supporting $G = 2$ DSS groups will have $Q_c = 256$ subcarriers, since in this case we have $T_s = 2T_c$.

5.5.1 MMSE-aided Versus MMSE-IGA-aided DSS/SSCH SDMA-OFDM

In Figure 5.8 we compare the BER performance of the TTCM assisted USSCH/SDMA-OFDM, DSS/USSCH SDMA-OFDM and conventional SDMA-OFDM systems, where the MMSE and MMSE-IGA MUDs were employed, respectively. The performance of the single-user SDMA-OFDM system employing the optimum ML MUD is also provided for reference. The same total throughput of $B_{\mathrm{T}} = 5120$ bits per OFDM symbol was maintained for all schemes, except for the single-user arrangement, where the throughput was 1024 bits per OFDM symbol, since we assumed that $Q_c = 512$ was the maximum number of subcarriers that can be accommodated in the fixed system bandwidth. Note that in the context of the conventional SDMA-OFDM benchmark system, since $L = 5$ users were supported by $P = 4$ receiver antenna elements, this scenario can be viewed as a moderately overloaded scenario. Explicitly, for the DSS and/or SSCH aided counterpart systems, the same implication of the overloaded scenario was also applicable, because the same total system throughput was maintained in these systems, which were equivalently overloaded.

From Figure 5.8 we can see that the MMSE-IGA aided systems significantly outperformed

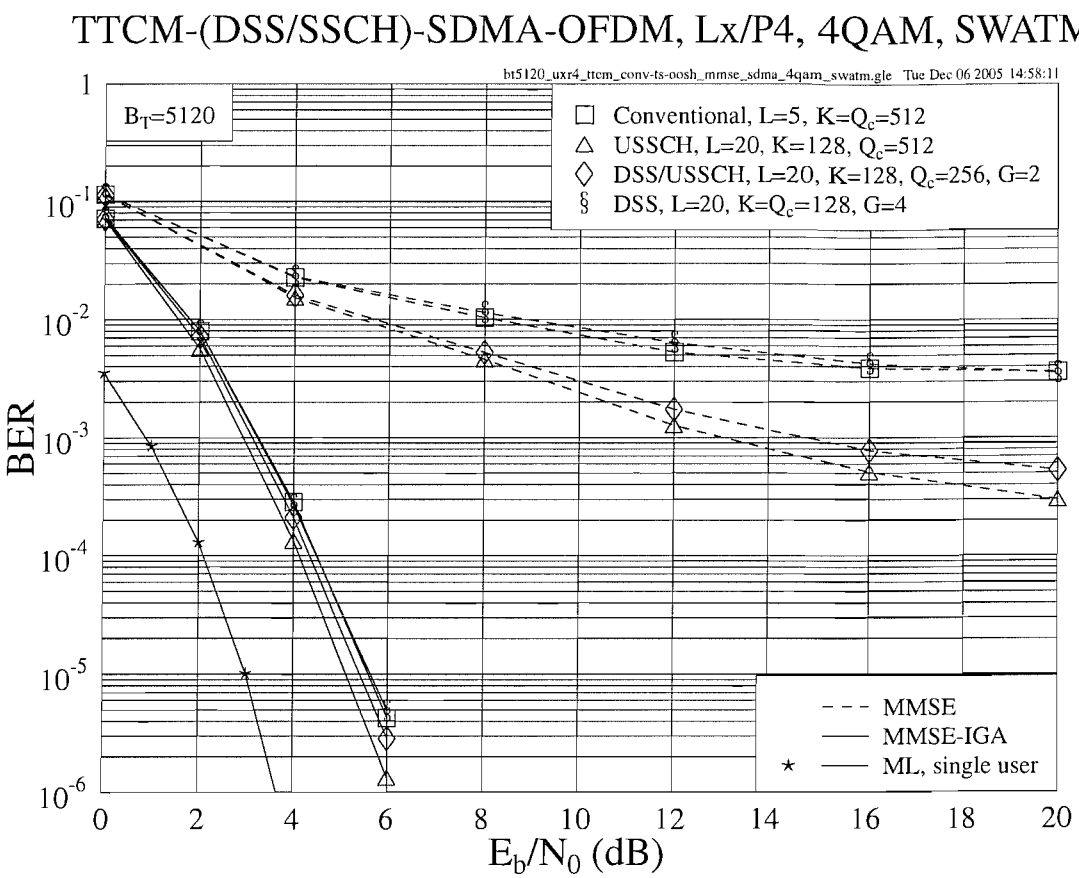

Figure 5.8: **BER** versus E_b/N_0 performance of the TTCM-assisted **conventional SDMA-OFDM**, **USSCH/SDMA-OFDM**, **DSS/SDMA-OFDM**, and **hybrid DSS/USSCH SDMA-OFDM** systems using the **MMSE** or the **MMSE-IGA** MUD, while employing a 4QAM scheme for transmission over the SWATM channel [3], where L number of users were supported with the aid of $P = 4$ receiver antenna elements. The associated overall system throughput was $\mathbf{B_T = 5120}$ bits. The basic simulation parameters and the notations used in the figure are summarized in Tables 5.1 and 5.2, respectively.

the MMSE aided systems. It is also observed that in the scenario, where the MMSE MUD was employed, the USSCH/SDMA-OFDM and DSS/USSCH SDMA-OFDM systems achieved a similar performance. The DSS/SDMA-OFDM and the conventional SDMA-OFDM systems also performed similarly to each other. However, both USSCH aided schemes were found to attain a better performance than those dispensing with USSCH. On the other hand, when using the MMSE-IGA MUD, the performances of the various systems were similar. This suggests that most of the MUI encountered can be effectively suppressed by the MMSE-IGA MUD in the moderately overloaded scenario associated with a throughput of $B_T = 5120$ bits.

5.5.2 SDMA-OFDM Using SFH and Hybrid DSS/SSCH Techniques

In Section 5.5.1 we have discussed the attractive performance of the MMSE-IGA MUD in the context of the hybrid SDMA-OFDM system. In this section, we will compare the attainable performance of various MMSE-IGA aided arrangements employing the SFH and the DSS/SSCH schemes.

5.5.2.1 Moderately Overloaded Scenarios

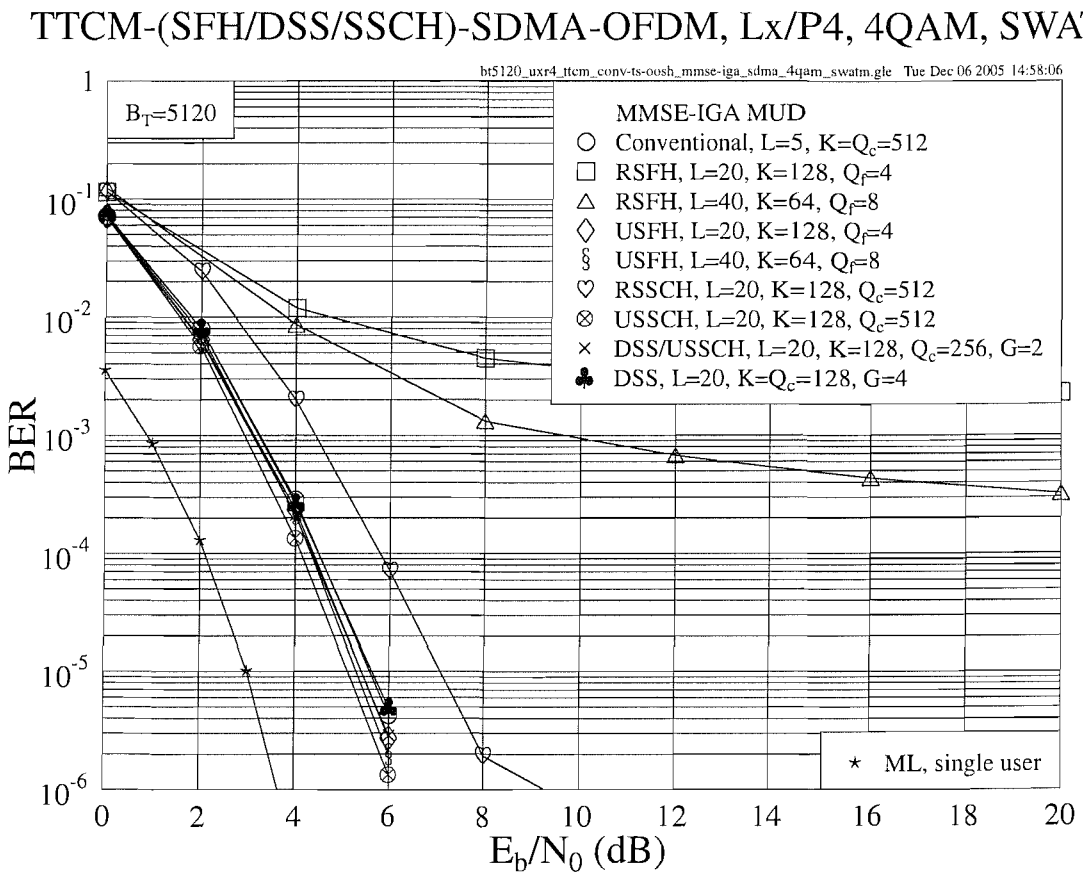

Figure 5.9: **BER** versus E_b/N_0 performance of the TTCM-assisted **conventional SDMA-OFDM, RSFH/USFH/RSSCH/USSCH SDMA-OFDM, DSS/SDMA-OFDM** and **hybrid DSS/USSCH SDMA-OFDM** systems employing a 4QAM scheme for transmission over the SWATM channel [3], where L number of users were supported with the aid of $P = 4$ receiver antenna elements. The associated overall system throughput was $\mathbf{B_T = 5120}$ bits. The basic simulation parameters and the notations used in the figure are summarized in Tables 5.1 and 5.2, respectively.

Figure 5.9 compares the BER performance of the various RSFH/RSSCH/USSCH aided SDMA-OFDM, DSS/USSCH aided SDMA-OFDM and conventional SDMA-OFDM systems, where TTCM and the MMSE-IGA MUD were employed. Note that according to the different

number of subcarriers K activated by the various schemes, the number of users was proportionately adjusted so that a total system throughput of $B_T = 5120$ bits per OFDM symbol was maintained for all the systems, apart from the ML-aided single-user reference scheme.

It is observed from Figure 5.9 that the RSFH/SDMA-OFDM scheme employing $K = 64$ subcarriers achieved a better performance than its counterpart, which used $K = 128$ subcarriers, when the E_b/N_0 value became higher than about 4dB. This is because in high-SNR scenarios the residual errors encountered are more likely to have been engendered by the average MUI, rather than by the noise. Furthermore, the RSFH system employing a lower number of subcarriers, or more precisely a larger number of sub-bands, results in less average MUI than the RSFH system, where fewer sub-bands are used, owing to supporting a reduced average number of users within each sub-band. More explicitly, this is because when a large number of users activate the same sub-band, all users' subcarriers located within this sub-band are severely corrupted and the signal carried by them may become unrecoverable even with the aid of channel codes. Moreover, at these high-MUI sub-bands the heavier the MUI, the larger the number of active users that are affected. Therefore, the RSFH scheme associated with wider sub-bands, each of which accommodates more subcarriers, will always suffer more from a MUI-induced performance degradation.

Moreover, an increased number of sub-bands also implies a potentially better exploitation of frequency diversity. In frequency-selective channels, when a deep frequency-selective channel fade occurs across a sub-band, a large portion of the subcarriers within this specific sub-band may be affected and the corresponding signal may become obliterated - a situation similar to that of a heavily MUI-infested sub-band. Although the effects imposed by a deep fade may not be worse than that by severe MUI, especially when the faded frequency-band is narrower than the sub-band's bandwidth, it does inflict a detrimental effect on the system and should be avoided or mitigated. This situation can be improved by invoking employing a large number of sub-bands, each having a low number of subcarriers. Explicitly, this facilitates a better exploitation of the frequency diversity offered by the system. Furthermore, if the subcarriers of a given user are arranged to be sufficiently far apart from each other in the frequency domain, they will experience independent FD fading, which in turn increases the TTCM channel decoder's chance of removing most - if not all - transmission errors.

This suggests that if the SFH sub-band of a specific user is further split into narrower bands, ideally each of which is as far from the others as possible, an improved performance may be achieved as a benefit of the associated frequency diversity. This argument is confirmed by the RSSCH-aided SDMA-OFDM system, which significantly outperformed both RSFH-aided arrangements, as a result of employing the subcarrier-based rather than the subband-based hopping approach, as observed in Figure 5.9.

However, note that the performance of the RSFH or RSSCH aided SDMA-OFDM system was worse than that of the conventional SDMA-OFDM system, since the use of random patterns inevitably results in an increased average BER, owing to the severe MUI arising from the subcarriers or sub-bands activated by an excessive number of users, as discussed in Section 5.4.2.1. By contrast, the employment of the uniform patterns calculated using the algorithm of Section 5.4.2.2 has the potential of improving the conventional system's performance, as shown in Figure 5.9. Furthermore, the achievable performance improvement becomes more significant, when the total system throughput is further increased, which will be discussed in the next section.

5.5.2.2 Highly Overloaded Scenarios

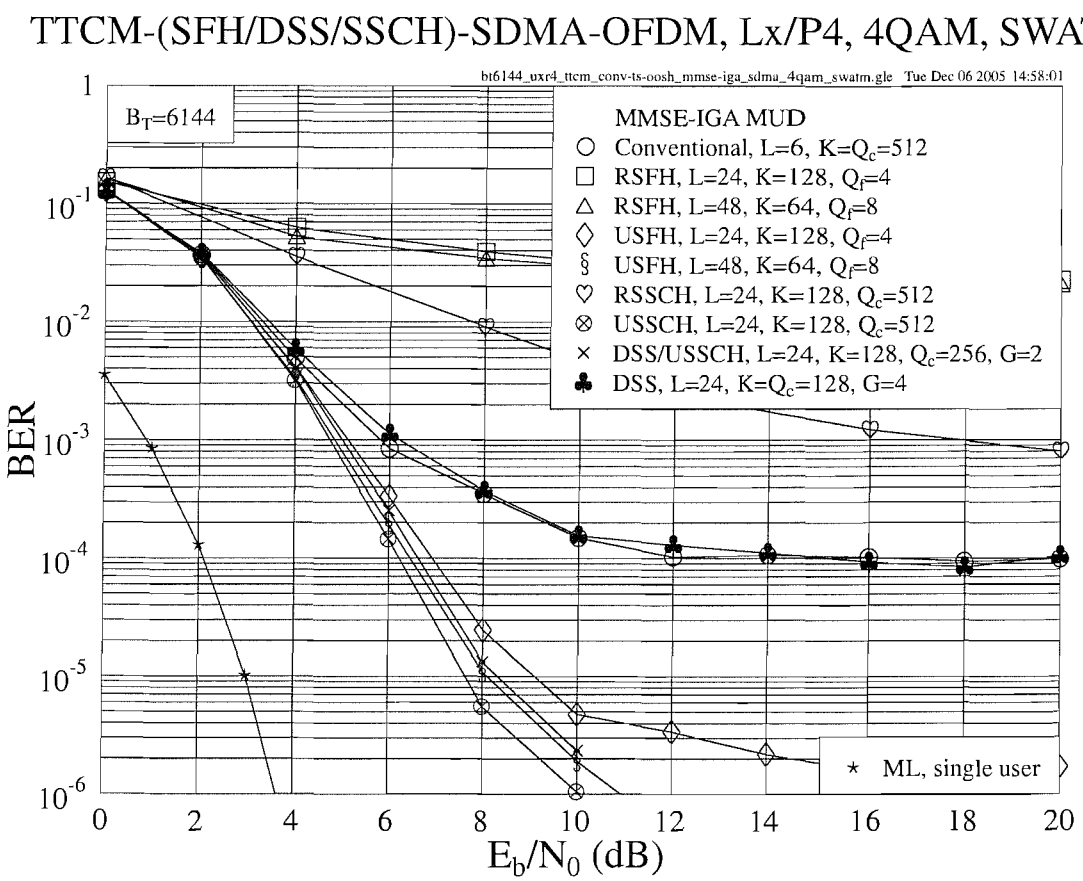

Figure 5.10: **BER** versus E_b/N_0 performance of the TTCM-assisted **conventional SDMA-OFDM, RSFH/USFH/RSSCH/USSCH SDMA-OFDM, DSS/SDMA-OFDM** and **hybrid DSS/USSCH SDMA-OFDM** systems employing a 4QAM scheme for transmission over the SWATM channel [3], where L number of users were supported with the aid of $P = 4$ receiver antenna elements. The associated overall system throughput was $\mathbf{B_T = 6144}$ bits. The basic simulation parameters and the notations used in the figure are summarized in Tables 5.1 and 5.2, respectively.

In this section, we investigate the various systems in the scenario, where the total system throughput was further increased to $B_T = 6144$ bits per OFDM symbol, as portrayed in Figure 5.10. From the figure, we can see that the USFH, the USSCH and the hybrid DSS/USSCH aided systems were capable of achieving a significantly better performance in comparison to the other systems, including the conventional SDMA-OFDM arrangement. More precisely, the RSFH/RSSCH SDMA-OFDM, the DSS/SDMA-OFDM and the conventional SDMA-OFDM systems gravely suffered from the excessive MUI and thus exhibited the corresponding error floors. By contrast, the schemes employing USFH/USSCH successfully suppressed the MUI and eliminated the associated error floor, as seen in Figure 5.10, while the USSCH/SDMA-OFDM system was found to be the best performer. This significant BER performance improvement was achieved as a benefit of the USSCH strategy presented in Section 5.4.2.2, which succeeded in exploiting the frequency diversity by dispersing the users' signals across the entire system bandwidth in a uniform-random manner. Hence, the TTCM decoder was capable of successfully correcting most of the near-uniformly scattered errors inherent in each user's transmitted signal, resulting in a significant BER performance improvement. For example, at an E_b/N_0 value of 10dB, the USSCH/SDMA-OFDM system reduced the BER by about two, three and four orders of magnitude in comparison to the conventional SDMA-OFDM, the RSSCH/SDMA-OFDM and the RSFH/SDMA-OFDM systems, respectively, as plotted in Figure 5.10.

Furthermore, as expected, the performance of the RSFH or USFH aided SDMA-OFDM system was further improved as the number of sub-bands was decreased. Moreover, the former system was outperformed by the RSSCH-aided scheme, while the latter by the USSCH-aided arrangement. On the other hand, the hybrid DSS/USSCH SDMA-OFDM system attained a performance between those of the USSCH/SDMA-OFDM and the DSS/SDMA-OFDM systems, while the DSS/SDMA-OFDM scheme achieved a similar performance to that of the conventional SDMA-OFDM system. Recall that when the total system bandwidth is fixed, the increased length of the DSS code, which implies a better exploitation of time diversity, is achieved at the cost of decreasing the number of available subcarriers, i.e. decreasing the attainable frequency diversity gain. Hence, the results shown in Figure 5.10 suggest that the frequency diversity benefits achieved by USSCH may be more significant than those of the time diversity attained by DSS. This implies that in such scenarios the fixed-bandwidth hybrid system should avoid using long DSS codes that result in a wider subcarrier bandwidth, so that a sufficiently high number of $Q > K$ subcarriers becomes available for the sake of maintaining a sufficiently high frequency diversity.

This characteristic is also confirmed by Figure 5.11, which shows the BER versus total system throughput performances of the various SDMA-OFDM systems, where a different number

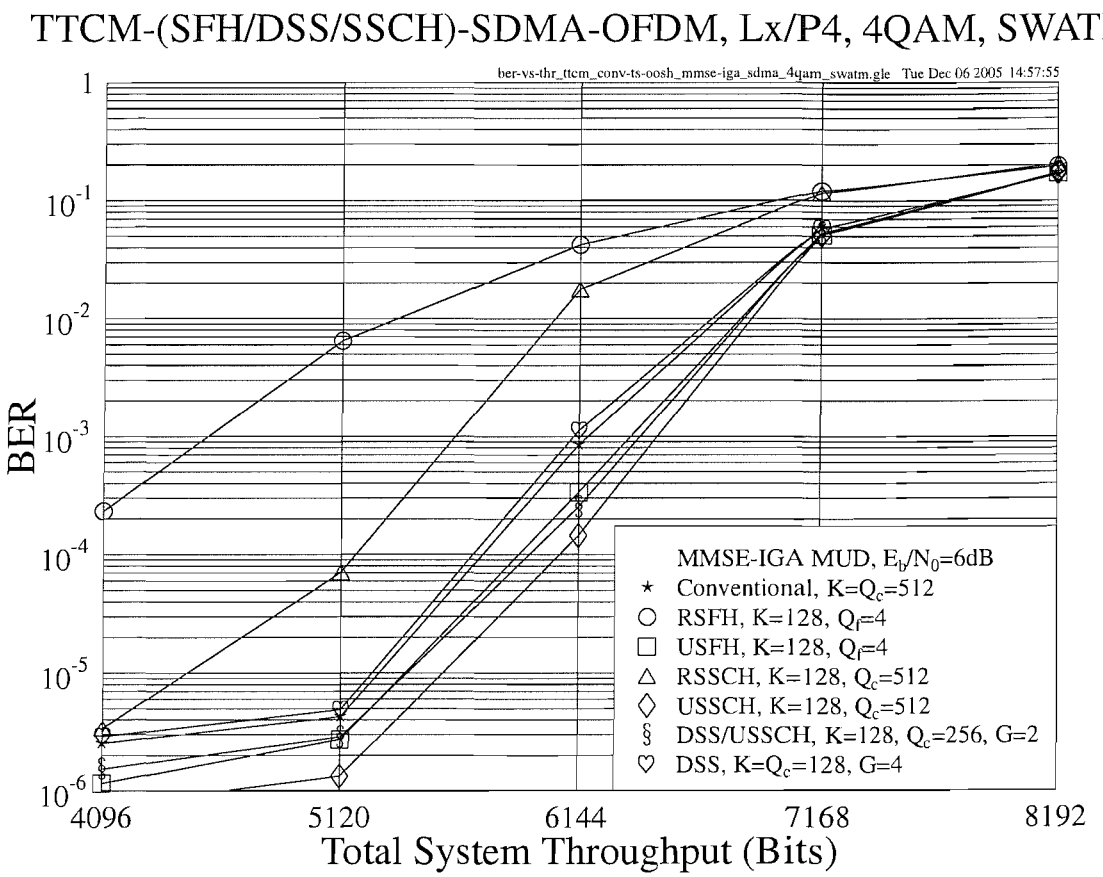

Figure 5.11: **BER** versus total system throughput performance of the TTCM-assisted **conventional SDMA-OFDM**, **RSFH/USFH/RSSCH/USSCH SDMA-OFDM**, **DSS/SDMA-OFDM** and **hybrid DSS/USSCH SDMA-OFDM** systems employing a 4QAM scheme for transmission over the SWATM channel [3], where $P = 4$ receiver antenna elements were used. The number of users supported increased proportionally to the total system throughput. The basic simulation parameters and the notations used in the figure are summarized in Tables 5.1 and 5.2, respectively.

of users was supported at the fixed E_b/N_0 value of 6dB. As inferred from Figure 5.11, when the total system throughput was increased, the performance of all the schemes degraded owing to the increased MUI. However, the systems using USSCH were found to outperform their counterparts dispensing with USSCH. Again, the USSCH/SDMA-OFDM system attained the best performance by exhibiting the highest robustness against MUI, which was, again, a direct benefit of the USSCH pattern assignment strategy of Section 5.4.2.2. This merit of the USSCH/SDMA-OFDM scheme was further evidenced by Figure 5.12, which shows the maximum total system throughput that can be supported by the various SFH/SSCH aided schemes without exceeding the target BER at different E_b/N_0 values. The number of subcarriers activated by each user was set to $K = 128$ for all schemes for the sake of a fair comparison. Specifically, the results attained for the target BER of 10^{-3} and 10^{-5} are portrayed at the

left-hand and right-hand sides of Figure 5.12, respectively. It is seen that in both scenarios for E_b/N_0 values beyond 8dB, the RSFH system was unable to tolerate more users, because its performance was limited by the MUI. By contrast, the other schemes were capable of providing a significant user capacity increase, while the USSCH/SDMA-OFDM system distinguished itself by providing the highest capacity. For example, at the E_b/N_0 value of 12dB, a capacity increase of about 4%, 13% and 44% was achieved by the USSCH scheme compared to the USFH, the RSSCH and the RSFH arrangement at the target BER of 10^{-3}, while 4%, 14% and 78% at the BER of 10^{-5}, respectively, as shown in Figure 5.12.

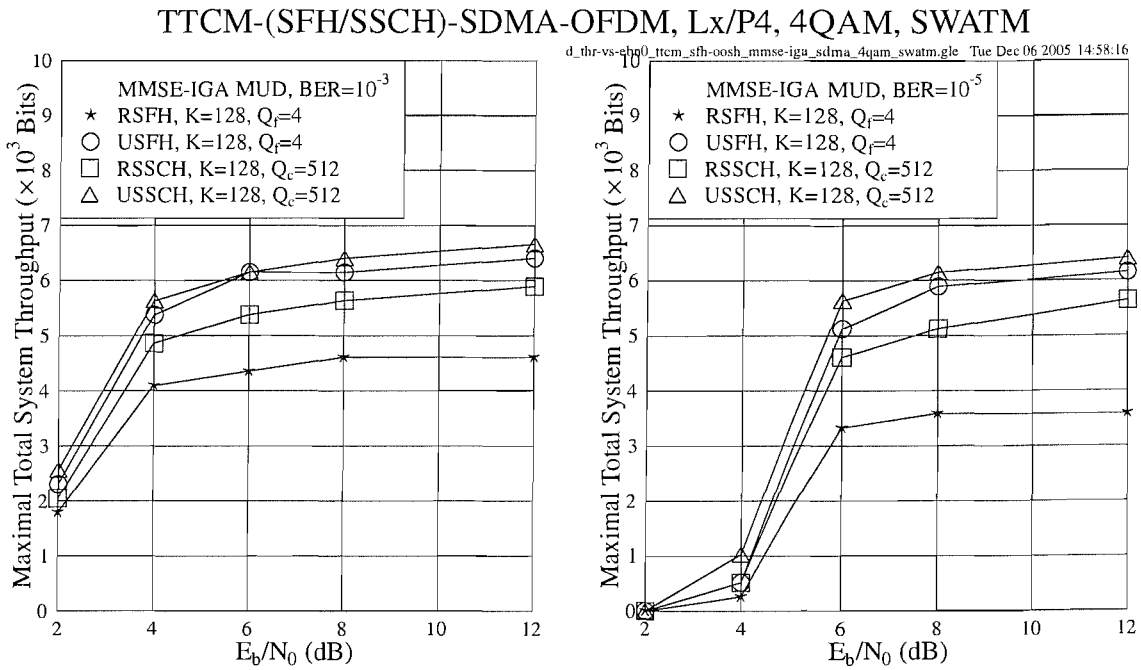

Figure 5.12: **Maximal total system throughput** versus E_b/N_0 performance of the TTCM-assisted **conventional SDMA-OFDM** and **RSFH/USFH/RSSCH/USSCH SDMA-OFDM** systems employing a 4QAM scheme for transmission over the SWATM channel [3], where $P = 4$ receiver antenna elements were used. The number of users supported increased proportionally to the maximal total system throughput. The basic simulation parameters and the notations used in the figure are summarized in Tables 5.1 and 5.2, respectively.

5.5.3 Performance Enhancements by Increasing Receiver Diversity

In the previous sections, the performance of the different SFH and SSCH aided SDMA-OFDM systems has been evaluated. Furthermore, the achievable performance of the different schemes can be potentially enhanced with the aid of a higher-order SDMA receiver diversity. Recall that in the context of SDMA-OFDM systems, the different users are distinguished by their spatial signatures, namely the associated channel CIRs. Hence, given a specific number of

simultaneous users, an increased receiver diversity order achieved by increasing the number of BS receiver antennas will directly attain a higher diversity gain for all the users supported by the system, and hence an overloaded system may be turned into one having a lower user load. Therefore, the MUD's efficiency can be enhanced with the advent of a higher degree of freedom in the context of multi-user detection.

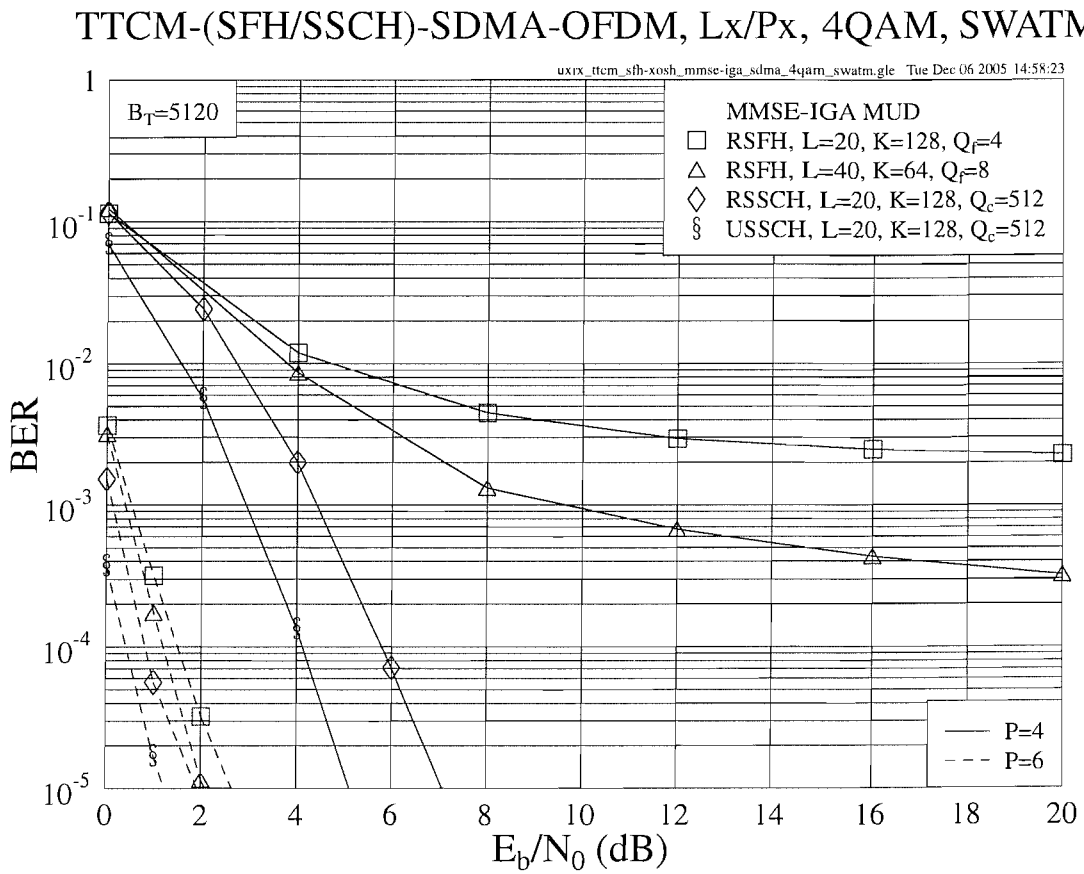

Figure 5.13: **BER** versus E_b/N_0 performance of the TTCM-assisted **RSFH/RSSCH/USSCH SDMA-OFDM** systems employing a 4QAM scheme for transmission over the SWATM channel [3], where L number of users were supported with the aid of **P=4** or **P=6** receiver antenna elements. The associated overall system throughput was $\mathbf{B_T = 5120}$ bits. The basic simulation parameters and the notations used in the figure are summarized in Tables 5.1 and 5.2, respectively.

In Figure 5.13, the various SFH/SSCH schemes are compared in the four-receiver and six-receiver SDMA-OFDM systems. In both scenarios, the throughput was fixed at $B_T = 5120$ bits per OFDM symbol. Clearly, when the number of receiver antenna elements was increased from four to six, the performance of all systems was improved, especially that of the RSFH/SDMA-OFDM arrangement. More precisely, the corresponding residual error floor observed in the four-antenna scenario was dramatically reduced or completely removed in the six-antenna scenario. Again, in both scenarios, the best solution was the USSCH assisted

system. However, the performance differences between the various schemes were substantially reduced in the higher-diversity scenario, since most of the achievable diversity gain of the SDMA system may be attained by increasing the number of BS receiver antennas, although at the cost of an increased hardware implementation complexity, especially in terms of channel estimation.

5.5.4 Performance Under Imperfect Channel Estimation

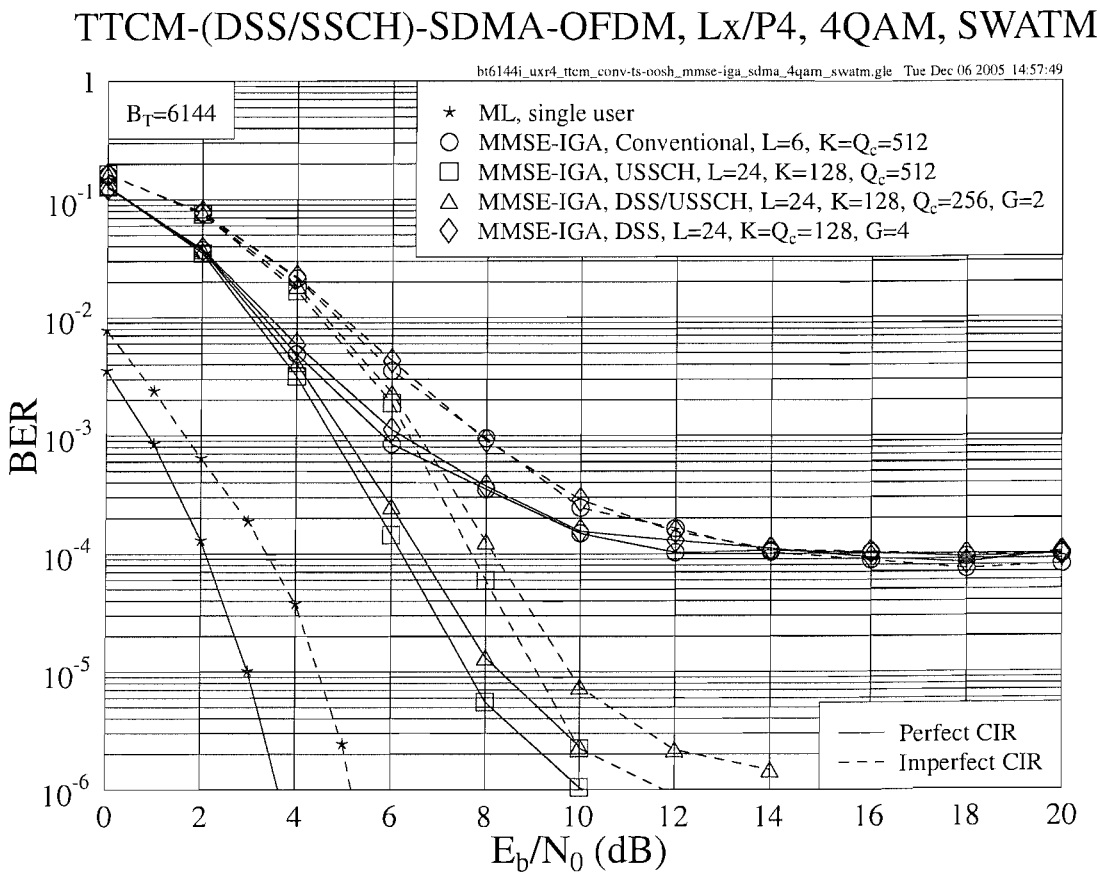

Figure 5.14: **BER** versus E_b/N_0 performance of the TTCM-assisted **conventional SDMA-OFDM**, **DSS SDMA-OFDM** and **hybrid DSS/USSCH SDMA-OFDM** systems employing a 4QAM scheme for transmission over the SWATM channel [3], where L number of users were supported with the aid of $P = 4$ receiver antenna elements. The associated overall system throughput was $\mathbf{B_T = 6144}$ bits. The basic simulation parameters and the notations used in the figure are summarized in Tables 5.1 and 5.2, respectively.

Similar to Section 4.3.2.2.3, we provide further simulation results for the scenario, where channel estimation was assumed to be imperfect. Again, the estimated SWATM CIRs were generated using Equation (4.19), while a snap shot of the SWATM channel has been plotted in Figure 4.25, which shows both the real and imaginary components of the FD-CHTFs

associated with both perfect and imperfect CIRs. The performance comparison of the various systems under the assumptions both of perfect and imperfect channel knowledge is given in Figure 5.14, where the total throughput was $B_T = 6144$ bits per OFDM symbol. As seen in Figure 5.14, the various DSS and/or USSCH aided SDMA-OFDM systems did not suffer a higher performance degradation than the single-user scheme, when the channel estimation was imperfect. This implies that the proposed hybrid system is capable of attaining an acceptable performance even without accurate channel knowledge.

5.6 Complexity Issues

The Q_c-point IFFT employed by the SSCH-aided system will inevitably impose a higher computational complexity than its SFH-aided counterpart, where a K-point IFFT is used, regardless whether the RSSCH or USSCH scheme is employed, since we have $K < Q_c$. However, it has been shown in Section 5.5 that SSCH systems typically achieve a significant performance improvement over the SFH arrangements considered, hence their additional complexity cost may be deemed justified. Furthermore, in SSCH systems the OFDM symbols modulate a single carrier frequency f_c, hence the frequency synthesizers necessary for both the SFH transmitter and receiver are eliminated, which simplifies the hardware implementation of the SSCH systems. Note that in SFH systems the subcarrier activation/deactivation operations may also be invoked in the baseband, so that the employment of the frequency synthesizers becomes unnecessary. However, in this case a Q_c-point IFFT will have to be invoked in the baseband-processing aided SFH systems, resulting in a similar complexity to that of the SSCH systems.

On the other hand, concerning the RSSCH and the USSCH systems, a similar SSCH transmitter invoking a Q_c-point IFFT is employed, thus the transmitter's complexity is similar in both systems. Nonetheless, the RSSCH arrangement imposes a potentially higher complexity at the receiver side. This is because the number of active users at each subcarrier is a random variable spanning from 1 to L, since a random SSCH pattern is employed. Therefore, a MUD that is capable of detecting a variable number of active users has to be employed, which will impose an increased complexity. Naturally, this problem exists in all the FH/SCH aided SDMA-OFDM systems using random hopping patterns. By contrast, a USSCH receiver has a complexity similar to that of conventional SDMA-OFDM systems, which employ a MUD designed for a fixed number of active users. This implementation benefit arises due to the characteristics of the USSCH system, since the users are uniformly distributed across the subcarriers, so that the number of users activating each subcarrier is similar. Specifically, if the condition of $L \ mod \ Q_g = L \ mod \ (\frac{Q_c}{K}) = 0$ is satisfied, namely if the number of users supported

by the system can be divided by the number of subcarriers within a subcarrier group, the number of users assigned to all subcarriers will be the same, as discussed in Section 5.4.2.2.2.

Note that without channel feedback the proposed USSCH pattern assignment algorithm may not be optimum in terms of combating the deleterious effects of deep channel fades. However, our proposed scheme has the advantage of low complexity and high MUI-resistance, since the USSCH patterns can be generated using offline pre-computation and yet achieve an attractive performance, as discussed in Section 5.4.2.4. This imposes a significantly lower computational complexity than that required by complicated adaptive algorithms requiring near-instantaneously channel knowledge.

5.7 Conclusions

From the investigations conducted in Section 5.5, we conclude that the proposed USSCH-aided SDMA-OFDM system was capable of achieving the best performance in comparison to all the other schemes considered, especially in high-throughput scenarios, when TTCM was employed. For example, in the overloaded scenario associated with $B_{\mathrm{T}} = 6144$ bits per OFDM symbol, the USSCH/SDMA-OFDM system reduced the BER recorded at an E_b/N_0 value of 8dB by one to four orders of magnitude in comparison to the DSS/USSCH SDMA-OFDM, the USFH/SDMA-OFDM, the DSS/SDMA-OFDM, the conventional SDMA-OFDM, the RSSCH/SDMA-OFDM and the RSFH/SDMA-OFDM systems, respectively, as shown in Figure 5.10. More specifically, the USSCH-aided system exhibits a high resilience against the excessive MUI incurred in high-throughput scenarios, owing to the characteristics of the proposed subcarrier assignment algorithm of Section 5.4.2.2. We also show that the attainable system performance may be further improved, if a higher-order receiver diversity is provided by the SDMA-OFDM system.

Furthermore, when compared to the conventional SDMA-OFDM system, the only additional computational complexity imposed by the USSCH/SDMA-OFDM system arises from the low-complexity USSCH algorithm. Moreover, it allows offline pre-computation of the patterns, as discussed in Section 5.4.2.4. Thus, the desirably high performance of the proposed USSCH/SDMA-OFDM system is not achieved at the cost of a significantly increased computational complexity, in comparison to its conventional counterpart.

5.8 Chapter Summary

In this chapter, we proposed a TTCM-assisted DSS/USSCH aided OFDM system operating with the aid of the MMSE-IGA MUD designed for the SDMA MIMO uplink channel intro-

duced in Section 3.2.1, and compared its performance to a range of different SDMA-OFDM systems.

In Section 5.1 the conventional SDMA-OFDM system was briefly reviewed, where we highlighted two of its disadvantages. On one hand, the conventional SDMA-OFDM cannot efficiently exploit frequency diversity, because all the users share all available subcarriers simultaneously. On the other hand, a high number of users will inevitably result in a high MUI across the entire bandwidth, which degrades all users' performance. In Section 5.2, an introduction to hybrid SDMA-OFDM systems was given, discussing how both of the above-mentioned problems encountered by the conventional SDMA-OFDM system may be overcome. Furthermore, in Section 5.3 we provided a comparison of the conventional SDMA-OFDM [3, 192], the SFH/SDMA-OFDM and the SSCH/SDMA-OFDM systems in terms of their frequency resource allocation strategies, where the SSCH scheme was considered to have more advantages than the others, such as for example its higher efficiency in terms of exploiting frequency diversity.

In Section 5.4, the proposed hybrid SDMA-OFDM system was introduced, which incorporated both direct sequence spreading and subcarrier-based FH techniques into conventional SDMA-OFDM systems. More specifically, an overview of the system's architecture was presented in Section 5.4.1, including the transmitter and receiver designs in Sections 5.4.1.1 and 5.4.1.2, respectively. Furthermore, two different SSCH pattern assignment strategies were considered in Section 5.4.2, namely the RSSCH scheme of Section 5.4.2.1 and the USSCH scheme of Section 5.4.2.2, where the USSCH strategy was considered to be more meritorious. This is because the USSCH algorithm designed in Section 5.4.2.2.1 assigns uniformly-distributed subcarriers to all users, so that the number of users activating each subcarrier becomes similar. Therefore, the average MUI across the whole system bandwidth can be minimized. In addition, with the advent of the USSCH strategy, the system's frequency diversity can be efficiently exploited. The random and uniform pattern assignment strategies can also be applied in SFH/SDMA-OFDM systems, as discussed in Section 5.4.2.3. Moreover, we pointed out in Section 5.4.2.4 that the USFH/USSCH patterns can be generated by offline pre-computation, which imposes a significantly lower computational complexity than that required by other adaptive algorithms benefitting from real-time channel knowledge. In order to offer an insight into the system design, we detailed in Section 5.4.3 the DSS despreading and SSCH demapping operations invoked at the SDMA receiver, followed by the discussion of the multi-user detection process in the context of the hybrid DSS/SSCH SDMA-OFDM system in Section 5.4.4.

Our simulation-based performance results associated with the SSCH/SDMA-OFDM system were provided in Section 5.5. Specifically, in Section 5.5.1 the attainable performance of

the DSS and/or SSCH aided SDMA-OFDM systems were compared, when using the classic MMSE MUD [3] discussed in Chapter 3 and the MMSE-IGA MUD proposed in Chapter 4. It was observed in Figure 5.8 that in the moderately overloaded scenario associated with a total system throughput of $B_{\mathrm{T}} = 5120$ bits, most of the MUI encountered can be effectively suppressed by the MMSE-IGA MUD, while the overloaded MMSE MUD results in a high error floor. In Section 5.5.2, the performance of the hybrid DSS/SSCH SDMA-OFDM system was characterized and compared to that of the conventional SDMA-OFDM and SFH-aided SDMA-OFDM systems, while employing the MMSE-IGA MUD. More specifically, a moderately overloaded scenario was considered in Section 5.5.2.1. The RSFH, the USFH and the RSSCH aided schemes were found to suffer from using random hopping patterns, which resulted in an increased average BER owing to the excessive MUI arising from the subcarriers or sub-bands activated by a high number of users. By contrast, the systems using the uniform patterns generated by the algorithm of Section 5.4.2.2 were capable of improving the achievable performance, as evidenced in Figure 5.9.

Furthermore, we demonstrated in Section 5.5.2.2 that the proposed uniform pattern assignment algorithm excelled, when the total system throughput was further increased. In the highly-overloaded scenario, where the total system throughput was increased to $B_{\mathrm{T}} = 6144$ bits per OFDM symbol, the USFH, the USSCH and the hybrid DSS/USSCH aided systems were capable of achieving a significantly better performance in comparison to the conventional SDMA-OFDM, the DSS/SDMA-OFDM as well as the RSFH/RSSCH aided SDMA-OFDM systems, as portrayed in Figure 5.10. More explicitly, the USSCH/SDMA-OFDM system was found to be the best design option, which successfully suppressed the MUI and eliminated the associated error floor as a benefit of the USSCH strategy presented in Section 5.4.2.2. For example, at an E_b/N_0 value of 10dB, the USSCH/SDMA-OFDM system reduced the BER by about two, three and four orders of magnitude in comparison to the conventional SDMA-OFDM, the RSSCH/SDMA-OFDM and the RSFH/SDMA-OFDM systems, respectively, as evidenced by Figure 5.10. On the other hand, it was concluded that the frequency diversity benefits achieved by USSCH may be more significant than those of the time diversity attained by DSS, since the hybrid DSS/USSCH SDMA-OFDM system attained a performance between those of the USSCH/SDMA-OFDM and the DSS/SDMA-OFDM systems, while the DSS/SDMA-OFDM scheme achieved a similar performance to that of the conventional SDMA-OFDM system. This suggests that the fixed-bandwidth hybrid system should avoid using long DSS codes that result in a wider subcarrier bandwidth, so that a sufficiently high number of $Q > K$ subcarriers becomes available for the sake of maintaining a sufficiently high frequency diversity. The proposed USSCH scheme's high robustness against MUI was further confirmed by the results of Figures 5.11 and 5.12. For example, at the E_b/N_0 value of 12dB, a capacity increase of about 4%, 13% and 44% was achieved by the USSCH scheme compared to

the USFH, the RSSCH and the RSFH arrangements, when aiming for the target BER of 10^{-3}, while 4%, 14% and 78% for the target BER of 10^{-5}, respectively, as shown in Figure 5.12. We also demonstrated that the attainable performance of the SSCH-aided SDMA-OFDM system can be further enhanced, when the receiver diversity order becomes higher, as discussed in Section 5.5.3. In Section 5.5.4, we demonstrated that the proposed hybrid system is capable of achieving an acceptable performance even without accurate channel knowledge. Finally, we pointed out that the superior performance of the USSCH-aided SDMA-OFDM system is achieved at a similar complexity to that of the conventional SDMA-OFDM arrangement, since the additional computational complexity imposed by the USSCH algorithm manifests itself in terms of the offline pre-computation, as discussed in Section 5.6.

From the perspective of practical applications, the efficient exploitation of frequency diversity and the robust MUI-suppression capability renders the channel-coded USSCH technique an attractive design option, resulting in flexible implementations. In fact, the USSCH/SDMA-OFDM scheme can be readily extended to a variable-rate system offering a high grade of flexibility, as required by future wireless multimedia services, where variable bit rates and different QoS requirements have to be satisfied. More specifically, each user may activate a different number of subcarriers depending on the type of service to be delivered or the bit rate to be supported. A modified version of the USSCH algorithm of Section 5.4.2.2 can be invoked for generating the users' uniform patterns, which takes into account their different rates. Furthermore, in SSCH-based systems the different subcarriers do not have to be contiguously allocated, which is a further attractive property, especially in the scenarios where several systems operated by different service providers have to coexist and/or fractional bandwidths have to be exploited. In addition, the different types of hybrid SFH/SSCH assisted SDMA-OFDM systems can be readily implemented by exploiting different number of sub-bands having different bandwidths, depending on the specific system requirements.

So far most of our investigations has been conducted under the assumption of perfect channel estimation. Naturally, this assumption is impractical in real applications. Hence, in the next chapter, we will continue our study by developing novel channel estimation techniques for SDMA-OFDM systems.

Chapter 6

Iterative Joint Channel Estimation and Multi-User Detection for High-Throughput Multiple-Antenna Aided OFDM Systems

6.1 Introduction

Multiple-Input Multiple-Output (MIMO) Orthogonal Frequency Division Multiplexing (OFDM) systems have recently attracted substantial research interest. On one hand, the employment of multiple antennas offers an opportunity to exploit both transmitter and receiver diversity, hence significantly increasing the system's transmission integrity [108]. On the other hand, as a further benefit, OFDM exhibits robustness against both frequency-selective fading as well as the Inter-Symbol Interference (ISI) imposed by multi-path propagation. Specifically, intensive research efforts have been invested both in Bell Labs Layered Space-Time architecture (BLAST) [106, 109, 318] and in Space Division Multiple Access (SDMA) based MIMO OFDM [3]. More specifically, in SDMA-OFDM systems the transmitted signals of L simultaneous uplink mobile users - each equipped with a single transmitter antenna - are received by the P different receiver antennas of the Base Station (BS). At the BS Multi-User Detection (MUD) [305] techniques are invoked for detecting the different users' transmitted signals with the aid of their unique, user-specific spatial signature constituted by their Frequency-Domain CHannel Transfer Functions (FD-CHTFs) or, equivalently, Channel Impulse Responses (CIRs). Since the same time-frequency resource is shared by simultaneous users, a higher bandwidth efficiency can be achieved by SDMA systems in comparison to

conventional multiplexing techniques, such as for example Time Division Multiple Access (TDMA) or Frequency Division Multiple Access (FDMA).

However, in these systems accurate channel estimation is required at the receiver for the sake of invoking both coherent demodulation and interference cancellation. Compared to Single-Input Single-Output (SISO) systems, channel estimation in the MIMO scenario becomes more challenging, since a significantly increased number of independent transmitter-receiver channel links have to be estimated simultaneously for each subcarrier. Moreover, the interfering signals of the other transmitter antennas have to be suppressed. All these factors render channel estimation for MIMO OFDM systems a new challenge.

In the literature, a number of blind channel estimation techniques have been proposed for MIMO OFDM systems [90, 216, 227, 250, 376, 377]. However, most of these approaches suffer from either a slow convergence rate or a performance degradation, owing to the inherent limitations of blind search mechanisms. By contrast, the techniques benefiting from explicit training with the aid of known reference/pilot signals, are typically capable of achieving a better performance at the cost of a reduced effective system throughput. For example, Li *et al.* [378] proposed an approach of exploiting both transmitter diversity and the delay profile characteristics of typical mobile channels, which was further simplified and enhanced in [131, 379] and [134], respectively. Other schemes employed Minimum Mean-Square Error (MMSE) [380], Constrained Least-Squares (CLS) [199], iterative Least-Squares (LS) [132,174], Second-Order Statistics (SOS) based sub-space [157] estimation algorithms as well as the QR Decomposition combined with the M-algorithm (QRD-M) [173, 381] or techniques based on Time-of-Arrivals (TOAs) [179], etc. Some researchers have their attention focused on designing optimum training patterns or structures [131, 133, 382]. Furthermore, various joint approaches combining channel estimation with data symbol detection at the receiver were also proposed for Code Division Multiple Access (CDMA) [377, 381], SISO OFDM [383] and MIMO OFDM [173, 384] systems. However, in the context of BLAST or SDMA type multi-user MIMO OFDM systems, all channel estimation techniques found in the literature were developed under the assumption that the number of users L is lower than [132, 157, 216, 227, 376, 380, 385] or equal to [133, 173, 179, 199, 250, 384, 386] the number of receiver antennas P. This assumption is critical for the following reasons. When we have $L > P$, which we refer to as an *overloaded* scenario, the $(P \times L)$-dimensional MIMO channel matrix representing the $(P \times L)$ number of channel links becomes singular, thus rendering the degree of freedom of the detector insufficient. This will catastrophically degrade the performance of numerous known detection approaches, such as for example the MMSE algorithm of [3, 305] and the QRD-M algorithm of [173]. Furthermore, the associated significant degradation of the MUD's performance in this overloaded scenario will inevitably result in severe error propagation in

decision-directed type channel estimators [3].

Against this background, in this chapter we propose a new Genetic Algorithm (GA) [319–323] assisted iterative Joint Channel Estimation and Multi-User Detection (GA-JCEMUD) approach for multi-user MIMO SDMA-OFDM systems, which provides an effective solution to the multi-user MIMO channel estimation problem in the above-mentioned overloaded scenario. Our ambitious goal of supporting a high number of users is physically possible, because the proposed GA-based technique dispenses with any constraints concerning the rank of the channel matrix. In the literature, only a few channel estimation schemes were proposed based on GAs. More specifically, Yen *et al.* [328] proposed a GA-aided multi-user CDMA single-antenna receiver, which jointly estimates the transmitted symbols and fading channel coefficients of all the users. A batch blind equalization scheme based on Maximum Likelihood (ML) concatenated channel and data estimation employing a micro genetic algorithm (μGA) and the Viterbi Algorithm (VA) was proposed in [387]. In [388,389], GA-based approaches were used for finding optimum training sequences for channel estimation in OFDM systems. However, to our best knowledge, no techniques employing GAs for joint channel and data optimization can be found in the literature in the context of multi-user MIMO OFDM. Furthermore, at the time of writing the GAs invoked in the data detection literature [45,326–328,390,391] can only provide a hard-decision output for the Forward Error Correction (FEC) or channel decoder, which inevitably limits the system's achievable performance. By contrast, our proposed GA is capable of providing "soft" outputs and hence it becomes capable of achieving an improved performance with the aid of FEC decoders.

The structure of this chapter is as follows. Firstly an overview of the proposed scheme is provided in Section 6.2, followed by the introduction of the proposed iterative GA-JCEMUD in Section 6.3. More specifically, the methods used to generate initial FD-CHTF estimates and initial symbol estimates are discussed in Sections 6.3.1 and 6.3.2, respectively. The GA-aided joint optimization process is detailed in Section 6.3.3, commencing with a discussion on the GA individual's structure in Section 6.3.3.1, followed by the description of the initialization process in Section 6.3.3.2, the analysis of the genetically joint channel estimation and symbol detection in Section 6.3.3.3 and the derivation of a novel soft-decoded GA in Section 6.3.3.4, respectively. Our simulation results are provided in Section 6.4, while Sections 6.5 and 6.6 conclude our findings.

6.2 System Overview

Figure 6.1 shows the schematic of a SDMA-OFDM uplink system using the proposed iterative GA-JCEMUD. As shown in the upper half of Figure 6.1, the information bit blocks

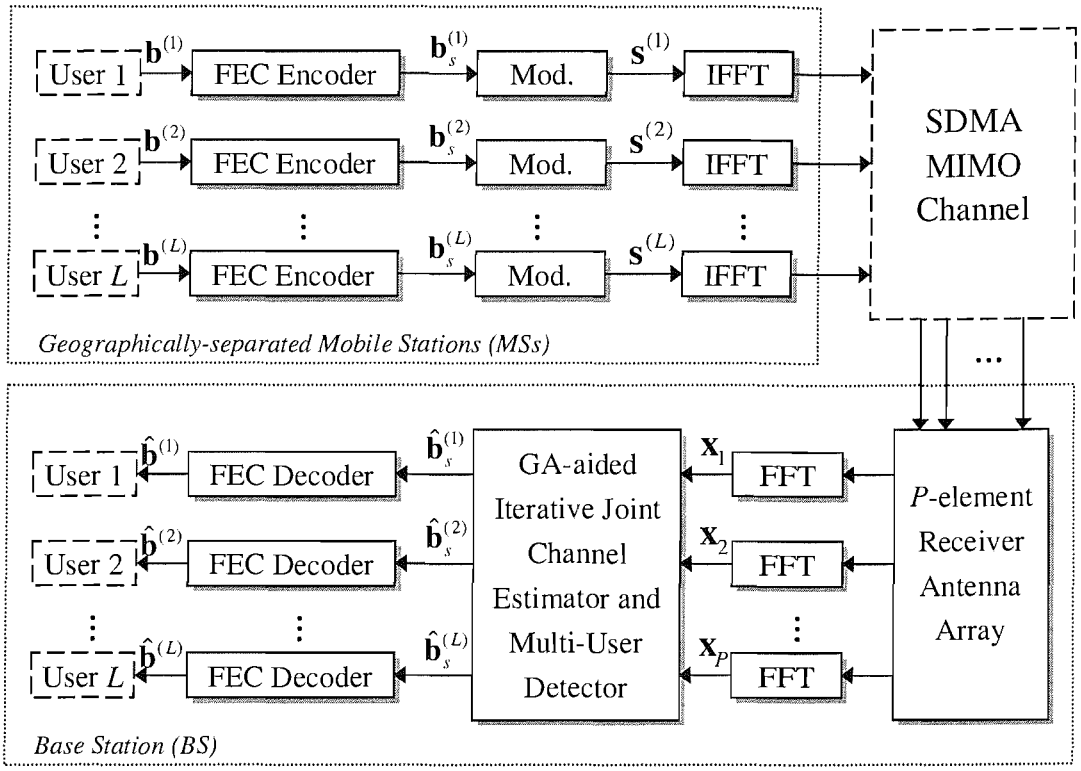

Figure 6.1: Schematic of the SDMA-OFDM uplink system employing the proposed GA-aided iterative joint channel estimator and multi-user detector.

$\mathbf{b}^{(l)}$ $(l = 1, \cdots, L)$ of the L number of mobile users are first encoded by the L independent FEC encoders. The resultant coded bits $\mathbf{b}_s^{(l)}$ are then mapped to Quadrature Amplitude Modulation (QAM) or Phase-Shift Keying (PSK) symbols $\mathbf{s}^{(l)}$, which are modulated by the Inverse Fast Fourier Transform (IFFT) based OFDM modulators and transmitted over the SDMA MIMO channel described in Section 3.2.1.

At the BS illustrated at the lower half of Figure 6.1, the received signal constituted by the noise-contaminated superposition of all users' transmitted signals is OFDM-demodulated at the P number of receiver antenna elements and forwarded to the iterative GA-JCEMUD for joint channel estimation and symbol detection, as it will be detailed in Section 6.3. Then the detected soft bits $\hat{\mathbf{b}}_s^{(l)}$ are generated, which are forwarded to the L independent FEC decoders for channel decoding.

6.3 GA-assisted Iterative Joint Channel Estimation and MUD

In this section, we will elaborate on the philosophy of the proposed iterative GA-JCEMUD, which is illustrated in Figure 6.2. We assume that each OFDM symbol consists of K subcarriers. All subcarriers of the first transmitted OFDM symbol of all the L users carry known

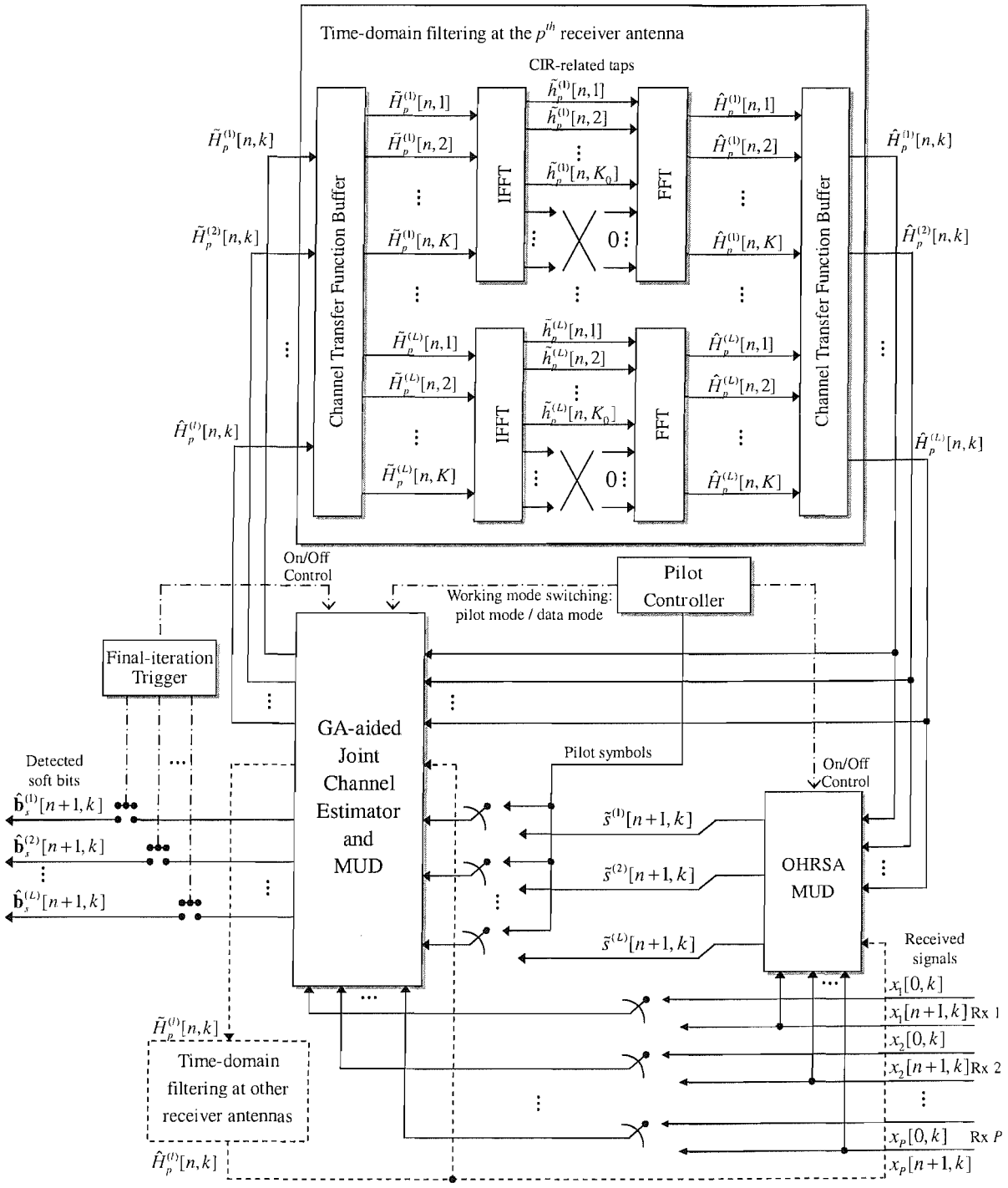

Figure 6.2: Structure of the proposed GA-aided iterative joint channel estimator and multi-user detector.

pilot QAM symbols, which are spread by user-specific spreading codes before transmission[1]. Within the first OFDM symbol duration ($n = 0$), the BS pilot controller seen in the middle of Figure 6.2 feeds the pilots to the GA-JCEMUD printed in grey, which simultaneously processes the received signals $x_p[0,k]$ ($p = 1, \cdots, P$; $k = 1, \cdots, K$) at the P receiver antenna elements. In order to simplify the analysis, we now focus our attention on the p^{th} receiver. Based on the pilots and the corresponding received signals, the initial estimates of the FD-CHTFs $\tilde{H}_p^{(l)}[0,k]$ ($l = 1, \cdots, L$; $k = 1, \cdots, K$) can be generated, which will be subjected to time-domain filtering invoked at the p^{th} receiver, as plotted at the top of Figure 6.2.

The time-domain filtering is invoked for each of the L users on an OFDM symbol basis. More specifically, for the l^{th} user, the K initial FD-CHTF estimates $\tilde{H}_p^{(l)}[n,k]$ ($k = 1, \cdots, K$) associated with the current, i.e. the n^{th} OFDM symbol are processed by a K-length IFFT, resulting in the set of K uncorrelated CIR-related taps $\tilde{h}_p^{(l)}[n,k]$. Then, only the first K_0 CIR tap coefficients are retained with the rest set to zero. The value of K_0 depends on the delay profile of the channel, which is not known *a priori* at the receiver. However, in many application scenarios it is possible to appropriately over-estimate K_0 on the basis of previous field experiments [227]. Generally speaking, the value of K_0 should be set to a sufficiently large number so that it exceeds the actual maximum delay spread of the channel. The reason for doing so is to ensure that the 'real' CIR taps are retained, while removing a significant part of the noise contaminating the high-delay, low-power CIR taps, and hence improving the initial CHTF estimates generated by the GA-JCEMUD. To elaborate a little further, on one hand, the output of the GA-JCEMUD may be noisy, owing to low SNRs and/or a high number of users as well as receiver antennas (i.e. more channel links to estimate, rendering the estimation job more difficult). On the other hand, in practical applications the value of K is usually chosen to be significantly higher than the number of CIR taps corresponding to the channel's maximum delay spread. Furthermore, most of the channel's output power is contributed by the first several CIR taps. In other words, provided that K_0 is higher than the maximum channel delay spread, the last $(K - K_0)$ CIR taps from the set of the total K time-domain CIR taps generated by the IFFT from the CHTF estimates contain nothing but noise. Therefore, when the last $(K - K_0)$ CIR taps are set to zero, most of the noise contaminating the channel estimates can be removed without failing to capture the channel's 'real' CIR taps. Based on the above analysis, we point out that a good choice of K_0 is constituted by the number of samples in the OFDM cyclic prefix. Additionally, the 'significant-tap catching' approaches of [131, 378] can be employed for improving the channel estimator's performance by further removing the low-power taps - those that are likely to be constituted by noise, rather than by 'real' CIR taps - within the range of $[1, \cdots, K_0]$ according to a pre-defined amplitude threshold. Following the CIR tap filtering process discussed above, the retained

[1] More details of the process will be discussed in Section 6.3.1.

CIR-related coefficients $\tilde{h}_p^{(l)}[n,k]$ $(k = 1, \cdots, K_0)$ are converted to the improved *a posteriori* FD-CHTF estimates $\hat{H}_p^{(l)}[n,k]$ $(k = 1, \cdots, K)$ by the Fast Fourier Transform (FFT). For more detailed discussions on these processes we refer to Chapters 15 and 16 of [3].

If in the $(n+1)^{th}$ OFDM symbol duration a data symbol rather than a pilot symbol was transmitted, the pilot controller will carry out the following actions:

- Enables a first-stage MUD for generating reference symbol estimates, and
- Switches the operating mode of the GA-JCEMUD from *pilot-aided channel estimation* mode to *joint channel estimation and data detection* mode.

More specifically, the Optimized Hierarchy Reduced Search Algorithm (OHRSA) aided MUD of [392–394] is employed as the first-stage MUD, as shown in Figure 6.2. It exploits the *a posteriori* FD-CHTF estimates $\hat{H}_p^{(l)}[n,k]$ associated with the previous OFDM symbol to invoke subcarrier-by-subcarrier based detection, yielding an initial guess of the L users' transmitted symbols $s^{(l)}[n+1,k]$ $(l = 1, \cdots, L;\ k = 1, \cdots, K)$. The resultant symbol estimates $\tilde{s}^{(l)}[n+1,k]$, the FD-CHTF estimates $\hat{H}_p^{(l)}[n,k]$ as well as the corresponding received signals $x_p[n+1,k]$ $(p = 1, \cdots, P;\ k = 1, \cdots, K)$ are then forwarded to the GA-JCEMUD, where the FD-CHTFs and data symbols associated with the $(n+1)^{th}$ OFDM symbol are jointly optimized on a subcarrier-by-subcarrier basis. The GA-optimized FD-CHTF estimates $\tilde{H}_p^{(l)}[n+1,k]$ are then forwarded to the time-domain filters for further enhancement, as mentioned earlier in this section. Now the cleansed *a posteriori* channel estimates $\hat{H}_p^{(l)}[n+1,k]$ are expected to be closer to their true values of $H_p^{(l)}[n+1,k]$ than the initially used estimates, i.e. $\hat{H}_p^{(l)}[n,k]$, which are associated with the previous OFDM symbol. Thus, based on the improved channel estimates, the OHRSA MUD is capable of providing a better initial guess of the transmitted symbols for the GA-JCEMUD. This decision-directed process can be invoked for a number of iterations for attaining a further performance enhancement. After the final iteration, the final-iteration trigger portrayed at the left-hand side of Figure 6.2 terminates the GA-JCEMUD's operation and enables the output links, generating the L users' detected soft bits $\hat{b}_s^{(l)}[n+1,k]$ $(l = 1, \cdots, L;\ k = 1, \cdots, K)$ corresponding to the $(n+1)^{th}$ OFDM symbol.

In the following sections, we will further detail the processes of obtaining initial FD-CHTF estimates with the aid of pilots, generating initial symbol estimates by the OHRSA MUD as well as jointly optimizing the FD-CHTFs and the data symbols using the GA, respectively.

6.3.1 Pilot-aided Initial Channel Estimation

In order to obtain an initial estimate of the FD-CHTFs, each user's pilot OFDM symbol is multiplied by a user-specific spreading code before it is transmitted[2]. With the aid of the spread pilot OFDM symbols, an initial FD-CHTF estimate is attainable at the receivers, where the Multi-User Interference (MUI) is effectively reduced proportionately to the spreading factor.

More specifically, the orthogonal Walsh-Hadamard Transform (WHT) [3] based codes of length L are chosen. The received symbol at the p^{th} receiver antenna element associated with the k^{th} subcarrier of the $n = 0^{th}$ OFDM symbol duration can be formulated as:

$$x_p[0,k] = \mathbf{c}\bar{\mathbf{H}}_p[0,k]\mathbf{s}[0,k] + n_p[0,k], \quad p = 1, \cdots, P, \tag{6.1}$$

where the pilot signal vector $\mathbf{s}[0,k]$ and the diagonal FD-CHTF matrix $\bar{\mathbf{H}}_p[0,k]$ are given by:

$$\mathbf{s}[0,k] = \left[s^{(1)}[0,k],\ s^{(2)}[0,k],\ \cdots,\ s^{(L)}[0,k] \right]^T, \tag{6.2}$$

$$\bar{\mathbf{H}}_p[0,k] = \mathrm{diag}\left[H_p^{(1)}[0,k],\ H_p^{(2)}[0,k],\ \cdots,\ H_p^{(L)}[0,k] \right], \tag{6.3}$$

respectively, and the user signature vector $\mathbf{c}$ is formulated as:

$$\mathbf{c} = \left[\mathbf{c}^{(1)},\ \mathbf{c}^{(2)},\ \cdots,\ \mathbf{c}^{(L)} \right], \tag{6.4}$$

where $\mathbf{c}^{(l)}$ $(l = 1, \cdots, L)$ represents the l^{th} user's WHT code sequence, which is the l^{th} row of the L-order recursive WHT matrix given by [3]:

$$\mathbf{U}_{\mathrm{WHT}_L} = \frac{1}{\sqrt{2}} \begin{bmatrix} 1 \cdot \mathbf{U}_{\mathrm{WHT}_{L/2}} & 1 \cdot \mathbf{U}_{\mathrm{WHT}_{L/2}} \\ 1 \cdot \mathbf{U}_{\mathrm{WHT}_{L/2}} & -1 \cdot \mathbf{U}_{\mathrm{WHT}_{L/2}} \end{bmatrix}, \tag{6.5}$$

while the lowest-order WHT unitary matrix is defined as:

$$\mathbf{U}_{\mathrm{WHT}_2} = \frac{1}{\sqrt{2}} \begin{bmatrix} 1 & 1 \\ 1 & -1 \end{bmatrix}. \tag{6.6}$$

Note that the pilot symbol vector $\mathbf{s}[0,k]$ of Equation (6.1) is known at the receivers. Furthermore, we can use the same unspread pilot QAM symbol for all users, i.e. $s^{(l)}[0,k] = s_0$ $(l = 1, \cdots, L)$. Hence, it directly follows from Equation (6.1) that:

$$\begin{aligned} \check{x}_p[0,k] &= \frac{s_0^*}{|s_0|^2} x_p[0,k] \\ &= \mathbf{c}\mathbf{H}_p^T[0,k] + \frac{s_0^*}{|s_0|^2} n_p[0,k], \quad p = 1, \cdots, P, \end{aligned} \tag{6.7}$$

[2]Note that no spreading is applied to the data OFDM symbols.

where $(\cdot)^*$ denotes complex conjugate and $\mathbf{H}_p[0,k]$ is the p^{th} row of the FD-CHTF matrix $\mathbf{H}$, given by:

$$\mathbf{H}_p[0,k] = \left[H_p^{(1)}[0,k],\ H_p^{(2)}[0,k],\ \cdots,\ H_p^{(L)}[0,k] \right]. \tag{6.8}$$

Thus, the initial FD-CHTF estimates can be obtained as follows:

$$\begin{aligned} \tilde{\mathbf{H}}_p^T[0,k] &= \mathbf{c}^T \check{x}_p[0,k] \\ &= \mathbf{H}_p^T[0,k] + \underbrace{\frac{s_0^*}{|s_0|^2} n_p[0,k]\mathbf{c}^T}_{n'_p[0,k]}, \quad p = 1, \cdots, P. \end{aligned} \tag{6.9}$$

After the time-domain CIR tap filtering operation shown in Figure 6.2, the refined channel estimates can then be used to assist the OHRSA MUD for detecting the unknown transmitted symbols within the next OFDM symbol duration. Afterwards, the GA-JCEMUD will be set to joint channel estimation and data detection mode, providing the FD-CHTF estimates associated with the forthcoming OFDM symbols.

Depending on the specific performance-versus-throughput design tradeoff targeted, this process of generating initial channel estimates can be invoked at pre-defined time intervals. Here we denote the pilot overhead as ϵ, which is defined by the ratio of the number of pilot OFDM symbols to the total number of transmitted OFDM symbols. We will show in Section 6.4 that a good performance is achievable by the proposed scheme with a small value of ϵ.

6.3.2 Generating Initial Symbol Estimates

As mentioned earlier, for each subcarrier, an initial symbol estimate is first obtained with the aid of the first-stage Optimized Hierarchy Reduced Search Algorithm (OHRSA) assisted MUD [392–394] shown in Figure 6.2, which exploits the *a postepriori* FD-CHTF estimates generated within the previous OFDM symbol duration. For the sake of notational convenience, in this section the index of $[n,k]$ is omitted. However, we note that the following analysis is conducted on a subcarrier basis.

As an extension of the Complex Sphere Decoder (CSD) method [314, 316], the OHRSA MUD is capable of achieving a near-optimum performance at a significantly reduced computational complexity. It is well known that the optimum ML MUD [3] employs an exhaustive search for finding the most likely transmitted signals. More explicitly, recall that the L-user symbol vector estimate $\hat{\mathbf{s}}_{\text{ML}}$ can be obtained by minimizing the following metric:

$$\hat{\mathbf{s}}_{\text{ML}} = \arg \left\{ \min_{\check{\mathbf{s}} \in \mathcal{M}^L} ||\mathbf{x} - \mathbf{H}\check{\mathbf{s}}||^2 \right\}, \tag{6.10}$$

where $\check{\mathbf{s}}$ is an *a priori* candidate vector of the set $\mathcal{M}^L$, which is constituted by 2^{mL} number of trial vectors, where m denotes the number of Bits Per Symbol (BPS). More specifically, $\mathcal{M}^L$ is formulated as:

$$\mathcal{M}^L = \left\{ \check{\mathbf{s}} = \left[\check{s}^{(1)}, \check{s}^{(2)}, \cdots, \check{s}^{(L)} \right]^T \middle| \check{s}^{(1)}, \check{s}^{(2)}, \cdots, \check{s}^{(L)} \in \mathcal{M}_c \right\}, \tag{6.11}$$

where $\mathcal{M}_c$ denotes the set containing the 2^m number of legitimate complex constellation points associated with the specific modulation scheme employed. Furthermore, it can be shown that Equation (6.10) is equivalent to [392–394]:

$$\hat{\mathbf{s}} = \arg \left\{ \min_{\check{\mathbf{s}} \in \mathcal{M}^L} ||\mathbf{V}(\check{\mathbf{s}} - \hat{\mathbf{s}}_{\text{MMSE}})||^2 \right\}, \tag{6.12}$$

where $\mathbf{V}$ is an upper-triangular matrix having positive real-valued elements on the main diagonal and satisfying

$$\mathbf{V}^H\mathbf{V} = \mathbf{H}^H\mathbf{H} + \sigma_n^2\mathbf{I}, \tag{6.13}$$

while

$$\hat{\mathbf{s}}_{\text{MMSE}} = (\mathbf{H}^H\mathbf{H} + \sigma_n^2\mathbf{I})^{-1}\mathbf{H}^H\mathbf{x} \tag{6.14}$$

is the unconstrained MMSE-based estimate[3] of the transmitted signal vector $\mathbf{s}$, with $\mathbf{I}$ and σ_n^2 are the identity matrix and the AWGN noise variance, respectively. Since $\mathbf{V}$ is an upper-triangular matrix, a specific cost function can be derived:

$$\begin{aligned} \Phi(\check{\mathbf{s}}) &= ||\mathbf{V}(\check{\mathbf{s}} - \hat{\mathbf{s}}_{\text{MMSE}})||^2 \\ &= (\check{\mathbf{s}} - \hat{\mathbf{s}}_{\text{MMSE}})^H\mathbf{V}^H\mathbf{V}(\check{\mathbf{s}} - \hat{\mathbf{s}}_{\text{MMSE}}) \\ &= \sum_{i=1}^{L} \left| \sum_{j=i}^{L} v_{ij}(\check{s}^{(j)} - \hat{s}^{(j)}_{\text{MMSE}}) \right|^2 \\ &= \sum_{i=1}^{L} \phi_i(\check{\mathbf{s}}_i), \end{aligned} \tag{6.15}$$

where $\phi(\check{\mathbf{s}}_i)$ is a set of sub-cost functions. Note that the outputs of both $\Phi(\check{\mathbf{s}})$ and $\phi(\check{\mathbf{s}}_i)$ are real-valued. Furthermore, we have:

$$\begin{aligned} \phi_i(\check{\mathbf{s}}_i) &= \left| \sum_{j=i}^{L} v_{ij}(\check{s}^{(j)} - \hat{s}^{(j)}_{\text{MMSE}}) \right|^2 \\ &= \left| v_{ii}(\check{s}^{(i)} - \hat{s}^{(i)}_{\text{MMSE}}) + \sum_{j=i+1}^{L} v_{ij}(\check{s}^{(j)} - \hat{s}^{(j)}_{\text{MMSE}}) \right|^2. \end{aligned} \tag{6.16}$$

[3]The unconstrained MMSE-based estimate denotes the resultant complex value calculated from Equation (6.14), as opposed to the constrained estimate, which is the hard-decoded version of the unconstrained estimate.

Based on Equation (6.16), $\Phi(\check{\mathbf{s}})$ can be re-defined as the Cumulative Sub-Cost (CSC) function:

$$\Phi_L(\check{\mathbf{s}}_L) = \phi_L(\check{\mathbf{s}}_L) = \left| v_{LL}(\check{s}^{(L)} - \hat{s}^{(L)}_{\text{MMSE}}) \right|^2, \quad i = L; \tag{6.17a}$$

$$\Phi_i(\check{\mathbf{s}}_i) = \Phi_{i+1}(\check{\mathbf{s}}_{i+1}) + \phi_i(\check{\mathbf{s}}_i), \quad i = L-1, \cdots, 1, \tag{6.17b}$$

where $\check{\mathbf{s}}_i$ represents the sub-vectors of $\check{\mathbf{s}}$, formulated as:

$$\check{\mathbf{s}}_i = \left[\check{s}^{(i)}, \ \check{s}^{(i+1)}, \ \cdots, \ \check{s}^{(L)} \right], \quad i \in \{1, \cdots, L\}. \tag{6.18}$$

In physically tangible terms, the Euclidean norm of Equation (6.17) can be interpreted as a weighted Euclidean distance between the candidate constellation point $\check{s}^{(l)}$ and the unconstrained MMSE estimate $\hat{s}^{(l)}_{\text{MMSE}}$ of the transmitted signal component $s^{(l)}$. Explicitly, the CSC functions obey the property:

$$\Phi(\check{\mathbf{s}}) = \Phi_1(\check{\mathbf{s}}_1) > \Phi_2(\check{\mathbf{s}}_2) > \cdots > \Phi_L(\check{\mathbf{s}}_L) > 0 \tag{6.19}$$

for all possible combinations of $\check{\mathbf{s}} \in \mathcal{M}^L$ and $\hat{\mathbf{s}}_{\text{MMSE}} \in \mathbb{C}^{L\times 1}$, where the L-dimensional complex space $\mathbb{C}^{L\times 1}$ contains all possible unconstrained MMSE estimates $\hat{\mathbf{s}}_{\text{MMSE}}$ of the transmitted signal vector $\mathbf{s}$.

Exploiting the monotonously increasing nature of the non-binary, i.e. multi-bit symbol based CSC functions of Equation (6.19), a bit-based recursive search algorithm can be developed [392–394], where the $(L_b = mL)$-dimensional bit vectors $\check{\mathbf{b}}$ constituting the L users' bits, rather than the symbol vectors $\check{\mathbf{s}}$ are used as the candidates for the CSC functions given by Equations (6.15) and (6.17). More specifically, two legitimate hypotheses of -1 and 1 are stipulated at each recursive step i of the search algorithm, concerning one of the bits of the bit-based trial vector $\check{\mathbf{b}}_i$. This allows us now to physically interpret the CSC functions as the Euclidian distance contribution of the specific $\check{\mathbf{b}}_i$, when considering a specific bit of a given symbol of a given user. The recursive search process commences with the evaluation of the CSC function of Equation (6.17a), followed by the calculation of the conditioned CSC function values of Equation (6.17b). Moreover, for each tentatively assumed value of $\check{\mathbf{b}}_i$ a successive recursive search step $(i-1)$ is invoked, which is conditioned on the hypotheses made in all preceding recursive steps $j = i, \cdots, L_b = mL$. Upon each arrival at the index $i = 1$ of the recursive process, a complete bit-based candidate vector $\check{\mathbf{b}}$ associated with a certain symbol vector $\check{\mathbf{s}}$ is hypothesized and the corresponding value of the cost function $\Phi(\check{\mathbf{b}})$ formulated in Equation (6.15) is evaluated. Furthermore, with the aid of a carefully-designed search strategy [392–394], the OHRSA is capable of arriving at the optimum ML estimate at a significantly reduced complexity. For more details on the OHRSA MUD, the interested reader is referred to [392–394].

6.3.3 GA-aided Joint Optimization Providing Soft Outputs

With the aid of the initial FD-CHTF estimates of Section 6.3.1 and the initial symbol estimates of Section 6.3.2, the proposed GA-JCEMUD printed in the grey block of Figure 6.2 is employed for jointly optimizing the estimates of the FD-CHTFs and multi-user data symbols.

6.3.3.1 Extended GA Individual Structure

In comparison to the pure GA-based MUDs [326, 327, 390], which optimize the multi-user data symbols only, the joint optimization work requires the FD-CHTFs to be simultaneously optimized along with the data symbols, as in [45, 328]. Furthermore, concerning the MIMO channel's structure, the GA *individuals*' representation of [45, 328] is extended to:

$$\begin{cases} \tilde{\mathbf{s}}_{(y,x)}[n,k] &= \left[\, \tilde{s}^{(1)}_{(y,x)}[n,k],\ \tilde{s}^{(2)}_{(y,x)}[n,k],\ \cdots,\ \tilde{s}^{(L)}_{(y,x)}[n,k] \,\right] \\ \tilde{\mathbf{H}}_{(y,x)}[n,k] &= \begin{bmatrix} \tilde{H}^{(1)}_{1,(y,x)}[n,k] & \tilde{H}^{(2)}_{1,(y,x)}[n,k] & \cdots & \tilde{H}^{(L)}_{1,(y,x)}[n,k] \\ \tilde{H}^{(1)}_{2,(y,x)}[n,k] & \tilde{H}^{(2)}_{2,(y,x)}[n,k] & \cdots & \tilde{H}^{(L)}_{2,(y,x)}[n,k] \\ \vdots & \vdots & \ddots & \vdots \\ \tilde{H}^{(1)}_{P,(y,x)}[n,k] & \tilde{H}^{(2)}_{P,(y,x)}[n,k] & \cdots & \tilde{H}^{(L)}_{P,(y,x)}[n,k] \end{bmatrix} \end{cases} \tag{6.20}$$

in the context of the k^{th} subcarrier of the n^{th} OFDM symbol, where the subscript (y,x) denotes the x^{th} $(x = 1, \cdots, X)$ individual at the y^{th} $(y = 1, \cdots, Y)$ *generation*. In compliance with classic GA terminology, any combination of a symbol vector $\tilde{\mathbf{s}}_{(y,x)}[n,k]$ and a FD-CHTF matrix $\tilde{\mathbf{H}}_{(y,x)}[n,k]$ represents a GA individual, where $\tilde{\mathbf{s}}_{(y,x)}[n,k]$ is referred to as the individual's *symbol chromosome* and $\tilde{\mathbf{H}}_{(y,x)}[n,k]$ as the associated *FD-CHTF chromosome*, respectively, while each element of a chromosome is termed as a *gene*. Note that the symbol genes and the channel genes belong to different sets. More specifically, we have $\tilde{s}^{(l)}_{(y,x)}[n,k] \in \mathcal{M}_c$ and $\tilde{H}^{(l)}_{p,(y,x)}[n,k] \in \mathbb{C}$, where $\mathbb{C}$ denotes the set of all complex numbers. This particular association of a pair of hypothesized channel and data estimates is reminiscent of the so-called Per-Survivor Processing (PSP) based blind detection techniques of [395, 396], however it distinguished itself by invoking a genetically guided efficient search strategy.

6.3.3.2 Initialization

During the stage of initialization, the GA generates a *population* of X individuals represented by Equation (6.20), based on the initial FD-CHTF estimates of Section 6.3.1 and the initial symbol estimates of Section 6.3.2. More explicitly, at the k^{th} subcarrier in the $(n+1)^{th}$ OFDM symbol duration, the genes of the $(y,x) = (1,1)^{st}$ individual are generated as:

$$\begin{cases} \tilde{s}^{(l)}_{(1,1)}[n+1,k] &= \tilde{s}^{(l)}[n+1,k] \\ \tilde{H}^{(l)}_{p,(1,1)}[n+1,k] &= \tilde{H}^{(l)}_{p}[n,k] \end{cases}, \quad l = 1, \cdots, L;\ p = 1, \cdots, P, \tag{6.21}$$

where $\tilde{s}^{(l)}[n+1,k]$ represents the initial symbol estimates provided by the OHRSA MUD, while $\tilde{H}_p^{(l)}[n,k]$ denotes the initial FD-CHTF estimates associated with the previous, i.e. the n^{th} OFDM symbol. The other $(X-1)$ individuals are then created by the GA's *mutation* operator:

$$\begin{cases} \tilde{s}^{(l)}_{(y,x)}[n+1,k] &= MUTATION\left(\tilde{s}^{(l)}_{(1,1)}[n+1,k]\right) \\ \tilde{H}^{(l)}_{p,(y,x)}[n+1,k] &= MUTATION\left(\tilde{H}^{(l)}_{p,(1,1)}[n+1,k]\right) \end{cases}, \\ x=2,\cdots,X;\ y=1,\cdots,Y;\ l=1,\cdots,L;\ p=1,\cdots,P. \tag{6.22}$$

The details of the mutation process are discussed in Section 6.3.3.3.2. After the creation of the $y=1^{st}$ generation, which consists of the population of the initially generated X individuals, the GA-based search process can be invoked for jointly optimizing the estimates of the multi-user symbols and FD-CHTFs.

6.3.3.3 Joint Genetic Optimization

The basic idea of the GA-based optimization is to find the optimum or a near-optimum solution according to a pre-defined *objective function (OF)*. In the context of the joint detection problem in SDMA-OFDM systems, the GA's OF can be based on the ML metric of Equation (6.10), formulated as:

$$\Omega\left(\tilde{\mathbf{H}}[n,k],\ \tilde{\mathbf{s}}[n,k]\right) = \left|\left|\ \mathbf{x}[n,k] - \tilde{\mathbf{H}}[n,k]\cdot\tilde{\mathbf{s}}[n,k]\ \right|\right|^2, \tag{6.23}$$

where each combination of the trial data vector $\tilde{\mathbf{s}}[n,k]$ and trial FD-CHTF matrix $\tilde{\mathbf{H}}[n,k]$ constitutes a GA individual defined in Equation (6.20). The output of the OF is referred to as the *Objective Score (OS)*, and the individual having a lower OS is considered to have a higher *fitness* value. Explicitly, the GA's ultimate aim is to find the individual that has the highest fitness value. This is achieved with the aid of the genetic operators invoked during the evolution process, such as *cross-over* and *mutation* [45, 319], where specific genes of the different individuals are exchanged and mutated to produce the corresponding *offspring*. The X number of resultant offspring individuals then constitute a new population, which forms the GA's next generation and is expected to have a statistically improved average fitness value in comparison to the parent population. Finally, the GA terminates, when the generation index reaches a pre-defined value Y. Conventionally, the highest-fitness individual of the final population will be considered as the GA's final solution, which consists of the genetically-improved FD-CHTF and data symbol estimates. For more details about the genetic optimization process we refer to Appendix A.1 and references [45, 326–328, 390].

Recall that the elements of the symbol chromosome $\tilde{\mathbf{s}}[n,k]$ of an individual belong to $\mathcal{M}_c$, i.e. to the legitimate constellation symbol set. Thus, the symbol mutation space is

discrete and is limited by the 2^m number of constellation points in $\mathcal{M}_c$. By contrast, the mutation space of the FD-CHTFs is continuous and infinite, simply because the value of a FD-CHTF sample can be an arbitrary value on the complex plane $\mathbb{C}$. Therefore, different cross-over/mutation operators have to be employed for the symbol chromosome and channel chromosome, respectively.

6.3.3.3.1 Cross-over Operator

In our system, the uniform cross-over [45] is used for mutating the symbol chromosomes. This cross-over operator exchanges specific symbol genes of two parent individuals in order to generate the offspring. Theoretically, it may also be applied to the FD-CHTF mutation process, where the channel chromosomes of parent individuals are swapped. However, this "exchange-only" mechanism neglects the continuous nature of the complex-valued FD-CHTFs, thus imposing a limitation during the cross-over process, when the genetic information is delivered from parents to offspring.

For the sake of improving the cross-over efficiency, the blend cross-over [397, 398] is invoked for combining the channel chromosomes from each of the two parent individuals into new channel chromosomes of the two offspring. More specifically, the offspring's channel chromosomes can be formulated as:

$$\begin{cases} \tilde{H}^{(l)}_{p,(y+1,1)}[n,k] &= \beta_1 \tilde{H}^{(l)}_{p,(y,1)}[n,k] + \beta_2 \tilde{H}^{(l)}_{p,(y,2)}[n,k] \\ \tilde{H}^{(l)}_{p,(y+1,2)}[n,k] &= \beta_2 \tilde{H}^{(l)}_{p,(y,1)}[n,k] + \beta_1 \tilde{H}^{(l)}_{p,(y,2)}[n,k] \end{cases}, \quad y = 1, \cdots, Y, \tag{6.24}$$

where the random weight factors $\beta_i \in [0,\ 1]$ $(i = 1, 2)$ satisfy:

$$\beta_1 + \beta_2 = 1. \tag{6.25}$$

Similar to the uniform cross-over operator invoked for symbol chromosomes, in the blend cross-over operator a random binary cross-over mask is also created for identifying the specific channel genes to be combined. Observing Equation (6.24), we note that the genes of the new channel chromosomes are actually the linearly biased or weighted results averaged between the two parents in the context of the $(P \times L)$-dimensional complex space. When we have $\beta_1 = \beta_2 = 0.5$, the result becomes an unbiased average of the channel chromosomes of the two parents. Explicitly, the blend cross-over operator exploits the continuous and infinite nature of the FD-CHTFs and hence it is capable of amalgamating the parental genetic information in a more meritorious manner.

6.3.3.3.2 Mutation Operator

Similar to the cross-over operator, the mutation operator also requires the employment of different methods for the symbol and channel chromosomes, respectively. The mutation schemes based on discrete character sets, for example the classic Uniform Mutation (UM) [45], can be applied to the symbol chromosomes. On the other hand, the approach of [328], which is referred to here as Step Mutation (SM), can be employed for mutating the channel chromosomes. To elaborate a little further, the offspring's channel chromosomes can be generated by:

$$\begin{cases} \Re\left(\tilde{H}^{(l)}_{p,(y+1,x)}[n,k]\right) = \Re\left(\tilde{H}^{(l)}_{p,(y,x)}[n,k]\right) + \theta_{\Re}\Delta^{(l)}_{p,(y,x)}[n,k] \\ \Im\left(\tilde{H}^{(l)}_{p,(y+1,x)}[n,k]\right) = \Im\left(\tilde{H}^{(l)}_{p,(y,x)}[n,k]\right) + \theta_{\Im}\Delta^{(l)}_{p,(y,x)}[n,k] \end{cases}, \\ x = 1,\cdots,X;\ y = 1,\cdots,Y;\ l = 1,\cdots,L;\ p = 1,\cdots,P, \tag{6.26}$$

where $\Delta^{(l)}_{p,(y,x)}[n,k]$ is a random number within $(0,\ \lambda_{max}]$, while $\Re$ and $\Im$ respectively, denote the real and imaginary components of the specific channel gene $\tilde{H}^{(l)}_{p,(y+1,x)}[n,k]$ to be mutated. The sign factors $\theta_{\Re}$ and $\theta_{\Im}$ of Equation (6.26) are uniformly and randomly generated, assuming values of $+1$ or -1.

We point out that the value of the maximum mutation step size λ_{max} is critical for the system's attainable performance, since it directly affects the convergence of the GA's optimization process. A low system performance will be expected, when λ_{max} is insufficiently high, where the GA may get trapped in local rather than global minima. However, an excessively high value of λ_{max} will result in a slow convergence rate. Generally speaking, the value of λ_{max} should be adjusted according to the Doppler frequency encountered. More specifically, when we have a higher Doppler frequency, the consecutive channel fades in the time domain experienced by each of the subcarriers become faster, thus requiring a higher λ_{max} value for assisting the GA in capturing the rapid changes of the channel fades. In low-Doppler scenarios, the situation is inverse. Therefore, it is desirable that the value of λ_{max} is adjusted as a function of the Doppler frequency. However, in this case it is a challenging task to develop a close-form function for quantifying the effects of the Doppler frequency, owing to the inherently nonlinear nature of the GA-based optimization process. Nonetheless, with the aid of computer simulations we can identify the appropriate values of λ_{max} for different Doppler frequencies, as it will be discussed in Section 6.4.1.

6.3.3.3.3 Comments on the Joint Optimization Process

Note that since the FD-CHTFs and data symbols are jointly optimized within the same genetic process, the individuals having better FD-CHTF estimates will have a higher probability of producing better symbol estimates and vice versa. Thus, this joint optimization

is a "self-adaptive" process with its native intuition leading towards the optimum solution. Furthermore, comparing to other techniques, for example that of [387], where the channel estimation and symbol detection are completed by the GA and the VA separately, the proposed joint scheme is capable of reducing the associated complexity, since the channel estimation is simultaneously achieved with the aid of the same GA process, thus incurring no additional complexity.

Moreover, it is worth pointing out that at the time of writing the GA-aided detection schemes found in the literature [45,326–328,390] are only capable of providing single-individual based hard-decoded symbol estimates, which inevitably limits the GA-aided system's attainable performance. In Section 6.3.3.4, we will introduce a method, which enables the GA to provide soft outputs based on the entire population.

6.3.3.4 Generating the GA's Soft Outputs

In this section we derive an algorithm that enables the GA to output soft information. For the sake of simplicity, again, we omit the index $[n, k]$ in this section.

The soft-bit value or Log-Likelihood Ratio (LLR) associated with the $(m_B)^{th}$ bit position of the l^{th} $(l = 1, \cdots, L)$ user's transmitted symbol $s^{(l)}$ can be formulated as [399]:

$$\mathcal{L}_{l,m_B} = \ln \frac{P(b_{l,m_B} = 1|\mathbf{x}, \mathbf{H})}{P(b_{l,m_B} = 0|\mathbf{x}, \mathbf{H})}, \tag{6.27}$$

which is the natural logarithm of the quotient of probabilities that the bit considered has a value of $b_{l,m_B} = 1$ or $b_{l,m_B} = 0$. Note that the probability $P(b_{l,m_B} = b|\mathbf{x}, \mathbf{H})$ that the symbol transmitted by the l^{th} user has the $(m_B)^{th}$ bit value of $b_{l,m_B} = b \in \{0, 1\}$, is given by the sum of all the probabilities of the symbol combinations which assume that $b_{l,m_B} = b$. Hence, Equation (6.27) can be equivalently rewritten as:

$$\mathcal{L}_{l,m_B} = \ln \frac{\sum_{\check{\mathbf{s}} \in \mathcal{M}^L_{l,m_B,1}} P(\check{\mathbf{s}}|\mathbf{x}, \mathbf{H})}{\sum_{\check{\mathbf{s}} \in \mathcal{M}^L_{l,m_B,0}} P(\check{\mathbf{s}}|\mathbf{x}, \mathbf{H})}, \tag{6.28}$$

where $\mathcal{M}^L_{l,m_B,b}$ denotes the specific subset associated with the l^{th} user, which is constituted by those specific trial vectors, whose l^{th} element's $(m_B)^{th}$ bit has a value of b, which is expressed as:

$$\mathcal{M}^L_{l,m_B,b} = \left\{ \check{\mathbf{s}} = \left[\check{s}^{(1)}, \check{s}^{(2)}, \cdots, \check{s}^{(L)} \right]^T \middle| \{ \check{s}^{(1)}, \check{s}^{(2)}, \cdots, \check{s}^{(L)} \in \mathcal{M}_c \} \wedge \{ b_{l,m_B} = b \} \right\}. \tag{6.29}$$

With the aid of Bayes' theorem [399], we have:

$$P(\check{\mathbf{s}}|\mathbf{x}, \mathbf{H}) = P(\mathbf{x}|\check{\mathbf{s}}, \mathbf{H}) \frac{P(\check{\mathbf{s}})}{P(\mathbf{x})}. \tag{6.30}$$

Upon substituting Equation (6.30) into Equation (6.28), we arrive at:

$$\mathcal{L}_{l,m_B} = \ln \frac{\sum_{\check{\mathbf{s}} \in \mathcal{M}^L_{l,m_B,1}} P(\mathbf{x}|\check{\mathbf{s}}, \mathbf{H})}{\sum_{\check{\mathbf{s}} \in \mathcal{M}^L_{l,m_B,0}} P(\mathbf{x}|\check{\mathbf{s}}, \mathbf{H})}. \tag{6.31}$$

Note that here we have assumed that the different (2^m)-ary symbol combination vectors $\check{\mathbf{s}}$ have the same probability, namely that $P(\check{\mathbf{s}}), \check{\mathbf{s}} \in \mathcal{M}_c$ is a constant. On the other hand, recall that in SDMA-OFDM systems we have:

$$\mathbf{x} = \mathbf{H}\mathbf{s} + \mathbf{n}. \tag{6.32}$$

It can be observed from Equation (6.32) that $\mathbf{x}$ is a random sample of the L-dimensional multi-variate complex Gaussian distribution, where the mean vector is $(\mathbf{Hs})$, while the $(P \times P)$-dimensional covariance matrix $\mathbf{R_n}$ is given by:

$$\mathbf{R_n} = E\{\mathbf{n}\mathbf{n}^H\} = \sigma_n^2 \mathbf{I}, \tag{6.33}$$

and the noise encountered at the P number of receiver antennas is assumed to be uncorrelated. Hence, the above-mentioned multi-variate complex Gaussian distribution can be described by [400]:

$$f(\mathbf{x}|\mathbf{s}, \mathbf{H}) = \frac{1}{\pi^P |\mathbf{R_n}|} \exp\Big\{ -(\mathbf{x} - \mathbf{Hs})^H \mathbf{R_n^{-1}} (\mathbf{x} - \mathbf{Hs}) \Big\}. \tag{6.34}$$

When substituting Equation (6.33) into Equation (6.34), we have:

$$f(\mathbf{x}|\mathbf{s}, \mathbf{H}) = \frac{1}{\pi^P \sigma_n^2} \exp\Big\{ -\frac{1}{\sigma_n^2} ||\mathbf{x} - \mathbf{Hs}||^2 \Big\}. \tag{6.35}$$

Note that $f(\mathbf{x}|\mathbf{s}, \mathbf{H}) = P(\mathbf{x}|\mathbf{s}, \mathbf{H})$ is the *a priori* probability that the vector $\mathbf{x}$ has been received under the condition that the vector $\mathbf{s}$ was transmitted over the MIMO channel characterized by the FD-CHTF matrix $\mathbf{H}$. Thus, Equation (6.31) can be further developed with the aid of Equation (6.35), yielding:

$$\mathcal{L}_{l,m_B} = \ln \frac{\sum_{\check{\mathbf{s}} \in \mathcal{M}^L_{l,m_B,1}} \frac{1}{\pi^P \sigma_n^2} \exp\Big\{ -\frac{1}{\sigma_n^2} ||\mathbf{x} - \mathbf{H}\check{\mathbf{s}}||^2 \Big\}}{\sum_{\check{\mathbf{s}} \in \mathcal{M}^L_{l,m_B,0}} \frac{1}{\pi^P \sigma_n^2} \exp\Big\{ -\frac{1}{\sigma_n^2} ||\mathbf{x} - \mathbf{H}\check{\mathbf{s}}||^2 \Big\}}. \tag{6.36}$$

In order to avoid the exponential computation imposed by Equation (6.36), the maximum-approximation [3] can be applied, yielding:

$$\mathcal{L}_{l,m_B} \approx -\frac{1}{\sigma_n^2} \Big[||\mathbf{x} - \mathbf{H}\check{\mathbf{s}}_{l,m_B,1}||^2 - ||\mathbf{x} - \mathbf{H}\check{\mathbf{s}}_{l,m_B,0}||^2 \Big], \tag{6.37}$$

where

$$\check{\mathbf{s}}_{l,m_B,b} = \arg \left\{ \min_{\check{\mathbf{s}} \in \mathcal{M}^L_{l,m_B,b}} \Big[||\mathbf{x} - \mathbf{H}\check{\mathbf{s}}||^2 \Big] \right\}, \quad b = 0, 1. \tag{6.38}$$

Furthermore, concerning the fact that the true FD-CHTF matrix $\mathbf{H}$ is unknown and using Equation (6.23), Equation (6.37) can be represented as:

$$\mathcal{L}_{l,m_B} \approx -\frac{1}{\sigma_n^2} \Big[\overline{\Omega}_{l,m_B,1} - \overline{\Omega}_{l,m_B,0} \Big], \tag{6.39}$$

where

$$\overline{\Omega}_{l,m_B,b} = \min\left[\ \Omega\left(\tilde{\mathbf{H}},\ \check{\mathbf{s}}_{l,m_B,b}\right),\ \omega\ \right],\quad b = 0, 1, \tag{6.40}$$

and $\omega = P \cdot L$ is a normalization factor. Equation (6.39) suggests that the LLRs can be obtained by evaluating the GA's OF. More explicitly, in order to calculate the LLR of the $(m_B)^{th}$ bit of the l^{th} $(l = 1, \cdots, L)$ user at the specific subcarrier considered, the X number of individuals in the GA's final generation are divided into two groups, where the first (or second) group is constituted by those individuals that have a value of one (or zero) at the $(m_B)^{th}$ bit of the l^{th} user's estimated transmitted symbol. The resultant lowest OS calculated in each of the two groups is then compared to ω, and the smaller of the two will be used in Equation (6.39) for calculating the corresponding LLR, which can therefore assist the channel decoder in improving the SDMA-OFDM system's performance.

It is worth pointing out that the proposed GA generating the above-mentioned population-based soft outputs only imposes a modest complexity increase in comparison to the conventional hard-decision aided individual-based GAs [45, 326–328, 390]. This is because the only additional operation required by the proposed scheme is to compare ω to the OSs, which are already available, since the results of the OF evaluation carried out by the conventional GAs can be readily used.

6.4 Simulation Results

In this section, we will quantify the performance of the MIMO SDMA-OFDM system using the proposed GA-aided iterative joint channel estimation and multi-user detection technique. Our attention was focused on overloaded scenarios, which has not been investigated in the literature in this specific context at the time of writing. Nonetheless, we point out that the proposed GA-JCEMUD scheme performs equally well in the conventional scenarios, where the number of users L is less than or equal to the number of receiver antenna elements P.

More specifically, an overloaded scenario where $L = 4$ users were supported by $P = 2$ receiver antenna elements was considered. As an example, a simple two-path Rayleigh fading channel model was employed, where the associated delay profile was $(0.7740 \cdot z^0 + 0.6332 \cdot z^{-1})$. The value of the parameter K_0 was set to $8 \gg 2$, which is a rather loose condition, potentially capable of tolerating an increase of the actual dispersion up to eight CIR taps. Each of the paths experienced independent Rayleigh fading having the same Doppler frequency of $F_D = f_d T_s$ normalized to the OFDM symbol rate, where f_d and T_s are the maximum Doppler frequency and the OFDM symbol duration including the cyclic prefix, respectively. The channel was assumed to be 'OFDM-symbol-invariant', implying that the CIR taps were assumed to be constant for the duration of one OFDM symbol, but they were faded at the

beginning of each symbol. Furthermore, the fading envelope of the $(P \times L)$ number of user-receiver channel links were assumed to be uncorrelated. Each user's associated transmit power or signal variance was assumed to be unity.

Both scenarios with and without FEC coding were investigated. In the FEC-coded scenario, as an example, a half-rate binary Low Density Parity Check (LDPC) [285, 294] code was employed. However, other FEC codes, for example Turbo Convolutional (TC) [2,286,287] codes are also applicable to the proposed system. For the reader's convenience, the simulation parameters are summarized in Table 6.1. For more details on the GA's configuration, the interested reader is referred to Section 6.3.3.3 and Chapter 4.

6.4.1 Effects of the Maximum Mutation Step Size

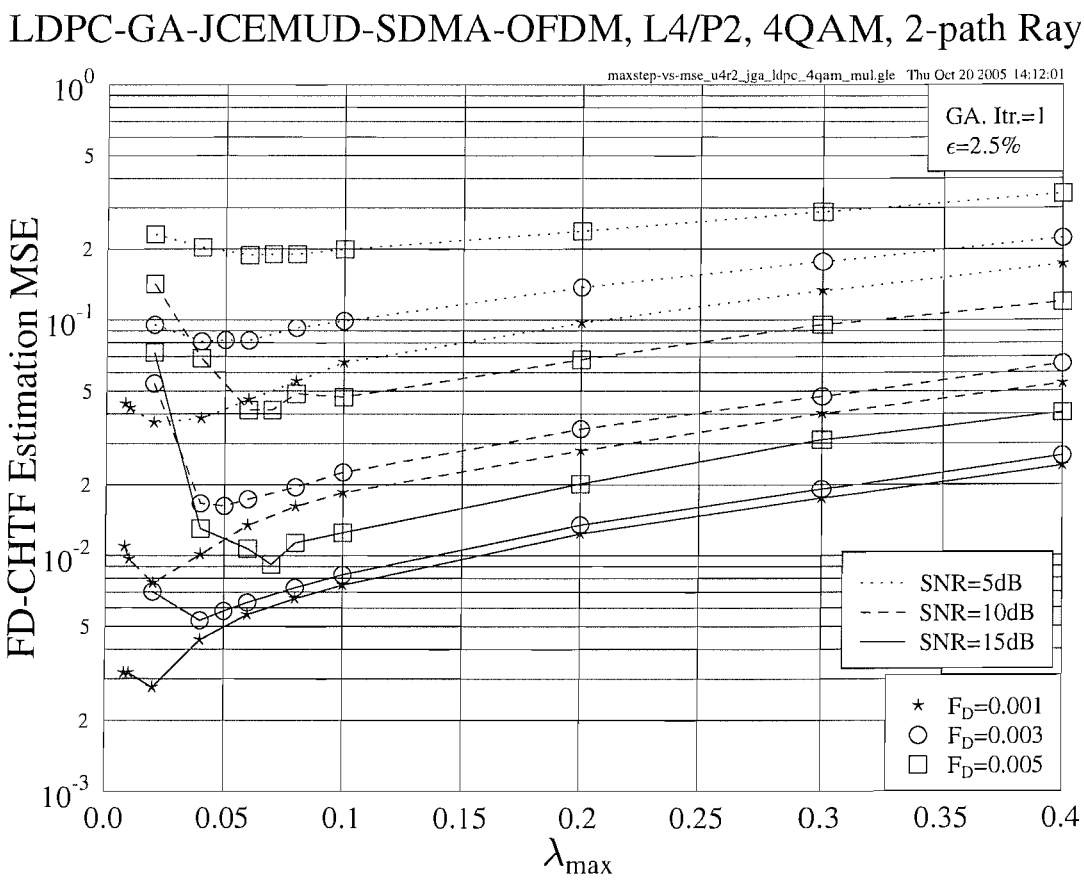

Figure 6.3: **FD-CHTF estimation MSE** versus λ_{max} performance of the **LDPC-coded iterative GA-JCEMUD assisted SDMA-OFDM** system in the overloaded scenario, where $L = 4$ users were supported with the aid of $P = 2$ receiver antenna elements, while assuming different values of the OFDM-symbol-normalized Doppler frequency F_D. The basic simulation parameters are given in Table 6.1.

LDPC parameters	Modem		4QAM
	Code rate		0.5
	Column weight		2.5
	Maximum iterations		10
	Block length of input bits		640 bits
GA-JCEMUD parameters	Symbol initialization		OHRSA [392–394]
	Mating pool creation strategy		Pareto-Optimality [320]
	Selection method		Fitness-Proportionate
	Cross-over scheme	FD-CHTF	Blend cross-over
		Symbol	Uniform cross-over
	Mutation scheme	FD-CHTF	Step mutation [45, 328]
		Symbol	Uniform mutation
	Mutation probability	FD-CHTF	0.20
		Symbol	0.15
	Maximum mutation step size λ_{max}		Varied (dependent on F_D)
	Elitism percentage		10%
	Incest prevention		Enabled
	Population size X		160
	Generations Y		5
	GA's output		Population-based
	Number of iterations		1 (unless specified)
	Pilot overhead ϵ		2.5% (unless specified)
Channel parameters	Paths		2
	Delay profile		$0.7740 \cdot z^0 + 0.6332 \cdot z^{-1}$
	K_0		8
	Subcarriers K		64
	Cyclic prefix		8
	F_D		0.003 (unless specified)

Table 6.1: Basic simulation parameters used in Section 6.4.

As a preliminary investigation, in this section we attempt to identify the appropriate choices of the maximum mutation step size λ_{max} in conjunction with different Doppler frequencies. Firstly, we characterize the average FD-CHTF estimation Mean-Square Error (MSE) performance of the GA-JCEMUD/SDMA-OFDM system using various values of λ_{max}, as shown in Figure 6.3, where the GA-JCEMUD invoked a single iteration and used a pilot overhead of $\epsilon = 2.5\%$. The average FD-CHTF estimation MSE is defined by:

$$\overline{\text{MSE}} = \frac{1}{N_T}\sum_{n=1}^{N_T}\overline{\text{MSE}}[n], \tag{6.41}$$

where N_T is the total number of OFDM symbols transmitted, while $\overline{\text{MSE}}[n]$ is the average FD-CHTF estimation MSE associated with the n^{th} OFDM symbol, given by:

$$\overline{\text{MSE}}[n] = \frac{1}{PLK}\sum_{p=1}^{P}\sum_{l=1}^{L}\sum_{k=1}^{K}\left|\hat{H}_p^{(l)}[n,k] - H_p^{(l)}[n,k]\right|^2. \tag{6.42}$$

Here we point out that the FD-CHTF estimation MSE performance of the GA-JCEMUD is the same both with and without employing FEC coding. This is because the GA-aided joint optimization process has no direct interaction with the outer FEC code and thus it becomes independent of the codec. Explicitly, we can see in Figure 6.3 that the choice of λ_{max} has a substantial effect on the system's FD-CHTF estimation MSE performance, regardless of both F_D as well as of Signal-to-Noise Ratio (SNR).

In Figure 6.4, the Bit Error Ratio (BER) versus λ_{max} performance of the LDPC-coded GA-JCEMUD aided SDMA-OFDM system is portrayed. It can be found that in scenarios associated with a higher SNR the effect of λ_{max} becomes more significant in terms of the achievable BER performance. The reason for this phenomenon is that at low SNRs the BER performance of the system is mainly dominated by the noise signal, while at high SNRs by the choice of λ_{max}, provided that the Doppler frequency is the same. Furthermore, a higher F_D value typically requires a higher λ_{max} for attaining the best achievable BER performance, as we have discussed in Section 6.3.3.3.2. According to Figure 6.4, the recommended values of λ_{max} in terms of achieving the best possible BER performance[4] are 0.4, 0.6 and 0.7 in conjunction with F_D values of 0.001, 0.003 and 0.005, respectively. These values of λ_{max} corresponding to the specific F_D values encountered were used for generating all the simulation results to be discussed in the rest of this chapter.

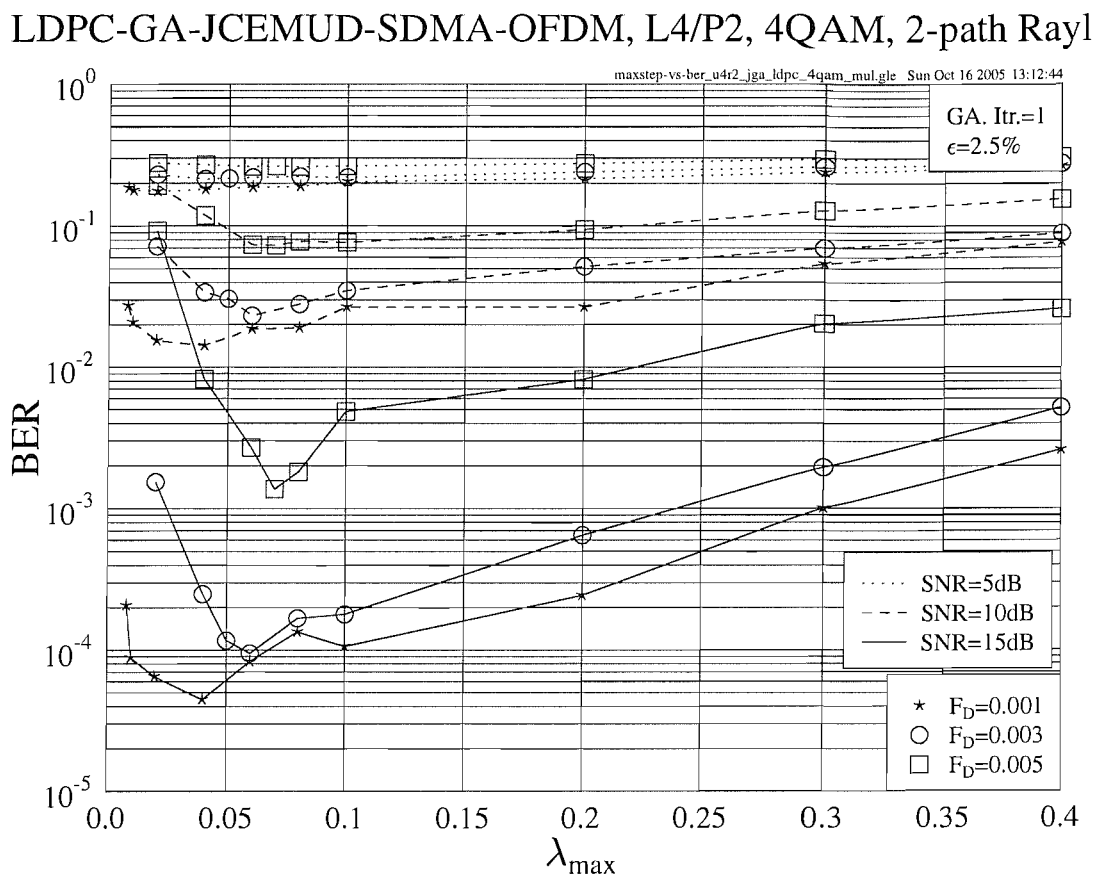

Figure 6.4: **BER** versus λ_{max} performance of the **LDPC-coded iterative GA-JCEMUD assisted SDMA-OFDM** system in the overloaded scenario, where $L = 4$ users were supported with the aid of $P = 2$ receiver antenna elements, while assuming different values of the OFDM-symbol-normalized Doppler frequency F_D. The basic simulation parameters are given in Table 6.1.

6.4.2 Effects of the Doppler Frequency

In Figure 6.5 we compare the BER versus SNR performance of both the uncoded and LDPC-coded GA-JCEMUD/SDMA-OFDM systems in conjunction with different values of F_D. The performances of the systems employing the linear MMSE MUD or the optimum ML MUD are also provided as references, both assuming perfect Channel State Information (CSI). A pilot overhead of $\epsilon = 2.5\%$ was assumed and the GA-JCEMUD used a single iteration. As shown in Figure 6.5, unsurprisingly, the performances of both the uncoded and coded GA-JCEMUD aided systems degraded, when F_D was increased, since a higher Doppler frequency implies that the channel fades more rapidly, which renders channel estimation more challenging. This is especially true for MIMO systems, even more so for overloaded MIMO systems, as

[4]Note that the best choice of λ_{max} for achieving the best BER performance may be similar to, but may not necessarily be the best choice for attaining the best FD-CHTF estimation MSE performance. This effect can be observed from Figures 6.3 and 6.4.

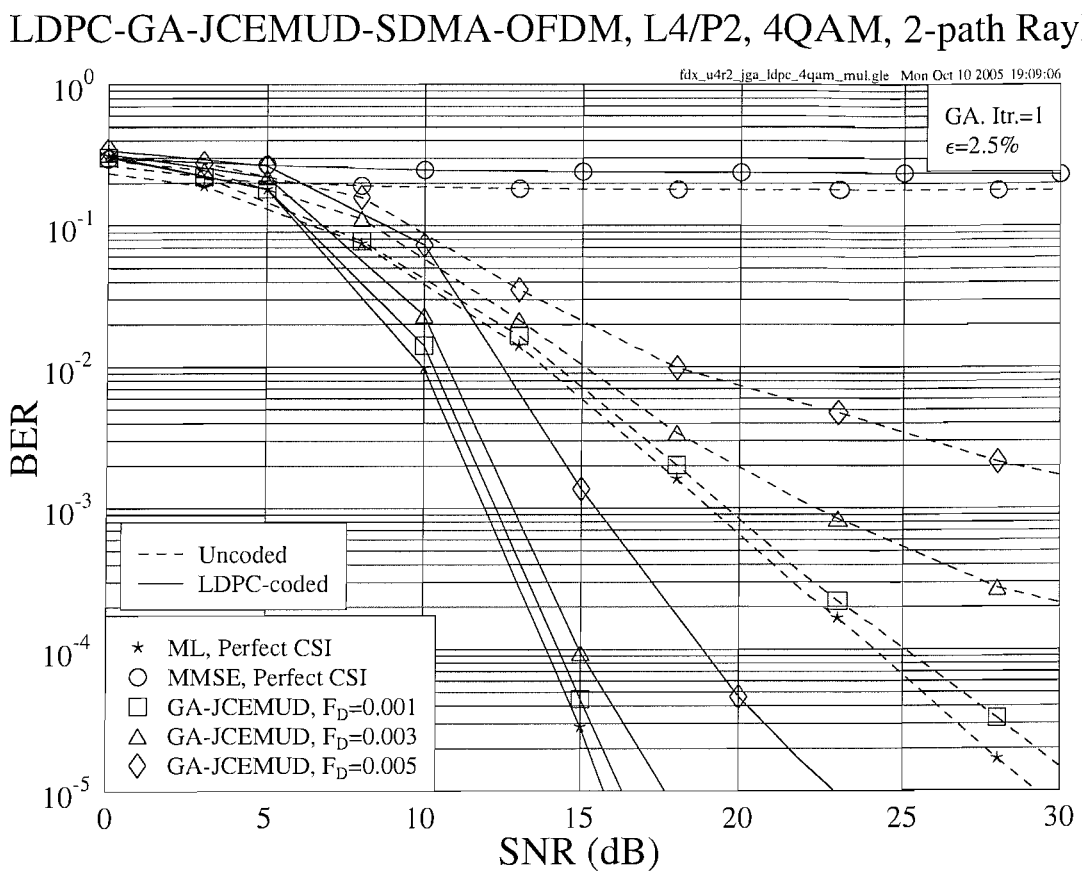

Figure 6.5: **BER** versus SNR performances of the **uncoded** and **LDPC-coded iterative GA-JCEMUD assisted SDMA-OFDM** systems in the overloaded scenario, where $L = 4$ users were supported with the aid of $P = 2$ receiver antenna elements, while assuming different values of the OFDM-symbol-normalized Doppler frequency F_D. The basic simulation parameters are given in Table 6.1.

discussed in Section 6.1. Nonetheless, with only a 2.5% pilot overhead, the proposed GA-JCEMUD/SDMA-OFDM system was capable of achieving a performance close to the perfect-CSI aided optimum ML MUD at $F_D = 0.001$. By contrast, the system employing the MMSE MUD completely failed even with the aid of perfect CSI, owing to the insufficient degree of detection freedom experienced in overloaded scenarios. Furthermore, compared to the uncoded scenario, the performance degradation of the LDPC-coded GA-JCEMUD incurred by higher Doppler frequencies was much less dramatic, as observed in Figure 6.5.

6.4.3 Effects of the Number of GA-JCEMUD Iterations

Figure 6.6 shows the achievable performance of the proposed system invoking different numbers of GA-JCEMUD iterations. It was assumed that we had $\epsilon = 2.5\%$ and $F_D = 0.003$. As

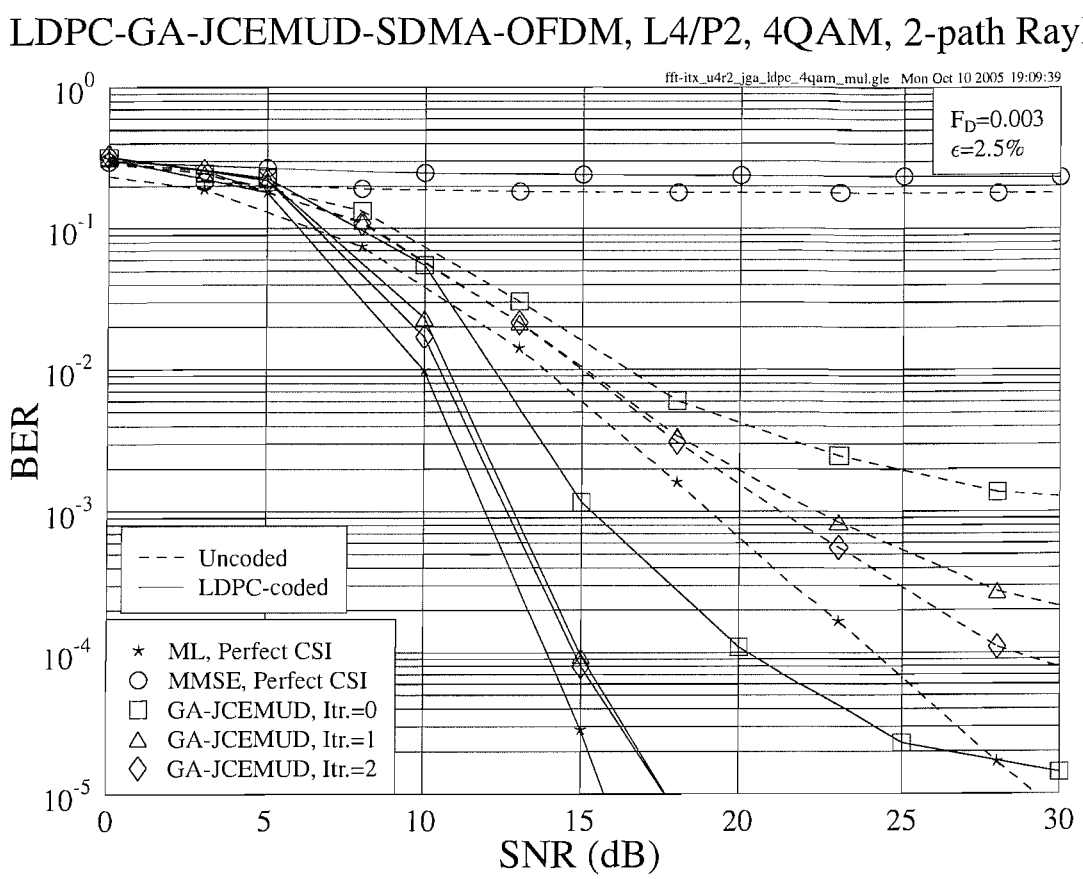

Figure 6.6: **BER** versus SNR performances of the **uncoded** and **LDPC-coded iterative GA-JCEMUD assisted SDMA-OFDM** systems in the overloaded scenario, where $L = 4$ users were supported with the aid of $P = 2$ receiver antenna elements, while invoking different numbers of GA-JCEMUD iterations. The basic simulation parameters are given in Table 6.1.

seen in Figure 6.6, a significant iteration gain was achieved, when the GA-JCEMUD invoked additional iterations. Furthermore, the performance of the uncoded system consistently improved as the number of iterations was increased, while in the LDPC-coded system most of the gain was attained by the first GA-JCEMUD iteration. In Figure 6.7, the average FD-CHTF estimation MSE performance of the GA-JCEMUD/SDMA-OFDM system as well as the performance of the reference system employing $\epsilon = 100\%$ pilot overhead are compared. Observe from Figure 6.7 that as expected, the FD-CHTF estimation MSE performance was improved, when the number of GA-JCEMUD iterations was increased. Moreover, when the SNR exceeded about 13dB, the GA-JCEMUD using $\epsilon = 2.5\%$ pilot overhead approached the best-case FD-CHTF estimation MSE performance associated with $\epsilon = 100\%$.

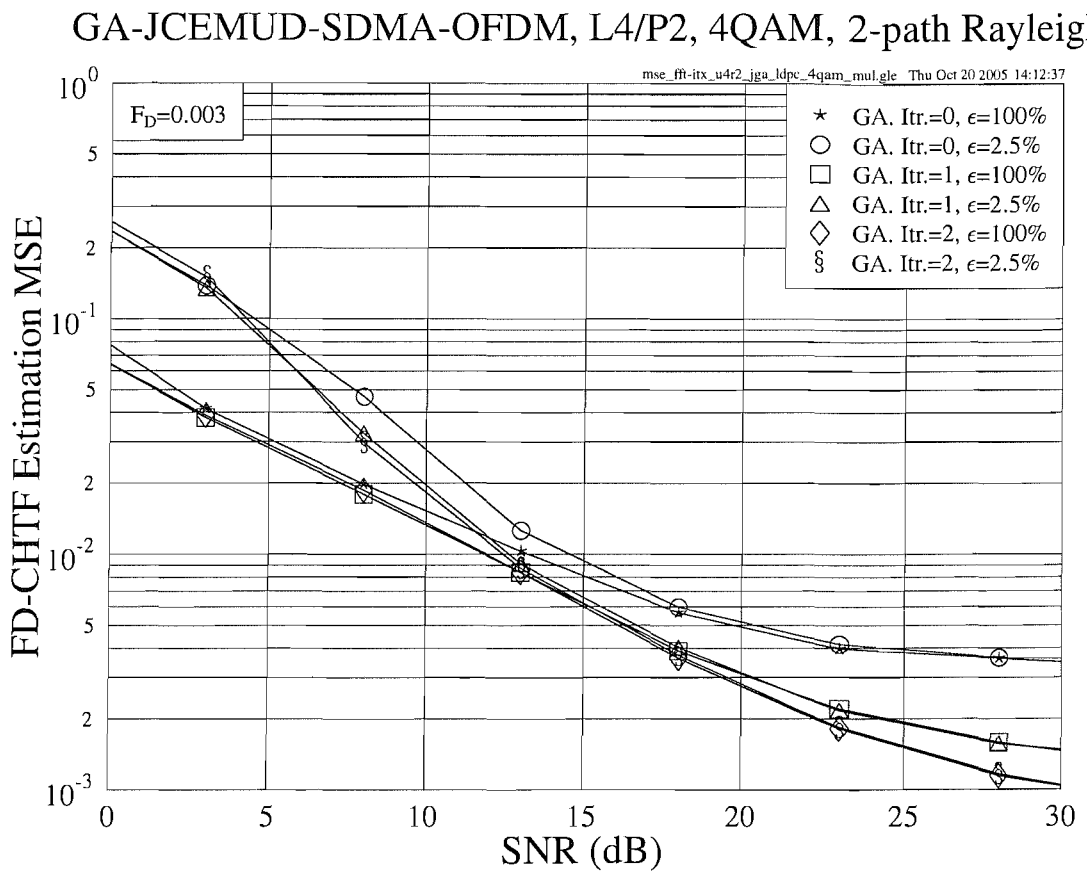

Figure 6.7: **FD-CHTF estimation MSE** versus SNR performance of the **iterative GA-JCEMUD assisted SDMA-OFDM** system in the overloaded scenario, where $L = 4$ users were supported with the aid of $P = 2$ receiver antenna elements, while invoking different numbers of GA-JCEMUD iterations. The basic simulation parameters are given in Table 6.1.

6.4.4 Effects of the Pilot Overhead

In Figure 6.8 the BER performance of the proposed system using different pilot overheads is investigated. In most cases, the GA-JCEMUD was capable of achieving a good performance using a pilot overhead as low as $\epsilon = 1.5 \sim 2.5\%$. Furthermore, the increase of pilot OFDM symbol overhead brings about more substantial benefits at the higher Doppler frequencies than at the lower ones, especially in the scenarios associated with higher SNRs, where an increasing fraction of the residual detection errors was inflicted by the inaccurate channel estimation.

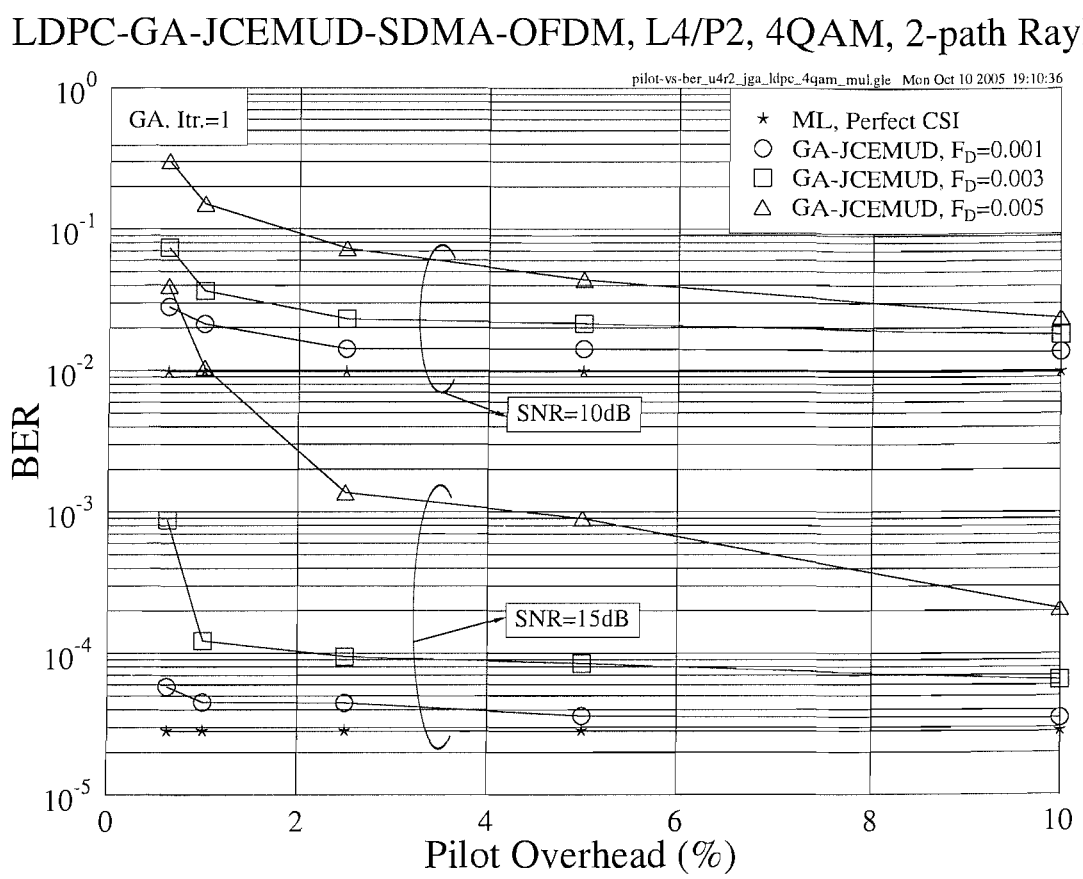

Figure 6.8: **BER** versus pilot overhead performance of the **LDPC-coded iterative GA-JCEMUD assisted SDMA-OFDM** system in the overloaded scenario, where $L = 4$ users were supported with the aid of $P = 2$ receiver antenna elements, while assuming different values of the OFDM-symbol-normalized Doppler frequency F_D. The basic simulation parameters are given in Table 6.1.

6.4.5 Joint Optimization Versus Separate Optimization

In order to further characterize the advantages of the proposed GA-aided joint optimization scheme, in Figure 6.9 we compare the performances of the GA-JCEMUD and its counterpart, referred to as the GA-based channel estimator assisted OHRSA MUD (GACE-OHRSA-MUD), where the OHRSA MUD is serially concatenated with the stand-alone GA-aided channel estimator. More specifically, in the GACE-OHRSA-MUD, channel estimation and symbol detection are separately accomplished by the GA-aided channel estimator and the OHRSA MUD, respectively. In other words, the symbol estimates offered by the OHRSA MUD are fixed during the GA-aided optimization process of the FD-CHTF estimates. Explicitly, in this case the effect of error propagation due to inaccurate symbol and/or channel estimates will become more severe, thus resulting in a dramatic BER performance degradation in comparison to the proposed joint optimization scheme, as evidenced in Figure 6.9. Furthermore, the

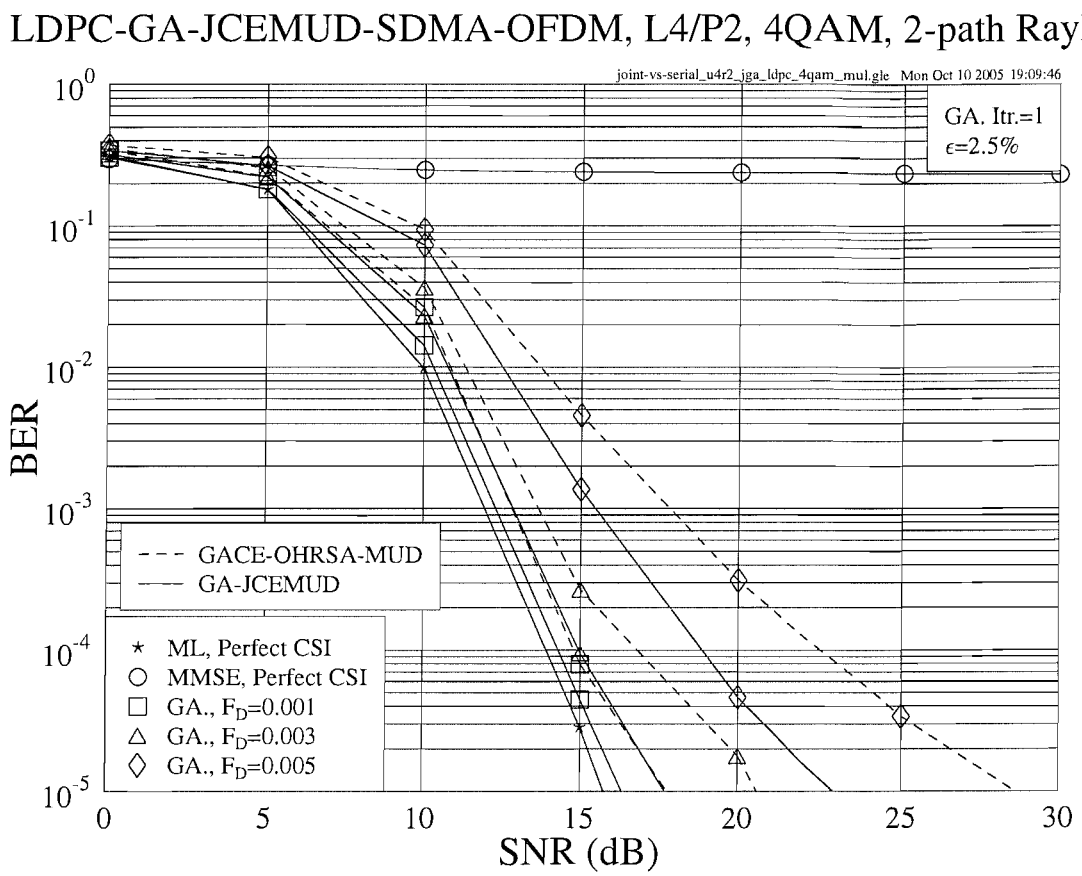

Figure 6.9: **BER** versus SNR performance of the **LDPC-coded SDMA-OFDM** system using either the **iterative GA-JCEMUD** or the **iterative GACE-OHRSA-MUD** in the overloaded scenario, where $L = 4$ users were supported with the aid of $P = 2$ receiver antenna elements, while assuming different values of the OFDM-symbol-normalized Doppler frequency F_D. The basic simulation parameters are given in Table 6.1.

superiority of the GA-JCEMUD becomes even more conspicuous in high-Doppler scenarios.

6.4.6 Comparison of GA-JCEMUDs Having Soft and Hard Outputs

In Figure 6.10, the performance comparison of the GA-JCEMUD providing either the conventional individual-based hard outputs [45, 326–328, 390] or the proposed population-based soft outputs is provided. As expected, with the advent of FEC codes, the proposed soft GA is capable of significantly outperforming the conventional arrangement, especially when the channel fades more rapidly. This result implies that the proposed GA exhibited a higher robustness against fast fading channels than the conventional GAs [45, 326–328, 390].

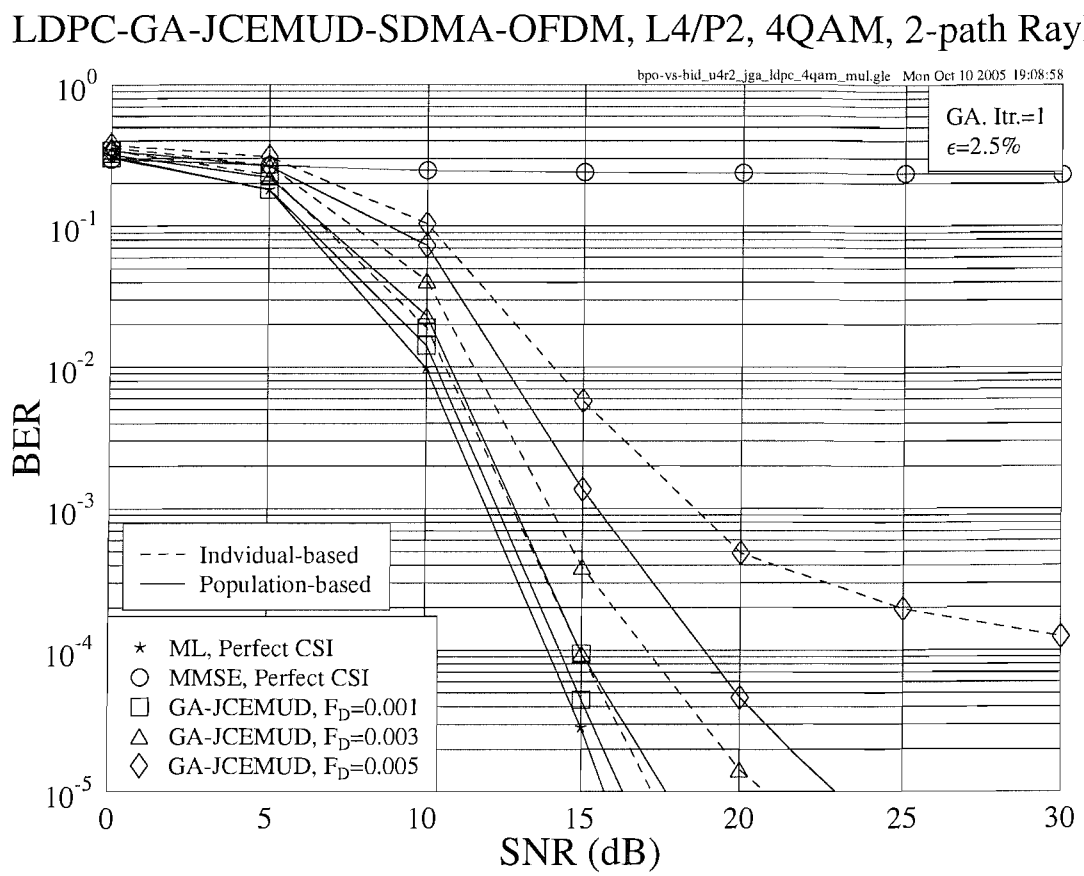

Figure 6.10: **BER** versus SNR performance of the **LDPC-coded SDMA-OFDM** system using either the conventional **individual-based** or the proposed **population-based** GA-JCEMUD in the overloaded scenario, where $L = 4$ users were supported with the aid of $P = 2$ receiver antenna elements, while assuming different values of the OFDM-symbol-normalized Doppler frequency F_D. The basic simulation parameters are given in Table 6.1.

6.4.7 MIMO Robustness

As a further investigation, a visual comparison of the true and estimated FD-CHTFs is portrayed in Figure 6.11. More specifically, the L users' FD-CHTFs associated with a specific receiver antenna element during a block of 40 consecutive OFDM symbols are plotted at a SNR value of 20dB. Each dot of the curves plotted in Figure 6.11 represents a complex-valued FD-CHTF at a specific subcarrier. By observing the perfect channel-knowledge based illustration at the top of Figure 6.11, we can see that the FD-CHTF at each subcarrier evolves over the duration of the 40 OFDM symbols, where the thickness of the ring-shaped formations indicates the amount of FD-CHTF change during this time interval. The full perimeter of the ring is constituted by the $K = 64$ spoke-like formations corresponding to the 64 OFDM subcarriers. Explicitly, the radiuses of the FD-CHTF rings associated with

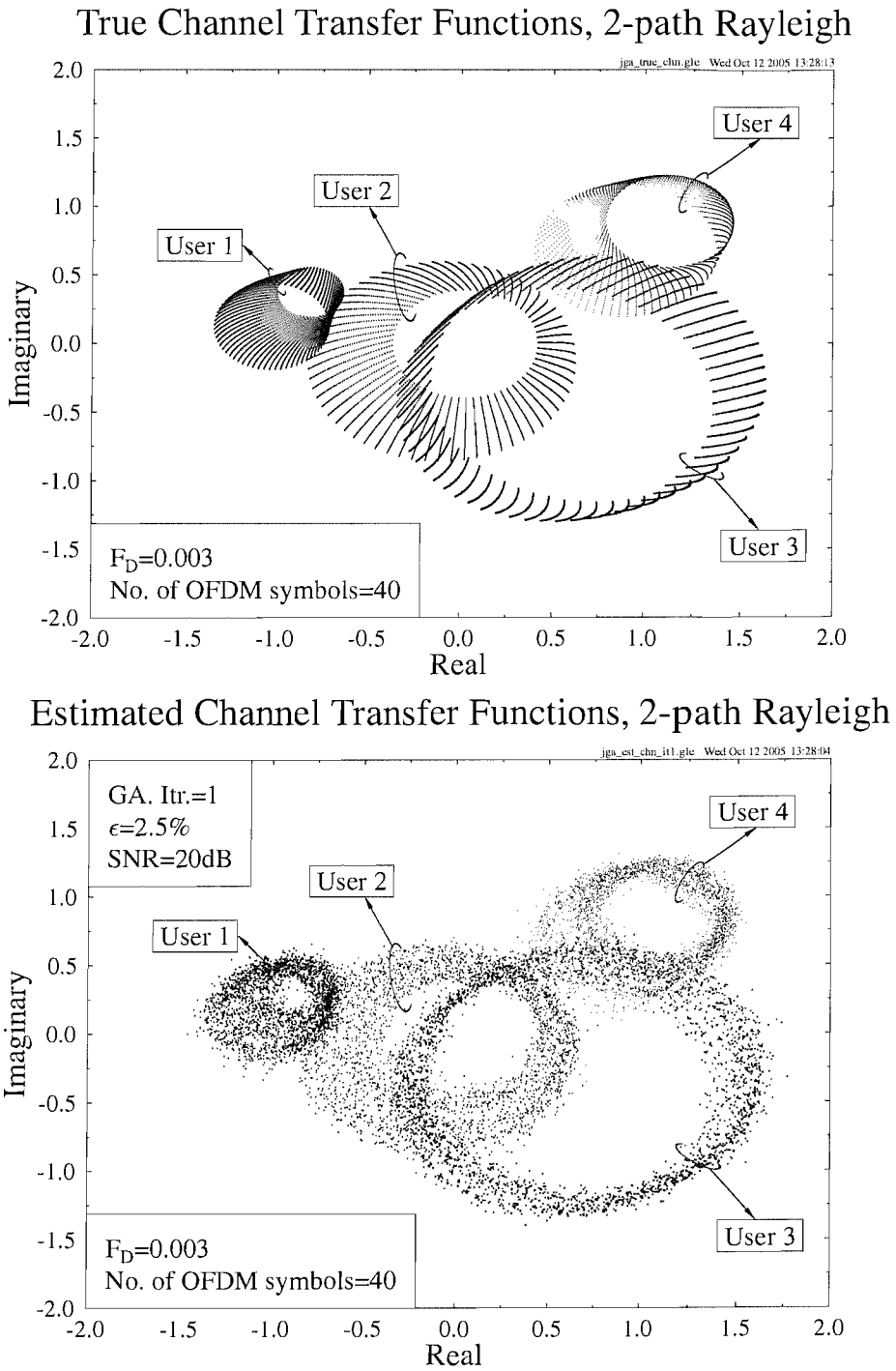

Figure 6.11: **Channel estimation** performance of the **iterative GA-JCEMUD assisted SDMA-OFDM** system in the overloaded scenario, where $L = 4$ users were supported with the aid of $P = 2$ receiver antenna elements. The estimated FD-CHTFs $\hat{H}_1^{(l)}[n,k]$ $(l = 1,\cdots,L;\ k = 1,\cdots,K)$ associated with $n = 1,\cdots,40$ consecutive OFDM symbols at the $p = 1^{st}$ receiver antenna are plotted at a SNR value of 20dB, and compared with the true FD-CHTFs. The basic simulation parameters are given in Table 6.1.

the four user-receiver channel links are significantly different. This is because each individual link is subjected to independent fading, and although the Doppler frequency encountered at the four links is identical, their short-term envelope fluctuation observed over the 40 OFDM symbol durations is different. However, by comparing the subfigures at the top and bottom of Figure 6.11, we can see that the FD-CHTF estimates closely match their true values, resulting in a similar FD-CHTF contour for each of the four channel links. This implies that the proposed GA-JCEMUD is capable of *simultaneously* capturing the fading envelope changes of *each* individual user-receiver link, regardless of its instant variety of fading. Since an equally good performance was attained over all the user-receiver links, this demonstrates the global robustness of the proposed approach in MIMO scenarios.

6.5 Conclusions

From our discussions in the previous sections, we conclude that the proposed GA-aided iterative joint channel estimation and multi-user detection scheme generating soft outputs constitutes an effective solution to the channel estimation problem in multi-user MIMO SDMA-OFDM systems. Furthermore, the GA-JCEMUD is capable of exhibiting a robust performance in overloaded scenarios, where the number of users is higher than the number of receiver antenna elements, either with or without FEC coding. This attractive property enables the SDMA-OFDM system to potentially support an increased number of users.

Note that in this chapter the GA-JCEMUD was used for estimating the CHTFs of a two-tap channel model, while the value of the parameter K_0 was set to 8, which is four times higher than the actual number of CIR taps. However, we point out that as long as the condition of $K_0 > 2$ is satisfied, the performance of the proposed scheme can be improved upon reducing the value of K_0, since more noise will be removed during the CIR tap filtering process. Furthermore, this implies that given a fixed value of K_0, which has to be higher than the maximum channel delay spread encountered, the more taps the channel has, the better the performance of the GA-JCEMUD, as a benefit of having an increased ratio of the 'real' number of CIR taps in comparison to K_0.

6.6 Chapter Summary

In MIMO OFDM systems accurate channel estimation is required at the receiver in order to carry out coherent demodulation and interference cancellation. However, channel estimation is more challenging in the MIMO scenario than in a SISO scenario, owing to an increased number of independent transmitter-receiver channel links as well as due to the interference

imposed by multiple transmitter antennas. Our discussions commenced in Section 6.1 with an extensive review of the family of channel estimation techniques found in the MIMO OFDM literature, where a number of channel estimation approaches including blind [90,216,227,250, 376,377], pilot-aided [131,132,134,199,378,379] and joint [173,384] estimation schemes have been proposed. However, in the context of BLAST or SDMA type multi-user MIMO OFDM systems, none of the channel estimation techniques found in the literature [133,157,173,179, 199,216,227,250,376,380,384,385] allows the number of users to exceed that of the receiver antennas. We refer to this as an overloaded scenario, where we have an insufficient detection degree of freedom, rendering the channel estimation an even more challenging task.

In an effort to overcome the channel estimation problem in overloaded MIMO OFDM systems, in this chapter a GA-assisted iterative Joint Channel Estimation and Multi-User Detection (GA-JCEMUD) approach was proposed. We commenced with an overview of the proposed scheme in Section 6.2, where we outlined our system schematic in Figure 6.1, followed by a detailed discussion in Section 6.3. The philosophy of the proposed iterative GA-JCEMUD was portrayed in Figure 6.2, accompanied by our corresponding elaborations. In Section 6.3.1, we generated initial estimates of the FD-CHTFs with the aid of pilot OFDM symbols spread by WHT-based spreading codes. On the other hand, the Optimized Hierarchy Reduced Search Algorithm (OHRSA) MUD [392–394] was employed as a first-stage detector in order to generate initial symbol estimates, as discussed in Section 6.3.2.

With the aid of the initial FD-CHTF and symbol estimates, the proposed GA-JCEMUD printed in the grey block of Figure 6.2 can be employed for jointly optimizing the estimates of the FD-CHTFs and multi-user data symbols. This process was detailed in Section 6.3.3. More specifically, concerning the MIMO channel's structure, in Section 6.3.3.1 we introduced the extended structure of the GA individuals. Following the description of the initialization process in Section 6.3.3.2, the GA-based joint optimization was presented in Section 6.3.3.3, which is constituted by the discussion of the cross-over operators in Section 6.3.3.3.1, the mutation operators in Section 6.3.3.3.2 and further discussions in Section 6.3.3.3.3. Furthermore, in order to overcome the limitations imposed by the conventional GA-aided MUDs, which can only provide single-individual based hard-decoded symbol estimates, a new algorithm was derived in Section 6.3.3.4 to enable the GA to provide soft outputs based on the entire population. Since the only additional operation required by the proposed scheme is to compare the normalization factor $\omega = P \cdot L$ to the OSs, which have already been calculated during the OF evaluation process carried out by the conventional GAs, the proposed GA generating the above-mentioned population-based soft outputs imposes only a modest complexity increase in comparison to its conventional hard-decision aided individual-based counterpart.

The numerical results of the proposed uncoded and LDPC-coded iterative GA-JCEMUD

aided SDMA-OFDM system were provided in Section 6.4. As a preliminary investigation, the effect of the maximum mutation step size λ_{max} used in the GA-JCEMUD was first identified in Section 6.4.1, where it was found that the choice of λ_{max} has a significant impact on the system's MSE as well as BER performance, and these effects became more substantial, when the SNR was increased. Furthermore, for the sake of attaining the best achievable BER performance, typically a higher λ_{max} is required in the scenario associated with a higher OFDM-symbol-normalized Doppler frequency F_D. This is because when we have a higher Doppler frequency, the consecutive time-domain channel fades experienced by each of the subcarriers become more rapidly fluctuating, thus requiring a higher λ_{max} value for assisting the GA in capturing the rapid changes of the channel fades. In addition, the values of λ_{max} required for attaining the best BER performance were identified for different values of F_D with the aid of Figure 6.4.

In Section 6.4.2, our research was dedicated to probing the effect of Doppler frequency. As expected, the performances of both the uncoded and coded GA-JCEMUD aided systems degraded, when F_D was increased. However, when using a low pilot overhead of $\epsilon = 2.5\%$, the proposed GA-JCEMUD/SDMA-OFDM system was capable of achieving a performance close to the perfect-CSI aided optimum ML MUD at $F_D = 0.001$, as evidenced in Figure 6.5, while the system employing the MMSE MUD completely failed even with the aid of perfect CSI. In Section 6.4.3, we showed that the proposed system's performance can be improved by increasing the number of GA-JCEMUD iterations, both with or without channel coding. At a SNR value of about 13dB, the GA-JCEMUD using $\epsilon = 2.5\%$ pilot overhead approached the best-case FD-CHTF estimation MSE performance associated with $\epsilon = 100\%$. When examining the effect of the pilot overhead ϵ, we observed that the GA-JCEMUD was capable of achieving a good performance using as low a pilot overhead as $\epsilon = 1.5 \sim 2.5\%$ in most of the scenarios considered, as shown in Figure 6.8 of Section 6.4.4.

In order to further characterize the advantages of the proposed joint optimization mechanism, in Section 6.4.5 we compared the performances of the GA-JCEMUD and its counterpart, namely the GACE-OHRSA-MUD, which serially concatenates the OHRSA MUD with the stand-alone GA-aided channel estimator. It was shown that the former outperformed the latter, especially in high-Doppler scenarios. This demonstrated the superiority of the joint optimization mechanism over the conventionally combined detection architecture. Moreover, Section 6.4.6 exhibits the further benefits of the proposed GA-JCEMUD scheme owing to its ability of providing soft outputs. With the advent of FEC codes, the proposed population-based soft-decoded GA of Section 6.3.3.4 was capable of significantly outperforming the conventional individual-based hard-decoded GAs [45, 326–328, 390], especially when the channel fades rapidly. This result implies that the proposed GA exhibited a higher ro-

bustness against fast fading channels than the conventional GAs. Finally, in Section 6.4.7 the GA-JCEMUD's robustness recorded in MIMO scenarios was verified. As shown in Figure 6.11, the proposed iterative GA-JCEMUD was capable of *simultaneously* capturing the fading envelope changes of *each* individual user-receiver link, regardless of its instant variety of fading, and thus achieving an equally good performance over all the user-receiver links. This result potently demonstrates the robustness of the proposed approach.

Chapter 7

Conclusions and Future Work

In this concluding chapter, we will summarize the main findings of our investigations presented in the thesis. This will be followed by a range of ideas concerning our future research.

7.1 Summary and Conclusions

7.1.1 Chapter 1

This chapter constitutes a general background of our studies throughout this thesis. More specifically, the milestones in the history of OFDM were presented in Section 1.1.1, where the key events and contributions across several decades were summarized in Tables 1.1-1.3. Furthermore, in Section 1.1.2.1 an overview of the MIMO techniques was provided, followed by the introduction to MIMO-OFDM systems in Section 1.1.2.2, where the associated contributions found in the literature were outlined in Tables 1.4-1.6. Moreover, our review of the SDMA and SDMA-OFDM literature outlined in Section 1.1.2.3 was summarized in Tables 1.7 and 1.8. Finally, we introduced the organization of the thesis in Section 1.2, while our novel contributions were highlighted in Section 1.3.

7.1.2 Chapter 2

Our research in Chapter 2 was conducted in the context of both single-user single-carrier and single-user OFDM systems, which constitutes the introductory and background work for the following chapters. Specifically, in Section 2.2, a general outline of Alamouti's simple scheme [278] using two transmitters in conjunction with a number of receivers for communications in non-dispersive Rayleigh fading channels was provided, followed by a brief review on various Space-Time Block Codes (STBCs) proposed by Tarokh *et al.* [279, 280], namely

the G_2, G_3, G_4, H_3 and H_4 codes, as well as their achievable performances over uncorrelated and correlated Rayleigh fading channels. The performances of all the space-time block codes considered are summarized in Table 2.2.

Following the above foundational work, in Section 2.3.1 the STBCs were combined with various Low Density Parity Check (LDPC) codes in order to improve the system's performance. It was found that provided that the same modulation scheme was used, a lower-rate LDPC code benefited the system more than a space-time code of a higher-diversity order did for transmission over the uncorrelated Rayleigh fading channels. On the other hand, when the same LDPC code was used, a lower-order modulation scheme tended to offer a higher performance improvement, than a space-time block code of a higher diversity order did. The performance of different LDPC-aided space-time block coded schemes was summarized in Table 2.5, where the half-rate LDPC-coded space-time block code G_2 was found to be the best option among all the LDPC-STBC concatenated schemes investigated. Furthermore, in Section 2.3.2, we compared the performance of a LDPC-aided G_2-coded scheme to a half-rate Turbo Convolutional (TC) code, namely to that of a TC(2,1,4) aided G_2-coded arrangement, which was found to be the best scheme in a range of TC-STBC-concatenated systems [2] designed for transmission over uncorrelated Rayleigh fading channels. From our coding gain versus complexity performance comparisons, it was concluded that the half-rate TC(2,1,4)-assisted space-time block code G_2 slightly outperforms the LDPC-assisted space-time block coded schemes. However, the LDPC-STBC concatenated schemes may be considered as better design options for complexity-sensitive systems, where the achievable performance does not necessarily have to be the highest possible, since the LDPC-aided schemes are capable of maintaining a lower complexity than the TC(2,1,4)-aided scheme is. In conclusion, the performance of the different schemes studied was summarized in Table 2.8.

Moreover, channel coding assisted space-time block coded single-user OFDM systems were studied in Section 2.4. More specifically, in Section 2.4.1 Trellis-Coded Modulation (TCM), Turbo Trellis-Coded Modulation (TTCM), Bit-Interleaved Coded Modulation (BICM) and iterative decoded BICM (BICM-ID) of the Coded Modulation (CM) family were amalgamated with a STBC G_2 aided OFDM system for communicating over wideband channels. Our corresponding simulation results were summarized in Table 2.11, which was followed by Section 2.4.2, where the performance of the TTCM and LDPC-assisted G_2-coded single-user OFDM systems was documented. It was found that the coding gain performance of the TTCM-aided G_2 schemes surpasses that of the LDPC-aided G_2 schemes, when the affordable complexity is higher than approximate 500, as observed in Figure 2.38. At a low complexity, namely below a value of about 500, however, the LDPC-aided schemes tend to achieve a higher coding gain than the TTCM-aided schemes. The associated results were summarized

in Table 2.13.

7.1.3 Chapter 3

In Chapter 3, our attention was focused on Space Division Multiple Access (SDMA) based uplink multi-user OFDM systems, where the various CM-assisted SDMA-OFDM schemes using the frequency-domain subcarrier-based Walsh-Hadamard Transform Spreading (WHTS) were investigated. In this chapter, the Minimum Mean-Square Error (MMSE) based Multi-User Detection (MUD) technique was considered. From the simulation results provided in Section 3.3, it was found that WHTS was capable of improving the system's performance, especially in uncoded scenarios, since the bursty subcarrier errors can be pseudo-randomly spread across the subcarriers of the entire WHT block. Furthermore, when we had two receiver antenna elements, the TTCM-aided WHTS-MMSE-SDMA-OFDM system achieved the best CodeWord Error Ratio (CWER) performance among all the CM- and WHTS-assisted schemes considered for transmission over the three-path SWATM channel of Figure 2.32. Comparing Figure 3.8 to Figure 3.10, we found that at the same user load level, for example at $\alpha_4 = \alpha_2 = 0.5$ or $\alpha_4 = \alpha_2 = 1.0$, the E_b/N_0 performance achieved by the four-receiver system was better than that of the two-receiver system, provided that the same CM-assisted scheme was used, since employing a higher number of SDMA receiver antennas offers a higher spatial diversity. Additionally, the performance of the various CM- and WHTS-assisted MMSE-SDMA-OFDM systems was evaluated in the context of the more dispersive twelve-path COST207 HT channel of Figure 3.12 in Section 3.3.2.2, including the two- and four-receiver scenarios in Section 3.3.2.2.1 and Section 3.3.2.2.2, respectively. It was found that with the aid of WHTS, the TTCM-assisted scheme constituted the best design option in terms of both the Bit Error Ratio (BER) and CWER in comparison to the other three CM-aided schemes. Furthermore, the spreading-induced E_b/N_0 gain achieved by all the schemes over the COST207 HT channel was higher than that achieved over the SWATM channel. This may suggest that in highly dispersive environments the channel-coded SDMA-OFDM system's performance may be further improved by employing WHTS.

In Table 3.4 we summarized the E_b/N_0 values required by the various CM- and WHTS-assisted MMSE-SDMA-OFDM schemes for achieving a BER of 10^{-5}, also showing the corresponding gains attained by the WHTS-assisted schemes. We observed that on one hand, when we had a specific user load, the spreading-induced E_b/N_0 gain achieved by a system having a lower diversity order was higher, regardless of the employment of CM. In other words, the subcarrier-based WHTS technique may be expected to attain a higher system performance improvement in relatively lower diversity-order scenarios. Moreover, if we supported a fixed number of users but varied the number of receiver antenna elements, similar conclusions may

be drawn. A plausible explanation for this fact may be that in the SDMA-MIMO system, a potentially higher space diversity gain may be achieved, when a higher number of receiver antenna elements is employed, and thus the benefits of WHTS may be less substantial. This may be particularly true in the context of the CM-aided systems, since most of the attainable gain has already been achieved by using the channel codes. On the other hand, when a given number of receiver antenna elements was used, the spreading-induced E_b/N_0 gains achieved in the context of the fully-loaded systems were higher than in the half-loaded systems, regardless of the employment of channel codes. This suggests that more benefits may arise from WHTS, especially in the fully-loaded scenarios, where the MUD suffers from a relatively low efficiency in differentiating the different users' signals.

Additionally, we provided the E_b/N_0 crossing points and the corresponding total gain achieved by the various CM-WHTS-MMSE-SDMA-OFDM schemes at the BER of 10^{-5}, in Figures 3.19 and 3.20, respectively. It was demonstrated that the performance gap between the different CM-aided schemes increased, as the user load increased. It was also found that when the user load was higher, namely when the Multi-User Interference (MUI) was increased, the performance degradation of the TTCM-aided schemes was lower than those of the TCM, BICM and BICM-ID-aided arrangements. By contrast, at a relatively low user load the various schemes provided a similar performance, because most of the attainable gain of the four-receiver SDMA-OFDM system had already been achieved.

The effects of using different WHT block sizes was studied in Section 3.3.2.3, in both the SWATM and COST207 HT channel scenarios, as seen in Figures 3.21 and 3.22, respectively. As expected, it was found that the system's performance was improved, while the WHT block size used was increased. In Section 3.3.2.4 the effects of the Doppler frequency was demonstrated. It was concluded that the maximum Doppler frequency does not significantly affect the performance of the WHTS-assisted MMSE-SDMA-OFDM system, regardless of the employment of CM, as for example portrayed in Figure 3.23.

From the investigations conducted in Chapter 3, it was concluded that the various CM schemes, namely TCM, TTCM, BICM and BICM-ID are capable of substantially improving the achievable performance of SDMA-OFDM systems. The employment of WHTS has the potential of further enhancing the system's performance in highly dispersive propagation environments. As a result, the TTCM- and WHTS-assisted scheme was found to have the best CWER performance in all the scenarios investigated. Furthermore, it was also the best design option in terms of the achievable E_b/N_0 gain expressed in dB, when communicating in highly dispersive environments, for example over the COST207 HT channel of Figure 3.12, while carrying a high user load of $\alpha_P \geq 0.5$.

7.1.4 Chapter 4

Since the performance of the linear MMSE MUD employed in Chapter 3 is limited, our work was carried forward in Chapter 4 towards the design of more sophisticated MUDs for the multi-user SDMA-OFDM systems. More specifically, we proposed a MMSE-aided Genetic Algorithm (GA) based MUD for employment in a TTCM-assisted SDMA-OFDM scheme.

In Section 4.2.1 we provided a system overview of the proposed GA-assisted TTCM-MMSE-SDMA-OFDM system. The antenna-specific optimization metric of Equation (4.3) designed for the proposed GA MUD was derived in Section 4.2.2.1 from that of the optimum Maximum Likelihood (ML) MUD. Moreover, in order to solve the decision conflict resulting from the P number of antenna-specific metrics, a joint metric of Equation (4.6) was employed in the GA MUD. Section 4.2.2.2 outlined the operation process of the concatenated MMSE-GA MUD, while its performance was evaluated in Section 4.2.3, where the GA-based schemes were shown to be capable of achieving a near-optimum performance. Additionally, a complexity comparison between the proposed GA MUD and the optimum ML MUD was provided in Section 4.2.4, where we showed that the complexity of the GA MUD was significantly lower than that of the ML MUD.

In order to further enhance the achievable performance of the TTCM-assisted MMSE-GA-SDMA-OFDM system, an improved GA MUD was proposed in Section 4.3. This was discussed in two steps. Firstly, we proposed the novel Biased Q-function Based Mutation (BQM) scheme in Section 4.3.1. This was constituted by a review of the conventional Uniform Mutation (UM) scheme in Section 4.3.1.1 and the detailed explanation of the BQM mechanism in Section 4.3.1.2. The proposed BQM-aided GA MUD exploits an effective mutation strategy, which significantly improves the mutation efficiency so that the GA's search space can be substantially compressed. Hence, the BQM-aided GA MUD is capable of achieving a better performance in comparison to its UM-aided counterpart, especially at high SNRs or high user loads, as evidenced by the simulation results given in Section 4.3.1.3. Furthermore, in Section 4.3.1.2.2 we pointed out that the BQM scheme can be readily simplified to the Closest-Neighbour Uniform Mutation (CNUM) scheme, which only considers a subset of all the theoretically possible mutation target symbols during the mutation process. The CNUM-related transition probability values associated with different modems were summarized in Table 4.4. As a result, the BQM-induced search space can be further reduced by the CNUM scheme without significantly degrading the achievable performance.

Secondly, an Iterative GA (IGA) aided MUD was introduced in Section 4.3.2. The theoretical foundations of the IGA MUD were presented in Section 4.3.2.1, where we characterized the IGA framework as well as its optimization potential. Specifically, the IGA MUD is ca-

pable of exploiting the benefits accruing both from improved TTCM-decoded initial symbol estimates and from the embedded two-dimensional joint optimization invoked in the codeword domain as well as the in frequency domain, as illustrated in Figure 4.15. From the numerical results provided in Section 4.3.2.2, the combined BQM-IGA aided system was found to give the best performance in all scenarios considered, while maintaining a modest computational complexity. More specifically, the underloaded and fully-loaded scenarios were first investigated in Section 4.3.2.2.1, where the number of users was assumed to be less than or equal to the number of receiver antenna elements. In low-throughput fully-loaded scenarios, for example in a six-user system employing a 4QAM modem, a two-iteration BQM-IGA MUD associated with $X = 20$ and $Y = 5$ was capable of achieving the same performance as the optimum ML-aided system at a complexity of 200, which is only about 50% and 5% of the MUD-related complexity imposed by the conventional UM-aided single-iteration IGA MUD and by the optimum ML MUD, respectively. On the other hand, in high-throughput six-user systems where for example a 16QAM modem was employed, the UM-aided GA or IGA MUDs suffered from a high residual error floor even when exploiting the iterative framework. By contrast, a two-iteration BQM-IGA MUD associated with $X = 40$ and $Y = 5$ achieved an E_b/N_0 gain of about 7dB over the MMSE MUD benchmarker at the BER of 10^{-5}.

Moreover, in Section 4.3.2.2.2 we demonstrated that the proposed BQM-IGA MUD is capable of providing a near-optimum performance even in the so-called overloaded scenarios, where the number of accommodated users is higher than the number of receiver antenna elements, while many conventional detection techniques suffer from an excessively high error floor. For instance, when we had $L = 8$ users and $P = 6$ receivers in Figure 4.20, the two-iteration based BQM-IGA MUD reduced the BER recorded at an E_b/N_0 value of 3dB by four orders of magnitude in comparison to the classic MMSE MUD aided benchmark system. This high robustness of the BQM-IGA MUD was achieved, since the high MUI experienced in overloaded scenarios was effectively suppressed. Moreover, the associated E_b/N_0 gain was attained at a modest complexity of 400 objective function evaluations, which is only 0.00238% of the excessive complexity imposed by the ML MUD that is prohibited from simulations in this case. As a further investigation, we demonstrated in Section 4.3.2.2.3 that the proposed system was capable of achieving a satisfactory performance even in conjunction with imperfect channel information.

In Section 4.3.3, a complexity analysis of the proposed BQM-IGA scheme was carried out, where we concluded that the complexity of the proposed detection scheme is only moderately higher than that imposed by the linear MMSE MUD, and is substantially lower than that imposed by the optimum ML MUD, as shown in Figures 4.27 and 4.28. We also showed that in both the fully-loaded scenario of Sections 4.3.1.3.2 and the overloaded scenario of 4.3.2.2.2.2

the complexity of the BQM approach can be further reduced by employing its simplified version, namely the CNUM scheme, at the cost of a slightly degraded system performance. Additionally, in Table 4.6 we further demonstrated the attractive performance-versus-complexity balance of the BQM-IGA scheme, which reduced the BER by up to five orders of magnitude in comparison to the MMSE MUD at the cost of only a moderate complexity.

Note that the system parameters of the IGA framework, such as the number of TTCM iterations, the number of IGA MUD iterations and the GA-related parameter settings, are all readily configurable, enabling us to strike an attractive tradeoff between the achievable performance and the complexity imposed. For specific scenarios, the TTCM scheme used in the system can also be conveniently substituted by other FEC schemes, for example the TC codes. Therefore, the facility provided by the proposed IGA MUD may make it possible to applications in multi-mode terminals, where good performance, low complexity and easy flexibility are all important criterions. It is also worth pointing out that the proposed BQM-aided IGA MUD can be readily incorporated into the multi-user CDMA systems, for example those of [45]. In this case, the initial detected signal supplied to the GA MUD for creating the first GA population is provided by the bank of matched filters installed at the CDMA BS, rather than by the MMSE MUD. However, the BQM scheme may remain unchanged.

7.1.5 Chapter 5

As we have seen in Chapter 4, in the so-called overloaded scenarios, the classic MMSE MUD results in an excessive residual BER, since the grade of freedom becomes insufficiently high. However, the GA-based MUDs are capable of supporting a higher number of users than the MMSE MUD. Furthermore, with the aid of a new Slow Frequency-Hopping (SFH) type technique, more users can be accommodated by the SDMA-OFDM system. This constituted our main objective in Chapter 5, where we proposed a TTCM-assisted SDMA-OFDM system employing the MMSE-IGA MUD of Chapter 4 with the aid of both Direct-Sequence Spreading (DSS) and the so-called Slow SubCarrier-Hopping (SSCH) techniques.

Firstly, the conventional SDMA-OFDM systems were briefly reviewed in Section 5.1, where its two disadvantages were identified. On one hand, conventional SDMA-OFDM is incapable of efficiently exploiting frequency diversity, because all the users simultaneously share the entire bandwidth for their own communications. On the other hand, in conventional SDMA-OFDM systems supporting a high number of bandwidth-sharing users will result in a high MUI across the entire bandwidth, inevitably degrading all users' performance. Against this background, in Section 5.2 we introduced the concept of hybrid SFH/SDMA-OFDM as well as the proposed SSCH/SDMA-OFDM schemes and discussed their potential benefits, aiming for finding an effective solution to the above-mentioned problems. In Section 5.3 a comparison

of conventional SDMA-OFDM, SFH/SDMA-OFDM and SSCH/SDMA-OFDM systems in terms of their frequency resource allocation strategies was given, where the SSCH scheme was considered to have more advantages than the others, such as for example its higher efficiency in exploiting frequency diversity.

Our design of the proposed hybrid DSS/SSCH SDMA-OFDM system was detailed in Section 5.4. More specifically, first an overview of the proposed hybrid system was provided in Section 5.4.1, followed by the design of the transmitter and receiver presented in Sections 5.4.1.1 and 5.4.1.2, respectively. Figures 5.3 and 5.4 provided an example of the architecture of the DSS/SSCH transmitter and receiver, respectively. In Section 5.4.2, we analyzed two SSCH pattern assignment strategies, namely the Random SSCH (RSSCH) scheme of Section 5.4.2.1 and the Uniform SSCH (USSCH) scheme of Section 5.4.2.2, where the USSCH strategy was considered to be better. On one hand, in order to mitigate the MUI, the USSCH strategy disperses rather than concentrates each user's high-MUI subcarriers across the FD. On the other hand, for the sake of combatting FD fading, the USSCH scheme uniformly distributed the subcarriers activated by the same user across the entire bandwidth, rather than consecutively mapping them to a small fraction of the entire bandwidth, and thus making it possible to efficiently exploit frequency diversity. As a result of employing the USSCH technique of Section 5.4.2.2.1, the number of users activating each subcarrier becomes similar, which in turn minimizes the average MUI across the whole system bandwidth. Moreover, we pointed out in Section 5.4.2.4 that the USSCH patterns can be generated by offline pre-computation, since their choice is not based on any channel knowledge. This requires a substantially lower computational complexity than that imposed by other adaptive algorithms exploiting real-time channel knowledge. The acquired patterns can also be reused according to pre-defined reuse time intervals, which should be sufficiently long for ensuring an efficient exploitation of frequency diversity. Additionally, for the sake of providing an insight into the hybrid DSS/SSCH SDMA-OFDM system, in Section 5.4.3 the DSS despreading and SSCH demapping operations invoked at the SDMA receiver were presented, followed by the discussion of the multi-user detection process in the context of the hybrid system in Section 5.4.4.

Section 5.5 compared the simulation results generated by the proposed DSS/SSCH SDMA-OFDM system to those of various other SDMA-OFDM systems. In Section 5.5.1, the performances of the DSS and/or SSCH aided SDMA-OFDM systems were compared, when employing either the classic MMSE MUD discussed in Chapter 3 or the MMSE-IGA MUD proposed in Chapter 4. More specifically, it was shown in Figure 5.8 that in the moderately overloaded scenario associated with a total system throughput of $B_{\mathrm{T}} = 5120$ bits per OFDM symbol, most of the MUI encountered can be effectively suppressed by the MMSE-IGA MUD, while the overloaded MMSE MUD results in a high error floor. This result achieved in the context

of the DSS/SSCH SDMA-OFDM system was consistent with our findings in Chapter 4, where the performance advantages of the MMSE-IGA MUD have been recognized.

In Section 5.5.2, we further compared the performances of various hybrid SDMA-OFDM as well as conventional SDMA-OFDM systems. More specifically, a moderately overloaded scenario was first considered in Section 5.5.2.1. It was observed that the Random SFH (RSFH), the Uniform SFH (USFH) and the RSSCH aided schemes suffered from the employment of random hopping patterns that resulted in an increased average BER owing to the high MUI encountered at the subcarriers or sub-bands activated by an excessive number of users. By contrast, the schemes exploiting the uniform patterns generated by the algorithm of Section 5.4.2.2 were capable of providing an improved performance, as shown in Figure 5.9.

Furthermore, we pointed out that the proposed uniform pattern assignment algorithm is capable of providing more benefits in the scenarios associated with a higher throughput. This argument was validated in Section 5.5.2.2, where a highly overloaded scenario corresponding to a total system throughput of $B_{\mathrm{T}} = 6144$ bits per OFDM symbol was considered. It was shown in Figure 5.10 that the USFH, the USSCH and the hybrid DSS/USSCH aided systems were capable of achieving a significantly better performance in comparison to the conventional SDMA-OFDM, the DSS/SDMA-OFDM as well as the RSFH/RSSCH aided SDMA-OFDM systems, while the USSCH/SDMA-OFDM system was found to be the best option. The superior performance of the USSCH scheme was attributed to its specific characteristics, which successfully suppressed the MUI and thus eliminated the associated error floor. For example, we observed in Figure 5.10 that at an E_b/N_0 value of 10dB, the USSCH/SDMA-OFDM system reduced the BER by about two, three and four orders of magnitude in comparison to the conventional SDMA-OFDM, the RSSCH/SDMA-OFDM and the RSFH/SDMA-OFDM systems, respectively. We also concluded that the frequency diversity benefits achieved by USSCH may be more significant than those of the time diversity attained by DSS, since the hybrid DSS/USSCH SDMA-OFDM system attained a performance between those of the USSCH/SDMA-OFDM and the DSS/SDMA-OFDM systems, while the DSS/SDMA-OFDM scheme achieved a similar performance to that of the conventional SDMA-OFDM system. This suggests that the fixed-bandwidth hybrid system should avoid using long DSS codes that result in a wider subcarrier bandwidth, so that a sufficiently high number of $Q > K$ subcarriers becomes available for the sake of maintaining a sufficiently high frequency diversity.

The proposed USSCH scheme's high robustness against MUI was further confirmed by Figures 5.11 and 5.12, where the USSCH/SDMA-OFDM system exhibited the best BER versus total system throughput performance as well as the best maximum total system throughput versus E_b/N_0 performance among the various SDMA-OFDM arrangements, respectively. For instance, as shown in Figure 5.12, at the E_b/N_0 value of 12dB, a capacity increase of about 4%,

13% and 44% was achieved by the USSCH scheme compared to the USFH, the RSSCH and the RSFH arrangement at the target BER of 10^{-3}, while 4%, 14% and 78% at the BER of 10^{-5}, respectively. In Section 5.5.4, we demonstrated that the proposed hybrid system is capable of achieving an acceptable performance even without accurate channel knowledge. Finally, we pointed out that the superior performance of the USSCH-aided SDMA-OFDM system is achieved at a similar complexity to that of the conventional SDMA-OFDM arrangement, since the additional computational complexity imposed by the USSCH algorithm manifests itself in terms of offline pre-computation.

The capability of effectively exploiting frequency diversity and suppressing high MUI renders the channel-coded USSCH technique an attractive design option, lending a beneficial flexibility to practical applications. Furthermore, the USSCH/SDMA-OFDM scheme can be readily extended to a variable-rate system offering a high grade of flexibility required by future wireless multimedia services, supporting variable bit rates and different QoS requirements. Each user may activate a different number of subcarriers, depending on the type of service to be delivered or the bit rate to be supported. In such scenarios, the USSCH algorithm of Section 5.4.2.2 can be modified by taking into account the different rates. Moreover, in SSCH-based systems the different subcarriers do not have to be contiguously allocated, which is a further attractive property, especially in the scenarios where several systems operated by different service providers have to coexist and/or fractional bandwidths have to be exploited. In addition, the different types of hybrid SFH/SSCH assisted SDMA-OFDM systems can be readily implemented by exploiting different number of sub-bands having different bandwidths, depending on the specific system requirements.

7.1.6 Chapter 6

The assumption of perfect channel estimation has been used in most of the previous chapters for the sake of simplifying the constraints. However, in practical MIMO OFDM systems accurate channel estimation is required at the receiver for invoking both coherent demodulation and interference cancellation. This task is more challenging than that in the SISO scenario, owing to an increased number of independent transmitter-receiver channel links as well as an increased interference level, as a result of employing multiple transmitter antennas. Aiming for overcoming the channel estimation challenge in MIMO OFDM systems, in Chapter 6 we proposed a GA-assisted iterative Joint Channel Estimation and Multi-User Detection (GA-JCEMUD) scheme, which constitutes an attractive and effective solution to this problem.

In Section 6.1, various channel estimation approaches designed for MIMO OFDM were outlined, where we pointed out that none of the methods proposed for the BLAST or SDMA type multi-user MIMO OFDM systems in the open literature allowed the number of users to

exceed that of the receiver antennas, which we refer to as an overloaded scenario, because the corresponding singular channel matrix results in an insufficient degree of freedom at the detector. Explicitly, in this overloaded scenario channel estimation becomes more challenging, especially in the context of decision-directed type channel estimators which are more vulnerable to error propagations. Against this background, we proposed an iterative joint channel estimation and symbol detection scheme benefitting from the GA 's optimization power, which was illustrated in Figure 6.1 of Section 6.2. A full discussion of the proposed iterative GA-JCEMUD approach was provided in Section 6.3, where the structure of the GA-JCEMUD was detailed in Figure 6.2. The joint optimization method first uses pilot OFDM symbols for generating initial Frequency-Domain CHannel Transfer Function (FD-CHTF) estimates, which are then improved by the time-domain filters, as elaborated on in Section 6.3.1. The improved channel estimates are used for assisting the Optimized Hierarchy Reduced Search Algorithm (OHRSA) of Section 6.3.2 in invoking a first-stage multi-user detection. The initially detected user signals and the FD-CHTF estimates associated with the previous OFDM symbol duration are then forwarded to the proposed GA-JCEMUD printed in the grey block of Figure 6.2 for jointly optimizing the estimates of both the FD-CHTFs and multi-user data symbols.

The GA-aided joint optimization process was detailed in Section 6.3.3. More specifically, we outlined the mathematical representation of the GA individuals according to the MIMO channel's structure in Section 6.3.3.1 and described the initialization of the joint optimization in Section 6.3.3.2. Furthermore, since the data symbols belong to the discrete legitimate constellation symbol set $\mathcal{M}_c$, while the FD-CHTFs are continuous-valued and can be potentially infinite across the complex plane $\mathbb{C}$, separate cross-over/mutation methods have to invoked for the symbol chromosome and the channel chromosome, as discussed in Sections 6.3.3.3.1 and 6.3.3.3.2. Additionally, in order to overcome the limitations imposed by the conventional GA-aided MUDs, which can only provide single-individual based hard-decoded symbol estimates, a new algorithm was derived in Section 6.3.3.4 for assisting the GA in generating soft outputs based on the entire population, where we also argued that the proposed GA generating the above-mentioned population-based soft outputs imposes only a modest complexity increase in comparison to its conventional hard-decision aided individual-based counterparts.

In Section 6.4 the numerical results generated by computer simulations were provided. As a preliminary investigation, in Section 6.4.1 we first identified the effect of the maximum mutation step size λ_{max} used in the GA-JCEMUD. It was shown in Figures 6.3 and 6.4 that the choice of λ_{max} has a significant effect on the system's performance, especially in high-SNR scenarios. In order to achieve the best possible performance, typically a higher λ_{max} value is required, when a higher OFDM-symbol-normalized Doppler frequency F_D is encountered, so

that the rapid changes of the channel fades can be successfully captured by the GA-JCEMUD. Based on Figure 6.4, the recommended values of λ_{max} in conjunction with different values of F_D in terms of achieving the best attainable BER performance can be identified. In Figure 6.5 of Section 6.4.2, the effect of different Doppler frequencies on the proposed scheme was evaluated, where it was noticed that the performances of both the uncoded and coded GA-JCEMUD aided systems degraded, as F_D was increased. Nonetheless, the proposed GA-JCEMUD-aided SDMA-OFDM system using a modest pilot overhead of $\epsilon = 2.5\%$ was capable of achieving a performance close to the perfect-CSI aided optimum ML MUD at $F_D = 0.001$, as seen in Figure 6.5, while the system employing the MMSE MUD completely failed even with the aid of perfect CSI. Furthermore, it was shown in Section 6.4.3 that the system's performance can be improved by invoking a higher number of GA-JCEMUD iterations, both with or without channel coding. Observe in Figure 6.7 that at a SNR value of about 13dB, the GA-JCEMUD using $\epsilon = 2.5\%$ pilot overhead approached the best-case FD-CHTF estimation MSE performance associated with $\epsilon = 100\%$. In an effort to investigate the effect of the pilot overhead ϵ, we argued that a satisfactory performance can be achieved with the aid of a pilot overhead as low as $\epsilon = 1.5 \sim 2.5\%$, as evidenced by Figure 6.8 of Section 6.4.4.

For the sake of further evaluating the benefits of the proposed joint optimization approach, in Section 6.4.5 we compared the performances of the GA-JCEMUD and its counterpart, namely the GACE-OHRSA-MUD, which serially concatenates the OHRSA MUD with the stand-alone GA-aided channel estimator. It was shown in Figure 6.9 that the GA-JCEMUD outperformed the GACE-OHRSA-MUD, especially in high-Doppler scenarios. This demonstrates the superiority of the joint optimization mechanism over conventional 'serially-concatenated' detection architectures. In Section 6.4.6, the merits of the proposed soft GA-JCEMUD scheme were identified in terms of its ability of providing soft outputs. Observe in Figure 6.10 that with the advent of FEC codes, the proposed population-based soft-decoded GA was capable of significantly outperforming the conventional individual-based hard-decoded GA, especially in high-Doppler scenarios, since it exhibited a higher robustness against fast fading channels than the conventional GAs. Last but not least, in Section 6.4.7 we examined the robustness of the GA-JCEMUD in MIMO scenarios. As portrayed in Figure 6.11, the proposed iterative GA-JCEMUD was capable of simultaneously capturing the fading envelope changes of each individual user-receiver link, regardless of its instantaneous fading envelope value, and thus achieving an equally good performance over all the user-receiver links. This result potently demonstrates the robustness of the GA-JCEMUD in MIMO scenarios.

7.2 Suggestions for Future Research

In this section, based on the work reported in this thesis, a few suggestions for future research are summarized.

7.2.1 Optimization of the GA's Configuration

The GA-based MUDs have found applications in diverse SDMA-OFDM systems investigated in this thesis. It is worth pointing out that the proposed GAs may be further improved in various ways. On one hand, its operators and parameters are all tunable, implying that the configurations we have invoked may not necessarily be optimum. For example, the value of the mutation probability p_m can be adapted according to:

- The number of users. A higher value of p_m can be used when more users' signals have to be detected, which may increase the chances of finding the optimum solution.
- The GA's generation index. During the early generations, p_m can be set to a high value for assisting the GA in identifying the more promising search branches. As the search process progresses, p_m can be reduced for the sake of achieving a better local fine-resolution of the search region.

The maximum mutation step size λ_{max} of the GA-JCEMUD of Chapter 6 can also be adjusted adaptively in accordance with the Doppler frequency, as discussed in Section 6.3.3.3.2. Other GA parameter control methods, for example those of [333], may also be employed for optimizing the GA's configurations.

On the other hand, in the context of generating the GA's soft output, in this thesis we only exploited the individuals of the final generation for calculating the soft information. However, a performance improvement may be achieved by introducing an 'individual log', which stores the OSs of all meritorious individuals throughout all generations and thus assists in improving the reliability of the GA's soft output.

Additionally, the GA individual's symbol chromosome, which consists of the multiple users' hard-decoded symbol estimates, may also be represented by the soft bit estimates, enabling the GA to benefit from the soft information provided by the channel decoders during the external iterative processing. This is expected to improve the performance of the iterative GAs, such as the IGA MUD of Section 4.3.2 and the GA-JCEMUD of Chapter 6.

7.2.2 Enhanced FD-CHTF Estimation

While the proposed GA-JCEMUD scheme of Chapter 6 uses the previous FD-CHTF estimates as a reference for the current FD-CHTF estimates, its mutation operator, namely the step mutation of Section 6.3.3.3.2, invokes the mutation process based on a uniform probability for all directions around the original FD-CHTF to be mutated, as implied by Equation (6.26). In other words, it does not exploit the 'directional' information of the time-domain correlation between the FD-CHTFs associated with the subcarriers of consecutive OFDM symbols. Here we recall Figure 6.11, which compared the real/imaginary values' evolution of the perfect as well as the GA-estimated FD-CHTFs. In the same spirit, an example of the above-mentioned directional correlation is illustrated in Figure 7.1, where the virtual contours of $n = 1, \cdots, 5$ OFDM symbols observed in five consecutive OFDM symbol durations at a specific user-receiver channel link are portrayed, which are constituted by the different dashed curves. Similarly to Figure 6.11, each black dot seen in Figure 7.1 represents the FD-CHTF at a specific subcarrier. The solid curves with arrows show the direction of evolution for the FD-CHTFs at each subcarrier in the context of the time domain.

Therefore, by borrowing the idea of the BQM approach proposed in Section 4.3.1.2, it would be beneficial to design a mutation operator, which is capable of tracking the direction of the FD-CHTF variation at each subcarrier in consecutive OFDM symbol durations. Similarly, the directional frequency-domain correlation between consecutive subcarriers in the same OFDM symbol can also be exploited. The mutation operator combining both the time-domain and the frequency-domain direction-tracking strategies may be expected to improve the performance of the GA-JCEMUD scheme.

Moreover, the joint channel estimation and symbol detection approach can be further enhanced by introducing a Soft-Input Soft-Output (SInSOu) mechanism. More specifically, not only the GA-optimized FD-CHTF estimates but also the GA-optimized symbol estimates can be forwarded to the OHRSA MUD of Section 6.3.2 for assisting in the initial symbol detection invoked in the next iteration. In this way the OHRSA MUD would be capable of benefitting from the GA in terms of both perspectives, thus improving the reliability of the initial symbol estimates, which in turn may be expected to result in a better overall system performance.

7.2.3 Radial Basis Function Assisted OFDM

Generally speaking, GAs belong to the family of Evolutionary Algorithms (EAs) [401, 402], which invokes the principles of natural evolution. With the aid of the advances in Artificial Intelligence (AI), a range of other problem-solving methods have also emerged. One of these

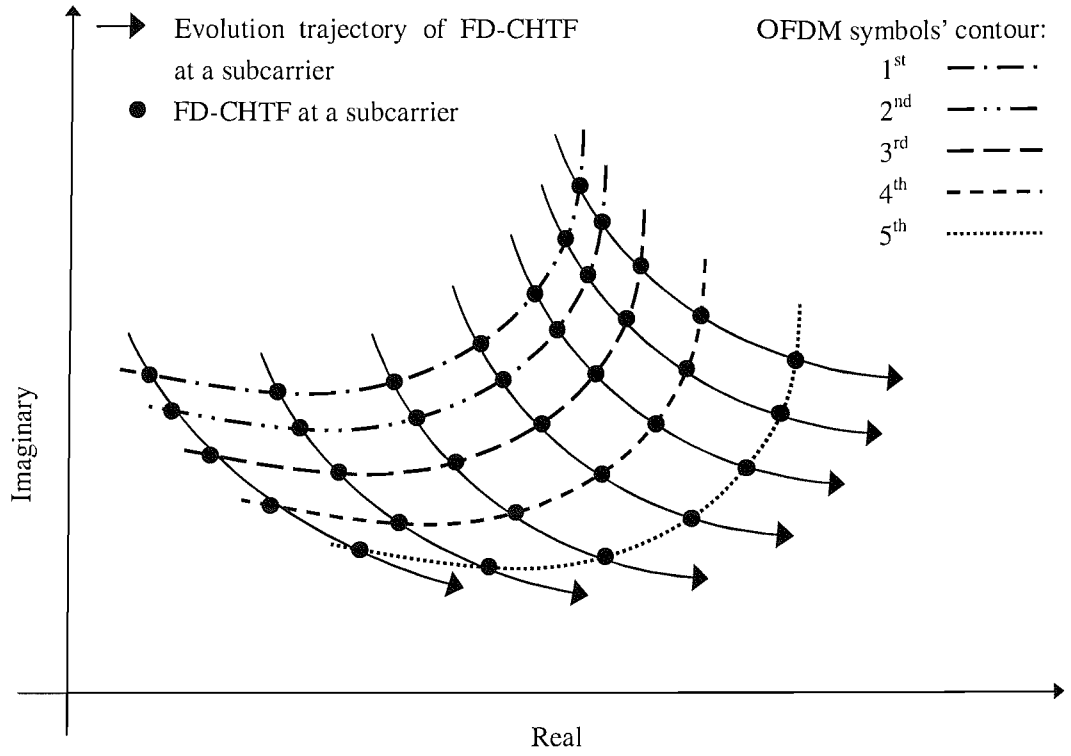

Figure 7.1: Illustration of the time-domain correlation of FD-CHTFs associated with $n = 1, \cdots, 5$ consecutive OFDM symbols at a specific user-receiver channel link. Similarly to Figure 6.11, each black dot represents the FD-CHTF at a specific subcarrier, while each of the five different dashed curves denotes the virtual contour of the corresponding OFDM symbol, respectively. The solid curves with arrows show the track and direction of the FD-CHTF variation at each subcarrier in the context of the time domain.

techniques is constituted by the family of Neural Networks (NNs) [403, 404], which is based on the models that mimick the operation of how biological neurons are connected in the human brain. Furthermore, EAs/GAs have been applied in constructing and training NNs in numerous research fields [397, 405, 406]. In the context of wireless communications, NNs also found employment in various fields, for example in channel equalization [407–409]. Moreover, NNs are also applicable to the field of multi-user detection. For example, the so-called Radial Basis Function (RBF) [407, 410, 411] based NNs have been proposed for multi-user detection in CDMA type systems [412–415]. However, hardly any research has been conducted in the context of RBF-assisted multi-user OFDM systems [416–419]. Explicitly, exploiting RBF with or without the aid of EAs/GAs for employment in OFDM, MIMO-OFDM, and SDMA-OFDM systems, especially for highly complicated nonlinear applications such as for example joint detection schemes, constitutes a wide research area. Alternatively, Minimum Bit Error Rate (MBER) type receivers [201, 420] may also be employed, which are capable of supporting up to twice the number of users in comparison to the classic MMSE MUD.

Appendix A

Appendix to Chapter 4

A.1 A Brief Introduction to Genetic Algorithms

The GAs [319–323] were first introduced by Holland [319] during the 1960s. Since then, a growing interest in GAs resulted in a rapid development in this area [320,421,422], since GAs have been shown to perform well in numerous robust global search and optimization problems, which may not be conveniently be solved by using traditional search methods.

In this section, we will briefly introduce the GAs in the context of multi-user SDMA-OFDM systems, in order to offer a better understanding of our proposed GA-based MUD of Chapter 4. Figure A.1 shows a flowchart of the GA MUD employed in our multi-user SDMA-OFDM system, while the actions of the GA-based search procedure during one generation are detailed in Figure A.2. Both of these figures will be referred to during our further discourse in this section.

Population Initialization At the beginning of the GA-based search, an initial *population* consisting X number of so-called *individuals* is created, each representing a possible solution of the optimization problem considered, either on a random basis or with the aid of *a priori* knowledge concerning the optimum solution. In the context of the SDMA-OFDM MUD, an individual is represented by a symbol vector containing L complex symbols, each of which belongs to one of the L number of users at the specific subcarrier considered. More specifically, the x^{th} individual of the y^{th} *generation* is expressed as:

$$\tilde{\mathbf{s}}_{(y,x)} = [\ \tilde{s}^{(1)}_{(y,x)},\ \tilde{s}^{(2)}_{(y,x)},\ \cdots,\ \tilde{s}^{(L)}_{(y,x)}\ ], \quad x = 1, \cdots, X;\ y = 1, \cdots, Y, \tag{A.1}$$

where $\tilde{s}^{(l)}_{(y,x)} \in \mathcal{M}_c$ denotes the l^{th} $(l = 1, \cdots, L)$ *gene* of the x^{th} individual, while $\mathcal{M}_c$ is the set containing the 2^m number of legitimate constellation symbols. For example, if the 4QAM modem constellation given in Figure A.3 is used, each gene $\tilde{s}^{(l)}_{(y,x)}$ of an individual

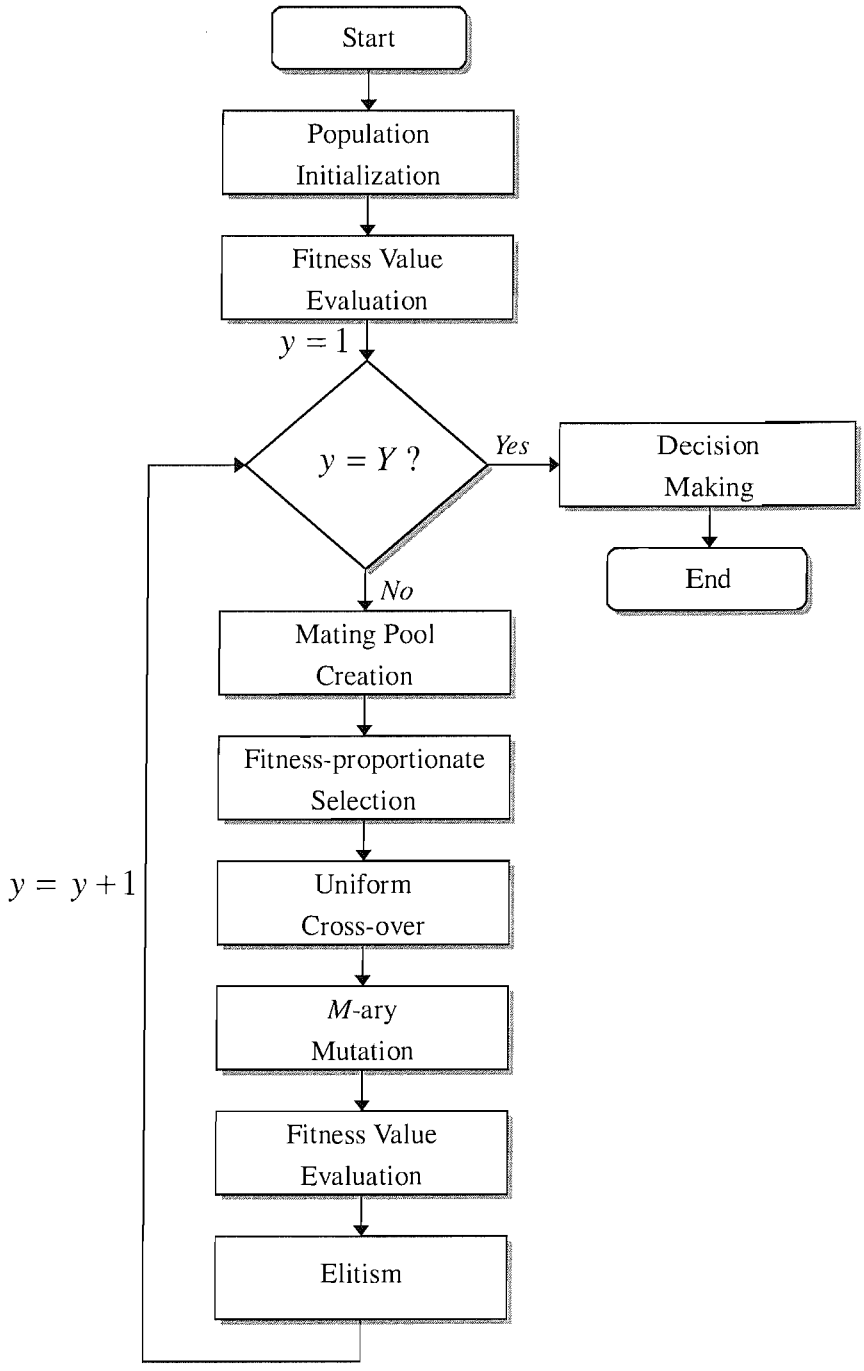

Figure A.1: The structure of the GA MUD used in the multi-user SDMA-OFDM system.

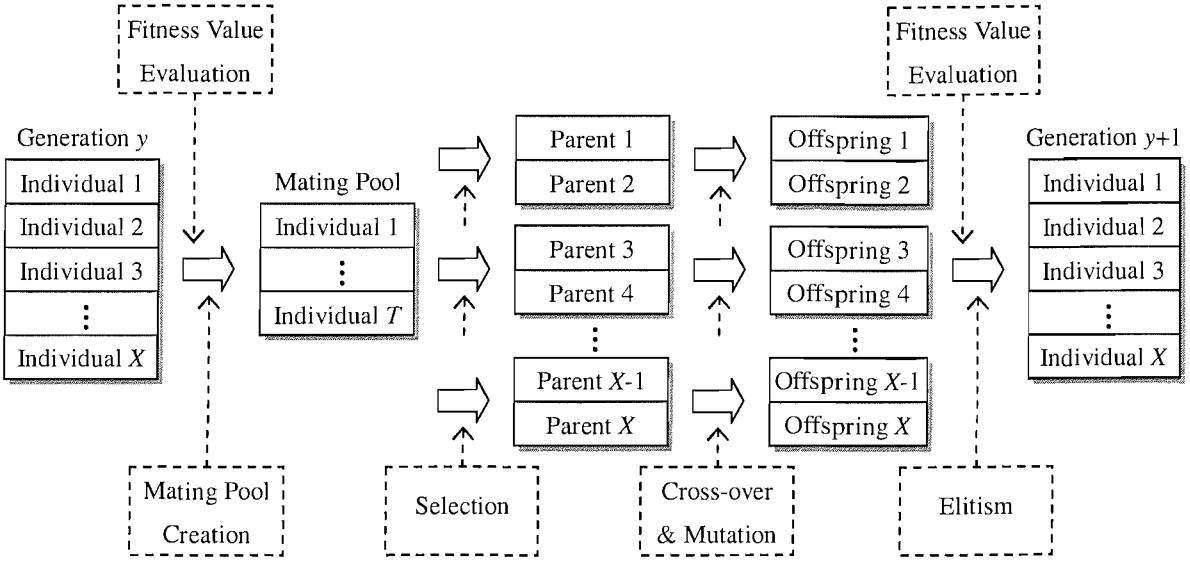

Figure A.2: The GA-based search procedure during one generation.

illustrated in Figure A.4, can be represented by the indices of the 4QAM constellation symbols, namely $\tilde{s}_{(y,x)}^{(l)} \doteq \{1, \cdots, 4\}$. For example, given $L = 6$ users, each employing 4QAM, the composite multi-user signal of each OFDM subcarrier may assume $4^6 = 4096$ possible symbol combinations. In this case the ML-aided MUD would have to find the most likely combination by invoking a full search of all the 4096 metric evaluations. By contrast, the GA-aided MUD typically finds this optimum solution by searching only a fraction of this search space. The population consisting of X number of individuals then forms the starting point of the optimization process, which is referred to as the $y = 1^{st}$ generation, as depicted in Figure A.2.

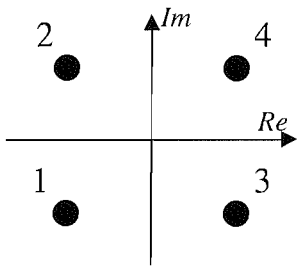

Figure A.3: The complex constellation symbols of a 4QAM modem, each of which corresponds to a gene of the L-gene GA individual.

Fitness Value Evaluation The GA's task is to find an individual, which is considered optimum or near-optimum in terms of minimizing the joint metric of Equation (4.6), which is based on the *Objective Function (OF)* given in Equation (4.3) in the context of a P-antenna SDMA-OFDM system. More explicitly, for each individual, an associated *Objective Score (OS)* can be derived by evaluating Equation (4.6). The OS is then converted to a

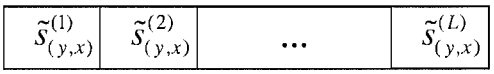

Figure A.4: An individual that contains L genes, each of which is one of the constellation symbols shown in Figure A.3.

corresponding *fitness* value, which indicates the fitness of the specific individual. This fitness calculation is carried out in the "Fitness Value Evaluation" block of Figure A.1.

Mating Pool Creation Based on the fitness values, T number of individuals that have the highest fitness values may be selected for creating the so-called *mating pool*, as shown in Figure A.2. However, for the SDMA-OFDM system, a better strategy of creating the mating pool is to follow the principle of *Pareto Optimality* [45, 320]. This strategy favours the so-called *non-dominated* individuals and ignores the so-called *dominated* individuals [45]. More specifically, the u^{th} L-symbol individual is considered to be dominated by the v^{th} individual, if we have [332]:

$$\begin{aligned} &\forall i \in \{1, \cdots, P\}: \ \Omega_i\left(\tilde{\mathbf{s}}_{(y,v)}\right) \leq \Omega_i\left(\tilde{\mathbf{s}}_{(y,u)}\right) \\ \wedge \ &\exists j \in \{1, \cdots, P\}: \ \Omega_j\left(\tilde{\mathbf{s}}_{(y,v)}\right) < \Omega_j\left(\tilde{\mathbf{s}}_{(y,u)}\right), \end{aligned} \tag{A.2}$$

where $\Omega_p(\cdot)$ is the OF associated with the p^{th} receiver antenna element, which is defined by Equation (4.3). If an individual is not dominated in the sense of Equation (A.2) by any other individuals in the population, then it is considered to be non-dominated. All the non-dominated individuals are then selected and placed in the mating pool, which will have a size of $2 < T \leq X$ [45].

Selection In order to evolve the population throughout the consecutive generations, the individuals in the mating pool are then selected as *parents* for producing *offspring*. The selection process is based on the so-called *fitness-proportionate* algorithm employed by the "Fitness-proportionate Selection" block of Figure A.1, which is widely used in the literature [423]. According to fitness-proportionate selection, each of the T number of individuals in the mating pool is first assigned a selection probability proportionate to its fitness value. More precisely, the individuals having higher fitness values will be assigned higher selection probabilities, based on which $X/2$ pairs of parents are selected, as illustrated in Figure A.2. Moreover, during the selection process the so-called *incest prevention* [424] technique can be invoked, which requires that the two individuals selected to form a pair of parents are different. This can effectively prevent the GA from premature convergence.

Cross-over For each pair of the $X/2$ selected parents, a genetic operation referred to as *cross-over* [321] is invoked, as shown in Figure A.2. The cross-over operation is a process during which some of the genes of a parent are exchanged with those of the other

parent, thus creating two offspring. In our proposed GA MUD, the well-known *uniform cross-over* [425] scheme corresponding to the "Uniform Cross-over" block of Figure A.1 is employed, as illustrated in Figure A.5. Suppose we have $L = 6$ users, hence each individual will have 6 genes accordingly, as portrayed in Figure A.5. Two individuals are then selected as parents from the mating pool, followed by the creation of a binary cross-over mask, which contains $L = 6$ randomly generated 1s and 0s. The genes, represented for example by the indices of the 4QAM constellation symbols given in Figure A.3, are then exchanged between the selected pair of parents at positions associated with a 1 in the cross-over mask, giving birth of two offspring.

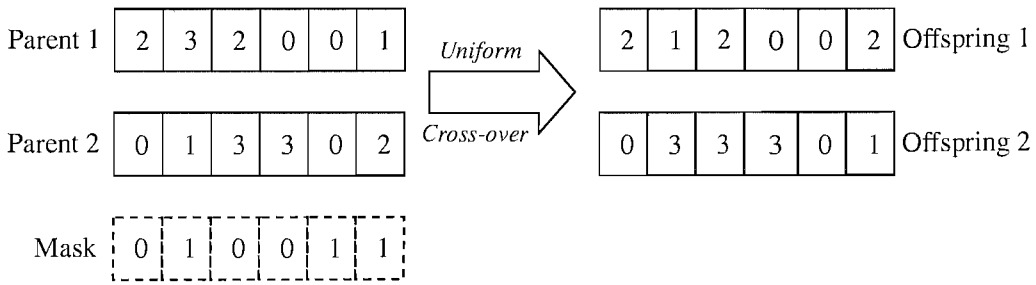

Figure A.5: An example of the uniform cross-over operation.

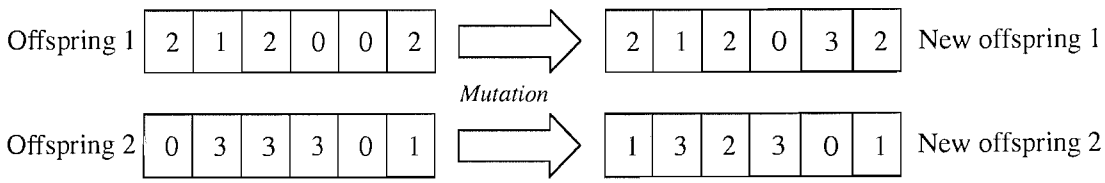

Figure A.6: An example of the mutation operation.

Mutation After the cross-over operation is applied to each pair of parents, X number of offspring are produced, which are then subjected to the so-called *mutation* [321] operation and some of the offspring's genes may be changed. More specifically, any gene of an offspring may be mutated to another legitimate gene under the control of the specific mutation strategy employed. Furthermore, the activation of the mutation process is governed by the so-called mutation probability p_m. An example of the mutation procedure following the cross-over operation of Figure A.5 is plotted in Figure A.6. Therefore, following the cross-over and mutation blocks illustrated in Figure A.1, the new population consists of X number of mutated offspring. It is worth pointing out that the mutation operation is critical to the success of the genetic evolution, since it ensures that sufficient diversity is maintained in the population, thus preventing the GA's search from being trapped at local optima.

Elitism While the cross-over and mutation operations offer the opportunity of improving

the average fitness of the population, they do not guarantee that each of the offspring is better than their parents in terms of their fitness values. In other words, the better individuals associated with the higher fitness values found in the y^{th} generation may not be retained in the $(y+1)^{th}$ generation. For the sake of ensuring that the high-fitness individuals are not lost from generation to generation, the best or a few of the best individuals of the parents population are copied into the new population, replacing the worst offspring. This technique is known as *elitism* [321], as illustrated in Figures A.1 and A.2.

The genetic operation cycle mentioned above forms the basis of the GA-aided optimization, yielding an offspring population having an improved average fitness. This evolution continues, until the generation index reaches its maximum. Then the operation of the GA is terminated and the highest-fitness individual of the last population will be considered as the final solution, which is the specific length-L symbol vector that contains the detected transmitted symbols of the L users at the specific OFDM subcarrier considered. If the population size X and/or the number of generations Y are sufficiently high, the GA's final solution approaches the optimum [45].

A.2 Normalization of the Mutation-Induced Transition Probability

Without loss of generality, let us first provide the following definitions:

$\mathcal{M}_c$: The set containing the 2^m number of legitimate constellation symbols $\hat{s}_i^{(l)}$ $(i = 1, \cdots, 2^m)$.

$\hat{s}_1^{(l)}$: The original gene (constellation symbol) of the l^{th} user, which is subjected to mutation.

$\hat{s}_2^{(l)}$: The target gene (constellation symbol) of the l^{th} user, which is the destination of mutation.

A: The event that the *current* gene is $\hat{s}_1^{(l)}$.

B: The event that the *next* gene is **not** $\hat{s}_1^{(l)}$.

C: The event that the *next* gene is $\hat{s}_2^{(l)}$.

According to conditional probability theory [335], we have:

$$\begin{cases} P(ABC) = P(A) \cdot P(B|A) \cdot P(C|AB) \\ P(ABC) = P(A) \cdot P(BC|A). \end{cases} \tag{A.3}$$

Based on Equation (A.3), the *normalized transition probability* $\tilde{p}_{mt}^{(12)}$ can be derived with the aid of the 2D transition probabilities:

$$\begin{aligned}
\tilde{p}_{mt}^{(12)} &= P(C|AB) && \text{(A.4)}\\
&= \frac{P(BC|A)}{P(B|A)} && \text{(A.5)}\\
&= \frac{P(C|A)}{P(B|A)} && \text{(A.6)}\\
&= \frac{p_{mt}^{(12)}}{\sum_{j=2}^{2^m} p_{mt}^{(1j)}} && \text{(A.7)}\\
&= \frac{p_{mt}^{(12)}}{1 - p_{mt}^{(11)}}, && \text{(A.8)}
\end{aligned}$$

where $p_{mt}^{(12)}$ and $p_{mt}^{(11)}$ are the corresponding 2D transition probabilities, which are given for example by Equations (4.16) and (4.17) in the context of 4QAM, respectively. Similarly, we can derive the normalized transition probabilities $\tilde{p}_{mt}^{(ij)}$ for all constellation symbols $\hat{s}_i^{(l)}$ ($i = 1, \cdots, 2^m$) of $\mathcal{M}_c$, although these calculations are not included here for reasons of space economy.

Glossary

E_b/N_0	Ratio of bit energy to noise power spectral density, 31
μGA	Micro Genetic Algorithm, 211
16QAM	16-level Quadrature Amplitude Modulation, 31
1D	One-Dimensional, 139
2D	Two-Dimensional, 140
3G	Third Generation, 8
4G	Fourth Generation, 5
64QAM	64-level Quadrature Amplitude Modulation, 33
8PSK	8-level Phase-Shift Keying, 31
ADC	Analogue-to-Digital Converter, 68
ADSL	Asymmetric Digital Subscriber Line, 2
AI	Artificial Intelligence, 255
AMPS	Advanced Mobile Phone Service, 15
ANSI	American National Standards Institute, 2
AWGN	Additive White Gaussian Noise, 67, 88
BCH	Bose-Chaudhuri-Hocquenghem, a class of FEC codes, 59
BER	Bit Error Ratio, 30
BICM	Bit-Interleaved Coded Modulation, 66, 87
BICM-ID	Iteratively Decoded Bit-Interleaved Coded Modulation, 66, 87
BLAST	Bell Labs Layered Space-Time architecture, 21
BPS	Bits Per Symbol, 30, 127
BPSK	Binary Phase-Shift Keying, 30
BQM	Biased Q-function Based Mutation, 139
BRAN	Broadband Radio Access Network, 2

BS	Base Station, 4, 86
BWMA	Broadband Wireless Multiple Access, 171
CATV	Cable Television, 171
CC	Convolutional Codes, 59
CCI	Co-Channel Interference, 10
CDD	Cyclic Delay Diversity, 12
CDF	Cumulative Dstribution Function, 16
CDMA	Code Division Multiple Access, 3, 86
CFO	Carrier Frequency Offset, 12
CIR	Channel Impulse Response, 71, 86
ClOFDM	Clustered Orthogonal Frequency Division Multiplexing, 171
CLS	Constrained Least-Squares, 210
CM	Coded Modulation, 66, 87
CNUM	Closest-Neighbour Uniform Mutation, 143
COFDM	Coded Orthogonal Frequency Division Multiplexing, 4
COST207 HT	COST207 Hilly Terrain channel, 104
CSC	Cumulative Sub-Cost, 219
CSD	Complex Sphere Decoder, 217
CSI	Channel State Information, 160
CWER	CodeWord Error Ratio, 96
DAB	Digital Audio Broadcasting, 2
DAC	Digital-to-Analogue Converter, 68
DAPSK	Differential Amplitude and Phase-Shift Keying, 6
DFT	Discrete Fourier Transform, 3
DMT	Discrete MultiTone, 2
DS-CDMA	Direct-Sequence Code Division Multiple Access, 170
DSS	Direct-Sequence Spreading, 171
DSSS	Direct-Sequence Spread Spectrum, 2
DVB	Digital Video Broadcasting, 2
DVB-H	Digital Video Broadcasting for Handheld terminals, 2
DVB-T	Digital Video Broadcasting for Terrestrial television, 2
EA	Evolutionary Algorithm, 255
EM	Expectation Maximization, 12

ETSI	European Telecommunication Standard Institute, 2
FD	Frequency Domain, 172
FD-CHTF	Frequency-Domain CHannel Transfer Functions, 88, 209
FDMA	Frequency Division Multiple Access, 3
FEC	Forward Error Correction, 87
FFH	Fast Frequency-Hopping, 174
FFT	Fast Fourier Transform, 68, 90
FH	Frequency-Hopping, 169
FH/SSMA	Frequency-Hopped SSMA, 170
FHSS	Frequency-Hopping Spread Spectrum, 2
FIR	Finite Impulse Response, 15
GA	Genetic Algorithm, 125
GA-JCEMUD	Joint Channel Estimation and Multi-User Detection, 211
GACE-OHRSA-MUD	GA-based Channel Estimation assisted OHRSA Multi-User Detection, 234
GMD	Geometric Mean Decomposition, 12
HDSL	High-bit-rate Digital Subscriber Line, 2
HSDPA	High Speed Downlink Packet Access, 8
ICI	Inter-Carrier Interference, 118
IEEE	The Institute of Electrical and Electronics Engineers, 2
IFFT	Inverse Fast Fourier Transform, 68, 89
IGA	Iterative Genetic Algorithm, 149
ISI	Inter-Symbol Interference, 67, 104
IWHT	Inverse Walsh-Hadamard Transform, 90
LAN	Local Area Network, 2
LDPC	Low Density Parity Check, 27, 227
LLR	Log-Likelihood Ratio, 224
LPF	Low-Pass Filter, 68
LS	Least-Squares, 86
MAC	Medium Access Control, 16

MAP	Maximum-A-Posteriori, 26
MB-OFDM	MultiBand Orthogonal Frequency Division Multiplexing, 2
MBER	Minimum Bit Error Rate, 256
MC-CDMA	Multi-Carrier Code Division Multiple Access, 86
MD	M-Dimensional, 142
MIMO	Multiple-Input Multiple-Output, 1, 209
ML	Maximum Likelihood, 26
MLD	Maximum Likelihood Detection, 86
MMSE	Minimum Mean-Square Error, 86
MRC	Maximum Ratio Combining, 20
MS	Mobile Station, 13, 87
MSE	Mean-Square Error, 229
MUD	Multi-User Detection/Detector, 86
MUI	Multi-User Interference, 98, 156
NN	Neural Network, 256
O-QAM	Orthogonal Quadrature Amplitude Modulation, 5
OF	Objective Function, 128, 221
OFDM	Orthogonal Frequency Division Multiplexing, 1
OFDMA	Orthogonal Frequency Division Multiple Access, 171
OHRSA	Optimized Hierarchy Reduced Search Algorithm, 215
OS	Objective Score, 130, 221
PAPR	Peak-to-Average Power Ratio, 4
PIC	Parallel Interference Cancellation, 86
PSK	Phase-Shift Keying, 212
PSP	Per-Survivor Processing, 220
QAM	Quadrature Amplitude Modulation, 3
QoS	Quality-of-Service, 3
QPSK	Quadrature Phase-Shift Keying, 28
QRD-M	QR Decomposition combined with the M-algorithm, 125
RBF	Radial Basis Function, 256
RLS	Recursive Least-Squares, 93

RSFH	Random Slow Frequency-Hopping, 186
RSSCH	Random Slow SubCarrier-Hopping, 181
SCH	SubCarrier-Hopping, 171
SD	Sphere Decoder, 125
SDM	Space Division Multiplexing, 18
SDMA	Space Division Multiple Access, 9, 86
SFH	Slow Frequency-Hopping, 171
SIC	Successive Interference Cancellation, 86
SINR	Signal to Noise and Interference Ratio, 11
SInSOu	Soft-Input Soft-Output, 255
SISO	Single-Input Single-Output, 8, 172
SM	Step Mutation, 223
SNR	Signal-to-Noise Ratio, 32, 138
SOS	Second-Order Statistics, 210
SS	Spread-Spectrum, 171
SSCH	Slow SubCarrier-Hopping, 171
SSMA	Spread-Spectrum Multiple Access, 170
STBC	Space-Time Block Code, 21
STC	Space-Time Code, 1
STTC	Space-Time Trellis Code, 25
SWATM	Short Wireless Asynchronous Transfer Mode channel, 71, 93
TBCH	Turbo Bose-Chaudhuri-Hocquenghem codes, 59
TC	Turbo Convolutional codes, 38, 87
TCM	Trellis Coded Modulation, 66, 87
TD-CDM-OFDM	Time-Division Code-Division Multiplexing Orthogonal Frequency Division Multiplexing, 12
TD-SCDMA	Time-Division Synchronous Code Division Multiple Access, 12
TDMA	Time Division Multiple Access, 3
TOA	Time-of-Arrival, 210
TTCM	Turbo Trellis Coded Modulation, 66, 87
UM	Uniform Mutation, 138
UMTS	Universal Mobile Telecommunications System, 8
USFH	Uniform Slow Frequency-Hopping, 186

USSCH	Uniform Slow SubCarrier-Hopping, 171
UWB	Ultra WideBand, 1
V-BLAST	Vertical Bell Labs Layered Space-Time architecture, 125
VA	Viterbi Algorithm, 211
VDSL	Very-high-speed Digital Subscriber Line, 2
WATM	Wireless Asynchronous Transfer Mode, 2, 71
WCDMA	Wideband Code Division Multiple Access, 86
WHT	Walsh-Hadamard Transform, 87
WHTS	Walsh-Hadamard Transform Spreading, 87
WLAN	Wireless Local Area Network, 2
WMAN	Wireless Metropolitan Area Network, 2
WPAN	Wireless Personal Area Network, 2
ZF	Zero-Forcing, 11

List of Symbols

$(\cdot)[n,k]$	The indices indicating the k^{th} subcarrier of the n^{th} OFDM symbol, 88
$(\cdot)^T$	The transposition operation, 189
$(\cdot)^H$	Hermitian transpose, 90
$(\cdot)^*$	Complex conjugate, 217
$\Im$	The imaginary component of a complex number, 223
$\Re$	The real component of a complex number, 223
π	The ratio of the circumference of a circle to the diameter, 225
$\exp(\cdot)$	The exponential operation, 225
$\mathbf{A}^{(l)}$	The remaining user set for the l^{th} iteration of the subcarrier-to-user assignment process, 183
α_P	The user load of an L-user and P-receiver conventional SDMA system, 96
B_{T}	The overall system throughput in bits per OFDM symbol, 193
b_{l,m_B}	The $(m_B)^{th}$ bit of the l^{th} user's transmitted symbol, 224
$\hat{b}_s^{(l)}[n,k]$	The l^{th} user's detected soft bit, 215
$\hat{\mathbf{b}}_s^{(l)}$	The detected soft bit block of the l^{th} user, 212
$\mathbf{b}^{(l)}$	The information bit block of the l^{th} user, 212
$\mathbf{b}_s^{(l)}$	The coded bit block of the l^{th} user, 212
$\mathbb{C}$	The complex space, 220
$\mathbb{C}^{(x\times y)}$	The $(x \times y)$-dimensional complex space, 90, 219
$\mathrm{CC}(n,k,K)$	Convolutional codes with the number of input bits k, the number of coded bits n and the constraint length K, 60

$c_{g_l}(t)$ The DSS signature sequence assigned to the l^{th} user and associated with the g^{th} DSS group, 187

$\bar{\mathbf{c}}_{G_q}$ The $(1 \times L_q)$-dimensional DSS code vector, 189

$\check{\mathbf{c}}_{G_q}$ The $(G_q \times 1)$-dimensional DSS code vector, 189

$\mathbf{c}_g$ The spreading code sequence associated with the g^{th} DSS group, 189

$\mathbf{c}$ The user signature vector, 216

$\mathbf{c}^{(l)}$ the l^{th} user's code sequence, 216

$\mathbf{c}_{g_l}$ The DSS code vector for the l^{th} user in the g^{th} DSS group, 177

$\Delta^{(l)}_{p,(y,x)}[n,k]$ The random step size for the $(p,l)^{th}$ channel gene during step mutation associated with the x^{th} individual of the y^{th} generation, 223

ϵ The pilot overhead, 217

F_D The OFDM-symbol-normalized Doppler frequency, 226

f'_d Normalized Doppler frequency, 71

f_c Carrier frequency, 187

f_d Maximum Doppler frequency, 72

f_q Carrier frequency associated with the q^{th} sub-band, 173

$f_{(y,x)}$ The fitness value associated with the x^{th} individual of the y^{th} generation, 130

G The number of DSS user groups in a DSS/SSCH system, 177

G_q The total number of different DSS codes used by the users activating the q^{th} subcarrier, 188

$\Gamma_\tau(t)$ The rectangular pulse within the duration of $[0,\tau)$, 188

$H^{(l)}_p$ The FD-CHTF associated with the l^{th} user and the p^{th} receiver antenna element, 89

$H^{(l)}_{p,q}$ The FD-CHTF associated with the specific link between the l^{th} user and the p^{th} receiver at the q^{th} subcarrier, 188

$H^{(l)}_p[n,k]$ The true FD-CHTF associated with the channel link between the l^{th} user and the p^{th} receiver, 215

$\hat{H}^{(l)}_p[n,k]$ The improved *a postepriori* FD-CHTF estimate associated with the channel link between the l^{th} user and the p^{th} receiver, 215

$\mathbf{H}$	The FD-CHTF matrix, 88
$\mathbf{H}^{(l)}$	The FD-CHTF vector associated with the l^{th} user, 88
$\mathbf{H}_{g,q}^{(l)}$	The $(P \times 1)$-dimensional FD-CHTF vector associated with the transmission paths between the l^{th} user's transmitter antenna and each element of the P-element receiver antenna array, corresponding to the g^{th} DSS group at the q^{th} subcarrier, 191
$\mathbf{H}_p$	The p^{th} row of the FD-CHTF matrix $\mathbf{H}$, 128
$\mathbf{H}_{g,q}$	The $(P \times l_g)$-dimensional FD-CHTF matrix associated with the g^{th} DSS group at the q^{th} subcarrier, 191
$\mathbf{H}_{p,g,q}$	The p^{th} row of the FD-CHTF matrix $\mathbf{H}_{g,q}$ associated with the g^{th} DSS group at the q^{th} subcarrier, 191
$\mathbf{H}_p[n,k]$	The initial FD-CHTF estimate matrix associated with all the channel links between each user and the p^{th} receiver, 217
$\bar{\mathbf{H}}_{p,q}$	The L_q users' $(L_q \times L_q)$-dimensional diagonal FD-CHTF matrix associated with the q^{th} subcarrier at the p^{th} receiver, 189
$\bar{\mathbf{H}}_p[n,k]$	The diagonal FD-CHTF matrix associated with all the channel links between each user and the p^{th} receiver, 216
$\tilde{\mathbf{H}}[n,k]$	The trial FD-CHTF matrix of the GA-JCEMUD, 221
$\tilde{\mathbf{H}}_{(y,x)}[n,k]$	The FD-CHTF chromosome of the GA-JCEMUD individual associated with the x^{th} individual of the y^{th} generation, 220
$\tilde{H}_{p,(y,x)}^{(l)}[n,k]$	The $(p,l)^{th}$ channel gene of the GA-JCEMUD FD-CHTF chromosome associated with the x^{th} individual of the y^{th} generation, 220
$\tilde{H}_p^{(l)}[0,k]$	The initial FD-CHTF estimate associated with the channel link between the l^{th} user and the p^{th} receiver at the k^{th} subcarrier in the first OFDM symbol duration, 214
$\tilde{h}_p^{(l)}[n,k]$	The initial estimate of the CIR-related taps associated with the channel link between the l^{th} user and the p^{th} receiver, 214
$\mathbf{I}$	Identity matrix, 90
K_0	The range of CIR-related taps to be retained, 214
L	Number of simultaneous mobile users supported in a SDMA system, 87
L_q	The number of users that activate the q^{th} subcarrier, 188

$\mathcal{L}_{l,m_B}$ The LLR associated with the $(m_B)^{th}$ bit position of the l^{th} user's transmitted symbol, 224

$\Lambda_q^{(l)}(t)$ The subcarrier activation function, 187

l_g The number of users in the g^{th} DSS group, 188

λ_{max} The maximum mutation step size of the step mutation, 223

M_{WHT} The WHT block size, 91

$\mathcal{M}^L$ The set consisting of 2^{mL} number of $(L \times 1)$-dimensional trial vectors, 127

$\mathcal{M}_{l,m_B,b}^L$ The specific subset associated with the l^{th} user, which is constituted by those specific trial vectors, whose l^{th} element's $(m_B)^{th}$ bit has a value of b, 224

$\mathcal{M}_c$ The set containing the 2^m number of legitimate complex constellation points associated with the specific modulation scheme employed, 127

m_B The bit position of a constellation symbol, 224

$\overline{\text{MSE}}$ The average FD-CHTF estimation MSE, 229

$\overline{\text{MSE}}[n]$ The average FD-CHTF estimation MSE associated with the n^{th} OFDM symbol, 229

N_T The total number of OFDM symbols transmitted, 229

$n_p(t)$ The AWGN at the p^{th} receiver, 188

$n_{p,q}$ The noise signal associated with the q^{th} subcarrier at the p^{th} receiver, 188

$\bar{\mathbf{n}}_{p,q}$ The $(G_q \times 1)$-dimensional effective noise vector associated with the q^{th} subcarrier at the p^{th} receiver, 189

$\mathbf{n}$ Noise signal vector, 88

ω_{ij} The cross-correlation coefficient of the i^{th} DSS group's and the j^{th} DSS group's signature sequence, 190

$\Omega(\cdot)$ The GA's joint objective function for all antennas, 128

$\Omega_{g,q}(\cdot)$ The GA's joint objective function for all antennas associated with the g^{th} DSS group at the q^{th} subcarrier, 191

$\Omega_{p,g,q}(\cdot)$ The GA's objective function associated with the g^{th} DSS group of the p^{th} antenna at the q^{th} subcarrier, 191

$\Omega_p(\cdot)$ The GA's objective function associated with the p^{th} antenna, 128

$\Omega_{y,T}$	The maximum GA objective score generated by evaluating the T individuals in the mating pool, 130
P	Number of receiver antenna elements employed by the BS in SDMA systems, 88
P_T	Transmitted signal power, 187
$\tilde{p}_{mt}^{(ij)}$	The normalized mutation-induced transition probability, 263
$p_{mt}^{(ij)}$	The 1D transition probability of mutating from a 1D symbol s_{Ri} to another 1D symbol s_{Rj}, 140
$p_{mt}^{(ii)}$	The original legitimate constellation symbol's probability of remaining unchanged, 142
$p_{mt}^{(ij)}$	The mutation-induced transition probability, which quantifies the probability of the i^{th} legitimate symbol becoming the j^{th}, 137
p_m	The mutation probability, which denotes the probability of how likely it is that a gene will mutate, 261
$\Phi(\cdot)$	The cost function of the OHRSA MUD, 218
$\Phi_i(\cdot)$	The cumulative sub-cost function of the OHRSA MUD at the i^{th} recursive step, 219
$\varphi^{(l)}$	The l^{th} user's phase angle introduced by carrier modulation, 187
$\phi(\cdot)$	The sub-cost function of the OHRSA MUD, 218
$Q(x)$	The Q-function, 139
$\mathbf{Q}_L$	The L-order full permutation set, 184
Q_c	The number of available subcarriers in conventional or SSCH systems, 173
Q_f	The number of available sub-bands in SFH systems, 173
Q_g	The number of subcarriers in a USSCH subcarrier group, 182
$\mathbf{q}_k$	The subcarrier vector generated for the k^{th} subcarrier group, 184
$\mathfrak{q}^{(l)}$	The USSCH pattern set of the l^{th} user, 184
R	Code rate, 24, 39
$\mathbf{R_n}$	The $(P \times P)$-dimensional covariance matrix, 225
$\bar{\mathbf{R}}_{G_q}$	The $(G_q \times L_q)$-dimensional cross-correlation matrix of the L_q users' DSS code sequences, 189
$r_p(t)$	The received signal at the p^{th} receiver, 188

$r_{p,q}$ The discrete signal received at the q^{th} subcarrier of the p^{th} receiver during an OFDM symbol duration, 188

$x_{p,g}(t)$ The despread signal of the g^{th} DSS group at the p^{th} receiver, 188

$\hat{s}_i^{(l)}$ The i^{th} constellation point of $\mathcal{M}_c$ as well as a possible gene symbol for the l^{th} user, 138

$s'^{(l)}_{g_l,q}(t)$ The transmitted signal at the q^{th} subcarrier associated with the l^{th} user in the g^{th} DSS group, 187

$s^{(l)}$ The transmitted signal of the l^{th} user at a subcarrier, 88

$s^{(l)}_{g_l,q}(t)$ The information signal at the q^{th} subcarrier associated with the l^{th} user in the g^{th} DSS group, 187

s_{Ri} The i^{th} 1D constellation symbol in the context of real axis, 139

$\overline{\mathbf{s}}_q$ The L_q users' $(L_q \times 1)$-dimensional information signal vector, 189

$\check{\mathbf{s}}$ The candidate trial vector, 218

$\check{\mathbf{s}}_i$ The sub-vector of $\check{\mathbf{s}}$ at the i^{th} OHRSA recursive step, 219

$\hat{\mathbf{s}}^{(l)}$ The l^{th} user's estimated information symbol block of the FFT length, 176

$\hat{\mathbf{s}}^{(l)}_{\mathrm{W}}$ The estimated l^{th} user's WHT-despreading signal block, 92

$\hat{\mathbf{s}}^{(l)}_{\mathrm{W},0}$ The estimated l^{th} user's WHT-despread signal block, 92

$\hat{\mathbf{s}}_{\mathrm{GA}}$ The estimated transmitted symbol vector detected by the GA MUD, 128

$\hat{\mathbf{s}}_{\mathrm{GA}_{g,q}}$ The GA-based estimated $(l_g \times 1)$-dimensional signal vector associated with the g^{th} DSS group at the q^{th} subcarrier, 191

$\hat{\mathbf{s}}_{\mathrm{MMSE}_{g,q}}$ The MMSE-based estimated $(l_g \times 1)$-dimensional signal vector associated with the g^{th} DSS group at the q^{th} subcarrier, 190

$\tilde{\mathbf{s}}[n,k]$ The trial data vector of the GA-JCEMUD, 221

$\tilde{\mathbf{s}}_{(y,x)}$ The x^{th} individual of the y^{th} generation, 129

$\tilde{\mathbf{s}}_{(y,x)}[n,k]$ The symbol chromosome of the GA-JCEMUD individual associated with the x^{th} individual of the y^{th} generation, 220

$\mathbf{s}$ Transmitted signal vector, 88

$\mathbf{s}^{(l)}$ The l^{th} user's information symbol block of the FFT length, 175

$\mathbf{s}^{(l)}_{\mathrm{W}}$ The l^{th} user's WHT-spread signal block, 91

$\mathbf{s}^{(l)}_{\mathrm{W},0}$ The l^{th} user's WHT-spreading signal block, 91

$\mathbf{s}_g$ The $(l_g \times 1)$-dimensional trial symbol vector for the GA's objective function associated with the g^{th} DSS group, 191

$\tilde{s}^{(l)}_{(y,x)}[n,k]$	The l^{th} symbol gene of the GA-JCEMUD symbol chromosome associated with the x^{th} individual of the y^{th} generation, 220
σ_l^2	Signal variance associated with the l^{th} user, 89
σ_n^2	Noise variance, 89
T_h	The FH dwell time, 174
$\mathrm{TC}(n,k,K)$	Turbo convolutional codes with the number of input bits k, the number of coded bits n and the constraint length K, 60
T_r	The reuse time interval of hopping patterns, 187
T_c	The DSS chip duration, 188
$\mathbf{U}_{\mathrm{WHT}_K}$	The K-order WHT matrix, 91
$u_{g_l}[c]$	The c^{th} element of the g^{th} row in the $(G \times G)$-dimensional WHT matrix, which is associated with the l^{th} user, 188
$\mathbf{V}$	The upper-triangular matrix having positive real-valued elements on the main diagonal, 218
ν	CM code memory, 69
W	System bandwidth, 173
W_{sc}	Subcarrier bandwidth, 173
$\mathbf{W}_{\mathrm{MMSE}}$	The MMSE-based weight matrix, 90
$\mathbf{W}_{\mathrm{MMSE}_{g,q}}$	The MMSE-based $(P \times l_g)$-dimensional weight matrix associated with the g^{th} DSS group at the q^{th} subcarrier, 191
X	GA population size, 129
x_p	The received signal at the p^{th} receiver at a subcarrier, 88
$\bar{\mathbf{x}}_{p,q}$	The despread signal associated with the q^{th} subcarrier at the p^{th} receiver, 189
$\mathbf{x}$	Received signal vector, 88
$\mathbf{x}_p$	The received symbol block of the FFT length at the p^{th} receiver, 176
$\mathbf{x}_{g,q}$	The $(P \times 1)$-dimensional despread signal vector associated with the g^{th} DSS group at the q^{th} subcarrier, 191
Y	Number of GA generations, 129

Bibliography

[1] W. C. Chung, N. J. August, and D. S. Ha, "Signaling and multiple access techniques for ultra wideband 4G wireless communication systems," *IEEE Wireless Communications*, vol. 12, no. 2, pp. 46–55, April 2005.

[2] L. Hanzo, T. H. Liew, and B. L. Yeap, *Turbo Coding, Turbo Equalisation and Space-Time Coding for Transmission Over Fading Channels.* New York, USA: IEEE Press - John Wiley & Sons Ltd., 2002.

[3] L. Hanzo, M. Münster, B. J. Choi, and T. Keller, *OFDM and MC-CDMA for Broadband Multi-user Communications, WLANs and Broadcasting.* IEEE Press - John Wiley & Sons Ltd., 2003.

[4] J. H. Winters, "Optimum Combining in Digital Mobile Radio with Cochannel Interference," *IEEE Journal on Selected Areas in Communications*, vol. 2, no. 4, pp. 528–539, July 1984.

[5] J. A. C. Bingham, "Multicarrier modulation for data transmission: an idea whose time has come," *IEEE Communications Magazine*, vol. 28, no. 5, pp. 5–14, May 1990.

[6] L. Hanzo, W. Webb, and T. Keller, *Single- and Multi-carrier Quadrature Amplitude Modulation*, 2nd ed. West Sussex, UK: IEEE Press - John Wiley & Sons Ltd., 2000, iSBN 0471492396.

[7] R. V. Nee and R. Prasad, *OFDM for wireless multimedia communications.* London, UK: Artech House, 2000.

[8] J. L. Holsinger, "Digital Communication over Fixed Time-Continuous Channels with Memory - with Special Application to Telephone Channels," MIT - Lincoln Laboratory, Cambridge, Massachusetts, USA, Technical Report No. 366, October 1964.

[9] J. M. Cioffi, *A Multicarrier Primer*, November 1991, ANSI T1E1.4/91-157.

[10] *A Technical Report on High-Bit-Rate Digital Subscriber Lines (HDSL)*, ANSI Committee T1-Telecommunications, February 1994, Technical Report No. 28.

[11] *Very-high-speed Digital Subscriber Lines: System Requirements*, September 1998, ANSI T1E1.4 VDSL SR: 98-043R5.

[12] *Transmission and Multiplexing (TM);Access transmission systems on metallic access cables;Very high speed Digital Subscriber Line (VDSL);Part 1: Functional requirements*, European Telecommunication Standard Institute, June 1998, ETSI TS 101 270-1 V1.1.2.

[13] *Digital Audio Broadcasting (DAB);DAB to mobile, portable and fixed Receivers*, European Telecommunication Standard Institute, February 1995, ETSI ETS 300 401 ed.1.

[14] *Digital Video Broadcasting (DVB);Framing structure, channel coding and modulation for digital terrestrial television (DVB-T)*, European Telecommunication Standard Institute, March 1997, ETSI ETS 300 744 ed.1.

[15] *Digital Video Broadcasting (DVB);Transmission System for Handheld Terminals (DVB-H)*, European Telecommunication Standard Institute, November 2004, ETSI EN 302 304 V1.1.1.

[16] *Radio Equipment and Systems (RES);HIgh PErformance Radio Local Area Network (HIPERLAN) Type 1;Functional specification*, European Telecommunication Standard Institute, October 1996, ETSI ETS 300 652 ed.1.

[17] *Broadband Radio Access Networks (BRAN);Inventory of broadband radio technologies and techniques*, European Telecommunication Standard Institute, May 1998, ETSI TR 101 173 V1.1.1.

[18] *IEEE Standard 802.11a: Wireless LAN Medium Access Control (MAC) and Physical Layer (PHY) specifications: high-speed physical layer in the 5 GHz band*, Institute of Electrical and Electronics Engineers, 1999.

[19] *IEEE Standard 802.11: Wireless Lan Medium Access Control (MAC) And Physical Layer (PHY) Specifications*, Institute of Electrical and Electronics Engineers, 18 November 1997.

[20] *IEEE Standard 802.11g: Wireless LAN Medium Access Control (MAC) and Physical Layer (PHY) specifications*, Institute of Electrical and Electronics Engineers, 2003.

[21] *IEEE Candidate Standard 802.11n: Wireless LAN Medium Access Control (MAC) and Physical Layer (PHY) specifications*, Institute of Electrical and Electronics Engineers, 2004, http://grouper.ieee.org/groups/802/11/Reports/tgn_update.htm.

[22] *IEEE Candidate Standard 802.15.3a: Wireless Medium Access Control (MAC) and Physical Layer (PHY) specifications for high rate Wireless Personal Area Networks (WPANs) involving imaging and multimedia*, Institute of Electrical and Electronics Engineers, 2004, http://www.ieee802.org/15/pub/TG3a.html.

[23] *IEEE Standard 802.15.3: Wireless Medium Access Control (MAC) and Physical Layer (PHY) specifications for high rate Wireless Personal Area Networks (WPANs)*, Institute of Electrical and Electronics Engineers, 2003.

[24] *IEEE Standard 802.16: Air Interface for Fixed Broadband Wireless Access Systems*, Institute of Electrical and Electronics Engineers, 2004.

[25] R. W. Chang, "Synthesis of Band-Limited Orthogonal Signals for Multichannel Data Transmission," *Bell System Technical Journal*, vol. 45, no. 11, pp. 1775–1796, December 1966.

[26] B. R. Saltzberg, "Performance of an Efficient Parallel Data Transmission System," *IEEE Transactions on Communications*, vol. 15, no. 6, pp. 805–811, December 1967.

[27] R. W. Chang and R. A. Gibby, "A Theoretical Study of Performance of an Orthogonal Multiplexing Data Transmission Scheme," *IEEE Transactions on Communications*, vol. 16, no. 4, pp. 529–540, August 1968.

[28] R. W. Chang, *U.S. Patent No. 3,488,445: Orthogonal Frequency Division Multiplexing*, filed November 14, 1966, issued January 6, 1970.

[29] S. B. Weinstein and P. M. Ebert, "Data Transmission by Frequency-Division Multiplexing Using the Discrete Fourier Transform," *IEEE Transactions on Communications*, vol. 19, no. 5, pp. 628–634, October 1971.

[30] A. Peled and A. Ruiz, "Frequency domain data transmission using reduced computational complexity algorithms," in *Proceedings of the 1980 IEEE International Conference on Acoustics, Speech, and Signal Processing (ICASSP '80)*, vol. 5, Denver, USA, 9-11 April 1980, pp. 964–967.

[31] L. Hanzo, S. X. Ng, T. Keller, and W. T. Webb, *Quadrature Amplitude Modulation: From Basics to Adaptive Trellis-Coded, Turbo-Equalised and Space-Time Coded OFDM, CDMA and MC-CDMA Systems*, 3rd ed. West Sussex, UK: IEEE Press - John Wiley & Sons Ltd., 2004.

[32] W. E. Keasler, D. L. Bitzer, and P. T. Tucker, *U.S. Patent No. 4,206,320: High-speed Modem Suitable for Operating with a Switched Network*, filed August 21, 1978, issued June 3, 1980.

[33] B. Hirosaki, "An Analysis of Automatic Equalizers for Orthogonally Multiplexed QAM Systems," *IEEE Transactions on Communications*, vol. 28, no. 1, pp. 73–83, January 1980.

[34] B. Hirosaki, "An Orthogonally Multiplexed QAM System Using the Discrete Fourier Transform," *IEEE Transactions on Communications*, vol. 29, no. 7, pp. 982–989, July 1981.

[35] B. Hirosaki, S. Hasegawa, and A. Sabato, "Advanced Groupband Data Modem Using Orthogonally Multiplexed QAM Technique," *IEEE Transactions on Communications*, vol. 34, no. 6, pp. 587–592, June 1986.

[36] L. J. Cimini Jr., "Analysis and Simulation of a Digital Mobile Channel Using Orthogonal Frequency Division Multiplexing," *IEEE Transactions on Communications*, vol. 33, no. 7, pp. 665–675, July 1985.

[37] I. Kalet, "The Multitone Channel," *IEEE Transactions on Communications*, vol. 37, no. 2, pp. 119–124, February 1989.

[38] M. Alard and R. Lassalle, "Principles of modulation and channel coding for digital broadcasting for mobile receivers," *EBU Technical Review*, no. 224, pp. 168–190, August 1987.

[39] K. Fazel and G. Fettweis, *Multi-carrier Spread Spectrum and Related Topics.* Kluwer, 2000, iSBN 0-7923-9973-0.

[40] T. Keller and L. Hanzo, "Adaptive multicarrier modulation: a convenient framework for time-frequency processing in wireless communications," *Proceedings of the IEEE*, vol. 88, no. 5, pp. 611–640, May 2000.

[41] L. Hanzo, B. J. Choi, and M. Münster, "A Stroll Along Multi-Carrier Boulevard towards Next-Generation Plaza - OFDM Background and History," *IEEE VTS News*, vol. 51, no. 4, pp. 4–10, November 2004.

[42] L. Hanzo, B. J. Choi, and M. Münster, "A Stroll Along Multi-Carrier Boulevard towards Next-Generation Plaza - Space-Time Coded Adaptive OFDM and MC-CDMA Comparison," *IEEE VTS News*, vol. 51, no. 4, pp. 10–19, November 2004.

[43] R. Steele and L. Hanzo, *Mobile Radio Communications: Second and Third Generation Cellular and WATM Systems*, 2nd ed. New York, USA: IEEE Press - John Wiley & Sons Ltd., 1999.

[44] A. J. Viterbi, *CDMA: Principles of Spread Spectrum Communication.* Addison-Wesley, 1995.

[45] L. Hanzo, L.-L. Yang, E.-L. Kuan, and K. Yen, *Single- and Multi-Carrier DS-CDMA: Multi-User Detection, Space-Time Spreading, Synchronisation and Standards.* IEEE Press - John Wiley & Sons Ltd., 2003.

[46] K. S. Zigangirov, *Theory of Code Division Multiple Access Communication.* IEEE Press - John Wiley & Sons Ltd., 2004, iSBN 0-471-45712-4.

[47] L. E. Miller and J. S. Lee, *CDMA Systems Engineering Handbook.* London, UK: Artech House, 1998.

[48] J. S. Lee, "Overview of the technical basis of Qualcomm's CDMA cellular telephone system design: A view of North American TIA/EIA IS-95," in *Proceedings of the 1994 International Conference on Communications Systems (ICCS '94)*, vol. 2, Singapore, 14-18 November 1994, pp. 353–358.

[49] I. Koffman and V. Roman, "Broadband Wireless Access Solutions Based on OFDM Access in IEEE 802.16," *IEEE Communications Magazine*, vol. 40, no. 4, pp. 96–103, April 2002.

[50] R. Laroia, S. Uppala, and J. Li, "Designing a Mobile Broadband Wireless Access Network," *IEEE Signal Processing Magazine*, vol. 21, no. 5, pp. 20–28, September 2004.

[51] P. Xia, S. Zhou, and G. B. Giannakis, "Bandwidth- and Power-Efficient Multicarrier Multiple Access," *IEEE Transactions on Communications*, vol. 51, no. 11, pp. 1828–1837, November 2003.

[52] Z. Cao, U. Tureli, and Y. Yao, "Deterministic Multiuser Carrier-Frequency Offset Estimation for Interleaved OFDMA Uplink," *IEEE Transactions on Communications*, vol. 52, no. 9, pp. 1585–1594, September 2004.

[53] R. Bercovich, "OFDM Enhances the 3G High-speed Data Access," in *GSPx 2004 Conference*, Santa Clara, USA, 27-30 September 2004, http://www.techonline.com/pdf/pavillions/gspx/2004/1084.pdf.

[54] T. May, H. Rohling, and V. Engels, "Performance analysis of Viterbi decoding for 64-DAPSK and 64-QAM modulated OFDM signals," *IEEE Transactions on Communications*, vol. 46, no. 2, pp. 182–190, February 1998.

[55] L. Lin, L. J. Cimini Jr., and C.-I. Chuang, "Comparison of convolutional and turbo codes for OFDM with antenna diversity in high-bit-rate wireless applications," *IEEE Communications Letters*, vol. 9, no. 4, pp. 277–279, September 2000.

[56] P. H. Moose, "A technique for orthogonal frequency division multiplexing frequency offset correction," *IEEE Transactions on Communications*, vol. 42, no. 10, pp. 2908–2914, October 1994.

[57] "OFDM for Mobile Data Communications," Flarion Technologies, Inc., Bedminster, USA, White Paper, March 2003.

[58] "FLASH-OFDM for 450MHz - Advanced Mobile Broadband Solution for 450MHz Operators," Flarion Technologies, Inc., Bedminster, USA, White Paper, November 2004.

[59] 3GPP, http://www.3gpp.org/.

[60] 3GPP2, http://www.3gpp2.org/.

[61] M. Yabusaki, "Asia Pacific Viewpoint and Activities: Introduction," 4G Forum, 27 May 2003.

[62] W. D. Warner and C. Leung, "OFDM/FM frame synchronization for mobile radio data communication," *IEEE Transactions on Vehicular Technology*, vol. 42, no. 3, pp. 302–313, August 1993.

[63] T. Pollet, M. V. Bladel, and M. Moeneclaey, "BER sensitivity of OFDM systems to carrier frequency offset and Wiener phase noise," *IEEE Transactions on Communications*, vol. 43, no. 2/3/4, pp. 191–193, February/March/April 1995.

[64] A. E. Jones, T. A. Wilkinson, and S. K. Barton, "Block coding scheme for reduction of peak to mean envelope power ratio of multicarrier transmission schemes," *Electronics Letters*, vol. 30, no. 25, pp. 2098–2099, December 1994.

[65] S. J. Shepherd, P. W. J. V. Eetvelt, C. W. Wyatt-Millington, and S. K. Barton, "Simple coding scheme to reduce peak factor in QPSK multicarrier modulation," *Electronics Letters*, vol. 31, no. 14, pp. 1131–1132, July 1995.

[66] D. Wulich, "Reduction of peak to mean ratio of multicarrier modulation using cyclic coding," *Electronics Letters*, vol. 32, no. 5, pp. 432–433, February 1996.

[67] D. Wulich, "Peak factor in orthogonal multicarrier modulation with variable levels," *Electronics Letters*, vol. 32, no. 20, pp. 1859–1861, September 1996.

[68] X. Li and L. J. Cimini Jr., "Effects of clipping and filtering on the performance of OFDM," in *Proceedings of the 1997 IEEE 47th Vehicular Technology Conference (VTC '97 Spring)*, vol. 3, Phoenix, Arizona, 4-7 May 1997, pp. 1634–1638.

[69] X. Li and L. J. Cimini Jr., "Effects of clipping and filtering on the performance of OFDM," *IEEE Communications Letters*, vol. 2, no. 5, pp. 131–133, May 1998.

[70] S. Hara and R. Prasad, "Overview of Multicarrier CDMA," *IEEE Communications Magazine*, vol. 35, no. 12, pp. 126–133, December 1997.

[71] Y. Li, L. J. Cimini Jr., and N. R. Sollenberger, "Robust channel estimation for OFDM systems with rapid dispersive fading channels," *IEEE Transactions on Communications*, vol. 46, no. 7, pp. 902–915, July 1998.

[72] Y. Li and N. R. Sollenberger, "Adaptive antenna arrays for OFDM systems with cochannel interference," *IEEE Transactions on Communications*, vol. 47, no. 2, pp. 217–229, February 1999.

[73] S. Armour, A. Nix, and D. Bull, "Pre-FFT equaliser design for OFDM," *Electronics Letters*, vol. 35, no. 7, pp. 539–540, April 1999.

[74] S. Armour, A. Nix, and D. Bull, "Performance analysis of a pre-FFT equalizer design for DVB-T," *IEEE Transactions on Consumer Electronics*, vol. 45, no. 3, pp. 544–552, August 1999.

[75] S. Armour, A. Nix, and D. Bull, "Complexity evaluation for the implementation of a pre-FFT equalizer in an OFDM receiver," *IEEE Transactions on Consumer Electronics*, vol. 46, no. 3, pp. 428–437, August 2000.

[76] B. Y. Prasetyo and A. H. Aghvami, "Simplified frame structure for MMSE-based fast burst synchronisation in OFDM systems," *Electronics Letters*, vol. 35, no. 8, pp. 617–618, April 1999.

[77] B. Y. Prasetyo, F. Said, and A. H. Aghvami, "Fast burst synchronisation technique for OFDM-WLAN systems," *IEE Proceedings - Communications*, vol. 147, no. 5, pp. 292–298, October 2000.

[78] P. Cherriman, T. Keller, and L. Hanzo, "Orthogonal frequency-division multiplex transmission of H.263 encoded video over highly frequency-selective wireless networks," *IEEE Transactions on Circuits and Systems for Video Technology*, vol. 9, no. 5, pp. 701–712, August 1999.

[79] C. Y. Wong, R. S. Cheng, K. B. Lataief, and R. D. Murch, "Multiuser OFDM with Adaptive Subcarrier, Bit, and Power Allocation," *IEEE Journal on Selected Areas in Communications*, vol. 17, no. 10, pp. 1747–1758, October 1999.

[80] C.-S. Lee, T. Keller, and L. Hanzo, "OFDM-based turbo-coded hierarchical and non-hierarchical terrestrial mobile digital video broadcasting," *IEEE Transactions on Broadcasting*, vol. 46, no. 1, pp. 1–22, March 2000.

[81] T. Keller and L. Hanzo, "Adaptive modulation techniques for duplex OFDM transmission," *IEEE Transactions on Vehicular Technology*, vol. 49, no. 5, pp. 1893–1906, September 2000.

[82] T. Keller, L. Piazzo, P. Mandarini, and L. Hanzo, "Orthogonal frequency division multiplex synchronization techniques for frequency-selective fading channels," *IEEE Journal on Selected Areas in Communications*, vol. 19, no. 6, pp. 999–1008, June 2001.

[83] B. Lu, X. Wang, and K. R. Narayanan, "LDPC-based space-time coded OFDM systems over correlated fading channels: performance analysis and receiver design," in *Proceedings of the 2001 IEEE International Symposium on Information Theory (ISIT '01)*, vol. 1, 24-29 June 2001, p. 313.

[84] B. Lu, X. Wang, and K. R. Narayanan, "LDPC-based space-time coded OFDM systems over correlated fading channels: Performance analysis and receiver design," *IEEE Transactions on Communications*, vol. 50, no. 1, pp. 74–88, January 2002.

[85] B. Lu, X. Wang, and Y. Li, "Iterative receivers for space-time block coded OFDM systems in dispersive fading channels," in *Proceedings of the 2001 IEEE Global Telecommunications Conference (GLOBECOM '01)*, vol. 1, 25-29 November 2001, pp. 514–518.

[86] B. Lu, X. Wang, and Y. Li, "Iterative receivers for space-time block-coded OFDM systems in dispersive fading channels," *IEEE Transactions on Wireless Communications*, vol. 1, no. 2, pp. 213–225, April 2002.

[87] P. J. Cherriman, T. Keller, and L. Hanzo, "Subband-adaptive turbo-coded OFDM-based interactive video telephony," *IEEE Transactions on Circuits and Systems for Video Technology*, vol. 12, no. 10, pp. 829–839, October 2002.

[88] O. Simeone, Y. Bar-Ness, and U. Spagnolini, "Pilot-based channel estimation for OFDM systems by tracking the delay-subspace," *IEEE Transactions on Wireless Communications*, vol. 3, no. 1, pp. 315–325, January 2004.

[89] J. Zhang, H. Rohling, and P. Zhang, "Analysis of ICI cancellation scheme in OFDM systems with phase noise," *IEEE Transactions on Broadcasting*, vol. 50, no. 2, pp. 97–106, June 2004.

[90] M. C. Necker and G. L. Stüber, "Totally blind channel estimation for OFDM on fast varying mobile radio channels," *IEEE Transactions on Wireless Communications*, vol. 3, no. 5, pp. 1514–1525, September 2004.

[91] A. Doufexi, S. Armour, A. Nix, P. Karlsson, and D. Bull, "Range and throughput enhancement of wireless local area networks using smart sectorised antennas," *IEEE*

Transactions on Wireless Communications, vol. 3, no. 5, pp. 1437–1443, September 2004.

[92] E. Alsusa, Y. Lee, and S. McLaughlin, "Channel-adaptive sectored multicarrier packet based systems," *Electronics Letters*, vol. 40, no. 19, pp. 1194–1196, September 2004.

[93] C. Williams, M. A. Beach, and S. McLaughlin, "Robust OFDM timing synchronisation," *Electronics Letters*, vol. 41, no. 13, pp. 751–752, June 2005.

[94] J. H. Winters, *U.S. Patent No. 4,639,914: Wireless PBX/LAN System With Optimum Combining*, filed December 6, 1984, issued January 27, 1987.

[95] J. Salz, "Digital transmission over cross-coupled linear channels," *AT&T Technical Journal*, vol. 64, no. 6, pp. 1147–1159, July-August 1985.

[96] J. H. Winters, "On the Capacity of Radio Communication Systems with Diversity in a Rayleigh Fading Environment," *IEEE Journal on Selected Areas in Communications*, vol. 5, no. 5, pp. 871–878, June 1987.

[97] J. H. Winters, "Optimum Combining for Indoor Radio Systems with Multiple Users," *IEEE Transactions on Communications*, vol. 35, no. 11, pp. 1222–1230, November 1987.

[98] S. Cheng and S. Verdu, "Gaussian multiaccess channels with ISI: capacity region and multiuser water-filling," *IEEE Transactions on Information Theory*, vol. 39, no. 3, pp. 773–785, May 1993.

[99] A. Duel-Hallen, "Equalizers for multiple input/multiple output channels and PAM systems with cyclostationary input sequences," *IEEE Journal on Selected Areas in Communications*, vol. 10, no. 3, pp. 630–639, April 1992.

[100] J. H. Winters, J. Salz, and R. D. Gitlin, "The impact of antenna diversity on the capacity of wireless communication systems," *IEEE Transactions on Communications*, vol. 5, no. 2/3/4, pp. 1740–1751, February/March/April 1994.

[101] J. Yang and S. Roy, "On joint transmitter and receiver optimization for multiple-input-multiple-output (MIMO) transmission systems," *IEEE Transactions on Communications*, vol. 42, no. 12, pp. 3221–3231, December 1994.

[102] J. Yang and S. Roy, "Joint transmitter-receiver optimization for multi-input multi-output systems with decision feedback," *IEEE Transactions on Information Theory*, vol. 40, no. 5, pp. 1334–1347, September 1994.

[103] J. H. Winters, "The diversity gain of transmit diversity in wireless systems with Rayleigh fading," *IEEE Transactions on Vehicular Technology*, vol. 47, no. 1, pp. 119–123, February 1998.

[104] J. H. Winters and J. Salz, "Upper bounds on the bit-error rate of optimum combining in wireless systems," *IEEE Transactions on Communications*, vol. 46, no. 12, pp. 1619–1624, December 1998.

[105] G. G. Raleigh and J. M. Cioffi, "Spatio-temporal coding for wireless communications," in *Proceedings of the 1996 IEEE Global Telecommunications Conference (GLOBECOM '96)*, vol. 3, 18-22 November 1996, pp. 1809–1814.

[106] G. J. Foschini, "Layered Space-Time Architecture for Wireless Communication in a Fading Environment When Using Multi-Element Antennas," *Bell Labs Technical Journal*, vol. Autumn, pp. 41–59, October 1996.

[107] G. G. Raleigh and J. M. Cioffi, "Spatio-temporal coding for wireless communication," *IEEE Transactions on Communications*, vol. 46, no. 3, pp. 357–366, March 1998.

[108] G. J. Foschini and M. J. Gans, "On limits of wireless communications in a fading environment when using multiple antennas," *Wireless Personal Communications*, vol. 6, no. 3, pp. 311–335, March 1998.

[109] G. J. Foschini, G. D. Golden, R. A. Valenzuela, and P. W. Wolniansky, "Simplified processing for high spectral efficiency wireless communication employing multi-element arrays," *IEEE Journal on Selected Areas in Communications*, vol. 17, no. 11, pp. 1841–1852, November 1999.

[110] B. Lu and X. Wang, "Iterative receivers for multiuser space-time coding systems," *IEEE Journal on Selected Areas in Communications*, vol. 18, no. 11, pp. 2322–2335, November 2000.

[111] S. Y. Kung, Y. Wu, and X. Zhang, "Bezout space-time precoders and equalizers for MIMO channels," *IEEE Transactions on Signal Processing*, vol. 50, no. 10, pp. 2499–2514, October 2002.

[112] F. Petré, G. Leus, L. Deneire, M. Engels, M. Moonen, and H. D. Man, "Space-time block coding for single-carrier block transmission DS-CDMA downlink," *IEEE Journal on Selected Areas in Communications*, vol. 21, no. 3, pp. 350–361, April 2003.

[113] L. Zhang, L. Gui, Y. Qiao, and W. Zhang, "Obtaining diversity gain for DTV by using MIMO structure in SFN," *IEEE Transactions on Broadcasting*, vol. 50, no. 1, pp. 83–90, March 2004.

[114] X. Zhu and R. D. Murch, "Layered space-frequency equalization in a single-carrier MIMO system for frequency-selective channels," *IEEE Transactions on Wireless Communications*, vol. 3, no. 3, pp. 701–708, May 2004.

[115] M. R. McKay and I. B. Collings, "Capacity and performance of MIMO-BICM with zero-forcing receivers," *IEEE Transactions on Communications*, vol. 53, no. 1, pp. 74–83, January 2005.

[116] J. Hoadley, "Building Future Networks with MIMO and OFDM," http://telephonyonline.com/wireless/technology/mimo_ofdm_091905/, 19 September 2005, Telephonyonline.com.

[117] A. J. Paulraj, D. A. Gore, R. U. Nabar, and H. Bölcskei, "An overview of MIMO communications - a key to gigabit wireless," *Proceedings of the IEEE*, vol. 92, no. 2, pp. 198–218, February 2004.

[118] "Using MIMO-OFDM Technology To Boost Wireless LAN Performance Today," Datacomm Research Company, St. Louis, USA, White Paper, June 2005.

[119] H. Sampath, S. Talwar, J. Tellado, V. Erceg, and A. J. Paulraj, "A fourth-generation MIMO-OFDM broadband wireless system: design, performance, and field trial results," *IEEE Communications Magazine*, vol. 40, no. 9, pp. 143–149, September 2002.

[120] Airgo Networks, http://www.airgonetworks.com/.

[121] H. Bölcskei, D. Gesbert, and A. J. Paulraj, "On the capacity of OFDM-based spatial multiplexing systems," *IEEE Transactions on Communications*, vol. 50, no. 2, pp. 225–234, February 2002.

[122] A. Ganesan and A. M. Sayeed, "A virtual input-output framework for transceiver analysis and design for multipath fading channels," *IEEE Transactions on Communications*, vol. 51, no. 7, pp. 1149–1161, July 2003.

[123] R. S. Blum, Y. Li, J. H. Winters, and Q. Yan, "Improved space-time coding for MIMO-OFDM wireless communications," *IEEE Transactions on Communications*, vol. 49, no. 11, pp. 1873–1878, November 2001.

[124] H. E. Gamal, A. R. Hammons Jr., Y. Liu, M. P. Fitz, and O. Y. Takeshita, "On the design of space-time and space-frequency codes for MIMO frequency-selective fading channels," *IEEE Transactions on Information Theory*, vol. 49, no. 9, pp. 2277–2292, September 2003.

[125] P. Dayal, M. Brehler, and M. K. Varanasi, "Leveraging coherent space-time codes for noncoherent communication via training," *IEEE Transactions on Information Theory*, vol. 50, no. 9, pp. 2058–2080, September 2004.

[126] W. Su, Z. Safar, M. Olfat, and K. J. R. Liu, "Obtaining full-diversity space-frequency codes from space-time codes via mapping," *IEEE Transactions on Signal Processing*, vol. 51, no. 11, pp. 2905–2916, November 2003.

[127] W. Su, Z. Safar, and K. J. R. Liu, "Full-rate full-diversity space-frequency codes with optimum coding advantage," *IEEE Transactions on Information Theory*, vol. 51, no. 1, pp. 229–249, January 2005.

[128] J. H. Moon, Y. H. You, W. G. Jeon, K. W. Kwon, and H. K. Song, "Peak-to-average power control for multiple-antenna HIPERLAN/2 and IEEE802.11a systems," *IEEE Transactions on Consumer Electronics*, vol. 49, no. 4, pp. 1078–1083, November 2003.

[129] Y. L. Lee, Y. H. You, W. G. Jeon, J. H. Paik, and H. K. Song, "Peak-to-average power ratio in MIMO-OFDM systems using selective mapping," *IEEE Communications Letters*, vol. 7, no. 12, pp. 575–577, December 2003.

[130] S. H. Han and J. H. Lee, "An overview of peak-to-average power ratio reduction techniques for multicarrier transmission," *IEEE Wireless Communications*, vol. 12, no. 2, pp. 56–65, April 2005.

[131] Y. Li, "Simplified Channel Estimation for OFDM Systems with Multiple Transmit Antennas," *IEEE Transactions on Wireless Communications*, vol. 1, no. 1, pp. 67–75, January 2002.

[132] I. Barhumi, G. Leus, and M. Moonen, "Optimal training design for MIMO OFDM systems in mobile wireless channels," *IEEE Transactions on Signal Processing*, vol. 51, no. 6, pp. 1615–1624, June 2003.

[133] M. Shin, H. Lee, and C. Lee, "Enhanced Channel-estimation Technique for MIMO-OFDM Systems," *IEEE Transactions on Vehicular Technology*, vol. 53, no. 1, pp. 262–265, January 2004.

[134] Y. Li, J. H. Winters, and N. R. Sollenberger, "MIMO-OFDM for Wireless Communications: Signal Detection with Enhanced Channel Estimation," *IEEE Transactions on Communications*, vol. 50, no. 9, pp. 1471–1477, September 2002.

[135] L. Giangaspero, L. Agarossi, G. Paltenghi, S. Okamura, M. Okada, and S. Komaki, "Co-channel interference cancellation based on MIMO OFDM systems," *IEEE Wireless Communications*, vol. 9, no. 6, pp. 8–17, December 2002.

[136] J. Li, K. B. Letaief, and Z. Cao, "Co-channel interference cancellation for space-time coded OFDM systems," *IEEE Transactions on Wireless Communications*, vol. 2, no. 1, pp. 41–49, January 2003.

[137] S. Y. Park and C. G. Kang, "Complexity-reduced iterative MAP receiver for interference suppression in OFDM-based spatial multiplexing systems," *IEEE Transactions on Vehicular Technology*, vol. 53, no. 5, pp. 1316–1326, September 2004.

[138] G. L. Stüber, J. R. Barry, S. W. McLaughlin, Y. Li, M. A. Ingram, and T. G. Pratt, "Broadband MIMO-OFDM wireless communications," *Proceedings of the IEEE*, vol. 92, no. 2, pp. 271–294, February 2004.

[139] C. Dubuc, D. Starks, T. Creasy, and Y. Hou, "A MIMO-OFDM prototype for next-generation wireless WANs," *IEEE Communications Magazine*, vol. 42, no. 12, pp. 82–87, December 2004.

[140] R. J. Piechocki, P. N. Fletcher, A. Nix, N. Canagarajah, and J. P. McGeehan, "Performance evaluation of BLAST-OFDM enhanced Hiperlan/2 using simulated and measured channel data," *Electronics Letters*, vol. 37, no. 18, pp. 1137–1139, August 2001.

[141] C.-N. Chuah, D. N. C. Tse, J. M. Kahn, and R. A. Valenzuela, "Capacity scaling in MIMO wireless systems under correlated fading," *IEEE Transactions on Information Theory*, vol. 48, no. 3, pp. 637–650, March 2002.

[142] S. Catreux, V. Erceg, D. Gesbert, and R. W. Heath Jr., "Adaptive modulation and MIMO coding for broadband wireless data networks," *IEEE Communications Magazine*, vol. 40, no. 6, pp. 108–115, June 2002.

[143] R. Piechocki, P. Fletcher, A. Nix, N. Canagarajah, and J. McGeehan, "A measurement based feasibility study of space-frequency MIMO detection and decoding techniques for next generation wireless LANs," *IEEE Transactions on Consumer Electronics*, vol. 48, no. 3, pp. 732–737, August 2002.

[144] A. F. Molisch, M. Z. Win, and J. H. Winters, "Space-time-frequency (STF) coding for MIMO-OFDM systems," *IEEE Communications Letters*, vol. 6, no. 9, pp. 370–372, September 2002.

[145] A. Stamoulis, S. N. Diggavi, and N. Al-Dhahir, "Intercarrier interference in MIMO OFDM," *IEEE Transactions on Signal Processing*, vol. 50, no. 10, pp. 2451–2464, October 2002.

[146] A. Doufexi, M. Hunukumbure, A. Nix, M. A. Beach, and S. Armour, "COFDM performance evaluation in outdoor MIMO channels using space/polarisation-time processing techniques," *Electronics Letters*, vol. 38, no. 25, pp. 1720–1721, December 2002.

[147] H. Bölcskei, M. Borgmann, and A. J. Paulraj, "Impact of the propagation environment on the performance of space-frequency coded MIMO-OFDM," *IEEE Journal on Selected Areas in Communications*, vol. 21, no. 3, pp. 427–439, April 2003.

[148] J. Cai, W. Song, and Z. Li, "Doppler spread estimation for mobile OFDM systems in Rayleigh fading channels," *IEEE Transactions on Consumer Electronics*, vol. 49, no. 4, pp. 973–977, November 2003.

[149] G. Leus and M. Moonen, "Per-tone equalization for MIMO OFDM systems," *IEEE Transactions on Signal Processing*, vol. 51, no. 11, pp. 2965–2975, November 2003.

[150] R. J. Piechocki, A. Nix, J. P. McGeehan, and S. M. D. Armour, "Joint blind and semi-blind detection and channel estimation," *IEE Proceedings - Communications*, vol. 150, no. 6, pp. 419–426, December 2003.

[151] P. Xia, S. Zhou, and G. B. Giannakis, "Adaptive MIMO-OFDM based on partial channel state information," *IEEE Transactions on Signal Processing*, vol. 52, no. 1, pp. 202–213, January 2004.

[152] D. Huang and K. B. Letaief, "Symbol-based space diversity for coded OFDM systems," *IEEE Transactions on Wireless Communications*, vol. 3, no. 1, pp. 117–127, January 2004.

[153] M. R. G. Butler and I. B. Collings, "A zero-forcing approximate log-likelihood receiver for MIMO bit-interleaved coded modulation," *IEEE Communications Letters*, vol. 8, no. 2, pp. 105–107, February 2004.

[154] B. Lu, G. Yue, and X. Wang, "Performance analysis and design optimization of LDPC-coded MIMO OFDM systems," *IEEE Transactions on Signal Processing*, vol. 52, no. 2, pp. 348–361, February 2004.

[155] A. V. Zelst and T. C. W. Schenk, "Implementation of a MIMO OFDM-based wireless LAN system," *IEEE Transactions on Signal Processing*, vol. 52, no. 2, pp. 483–494, February 2004.

[156] A. Pascual-Iserte, A. I. Pérez-Neira, and M. A. Lagunas, "On power allocation strategies for maximum signal to noise and interference ratio in an OFDM-MIMO system," *IEEE Transactions on Wireless Communications*, vol. 3, no. 3, pp. 808–820, May 2004.

[157] Y. Zeng and T. S. Ng, "A Semi-blind Channel Estimation Method for Multiuser Multi-antenna OFDM Systems," *IEEE Transactions on Signal Processing*, vol. 52, no. 5, pp. 1419–1429, May 2004.

[158] B. Alien, R. Brito, M. Dohler, and A. H. Aghvami, "Performance comparison of spatial diversity array topologies in an OFDM based wireless LAN," *IEEE Transactions on Consumer Electronics*, vol. 50, no. 2, pp. 420–428, May 2004.

[159] J. Tan and G. L. Stüber, "Multicarrier delay diversity modulation for MIMO systems," *IEEE Transactions on Wireless Communications*, vol. 3, no. 5, pp. 1756–1763, September 2004.

[160] X. Wang, Y. R. Shayan, and M. Zeng, "On the code and interleaver design of broadband OFDM systems," *IEEE Communications Letters*, vol. 8, no. 11, pp. 653–655, November 2004.

[161] Y. Pan, K. B. Letaief, and Z. Cao, "Dynamic spatial subchannel allocation with adaptive beamforming for MIMO/OFDM systems," *IEEE Transactions on Wireless Communications*, vol. 3, no. 6, pp. 2097–2107, November 2004.

[162] C. Tepedelenlioğlu and R. Challagulla, "Low-complexity multipath diversity through fractional sampling in OFDM," *IEEE Transactions on Signal Processing*, vol. 52, no. 11, pp. 3104–3116, November 2004.

[163] M. S. Baek, M. J. Kim, Y. H. You, and H. K. Song, "Semi-blind channel estimation and PAR reduction for MIMO-OFDM system with multiple antennas," *IEEE Transactions on Broadcasting*, vol. 50, no. 4, pp. 414–424, December 2004.

[164] G. Barriac and U. Madhow, "Space-time communication for OFDM with implicit channel feedback," *IEEE Transactions on Information Theory*, vol. 50, no. 12, pp. 3111–3129, December 2004.

[165] J. Zhang, A. Kavcic, and K. M. Wong, "Equal-diagonal QR decomposition and its application to precoder design for successive-cancellation detection," *IEEE Transactions on Information Theory*, vol. 51, no. 1, pp. 154–172, January 2005.

[166] Y. Yao and G. B. Giannakis, "Blind carrier frequency offset estimation in SISO, MIMO, and multiuser OFDM systems," *IEEE Transactions on Communications*, vol. 53, no. 1, pp. 173–183, January 2005.

[167] K. Zheng, L. Huang, W. Wang, and G. Yang, "TD-CDM-OFDM: Evolution of TD-SCDMA toward 4G," *IEEE Communications Magazine*, vol. 43, no. 1, pp. 45–52, January 2005.

[168] H. Yang, "A road to future broadband wireless access: MIMO-OFDM-Based air interface," *IEEE Communications Magazine*, vol. 43, no. 1, pp. 53–60, January 2005.

[169] Y. Zhang and K. B. Letaief, "An efficient resource-allocation scheme for spatial multiuser access in MIMO/OFDM systems," *IEEE Transactions on Communications*, vol. 53, no. 1, pp. 107–116, January 2005.

[170] X. Ma, M. K. Oh, G. B. Giannakis, and D. J. Park, "Hopping pilots for estimation of frequency-offset and multiantenna channels in MIMO-OFDM," *IEEE Transactions on Communications*, vol. 53, no. 1, pp. 162–172, January 2005.

[171] M. Fozunbal, S. W. McLaughlin, and R. W. Schafer, "On space-time-frequency coding over MIMO-OFDM systems," *IEEE Transactions on Wireless Communications*, vol. 4, no. 1, pp. 320–331, January 2005.

[172] S. Nanda, R. Walton, J. Ketchum, M. Wallace, and S. Howard, "A high-performance MIMO OFDM wireless LAN," *IEEE Communications Magazine*, vol. 43, no. 2, pp. 101–109, February 2005.

[173] K. J. Kim, J. Yue, R. A. Iltis, and J. D. Gibson, "A QRD-M/Kalman Filter-based Detection and Channel Estimation Algorithm for MIMO-OFDM Systems," *IEEE Transactions on Wireless Communications*, vol. 4, no. 2, pp. 710–721, March 2005.

[174] Y. Qiao, S. Yu, P. Su, and L. Zhang, "Research on An Iterative Algorithm of LS Channel Estimation in MIMO OFDM Systems," *IEEE Transactions on Broadcasting*, vol. 51, no. 1, pp. 149–153, March 2005.

[175] H. Sampath, V. Erceg, and A. Paulraj, "Performance analysis of linear precoding based on field trials results of MIMO-OFDM system," *IEEE Transactions on Wireless Communications*, vol. 4, no. 2, pp. 404–409, March 2005.

[176] F. Rey, M. Lamarca, and G. Vazquez, "Robust power allocation algorithms for MIMO OFDM systems with imperfect CSI," *IEEE Transactions on Signal Processing*, vol. 53, no. 3, pp. 1070–1085, March 2005.

[177] Y. Sun, Z. Xiong, and X. Wang, "EM-based iterative receiver design with carrier-frequency offset estimation for MIMO OFDM systems," *IEEE Transactions on Communications*, vol. 53, no. 4, pp. 581–586, April 2005.

[178] A. Lodhi, F. Said, M. Dohler, and A. H. Aghvami, "Performance comparison of space-time block coded and cyclic delay diversity MC-CDMA systems," *IEEE Wireless Communications*, vol. 12, no. 2, pp. 38–45, April 2005.

[179] Z. Wang, Z. Han, and K. J. R. Liu, "A MIMO-OFDM Channel Estimation Approach Using Time of Arrivals," *IEEE Transactions on Wireless Communications*, vol. 4, no. 3, pp. 1207–1213, May 2005.

[180] C. K. Wen, Y. Y. Wang, and J. T. Chen, "A low-complexity space-time OFDM multiuser system," *IEEE Transactions on Wireless Communications*, vol. 4, no. 3, pp. 998–1007, May 2005.

[181] W. Su, Z. Safar, and K. J. R. Liu, "Towards maximum achievable diversity in space, time, and frequency: performance analysis and code design," *IEEE Transactions on Wireless Communications*, vol. 4, no. 4, pp. 1847–1857, July 2005.

[182] M. Tan, Z. Latinović, and Y. Bar-Ness, "STBC MIMO-OFDM peak-to-average power ratio reduction by cross-antenna rotation and inversion," *IEEE Communications Letters*, vol. 9, no. 7, pp. 592–594, July 2005.

[183] K. W. Park and Y. S. Cho, "An MIMO-OFDM technique for high-speed mobile channels," *IEEE Communications Letters*, vol. 9, no. 7, pp. 604–606, July 2005.

[184] L. Shao and S. Roy, "Rate-one space-frequency block codes with maximum diversity for MIMO-OFDM," *IEEE Transactions on Wireless Communications*, vol. 4, no. 4, pp. 1674–1687, July 2005.

[185] T. C. W. Schenk, X. Tao, P. F. M. Smulders, and E. R. Fledderus, "On the influence of phase noise induced ICI in MIMO OFDM systems," *IEEE Communications Letters*, vol. 9, no. 8, pp. 682–684, August 2005.

[186] M. Borgmann and H. Bölcskei, "Noncoherent space-frequency coded MIMO-OFDM," *IEEE Journal on Selected Areas in Communications*, vol. 23, no. 9, pp. 1799–1810, September 2005.

[187] A. Tarighat and A. H. Sayed, "MIMO OFDM Receivers for Systems With IQ Imbalances," *IEEE Transactions on Signal Processing*, vol. 53, no. 9, pp. 3583–3596, September 2005.

[188] Y. Jiang, J. Li, and W. W. Hager, "Joint transceiver design for MIMO communications using geometric mean decomposition," *IEEE Transactions on Signal Processing*, vol. 53, no. 10, pp. 3791–3803, October 2005.

[189] J. Choi and R. W. Heath Jr., "Interpolation Based Transmit Beamforming for MIMO-OFDM With Limited Feedback," *IEEE Transactions on Signal Processing*, vol. 53, no. 11, pp. 4125–4135, November 2005.

[190] M. S. Baek, H. J. Kook, M. J. Kim, Y. H. You, and H. K. Song, "Multi-Antenna Scheme for High Capacity Transmission in the Digital Audio Broadcasting," *IEEE Transactions on Broadcasting*, vol. 51, no. 4, pp. 551–559, December 2005.

[191] T.-H. Liew and L. Hanzo, "Space-Time Trellis and Space-Time Block Coding Versus Adaptive Modulation and Coding Aided OFDM for Wideband Channels," *IEEE Transactions on Vehicular Technology*, vol. 55, no. 1, pp. 173–187, January 2006.

[192] P. Vandenameele, L. V. D. Perre, and M. Engels, *Space Division Multiple Access for Wireless Local Area Networks.* London, UK: Kluwer, 2001.

[193] I. P. Kovalyov, *SDMA for Multipath Wireless Channels: Limiting Characteristics and Stochastic Models*, 1st ed. Springer, 2004, iSBN 3-540-40225-X.

[194] D. Tse and P. Viswanath, *Fundamentals of Wireless Communication.* Cambridge, UK: Cambridge University Press, 2005, iSBN-13 978-0-521-84527-4.

[195] M. Cooper and M. Goldburg, "Intelligent Antennas: Spatial Division Multiple Access," *ArrayComm: Annual Review of Communications*, pp. 999–1002, 1996.

[196] P. Vandenameele, L. V. D. Perre, M. Engels, B. Gyselinckx, and H. D. Man, "A Novel Class of Uplink OFDM/SDMA Algorithms: A Statistical Performance Analysis," in *Proceedings of the 1999 IEEE 50th Vehicular Technology Conference (VTC '99 Fall)*, vol. 1, Amsterdam, Netherlands, 19-22 September 1999, pp. 324–328.

[197] P. Vandenameele, L. V. D. Perre, M. Engels, B. Gyselinckx, and H. D. Man, "A Combined OFDM/SDMA Approach," *IEEE Journal on Selected Areas in Communications*, vol. 18, no. 11, pp. 2312–2321, November 2000.

[198] S. Thoen, L. V. D. Perre, M. Engels, and H. D. Man, "Adaptive loading for OFDM/SDMA-based wireless networks," *IEEE Transactions on Communications*, vol. 50, no. 11, pp. 1798–1810, November 2002.

[199] S. Thoen, L. Deneire, L. V. D. Perre, M. Engels, and H. D. Man, "Constrained Least Squares Detector for OFDM/SDMA-based Wireless Networks," *IEEE Transactions on Wireless Communications*, vol. 2, no. 1, pp. 129–140, January 2003.

[200] A. T. Alastalo and M. Kahola, "Smart-antenna operation for indoor wireless local-area networks using OFDM," *IEEE Transactions on Wireless Communications*, vol. 2, no. 2, pp. 392–399, March 2003.

[201] M. Y. Alias, A. K. Samingan, S. Chen, and L. Hanzo, "Multiple Antenna Aided OFDM Employing Minimum Bit Error Rate Multiuser Detection," *Electronics Letters*, vol. 39, no. 24, pp. 1769–1770, November 2003.

[202] X. Dai, "Carrier frequency offset estimation for OFDM/SDMA systems using consecutive pilots," *IEE Proceedings - Communications*, vol. 152, no. 5, pp. 624–632, October 2005.

[203] Y. S. Yeh and D. Reudink, "Efficient Spectrum Utilization for Mobile Radio Systems Using Space Diversity," *IEEE Transactions on Communications*, vol. 30, no. 3, pp. 447-455, March 1982.

[204] K. T. Ko and B. Davis, "A Space-Division Multiple-Access Protocol for Spot-Beam Antenna and Satellite-Switched Communication Network," *IEEE Journal on Selected Areas in Communications*, vol. 1, no. 1, pp. 126–132, January 1983.

[205] S. C. Swales, M. A. Beach, and D. J. Edwards, "Multi-beam adaptive base-station antennas for cellular land mobile radio systems," in *Proceedings of the 1989 IEEE 39th Vehicular Technology Conference (VTC '89 Spring)*, vol. 1, 1-3 May 1989, pp. 341–348.

[206] S. C. Swales, M. A. Beach, D. J. Edwards, and J. P. McGeehan, "The performance enhancement of multibeam adaptive base-station antennas for cellular land mobile radio systems," *IEEE Transactions on Vehicular Technology*, vol. 39, no. 1, pp. 56–67, February 1990.

[207] B. G. Agee, S. V. Schell, and W. A. Gardner, "Spectral self-coherence restoral: a new approach to blind adaptive signal extraction using antenna arrays," *Proceedings of the IEEE*, vol. 78, no. 4, pp. 753–767, April 1990.

[208] S. Anderson, M. Millnert, M. Viberg, and B. Wahlberg, "An adaptive array for mobile communication systems," *IEEE Transactions on Vehicular Technology*, vol. 40, no. 1, pp. 230–236, February 1991.

[209] P. Balaban and J. Salz, "Optimum diversity combining and equalization in digital data transmission with applications to cellular mobile radio. Part I: Theoretical considerations," *IEEE Transactions on Communications*, vol. 40, no. 5, pp. 885–894, May 1992.

[210] P. Balaban and J. Salz, "Optimum diversity combining and equalization in digital data transmission with applications to cellular mobile radio. Part II: Numerical results," *IEEE Transactions on Communications*, vol. 40, no. 5, pp. 895–907, May 1992.

[211] G. Xu, H. Liu, W. J. Vogel, H. P. Lin, S. S. Jeng, and G. W. Torrence, "Experimental studies of space-division-multiple-access schemes for spectral efficient wireless communications," in *Proceedings of the 1994 IEEE International Conference on Communications (ICC '94)*, vol. 2, New Orleans, USA, 1-5 May 1994, pp. 800–804.

[212] S. Talwar, M. Viberg, and A. Paulraj, "Blind estimation of multiple co-channel digital signals using an antenna array," *IEEE Signal Processing Letters*, vol. 1, no. 2, pp. 29–31, February 1994.

[213] A. J. V. D. Veen, S. Talwar, and A. Paulraj, "Blind estimation of multiple digital signals transmitted over FIR channels," *IEEE Signal Processing Letters*, vol. 2, no. 5, pp. 99–102, May 1995.

[214] B. H. Khalaj, A. Paulraj, and T. Kailath, "Spatio-temporal channel estimation techniques for multiple access spread spectrum systems with antenna arrays," in *Proceedings of the 1995 IEEE International Conference on Communications (ICC '95)*, vol. 3, Seattle, USA, 18-22 June 1995, pp. 1520–1524.

[215] K. Anand, G. Mathew, and V. U. Reddy, "Blind separation of multiple co-channel BPSK signals arriving at an antenna array," *IEEE Signal Processing Letters*, vol. 2, no. 9, pp. 176–178, September 1995.

[216] H. Liu and G. Xu, "Smart Antennas in Wireless Systems: Uplink Multiuser Blind Channel and Sequence Detection," *IEEE Transactions on Communications*, vol. 45, no. 2, pp. 187–199, February 1997.

[217] G. Tsoulos, M. A. Beach, and J. McGeehan, "Wireless personal communications for the 21st century: European technological advances in adaptive antennas," *IEEE Communications Magazine*, vol. 35, no. 9, pp. 102–109, September 1997.

[218] L. Deneire and D. T. M. Slock, "Blind channel identification based on cyclic statistics," *IEE Proceedings - Radar, Sonar and Navigation*, vol. 145, no. 1, pp. 58–62, February 1998.

[219] G. Tsoulos, J. McGeehan, and M. A. Beach, "Space division multiple access (SDMA) field trials. Part I: Tracking and BER performance," *IEE Proceedings - Radar, Sonar and Navigation*, vol. 145, no. 1, pp. 73–78, February 1998.

[220] G. Tsoulos, J. McGeehan, and M. A. Beach, "Space division multiple access (SDMA) field trials. Part II: Calibration and linearity issues," *IEE Proceedings - Radar, Sonar and Navigation*, vol. 145, no. 1, pp. 79–84, February 1998.

[221] V. A. N. Barroso, J. M. F. Moura, and J. Xavier, "Blind array channel division multiple access (AChDMA) for mobile communications," *IEEE Transactions on Signal Processing*, vol. 46, no. 3, pp. 737–752, March 1998.

[222] F. Demmerle and W. Wiesbeck, "A biconical multibeam antenna for space-division multiple access," *IEEE Transactions on Antennas and Propagation*, vol. 46, no. 6, pp. 782–787, June 1998.

[223] B. Lindmark, S. Lundgren, J. R. Sanford, and C. Beckman, "Dual-polarized array for signal-processing applications in wireless communications," *IEEE Transactions on Antennas and Propagation*, vol. 46, no. 6, pp. 758–763, June 1998.

[224] B. Suard, G. Xu, H. Liu, and T. Kailath, "Uplink channel capacity of space-division-multiple-access schemes," *IEEE Transactions on Information Theory*, vol. 44, no. 4, pp. 1468–1476, July 1998.

[225] S. S. Jeng, G. Xu, H. P. Lin, and W. J. Vogel, "Experimental studies of spatial signature variation at 900 MHz for smart antenna systems," *IEEE Transactions on Antennas and Propagation*, vol. 46, no. 7, pp. 953–962, July 1998.

[226] P. Petrus, R. B. Ertel, and J. H. Reed, "Capacity enhancement using adaptive arrays in an AMPS system," *IEEE Transactions on Vehicular Technology*, vol. 47, no. 3, pp. 717–727, August 1998.

[227] J. M. F. Xavier, V. A. N. Barroso, and J. M. F. Moura, "Closed-form Blind Channel Identification and Source Separation in SDMA Systems Through Correlative Coding," *IEEE Journal on Selected Areas in Communications*, vol. 16, no. 8, pp. 1506–1517, October 1998.

[228] C. Farsakh and J. A. Nossek, "Spatial covariance based downlink beamforming in an SDMA mobile radio system," *IEEE Transactions on Communications*, vol. 46, no. 11, pp. 1497–1506, November 1998.

[229] G. V. Tsoulos, "Smart antennas for mobile communication systems: benefits and challenges," *Electronics and Communication Engineering Journal*, vol. 11, no. 2, pp. 84–94, April 1999.

[230] F. Piolini and A. Rolando, "Smart channel-assignment algorithm for SDMA systems," *IEEE Transactions on Microwave Theory and Techniques*, vol. 47, no. 6, pp. 693–699, June 1999.

[231] G. M. Galvan-Tejada and J. G. Gardiner, "Theoretical blocking probability for SDMA," *IEE Proceedings - Communications*, vol. 146, no. 5, pp. 303–306, October 1999.

[232] G. M. Galvan-Tejada and J. G. Gardiner, "Theoretical model to determine the blocking probability for SDMA systems," *IEEE Transactions on Vehicular Technology*, vol. 50, no. 5, pp. 1279–1288, September 2001.

[233] G. V. Tsoulos, "Experimental and theoretical capacity analysis of space-division multiple access (SDMA) with adaptive antennas," *IEE Proceedings - Communications*, vol. 146, no. 5, pp. 307–311, October 1999.

[234] U. Vornefeld, C. Walke, and B. Walke, "SDMA techniques for wireless ATM," *IEEE Communications Magazine*, vol. 37, no. 11, pp. 52–57, November 1999.

[235] P. Djahani and J. M. Kahn, "Analysis of infrared wireless links employing multibeam transmitters and imaging diversity receivers," *IEEE Transactions on Communications*, vol. 48, no. 12, pp. 2077–2088, December 2000.

[236] F. Shad, T. D. Todd, V. Kezys, and J. Litva, "Dynamic slot allocation (DSA) in indoor SDMA/TDMA using a smart antenna basestation," *IEEE/ACM Transactions on Networking*, vol. 9, no. 1, pp. 69–81, February 2001.

[237] R. Kuehner, T. D. Todd, F. Shad, and V. Kezys, "Forward-link capacity in smart antenna base stations with dynamic slot allocation," *IEEE Transactions on Vehicular Technology*, vol. 50, no. 4, pp. 1024–1038, July 2001.

[238] S. S. Jeon, Y. Wang, Y. Qian, and T. Itoh, "A novel smart antenna system implementation for broad-band wireless communications," *IEEE Transactions on Antennas and Propagation*, vol. 50, no. 5, pp. 600–606, May 2002.

[239] S. Bellofiore, C. A. Balanis, J. Foutz, and A. S. Spanias, "Smart-antenna systems for mobile communication networks. Part 1: Overview and antenna design," *IEEE Antennas and Propagation Magazine*, vol. 44, no. 3, pp. 145–154, June 2002.

[240] S. Bellofiore, C. A. Balanis, J. Foutz, and A. S. Spanias, "Smart-antenna systems for mobile communication networks. Part 2: Beamforming and network throughput," *IEEE Antennas and Propagation Magazine*, vol. 44, no. 4, pp. 106–114, August 2002.

[241] X. Fang, "More realistic analysis for blocking probability in SDMA systems," *IEE Proceedings - Communications*, vol. 149, no. 3, pp. 152–156, June 2002.

[242] A. Arredondo, K. R. Dandekar, and G. Xu, "Vector channel modeling and prediction for the improvement of downlink received power," *IEEE Transactions on Communications*, vol. 50, no. 7, pp. 1121–1129, July 2002.

[243] C. M. Walke and T. J. Oechtering, "Analytical expression for uplink C/I-distribution in interference-limited cellular radio systems," *Electronics Letters*, vol. 38, no. 14, pp. 743–744, July 2002.

[244] T. Zwick, C. Fischer, and W. Wiesbeck, "A stochastic multipath channel model including path directions for indoor environments," *IEEE Journal on Selected Areas in Communications*, vol. 20, no. 6, pp. 1178–1192, August 2002.

[245] S. A. Zekavat, C. R. Nassar, and S. Shattil, "Oscillating-beam smart antenna arrays and multicarrier systems: achieving transmit diversity, frequency diversity, and directionality," *IEEE Transactions on Vehicular Technology*, vol. 51, no. 5, pp. 1030–1039, September 2002.

[246] J. L. Pan and P. M. Djurić, "Multibeam cellular mobile communications with dynamic channel assignment," *IEEE Transactions on Vehicular Technology*, vol. 51, no. 5, pp. 1252–1258, September 2002.

[247] C. C. Cavalcante, F. R. P. Cavalcanti, and J. C. M. Mota, "Adaptive blind multiuser separation criterion based on log-likelihood maximisation," *Electronics Letters*, vol. 38, no. 20, pp. 1231–1233, September 2002.

[248] H. Yin and H. Liu, "Performance of space-division multiple-access (SDMA) with scheduling." *IEEE Transactions on Wireless Communications*, vol. 1, no. 4, pp. 611–618, October 2002.

[249] M. Rim, "Multi-user downlink beamforming with multiple transmit and receive antennas," *Electronics Letters*, vol. 38, no. 25, pp. 1725–1726, December 2002.

[250] I. Bradaric, A. P. Pertropulu, and K. I. Diamantaras, "Blind MIMO FIR Channel Identification Based on Second-order Spectra Correlations," *IEEE Transactions on Signal Processing*, vol. 51, no. 6, pp. 1668–1674, June 2003.

[251] M. Y. Alias, S. Chen, and L. Hanzo, "Multiple-antenna-aided OFDM employing genetic-algorithm-assisted minimum bit error rate multiuser detection," *IEEE Transactions on Vehicular Technology*, vol. 54, no. 5, pp. 1713–1721, September 2005.

[252] Q. H. Spencer, A. L. Swindlehurst, and M. Haardt, "Zero-forcing methods for downlink spatial multiplexing in multiuser MIMO channels," *IEEE Transactions on Signal Processing*, vol. 52, no. 2, pp. 461–471, February 2004.

[253] J. Li, K. B. Letaief, and Z. Cao, "A reduced-complexity maximum-likelihood method for multiuser detection," *IEEE Transactions on Communications*, vol. 52, no. 2, pp. 289–295, February 2004.

[254] L. U. Choi and R. D. Murch, "A pre-BLAST-DFE technique for the downlink of frequency-selective fading MIMO channels," *IEEE Transactions on Communications*, vol. 52, no. 5, pp. 737–743, May 2004.

[255] W. Ajib and D. Haccoun, "An overview of scheduling algorithms in MIMO-based fourth-generation wireless systems," *IEEE Network*, vol. 19, no. 5, pp. 43–48, September-October 2005.

[256] M. Münster and L. Hanzo, "Parallel-interference-cancellation-assisted decision-directed channel estimation for OFDM systems using multiple transmit antennas," *IEEE Transactions on Wireless Communications*, vol. 4, no. 5, pp. 2148–2162, September 2005.

[257] K. M. Nasr, F. Costen, and S. K. Barton, "A Wall Imperfection Channel Model for Signal Level Prediction and its Impact on Smart Antenna Systems for Indoor Infrastructure WLAN," *IEEE Transactions on Antennas and Propagation*, vol. 53, no. 11, pp. 3767–3775, November 2005.

[258] M. Jiang, S. X. Ng, and L. Hanzo, "TCM, TTCM, BICM and BICM-ID Assisted MMSE Multi-User Detected SDMA-OFDM Using Walsh-Hadamard Spreading," in *Proceedings of the 2004 IEEE 59th Vehicular Technology Conference (VTC '04 Spring)*, vol. 2, Milan, Italy, 17-19 May 2004, pp. 1129–1133.

[259] M. Jiang and L. Hanzo, "SDMA-OFDM Using Channel Coding and Spreading," University of Southampton, Southampton, UK, Mobile VCE Core 3 Programme - Wireless Enablers 2.2: Deliverable D-WE2.2.1(P2), December 2003.

[260] M. Jiang and L. Hanzo, "Genetically Enhanced TTCM Assisted MMSE Multi-User Detection for SDMA-OFDM," in *Proceedings of the 2004 IEEE 60th Vehicular Technology Conference (VTC '04 Fall)*, vol. 3, Los Angeles, USA, 26-29 September 2004, pp. 1954–1958.

[261] M. Jiang and L. Hanzo, "Improved Hybrid MMSE Detection for Turbo Trellis Coded Modulation Assisted Multi-User OFDM Systems," *Electronics Letters*, vol. 40, no. 16, pp. 1002–1003, August 2004.

[262] M. Jiang and L. Hanzo, "Iterative Hybrid Multi-User Detection Using Genetic Algorithm and Biased Mutation," in *Proceedings of the 2005 IEE 6th International Conference on 3G and Beyond (3G '05)*, London, UK, 7-9 November 2005, pp. 297–301.

[263] M. Jiang, S. X. Ng, and L. Hanzo, "Hybrid Iterative Multi-User Detection for Channel Coded Space Division Multiple Access OFDM Systems," *IEEE Transactions on Vehicular Technology*, vol. 55, no. 1, pp. 115–127, January 2006.

[264] M. Jiang and L. Hanzo, "Novel MUD Techniques Designed for OFDM/MC-CDMA," University of Southampton, Southampton, UK, Mobile VCE Core 3 Programme - Wireless Enablers 2.2: Deliverable D-WE2.2.2(P2), June 2004.

[265] M. Jiang, J. Akhtman, and L. Hanzo, "Near-Optimum Nonlinear Soft Detection for Multiple-Antenna Assisted OFDM," in *Proceedings of the 2006 IEEE Wireless Communications and Networking Conference (WCNC '06)*, Las Vegas, USA, 3-6 April 2006.

[266] M. Jiang, J. Akhtman, and L. Hanzo, "Soft-information Assisted Near-optimum Nonlinear Detection for BLAST-type Space Division Multiplexing OFDM Systems," *accepted by IEEE Wireless Communications Letters*, December 2006.

[267] M. Jiang, S. X. Ng, and L. Hanzo, "Slow Subcarrier-Hopped Space Division Multiple Access OFDM Systems," in *Proceedings of the 2005 IEEE 62nd Vehicular Technology Conference (VTC '05 Fall)*, Dallas, USA, 25-28 September 2005.

[268] M. Jiang and L. Hanzo, "Multi-User MIMO OFDM Systems Using Subcarrier-Hopping," *submitted to IEE Proceedings - Communications*, August 2005.

[269] M. Jiang, L.-L. Yang, and L. Hanzo, "Direct-Sequence-Spreading and Slow-Subcarrier-Hopping Aided Multi-User OFDM Systems," *submitted to IEEE Transactions on Vehicular Technology*, June 2005.

[270] M. Jiang and L. Hanzo, "Subband-Hopped and Subcarrier-Hopped Multi-User SDMA/OFDM Systems," University of Southampton, Southampton, UK, Mobile VCE Core 3 Programme - Wireless Enablers 2.2: Deliverable D-WE2.2.3(P2), December 2004.

[271] M. Jiang, J. Akhtman, F. Guo, and L. Hanzo, "Iterative Joint Channel Estimation and Multi-User Detection for High-Throughput Multiple-Antenna Aided OFDM Systems," in *Proceedings of the 2006 IEEE 63rd Vehicular Technology Conference (VTC '06 Spring)*, Melbourne, Australia, 7-10 May 2006.

[272] M. Jiang, J. Akhtman, and L. Hanzo, "Iterative Joint Channel Estimation and Multi-User Detection for Multiple-Antenna Aided OFDM Systems," *submitted to IEEE Transactions on Wireless Communications*, October 2005.

[273] M. Jiang and L. Hanzo, "Joint Channel Estimation and Multi-User Detection for Multiple-Antenna Aided OFDM," University of Southampton, Southampton, UK, Mobile VCE Core 3 Programme - Wireless Enablers 2.2: Deliverable D-WE2.2.4(P2), October 2005.

[274] L. Hanzo and T. Keller, *An OFDM and MC-CDMA Primer*. IEEE Press - John Wiley & Sons Ltd., 2006.

[275] P. Chaudhury, W. Mohr, and S. Onoe, "The 3GPP Proposal for IMT-2000," *IEEE Communications Magazine*, vol. 37, no. 12, pp. 72–81, December 1999.

[276] B. Glance and L. Greestein, "Frequency-selective fading effects in digital mobile radio with diversity combining," *IEEE Transactions on Communications*, vol. 31, no. 9, pp. 1085–1094, September 1983.

[277] F. Adachi and K. Ohno, "BER performance of QDPSK with postdetection diversity reception in mobile radio channels," *IEEE Transactions on Vehicular Technology*, vol. 40, no. 1, pp. 237–249, February 1991.

[278] S. M. Alamouti, "A Simple Transmit Diversity Technique for Wireless Communications," *IEEE Journal on Selected Areas in Communications*, vol. 16, no. 8, pp. 1451–1458, October 1998.

[279] V. Tarokh, H. Jafarkhani, and A. R. Calderbank, "Space-time Block Codes from Orthogonal Designs," *IEEE Transactions on Information Theory*, vol. 45, no. 5, pp. 1456–1467, May 1999.

[280] V. Tarokh, H. Jafarkhani, and A. R. Calderbank, "Space-Time Block Coding for Wireless Communications: Performance Results," *IEEE Journal on Selected Areas in Communications*, vol. 17, no. 3, pp. 451–460, March 1999.

[281] V. Tarokh, N. Seshadri, and A. R. Calderbank, "Space-Time Codes for High Data Rate Wireless Communication: Performance Criterion and Code Construction," *IEEE Transactions on Information Theory*, vol. 44, no. 2, pp. 744–765, March 1998.

[282] V. Tarokh, A. Naguib, N. Seshadri, and A. R. Calderbank, "Space-Time Codes for High Data Rate Wireless Communication: Performance Criteria in the Presence of Channel Estimation Errors, Mobility, and Multile Paths," *IEEE Transactions on Communications*, vol. 47, no. 2, pp. 199–207, February 1999.

[283] V. Tarokh, A. Naguib, N. Seshadri, and A. Calderbank, "Space-Time Codes for High Data Rate Wireless Communication: Mismatch Analysis," in *Proceedings of the 1997 IEEE International Conference on Communications (ICC '97)*, vol. 1, Montreal, Canada, 8-12 June 1997, pp. 309–313.

[284] N. Seshadri, V. Tarokh, and A. Calderbank, "Space-Time Codes for Wireless Communication: Code Construction," in *Proceedings of the 1997 IEEE 47th Vehicular Technology Conference (VTC '97 Spring)*, vol. 2, Phoenix, Arizona, 4-7 May 1997, pp. 637–641.

[285] R. Gallager, "Low-density parity-check codes," *IEEE Transactions on Information Theory*, vol. 8, no. 1, pp. 21–28, January 1962.

[286] C. Berrou, A. Glavieux, and P. Thitimajshima, "Near Shannon Limit Error-Correcting Coding and Decoding: Turbo-Codes (1)," in *Proceedings of the 1993 IEEE International*

Conference on Communications (ICC '93), vol. 2, Geneva, Switzerland, 23-26 May 1993, pp. 1064–1070.

[287] C. Berrou and A. Glavieux, "Near optimum error correcting coding and decoding: Turbo-codes," *IEEE Transactions on Communications*, vol. 44, no. 10, pp. 1261–1271, October 1996.

[288] G. Bauch, "Concatenation of Space-Time Block Codes and Turbo-TCM," in *Proceedings of the 1999 IEEE International Conference on Communications (ICC '99)*, vol. 2, Vancouver, Canada, 6-10 June 1999, pp. 1202–1206.

[289] W. Koch and A. Baier, "Optimum and Sub-Optimum Detection of Coded Data Distributed by Time-Varying Inter-Symbol Interference," in *Proceedings of the 1990 IEEE Global Telecommunications Conference (GLOBECOM '90)*, vol. 3, 2-5 December 1990, pp. 1679–1684.

[290] J. Erfanian, S. Pasupathy, and G. Gulak, "Reduced Complexity Symbol Detectors with Parallel Structures for ISI Channels," *IEEE Transactions on Communications*, vol. 42, no. 2/3/4, pp. 1661–1671, February/March/April 1994.

[291] P. Robertson, E. Villebrun, and P. Höher, "A Comparison of Optimal and Sub-Optimal MAP Decoding Algorithms Operating in the Log Domain," in *Proceedings of the 1995 IEEE International Conference on Communications (ICC '95)*, vol. 2, Seattle, USA, 18-22 June 1995, pp. 1009–1013.

[292] D. J. C. Mackay and R. M. Neal, "Near Shannon Limit Performance of Low Density Parity Check Codes," *Electronics Letters*, vol. 33, no. 6, pp. 457–458, March 1997.

[293] M. G. Luby, M. Mitzenmacher, M. A. Shokrollahi, and D. A. Spielman, "Improved low-density parity-check codes using irregular graphs," *IEEE Transactions on Information Theory*, vol. 47, no. 2, pp. 585–598, February 2001.

[294] M. C. Davey, "Error-Correction Using Low Density Parity Check Codes," Ph.D. dissertation, University of Cambridge, Cambridge, UK, 1999.

[295] J. Hou, P. H. Siegel, and L. B. Milstein, "Performance Analysis and Code Optimization of Low Density Parity-Check Codes on Rayleigh Fading Channels," *IEEE Journal on Selected Areas in Communications*, vol. 19, no. 5, pp. 924–934, May 2001.

[296] M. Chiani, A. Conti, and A. Ventura, "Evaluation of low-density parity-check codes over block fading channels," *Proceedings of the 2000 IEEE International Conference on Communications (ICC '00)*, vol. 3, pp. 1183–1187, 18-22 June 2000.

[297] F. Guo, S. X. Ng, and L. Hanzo, "LDPC Assisted Block Coded Modulation for Transmission over Rayleigh Fading Channels," in *Proceedings of the 2003 IEEE 57th Vehicular Technology Conference (VTC '03 Spring)*, vol. 3, Jeju Island, Korea, 22-25 April 2003, pp. 1867–1871.

[298] J. Hagenauer, E. Offer, and L. Papke, "Iterative decoding of binary block and convolutional codes," *IEEE Transactions on Information Theory*, vol. 42, no. 2, pp. 429–445, March 1996.

[299] M. Y. Alias, F. Guo, S. X. Ng, T. H. Liew, and L. Hanzo, "LDPC and Turbo Coding Assisted Space-Time Block Coded OFDM," in *Proceedings of the 2003 IEEE 57th Vehicular Technology Conference (VTC '03 Spring)*, vol. 4, Jeju Island, Korea, 22-25 April 2003, pp. 2309–2313.

[300] G. Ungerböeck, "Channel Coding with Multilevel/Phase Signals," *IEEE Transactions on Information Theory*, vol. 28, no. 1, pp. 55–67, January 1982.

[301] P. Robertson and T. Wörz, "Bandwidth Efficient Turbo Trellis-Coded Modulation Using Punctured Component Codes," *IEEE Journal on Selected Area on Communications*, vol. 16, no. 2, pp. 206–218, February 1998.

[302] E. Zehavi, "8-PSK trellis codes for a Rayleigh channel," *IEEE Transactions on Communications*, vol. 40, no. 5, pp. 873–883, May 1992.

[303] X. Li and J. A. Ritcey, "Bit-interleaved coded modulation with iterative decoding using soft feedback," *Electronics Letters*, vol. 34, no. 10, pp. 942–943, May 1998.

[304] Z. Guo and W. Zhu, "Performance study of OFDMA vs. OFDM/SDMA," in *Proceedings of the 2002 IEEE 55th Vehicular Technology Conference (VTC '02 Spring)*, vol. 2, 6-9 May 2002, pp. 565–569.

[305] S. Verdu, *Multiuser Detection.* Cambridge University Press, 1998.

[306] C. Z. W. H. Sweatman, J. S. Thompson, B. Mulgrew, and P. M. Grant, "A Comparison of Detection Algorithms including BLAST for Wireless Communication using Multiple Antennas," in *Proceedings of the 2000 IEEE International Symposium on Personal, Indoor and Mobile Radio Communications (PIMRC '00)*, vol. 1, London, UK, 18-21 September 2000, pp. 698–703.

[307] M. Münster and L. Hanzo, "Co-Channel Interference Cancellation Techniques for Antenna Array Assisted Multiuser OFDM Systems," in *Proceedings of the 2000 IEE 1st International Conference on 3G Mobile Communication Technologies (3G '00)*, vol. 1, London, Great Britain, 27-29 March 2000, pp. 256–260.

[308] M. Sellathurai and S. Haykin, "A Simplified Diagonal BLAST Architecture with Iterative Parallel-Interference Cancellation Receivers," in *Proceedings of the 2001 IEEE International Conference on Communications (ICC '01)*, vol. 10, Helsinki, Finnland, 11-14 June 2001, pp. 3067–3071.

[309] M. Münster and L. Hanzo, "Performance of SDMA Multiuser Detection Techniques for Walsh-Hadamard-Spread OFDM Schemes," in *Proceedings of the 2001 IEEE 54th Vehicular Technology Conference (VTC '01 Fall)*, vol. 4, Atlantic City, USA, 7-11 October 2001, pp. 2319–2323.

[310] "COST207, Digital Land Mobile Radio Communications," Commission of the European Communities, Luxembourg, Final report, 1989.

[311] U. Fincke and M. Pohst, "Improved methods for calculating vectors of short length in a lattice, including a complexity analysis," *Mathematics of Computation*, vol. 44, no. 170, pp. 463–471, April 1985.

[312] E. Viterbo and J. Boutros, "A universal lattice code decoder for fading channels," *IEEE Transactions on Information Theory*, vol. 45, no. 5, pp. 1639–1642, July 1999.

[313] M. O. Damen, A. Chkeif, and J.-C. Belfiore, "Lattice code decoder for space-time codes," *IEEE Communications Letters*, vol. 4, no. 5, pp. 161–163, May 2000.

[314] B. M. Hochwald and S. ten Brink, "Achieving Near-Capacity on a Multiple-Antenna Channel," *IEEE Transactions on Communications*, vol. 51, no. 3, pp. 389–399, March 2003.

[315] L. Brunel, "Multiuser Detection Techniques Using Maximum Likelihood Sphere Decoding in Multicarrier CDMA Systems," *IEEE Transactions on Wireless Communications*, vol. 3, no. 3, pp. 949–957, May 2004.

[316] D. Pham, K. R. Pattipati, P. K. Willet, and J. Luo, "An Improved Complex Sphere Decoder for V-BLAST Systems," *IEEE Signal Processing Letters*, vol. 11, no. 9, pp. 748–751, September 2004.

[317] T. Cui and C. Tellambura, "Approximate ML Detection for MIMO Systems Using Multistage Sphere Decoding," *IEEE Signal Processing Letters*, vol. 12, no. 3, pp. 222–225, March 2005.

[318] P. W. Wolniansky, G. J. Foschini, G. D. Golden, and R. A. Valenzuela, "V-BLAST: an architecture for realizing very high data rates over the rich-scattering wireless channel," in *URSI International Symposium on Signals, Systems, and Electronics, 1998 (ISSSE '98)*, Pisa, Italy, 29 September-2 October 1998, pp. 295–300.

[319] J. Holland, *Adaptation in Natural and Artificial Systems.* Ann Arbor, Michigan: University of Michigan Press, 1975.

[320] D. E. Goldberg, *Genetic Algorithms in Search, Optimization, and Machine Learning.* Reading, Massachusetts: Addison-Wesley, 1989.

[321] M. Mitchell, *An Introduction to Genetic Algorithms.* Cambridge, Massachusetts: MIT Press, 1996.

[322] D. Whitley, "A Genetic Algorithm Tutorial," *Statistics and Computing*, vol. 4, no. 2, pp. 65–85, June 1994.

[323] S. Forrest, "Genetic Algorithms: Principles of Natural Selection Applied to Computation," *Science*, vol. 261, no. 5123, pp. 872–878, August 1993.

[324] M. J. Juntti, T. Schlösser, and J. O. Lilleberg, "Genetic Algorithms for Multiuser Detection in Synchronous CDMA," in *Proceedings of the 1997 IEEE International Symposium on Information Theory (ISIT '97)*, Ulm, Germany, 29 June-4 July 1997, p. 492.

[325] X. F. Wang, W.-S. Lu, and A. Antoniou, "A genetic-algorithm-based multiuser detector for multiple-access communications," in *Proceedings of the 1998 IEEE International Symposium on Circuits and Systems (ISCAS '98)*, vol. 4, Monterey, USA, 31 May-3 June 1998, pp. 534–537.

[326] C. Ergün and K. Hacioglu, "Multiuser Detection Using a Genetic Algorithm in CDMA Communications Systems," *IEEE Transactions on Communications*, vol. 48, no. 8, pp. 1374–1383, August 2000.

[327] K. Yen and L. Hanzo, "Antenna-diversity-assisted genetic-algorithm-based multiuser detection schemes for synchronous CDMA systems," *IEEE Transactions on Communications*, vol. 51, no. 3, pp. 366–370, March 2003.

[328] K. Yen and L. Hanzo, "Genetic Algorithm Assisted Joint Multiuser Symbol Detection and Fading Channel Estimation for Synchronous CDMA Systems," *IEEE Journal on Selected Areas in Communications*, vol. 19, no. 6, pp. 985–998, June 2001.

[329] S. Abedi and R. Tafazolli, "Genetically modified multiuser detection for code division multiple access systems," *IEEE Journal on Selected Areas in Communications*, vol. 20, no. 2, pp. 463–473, February 2002.

[330] U. Fawer and B. Aazhang, "A Multiuser Receiver for Code Division Multiple Access Communications over Multipath Channels," *IEEE Transactions on Communications*, vol. 43, no. 2-4, pp. 1556–1565, February-April 1995.

[331] T. Blickle and L. Thiele, "A Comparison of Selection Schemes Used in Evolutionary Algorithms," *Evolutionary Computation*, vol. 4, no. 4, pp. 361–394, January 1996.

[332] E. Zitzler and L. Thiele, "Multiobjective Evolutionary Algorithms: A Comparative Case Study and the Strength Pareto Approach," *IEEE Transactions on Evolutionary Computation*, vol. 3, no. 4, pp. 257–271, November 1999.

[333] A. E. Eiben, R. Hinterding, and Z. Michalewicz, "Parameter Control in Evolutionary Algorithms," *IEEE Transactions on Evolutionary Computation*, vol. 3, no. 2, pp. 124–141, July 1999.

[334] J. G. Proakis, *Digital Communications*, 4th ed. McGraw-Hill International Edition, 2001.

[335] W. Ledermann and E. Lloyd, *Handbook of Applicable Mathematics, Volume II: Probability.* John Wiley & Sons Ltd., 1980, vol. 2.

[336] M. K. Simon, J. K. Omura, R. A. Scholtz, and B. K. Levitt, *Spread Spectrum Communications: Volume I.* Maryland, USA: Computer Science Press, 1985.

[337] M. K. Simon, J. K. Omura, R. A. Scholtz, and B. K. Levitt, *Spread Spectrum Communications: Volume II.* Maryland, USA: Computer Science Press, 1985.

[338] M. K. Simon, J. K. Omura, R. A. Scholtz, and B. K. Levitt, *Spread Spectrum Communications: Volume III.* Maryland, USA: Computer Science Press, 1985.

[339] R. E. Ziemer and R. L. Peterson, *Digital Communications and Spread Spectrum System.* New York, USA: Macmillan Publishing Company, 1985.

[340] G. Einarsson, "Address Assignment for a Time-Frequency-Coded, Spread-Spectrum System," *Bell System Technical Journal*, vol. 59, no. 7, pp. 1241–1255, September 1980.

[341] D. J. Goodman, P. S. Henry, and V. K. Prabhu, "Frequency-Hopped Multilevel FSK for Mobile Radio," *Bell System Technical Journal*, vol. 59, no. 7, pp. 1257–1275, September 1980.

[342] A. W. Lam and D. P. Sarwate, "Time-Hopping and Frequency-Hopping Multiple-Access Packet Communications," *IEEE Transactions on Communications*, vol. 38, no. 6, pp. 875–888, June 1990.

[343] U. Fiebig, "Iterative Interference Cancellation for FFH/MFSK MA Systems," *IEE Proceedings - Communications*, vol. 143, no. 6, pp. 380–388, December 1996.

[344] L.-L. Yang and L. Hanzo, "Slow Frequency-Hopping Multicarrier DS-CDMA for Transmission over Nakagami Multipath Fading Channels," *IEEE Journal on Selected Areas In Communications*, vol. 19, no. 7, pp. 1211–1221, July 2001.

[345] L.-L. Yang and L. Hanzo, "Blind Joint Soft-Detection Assisted Slow Frequency-Hopping Multicarrier DS-CDMA," *IEEE Transactions on Communications*, vol. 48, no. 9, pp. 1520–1529, September 2000.

[346] E. A. Geraniotis, "Coherent Hybrid DS-SFH Spread-Spectrum Multiple-Access Communications," *IEEE Journal on Selected Area on Communications*, vol. 3, no. 5, pp. 695–705, September 1985.

[347] J. Wang and H. Huang, "Multicarrier DS/SFH-CDMA Systems," *IEEE Transactions on Vehicular Technology*, vol. 51, no. 5, pp. 867–876, September 2002.

[348] M. Jankiraman and R. Prasad, "A novel solution to wireless multimedia application: the hybrid OFDM/CDMA/SFH approach," in *Proceedings of the 2000 IEEE International Symposium on Personal, Indoor and Mobile Radio Communications (PIMRC '00)*, vol. 2, London, UK, 18-21 September 2000, pp. 1368–1374.

[349] K. Hamaguchi and L. Hanzo, "Time-Frequency Spread OFDM/FHMA," in *Proceedings of the 2003 IEEE 57th Vehicular Technology Conference (VTC '03 Spring)*, vol. 2, Jeju Island, Korea, 22-25 April 2003, pp. 1248–1252.

[350] E. A. Geraniotis, "Noncoherent Hybrid DS-SFH Spread-Spectrum Multiple-Access Communications," *IEEE Transactions on Communications*, vol. 34, no. 9, pp. 862–872, September 1986.

[351] Y. Li and N. R. Sollenberger, "Clustered OFDM with Channel Estimation for High Rate Wireless Data," *IEEE Transactions on Communications*, vol. 49, no. 12, pp. 2071–2076, December 2001.

[352] B. Daneshrad, L. J. Cimini Jr., M. Carloni, and N. Sollenberger, "Performance and Implementation of Clustered OFDM for Wireless Communications," *ACM Journal on Mobile Networks and Applicaitons (MONET) special issue on Personal Communications Services*, vol. 2, no. 4, pp. 305–314, January 1998.

[353] H. Niu, M. Shen, J. A. Ritcey, and H. Liu, "Performance of clustered OFDM with low density parity check codes over dispersive channels," in *Conference Record of the 36th Asilomar Conference on Signals, Systems and Computers*, vol. 1, 3-6 November 2002, pp. 160–164.

[354] G. Parsaee and A. Yarali, "OFDMA for the 4th Generation Cellular Networks," in *Canadian Conference on Electrical and Computer Engineering*, vol. 4, 2-5 May 2004, pp. 2325–2330.

[355] H. Sari and G. Karam, "Orthogonal frequency-division multiple access and its application to CATV network," *European Transactions on Telecommunications*, vol. 9, pp. 507–516, November/December 1998.

[356] J. Jang and K. B. Lee, "Transmit Power Adaptation for Multiuser OFDM Systems," *IEEE Journal on Selected Areas in Communications*, vol. 21, no. 2, pp. 171–178, February 2003.

[357] C. Y. W. amd C. Y. Tsui, R. S. Cheng, and K. B. Lataief, "A Real-time Sub-carrier Allocation Scheme for Multiple Access Downlink OFDM Transmission," in *Proceedings of the 1999 IEEE 50th Vehicular Technology Conference (VTC '99 Fall)*, vol. 2, 19-22 September 1999, pp. 1124–1128.

[358] D. Kivanc, G. Li, and H. Liu, "Computationally Efficient Bandwidth Allocation and Power Control for OFDMA," *IEEE Transactions on Wireless Communications*, vol. 2, no. 6, pp. 1150–1158, November 2003.

[359] D. Kivanc and H. Liu, "Subcarrier Allocation and Power Control for OFDMA," in *Conference Record of the 34th Asilomar Conference on Signals, Systems and Computers*, vol. 1, 29 October-1 November 2000, pp. 147–151.

[360] I. Kim, H. L. Lee, B. Kim, and Y. H. Lee, "On the use of linear programming for dynamic subchannel and bit allocation in multiuser OFDM," in *Proceedings of the 2001 IEEE Global Telecommunications Conference (GLOBECOM '01)*, vol. 6, 25-29 November 2001, pp. 3648–3652.

[361] W. Rhee and J. M. Cioffi, "Increase in capacity of multiuser OFDM system using dynamic subchannel allocation," in *Proceedings of the 2000 IEEE 51st Vehicular Technology Conference (VTC '00 Spring)*, vol. 2, Tokyo, Japan, 15-18 May 2000, pp. 1085–1089.

[362] S. Das and G. D. Mandyam, "An efficient sub-carrier and rate allocation scheme for M-QAM modulated uplink OFDMA transmission," in *Proceedings of the 2003 IEEE 37th Asilomar Conference on Signals, Systems and Computers (ACSSC '03)*, vol. 1, 9-12 November 2003, pp. 136–140.

[363] S. Pietrzyk and G. J. M. Janssen, "Multiuser subcarrier allocation for QoS provision in the OFDMA systems," in *Proceedings of the 2002 IEEE 56th Vehicular Technology Conference (VTC '02 Fall)*, vol. 2, 24-28 September 2002, pp. 1077–1081.

[364] Z. Hu, G. Zhu, Y. Xia, and G. Liu, "Multiuser subcarrier and bit allocation for MIMO-OFDM systems with perfect and partial channel information," in *Proceedings of the 2004 IEEE Wireless Communications and Networking Conference (WCNC '04)*, vol. 2, 21-25 March 2004, pp. 1188–1193.

[365] S. Zhou, G. B. Giannakis, and A. Scaglione, "Long codes for generalized FH-OFDMA through unknown multipath channels," *IEEE Transactions on Communications*, vol. 49, no. 4, pp. 721–733, April 2001.

[366] Z. Cao, U. Tureli, and P. Liu, "Optimum subcarrier assignment for OFDMA uplink," in *Conference Record of the 37th Asilomar Conference on Signals, Systems and Computers*, vol. 1, 9-12 November 2003, pp. 708–712.

[367] Y. H. Kim, K. S. Kim, and J. Y. Ahn, "Iterative estimation and decoding for an LDPC-coded OFDMA system in uplink environments," in *Proceedings of the 2004 IEEE International Conference on Communications (ICC '04)*, vol. 4, 20-24 June 2004, pp. 2478–2482.

[368] H. Sari, Y. Levy, and G. Karam, "An analysis of orthogonal frequency-division multiple access," in *Proceedings of the 1997 IEEE Global Telecommunications Conference (GLOBECOM '97)*, vol. 3, 3-8 November 1997, pp. 1635–1639.

[369] T. Kurt and H. Delic, "Collision avoidance in space-frequency coded FH-OFDMA," in *Proceedings of the 2004 IEEE International Conference on Communications (ICC '04)*, vol. 1, 20-24 June 2004, pp. 269–273.

[370] H. H. Chen, Y. C. Yeh, C. H. Tsai, and W. H. Chang, "Uplink synchronisation control technique and its environment-dependent performance analysis," *Electronics Letters*, vol. 39, no. 24, pp. 1755–1757, November 2003.

[371] J.-J. V. D. Beek, P. O. Börjesson, M.-L. Boucheret, D. Landström, J. M. Arenas, P. Ödling, C. Östberg, M. Wahlqvist, and S. K. Wilson, "A time and frequency synchronization scheme for multiuser OFDM," *IEEE Journal on Selected Areas in Communications*, vol. 17, no. 11, pp. 1900–1914, November 1999.

[372] M. Pompili, S. Barbarossa, and G. B. Giannakis, "Channel-independent non-data aided synchronization of generalized multiuser OFDM," in *Proceedings of the 2001 IEEE International Conference on Acoustics, Speech, and Signal Processing (ICASSP '01)*, vol. 4, 7-11 May 2001, pp. 2341–2344.

[373] S. T. Wu and K. C. Chen, "Programmable multiuser synchronization for OFDM-CDMA," in *Proceedings of the 2001 IEEE 53rd Vehicular Technology Conference (VTC '01 Spring)*, vol. 2, 6-9 May 2001, pp. 830–834.

[374] S. Lipschutz and M. L. Lipson, *Schaum's Outline of Theory and Problems of Probability*, 2nd ed., ser. Schaum's Outline Series. USA: McGraw-Hill, 2000.

[375] M. K. Simon, J. K. Omura, R. A. Scholtz, and B. K. Levitt, *Spread Spectrum Communications: Volume I, II, III.* Maryland, USA: Computer Science Press, 1985.

[376] J. Xavier, V. A. N. Barroso, and J. M. F. Moura, "Closed-form correlative coding (CFC2) blind identification of MIMO channels: isometry fitting to second order statistics," *IEEE Transactions on Signal Processing*, vol. 49, no. 5, pp. 1073–1086, May 2001.

[377] W. Nabhane and H. V. Poor, "Blind Joint Equalization and Multiuser Detection in Dispersive MC-CDMA/MC-DS-CDMA/MT-CDMA Channels," in *Proceedings of the 2002 IEEE Military Communications Conference (MILCOM '02)*, vol. 2, 7-10 October 2002, pp. 814–819.

[378] Y. Li, N. Seshadri, and S. Ariyavisitakul, "Channel Estimation for OFDM Systems With Transmitter Diversity in Mobile Wireless Channels," *IEEE Journal on Selected Areas in Communications*, vol. 17, no. 3, pp. 461–471, March 1999.

[379] H. Minn, D. I. Kim, and V. K. Bhargava, "A Reduced Complexity Channel Estimation for OFDM Systems With Transmit Diversity in Mobile Wireless channels," *IEEE Transactions on Communications*, vol. 50, no. 5, pp. 799–807, May 2002.

[380] F. W. Vook and T. A. Thomas, "MMSE Multi-user Channel Estimation for Broadband Wireless Communications," in *Proceedings of the 2001 IEEE Global Telecommunications Conference (GLOBECOM '01)*, vol. 1, San Antonio, USA, 25-29 November 2001, pp. 470–474.

[381] K. J. Kim and R. A. Iltis, "Joint Detection and Channel Estimation Algorithms for QS-CDMA Signals Over Time-varying Channels," *IEEE Transactions on Communications*, vol. 50, no. 5, pp. 845–855, May 2002.

[382] F. Horlin and L. V. D. Perre, "Optimal Training Sequences for Low Complexity ML Multi-channel Estimation in Multi-user MIMO OFDM-based Communications," in *Proceedings of the 2004 IEEE International Conference on Communications (ICC '04)*, vol. 4, 20-24 June 2004, pp. 2427–2431.

[383] T. Cui and C. Tellambura, "Joint channel estimation and data detection for OFDM systems via sphere decoding," in *Proceedings of the 2004 IEEE Global Telecommunications Conference (GLOBECOM '04)*, vol. 6, 29 November-3 December 2004, pp. 3656–3660.

[384] H. Zhu, B. Farhang-Boroujeny, and C. Schlegel, "Pilot Embedding for Joint Channel Estimation and Data Detection in MIMO Communication Systems," *IEEE Communications Letters*, vol. 7, no. 1, pp. 30–32, January 2003.

[385] J. Wang and K. Araki, "Pilot-symbol Aided Channel Estimation in Spatially Correlated Multiuser MIMO-OFDM Channels," in *Proceedings of the 2004 IEEE 60th Vehicular Technology Conference (VTC '04 Fall)*, vol. 1, Los Angeles, USA, 26-29 September 2004, pp. 33–37.

[386] J. Siew, J. Coon, R. J. Piechocki, A. Dowler, A. Nix, M. A. Beach, S. Armour, and J. McGeehan, "A channel estimation algorithm for MIMO-SCFDE," *IEEE Communications Letters*, vol. 8, no. 9, pp. 555–557, September 2004.

[387] S. Chen and Y. Wu, "Maximum likelihood joint channel and data estimation using genetic algorithms," *IEEE Transactions on Signal Processing*, vol. 46, no. 5, pp. 1469–1473, May 1998.

[388] Y. S. Zhang, Y. Du, W. Zhang, X. Z. Wang, and J. Li, "A data-aided time domain channel estimation method," in *Proceedings of the 2004 Joint Conference of the 10th Asia-Pacific Conference on Communications and the 5th International Symposium on Multi-Dimensional Mobile Communications*, vol. 1, 29 August-1 September 2004, pp. 469–473.

[389] C. E. Tan and I. J. Wassell, "Near-optimum training sequences for OFDM systems," in *The 9th Asia-Pacific Conference on Communications (APCC '03)*, vol. 1, 21-24 September 2003, pp. 119–123.

[390] K. Yen and L. Hanzo, "Genetic-algorithm-assisted multiuser detection in asynchronous CDMA communications," *IEEE Transactions on Vehicular Technology*, vol. 53, no. 5, pp. 1413–1422, September 2004.

[391] X. Wu, T. C. Chuah, B. S. Sharif, and O. R. Hinton, "Adaptive robust detection for CDMA using a genetic algorithm," *IEE Proceedings - Communications*, vol. 150, no. 6, pp. 437–444, 10 December 2003.

[392] J. Akhtman and L. Hanzo, "Reduced-Complexity Maximum-Likelihood Detection in Multiple-Antenna-Aided Multicarrier Systems," in *Proceedings of the 5th International Workshop on Multi-Carrier Spread Spectrum Communications*, Oberpfaffenhofen, Germany, 14-16 September 2005.

[393] J. Akhtman and L. Hanzo, "An Optimized-Hierarchy-Aided Maximum Likelihood Detector for MIMO-OFDM," in *Proceedings of the 2006 IEEE 63rd Vehicular Technology Conference (VTC '06 Spring)*, Melbourne, Australia, 7-10 May 2006.

[394] J. Akhtman and L. Hanzo, "Novel Optimized-Hierarchy RSA-aided Space-Time Processing Method," University of Southampton, Southampton, UK, Mobile VCE Core 3 Programme - Wireless Enablers 2.2: ICR-WE2.2.1, May 2005.

[395] N. Seshadri, "Joint data and channel estimation using blind trellis search techniques," *IEEE Transactions on Communications*, vol. 42, no. 2-4, pp. 1000–1011, February-April 1994.

[396] R. Raheli, A. Polydoros, and C. K. Tzou, "Per-Survivor Processing: a general approach to MLSE in uncertain environments," *IEEE Transactions on Communications*, vol. 43, no. 2-4, pp. 354–364, February-April 1995.

[397] R. L. Haupt and S. E. Haupt, *Practical Genetic Algorithms*, 2nd ed. New Jersey, USA: John Wiley & Sons, Ltd., 2004, iSBN 0-471-45565-2.

[398] Z. Michalewicz, *Genetic Algorithms + Data Structures = Evolution Programs*, 2nd ed. New York, USA: Springer-Verlag, 1994.

[399] T. K. Moon and W. C. Stirling, *Mathematical Methods and Algorithms for Signal Processing.* Prentice Hall, 2002.

[400] S. Kay, *Fundamentals of Statistical Signal Processing, Estimation Theory.* New Jersey, USA: Prentice Hall, 1993.

[401] T. Bäck, *Evolutionary Algorithms in Theory and Practice: Evolution Strategies, Evolutionary Programming, Genetic Algorithms.* New York, USA: Oxford University Press, 1996.

[402] D. B. Fogel, "An Introduction to Simulated Evolutionary Optimization," *IEEE Transactions on Neural Networks*, vol. 5, no. 1, pp. 3–14, January 1994.

[403] S. Haykin, *Neural Networks*, 2nd ed. Prentice Hall, 1999.

[404] L. Fausett, *Fundamentals of Neural Networks: Architectures, Algorithms and Applications.* Prentice-Hall, 1994.

[405] V. W. Porto and D. B. Fogel, "Alternative Neural Network Training Methods," *IEEE Expert*, vol. 10, no. 3, pp. 16–22, June 1995.

[406] K. Chellapilla and D. Fogel, "Evolving an expert checkers playing program without using human expertise," *IEEE Transactions on Evolutionary Computation*, vol. 5, no. 4, pp. 422–428, August 2001.

[407] L. Hanzo, C. H. Wong, and M. S. Yee, *Adaptive Wireless Tranceivers.* IEEE Press - John Wiley & Sons Ltd., 2002.

[408] G. Kechriotis, E. Zervas, and E. S. Manolakos, "Using Recurrent Neural Networks for Adaptive Communication Channel Equalization," *IEEE Transactions on Neural Networks*, vol. 5, no. 2, pp. 267–278, March 1994.

[409] R. Parisi, E. D. D. Claudio, G. Orlandi, and B. D. Rao, "Fast Adaptive Digital Equalization by Recurrent Neural Networks," *IEEE Transactions on Signal Processing*, vol. 45, no. 11, pp. 2731–2739, November 1997.

[410] M. D. Buhmann, *Radial Basis Functions: Theory and Implementations.* Cambridge University Press, 2003.

[411] P. V. Yee and S. Haykin, *Regularized Radial Basis Function Networks: Theory and Applications.* USA: John Wiley & Sons Ltd., 2001.

[412] U. Mitra and H. V. Poor, "Neural network techniques for adaptive multiuser demodulation," *IEEE Journal on Selected Areas in Communications*, vol. 12, no. 9, pp. 1460–1470, December 1994.

[413] K. Ko, S. Choi, C. Kang, and D. Hong, "RBF multiuser detector with channel estimation capability in a synchronous MC-CDMA system," *IEEE Transactions on Neural Networks*, vol. 12, no. 6, pp. 1536–1539, November 2001.

[414] C. Ahn and I. Sasase, "Adaptive array antenna based on radial basis function network as multiuser detection for WCDMA," *Electronics Letters*, vol. 38, no. 20, pp. 1208–1210, September 2002.

[415] H. Wei and L. Hanzo, "Reduced-Complexity Genetic Algorithm Aided and Radial Basis Function Assisted Multiuser Detection for Synchronous CDMA," in *Proceedings of the 2004 European Signal Processing Conference (EUSIPCO '04)*, Vienna, Austria, September 2004, pp. 157–160.

[416] X. Zhou and X. Wang, "Channel Estimation for OFDM Systems Using Adaptive Radial Basis Function Networks," *IEEE Transactions on Vehicular Technology*, vol. 52, no. 1, pp. 48–59, January 2003.

[417] G. Charalabopoulos, P. Stavroulakis, and A. H. Aghvami, "A frequency-domain neural network equalizer for OFDM," in *Proceedings of the 2003 IEEE Global Telecommunications Conference (GLOBECOM '03)*, vol. 2, 1-5 December 2003, pp. 571–575.

[418] S. Lerkvaranyu, K. Dejhan, and Y. Miyanaga, "M-QAM demodulation in an OFDM system with RBF neural network," in *Proceedings of the 2004 IEEE 47th Midwest Symposium on Circuits and Systems (MWSCAS '04)*, vol. 2, 25-28 July 2004, pp. 581–584.

[419] T. Cui and C. Tellambura, "Channel estimation for OFDM systems based on adaptive radial basis function networks," in *Proceedings of the 2004 IEEE 60th Vehicular Technology Conference (VTC '04 Fall)*, vol. 1, Los Angeles, USA, 26-29 September 2004, pp. 608–611.

[420] S. Chen, A. K. Samingan, B. Mulgrew, and L. Hanzo, "Adaptive minimum-BER linear multiuser detection for DS-CDMA signals in multipath channels," *IEEE Transactions on Signal Processing*, vol. 49, no. 6, pp. 1240–1247, June 2001.

[421] H. Mühlenbein, *Foundations of Genetic Algorithms*, G. Rawlins, Ed. California, USA: Morgan Kaufmann, 1991.

[422] J. J. Grefenstette and J. E. Baker, "How Genetic Algorithms Work: A critical look at implicit parallelism," in *Proceedings of the 3rd International Conference on Genetic Algorithms*, J. D. Schaffer, Ed. California, USA: Morgan Kaufmann, 1989, pp. 20–27.

[423] B. L. Miller and D. E. Goldberg, "Genetic Algorithms, Selection Schemes and the Varying Effects of Noise," *Evolutionary Computation*, vol. 4, no. 2, pp. 113–131, Summer 1996.

[424] L. J. Eshelman and J. D. Schaffer, "Preventing premature convergence in Genetic Algorithms by preventing incest," in *Proceedings of the 4th International Conference on Genetic Algorithms*, R. K. Belew and L. B. Booker, Eds. California, USA: Morgan Kaufmann, 1991, pp. 115–122.

[425] G. Syswerda, "Uniform Crossover in Genetic Algorithms," in *Proceedings of the 3rd International Conference on Genetic Algorithms*, J. D. Schaffer, Ed. California, USA: Morgan Kaufmann, 1989, pp. 2–9.

Index

Author Index

C

D

E

F

G

H

I

M

N

O

S

T

X

Y

Z